

U.S. DEPARTMENT OF THE INTERIOR

U.S. GEOLOGICAL SURVEY

**CONTRIBUTIONS TO THE GOLD METALLOGENY
OF NORTHERN NEVADA**

Richard M. Tosdal
editor

Open-File Report

98-338- B

This report is preliminary and has not been reviewed for conformity with U.S. Geological Survey editorial standards or with the North American Stratigraphic Code. Any use of trade, product or firm names is for descriptive purposes only and does not imply endorsement by the U.S. Government.

U.S. Geological Survey, Menlo Park, CA

TABLE OF CONTENTS

Contributions to the gold metallogeny of northern Nevada—Preface <i>R.M. Tosdal</i>	1
Crustal structure	
Progress on understanding the crustal structure near the Battle Mountain-Eureka mineral trend from geophysical constraints <i>V.J.S. Grauch, D.P. Klein, Brian D. Rodriguez</i>	8
Regional crustal structure beneath the Carlin Trend, Nevada, based on deep electrical geophysical measurements <i>Brian D. Rodriguez</i>	15
Pb isotopic mapping of crustal structure in the northern Great Basin and relationships to Au deposit trends <i>J.L. Wooden, R.W. Kistler, and R.M. Tosdal</i>	20
Crustal structure and its relation to gold belts in north-central Nevada: Overview and progress report <i>V.J.S. Grauch</i>	34
Carlin-type gold deposits	
Preliminary facies analysis of Silurian and Devonian autochthonous rocks that host gold along the Carlin trend, Nevada <i>Augustus K. Armstrong, Ted G. Theodore, Robert L. Oscarson, Boros B. Kotlyar, Anita G. Harris, Keith H. Bettles, Eric A. Lauha, Richard A. Hipsley, Gregory L. Griffin, Earl W. Abbott, and J. Kelly Cluer</i>	38
Geology of the northern terminus of the Carlin trend, Nevada: Links between crustal shortening during the late Paleozoic Humboldt orogeny and northeast-striking faults <i>Ted G. Theodore, Augustus K. Armstrong, Anita G. Harris, Calvin H. Stevens, and Richard M. Tosdal</i>	69
Evidence for the Crescent Valley-Independence Lineament, north-central Nevada <i>Stephen G. Peters</i>	106
Initial results of stratigraphic and structural framework studies in The Cedars quadrangle, southern Shoshone Range <i>Thomas E. Moore and Benita L. Murchey</i>	119
Recognition and significance of Eocene deformation in the Alligator Ridge area, central Nevada <i>C.J. Nutt and S.C. Good</i>	141
Tungsten-polymetallic- and barite-mineralized rocks in the Ruby Mountains, Nevada <i>Vladimir I. Berger and Robert L. Oscarson</i>	151
Age and possible source of air-fall tuffs of the Miocene Carlin Formation, northern Carlin trend <i>Robert J. Fleck, Ted G. Theodore, Andrei Sarna-Wojcicki, and Charles E. Meyer</i>	176
Importance of clay characterization to interpretation of $^{40}\text{Ar}/^{39}\text{Ar}$ dates on illite from Carlin-type gold deposits: Insights from Jerritt Canyon, Nevada <i>H.W. Folger, A. H. Hofstra, D.D. Eberl, and L.W. Snee</i>	193

δD and $\delta^{18}O$ data from Carlin-type gold deposits—Implications for genetic models <i>Albert H. Hofstra and Robert O. Rye</i>	202
Geochemical modeling of alteration and gold deposition in the Betze deposit, Eureka County, Nevada <i>M. B. Woitsekhowskaya and S.G. Peters</i>	211
Mixed sources of Pb in sedimentary-rock-hosted Au deposits, northern Nevada <i>R.M. Tosdal, J.S. Cline, A.H. Hofstra, S.G. Peters, J.L. Wooden, M.N. Young- Mitchell</i>	223
Regional analysis of the distribution of gold deposits in northeast Nevada using NURE arsenic and geophysical data <i>Boris B. Kotlyar, Donald A. Singer, Robert C. Jachens, and Ted G. Theodore</i>	234
Soil gas studies along Carlin trend, Eureka and Elko counties, Nevada <i>Howard McCarthy and Emmet McGuire</i>	243

Pluton related gold deposits in the Battle Mountain Mining District

Pluton-related Au in the Battle Mountains Mining District—An overview <i>Ted G. Theodore</i>	251
Large distal-disseminated precious-metal deposits, Battle Mountain Mining District, Nevada <i>Ted G. Theodore</i>	253
Multilevel geochemical patterns at the Fortitude gold skarn, Battle Mountain Mining District, Nevada <i>Boris B. Kotlyar and Ted G. Theodore</i>	259

Hot-spring Au deposits

New studies on Tertiary volcanic rocks and mineral deposits, northern Nevada Rift <i>A.R. Wallace and D.A. John</i>	264
Geology and mineralization of the Eocene Tuscarora Volcanic Field, Elko County, Nevada <i>Christopher D. Henry, David R. Boden, and Steven B. Castor</i>	279

CONTRIBUTORS TO THIS VOLUME

**U.S. Geological Survey
345 Middlefield Road
Menlo Park, CA 94025**

*Augusta K. Armstrong
Vladimir I. Berger
Boris B. Kotlyar
Robert J. Fleck
Robert C. Jachens
David A. John
Ronald W. Kistler
Charles E. Meyer
Thomas E. Moore
Benita L. Murchey
Robert L. Oscarson
Andrei Sarna-Wojcicki
Donald A. Singer
Ted G. Theodore
Richard M. Tosdal
Joseph L. Wooden*

**U.S. Geological Survey
Mackay School of Mines
University of Nevada
Reno, NV 89557**

*Howard McCarthy
Emmet McGuire
Stephen G. Peters
Alan R. Wallace*

**U.S. Geological Survey
Box 25046 Denver Federal Center
Denver, CO 80225**

*D.D. Eberl
Helen W. Folger
Carol A. Gent
V.J.S. Grauch
Albert H. Hofstra
Douglas P. Klein
Constance J. Nutt
Brian D. Rodriguez
Robert O. Rye
Lawrence W. Snee*

**U.S. Geological Survey
National Center
Reston, VA 22092**

Anita G. Harris

OTHER CONTRIBUTORS

Earl W. Abbott
Consultant
Reno, NV 89502

Keith H. Bettles
Eric G. Lauha
Richard A. Hipsley
Gregory L. Griffin
Barrick Goldstrike Mines, Inc.
Elko, Nevada 89803

David R. Boden
1445 High Chaparral Drive
Reno, NV 89511

J. S. Cline
Department of Geoscience
University of Nevada, Las Vegas
Las Vegas, NV

J. Kelly Cluer
Uranerz U.S.A. Inc.
Reno, Nevada 89502

S.C. Good
Department of Geology and Astronomy
West Chester University
West Chester, PA. 19383

Christopher D. Henry
Steven B. Kastor
Nevada Bureau of Mines and Geology
University of Nevada
Reno, NV 89557

Calvin H. Stevens
Department of Geology
San Jose State University
San Jose, CA 95192

Michaela Young-Griffin
Department of Geosciences
University of Arizona
Tucson, AZ 85721

Maria B. Woitsekhowskaya
Mackay School of Mines
University of Nevada
Reno, NV 89557

CONTRIBUTIONS TO THE GOLD METALLOGENY OF NORTHERN NEVADA—PREFACE

By R.M. Tosdal

INTRODUCTORY COMMENTS

The northern Great Basin, specifically northern Nevada, is one of the Earth's premier Au producing regions. Here, gold (Au) and silver (Ag) are produced from a range of deposit types, with production being dominated by sedimentary-rock-hosted deposits, particularly those that lie along the Carlin trend (fig. 1) (Christensen, 1993, 1996). This small area is North America's most prolific gold mining district. Across the state of Nevada, gold production during 1998 will account for approximately 64 percent of U.S and 9 percent of the world total. Clearly the impact of these deposits on nearby local economies and on our national balance of payments will be profound well into the next century.

Knowledge of the major Au-Ag deposit types as well as crustal structure is critical to understanding the gold metallogeny of northern Nevada. This information is a basis for mineral exploration, for land-use planning decisions, and for environmental questions. Of principal importance in this region are the giant, sedimentary-rock-hosted or Carlin-type deposits, which are some of the largest deposits in the world. Despite their economic importance, their genesis is not fully understood, even though aspects of them have been investigated for over 35 years. For example, there still is no agreement as to the source of gold, the age of gold deposition, the source of heat driving hydrothermal convection systems, and the geologic reasons for linear arrays of deposits (Christensen, 1993, 1996; Arehart, 1996). In contrast to the uncertain origin of the Carlin-type deposits, other sedimentary-rock hosted deposits in northern Nevada, known as the distal-disseminated Ag-Au type (Theodore, 1998), are genetically related to shallow plutonic complexes (Theodore, 1998, this volume). These sedimentary-rock-hosted deposits bear many similarities to a typical Carlin-type deposit, an observation that has led to models linking them to the plutonic environment (Sillitoe and Bonham, 1990). Hot-spring Au-Ag systems associated with Tertiary volcanic rocks represent a third type of precious metal deposit in northern Nevada. These deposits, although generally smaller than the sedimentary-rock-hosted gold deposits, are important gold resources.

Aspects important to the varied geologic environments of these different gold deposits in northern Nevada (fig. 1), which are the focus of ongoing research, are addressed in

the twenty-two chapters that compose this volume. These chapters are organized along four themes: (1) crustal structure; (2) Carlin-type deposits; (3) pluton-related Au-Ag deposits near Battle Mountain; and (4) hot-spring Au-Ag deposits. The chapters represent contributions from scientists of the U.S. Geological Survey, University of Nevada at Reno, University of Nevada at Las Vegas, Nevada Bureau of Mines and Geology, University of Arizona, West Chester University, San Jose State University, Barrick Goldstrike Mines Inc., Uranerz U.S.A. Inc., and Sierra Exploration Inc.

CRUSTAL STRUCTURE

Linear arrays of Au-Ag deposits in northern Nevada, the Carlin trend and the Battle Mountain-Eureka mineral belt (fig. 1), are thought to reflect a fundamental deep crustal structural control on ore deposition (Shawe, 1991), although other tectonic models have been proposed (Madrid and Roberts, 1991). Understanding the control these inferred crustal-scale faults exerted on ore formation is not straightforward. There is neither structural evidence linking ore formation to the inferred north-northwest trending deep crustal faults, nor is there surface outcrops of such faults (Christensen, 1995), nor is there widespread evidence suggesting their geometry or crustal persistence. Grauch and others (1995) have observed a major northwest-trending gravity gradient that is coincident with the Battle Mountain-Eureka mineral trend and partially coincident with the northern Nevada rift. Combining this gravity gradient with other geophysical evidence, Grauch and others (this volume) demonstrate a discontinuity in geophysical properties coincident with the Battle Mountain-Eureka mineral belt. They interpret the discontinuity to reflect a crustal-scale fault. Rodriguez (1997, this volume) extended the magnetotelluric profile of Grauch and others (this volume) across northern Nevada crossing the Carlin trend where a similar discontinuity in crustal resistivity is evident. This implies that the Carlin trend also lies along a major crustal fault system.

Whereas the geophysical data are interpreted to indicate that the Battle Mountain-Eureka mineral belt and the Carlin trend are indeed associated with faults, or fault zones, penetrating deep in the crust, these data provide little

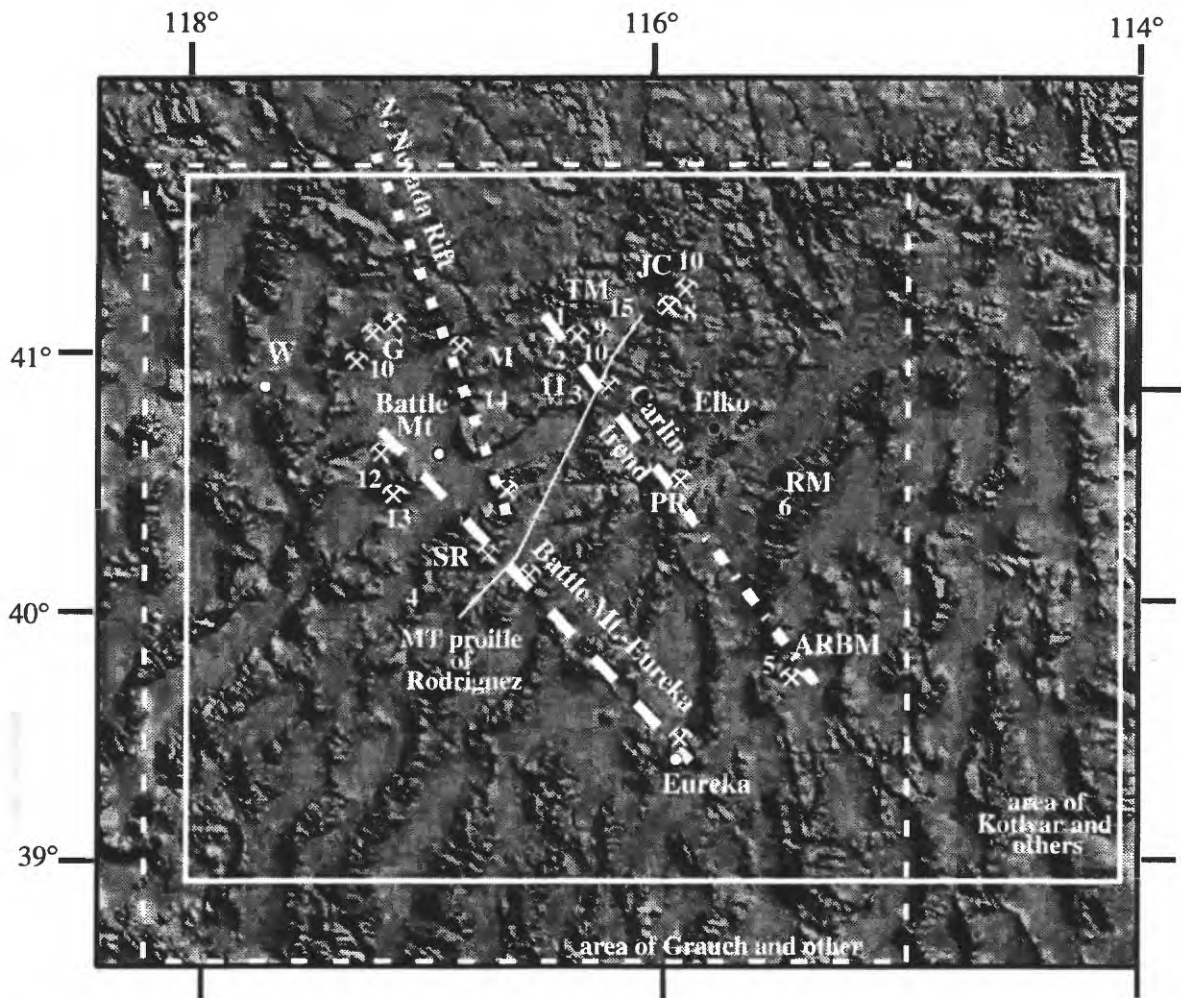


Figure 1. Shaded digital topographic map of northern Nevada showing location of geophysical and isotopic studies described herein, selected geographic locations and mines, Battle Mountain-Eureka mineral belt, Carlin trend and the southeastern extension to Alligator Ridge (dash-dot line), and the northern Nevada Rift. ARBM, Alligator Ridge-Bald Mountain; G, Getchell Mine; JC, Jerritt Canyon Mining District; M, Midas; RM, Ruby Mountains, SR, Shoshone Range; TM, Tuscarora Mountains; and W, Winnemucca.

Area of study by Grauch and others (this volume) included within large box outlined by white dashed lines. Magnetotelluric traverse of Rodriguez (this volume) is shown in solid white line. Area of Pb and Sr isotopic mapping described by Wooden and others (this volume) extends beyond the area of the map. Grauch (this volume) summarized these contributions across a traverse broadly parallel to the magnetotelluric profile of Rodriguez (this volume). Area of regional geochemical and geophysical analysis by Kotlyar and others (this volume) is outlined in the box (solid white line). Stable isotopic study by Hofstra and Rye (this volume) covers the central part of the map. Site specific studies are: 1, Armstrong and others (this volume); 2, Theodore and others (this volume); 3, Peters (this volume); 4, Moore and Murchey (this volume); 5, Nutt and Good (this volume); 6, Berger and others (this volume); 7, Fleck and others (this volume); 8, Folger and others (this volume); 9, Woitsekhowskaya and Peters (this volume); 10, Tosdal and others (this volume); 11, McCarthy and McGuire; 12, Battle Mountain Mining District summarized by Theodore (this volume), 13, Kotlyar and Theodore (this volume); 14, John and Wallace (this volume), and 15, Henry and others (this volume).

evidence as to their origin. To address this question, Wooden and others (this volume), using Pb and Sr isotopic maps of Mesozoic and Tertiary igneous rocks, recognize regional differences in the composition of the lower and middle crust. Combining the Pb and Sr isotopic maps with stratigraphic facies variations (Elison and others, 1990), they propose that isotopic provinces, and the boundaries between them, were

established during rifting along the western (present coordinates) margin of North America in the late Proterozoic and early Paleozoic. The Carlin trend lies along the Pb isotopic boundary which separates relatively intact and largely unmodified Archean and Proterozoic crust to the east from transitional continental crust to the west. This places most large gold deposits in the Great Basin over transitional

continental crust and west of relatively intact and unmodified crust in northeastern Nevada, an observation also made by Cunningham (1988) using other data.

Integrating the geophysical constraints with the radiogenic isotopic data permit Grauch (this volume) to present a schematic cross section across northern Nevada. Deeply penetrating fault zones are interpreted to coincide with the Battle Mountain-Eureka and Carlin trends. These faults separate broad west to east changes in crustal composition, and mark fundamental changes from oceanic crust to thinned transitional continental crust to relatively intact and unmodified continental crust.

CARLIN-TYPE GOLD DEPOSITS

Sedimentary-rock-hosted or Carlin-type deposits represent the major gold deposit-type in northern Nevada. The largest concentration of these deposits lies in the Carlin trend (fig. 1), a 60-km-long array of deposits and prospects, which has produced approximately 21 million ounces of gold since 1965 (Christensen, 1996). The many studies of these deposits have recognized the importance of reactive calcareous sedimentary rocks to their formation (summarized by Christensen, 1993, 1995, 1996; and Arehart, 1996). A facies analysis of Silurian and Devonian rocks, the principal host rocks in the northern Carlin trend (fig. 1), by Armstrong and others (this volume) suggest that essential attributes derived from their depositional environments contributed significantly to subsequent gold deposition. They point out that the vast bulk of Carlin-type deposits are hosted in the Roberts Mountains and Popovich Formations because these rocks had porosity at the time of gold deposition due to early diagenetic crystallization of dolomite in a lime mud. Abundant intercrystalline sulfur-rich carbon also contributed to their being favorable host rocks.

Structure, particularly an allochthonous thrust sheet of deep-water eugeoclinal rocks emplaced over reactive calcareous rocks along the Devonian and early Mississippian Roberts Mountains thrust system, is another important aspect of Carlin-type deposits (Roberts, 1966; Christensen, 1995, 1996). Younger contractile late Paleozoic and Mesozoic deformations further complicate the structural architecture of the deposits (Ketner, 1977, 1998), but their impact on the structural fabric of the Carlin trend is not widely appreciated. Theodore and others (this volume), building upon geologic mapping at the northern end of the Carlin trend, (fig. 1) outline the regional importance of southward shortening in the Late Paleozoic Humboldt orogeny. Deformation at this time was marked by west-northwest to northwest trending folds, thrust faults, and moderate-dipping reverse faults. These faults cut at high angles across the northerly striking Devonian and early Mississippian Roberts Mountains thrust system. The Rain fault in the northern Piñon Range, along which the Rain

Carlin-type deposit is localized (Longo and Williams *in* Teal and Jackson, 1997), is one of these late Paleozoic contractile structures (Theodore and others, this volume).

Peters (this volume) describes a north-northeast trending lineament, the Crescent Valley-Independence lineament, which extends from the Independence Mountains on the northeast to near Cortez, Nevada, on the southwest (fig. 1). This lineament is formed by the alignment of modern physiographic and geologic features. The central part of the Crescent Valley-Independence lineament is marked by tectonized rocks characterized by melange fabrics. Peters (this volume) argues that the lineament is a long-lived structural feature that has been reactivated multiple times since formation in the Paleozoic. It is also suggested to have focused hydrothermal fluid flow leading to the formation of Carlin-type deposits.

To the west near the Battle Mountains-Eureka mineral belt, Moore and Murchey (this volume) outline the Paleozoic stratigraphic, biostratigraphic, and structural framework of a part of the Shoshone Range (fig. 1). Here, eugeoclinal rocks of the Roberts Mountain allochthon are unconformably overlain by the upper Paleozoic Antler overlap sequence, consisting of a shoaling upward sequence of clastic rocks and minor limestone. These rocks regionally are structurally buried beneath deep-water upper Paleozoic rocks of the Golconda allochthon in the late Paleozoic (Stewart, 1980). However in the northern Shoshone Range, new fossil data suggest that the transition from the overlap sequence to the deeper water sedimentary rocks is not obviously a major thrust fault, as would be expected based upon regional relations. Evidently, there are structural complexities of regional importance that need to be resolved.

In the Alligator Ridge-Bald Mountain area at the southeastern terminus of the Carlin trend (fig. 1), Nutt and Good (this volume) document Eocene transpressive deformation. Hydrothermal circulation and silicification of similar style to Carlin-type deposits accompanied deformation. Strike-slip faulting, block rotation, and folding in this area record Eocene sinistral slip across a deeper fault in the subsurface. This fault reactivates an old crustal boundary (see Wooden and others, this volume) and separates Eocene and subsequently Oligocene and Miocene deformation into discrete domains of differential extensional strain and kinematics (Gans and Miller, 1983). How far along strike to the northwest into the northern Carlin trend Eocene transpressional strain extends is an important unresolved question, although Eocene folding and normal faulting is known in this area (Henry and Boden, 1997; Henry and others, this volume; Ketner and Alpha, 1988). As flow of auriferous hydrothermal fluids in the northern Carlin trend was controlled by the fault architecture (Teal and Jackson, 1997), and in view of the opinion Carlin-type deposits are of Eocene age (Henry and Boden, 1997; Ilchik and Barton, 1997; but see Arehart, 1996, for a dissenting opinion), understanding

regional Eocene strain patterns will constrain genetic model of Carlin-type deposits, as well as provide exploration criteria.

Large-scale crustal extension in the Oligocene and Miocene formed metamorphic core complexes in the Ruby and Snake Mountains (fig. 1) (Gans and Miller, 1983; MacCready and others, 1997). Implicit in these models is the possibility that the mid-crustal plutonic-metamorphic environment now outcropping in the Ruby Mountains core complex to the east of the Carlin trend may be the deep crustal roots to the upper crustal Carlin-type deposits. Analysis of the varied ore deposits formed at different crustal levels within the Ruby Mountains by Berger and Oscarson (this volume) indicates that this was not the case. In fact the deposits represent a zoned magmatic-hydrothermal system peripheral to plutons. The deposits are also generally impoverished in gold.

Unconformably overlying gold deposits in the Carlin trend is the middle Miocene Carlin Formation. Precise $^{40}\text{Ar}/^{39}\text{Ar}$ laser-fusion ages of alkali-feldspar-bearing air-fall tuff interbedded in the middle of the Carlin Formation at the northern end of the Carlin trend (fig. 1) demonstrate emplacement of the tuff occurred over a short period of time between 14.4 and 15.1 Ma (Fleck and others, this volume). Evidently, deposition took place after local silicic volcanic centers, such as those in the Midas and Ivanhoe Mining Districts, were active (Wallace and John, this volume). The mid-Miocene age and major-element chemistry of glass shards composing the tuffs suggest their derivation not from local sources but from distal silicic volcanic centers associated with the Yellowstone hotspot or with the northern Nevada rift.

Stable isotopic compositions of minerals and fluid inclusions indicate that the hydrothermal fluids which formed most Carlin-type gold deposits were variably exchanged meteoric water, except along the Getchell Trend (fig. 1) where ore fluids contained an additional component of magmatic or metamorphic fluids (Hofstra and others, this volume). The unusually low $\delta\text{D}_{\text{H}_2\text{O}}$ values of these fluids also suggests ore deposition during a cool climate, which characterized the mid-Tertiary (42 to 30 Ma), and not during a warm climate, which typified the Late Jurassic and Cretaceous.

Several of the problems which have inhibited development of a genetic model for Carlin-type deposits are the uncertainties regarding the age, or ages, of mineralization, the fluid evolution, and the source of gold (Christensen, 1993). Much of the debate regarding the age, or ages, of Carlin-type deposits stems from the interpretation of K-Ar and $^{40}\text{Ar}/^{39}\text{Ar}$ ages of illite (Arehart, 1996; Hofstra, 1995; Ilchik, 1995). Illite in the deposits is of detrital, diagenetic, and hydrothermal origin (Folger and others, this volume). Folger and others (this volume) address the ambiguity of K-Ar and $^{40}\text{Ar}/^{39}\text{Ar}$ ages of illite by comparing $^{40}\text{Ar}/^{39}\text{Ar}$ ages for different grain sizes recovered from unaltered and altered

calcareous rocks that host <40.8-Ma Carlin-type deposits in the Jerritt Canyon Mining District (fig. 1). In all size fractions of illite, including the smallest (<0.1-micron) which is dominated by neoformed hydrothermal illite, the $^{40}\text{Ar}/^{39}\text{Ar}$ ages are too old. This age discrepancy is due to the influence of older detrital or diagenetic illite.

The evolution of ore fluids and mechanism of ore deposition are critical to formation of ore deposits. Voitsekhowskaya and Peters (this volume) modeled fluid evolution during formation of the giant Betze deposit in the northern Carlin trend (fig. 1). They conclude that the natural evolution of a CO_2 , H_2S , and NaCl bearing fluid as it moves from below the site of ore deposition through reactive calcareous sedimentary rocks at the site of ore deposition can explain the distribution of alteration mineral phases in the deposit. Gold precipitation in association with arsenic in pyrite resulted from sulfidation of reactive iron in host rocks. Sulfidation resulted in higher hydrogen and lower aqueous sulfur activity and destabilization of arsenic- and gold-bearing aqueous complexes.

Establishing the source, or sources, of gold in Carlin-type deposits is also critical to genetic models for their formation (Christensen, 1993). Tosdal and others (this volume) address this question using Pb isotopic compositions of sulfide minerals in three Carlin-type deposits (fig. 1) along with Pb isotopic data for miogeoclinal and eugeoclinal sedimentary rocks and for Mesozoic and Eocene igneous rocks (Wooden and others, this volume). They demonstrate that mixing of two distinct Pb isotopic sources occurred during ore formation, a conclusion consistent with much geochemical information (summarized by Arehart, 1996).

On a regional scale, Kotlyar and others (this volume) modeled NURE geochemical surveys, gravity surveys, and magnetic surveys (fig. 1). They demonstrate that regional-scale distribution patterns of stream-sediment arsenic anomalies in northeast Nevada bear striking similarities to some important mineralized trends. The arsenic anomalies also correspond to some isostatic residual gravity anomalies and their gradients, which result from density distributions in the pre-Cenozoic rocks of the middle and upper crust. This coincidence of geochemical and geophysical data suggests that arsenic, as well as precious metals, may have been derived from the middle and upper crust, and then concentrated along linear structural zones during regional fluid flow.

Lastly, McCarthy and McGuire (this volume) conducted soil-gas surveys measuring inorganic and organic gases along widely spaced traverses that crossed the Carlin trend. Gas anomalies were found 7-11 km west and east of the center of the Carlin trend where the gold deposits are localized. The flanking gas anomalies extend northwest of the last known gold deposit along the Carlin trend. If the gas anomalies are in some way a reflection of the Carlin trend, then the northwestward extension of flanking gas anomalies

suggests some exploration potential for this region.

PLUTON-RELATED GOLD DEPOSITS IN THE BATTLE MOUNTAIN AREA

The Battle Mountain Mining District, near the northwest terminus of the Battle Mountain-Eureka mineral belt in north central Nevada, contains a copious and varied metal endowment. Included in the mining district are four Tertiary porphyry Cu-Au and three Cretaceous stockwork Mo systems (fig. 1) (Theodore, 1998, this volume). A large number of distal-disseminated Ag-Au deposits and Cu-Au skarns are spatially and genetically related to Tertiary porphyry Cu systems (Theodore, 1998, this volume). Deposits in the northern part of the mining district represent shallow levels of zoned hydrothermal and plutonic systems. The southern part of the mining district represents deeper crustal levels of magmatic-hydrothermal systems where porphyry cores and flanking auriferous skarn deposits are concentrated along with more peripheral sedimentary-rock-hosted Ag-Au deposits. In the Copper Canyon area (fig. 1) Kotlyar and others (this volume), using three-dimensional modeling of geochemical data provided by Battle Mountain Gold Co., demonstrate district-scale geochemical zoning patterns that emanate outward from a Cu-Au core through the peripheral Fortitude Au skarn to a distal Pb-Zn halo.

HOT-SPRING GOLD DEPOSITS

Hot-spring Au-Ag deposit, the third major deposit type in northern Nevada, are near-surface deposits representing the shallowest setting of ore genesis. They provide a critical link between magmatic and hydrologic environments (Hedenquist and Lowenstern, 1994). Of importance in defining their genesis and role in the metallogeny of the region is understanding their environments, their age, and relationship to tectonomagmatic events in the Tertiary. Wallace and John (this volume) describe the geologic framework of Miocene volcanic complexes along the Northern Nevada Rift in the Shoshone and Sheep Creek Ranges and Snowstorm Mountains (fig. 1). Here, the interplay between east-northeast-directed extension and compositionally expanded magmatism localized precious metal mineralization in hot-spring deposits. The Mule Canyon deposit (~1 million oz Au) is the largest of the hot-spring type deposit (fig. 1).

In the Tuscarora Mountains (fig. 1), Henry and Boden (this volume) describe the complex volcanic history of the Eocene Tuscarora volcanic field. They demonstrate that a

large quantity of igneous rocks were erupted or emplaced in different volcanic-plutonic environments over less than 1 m.y. In the Tuscarora Mining District, low-sulfidation hot-spring deposits formed during the waning stages of volcanism. Here, two spatially related but separate hydrothermal systems, one Au-rich and the other Ag-rich, were partially superposed. The superposition of hydrothermal systems of differing metal associations suggests that complex fluid circulation systems were established during the waning stages of volcanism.

REFERENCES CITED

- Arehart, G.B., 1996, Characteristics and origin of sediment-hosted disseminated gold deposits: a review: *Ore Geology Reviews*, v. 11, p. 383-403.
- Arehart, G.B., Foland, K.A., Naeser, C.W., and Kesler, S.E., 1993, $^{40}\text{Ar}/^{39}\text{Ar}$, K/Ar, and fission track geochronology of sediment-hosted disseminated gold deposits at Post/Betze, Carlin Trend, northeastern Nevada: *Economic Geology*, v. 88, p. 622-646.
- Armstrong, A.K., Theodore, T.G., Oscarson, R.L., Kotlyar, B.B., Harris, Anita, Bettles, K.H., Lauha, E.G., Hipsley, R.A., Griffin, G.L., Abbott, E.W., and Cluer, J.K., (this volume), Preliminary facies analysis of Silurian and Devonian autochthonous rocks that host gold along the Carlin trend, Nevada, *in* Tosdal, R.M., ed., *Contributions to the gold metallogeny of northern Nevada*: U.S. Geological Survey Open-File Report.
- Berger, Vladimir I., and Oscarson, Robert L., (this volume), Tungsten-polymetallic- and barite-mineralized rocks in the Ruby Mountains, Nevada, *in* Tosdal, R.M., ed., *Contributions to the gold metallogeny of northern Nevada*: U.S. Geological Survey Open-File Report.
- Christensen, O.D., 1993, Carlin trend geologic overview, *in* Christensen, O.D., ed., *Gold deposits of the Carlin Trend, Nevada*: Society of Economic Geologists Guidebook Series, v. 18, p. 12-26.
- Christensen, O.D., 1995, The Carlin trend giant gold camp: is it the strata, the structure or the stocks, *in* Clark, A.H., ed., *Giant ore deposits II, controls on the scale of orogenic magmatic-hydrothermal mineralization: Proceedings of the Second Giant Ore Deposits Symposium*, Kingston, Ontario, April, 1995, p. 340-352.
- Christensen, O.D., 1996, Carlin trend geologic overview, *in* Peters, S.G., Williams, C.L., and Volk, Jeff, *Field trip guidebook for Trip B—Structural geology of the Carlin trend*, *in* Green, S.M., and Struhsacker, Eric, eds., *Field Trip Guidebook Compendium*: Reno, Nevada, Geological Society of Nevada, *Geology and ore deposits of the American Cordillera*, p. 147-156.
- Cunningham, C.G., 1988, The relationship between some disseminated gold deposits, the western edge of the Precambrian craton, and paleothermal anomalies in Nevada, *in* Schafer, R.W., Cooper, J.J., and Vikre, P.G., eds., *Bulk mineable precious metal deposits of the western United States; Symposium proceedings*: Reno, Nevada, Geological Society of Nevada, p. 35-48.
- Elison, M.W., Speed, R.C., and Kistler, R.W., 1990, *Geologic and*

- isotopic constraints on the crustal structure of the northern Great Basin: *Geological Society of America Bulletin*, v. 102, p. 1077-1092.
- Fleck, R.J., Theodore, T.G., Sarna-Wojcicki, Andrei, and Meyer, C.E., (this volume), Age and possible source of air-fall tuffs of the Miocene Carlin Formation, northern Carlin trend, *in* Tosdal, R.M., ed., *Contributions to the gold metallogeny of northern Nevada*: U.S. Geological Survey Open-File Report.
- Folger, H.W., Hofstra, A.H., Snee, L.W., and Eberl, D.D., (this volume), K-Ar and $^{40}\text{Ar}/^{39}\text{Ar}$ dating of illites from Carlin-type gold deposits—Nature of the problem and guidelines for future studies, *in* Tosdal, R.M., ed., *Contributions to the gold metallogeny of northern Nevada*: U.S. Geological Survey Open-File Report.
- Gans, P.B., and Miller, E.L., 1983, Styles of mid-Tertiary extension in east-central Nevada, *in* Gurgel, K.D., ed., *Geologic excursions in the overthrust belt and metamorphic core complexes of the Intermountain region, Nevada*: Utah Geological and Mineral Survey Special Studies 59, p. 107-160.
- Grauch, V.J.S., (this volume), Crustal structure and relation to gold belts in north-central Nevada: overview and progress report, *in* Tosdal, R.M., ed., *Contributions to the gold metallogeny of northern Nevada*: U.S. Geological Survey Open-File Report.
- Grauch, V.J.S., Jachens, R.C., and Blakely, R.J., 1995, Evidence for a basement feature related to the Cortez disseminated gold trend and implications for regional exploration in Nevada: *Economic Geology*, v. 90, p. 203–207.
- Grauch, V.J.S., Klein, D.P., and Rodriguez, B.D., (this volume), Progress on understanding the crustal structure near the Battle Mountain-Eureka mineral trend from geophysical constraints, *in* Tosdal, R.M., ed., *Contributions to the gold metallogeny of northern Nevada*: U.S. Geological Survey Open-File Report.
- Hedenquist, J.W. and Lowenstern, J.B., 1994, The role of magmas in the formation of hydrothermal ore deposits: *Nature*, v. 370, p. 519-527.
- Henry, C.D., and Boden, D.R., 1997, Eocene magmatism of the Tuscarora volcanic field, Elko County, Nevada, and implications for Carlin-type mineralization, *in* Vikre, P., Thompson, T.B., Bettles, K., Christensen, O., and Parratt, R., eds., *Carlin-type gold deposits field conference*: Society of Economic Geology Guidebook Series, v. 28, p. 193–202.
- Henry, C.D., Boden, D.R., and Castor, S.B., (this volume), Geology and mineralization of the Eocene Tuscarora Volcanic Field, Elko County, Nevada, *in* Tosdal, R.M., ed., *Contributions to the gold metallogeny of northern Nevada*: U.S. Geological Survey Open-File Report.
- Hofstra, A.H., 1995, Timing and duration of Carlin-type gold deposits in Nevada and Utah—Relation to back-arc extension and magmatism: *Geological Society of America Abstracts with Programs*, v. 27, no. 6, pp. A-329.
- Hofstra, A.H. and Rye, R.O., (this volume), δD and $\delta^{18}\text{O}$ data from Carlin-type gold deposits—Implications for genetic models, *in* Tosdal, R.M., ed., *Contributions to the gold metallogeny of northern Nevada*: U.S. Geological Survey Open-File Report.
- Ilchik, R.P., 1995, $^{40}\text{Ar}/^{39}\text{Ar}$, K-Ar, and fission track geochronology of the sediment-hosted disseminated gold deposits at Post-Betze, Carlin trend, northeastern Nevada—a discussion: *Economic Geology*, v. 90, p. 208-210.
- Ilchik, R.P., and Barton, M.D., 1997, An amagmatic origin of Carlin-type gold deposits: *Economic Geology*, v. 92, p. 269-288.
- Ketner, K.B., 1977, Deposition and deformation of lower Paleozoic western facies rocks, northern Nevada, *in* Stewart, J.H., Stevens, C.H., and Fritsche, A.E., eds., *Paleozoic paleogeography of the western United States*: Pacific Coast Paleogeography Symposium 1: Los Angeles, Society of Economic Paleontologists and Mineralogists, Pacific Section, p. 251–258.
- Ketner, K.B., 1998, The nature and timing of tectonism in the western facies terrane of Nevada and California—An outline of evidence and interpretations derived from geologic maps of key areas: U.S. Geological Survey Professional Paper 592, 19 p.
- Ketner, K.B., and Alpha, A.G., 1988, Mesozoic and Tertiary rocks near Elko, Nevada—Evidence for Jurassic to Eocene folding and low-angle faulting: U.S. Geological Survey Bulletin 1988-C, 13 p.
- Kotlyar, B.B., and Theodore, T.G., (this volume), Multilevel geochemical patterns at the Fortitude gold skarn, Battle Mountain Mining District, Nevada, *in* Tosdal, R.M., ed., *Contributions to the gold metallogeny of northern Nevada*: U.S. Geological Survey Open-File Report.
- Kotlyar, B.B., Singer, D.A., Jachens, R.C., and Theodore, T.G., (this volume) Regional analysis of the distribution of gold deposits in northeast Nevada using NURE arsenic and geophysical data, *in* Tosdal, R.M., ed., *Contributions to the gold metallogeny of northern Nevada*: U.S. Geological Survey Open-File Report.
- MacCready, T., Snoke, A.W., Wright, J.E., and Howard, K.A., 1997, Mid-crustal flow during Tertiary extension in the Ruby Mountains core complex, Nevada: *Geological Society of America Bulletin*, v. 109, p. 1576-1594.
- Madrid, R.J. and Roberts, R.J., 1991, Origin of gold belts in north central Nevada, *in* Buffa, R.H., and Coyner, A.R., eds., *Geology and ore deposits of the Nevada*: Geological Society of Nevada Field Trip Guidebook Compendium, Reno, NV, 1990, p. 927-939.
- McCarthy, Howard, and McGuire, Emmet, (this volume), Soil gas studies along the Carlin trend, Eureka and Elko counties, Nevada, *in* Tosdal, R.M., ed., *Contributions to the gold metallogeny of northern Nevada*: U.S. Geological Survey Open-File Report.
- Moore, T.E., and Murchey, B.L., (this volume), Stratigraphic and structural framework studies in the southern Battle Mountain trend, The Cedars area, Shoshone Range, *in* Tosdal, R.M., ed., *Contributions to the gold metallogeny of northern Nevada*: U.S. Geological Survey Open-File Report.
- Nutt, C.J., and Good, S.C., (this volume), Recognition and significance of Eocene deformation in the Alligator Ridge area, central Nevada, *in* Tosdal, R.M., ed., *Contributions to the gold metallogeny of northern Nevada*: U.S. Geological Survey Open-File Report.

- Peters, S.G., (this volume), Regional implications of the Crescent Valley-Independence Lineament, north-central Nevada, *in* Tosdal, R.M., ed., Contributions to the gold metallogeny of northern Nevada: U.S. Geological Survey Open-File Report.
- Roberts, R.J., 1966, Metallogenic provinces and mineral belts in Nevada: Nevada Bureau of Mines Report 13, pt. A, p. 47-72.
- Rodriguez, B.D., 1997, Deep regional resistivity structure across the Carlin trend, *in* Vikre, P., Thompson, T.B., Bettles, K., Christensen, O., Parratt, R., eds., Carlin-type gold deposits field conference: Society of Economic Geologist Guidebook Series, v. 28. p.39-45.
- Rodriguez, B.D., (this volume), Regional crustal structure beneath the Carlin Trend, Nevada based on deep electrical geophysical measurements, *in* Tosdal, R.M., ed., Contributions to the Au metallogeny of northern Nevada: U.S. Geological Survey Open-File Report.
- Shawe, D. R., 1991, Structurally controlled gold trends imply large gold resources in Nevada, *in* Raines, G. L., Lisle, R. E., Schafer, R. W., and Wilkinson, W. H., Eds., Geology and ore deposits of the Great Basin: Geological Society of Nevada, Reno, Nevada, p. 199-212.
- Sillitoe, R.H., and Bonham, H.F., 1990, Sediment-hosted gold deposits—Distal products of magmatic-hydrothermal systems: *Geology*, v. 18, p. 157-161.
- Smith, J.F., and Ketner, K.B., 1976, Stratigraphy of post-Paleozoic rocks and summary of resources in the Carlin-Pinon Range area, Nevada: U.S. Geological Survey Professional Paper 867-B, p. B1-B48.
- Stewart, J.H., 1980, Geology of Nevada: Nevada Bureau of Mines and Geology Special Publication 4, 136 p.
- Teal, L., and Jackson, M., 1997, Geologic overview of the Carlin Trend gold deposits and description of recent deep discoveries: Society of Economic Geologist Newsletter, no. 31.
- Theodore, T.G., 1998, Geology of pluton-related gold mineralization at Battle Mountain, Nevada: Tucson, Arizona, University of Arizona and U.S. Geological Survey Center for Mineral Resources Monograph 2 (in press).
- Theodore, T.G., (this volume), Pluton-related Au in the Battle Mountains Mining District— Overview, *in* Tosdal, R.M., ed., Contributions to the gold metallogeny of northern Nevada: U.S. Geological Survey Open-File Report.
- Theodore, T.G., (this volume), Large distal-disseminated precious-metal deposits, Battle Mountain Mining District, Nevada *in* Tosdal, R.M., ed., Contributions to the gold metallogeny of northern Nevada: U.S. Geological Survey Open-File Report.
- Theodore, T.G., Armstrong, A.K., Harris, A.G., Stevens, C.H., and Tosdal, R.M., (this volume), Geology of the northern terminus of the Carlin trend, Nevada: Links between crustal shortening during the late Paleozoic Humboldt orogeny and northwest-striking faults, *in* Tosdal, R.M., ed., Contributions to the gold metallogeny of northern Nevada: U.S. Geological Survey Open-File Report.
- Tosdal, R.M., Cline, J.S., Hofstra, A.H., Peters, S.G., Wooden, J.L., Young-Mitchell, M.N., (this volume), Mixed sources of Pb in sedimentary-rock-hosted Au deposits, northern Nevada, *in* Tosdal, R.M., ed., Contributions to the gold metallogeny of northern Nevada: U.S. Geological Survey Open-File Report.
- Wooden, J.L., Tosdal, R.M., and Kistler, R.W., 1997, Pb and Sr isotopic mapping of crustal structure in the Northern Great Basin, *in* Vikre, P., Thompson, T.B., Bettles, K., Christensen, O., Parratt, R., eds., Carlin-type gold deposits field conference: Society of Economic Geologist Guidebook Series, v. 28. p. 47-53.
- Wooden, J.L., Kistler, R.W., and Tosdal, R.M., (this volume), Pb isotopic mapping of crustal structure in the northern Great Basin and relationships to Au deposit trends, *in* Tosdal, R.M., ed., Contributions to the gold metallogeny of northern Nevada: U.S. Geological Survey Open-File Report.
- Wallace, A.R., and John, D.A., (this volume), New studies on Tertiary volcanic rocks and mineral deposits, northern Nevada rift *in* Tosdal, R.M., ed., Contributions to the gold metallogeny of northern Nevada: U.S. Geological Survey Open-File Report.
- Woitsekhovskaya, M.B., and Peters, S.G., (this volume), Geochemical modeling of alteration and gold deposition in the Betze deposit, Eureka County, Nevada *in* Tosdal, R.M., ed., Contributions to the gold metallogeny of northern Nevada: U.S. Geological Survey Open-File Report.

PROGRESS ON UNDERSTANDING THE CRUSTAL STRUCTURE NEAR THE BATTLE MOUNTAIN- EUREKA MINERAL TREND FROM GEOPHYSICAL CONSTRAINTS

By V.J.S. Grauch, Douglas P. Klein, and Brian D. Rodriguez

ABSTRACT

Information from magnetic, gravity, seismic-reflection, and MT data were integrated along a southwest-northeast profile crossing the Battle Mountain-Eureka trend to better understand crustal structure related to the trend. Most importantly, the mineral trend coincides with a change in density and resistivity of upper crustal rocks from high-density, high-resistivity rocks on the east to lower density, less resistive rocks on the west. An electrically conductive zone separates the areas of different resistivities and corresponds in part to the mineral trend. The observations are consistent with an interpretation that carbonate rocks with some igneous intrusion dominate the upper crust on the east and that on the west consists primarily of volcanic and clastic sedimentary rocks. We infer that the two regions are separated by a deeply penetrating crustal fault, of unknown slip. The fault may be a multiply reactivated rift-basin margin, related to Late Proterozoic rifting of North America, that represents a long-lived crustal conduit for mineralizing fluids. Many questions remain about the tectonic origin of the fault zone, its activity throughout geologic history, the relation to other tectonic features such as the northern Nevada rift, the source of fluids, and the source of gold.

INTRODUCTION

Roberts (1966) first pointed out and named alignments of geologic structures and mineral deposits in north-central Nevada. Since then, mining geologists have used the alignments as exploration guides for discovering new precious-metal deposits, with most success along the parallel Battle Mountain-Eureka and Carlin trends (fig. 1). Buried crustal structures that helped localize mineralization were usually invoked to explain the alignments (e.g., Shawe, 1991), although evidence for them was only conjectural.

We seek to explain the origin of the Battle Mountain-Eureka trend by examining geophysical data for evidence of buried crustal features that correspond to the trend. We focus

on gravity, magnetic, seismic, and new magnetotelluric data. Based on preliminary examination, we propose that the mineral trend follow a deep and long-lived crustal zone of enhanced permeability that has served as a conduit for mineralizing fluids.

GEOPHYSICAL DATA

Regional structures and major differences in lithology, porosity, or pore fluid composition are commonly reflected in contrasts in physical properties of the crust. Therefore, geophysical techniques, which are sensitive to certain physical properties of the subsurface, can be used to infer crustal structure. However, each geophysical method resolves different aspects of geologic features. Therefore, an understanding of the subsurface comes from the integrated application of several different geophysical methods, combined with constraints from geologic maps and isotopic data that reflect crustal chemistry. Geophysical data discussed in this report include gravity, magnetic, magnetotelluric (MT), and seismic-reflection data.

Variations in gravity are caused by lateral variations in crustal density. Gravity anomalies occur over volumes of rock having densities that contrast with the surrounding rock. Gravity measurements are useful for detecting geologic features such as near-vertical faults that juxtapose rock types of contrasting density, and anticlines or folds containing layers of contrasting density.

A technique developed by Jachens and Moring (1990) isolates gravity anomalies due to density variations in underlying rocks (basement gravity data) from the gravity signature of shallower, younger, basin features. To a first order, the resulting basement gravity map expresses major density variations within the pre-Tertiary basement, including younger intrusions within the basement (fig. 2) (Jachens and others, 1996). Jachens and Moring's method focuses on the gravity effects of sources within the top 10 km of the crust. Its accuracy and resolution are limited by the distribution of pre-Tertiary basement outcrops, gravity station coverage, and

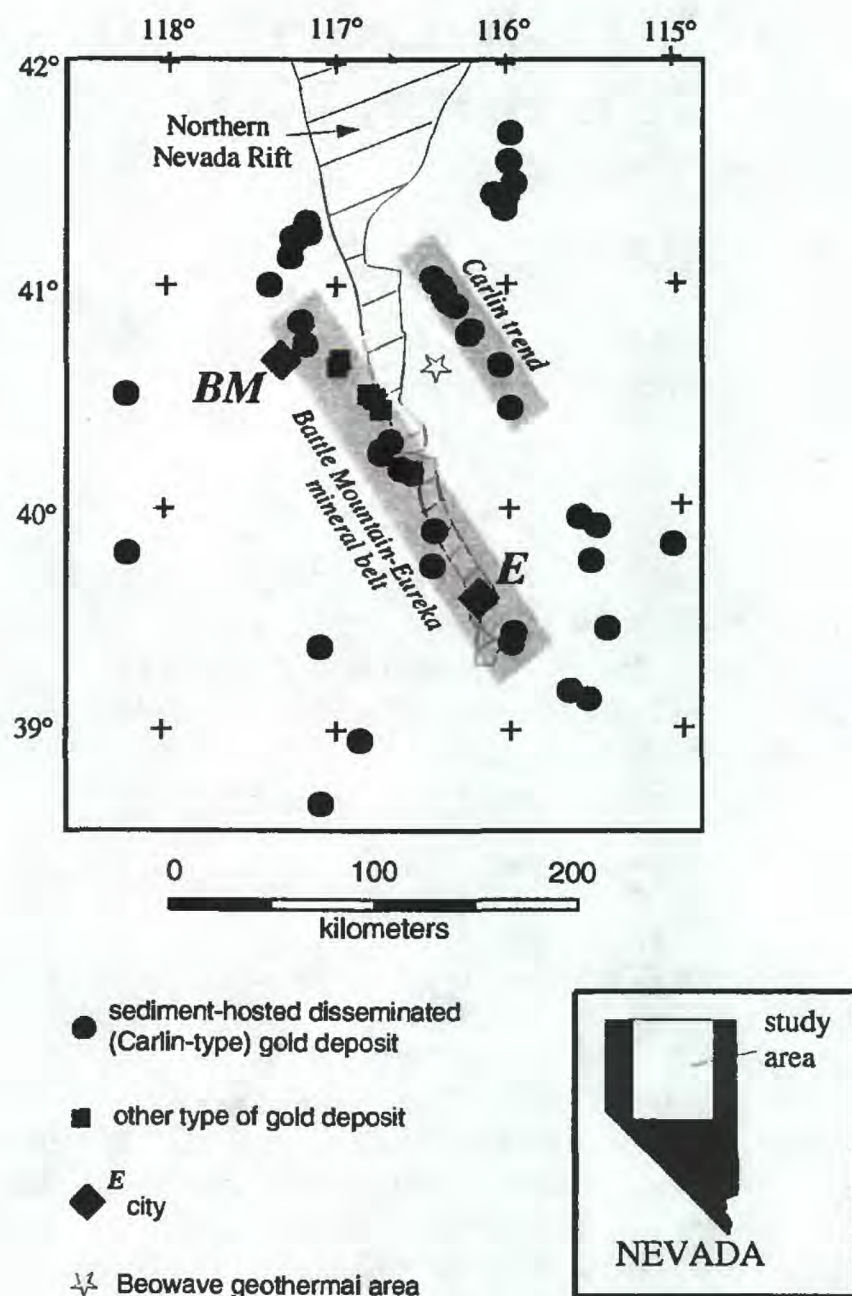


Figure 1. Location of mineral trends and other geologic and geographic features in the study area. Locations of sediment-hosted, disseminated ("Carlin-type") gold and other deposits that help define the trends are also shown. The northern Nevada rift (Zoback and others, 1994) is delineated by its magnetic expression. The cities of Battle Mountain (BM) and Eureka (E) are located by solid diamonds; Beowave geothermal area by a star.

simplifying assumptions about density and rock type within basins and volcanic areas (Jachens and Moring, 1990; Jachens and others, 1996; Saltus and Jachens, 1995).

With the new view of pre-Tertiary basement provided by the basement gravity map, Grauch and others (1995) recognized a major gravity gradient associated with the alignment of sediment-hosted, disseminated gold ("Carlin-type") deposits along the Battle Mountain-Eureka trend (fig. 2). The gradient separates lower gravity values on the southwest from higher values on the northeast, indicating an abrupt change in crustal density. This density contrast is an expression of a crustal boundary, such as a significant lateral offset of the crust, vertical uplift, or a suture between different types of crust. The boundary's correspondence to the alignment of deposits, geologic structures, and intrusions

along the Battle Mountain-Eureka trend suggests it controlled their spatial distribution as they formed and is at least Jurassic in age (Grauch and others, 1995). The basement gravity gradient has provided the focus for investigations using other geophysical methods.

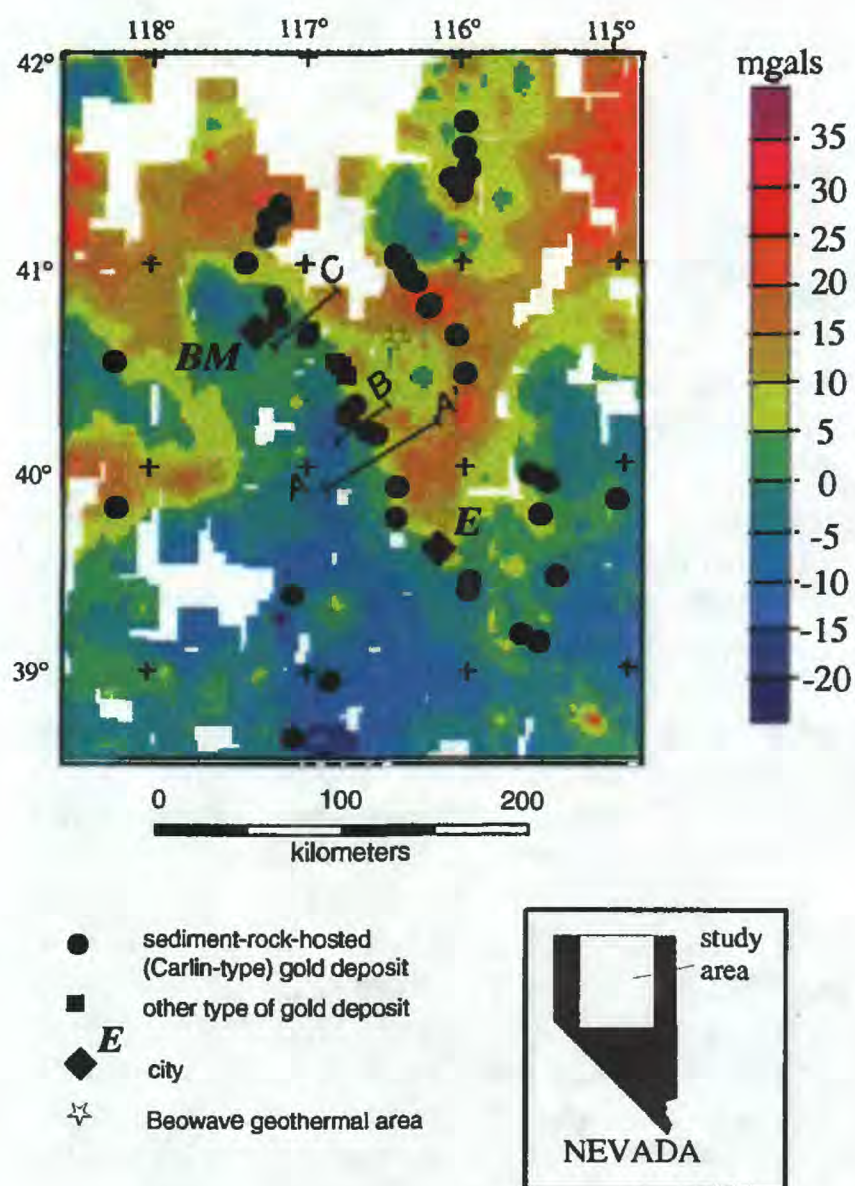


Figure 2. Basement gravity map for the study area from Jachens and Moring (1990), with gold deposits and geographic features of Figure 1. The location of gravity gradients generally can be resolved to within 2 to 10 km; blank areas show where information required to construct the map was inadequate. Data for profile A-A' are shown in subsequent figures; profiles B and C indicate MT profiles that have been collected but are not presented in this report.

Magnetic map

Magnetic methods conventionally measure variations in the strength of the earth's magnetic field produced by the magnetization of rocks containing significant amounts of magnetic minerals (commonly magnetite). The most common rock types containing a significant quantity of

magnetite are igneous rocks and certain metamorphic rocks. Magnetic data for Nevada were pieced together from individual aeromagnetic surveys (Hildenbrand and Kucks, 1988). The resulting data set gives a coherent picture for regional interpretation of volcanic rocks, intrusions, and related tectonic features, especially within the top 10 km of the crust. Magnetic data for north-central Nevada are dominated by the signature of shallow igneous rocks (Blakely and Jachens, 1991). One of the most prominent magnetic features is a linear high associated with the mid-Miocene northern Nevada rift (fig. 1), an alignment of dikes, intrusions, and graben-filling lava flows extending for at least 250 km in north-central Nevada (Zoback and others, 1994). The alignment follows a trend east of and slightly divergent from the Battle Mountain-Eureka mineral trend (fig. 1). Although the proximity of the rift to the Battle Mountain-Eureka mineral trend suggests a cause-and-effect relation between them, most of the gold deposits along the trend were formed earlier than the mid-Miocene rifting, during Late Cretaceous to Oligocene time (Maher and others, 1993; Seedorff, 1991).

Seismic-Reflection Profile

Seismic-reflection data, collected as part of the Consortium for Continental Reflection Profiling (COCORP) program, are available corresponding to most of profile A-A' (figs. 2 and 3) (Potter and others, 1987). Seismic-reflection methods induce acoustic or sonic waves into the ground and observe the arrival times of waves returning from reflectors in the subsurface. "Reflectors" occur at semi-horizontal contrasts in elastic properties of the Earth, which are commonly associated with interfaces between layered rock units of contrasting lithologies.

COCORP deep seismic-reflection data were designed to provide cross-sectional information about the crust to depths of 35-40 km (Allmendinger and others, 1987). In a segment of COCORP data corresponding to profile A-A' (fig. 2), Potter and others (1987) observed a pronounced zone of subhorizontal reflectors 18-33 km (fig. 3B), which they interpreted as mafic intrusions related to the northern Nevada rift. The layering of this zone is considered to be a better-developed portion of a more widespread, mid- to lower-crustal reflective zone observed across northern Nevada (Allmendinger and others, 1987; Holbrook and others, 1991; Hyndman and others, 1991). Potter and others (1987) also interpreted several reflectors between depths of 8-15 km (fig. 3B), which probably originate near the top of crystalline basement or within the overlying sedimentary rocks. They suggest reflector Y (fig. 3B) may represent either an inclined feeder to the northern Nevada rift, a Mesozoic thrust fault, or in conjunction with reflector Z (fig. 3B) the upper boundary of a lens produced by irregular extension of the mid-crust.

Magnetotelluric Profiles

The magnetotelluric (MT) method (Vozoff, 1991) measures the natural, time-varying electric and magnetic fields at the surface of the Earth to yield information on the patterns of electrical resistivity (the inverse of conductivity) in the subsurface. Sources of natural magnetic and electric fields are lightning and ionospheric electrical currents found across the globe at a range of frequencies. The range of frequencies produced by the fields allows experimental design to adjust the depths of investigation from tens of meters to tens of kilometers.

Laboratory studies have shown that factors that affect resistivity in the Earth's crust are the composition and temperature of pore-fluids, melting, and the presence of clay minerals, graphite, or certain metallic minerals (Keller, 1989). Any of these factors can measurably decrease the resistivity of carbonate and silicate rocks that constitute most of the crust, and thus allow certain inferences on lithology and structure.

Previous MT investigations were conducted as part of geothermal exploration in central Nevada near the northwestern and the southeastern part of the basement gravity gradient. Swift (1979) and Park (1985) regarded MT measurements in the Beowawe geothermal area (fig. 1) as consistent with a north-northwest trending zone of electrically conductive and anisotropic rocks extending to depths of about 6 km. The zone is associated with the northern Nevada Rift in this area (fig. 1; Zoback and others, 1994). Chau (1989) and Chau and Park (1990) evaluated MT observations across the gravity gradient to the northwest of Eureka (fig. 1). Two-dimensional analysis of the data (Chau, 1989) suggested a conductive zone similar to that in the Beowawe geothermal area that trends north-northwest in the vicinity of the gravity gradient and the northern Nevada Rift. However, in the final three-dimensional analysis, Chau and Park (1990) concluded that this zone is confined to the upper two kilometers of the crust and related to contrasts between bedrock and alluvial fill within valleys.

Magnetotelluric experiment

An electromagnetic experiment using the magnetotelluric (MT) method was conducted in 1994 to characterize the crustal resistivity across the basement gravity gradient. The initial objective was to establish whether crustal resistivity could identify resistivity contrasts associated with the tectonic feature inferred from the gradient. MT observations were established near profile A-A', corresponding to the COCORP deep seismic-reflection data (Potter and others, 1987) and along profile B (fig. 2). Based on preliminary analysis of the MT observations, we concluded that resistivity structure might

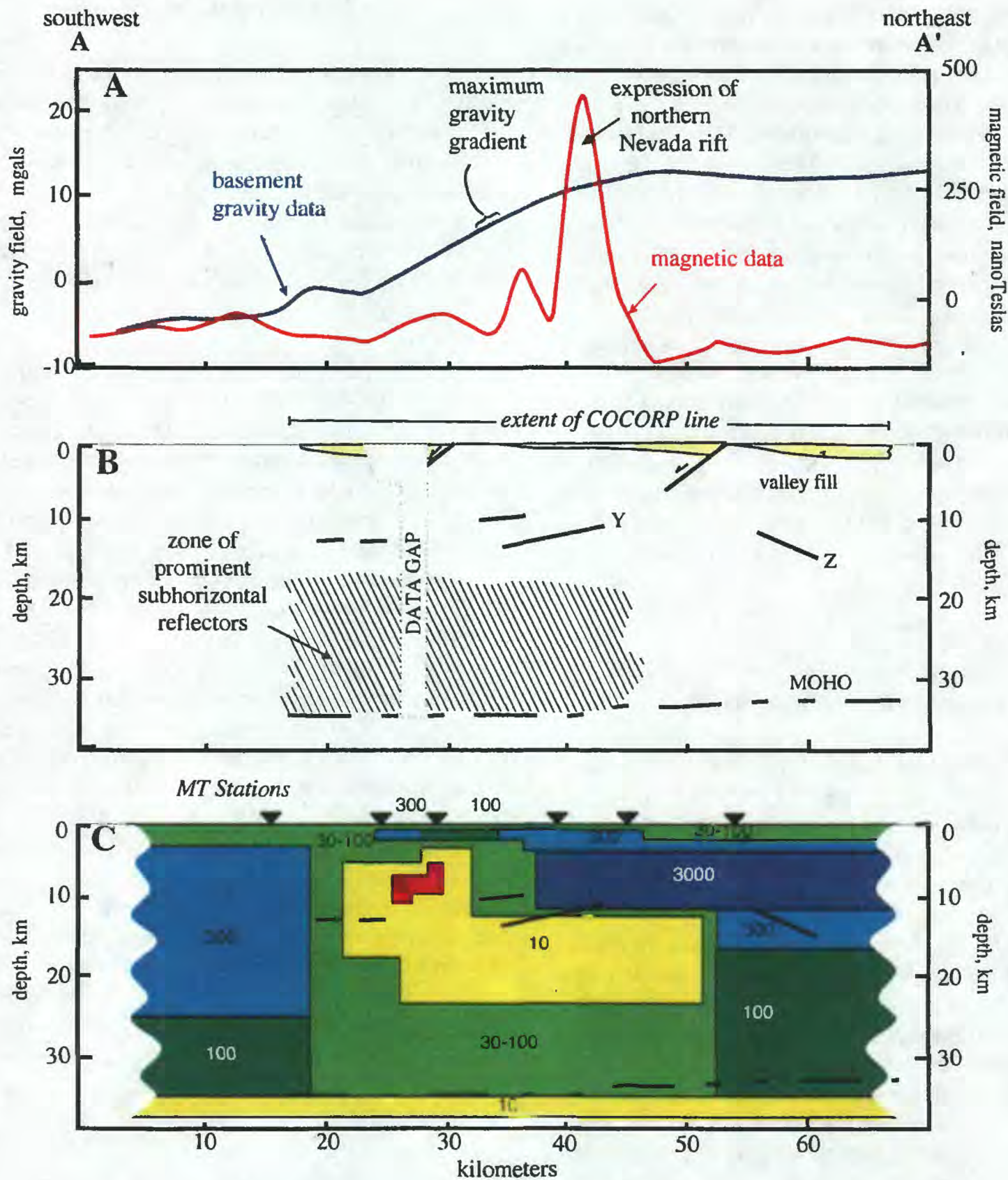


Figure 3. Basement-gravity, magnetic, and seismic-reflection data and MT model for profile A-A' located on Figure 2. For simplicity, topography is not shown. (A) Basement gravity and magnetic profiles extracted from Jachens and Moring (1990) and Hildenbrand and Kucks (1988), respectively. Basement gravity does not contain the effects of shallow basins and deep sources (>10 km). Noted are the magnetic high associated with the northern Nevada rift (Zoback and others, 1994) and the maximum gravity gradient that locates the inferred crustal boundary coinciding with the Battle Mountain-Eureka mineral trend (Grauch and others, 1995). (B) Interpreted depth section from COCORP seismic-reflection data modified from Potter and others (1987) and projected to the profile. Interpreted basin and range features are shown schematically. Solid black lines are reflectors of Potter and others (1987); Y and Z are discussed in the text. The dash-dot-dot line indicates the Moho. The zone of prominent subhorizontal reflectors was considered by Potter and others (1987) to be a better-developed portion of a more widespread lower-crustal reflective zone. (C) Diagram of the result of two-dimensional MT modeling, projected to the profile and overlain by seismic reflectors and the Moho as shown in B. MT stations are located by inverted triangles. Resistivities of model layers are shown in units of ohm-m. The change in basement gravity values in A corresponds to a change in the upper crust from high-resistivity rocks on the east to less resistive rocks on the west, with an intervening electrically conductive zone. We interpret the conductive zone to represent a crustal fault or fault zone that may have been a long-lived crustal conduit for mineralizing fluids.

provide useful constraints for understanding the other geophysical data. Additional observations across the gravity gradient north of the initial experiment were acquired in 1997 (profile C, fig. 2). Discussion of these latter observations will be reported elsewhere.

A 2-D model of MT observations corresponding to profile A-A' was created using the inversion algorithm of Smith and Booker (1991). This algorithm results in models showing slow changes, representing average resistivity, as opposed to abrupt resistivity contrasts. Results of the 2-dimensional inversion for profile A-A' are summarized in figure 3C, a schematic view of the important aspects of the model.

Although the model may share features in common with the Earth, several criteria of dimensionality in the data and misfit statistics of the model indicate that a two-dimensional representation may not be adequate. The effects of three-dimensional bodies at shallow depths (upper 1-3 km) could account for some two-dimensional representation of contrasts extending into the lower crust, as shown by Chau and Park (1990) elsewhere. Moreover, studies of shallow, rectangular conductive bodies similar in dimensions to the basins of the present study area (Wannamaker and others, 1984) have demonstrated that the basin configurations are an important influence on MT data in Basin and Range Province.

Thus, with caveats that the 2-dimensional model (fig. 3C) is a rough representation of the resistivity structure along profile A-A' the main features and suggested origins are as follows:

1. A conductive zone is located near the gravity gradient and penetrates from near surface to mid-crustal depths. The zone could be associated with intrusion and alteration associated with a crustal suture or fault zone.
2. A high-resistivity (about 3000 ohm-m) upper crust borders the conductive zone on the east. It may represent resistive carbonate shelf rocks or unaltered intrusions.
3. A moderate-resistivity (several hundred ohm-m) upper crust borders the conductive zone on the west. It may signify a larger portion of volcanic and clastic sedimentary rocks in the upper crust compared to crust on the east.
4. A moderately-conductive (30-100 ohm-m) lower crust seems to extend across the profile. It is similar to a conductive zone inferred further east near the Ruby Range that may represent small percentages (<5%) of high-temperature, metamorphic-derived brines (Wannamaker and others, 1997).

CONCLUSIONS

Magnetic, gravity, seismic-reflection, and MT information along profile A-A' have been combined onto one cross-section on figure 3. Integrating this information helps constrain different aspects of the subsurface in the vicinity of the Battle Mountain-Eureka trend. Preliminary conclusions about the relations between these data sets follow.

A major change in gravity values originating in upper crustal rocks corresponds to the Battle Mountain-Eureka mineral belt, as discussed by Grauch and others (1995). Along profile A-A' the change in gravity values corresponds to a change from high-resistivity rocks on the east to less resistive rocks on the west, with an intervening electrically conductive zone that penetrates from near surface to mid-crustal depths (fig. 3). In addition, the magnetic data indicate igneous rocks at depth coinciding with the northern Nevada rift (Zoback and others, 1994). These observations are consistent with an interpretation that the upper crust on the east is dominated by carbonate rocks, intruded by igneous rocks in the vicinity of the northern Nevada rift, whereas the upper crust on the west consists primarily of volcanic and clastic sedimentary rocks. The intervening conductive zone and the steepness and linearity of the gravity gradient in map view (fig. 2; Grauch and others, 1995) are evidence for a deeply penetrating crustal fault, which offsets crust of different composition either vertically, laterally, or both. The fault may be a multiply reactivated rift-basin margin, related to Late Proterozoic rifting of North America, as suggested for this and other areas in northern Nevada from isotopic evidence (Wooden and others, 1997). This scenario is also consistent with paleo-carbonate basin escarpments interpreted in the subsurface along the Carlin trend (Teal and Jackson, 1997). The conductive fault zone encompasses a larger area than known geothermal activity at the surface, which leads us to suggest it may represent a long-lived crustal conduit for mineralizing fluids.

The MT model and seismic-reflection depth-section show several commonalities in the picture of the mid- to lower crust (below about 10 km) along profile A-A' (fig. 3C), but their significance is unclear. COCORP reflectors Y and Z (fig. 3B; Potter and others, 1987) generally coincide with large vertical contrasts in resistivity at about 12 km depth in the MT model. The zone of prominent reflectors and the conductive zone (less than 100 ohm-m) in the middle of profile A-A' coincides for the most part. The reflection Moho apparently corresponds to the top of extensive conductive zone at about 33-35 km depth. However, the resistivity distribution at these depths has not been sufficiently evaluated to warrant further discussion.

The current state of our study has produced some

encouraging leads that point to an explanation of the alignment of mineral deposits along the Battle Mountain-Eureka trend. A crustal fault or fault zone generally coincident with the trend may have developed as a system of deep faults and fractures that enhanced permeability and allowed magmatic, metamorphic, or deeply penetrating surface fluids to circulate upward, resulting in a locus of mineralization along the boundary. Many questions remain about the tectonic origin of the fault zone, its activity throughout geologic history, the relation to other tectonic features such as the northern Nevada rift, the source of fluids, and the source of gold.

Our focus for the near future is to test and expand our geophysical models. The current MT model has to be evaluated for its sensitivity to data noise and against the possible influence of the 3-D basin configuration. Additional MT profiles will help establish a consistent resistivity signature at several points along the basement gravity gradient. We have recently acquired the additional profile C-C' in the Battle Mountain area (fig. 2), and our current priority is to develop a model for this new data. Gravity models must be revised in light of constraints provided by the new MT data, by exposed and inferred geology, and by isotopic information. Eventually, we must look to other disciplines, such as geology and geochemistry, to constrain these tectonic questions and to make a connection between mineralizing fluids and the crustal fault.

REFERENCES

- Allmendinger, R. W., Hauge, T. A., Hauser, E. C., Potter, C. J., Klempner, S. L., Nelson, K. D., Knuepfer, P., and Oliver, J., 1987, Overview of the COCORP 40°N Transect, western United States: The fabric of an orogenic belt: *Geological Society of America Bulletin* v. 98, p. 308-319.
- Blakely, R. J., and Jachens, R. W., 1991, Regional study of mineral resources in Nevada: insights from three-dimensional analysis of gravity and magnetic anomalies: *Geological Society of America Bulletin*, v. 103, p. 795-803.
- Chau, L. L., 1989, A magnetotelluric study of electrical conductivity structure in the northern Nevada rift zone: Implications on Tertiary extension in the central Basin and Range: Riverside, University of California, MS Thesis, 132 p.
- Chau, L. L., and Park, S. K., 1990, Implications of electrical conductivity structure inferred from magnetotelluric data on Tertiary extension in central Nevada: expanded abstract: *Society of Exploration Geophysicists Annual Meeting 1990, Abstracts and Bibliographies*, p. 565-568.
- Grauch, V. J. S., Jachens, R. C., and Blakely, R. J., 1995, Evidence for a basement feature related to the Cortez disseminated gold trend and implications for regional exploration in Nevada: *Economic Geology*, v. 90, p. 203-207.
- Hildenbrand, T. G., and Kucks, R. P., 1988, Total intensity magnetic anomaly maps of Nevada: Nevada Bureau of Mines and Geology Map 93A, scale 1:1,000,000.
- Holbrook, W. S., Catchings, R. D., and Jarchow, C. M., 1991, Origin of deep crustal reflections: Implications of coincident seismic refraction and reflection data in Nevada: *Geology*, v. 19, p. 175-179.
- Hyndman, R. D., Lewis, T. J., and Marquis, G., 1991, Comment on "Origin of deep crustal reflections: Implications of coincident seismic refraction and reflection data in Nevada": *Geology*, v. 19, p. 1243-1244.
- Jachens, R. C., and Moring, B. C., 1990, Maps of the thickness of Cenozoic deposits and the isostatic residual gravity over basement for Nevada: U. S. Geological Survey Open-File Report 90-404, 15 p., 2 sheets, scale 1:1,000,000.
- Jachens, R. C., Moring, B. C., and Schruben, P. G., 1996, Thickness of Cenozoic deposits and the isostatic residual gravity over basement, in Singer, D. A., ed., *An analysis of Nevada's metal-bearing mineral resources: Nevada Bureau of Mines and Geology Open-File Report 96-2*, p. 2-1 through 2-10, 1 sheet, scale 1:1,000,000.
- Keller, G. V., 1989, Electrical properties, in Carmichael, R. S., ed., *Practical handbook of physical properties of rocks and minerals*: Boca Raton, CRC Press, p.359-427.
- Maher, B. J., Browne, Q. J., and McKee, E. H., 1993, Constraints on the age of gold mineralization and metallogenesis in the Battle Mountain-Eureka mineral belt, Nevada: *Economic Geology*, v. 88, p. 469-478.
- Park, S. K., 1985, Distortion of magnetotelluric sounding curves by three-dimensional structures: *Geophysics*, v. 50, p. 785-797.
- Potter, C. J., Liu, C-S., Huang, J., Zheng, L., Hauge, T. A., Hauser, E. C., Allmendinger, R. W., Oliver, J. E., Kaufman, S., and Brown, L., 1987, Crustal structure of north-central Nevada: results from COCORP deep seismic profiling: *Geological Society of America Bulletin*, v. 98, p. 330-337.
- Roberts, R. J., 1966, Metallogenic provinces and mineral belts in Nevada: Nevada Bureau of Mines Report 13, p. 47-72.
- Saltus, R. W., and Jachens, R. C., 1995, Gravity and basin-depth maps of the Basin and Range province, western United States: U. S. Geological Survey Geophysical Investigations map GP-1012, scale 1:2,500,000.
- Seedorff, Eric, 1991, Magmatism, extension, and ore deposits of Eocene to Holocene age in the Great Basin—Mutual effects and preliminary proposed genetic relationships, in Raines, G. L., Lisle, R. E., Schafer, R. W., and Wilkinson, W. H., eds., *Geology and ore deposits of the Great Basin: Geological Society of Nevada, Reno, Nevada*, p. 133-178.
- Shawe, D. R., 1991, Structurally controlled gold trends imply large gold resources in Nevada, in Raines, G. L., Lisle, R. E., Schafer, R. W., and Wilkinson, W. H., eds., *Geology and ore deposits of the Great Basin: Geological Society of Nevada, Reno, Nevada*, p. 199-212.
- Smith, J. T., and Booker, J. R., 1991, Rapid inversion of two- and three-dimensional magnetotelluric data: *Journal of Geophysical Research*, v. 96, p. 3, 903-3,922.
- Swift, C. M., Jr., 1979, Geophysical data, Beowawe geothermal area, Nevada: *Transactions, Geothermal Resources Council*, v. 3, p. 701-703.
- Teal, L., and Jackson, M., 1997, Geologic overview of the Carlin

- Trend gold deposits and descriptions of recent deep discoveries: Society of Economic Geologists Newsletter, no. 31, p. 1 and 13-25.
- Vozoff, K., 1991, The Magnetotelluric Method, Chapter 8, *in* Nabighian, M.N., ed., *Electromagnetic Methods in Applied Geophysics*, v. 2; Application, Parts A and B: Tulsa, Oklahoma, Society of Exploration Geophysicists, *Investigations in Geophysics* No. 3, p. 641-712.
- Wannamaker, P. E., Hohmann, G. W., and Ward, S. H., 1984, Magnetotelluric responses of three-dimensional bodies in layered earths: *Geophysics*, v. 49, p. 1517-1533.
- Wannamaker, P. E., Doerner, W. M., Stodt, J. A., Johnston, J. M., 1997, Subdued state of tectonism of the Great Basin interior relative to its eastern margin based on deep resistivity structure: *Earth and Planetary Science Letters*, v. 150, p. 41-53.
- Wooden, J.L., Tosdal, R.M., and Kistler, R.W., this volume, Pb isotopic mapping of crustal structure in the northern Great Basin and relationships to Au deposit trends, *in* Tosdal, R.M., ed., 1998, *Toward a better understanding of the gold metallogeny of northern Nevada: U.S. Geological Survey Open-File Report*.
- Wooden, J. L., Tosdal, R. M., and Kistler, R. W., 1997, Pb and Sr isotopic mapping of crustal structure in northern Great Basin: Society of Economic Geologists Guidebook Series, v. 28, p. 47-51.
- Zoback, M. L., McKee, E. H., Blakely, R. J., and Thompson, G. A., 1994, The northern Nevada rift: Regional tectono-magmatic relations and Miocene stress direction: *Geological Society of America Bulletin*, v. 106, p. 371-382.

REGIONAL CRUSTAL STRUCTURE BENEATH THE CARLIN TREND, NEVADA BASED ON DEEP ELECTRICAL GEOPHYSICAL MEASUREMENTS

By Brian D. Rodriguez

ABSTRACT

Gold deposits along the Carlin trend in northern Nevada are interpreted to have been controlled by deep regional fault systems. Magnetotelluric data along a regional southwest to northeast profile have revealed deeply-penetrating resistivity structures beneath the Carlin and Battle Mountain-Eureka mineral trends which appear consistent with tectonic breaks in the crust and which possibly serve as channels for hydrothermal fluids. The resistivity model shows a high crustal resistivity (1,000 ohm-m) beneath the Carlin trend, a feature that is characteristic of intrusive complexes. Southwest of the Carlin trend, a high-angle, southwest dipping, low resistivity (5-30 ohm-m) zone may be interpreted as a crustal-dimension fault, possibly extending to 15 to 20 kilometers depth. Crustal resistivity across the eastern part of the Battle Mountain-Eureka trend (2,000 ohm-m) is also characteristic of igneous bodies or intruded rocks. The western edge of this crustal high resistivity also corresponds to the Northern Nevada Rift. Southwest of this high resistivity body, a high-angle, northeast dipping low resistivity (10-30 ohm-m) zone may be interpreted as a crustal-dimension fault, probably extending to about 10 kilometers depth.

INTRODUCTION

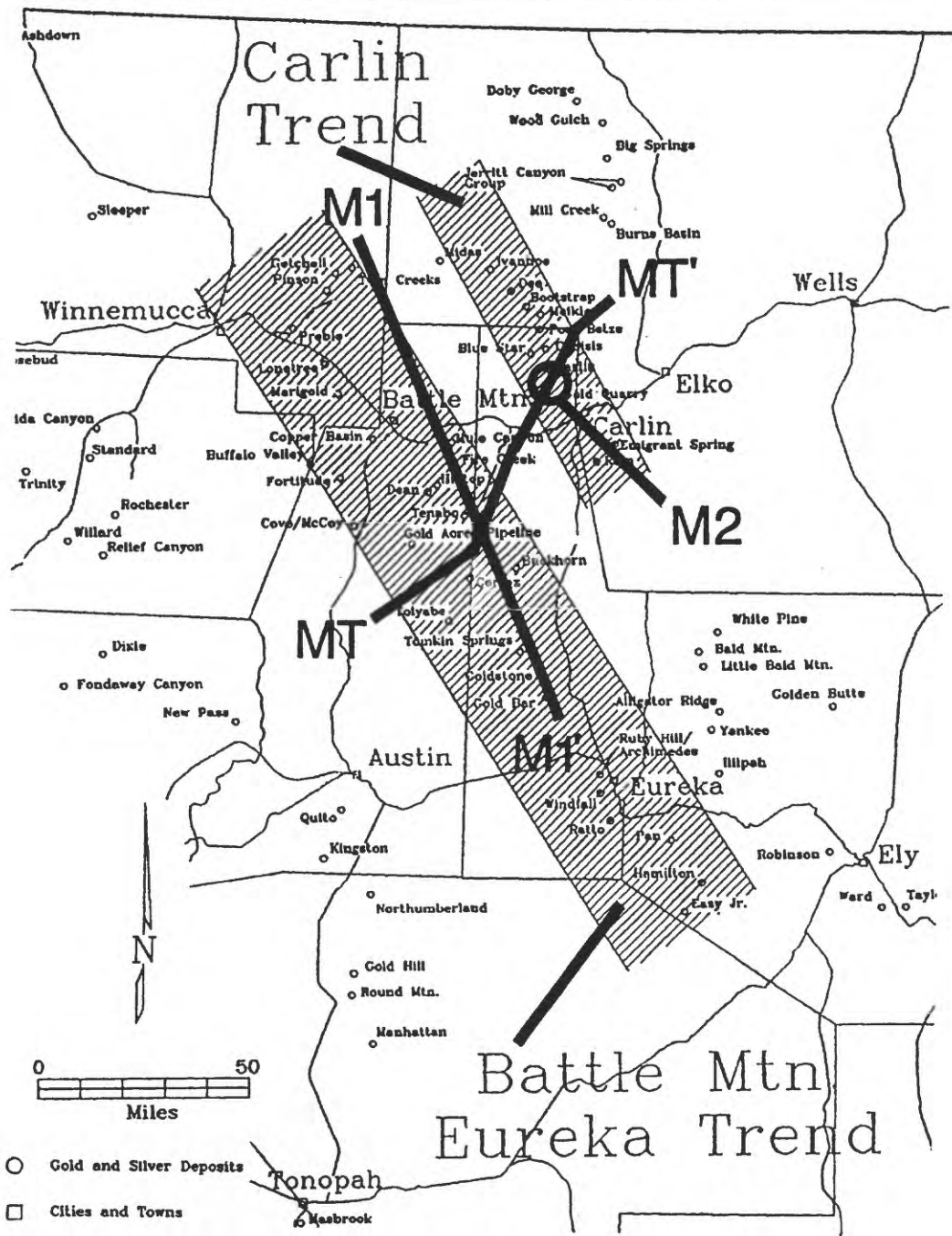
Genesis of gold deposits along the Carlin trend in northern Nevada is not fully understood and subject to conflicting models (e.g. Arehart and others, 1993; Illchik and Barton, 1997; Radtke, 1985; Shawe, 1991; Sillitoe and Bonham, 1990). These deposits, and other deposits along the subparallel Battle Mountain-Eureka mineral belt, are interpreted to have been controlled by deep regional fault systems. These structures controlled emplacement of magmas generated in the lower crust or upper mantle, and channeled magmatic-derived hydrothermal fluids or heated meteoric waters that transported and deposited the gold ores. To investigate crustal processes that may have contributed to the genesis of gold deposits along the Carlin trend, a regional southwest to northeast profile of

magnetotelluric (MT) soundings was acquired in 1996 (line MT-MT', fig. 1). Two-dimensional modeling of the MT profile was used to derive the resistivity structure and investigate its implication on possible heat or magma sources and possible tectonic controls on the linear distribution of mineral deposits.

MAGNETOTELLURIC METHOD

The magnetotelluric method is a passive surface geophysical technique, which uses the earth's natural electromagnetic fields to investigate the resistivity structure of the subsurface. The resistivity of geologic units is largely dependent upon their fluid content, porosity, fracturing, temperature, and conductive mineral content (Keller and Frischknecht, 1966). Saline fluids within the pore spaces and fracture openings can reduce resistivities in a resistive rock matrix. Also, resistivity can be lowered by the presence of conductive clay minerals, graphitic carbon, and metallic mineralization. It is common for altered volcanic rocks to contain authigenic minerals that have resistivities ten times lower than those of the surrounding rocks (Nelson and Anderson, 1992). Increased temperatures cause higher ionic mobility and mineral activation energy, reducing rock resistivities significantly. Unaltered, unfractured igneous rocks are normally very resistive (typically 1,000 ohm-m or greater), whereas faults will show low resistivity (less than 100 ohm-m) when they are comprised of rocks fractured enough to have hosted fluid transport and consequent mineralogical alteration. Carbonate rocks are moderately to highly resistive (hundreds to thousands of ohm-m) dependent upon their fluid content, porosity, fracturing, and impurities. Marine shales, mudstones, and clay-rich alluvium are normally very conductive (a few ohm-m to tens of ohm-m). Metamorphic rocks (non-graphitic) are moderately to highly resistive (hundreds to thousands of ohm-m). Tables of electrical resistivity for a variety of rocks, minerals and geological environments may be found in Keller (1987) and Palacky (1987).

The MT method (Vozoff, 1991) allows us to probe the crust from depths of tens of meters to depths of tens of



kilometers by measuring natural variations of the Earth's magnetic and electric field due to world-wide lightning activity at frequencies of 10,000 Hz to 1 Hz and geomagnetic micropulsation at frequencies of 1 Hz to 0.0001 Hz. The natural electric and magnetic fields propagate vertically in the earth because the very large resistivity contrast between the air and the earth causes a vertical refraction of both fields

transmitted into the earth (Vozoff, 1972). Using a computer-based data-acquisition and processing system, the natural electric and magnetic fields are recorded in two orthogonal, horizontal directions (the vertical magnetic field is sometimes recorded as well). The resulting time-series signals are used to derive earth tensor apparent resistivities and phases. Generally, a rotated coordinate system that

corresponds to apparent resistivity measured along electrical strike (called the transverse electric, TE direction) and normal to strike (called the transverse magnetic, TM direction) is used. The MT method is well suited for studying complicated geological environments because the electric and magnetic relations are sensitive to vertical and horizontal variations in resistivity. The method is capable of establishing whether the electromagnetic fields are responding to subsurface rock bodies of effectively 1-, 2-, or 3-dimensions.

MAGNETOTELLURIC SURVEY

Twenty-seven MT soundings were located along profile MT-MT' (fig. 1) with spacing that varied from 1.5 to 12.4 kilometers. The profile orientation is oblique to the trends of the mineral belts in the center of the profile in order to take advantage of other MT data (Grauch and others, this volume) and to optimize station locations for proximity to roads. This logistical arrangement was required by the U.S. Geological Survey truck-mounted MT system, and by the need to avoid electrical noise, such as power lines. Frequencies sampled ranged from 300 to 0.004 Hz using single station recordings of both orthogonal horizontal components of the electric and magnetic fields. Sampling these frequencies in the Carlin trend area allowed us to probe the crust from depths of hundreds of meters to depths of tens of kilometers.

MAGNETOTELLURIC MODEL

Wannamaker (1983) has found that MT responses in the northern Basin and Range are fundamentally 3-D in nature. However, because 3-D modeling is prohibitively time-consuming, 2-D modeling was used to construct the schematic cross-section of resistivity (fig. 2) along profile MT-MT' (fig. 1).

The MT data were modeled with a 2-D inversion algorithm (Smith and Booker, 1991) called rapid relaxation inverse (RRI). The RRI method provides a rapid means of 2-D modeling and uses a minimum-structure criterion (Smith and Booker, 1988), which substantially reduces unnecessary structural elements in the final solution. The final inversion model generally fit the TM data (misfit 4%) better than the TE data (misfit 12%). The gross structure of the model came from fitting the TM data. Wannamaker and others, (1984) have shown in 3-D MT modeling that approximating 3-D structure beneath a centrally located profile with 2-D modeling is best achieved when fitting the TM curve even at the expense of fitting the TE curve. However, because TM data are quite insensitive to the depth extent of a subsurface body (Eberhart-Phillips and others, 1995), the depths to the base of the bodies in the model are not well constrained. Clarifying the limits of the models with further 2-D and 3-D MT analysis is needed.

DISCUSSION

The resistivity model (fig. 2) shows a high crustal resistivity (1,000 ohm-m) beneath the Carlin trend, characteristic of igneous bodies. Exposures of Cretaceous quartz monzonite near MT station 18, Tertiary granodiorite about one mile southeast of station 16, widespread recrystallized carbonates in these areas (Evans, 1980), and a broad magnetic high (M2 in fig. 2) support the presence of a large, concealed, composite pluton (Grauch, 1996). Southwest of the Carlin trend, a high-angle, southwest dipping, low resistivity (5-30 ohm-m) zone may be interpreted as a crustal-dimension fault, possibly extending to 15 to 20 kilometers depth. This zone may represent a crustal conduit for fluids. This zone would have to contain hot fluids, or clay minerals from hydrothermal alteration in fractures, or even conductive sulfide or graphitic minerals from contact metamorphism to maintain such a low resistivity that extends so deep in the crust. The low resistivity (5-30 ohm-m) zone beneath the northeastern Carlin trend and to the northeast are probably comprised of approximately 5 km of alluvial fill (Jachens and others, 1996) and carbonaceous rocks. Beneath the eastern Carlin trend, and to the northeast end of the MT profile (stations 21 to 27) the change to 1,000 ohm-m at 12 km depth could be the base of the sedimentary section on top of crystalline basement rocks. The moderately resistive (30-100 ohm-m) rocks northeast of the Carlin trend and ubiquitously southwest probably correspond to carbonates in the near surface where local outcrops exist (stations 2, 3, 4, 12, 13, 14, 15, 19, 26, and 27) and other unknown volcanic and/or clastic sedimentary rocks at depth. The low resistivity (5 ohm-m) zone beneath stations 10 and 11 correlates with a known geothermal resource area (Beowawe KGRA near the center of MT profile, fig. 2).

Crustal resistivity across the eastern part of the Battle Mountain-Eureka trend (2,000 ohm-m, between stations 7 and 10, fig. 2) is also characteristic of igneous bodies or intruded rocks. The western edge of this crustal high resistivity also corresponds to the Northern Nevada Rift (M1 in fig. 2, see fig. 1 in Grauch and others, this volume). Southwest of this high resistivity body, a high-angle, northeast dipping low resistivity (10-30 ohm-m) zone may be interpreted as a crustal-dimension fault, probably extending to about 10 kilometers depth. A similar conductive feature is seen across a MT profile about 10-km south (see fig. 3 in Grauch and others this volume). The low resistivity (5 ohm-m) zone embedded at the top of this inferred fault is probably comprised of approximately 5 km of alluvial fill (Jachens and others, 1996) and possibly clay-rich or carbonaceous rocks, similar in size and resistivity to the valley fill northeast of the Carlin trend. At the southwest end of the MT profile, a southwest dipping, low resistivity (10-30 ohm-m) zone beneath stations 1 and 2 probably is valley fill.

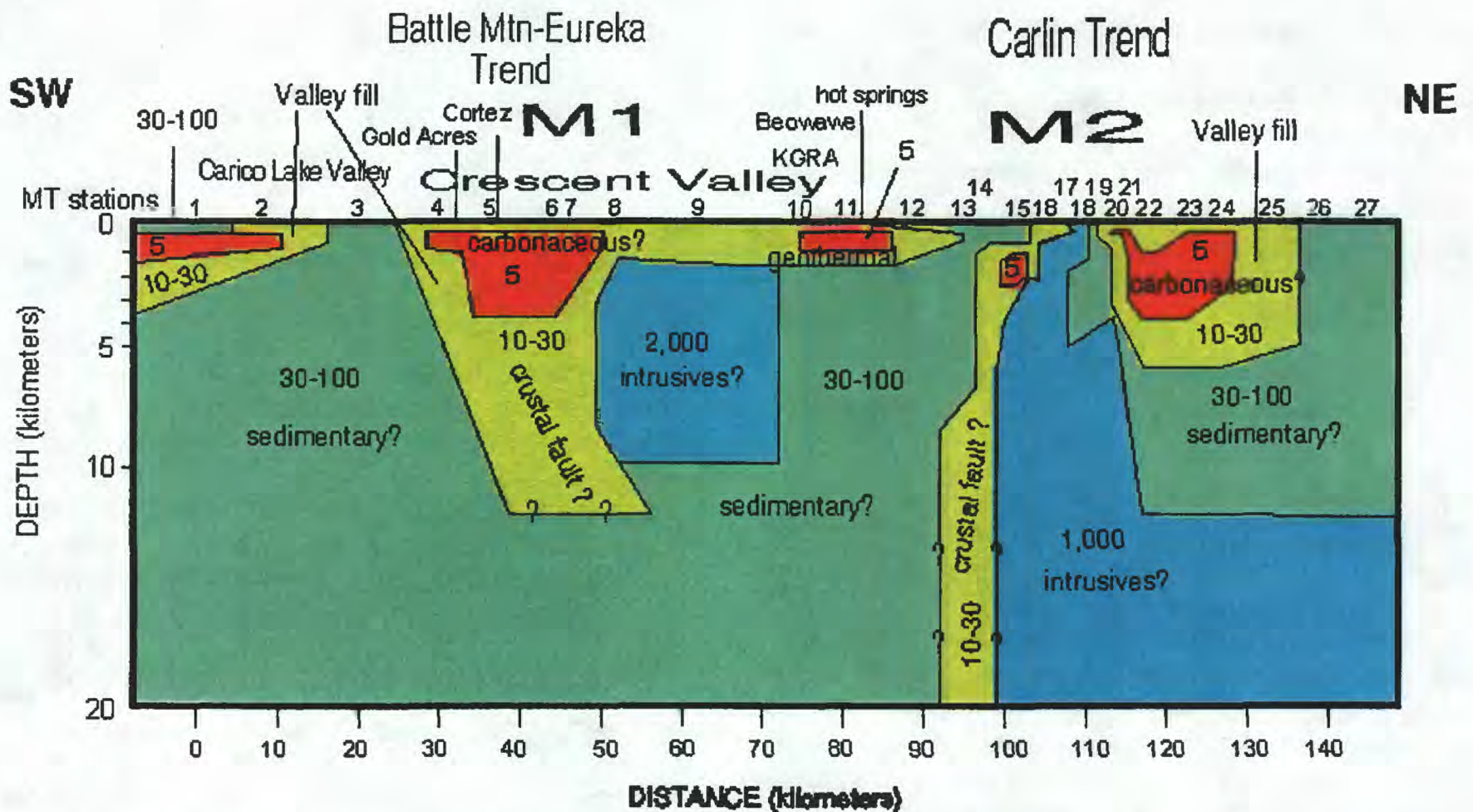


Figure 2. Two-dimensional resistivity model of crustal structure for the magnetotelluric transect (MT-MT' on figure 1) that was acquired in 1996 across the Carlin trend and Battle Mountain-Eureka mineral belt in northeastern Nevada. M1 is an anomalous linear magnetic high (Northern Nevada Rift) and M2 is a broad magnetic high anomaly (see figure 1). Numbers assigned to interpreted bodies are modeled resistivity in ohm-meters. Vertical exaggeration is approximately four. The bend in the profile (MT-MT' on figure) between MT stations 7 and 10 cause features in the resistivity model to appear wider than they really are because they are projected obliquely with respect to the rest of the profile.

SUMMARY

Strengthening the suggestion of Shawe (1991), the MT data have revealed deeply-penetrating resistivity structures beneath the Carlin and Battle Mountain-Eureka trends which appear consistent with tectonic breaks in the crust and which possibly serve as channels for hydrothermal fluids. In order to confirm whether these crustal structures continue to conform with the location of the linear arrays of gold deposits, new MT data should be added along parallel profiles across adjacent parts and even near the apparent terminations of the gold trends.

REFERENCES CITED

- Arehart, G. B., Foland, K. A., Naeser, C. W., and Kesler, S. E., 1993, $^{40}\text{Ar}/^{39}\text{Ar}$, K/Ar, and fission track geochronology of sediment-hosted disseminated gold deposits at Post-Betze, Carlin Trend, northeastern Nevada: *Economic Geology*, v. 88, p. 622-646.
- Doeblich, J. L., Wotruba, P. R., Theodore, T. G., McGibbon, D. H., and Felder, R. P., 1995, *Field guide for geology and ore deposits of the Battle Mountain mining district, Humboldt and Lander counties, Nevada*, in *Geology and ore deposits of the American Cordillera symposium: Geological Society of Nevada, U.S. Geological Survey, and Sociedad Geológica de Chile*, 121 p.
- Eberhart-Phillips, D., Stanley, W. D., Rodriguez, B. D., and Lutter, W. J., 1995, Surface seismic and electrical methods to detect fluids related to faulting: *Journal of Geophysical Research*, v. 100, no. B7, p. 12,919-12,936.
- Evans, J. G., 1980, *Geology of the Rodeo Creek NE and Welches Canyon quadrangles, Eureka county, Nevada*: U.S. Geological Survey Bulletin 1473, 81p.
- Grauch, V. J. S., 1996, Magnetically interpreted, granitoid plutonic bodies, in Singer, D. A., ed., *An analysis of Nevada's metal-bearing mineral resources: Nevada Bureau of Mines and Geology Open-File Report 96-2*, p. 7-1 to 7-16.
- Grauch, V.J.S., Klein, D.P., and Rodriguez, Brian, (this volume), Progress on understanding the crustal structure near the Battle Mountain-Eureka mineral trend from geophysical constraints, in Tosdal, R.M., ed., *Contributions to the gold metallogeny of northern Nevada: U.S. Geological Survey Open-File Report*.
- Ilchik, R. P. and Barton, M. D., 1997, An amagmatic origin of Carlin-type gold deposits: *Economic Geology*, v. 92, no. 3, p. 269-288.

- Jachens, R. C., Moring, B. C., and Schruben, P. G., 1996, Thickness of Cenozoic deposits and the isostatic residual gravity over basement for Nevada, *in* Singer, D. A., An analysis of Nevada's metal-bearing mineral resources: Nevada Bureau of Mines and Geology Open-File Report 96-2, p. 2-1 through 2-10, 1 plate, scale 1:1,000,000.
- Keller, G. V. and Frischknecht, F. C., 1966, Electrical methods in geophysical prospecting: Pergamon Press, New York, 517 p.
- Keller, G. V., 1987, Rock and mineral properties, *in* M. N. Nabighian, ed., Electromagnetic Methods in Applied Geophysics Theory: Tulsa, Oklahoma, Society of Exploration Geophysicists, v. 1, p. 13-51.
- Nelson, P. H. and Anderson, L. A., 1992, Physical properties of ash flow tuff from Yucca Mountain, Nevada: Journal of Geophysical Research, v. 97, no. B5, p. 6823-6841.
- Palacky, G. J., 1987, Resistivity characteristics of geologic targets, in Electromagnetic Methods, *in* M. N. Nabighian, ed., Applied Geophysics-Theory: Tulsa, Oklahoma, Society of Exploration Geophysicists, v. 1, p. 53-129.
- Radtke, A. S., 1985, Geology of the Carlin gold deposit, Nevada: U. S. Geological Survey Professional Paper 1267, 124 p.
- Shawe, D. R., 1991, Structurally controlled gold trends imply large gold resources in Nevada, *in* Raines, G. L., Lisle, R. E., Schafe, R. W., Wilkinson, W. H., eds., Geology and ore deposits of the Great Basin, Symposium Proceedings: Geological Society of Nevada, Reno, v. 1, p. 199-212.
- Sillitoe, R. H. and Bonham, H. F., 1990, Sediment-hosted gold deposits; distal products of magmatic-hydrothermal systems: Geology, v. 18, no. 2, p. 157-161.
- Smith, J. T., and Booker, J. R., 1988, Magnetotelluric inversion for minimum structure: Geophysics, v. 53, p. 1565-1576.
- _____, 1991, Rapid inversion of two- and three-dimensional magnetotelluric data: Journal of Geophysical Research, v. 96, p. 3905-3922.
- Vozoff, K., 1972, The magnetotelluric method in the exploration of sedimentary basins: Geophysics, v. 37, p. 98-141.
- _____, 1991, The magnetotelluric method, *in* M. N. Nabighian, ed., Electromagnetic methods in applied geophysics: Tulsa, Oklahoma, Society of Exploration Geophysicists, v. 2, part B, p. 641-711.
- Wannamaker, P. E., 1983, Resistivity structure of the northern Basin and Range: Geothermal Resources Council, Special Report No. 13, p. 345-361.
- Wannamaker, P. E., Hohmann, G. W. and Ward, S.H., 1984, Magnetotelluric responses of three-dimensional bodies in layered earths: Geophysics, v. 49, no. 9, p. 1517-1533.

Pb ISOTOPIC MAPPING OF CRUSTAL STRUCTURE IN THE NORTHERN GREAT BASIN AND RELATIONSHIPS TO Au DEPOSIT TRENDS

By J.L. Wooden, R.W. Kistler, and R.M. Tosdal

ABSTRACT

A regional common Pb isotopic study of Mesozoic and Tertiary granitoids and some Tertiary volcanic rocks in the northern Great Basin provides a better understanding of the regional crustal structure and composition, and their relationship to the apparent linear alignment of gold deposits along the Carlin and Battle Mountain - Eureka trends. The Pb isotopic data allow for the subdivision of the northern Great Basin into western, central, and eastern provinces. The boundary between the western and central provinces closely follows the previously documented initial Sr ($ISr = 0.706$) line and represents a narrow zone in which initial Pb and Sr isotopic ratios increase rapidly. Initial Pb vs. Pb and Pb vs. Sr isotopic ratios show strong positive correlation, and initial Pb and Sr isotopic ratios increase from west to east across these two provinces. The eastern province is characterized by plutons in which the Pb and Sr isotopic ratios are not strongly correlated and exhibit much greater variability than those in plutons from the two provinces to the west. The boundary between the central and eastern provinces is sharp and is approximately coincident with the Carlin trend in north-central Nevada. It is suggested that this isotopic boundary and the Carlin trend mark the locus of a cryptic major crustal discontinuity. The Battle Mountain - Eureka trend lies within the central province and is generally parallel to both the Carlin trend and the north-south oriented portion of the boundary between the western and central provinces as marked by the $ISr = 0.706$ line. It is proposed that the Pb province boundaries, the $ISr = 0.706$ line, and the gold deposit trends are related to crustal-scale discontinuities formed during continent-scale rifting along western North America in the latest Precambrian and that these discontinuities, which probably were originally fault systems, were reactivated or utilized by subsequent tectonic and magmatic events in the Phanerozoic.

INTRODUCTION

Two subparallel north-northwest to northwest-trending mineral belts in Nevada, the Battle Mountain-Eureka trend on the SW and the Carlin trend on the NE (fig. 1), are thought to reflect

deep-seated, pre-Cenozoic crustal structures. These structures may be pre-Cenozoic faults, Mesozoic and/or Paleozoic fold axes, or uncertain features of the Precambrian basement. Both geophysical and geochemical-isotopic studies can complement field based geologic studies of these features,

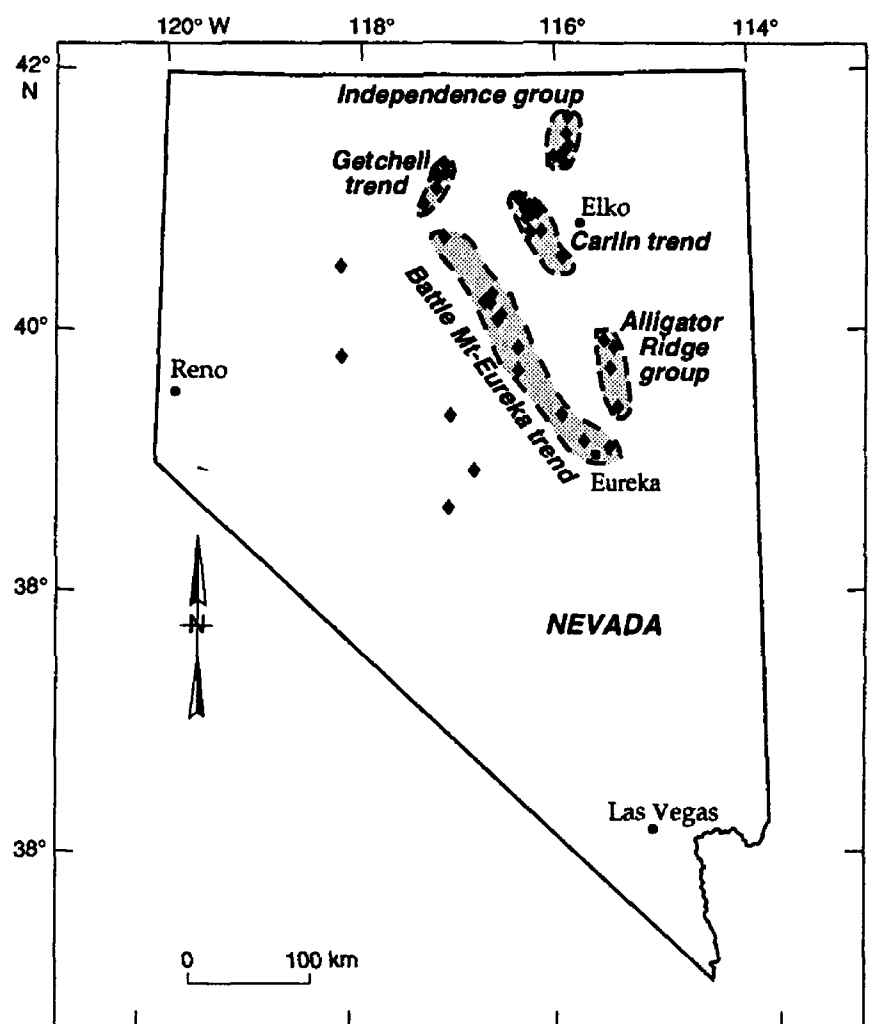


Figure 1. Location of major belts of precious metal deposits in north-central Nevada.

and both have been successfully applied in studies of crustal structure in the northern Great Basin and the western U.S (for example Blakely and Jachens, 1991; Grauch and others, 1995; Zoback and others, 1994; Kistler and Peterman, 1973, 1978; and Kistler, 1983, 1991). Geophysical studies measure time-integrated physical parameters and attempt to distinguish

shallow from deep and younger from older features but are limited in temporal distinctions because the basic data are tied to present conditions and may be dominated by recent crust-mantle events. Isotopic studies have the advantage of investigating time-related features by comparing the isotopic compositions of rocks formed at different times during the geologic history of a region for systematic or significant changes. However, the sampling interval for isotopic studies is controlled by the present-day outcrop distribution of the rocks to be studied, and the result can be a very uneven geographic distribution. In comparison, the sampling interval for geophysical studies is not tied to the outcrop patterns and can be designed to provide an even geographic coverage at a chosen scale. The isotopic signatures of igneous rocks largely reflect the average characteristics of their source regions plus any later interaction with the crustal column through which they moved or into which they were emplaced and any later modification by metamorphism or hydrothermal alteration. In general isotopic signatures of granitoid rocks reflect the geochemical properties of the lower and middle crust and the mantle from which they were melted and are unlikely to reflect the upper crust, the structure of which is more readily revealed by geophysical methods. Since one goal of this study is to provide a basis for the comparison of the geophysical and isotopic data sets with respect to the crustal structure of Nevada, it is important to remember that the two methods have some fundamental differences in what features of the crust and mantle system are providing the basic data.

Kistler and Peterman (1973, 1978) and Kistler (1983, 1991) demonstrated that the distribution of Sr isotopic compositions of granitoid rocks in the northern Great Basin delineated crustal structure, particularly the location of the boundary between continental and oceanic crust as marked by the initial $^{87}\text{Sr}/^{86}\text{Sr}$ (ISr) = 0.706 line (fig. 2). Elison and others (1990) showed that the ISr = 0.706 line correlates well with the shelf-slope break defined by Early Paleozoic and Triassic strata. Farmer and DePaolo (1983, 1984) used combined Nd and Sr isotopic compositions of Great Basin granitoids to study the petrogenesis of these rocks and regional crustal structure; however, their pioneering studies were limited by the small sample suite for which Nd isotopic data were available. Bennett and DePaolo (1987) and DePaolo and others (1991) present examples of the application of Nd isotopic studies to understanding the distribution of Precambrian crustal provinces in, and the more general crustal structure of, the southwestern U.S. Farmer and Ball (1997) provide an excellent example of using Nd isotopic characteristics of Precambrian crustal provinces to determine provenance of Late Precambrian to early Paleozoic sedimentary rocks in the Great Basin. Since these rocks are potential sources for Pb in the ore minerals associated with the gold deposits in Nevada (Tosdal and others, this volume), the conclusions reached in Farmer and Ball (1997) are of

general interest to the present study.

Pb and Sr isotopic data are suitable for regional scale studies because the data are relatively easy to acquire for regional-scale sample suites. Rocks and magmas derived from the mantle have low Pb concentrations (1-2 ppm or less) relative to feldspar-rich crustal rocks that typically have 10-30 ppm Pb. Because of this strong contrast in Pb concentration, the Pb isotopic composition of most granitoid rocks reflects that of the crust with which it is associated even if the magma had a significant mantle contribution to its formation. Doe and Delevaux (1973) report an early example of the application of Pb isotopic studies to Mesozoic granitoids in the western U.S. Chen and Tilton (1991) have demonstrated the usefulness of combined Pb and Sr isotopic studies in the southern Sierra Nevada. Building on the work of Zartman (1974), Wooden and others (1988), Wooden and Miller (1990) and Wooden and DeWitt (1991) used the Pb isotopic compositions of Proterozoic and Phanerozoic rocks to better define the extent and nature of the crustal provinces in the southwestern U.S. Wooden and Mueller (1988) provide a Pb isotopic characterization for the Archean Wyoming province. These studies provide the background necessary to interpret the Pb isotopic signatures of the Great Basin granitoids. It should be pointed out that the Precambrian crustal provinces of the southwestern U.S. as defined by the Pb and Nd isotopic studies mentioned above are similar in their geographic extent, but not the same (compare figures in Wooden and DeWitt, 1991, to those in Farmer and Ball, 1997). One of the areas of disagreement is the extent of the Mojave crustal province in the Nevada, Utah, and Arizona, but this difference mostly effects the details, not the main thesis, of the data interpretation provided below. Given that there are fundamental differences in the geochemical basis of the Pb and Nd isotopic systems, these differences in the extent of the crustal provinces may be real and/or rooted in sample distribution, sample types, and interpretation. A large database of Sr isotopic data and crystallization ages is already available for granitoids from the northern Great Basin. We report here on the results derived from the determination of initial Pb isotopic compositions for many of the same samples used in the studies by Kistler and co-workers (see references above and below) and for other new samples.

DATA SOURCES AND ANALYTICAL PROCEDURES

The data used herein have been determined over about a ten year period in the Pb isotopic laboratory at the U.S. Geological Survey in Menlo Park for a number of topical studies (e.g. Wright and Wooden, 1991) mostly focused on magmatic and tectonic histories and processes. Most of the data represent feldspar separates made from whole-rock crushes by conventional magnetic and heavy-liquid separation techniques.

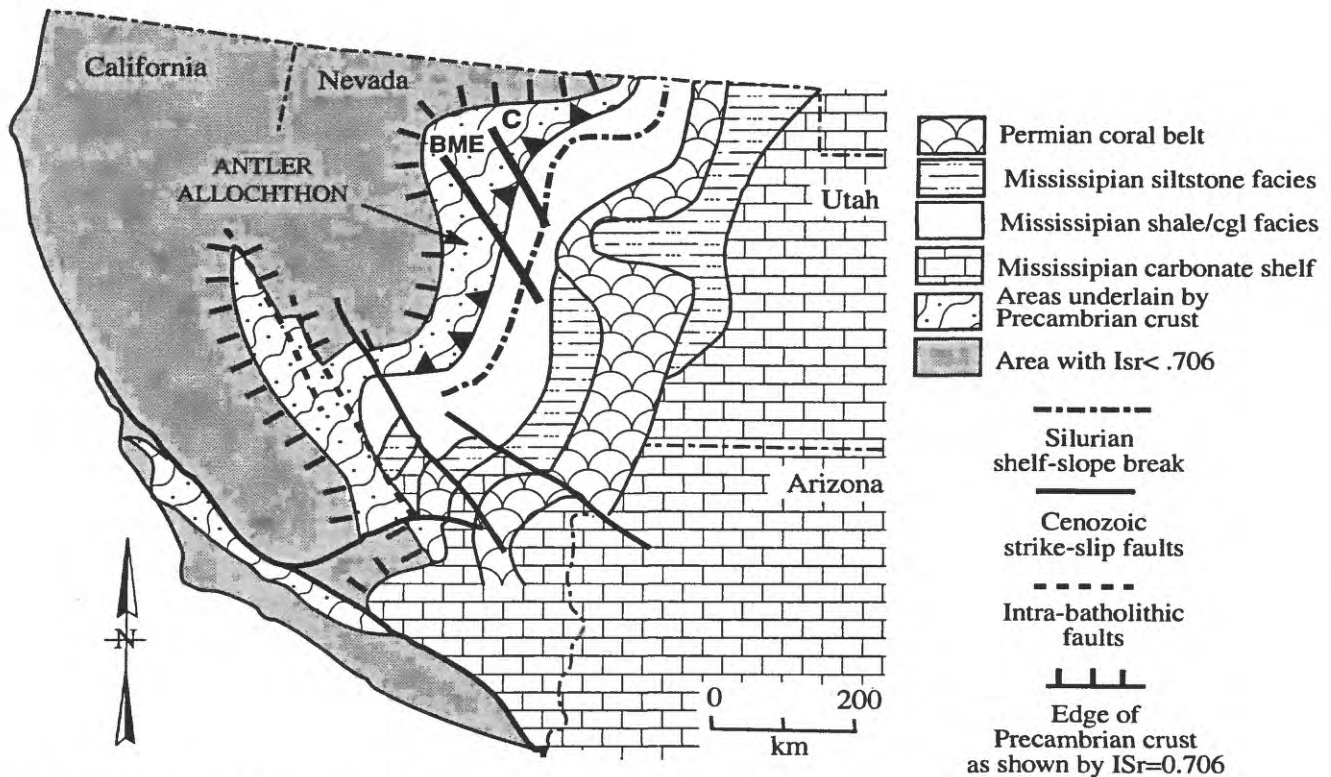


Figure 2. Outline map of California and Nevada showing the $ISr = 0.706$ line and Paleozoic facies boundaries (from Kistler and Fleck, 1994; Stevens and others, 1992; and Kistler, 1990). BME, Battle Mountain-Eureka mineral belt; C, Carlin.

Sodium- and particular K-rich feldspars from granitoid rocks have relatively high concentrations of Pb and very low concentrations of U and Th. The very low U/Pb and Th/Pb ratios of feldspars mean that the Pb isotopic composition of feldspars changes little with time, and a present-day isotopic composition of feldspar is a good estimate of the initial Pb isotopic composition of the feldspar and the magma (assuming equilibrium) at the time of crystallization. In the rare cases where a feldspar has a significant U/Pb or Th/Pb ratio, failure to correct for the added radiogenic Pb will make the measured Pb isotopic ratios higher than the true initial values. The Pb isotopic composition of feldspar is subject to resetting during heating events that reach about 300° C or approximately the same temperature range in which biotite K-Ar and Rb-Sr ages are reset. During such a heating event, radiogenic Pb produced in minerals or along grain boundaries where high U/Pb and Th/Pb exist migrates and is taken into the feldspar crystal structure. The Pb isotopic composition of such a feldspar will be more radiogenic than the initial composition. In Paleozoic and younger systems, the Pb isotopic ratio that is most likely to be effected by failure to correct for a significant U/Pb or Th/Pb ratio or for thermal resetting is $^{206}\text{Pb}/^{204}\text{Pb}$ because most of the U present during this time is ^{238}U , the parent of ^{206}Pb ; ^{235}U (parent of ^{207}Pb)

has mostly disappeared because of its much higher decay rate compared to ^{238}U , and ^{232}Th (parent of ^{208}Pb) has a lower decay rate than ^{238}U .

Some analyses used herein are from whole-rock powders used in the regional geochemical and isotopic studies of Lee (1984) and Kistler and Lee (1989). For these samples the present-day Pb isotopic composition of the whole-rock powder has been determined along with a Pb concentration by the isotope dilution technique. These data have been combined with U and Th concentration and crystallization age data (Lee, 1984; Kistler and Lee, 1989) to calculate an initial Pb isotopic concentration. Initial Pb isotopic ratios calculated from whole-rock samples carry a higher uncertainty than those measured in feldspar mineral separates because of the analytical uncertainties associated with the U and Th concentrations, and the tendency of medium- and coarse-grained granitic samples to lose U in surficial weathering environments. The most common error in initial Pb ratios calculated from whole-rock powders is for the present-day $^{206}\text{Pb}/^{204}\text{Pb}$ ratios to be under-corrected because the measured U concentration is too low as a result of U-loss during weathering. The $^{206}\text{Pb}/^{204}\text{Pb}$ ratio experiences the most change in Phanerozoic materials because of the very high ratio of ^{238}U to ^{235}U for this time interval.

Pb was separated from feldspar and whole-rock samples using the standard anion exchange resin process that utilizes HBr and HCl. All feldspar mineral separates were leached with HCl, HNO₃, and weak HF to remove labile Pb before dissolution. Pb isotopic compositions were determined in static-collection mode on a MAT 262 mass spectrometer. Thermal fractionation is monitored by running NBS-981 and -982. The empirical fractionation correction factor is 0.0011 per mass unit and its uncertainty is the largest contribution to the total analytical uncertainty of about 0.1% associated with the Pb isotopic ratios.

RESULTS

There are approximately 400 samples for which common Pb isotopic data are available (fig. 3). Sr isotopic data produced from separate studies are available for most of these samples, and the existence of these previously analyzed sample suites and Sr isotopic data was a great asset in the conduct of the present study. Observations made in the early stages of this study were that for most of the samples a strong positive correlation exists between the three Pb isotopic ratios and between the initial Sr ratio and

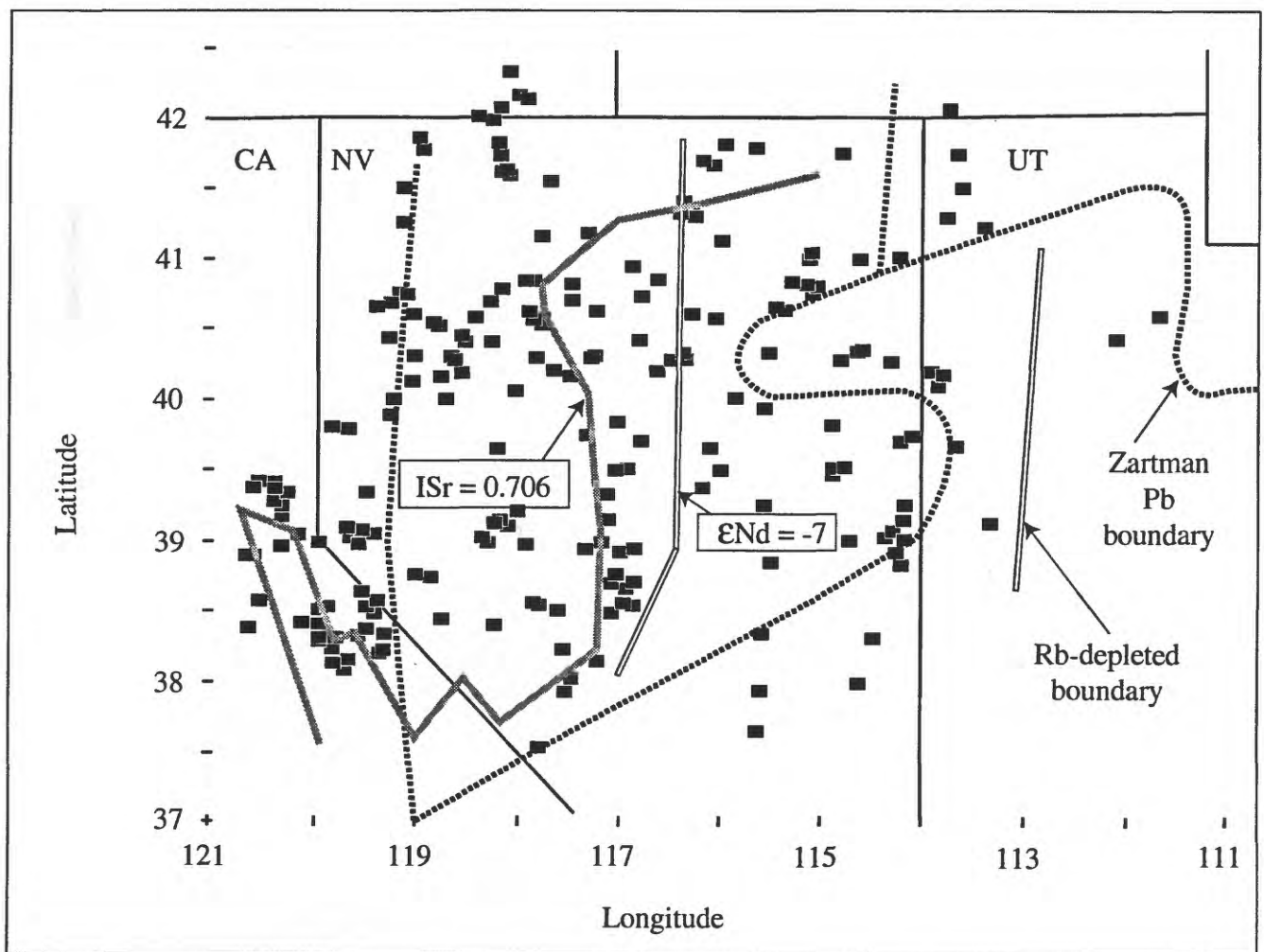


Figure 3. Outline map of California (CA), Nevada (NV), and Utah (UT) showing distribution of igneous samples used for the Pb isotopic study. The approximate boundary of the $I_{Sr} = 0.706$ line is shown as are the boundaries (heavy dashed lines) for the Pb isotopic provinces of Zartman (1974) and two boundaries (Rb-depleted and $\epsilon_{Nd} = -7$) proposed by Farmer and DePaolo (1983) from their Nd and Sr isotopic data. See text for additional discussion.

each of the Pb isotopic ratios (Wooden and Stacey, 1987; Wright and Wooden, 1991). These positive correlations, however, were not observed for many samples from eastern Nevada (fig. 4; Wooden and others, 1991, 1993). These observations were consistent with those made by Chen and Tilton (1991) for a transect in the southern Sierra Nevada. That transect in some aspects represents a telescoped version of the Nevada data set including the fact that the strong correlation between isotopic ratios is no longer observed at its eastern end. Since previous Sr isotopic studies (Kistler and Peterman, 1973, 1978; Kistler, 1983, 1991) had already established a correlation between geographic position and Sr isotopic ratio (i.e. the $ISr = 0.706$ line), the positive correlation between Sr and Pb isotopic ratios indicates that the Pb isotopic ratios must also be related in a regular way to geographic position. Simple plots of sample longitude vs. Pb (and Sr) isotopic values confirm this situation and demonstrate that the Pb isotopic data indicated a general increase in Pb isotopic ratios from west to east (fig. 5). However, the changes in orientation of the $ISr = 0.706$ line from northerly in western Nevada to east-northeast in northern Nevada and the loop defined in west-central Nevada and California (Kistler, 1983, 1991; Elison and others, 1990) indicate that no simple west to east geographic distribution of the Sr isotopic data exists across the full N-S extent of Nevada (fig. 2), and consequently none should be expected for the Pb isotopic data either. Another complication for the interpretation of the Pb and Sr isotopic data is that local geographic variations occur in the distribution of the ratios. In other words somewhat anomalous values, either higher or lower, with respect to the average of surrounding values are fairly common, and the occurrence of these values prevents a simple, monotonic contouring of the data. Some of the analytical reasons for these anomalies were discussed above, but the anomalies may also be geologic in origin and related to variations in the age and geochemical properties of the sources and/or magmatic interaction with upper crustal rocks. Regardless of the reason for the anomalies, it becomes simpler to examine the geographic distribution of the data sets in terms of ranges of values rather than simple monotonic contours. Figures 6 and 7 show the geographic distribution of selected ranges of $^{206}Pb/^{204}Pb$ (<18.7 , $18.7-19.1$, $19.1-19.3$, $19.3-19.6$, >19.6) and $^{208}Pb/^{204}Pb$ (<38.8 , $38.8-39.0$, $39.0-39.7$, >39.7); geographic plots for $^{207}Pb/^{204}Pb$ are not shown because the much more limited range of these data result in poorer geographic resolution. Only two to three ranges of data are shown on each figure in order to minimize the problem of overlapping data points during plotting which obscure the geographic distribution of the data. The breaks at $^{206}Pb/^{204}Pb = 19.1$ and $^{208}Pb/^{204}Pb = 38.8$ were chosen from the Pb isotopic ratio vs. ISr plots to correspond generally to $ISr = 0.706$ (fig. 4B).

The geographic distribution of these Pb isotopic data

intervals in the northern Great Basin indicates a subdivision of the region into three major provinces which for descriptive purposes will be referred to as western, central and eastern (fig. 8). The boundary between the western and central provinces corresponds closely, but not exactly, to the $ISr = 0.706$ line reflecting the selection criteria of the Pb isotopic data intervals. The observation that this boundary represents a narrow geographic zone across which Pb (and Sr) isotopic ratios change rapidly (figs. 5A, 6B and 7B) is confirmation that this boundary represents more than just a numerical division of the data set. This zone separates a broad region in central-western, northwestern, and central-northern Nevada (western province) where $^{206}Pb/^{204}Pb = 18.75-19.1$, $^{208}Pb/^{204}Pb = 38.45-38.8$, and $ISr = 0.704-0.706$, from a region in central Nevada (central province) where the corresponding ratios are $19.3-19.6$, $39.0-39.7$, and $0.707-0.710$.

The boundary between the central and eastern provinces is best defined by the occurrence of samples with $^{208}Pb/^{204}Pb$ greater than 39.7. The western edge of this field of values defines a fairly sharp boundary that trends north-northwest and is approximately coincident with the Carlin trend (figs. 7B-8A). The distribution of samples with $^{206}Pb/^{204}Pb$ either greater than 19.6 or less than 18.7 suggests a similar but more poorly defined boundary (fig. 6B). Pb isotopic variations in the eastern province are more irregular than in the western and central provinces. Notable features are the reappearance of samples with $^{208}Pb/^{204}Pb$ less than 39.0 and $^{206}Pb/^{204}Pb$ less than 19.3. The eastern province may be divisible into northern and southern areas based on the occurrence of samples with $^{206}Pb/^{204}Pb$ either greater than 19.6 or less than 19.1 and $^{208}Pb/^{204}Pb$ less than 39.7 (figs. 6B-7B). The data do not define a sharp boundary between these two areas, but only a broad zone. Possible reasons for the irregular isotopic variations of the eastern province will be discussed below. The paucity of samples for Utah and southernmost Nevada prevent the clear extension of these three Pb isotopic provinces or the definition of province boundaries. However, a sufficient body of Pb isotopic data exists both for Precambrian and Phanerozoic rocks in southeastern California and for Precambrian rocks in western Arizona to conclude that the Proterozoic Mojave crustal province exists in this region (Wooden and Miller, 1990; Wooden and DeWitt, 1991). The Pb isotopic signature of Mesozoic and Tertiary igneous rocks in the Mojave crustal province is very similar to that observed for the eastern province in Nevada. It is an inescapable conclusion that the southward extension of the boundary between the central and eastern Pb provinces of Nevada must turn back to the west. Furthermore the boundary must remain north of the Proterozoic outcrops in the Mojave Desert and in the Death Valley region (unpublished Pb isotopic data show these to belong to the Mojave crustal province, Wooden and Calzia,

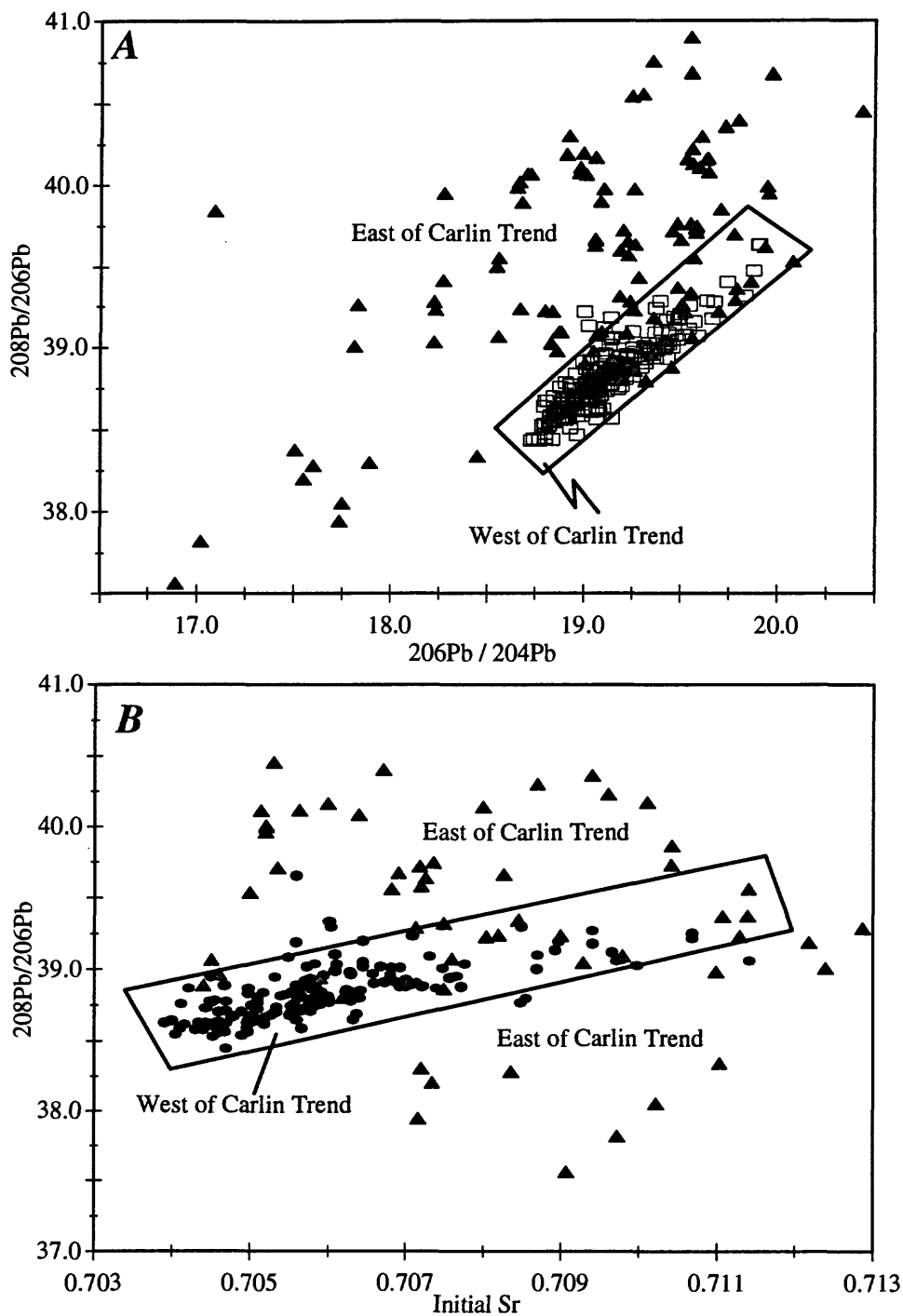


Figure 4. (A) Initial $^{206}\text{Pb}/^{204}\text{Pb}$ vs. initial $^{208}\text{Pb}/^{204}\text{Pb}$ for all samples. Pb isotopic compositions for samples west of the Carlin trend (open squares, within rectangular box) show a strong, tight positive correlation. Pb isotopic compositions for samples east of the Carlin trend (solid triangles) are not well correlated, and many have much higher $^{208}\text{Pb}/^{204}\text{Pb}$ relative to $^{206}\text{Pb}/^{204}\text{Pb}$ than samples west of the Carlin trend. (B) Initial Sr isotopic ratio vs. $^{208}\text{Pb}/^{204}\text{Pb}$ for all samples. Sr and Pb isotopic compositions for samples west of the Carlin trend show a strong positive correlation (solid circles, within rectangular box) while those from samples east of the Carlin trend (triangles) are poorly correlated and have a larger range of values.

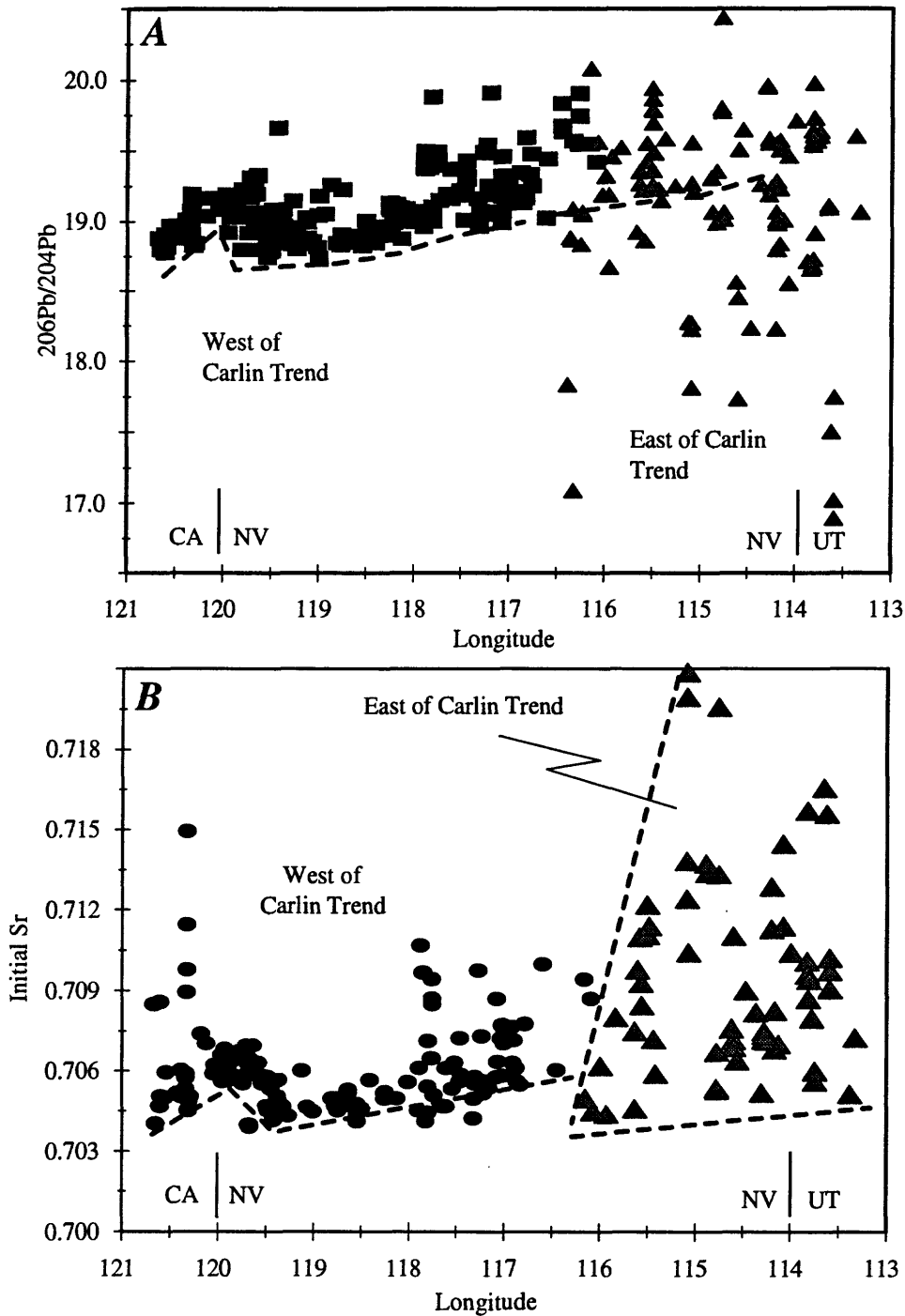


Figure 5. Variation of (A) initial $^{206}\text{Pb}/^{204}\text{Pb}$ Pb and (B) initial Sr with west longitude in degrees for all samples. Initial isotopic compositions for samples located west of the Carlin trend (solid circles) show regular variations from west to east while those east of the Carlin trend (solid triangles) range to much lower ($^{206}\text{Pb}/^{204}\text{Pb}$) and higher (initial Sr) values. These composite west to east transects indicate more apparent variation for western samples than actually exists because isotopic isopleths do not have simple north to south orientations. For example the $\text{ISr} = 0.706$ line and corresponding Pb isotopic values cross from 117° and 118° in central Nevada (see fig. 6-8) and then loops back to the east producing the two increasing trends in initial $^{206}\text{Pb}/^{204}\text{Pb}$ at 118° and 117° degrees longitude.

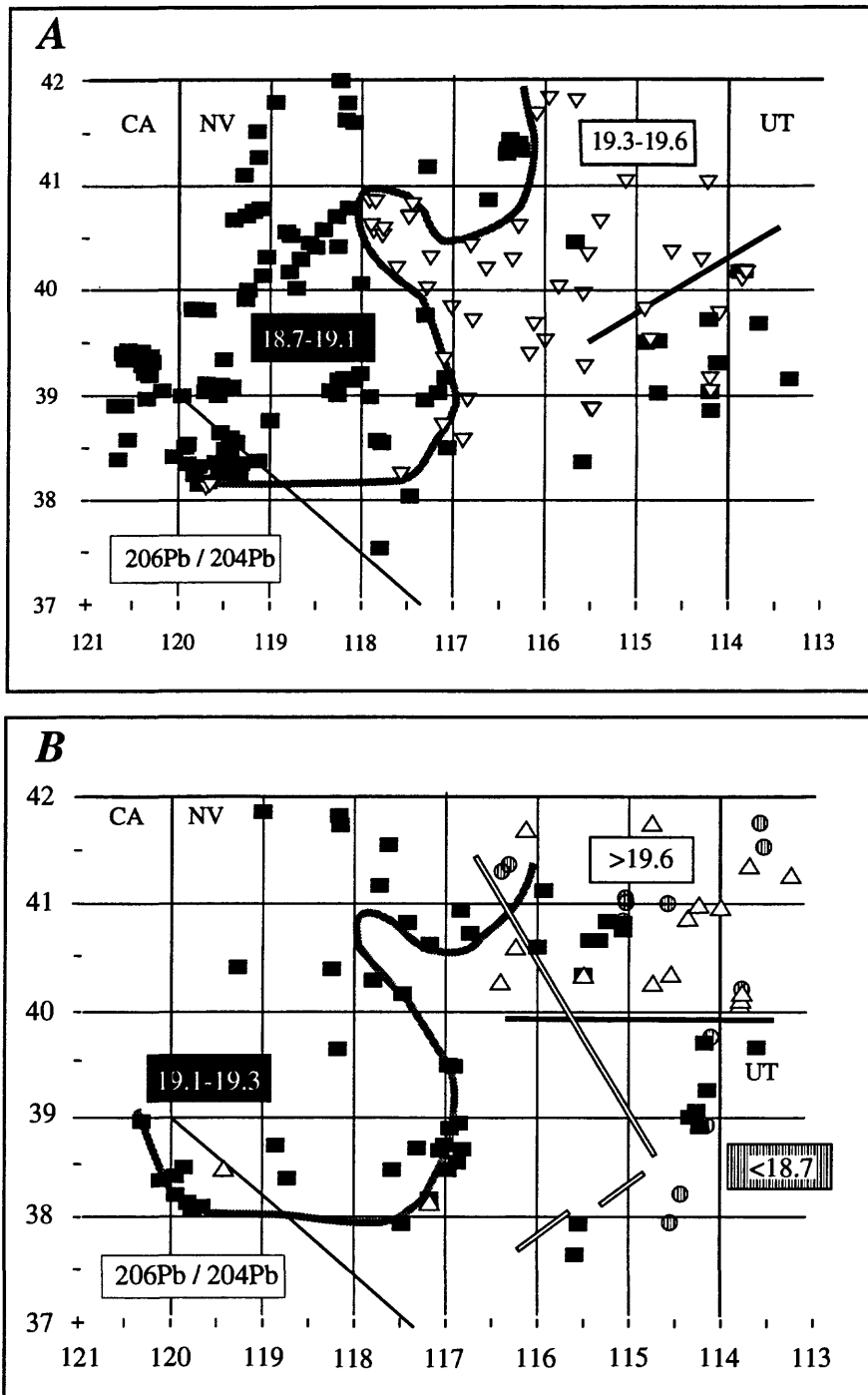


Figure 6. The geographic distribution of samples with selected ranges of initial $^{206}\text{Pb}/^{204}\text{Pb}$ in Nevada and adjoining areas of California and Utah. (A) Distribution of samples for only two non-overlapping ranges of $^{206}\text{Pb}/^{204}\text{Pb}$, 18.7 to 19.1 and 19.3 to 19.6. (B) Distribution for three ranges - less than 18.7, 19.1 to 19.3, and greater than 19.6. The ranges were plotted separately in this figure and in figure 7 to avoid visual clutter. The break at 19.1 was chosen to correspond approximately to $\text{ISr} = 0.706$ based on the correlation between ISr and initial $^{206}\text{Pb}/^{204}\text{Pb}$ and marks the boundary between the proposed western and central Pb isotopic provinces. The occurrence of samples with initial $^{206}\text{Pb}/^{204}\text{Pb}$ less than 19.1 in eastern Nevada and Utah indicates more heterogeneous crust and may imply an age difference across the marked east to west and northeast trending lines. See text for further discussion.

1995; see Ramo and Calzia, 1996, for Nd data), and connect to the eastern portion of the transect of Chen and Tilton (1991). The southern edge of the basement gravity low of Blakely and Jachens (1991) may be related to the edge of the preserved Precambrian craton in southern Nevada. In general, the boundary between the central and eastern Pb provinces probably roughly parallels the $ISr = 0.706$ line and western-central Pb province boundary in Nevada until it reaches the east side of the Sierra Nevada batholith where the boundary appears to run southerly toward the Garlock fault. This boundary can be traced south of the Garlock fault through the western Mojave Desert as the western edge of the Mojave crustal province (Martin and Walker, 1992). It is possible to define provinces roughly similar to the western and central Pb provinces in Nevada there also; however, the need to restore the Tertiary tectonic disruption of this region and other geologic differences (Kistler, 1990; Miller and Glazner, 1995) make that discussion beyond the scope of this paper.

DISCUSSION AND CONCLUSIONS

Pb vs. Pb and Pb vs. Sr isotopic ratios within the western and central provinces of Nevada as defined above show strong positive correlations, increase generally west to east, have the same trends regardless of pluton age, and mimic two component mixing systems. These features are at least partially attributed to the process of averaging tens of cubic kilometers of the source region during the melting that accompanies magma production. The isotopic signature of granitoids in the western province is not entirely oceanic as compared to that of granitoids in the Klamath region of northern California (Barnes and others, 1992) and must contain a significant component derived from the continental lithosphere. The granitoid source region for the central province must have a dominant crustal component and probably represents thinned Precambrian crust and subcontinental mantle and an (underplated?) oceanic component. The Battle Mountain-Eureka mineral belt lies within the central province and roughly parallels the north-northwest-trending section of the $ISr = 0.706$ line (fig. 8A). This mineral belt lies along the east side of an area from the East Range to Battle Mountain that contains unusually radiogenic Pb and Sr isotopic compositions with respect to their geographic position (Figs. 5 and 8). The $ISr = 0.706$ line makes a noticeable bend around the west and north sides of this area as it turns to the east-northeast (fig. 8). These more radiogenic isotopic values are more similar to those at the eastern edge of the central province (near Carlin), and it is possible that this area has been displaced tectonically toward the west at some unknown time. The limited data set presently available indicates that less radiogenic Pb isotopic values are found immediately east of this more radiogenic area which

allows for a southerly embayment in the Pb isotopic isopleths into the northern part of the Battle Mountain-Eureka mineral belt (figs. 6-8). This area of less radiogenic isotopic values is roughly coincident with the geophysical basement feature defined by Grauch and others (1995) and the northern Nevada rift of Zoback and others (1994). At the present time, however, it is not possible to correlate an isotopic feature with the south-southeastward extension of the Battle Mountain - Eureka mineral belt. This trend may simply represent the reactivation of an old major crustal fault largely within the region of a thinned continental crust.

These well-organized isotopic trends end abruptly along the north-northwest-trending boundary that marks the western edge of the eastern province and approximates the position of the Carlin trend. East of this boundary, the sharpness of which suggests a major crustal fault or suture, most samples exhibit high to very high $^{208}Pb/^{204}Pb$ (and many have high $^{207}Pb/^{204}Pb$) relative to $^{206}Pb/^{204}Pb$, the range of Pb and Sr isotopic ratios expands greatly, and isotopic ratios show no simple correlation trends (figs. 4, 5, and 9). Farmer and DePaolo (1983) defined a Nd isotopic boundary based on the occurrence of granitoids with very low epsilon Nd values in this general location. The eastern province represents Precambrian crust (and subcontinental mantle?) that has experienced the least amount of modification by Late Precambrian and Phanerozoic events. As noted above, and by Wright and Wooden (1991), this province can be divided on the basis of $^{206}Pb/^{204}Pb$, $^{207}Pb/^{204}Pb$, and $^{208}Pb/^{204}Pb$ ratios into northern and southern regions along a broad east-northeasterly trending belt. The distinction between northern and southern regions is particularly sharp in the isotopic data for Tertiary igneous rocks, which can show significant differences from the isotopic data of Jurassic rocks in the same area. The characteristics of the isotopic data (fig. 9) suggest that the northern region represents the Archean Wyoming province and the southern region an Early Proterozoic province most similar to the Mojave crustal province of Wooden and Miller (1990). Wright and Snoke (1993) suggest that in the Ruby Mountains and East Humboldt Range this east-northeast-trending boundary is a relatively sharp feature that represents the continuation of the Cheyenne belt into northeast Nevada. The Nd isotopic study of the Cheyenne belt in southern Wyoming by Ball and Farmer (1991) also suggested a relatively sharp boundary that may have resulted in large part from erosion of overthrust crust. The regional isotopic data in eastern Nevada can also be modeled, however, as a broad zone of crustal mixing probably established by a combination of tectonic, magmatic, and sedimentary processes during the juxtaposition of these terranes in the Early Proterozoic and, as such, would be similar to the boundary zone between the Mojave and Arizona crustal provinces (Wooden and DeWitt, 1991). This model is preferred.

The west to east sequence of isotopic provinces across Nevada is a unique feature in the western U.S., and possibly

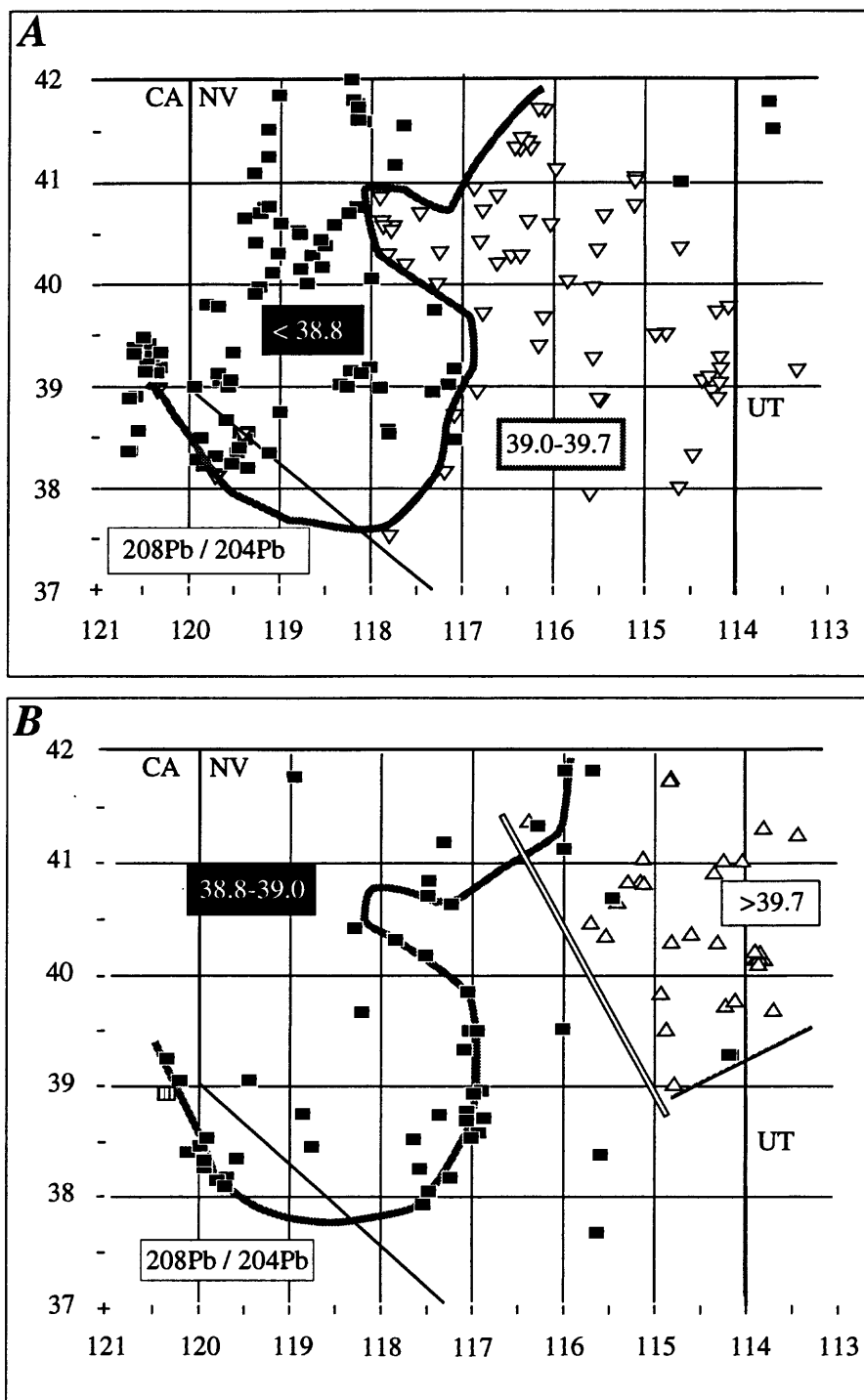


Figure 7. The geographic distribution of samples with selected ranges of initial $^{208}\text{Pb}/^{204}\text{Pb}$ in Nevada and adjoining areas of California and Utah. (A) Distribution of samples for two, non-overlapping ranges of initial $^{208}\text{Pb}/^{204}\text{Pb}$, less than 38.8 and 39.0 to 39.7. (B) Distribution for the ranges 38.8 to 39.0 and greater than 39.7. The break at 38.8 was chosen to correspond to an ISr of 0.706 and represents the boundary between the proposed western and central Pb isotopic provinces. Note the concentration of samples with $^{208}\text{Pb}/^{204}\text{Pb}$ between 38.8 and 39.0 along the western-central province boundary. The western edge of the distribution of samples with $^{208}\text{Pb}/^{204}\text{Pb}$ greater than 39.7 is proposed to mark the boundary between the central and eastern provinces. The southern extent of this range may also denote a crustal age difference in the eastern province. See text for further discussion.

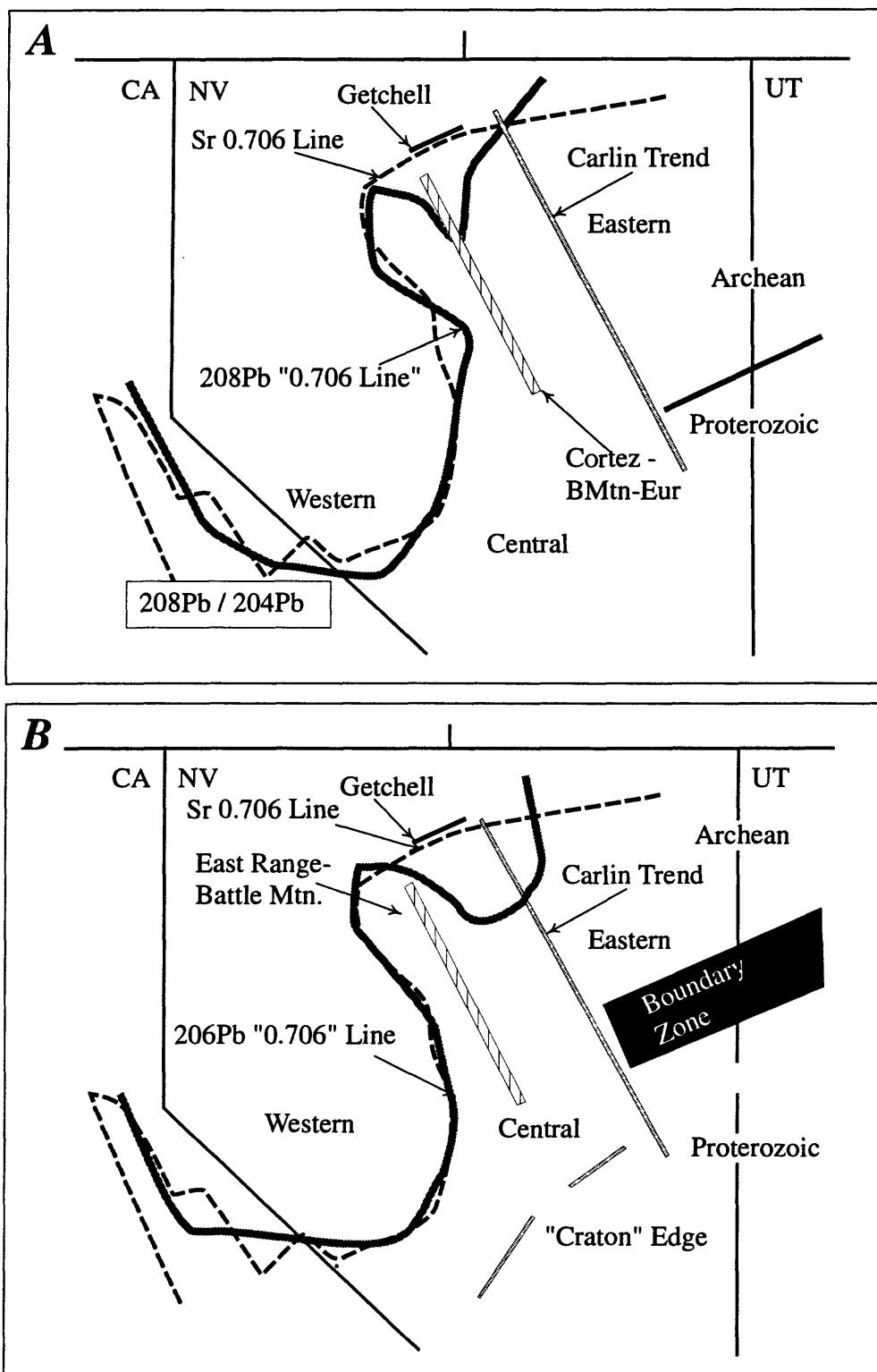


Figure 8. Summary maps of the boundaries and regions defined by (A) initial $^{208}\text{Pb}/^{204}\text{Pb}$ and (B) initial $^{206}\text{Pb}/^{204}\text{Pb}$ for Nevada and adjoining parts of California and Utah and a comparison to the $\text{ISr} = 0.706$ line and to Carlin, Battle Mountain-Eureka, and Getchell mineral trends. Note the difference in north-central Nevada between the $\text{ISr} = 0.706$ line and the lines defined by the Pb isotopic data. The break between Archean and Proterozoic crust in the eastern province is not clearly defined and probably is indicative of a gradational boundary.

in western North America. Although isotopic patterns similar to parts of what is present in Nevada can be observed elsewhere (e.g. the northern Peninsular Range is similar to the western and part of the central province), there appears to be nowhere else that the complete transition is preserved. Given the tectonic history of western North America in the Phanerozoic, particularly the north-south movement by strike-slip faults along the continental edge, it is not surprising that the character of a continental margin created in the Late Precambrian would be greatly disrupted. It is also unclear if the Late Precambrian continental margin would have experienced the exact same processes along the entire rifted margin. The general preservation of the isotopic zoning in Nevada since the Late Precambrian does, however, place constraints on the relative displacements of crust and mantle in the Phanerozoic. Although the continental margin in Nevada has experienced several shorting events, none of them

could have been so severe as to greatly displace the regular pattern of isotopic zoning. Therefore a model calling for over a hundred kilometers of eastward thrusting as suggested by Wright and Wooden (1991) seems unlikely, and the contrast in the isotopic signatures between Jurassic and Tertiary intrusions in the eastern Pb province, that stimulated this model, is probably more related to differences in the depth of melting in the same crust-mantle system than to lateral movements of the upper crust. Similar arguments also hold for the Tertiary extensional events that produced the modern geomorphic pattern of the northern Great Basin. In spite of the variable geographic distribution of this extension, the zoning patterns have been preserved perhaps in part because the extension is mostly normal or parallel to the strike of the isotopic provinces and breaks the crust into discrete extensional domains of smaller scale than that proposed for thrusting events.

The most significant Pb isotopic boundary identified in

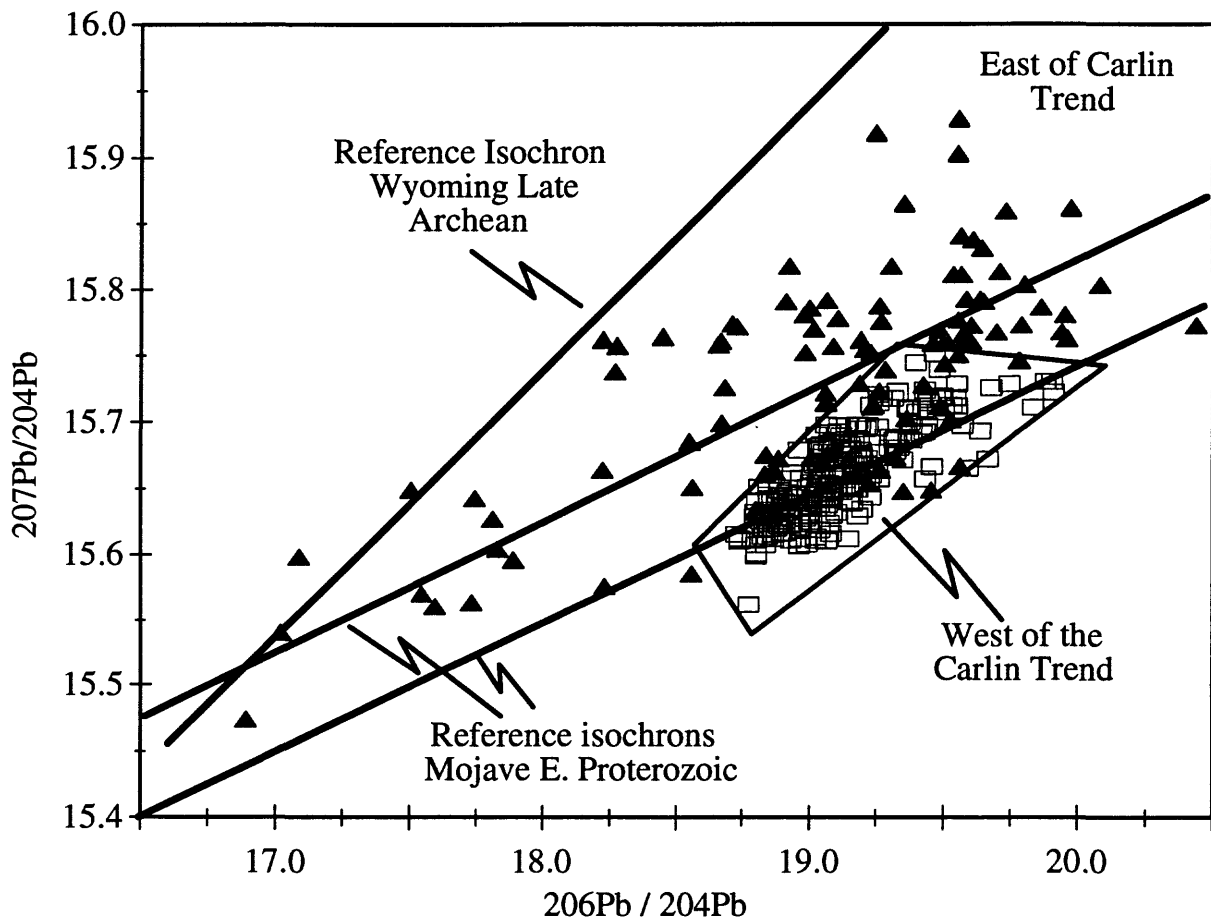


Figure 9. $206\text{Pb}/204\text{Pb}$ vs. initial $207\text{Pb}/204\text{Pb}$ on a Pb isochron diagram for all samples in this study. Samples located west of the Carlin trend (open squares) define a relatively small field compared to those east of the Carlin trend (solid triangles). Reference isochrons are shown for the Early Proterozoic Mojave crustal province (two parallel lines) and the Late Archean rocks of the Wyoming Province (steeper single line) and encompass most of the eastern samples. See text for additional discussion.

this study lies between the eastern and central provinces; this boundary corresponds in location and orientation to the Carlin trend. The Battle Mountain-Eureka or Cortez mineral belt shares the orientation of this boundary but is not distinguished by isotopic data. The north-trending part of the boundary between the western and central provinces that matches in location this part of the ISr = 0.706 line shares the same general north-northwest trend as the two mineral belts. The Pb province boundaries and the ISr = 0.706 line indicate the presence of major crustal-scale features. The common orientation of the Battle Mountain - Eureka mineral belt suggests that its location may have resulted from the same process that formed the other two crustal-scale features. Our interpretation of these crustal-scale features is that most resemble a regional fault system and/or sutures. Interestingly published gravity data (Grauch and others, 1995) are most supportive of this conclusion for the Battle Mountain-Eureka mineral belt, which the isotopic data do not distinguish as a major crustal boundary. These gravity data, however, are at least suggestive that the Carlin trend may also represent a geophysical discontinuity. The combination of north-northwest-trending crustal boundaries and their high angle of intersection with the east-northeast trend of the ISr = 0.706 line and stratigraphic trends in north-central and northeastern Nevada suggests a model in which major northwest-striking normal fault systems developed to accommodate an extending and thinning continental margin during Late Proterozoic rifting of the western margin of North America. Phanerozoic reactivation of these fault systems has focused younger tectonic, magmatic, hydrothermal and mineralization events, and possibly influenced even the orientations of the modern basins and ranges.

ACKNOWLEDGMENTS

Thanks are due to our USGS colleagues in the Western Region Au project, Dave John, Jim Wright, Al Robinson, and Chris Henry for utilization of their sample collections and accompanying geologic knowledge, and to Charles Holdsworth for laboratory support. The constructive criticism of Bob Fleck and Dave Miller has improved the manuscript.

REFERENCES CITED

- Ball, T.T., and Farmer, G.L., 1991, Identification of 2.0 to 2.4 Nd model age crustal material in the Cheyenne belt, southeastern Wyoming: Implications for Proterozoic accretionary tectonics at the southern margin of the Wyoming craton: *Geology*, v. 19, p. 360-363.
- Barnes, C.G., Petersen, S.W., Kistler, R.W., Prestvik, T., and Sundvoll, B., 1992, Tectonic implications of isotopic variations among the Jurassic and Early Cretaceous plutons, Klamath Mountains: *Geological Society of America Bulletin*, v. 104, p. 117-126.
- Bennett, V.C., and DePaolo, D.J., 1987, Proterozoic crustal history of the western United States as determined by neodymium isotopic mapping: *Geological Society of America Bulletin*, v. 99, p. 674-685.
- Blakely, R.J., and Jachens, R.C., 1991, Regional study of mineral resources in Nevada: Insights from three-dimensional analysis of gravity and magnetic anomalies: *Geological Society of America Bulletin*, v. 103, p. 795-803.
- Chen, J.H., and Tilton, G.R., 1991, Applications of lead and strontium isotopic relationships to the petrogenesis of granitoid rocks, central Sierra Nevada batholith, California: *Geological Society of America Bulletin*, v. 103, p. 439-447.
- DePaolo, D.J., 1981, A neodymium and strontium isotopic study of the Mesozoic calc-alkaline granitic batholiths of the Sierra Nevada and Peninsular Ranges, California: *Journal of Geophysical Research*, v. 86, p. 10,470-10,488.
- DePaolo, D.J., Linn, A.M., and Schubert, 1991, The continental crustal age distribution: Methods of determining mantle separation ages from Sm-Nd isotopic data and application to the southwestern United States: *Journal of Geophysical Research*, v. 96, p. 2071-2088.
- Doe, B.R., and Delevaux, M.H., 1973, Variations in lead isotopic compositions in Mesozoic granitic rocks of California - A preliminary investigation: *Geological Society America Bulletin*, v. 84, p. 3513-3526.
- Elison, M.W., Speed, R.C., and Kistler, R.W., 1990, Geologic and isotopic constraints on the crustal structure of the northern Great Basin: *Geological Society America Bulletin*, v. 102, p. 1077-1092.
- Farmer, G.L., 1988, Isotope geochemistry of Mesozoic and Tertiary igneous rocks in the western United States and implications for the structure and composition of the deep continental lithosphere, in Ernst, W.G., ed., *Metamorphism and crustal evolution of the western United States*: Englewood Cliffs, New Jersey, Prentice Hall, W.W. Rubey v. VII, p. 87-109.
- Farmer, G.L., and Ball, T.T., 1997, Sources of Middle Proterozoic to Early Cambrian siliciclastic sedimentary rocks in the Great Basin: A Nd isotope study: *Geological Society America Bulletin*, v. 109, p. 1193-1205.
- Farmer, G.L., and DePaolo, D.J., 1983, Origin of Mesozoic and Tertiary granite in the western United States and implications for pre-Mesozoic crustal structure; 1, Nd and Sr isotopic studies in the geocline of the northern Great Basin: *Journal of Geophysical Research*, v. 88, p. 3379-3401.
- Farmer, G.L., and DePaolo, D.J., 1984, Origin of Mesozoic and Tertiary granite in the western United States and implications for pre-Mesozoic crustal structure; 2, Nd and Sr studies of unmineralized and Cu- and Mo-mineralized granites in the Precambrian craton: *Journal of Geophysical Research*, v. 89, p. 10141-10160.
- Grauch, V.J.S., Jachens, R.C., and Blakely, R.J., 1995, Evidence for a basement feature related to the Cortez disseminated gold trend and implications for regional exploration in Nevada: *Economic Geology*, v. 90, p. 203-207.
- Kistler, R.W., 1983, Isotope geochemistry of plutons in the northern Great Basin: *Geothermal Resources Council Special Report* 13, p. 3-8.
- Kistler, R.W., 1990, Two different lithosphere types in the Sierra Nevada, California, in Anderson, J.L., ed., *The nature and origin of Cordilleran magmatism*: *Geological Society of America*

- Memoir 174, p. 271-281.
- Kistler, R.W., 1991, Chemical and isotopic characteristics of plutons in the Great Basin: Geology and Ore Deposits of the Great Basin Symposium, Reno 1990, Proceedings, p. 107-109.
- Kistler, R.W., 1993, Mesozoic interbatholithic faulting, Sierra Nevada, California, *in* Dunn, G., and McDougall, K., ed., Mesozoic Paleogeography of the Western United States - II: Pacific Section Society of Economic Paleontologists and Mineralogists, Book 71, p. 247-262.
- Kistler, R.W., and Fleck, R.J., 1994, Field guide for a transect of the central Sierra Nevada, California: Geochronology and isotope geology: U.S. Geological Survey Open-File Report 94-267, 51p.
- Kistler, R.W., Ghent, E.D., and O'Neil, J.R., 1981, Petrogenesis of garnet two-mica granites in the Ruby Mountains, Nevada: *Journal of Geophysical Research*, v. 86, p. 10591-10606.
- Kistler, R.W., and Lee, D.E., 1989, Rubidium, strontium, and strontium isotopic data for a suite of granitoid rocks from the Basin and Range Province, Arizona, California, Nevada, and Utah: U.S. Geological Survey Open-File Report 89-199, 13p.
- Kistler and Peterman, 1973, Variations in Sr, Rb, K, Na, and initial $^{87}\text{Sr}/^{86}\text{Sr}$ in Mesozoic granitic rocks and intruded wall rocks in central California: *Geological Society of America Bulletin*, v. 84, p. 3489-3512;
- Kistler and Peterman, 1978, Reconstruction of crustal blocks of California on the basis of initial strontium isotopic compositions of Mesozoic granitic rocks: U.S. Geological Survey Professional Paper 1071, 17 p.
- Kistler, R.W., and Ross, D.C., 1990, A strontium isotopic study of plutons and associated rocks of the southern Sierra Nevada and vicinity, California: U.S. Geological Survey Bulletin 1920, 20 p.
- Lee, D.E., 1984, Analytical data for a suite of granitoid rocks from the Basin and Range Province: U.S. Geological Survey Bulletin 1602, 54 p.
- Lee, D.E., Friedman, I., and Gleason, J.D., 1981, Map showing oxygen isotope compositions of granitoid rocks of the Basin and Range Province: U.S. Geological Survey Miscellaneous Field Studies Map MF-1305, scale 1:3,168,000.
- Lee, D.E., Kistler, R.W., and Robinson, A.C., 1986, The strontium isotope composition of granitoid rocks of the southern Snake Range: U.S. Geological Survey Bulletin 1622, p. 171-179.
- Martin, M.W., and Walker, J.D., 1992, Extending the western North American Proterozoic and Paleozoic continental crust through the Mojave Desert: *Geology*, v. 20, p. 753-756.
- Miller, J.S., and Glazner, A.F., 1995, Jurassic plutonism and crustal evolution in the central Mojave Desert, California: *Contributions to Mineralogy and Petrology*, v. 118, p. 379-395.
- Ramo, O.T., and Calzia, J.P., 1996, Neodymium isotopic composition of cratonic rocks in the southern Death Valley region, California: Evidence for a substantial Archean source component: *Geological Society of America Abstracts with Programs*, v. 28, p. A316.
- Solomon, G.C., and Taylor, H.P., Jr., 1989, Isotopic evidence for the origin of Mesozoic and Cenozoic granitic plutons in the northern Great Basin: *Geology*, v. 17, p. 591-594.
- Stacey, J.S., and Zartman, R.E., 1978, A lead and strontium isotopic study of igneous rocks and ores from the Gold Hill Mining district, Utah: *Utah Geology*, v. 5, p. 1-15.
- Tosdal, R.M., Cline, J.S., Hofstra, A.H., Peters, S.G., Wooden, J.L., and Young-Mitchell, M.N., 1998, Some constraints on Pb sources in sediment-hosted Au deposits, northern Nevada, *in* Tosdal, R.M., ed., Contributions to the Au metallogeny of northern Nevada: U.S. Geological Survey Open-File Report.
- Wooden, J.L., and DeWitt, Ed, 1991, Pb isotopic evidence for the boundary between the Early Proterozoic Mojave and Central Arizona crustal provinces in western Arizona, *in* Karlstrom, K., and DeWitt, E, eds., Proterozoic Geology and Ore Deposits of Arizona: Tucson, Arizona Geological Society Digest 19, p. 27-50.
- Wooden, J.L., Kistler, R.W., Morton, D.M., and Lichte, F.E., 1994, A Pb, Sr, and O isotopic transect across the northern Peninsular Ranges batholith, southern California: *Transactions of the American Geophysical Union*, v. 75, p. 701.
- Wooden, J.L., Kistler, R.W., Robinson, A.C., Tosdal, R.M., and Wright, J.E., 1991, A comparison of isotopic signatures of Mesozoic and Tertiary plutonism in the western U.S.: Northern Great Basin vs. southern Basin and Range: *Transactions of the American Geophysical Union*, v. 72, p. 302.
- Wooden, J.L., Kistler, R.W., Robinson, A.C., Tosdal, R.M., and Wright, J.E., 1993, Character of the pre-Mesozoic basement along the edge of the western U.S. craton: Pb isotopic evidence from Mesozoic plutonism: *Geological Society America Abstracts with Programs*, v. 25, p 166.
- Wooden, J.L., and Miller, D.M., 1990, Chronologic and isotopic framework for Early Proterozoic crustal evolution in the eastern Mojave Desert region, SE California: *Journal of Geophysical Research*, v. 95, p. 20,133-20,146.
- Wooden, J.L., and Mueller, P.A., 1988, Pb, Sr, and Nd isotopic compositions of a suite of Late Archean, igneous rocks, eastern Beartooth Mountains: Implications for crust-mantle evolution: *Earth Planetary Science Letters*, v. 87, p. 59-72.
- Wooden, J.L., and Stacey, J.S., 1987, Lead isotopic constraints on the origin of Cordilleran granitic magmatism in the western U.S.: *Geological Society of America Abstracts with Programs*, v. 19, p. 465.
- Wooden, J.L., Stacey, J.S., Howard, K.A., Doe, B.R., and Miller, D.M., 1988, Pb isotopic evidence for the formation of Proterozoic crust in the southwestern United States, *in* Ernst, W.G., ed., Metamorphism and crustal evolution of the western United States: Englewood Cliffs, New Jersey, Prentice Hall, W.W. Rubey v. VII, p. 68-86.
- Wright, J.E., and Snoke A.W., 1993, Tertiary magmatism and mylonitization in the Ruby-East Humboldt metamorphic core complex, northeastern Nevada: U-Pb geochronology and Sr, Nd, and Pb isotope geochemistry: *Geological Society of America Bulletin*, v. 105, p. 935-952.
- Wright, J.E., and Wooden, J.L., 1991, New Sr, Nd, and Pb isotopic data from plutons in the northern Great Basin: Implications for crustal structure and granite petrogenesis in the hinterland of the Sevier thrust belt: *Geology*, v. 19, p. 457-460.
- Zartman, 1974, Lead isotopic provinces in the Cordillera of the western United States and their geologic significance: *Economic Geology*, v. 69, p. 792-805.
- Zoback, M.L., McKee, E.H., Blakely, R.J., and Thompson, G.A., 1994, The northern Nevada rift - regional tectono-magmatic relations and middle Miocene stress directions: *Geological Society of America Bulletin*, v. 106, p. 371-382.

CRUSTAL STRUCTURE AND ITS RELATION TO GOLD BELTS IN NORTH-CENTRAL NEVADA: OVERVIEW AND PROGRESS REPORT

By V. J. S. Grauch

ABSTRACT

A schematic cross-sectional view of the crustal structure across north-central Nevada was derived from results presented in papers in this section. The main elements of this preliminary view are that deeply penetrating fault zones generally coincide with the Carlin and Battle Mountain-Eureka mineral trends and separate large blocks of dominantly carbonate upper crust. The faults may be the underlying controls on the alignment of mineral deposits. Many questions remain about the tectonic evolution of the crustal structure and the relation between crustal structure and mineralization processes.

INTRODUCTION

Much attention has been given to alignments of mineral deposits in Nevada since Roberts (1966) first named some mineral belts and described their association with the alignment of structural windows in the Roberts Mountains allochthon. Exploration for new discoveries along these alignments has been fairly successful for sediment-hosted disseminated ("Carlin-type") gold deposits along the Carlin and Battle Mountain-Eureka mineral trends in north-central Nevada (fig. 1). These mineral alignments are commonly attributed to pre-Tertiary structural features that regionally controlled the spatial distribution of structural windows and mineralization (for example Shawe, 1991). However, geologic evidence for deep-seated regional structures is indirect.

This section includes three papers describing geophysical and geochemical-isotopic methods applied to understanding different aspects of subsurface crustal structure in north-central Nevada. The resultant view of the subsurface crustal structure (presented below) helps us understand the tectonic evolution of deep-seated regional structures or crustal provinces and their role in controlling the spatial distribution of mineral deposits at the surface. The paper by Grauch and others (this volume) applies gravity, magnetic, seismic-reflection, and magneto-telluric methods to develop a preliminary cross-sectional model of crustal structure across the Battle Mountain-Eureka trend. The paper by Rodriguez

(this volume) presents a preliminary magnetotelluric profile model across both the Battle Mountain-Eureka and Carlin trends. Wooden and others (this volume) use Pb and Sr isotopes collected from igneous rocks across north-central Nevada to map crustal provinces and infer their origin.

VIEWING THE SUBSURFACE

Geophysical and geochemical-isotopic methods can provide evidence of major subsurface structures and changes in crustal composition insofar as they are expressed by changes

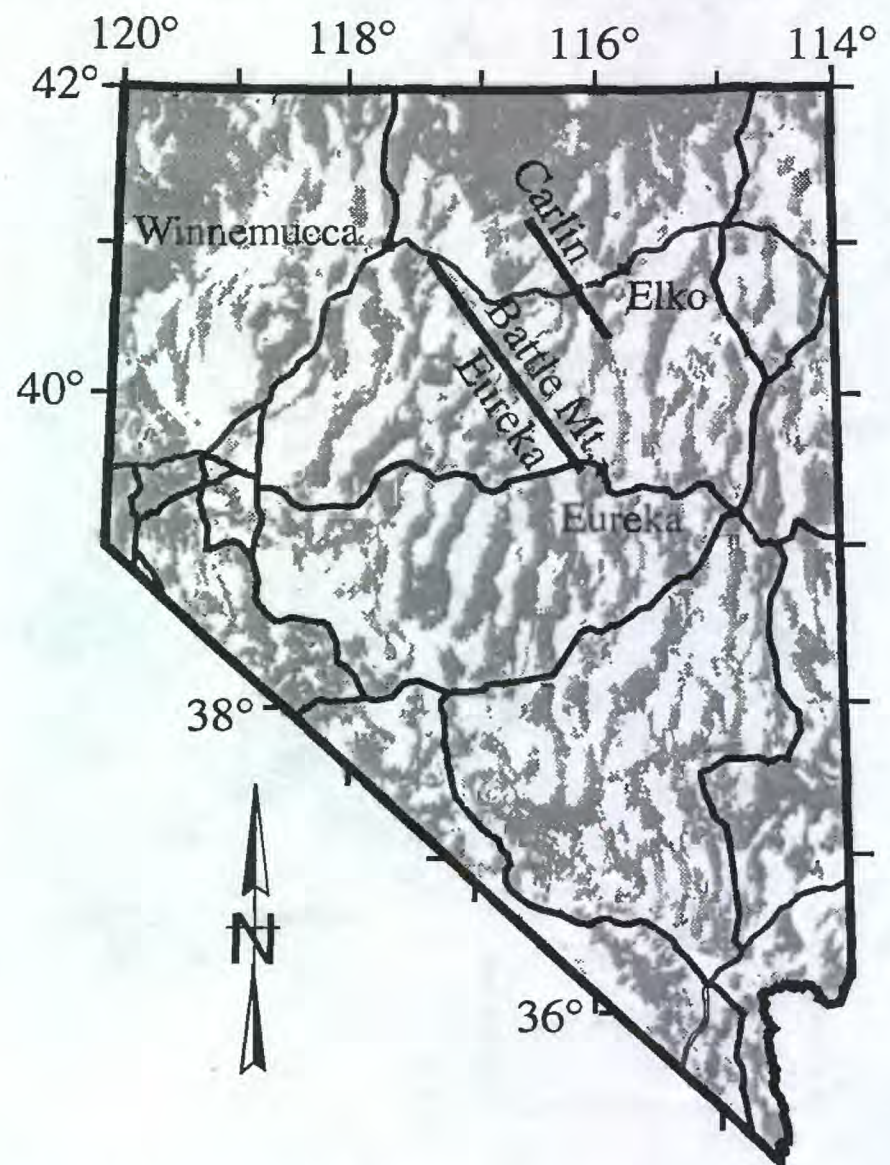


Figure 1. Location of Battle Mountain-Eureka mineral belt and the Carlin trend in Nevada. Outline of modern ranges (shaded) and major roads are also shown.

in rock properties or can be understood from chemical analyses of rocks at the surface. Geochemical-isotopic methods also provide information on crustal structure at different times. However, each method only provides information about certain aspects of the overall crustal structure, which necessitates an integrated approach combining several different geophysical methods, geochemical-isotopic studies, and constraints from geologic knowledge.

Figure 2 demonstrates the range of data available from geophysical and geochemical-isotopic studies for integration into a preliminary picture of crustal structure. These data are described in more detail in the previous papers contained in this section. The figure also exemplifies how information from the data sets can be complimentary. Shown are the basement gravity map (Grauch and others) and Pb and Sr isotopic

province boundaries (Wooden and others). The basement gravity data show changes in density in the upper crust that are related to lithologic changes and/or regional structures. In particular, an abrupt change in density coincides with the Battle Mountain-Eureka mineral belt (Grauch and others, 1995). The isotopic provinces provide information about chemical compositions in the middle and lower crust in the past. As shown on figure 2, the Carlin trend coincides with a boundary between two Pb isotopic provinces and the northern part of the Battle Mountain-Eureka trend coincides with a deflection in the another province boundary (Wooden and others, this volume). The basement-gravity and Pb-Sr isotopic province boundaries together provide evidence that deep-seated regional structures and changes in crustal composition are related to the mineral trends.

VIEWING THE SUBSURFACE USING MULTIPLE DATA SETS

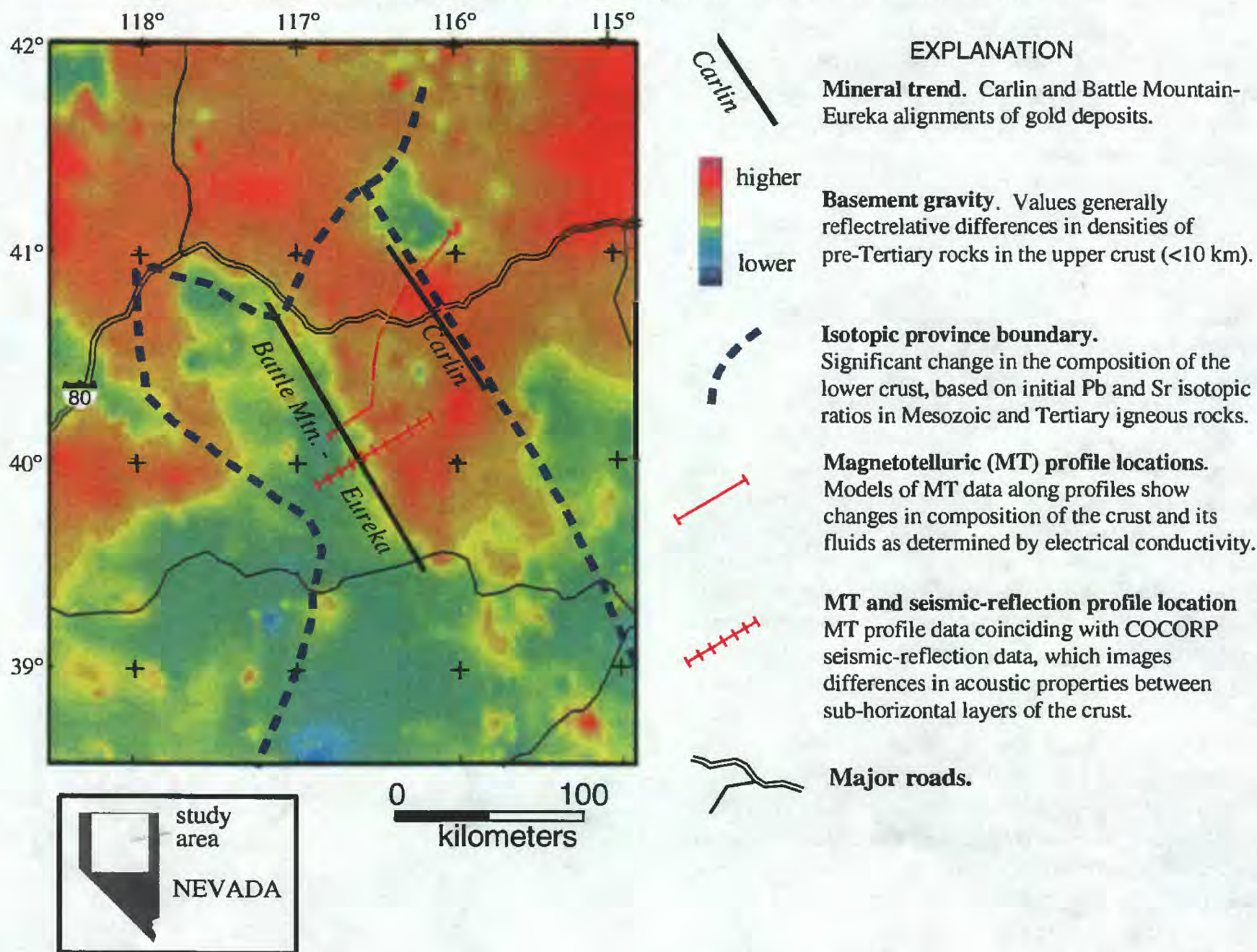


Figure 2. Map of basement gravity values overlain by isotopic province boundaries and locations of magnetotelluric and seismic-reflection profiles. Magnetic data cover the same map area but are not shown

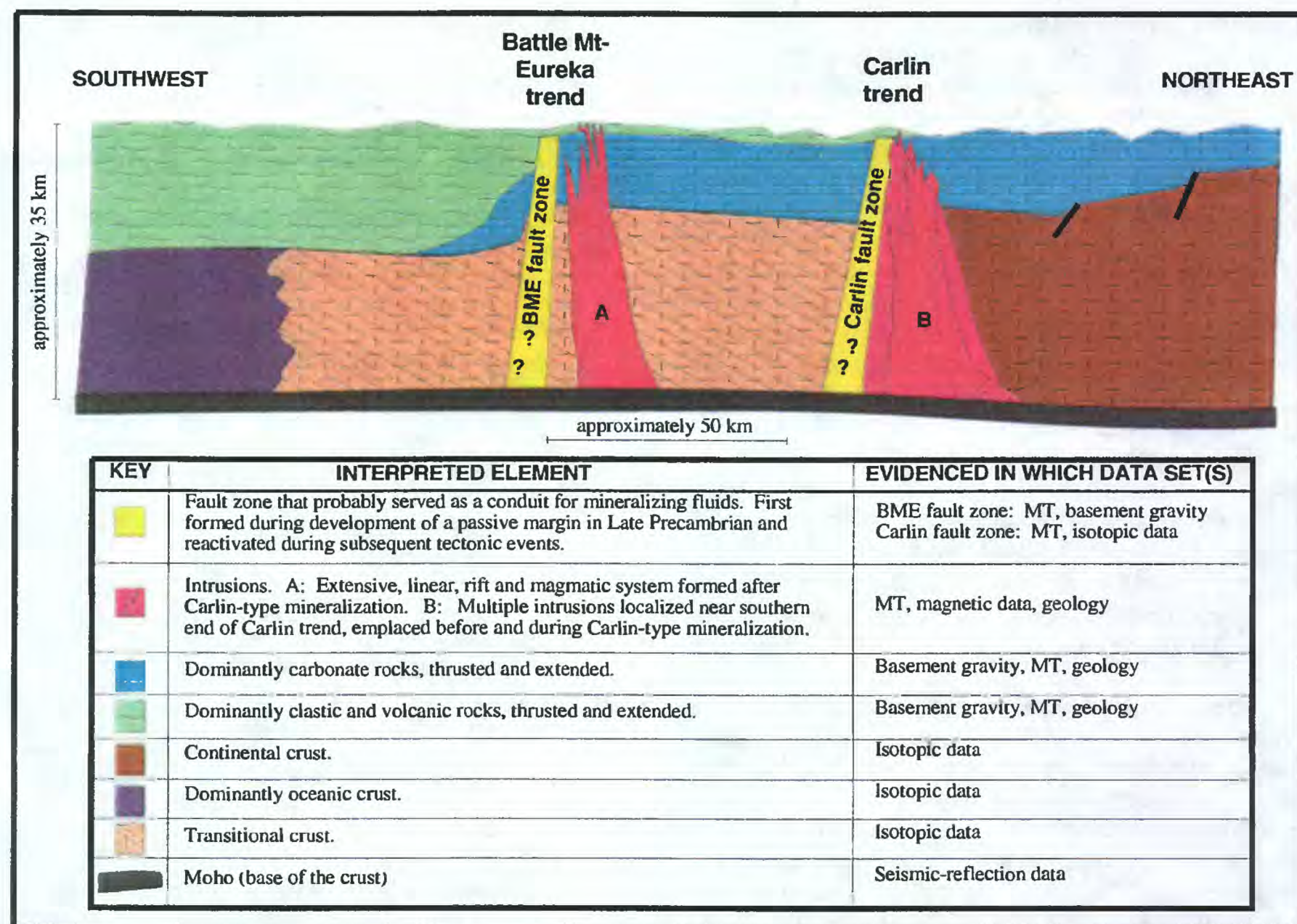


Figure 3. Schematic southwest-northeast cross-section across the Battle Mountain-Eureka and Carlin trends showing a preliminary hypothesis of the crustal structure. The table explains each interpreted element and which data set(s) provide(s) the evidence.

PRELIMINARY HYPOTHESIS

Integration of the results given by the papers in this section provides a schematic cross-sectional view of the crustal structure across the Battle Mountain-Eureka and Carlin trends along a southwest-northeast line (fig. 3). The major elements of the cross-section are as follows:

Fault zones: Deep crustal penetrating fault zones generally coinciding with the Battle Mountain-Eureka and Carlin trends are evident from electrically conductive zones in magnetotelluric data (Grauch and others, this volume; Rodriguez, this volume). Additional evidence for a fault coinciding with the Battle Mountain-Eureka trend is provided by the abrupt, linear change in gravity values in the basement gravity map (fig. 2). The geochemical-isotopic studies (Wooden and others, this volume) suggest the faults separate large crustal blocks of differing lithology or chemistry. These blocks probably originated during Late Proterozoic continental rifting, and remained

fairly intact during reactivation of the faults in subsequent tectonic events (Tosdal and Wooden, 1997; Wooden and others, this volume).

Intrusions: Large intrusions are shown near the mineral trends on figure 3, but they are not consistently located next to the fault zones in map view. The intrusion near the Battle Mountain-Eureka trend (A, fig. 3) is associated with the mid-Miocene northern Nevada rift of Zoback and others (1994). The rift diverges from the mineral belt toward the north and northeast. It was formed after most of the mineral deposits along the trend (Maher and others, 1993; Seedorff, 1991). The intrusion shown near the Carlin trend (B, fig. 3) does not extend to the northwest and southeast beyond the middle of the trend. It consists of intrusions of Jurassic, Cretaceous, and Eocene age (Teal and Jackson, 1997).

East-west change in upper crust composition: The Battle Mountain-Eureka trend coincides with a change from

lower-density, lower-resistivity upper crust on the southwest to high-density, high-resistivity upper crust on the northeast, as evidenced in basement gravity and magnetotelluric data (Grauch and others, this volume; Rodriguez, this volume). The western upper crust is interpreted as dominantly clastic and volcanic (eugeoclinal) rocks and the eastern upper crust as dominantly carbonate (miogeoclinal) rocks. Both the western and eastern upper crusts consist of numerous thrust sheets and extensional blocks, as evidenced at the surface. However, these structures lack much expression at deeper levels of the crust, as inferred from the geophysical data (fig 2; Grauch and others, this volume; Rodriguez, this volume).

West to east progression from oceanic to continental crust:

Isotopic provinces indicate a progression from dominantly oceanic crust on the west to relatively unmodified continental crust on the east (Wooden and others, this volume). The change from transitional crust to continental crust occurs abruptly at the Carlin trend.

The general coincidence of the fault zones and the mineral belts suggest that the deeply penetrating faults focused magmatism and hydrothermal circulation. However, many questions remain. For example, what was the source of hydrothermal fluids? What was the source of gold? What was the interaction between the fluids, the gold, and the crustal structure? What is the relation of the faults to other tectonic features such as the northern Nevada rift? These questions may be answered with additional geologic, geochemical, and geophysical study.

REFERENCES CITED

- Grauch, V. J. S., Jachens, R. C., and Blakely, R. J., 1995, Evidence for a basement feature related to the Cortez disseminated gold trend and implications for regional exploration in Nevada: *Economic Geology*, v. 90, p. 203-207.
- Grauch, V.J.S., Klein, D.P., and Rodriguez, B.D., (this volume), Progress on understanding the crustal structure near the Battle Mountain-Eureka mineral trend from geophysical constraints, *in* Tosdal, R.M., ed., Contributions to the Au metallogeny of northern Nevada: U.S. Geological Survey Open-File Report.
- Maher, B. J., Browne, Q. J., and McKee, E. H., 1993, Constraints on the age of gold mineralization and metallogenesis in the Battle Mountain-Eureka mineral belt, Nevada: *Economic Geology*, v. 88, p. 469-478.
- Roberts, R. J., 1966, Metallogenic provinces and mineral belts in Nevada: Nevada Bureau of Mines Report 13, p. 47-72.
- Rodriguez, B.D., (this volume), Regional crustal structure beneath the Carlin Trend, Nevada based on deep electrical geophysical measurements, *in* Tosdal, R.M., ed., Contributions to the Au metallogeny of northern Nevada: U.S. Geological Survey Open-File Report.
- Seedorff, Eric, 1991, Magmatism, extension, and ore deposits of Eocene to Holocene age in the Great Basin—mutual effects and preliminary proposed genetic relationships, *in* Raines, G. L., Lisle, R. E., Schafer, R. W., and Wilkinson, W. H., eds., *Geology and ore deposits of the Great Basin*: Geological Society of Nevada, Reno, Nevada, p. 133-178.
- Shawe, D. R., 1991, Structurally controlled gold trends imply large gold resources in Nevada, *in* Raines, G. L., Lisle, R. E., Schafer, R. W., and Wilkinson, W. H., eds., *Geology and ore deposits of the Great Basin*: Geological Society of Nevada, Reno, Nevada, p. 199-212.
- Teal, L., and Jackson, M., 1997, Geologic overview of the Carlin Trend gold deposits and descriptions of recent deep discoveries: *Society of Economic Geologists Newsletter*, no. 31, p. 1 and 13-25.
- Tosdal, R. M., and Wooden, J. L., 1997, Granites, Pb isotopes, and the Carlin and Battle Mt.-Eureka trends, Nevada: *Geological Society of America Abstracts with Programs*, v. 29, no. 6, p. A-61.
- Wooden, J. L., Tosdal, R. M., and Kistler, R. W., 1997, Pb and Sr isotopic mapping of crustal structure in the northern Great Basin: *Society of Economic Geologists Guidebook Series*, v. 28, p. 47-51.
- Wooden, J.L., Tosdal, R.M., and Kistler, R.W., (this volume), Pb isotopic mapping of crustal structure in the northern Great Basin and relationships to Au deposit trends, *in* Tosdal, R.M., ed., Contributions to the Au metallogeny of northern Nevada: U.S. Geological Survey Open-File Report.
- Zoback, M. L., McKee, E. H., Blakely, R. J., and Thompson, G. A., 1994, The northern Nevada rift: Regional tectono-magmatic relations and Miocene stress direction: *Geological Society of America Bulletin*, v. 106, p. 371-382.

PRELIMINARY FACIES ANALYSIS OF SILURIAN AND DEVONIAN AUTOCHTHONOUS ROCKS THAT HOST GOLD ALONG THE CARLIN TREND, NEVADA

By Augustus K. Armstrong, Ted G. Theodore, Robert L. Oscarson, Boris B. Kotlyar, Anita G. Harris, Keith H. Bettles, Eric A. Lauha, Richard A. Hipsley, Gregory L. Griffin, Earl W. Abbott, and J. Kelly Cluer

ABSTRACT

Sedimentary platform rocks in northern Nevada serve as hosts for the bulk of the gold in Carlin-type gold deposits. These deposits largely account for this region comprising the most significant gold province in North America. The most prolific part of the Carlin trend is the northern half, which extends from the Gold Quarry Mine on the south to the Dee Mine on the north. Although sedimentary rocks constitute a fundamental element of genetic models for Carlin-type deposits, the implications and impacts of Paleozoic sedimentary fabrics and diagenetic processes on deposit genesis have not been investigated as thoroughly as have the associated alteration, chemistry of the mineralizing fluids, and structural setting(s) of the deposits. Five Silurian-Devonian rock units below the Roberts Mountains thrust are the principal gold-hosting units in the Carlin trend; these are the Hanson Creek Formation, Roberts Mountains Formation, Bootstrap limestone, Popovich Formation, and the Rodeo Creek unit. Of these units, only the Roberts Mountains and Popovich Formations have the mineralogy and porosity which favors gold mineralization. In both the Roberts Mountains and the Popovich Formations, the sedimentary rocks are typically calcitic dolostones with primary intercrystalline vug porosity resulting essentially from diagenetic crystallization of dolomite. The Roberts Mountains and Popovich Formations thus had an inherent porosity due to primary early crystallization of dolomite in lime mud (micrite) and an abundance of intercrystalline sulfur-rich carbon has subsequently enhanced its reactivity to gold-bearing fluids that circulated there during the Cretaceous and (or) Tertiary.

The sequence of rocks discussed in this report lies below the regionally extensive Roberts Mountains thrust. They include a number of structurally autochthonous units: (1) The Ordovician to Silurian Hanson Creek Formation, which is composed of arenaceous dolostones, is the lowest unit studied. These sedimentary rocks were deposited as arenaceous, pellet, peloid, ooid, packstone, and grainstone in a shallow water, shoaling environment as the final phase in a thick, upward shoaling sequence. (2) The Silurian and Devonian Roberts Mountains Formation, lying

disconformably above the Hanson Creek Formation, is a quartz silt, dolomitic, lime mudstone to packstone, and generally black in color due to carbon. Fossil fragments are common and usually include echinoderms and brachiopods. Siliciclastic sediments are angular silt-size quartz, and have abundant white mica, feldspar fragments, and rare zircons. (3) The Silurian and Devonian informally named Bootstrap limestone unit is typically a shallow marine carbonate shelf limestone that is dominated by multiple shoaling upward sequences. The Bootstrap limestone in core from the area of the Ren Mine has dolostones with intercrystalline pores and large vugs. Although the dolostones are vuggy, very low to no permeability is present. The dolomite rhombs, 0.1 to 3 mm in size, are subhedral to anhedral. Essentially all the dolomite rhombs, whether matrix or void filling, are cloudy. (4) The Devonian Popovich Formation is conformably above the Bootstrap limestone unit. It is composed of detrital silt size, angular to subrounded quartz, with minor amounts of feldspar, and some clay minerals. Carbonate minerals make up various percentages (approximately 15 to 40 volume percent) of the Popovich Formation, and are 30 to 100 μ m-size rhombs of calcite and euhedral dolomite. The rock is typically a calcitic dolostone with some intercrystalline vug porosity. The Popovich Formation has four units that have been delineated in the area of the Meikle and Betze-Post gold deposits. From bottom to top, they are a sedimentary breccia/wispy unit, a fossil hash/planar unit, a soft-sediment-deformation (SSD) unit, and an upper limey mud to mud lime unit. The formation was deposited in a progressively drowned and deeper water environment. Sedimentation went from the foreslope to basin euxinic environments. (5) An additional ore host, the informally named late Middle to Late Devonian age Rodeo Creek unit, represents a largely siliceous sequence of sediments that lie conformably above the Popovich Formation in the West Carlin pit and at the Gold Quarry Mine. The Rodeo Creek unit is the highest stratigraphic unit present below the Roberts Mountains thrust in the area of the Carlin trend. Quartz silt, dolostone and quartz silt-dolomite, and argillaceous chert form the Rodeo Creek unit. The environment of its deposition was deep-water euxinic to toe-of-slope.

INTRODUCTION

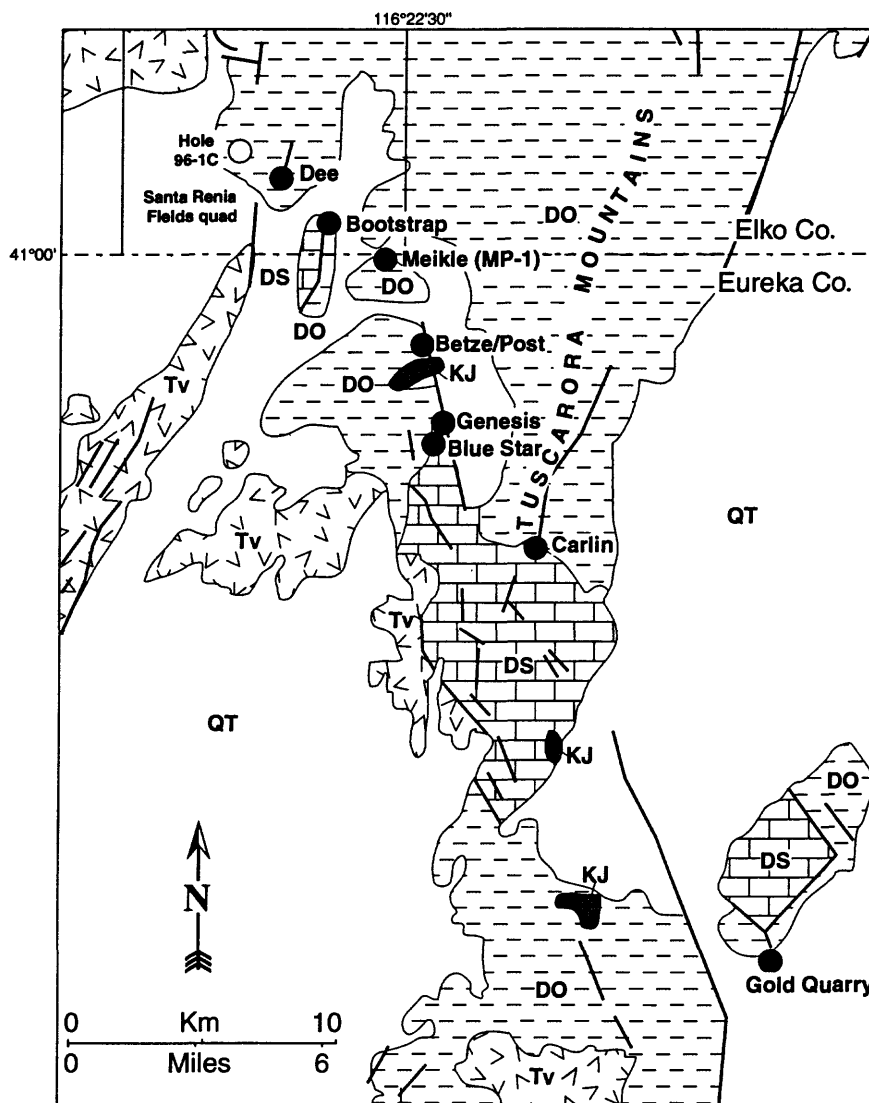
Middle Paleozoic sedimentary platform rocks in northern Nevada serve as hosts for the bulk of the gold introduced into Carlin-type gold deposits (Roberts, 1966; Arehart and others, 1993a; Christensen, 1996). These deposits largely account for this region comprising the most significant gold province in North America. In 1998, approximately 7 million oz Au will be produced from the province, which amounts to approximately 64 percent of United States and 9 percent of world production (Dobra, 1997). Production since 1965 from the Carlin trend of deposits totals about 21 million oz Au (Christensen, 1996). The most prolific part of the 40 mile-long Carlin trend is its northern half which extends from the Gold Quarry Mine on the south to the Dee Mine on the north (fig. 1). Although sedimentary rocks constitute a fundamental element of the genetic model for Carlin-type deposits (Cox and Singer, 1986), the implications and impacts of Paleozoic sedimentary fabrics and diagenetic processes on the genesis of these deposits have not been investigated as thoroughly as have the types of associated alteration, chemistry of the mineralizing fluids, and structural setting(s) of the deposits. Cook (1993) in his discussion of submarine carbonate sedimentary breccias in Paleozoic carbonate of the eastern Great Basin suggests that diagenetically altered carbonate turbidites and megabreccias could form reservoirs for disseminated gold in the Roberts Mountains, Denay, Devils Gate, Pilot and other formations.

The purpose of this report is two fold: (1) to present a facies and diagenesis analysis of autochthonous Silurian and Devonian rocks that are the principal hosts for gold in the northern part of the Carlin trend (fig. 2); and (2) to suggest that some depositional and diagenetic parameters of these rocks contributed significantly to their becoming premier gold hosts.

The sequence of rocks discussed herein lies below the regionally extensive Roberts Mountains thrust (Roberts and others, 1967). It includes three distinct packages of autochthonous units, listed from base to top (fig. 2): (1) The Ordovician and Silurian Hanson Creek Formation, Silurian and Devonian Roberts Mountains Formation, Devonian Bootstrap limestone unit, an informally named unit in the uppermost part of the Silurian and Devonian Roberts Mountains Formation (see also, Merriam, 1940; Merriam and Anderson, 1942; Evans and Mullens, 1976; Mullens, 1980; Armstrong and others, 1987). (2) The Devonian Popovich Formation (Hardie, 1966; Evans, 1974; Ettner, 1989) which is dolomitic and calcareous rocks deposited conformably above the Bootstrap limestone unit. And (3) the informally named late Middle to Late Devonian Rodeo Creek unit (Ettner, 1989; Ettner and others, 1989). The Rodeo Creek is a mostly siliceous package of rocks which lies conformably above the Popovich Formation in the West Carlin pit and at the Gold Quarry Mine (F.G. Poole, oral commun., 1997). It also is present at the Meikle Mine and elsewhere in the northern part of the Carlin

trend (fig. 1). Locally, there is some evidence that the contact between the Rodeo Creek unit and the Popovich Formation is depositional, although there may be a possible hiatus, with karsting. There is also evidence of faulting and the localization of intrusive sills along the contact between the two units in the Meikle and Betze-Post area (Volk and others, 1996). The Rodeo Creek unit probably is age equivalent to parts of the Devonian Woodruff Formation. The Woodruff Formation originally was described in the Carlin-Piñon Range area (Smith and Ketner, 1968, 1975), and it is equivalent in age to the Devonian Scott Canyon Formation (Roberts, 1964; Jones and others, 1978) and the Devonian Slaven Chert (Gilluly and Gates, 1965). The latter two units presumably make up part of the allochthonous siliceous assemblage overlying the Roberts Mountains thrust approximately 50 miles west of the Carlin trend. However, some parts of the Scott Canyon Formation in the Battle Mountain Range and the Slaven Chert in the Shoshone Range may, in fact, represent autochthonous rock packages that lie below the Roberts Mountains thrust rather than above the thrust as has been traditionally proposed (Roberts and others, 1958; Roberts, 1964; Gilluly and Gates, 1965). These two formations, if the herein amended regional tectonostratigraphic interpretations prove to be valid, then could be considered deep water, rifted margin equivalents of the Rodeo Creek unit, because of the presence in them of significant volumes of submarine basaltic rock (see also, Madrid, 1987). However, the presence of lower Paleozoic carbonate sequences of rock in the East Range approximately 40 miles west of the Battle Mountain Range, (Whitebread, 1994) appears to argue against such a hypothesis. The Rodeo Creek unit is the highest stratigraphic unit present below the Roberts Mountains thrust in the area of the Carlin trend (see also, Ettner, 1989).

This preliminary study is based on a large number of samples systematically collected and made into thin sections and polished sections from 12 deep exploration drill holes in the general area of gold deposits along the Carlin trend. Barrick Gold Corporation, Minorca Resources Inc., and Uranerz U. S. A., Inc. provided access to these drill holes. All samples were examined using standard petrographic techniques, and many polished sections were studied by scanning electron microscope (SEM). In addition, hand-specimen-scale structures and textural relations in all cores were studied; these examinations supplemented those previously completed by company geologists who initially logged the cores during their drilling. Our study also included material from a number of underground horizontal drill holes into the orebody at Barrick's Meikle Mine (fig. 1). Most deep holes penetrated a relatively intact sequence of autochthonous rocks below the Roberts Mountains thrust near the northwest end of the Carlin trend. They provide an extraordinary opportunity to construct depositional environments during the Paleozoic for many rocks that host the bulk of the gold in the most significant gold province in North America. We emphasize that this report is a



EXPLANATION

<p>QT Quaternary alluvial and playa deposits and Tertiary sedimentary, tuffaceous, and lacustrine rocks</p> <p>VOLCANIC AND SHALLOW INTRUSIVE ROCKS</p> <p>TV Tertiary volcanic rocks including andesite flows and breccias, rhyolite flows, shallow intrusive rocks, and ash-flow tuffs</p> <p>INTRUSIVE ROCKS</p> <p>KJ Intrusive rocks of granitic to dioritic composition</p>	<p>SEDIMENTARY ROCKS</p> <p>DO Devonian Woodruff and (or) Slaven Chert and Ordovician and Silurian Vinini Formation: shale, chert, siliceous argillite, limestone, minor quartzite, and greenstone</p> <p>DS Devonian limestone and Silurian and Devonian Roberts Mountains Formation: limestone, dolomite, and calcareous siltstone. Locally includes Devonian Rodeo Creek unit, Popovich Formation, as well as several other Silurian and Devonian carbonate platform units</p> <p>● Gold deposits</p>
--	---

Figure 1. Geologic sketch map of the southern Tuscarora Mountains, Elko and Eureka Counties, Nevada. Modified from Christensen (1996).

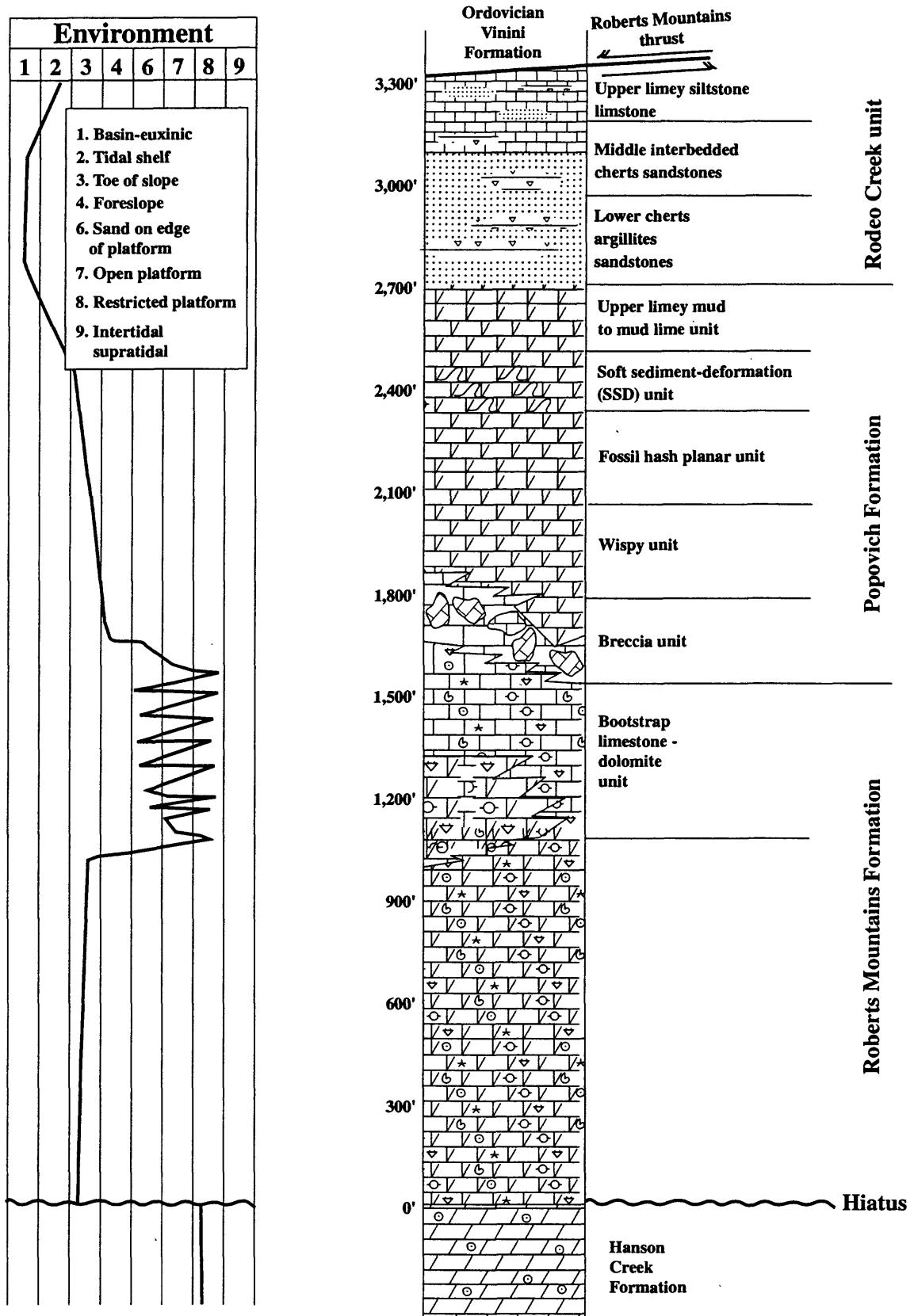


Figure 2. Schematic stratigraphic column in the general area of the Goldstrike Mine. In part modified from Volk and others (1996).

work in progress, and it represents a contribution towards establishment of a consistent regional stratigraphic nomenclature and understanding.

The carbonate classification used in this study is Dunham's (1962).

STRATIGRAPHY

Hanson Creek Formation

The name Hanson Creek Formation was first applied to upper Ordovician limestone beds in the Roberts Mountains (Merriam, 1940), approximately 70 miles south of the northern Carlin trend, where the type section is situated on Pete Hanson Creek (Merriam, 1963).

Within the general area of the northern terminus of the Carlin trend, exploration drilling has encountered only the upper part of the Hanson Creek Formation. The rocks are arenaceous dolostone. The sediments were deposited as arenaceous, pellet, peloid, ooid, packstone and grainstone in a shallow water environment as the final phase in a thick shoaling upwards sequence. The quartz sand is subrounded to rounded 0.3 to 1-mm sand grains and is supported by a dolomite matrix.

Diagenesis

Dunham and Olson (1980) published a study of the Hanson Creek Formation of Eureka County, Nevada. Their research included petrographic studies combined with the examination of trace element and isotope data. Their interpretation is that major dolomitization events which affected the Hanson Creek strata took place in the shallow subsurface as a result of the mixing of meteoric derived ground water and marine pore water in the Early Silurian. IncurSION of freshwater into subtidally deposited sediments took place as a result of vertical and lateral extensions of freshwater lenses that developed beneath subaerially exposed tracts of an inner carbonate platform. Dolomite to limestone transition marked the maximum extent of freshwater lenses in the subsurface. Their study indicates that although the dolomite is diagenetic, it is not related to the depositional environment of the original carbonate sediment. The dolomite is early diagenetic, formed through surface-related processes before deposition of the overlying Roberts Mountains Formation. Regional stratigraphic evidence shows subaerial erosion at the top of the Hanson Creek Formation. Conodont data indicate the top of the Hanson Creek is early Silurian (middle Llandovery), and the base of the Roberts Mountain Formation is late Llandovery (late Early Silurian). Thus a depositional hiatus equivalent to the length of the middle Llandovery separates the Hanson Creek from the Roberts Mountains Formation. Hanson Creek dolomitization occurred during this hiatus (3 to 5 m.y.), probably early on, when the Hanson Creek marine carbonate sequences were exposed to fresh water recharge,

and as a result of the mixing of meteoric derived ground water and marine pore water.

Roberts Mountains Formation

Many geologists (Merriam and Anderson, 1942; Nolan and others, 1956; Merriam, 1963, Roberts and others, 1958; Roberts, 1964, Gilluly and Gates, 1965; Smith and Ketner, 1968, 1975; Stewart and McKee, 1977, and Stewart and Poole, 1974) have studied the Roberts Mountain Formation.

Mullens (1980) presents an excellent discussion of the regional distribution of the Roberts Mountains Formation for north-central Nevada. In the Roberts Mountains, the Roberts Mountain Formation interfingers with the shoal water equivalent of the Lone Mountain Dolomite. Within the Carlin trend, the Roberts Mountains Formation is quartz silt and dolomitic limestone (lime mudstone to packstone). Fossil fragments are common and are usually characterized by abundant echinoderms and brachiopods. Detrital sediments are angular silt-size quartz, abundant white mica, feldspar fragments, and rare zircons. Calcite was deposited as lime mud or micrite, pellets, well-worn rounded fossil bioclasts and occasionally large fragments of brachiopods and echinoderms. The Roberts Mountain Formation contains abundant carbonate turbidites comprised of allodapic components. Dolomite rhombs are abundant, are found in various amounts, and generally are floating in a matrix of calcite and quartz silt. The dolomite rhombs are typically subhedral to euhedral and are from 5 to 80 μm in size (fig. 4). Pyrite is abundant and is 1 to 30 μm in size, commonly framboidal, and believed to be primarily early diagenetic and related to sea floor organic (bacterial) activity. Pyrite is concentrated between the carbonate grains or crystals, and is most abundant in the dark carbon rich, millimeter laminations. Sphalerite (ZnS) crystals in the 1 to 30 μm size are not uncommon in the carbonate matrix.

Millimeter laminations are the most distinguishing characteristic of the Roberts Mountains Formation (Mullens, 1980). SEM studies show the intercrystalline spaces contain sulfur-rich carbon, which is interpreted as derived from "thermally altered" hydrocarbons.

Environment of Deposition.

The presence of pyrite, in particular framboidal pyrite, and the preservation of the laminations indicates a reducing environment existed during deposition and was toxic to an infauna or boring organisms (Mullens, 1980). The core samples indicate the Roberts Mountains Formation was deposited in an anoxic, "deep" water shelf or slope to basin, environment. The core samples studied have a consistency in mineralogy and petrology that indicates a relatively stable environment of deposition through time. Thin bands of bioclastic material, composed of large brachiopod and

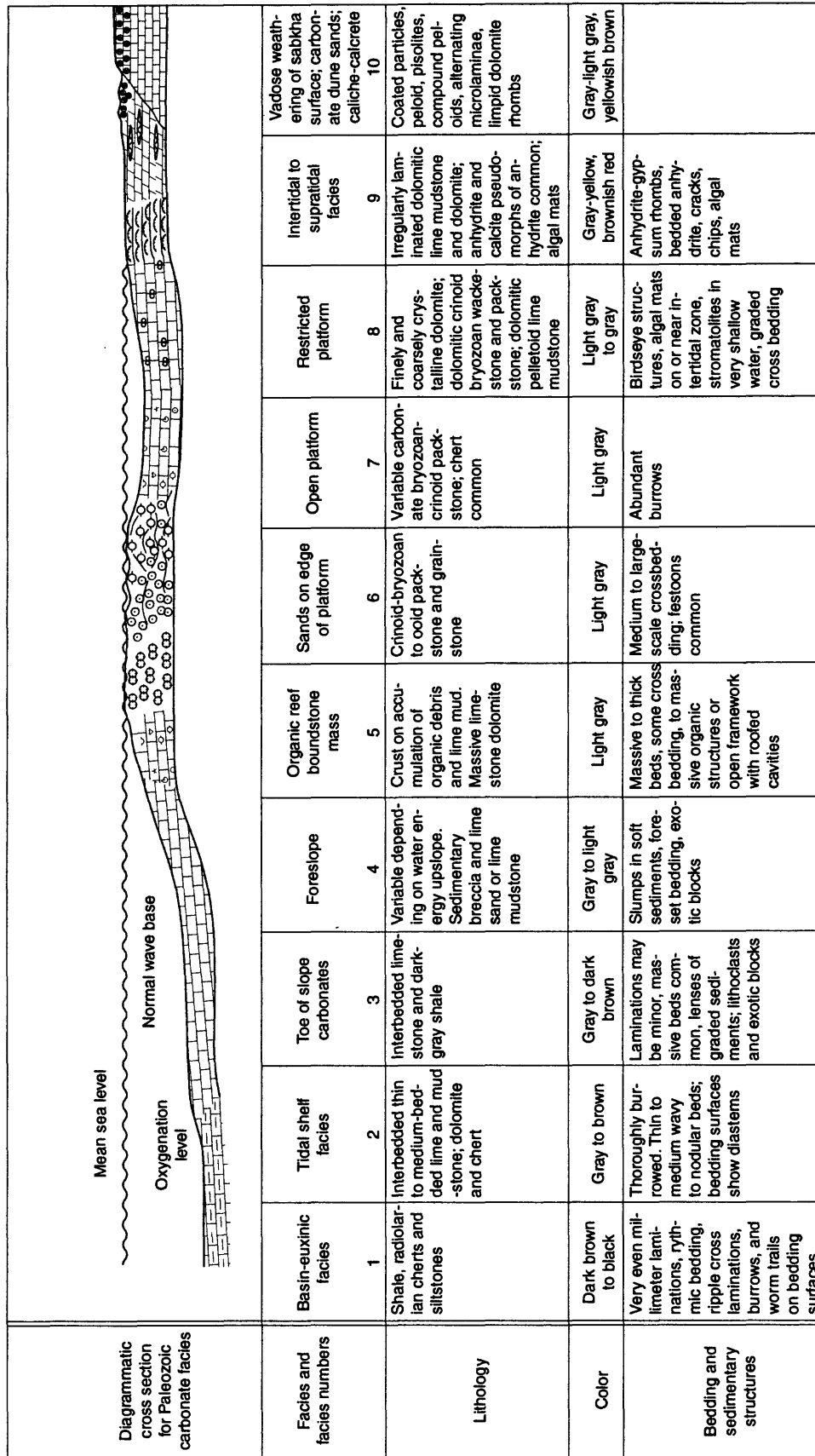


Figure 3. Idealized sequence of facies belts for the Silurian and Devonian, including, Hanson Creek Formation, Roberts Mountains Formation, Bootstrap limestone, Popovich Formation, and Rodeo Creek unit. Concept modified from Wilson (1975).

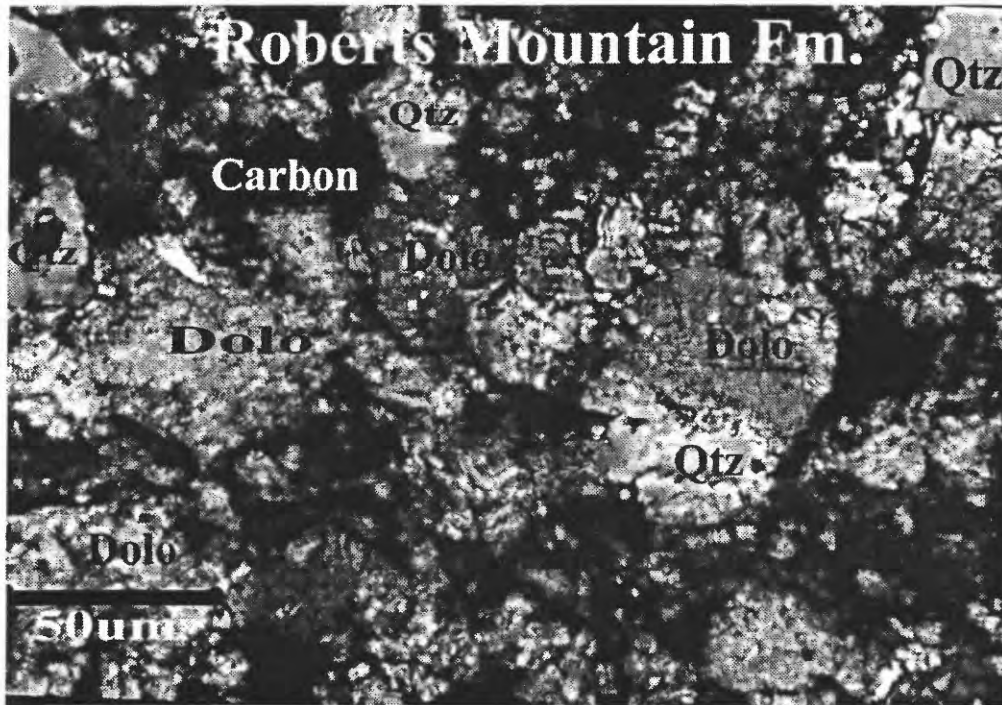


Figure 4. Photomicrograph of the carbon rich Roberts Mountains Formation. Rhombs of dolomite and detrital quartz silt in a matrix of black carbon. Polarized light.

echinoderm fragments, indicate a nearby source of shell material which, when alive, had to exist in normal, oxygenated seawater. No oolites were seen, but mud lumps and soft peloids were observed in some thin debris beds. Extensive soft-sediment deformation is absent within these specimens of the Roberts Mountains Formation. Nothing comparable to the soft sediment deformation (SSD) unit (see below) of the Popovich Formation was found. The mineralogy and petrography of the Roberts Mountains Formation, however, are similar to that in the Popovich Formation wispy unit, fossil hash/planar unit, and soft sediment unit.

The Roberts Mountains Formation was deposited in a tectonically stable euxinic basin. Deposition began on an eroded Hanson Creek dolomite surface. The depositional hiatus that separates the two formations encompass middle Llandovery time (Dunham and Olson, 1980). The basal Roberts Mountains Formation is a black, finely laminated carbonate mudstone which is dolomitic and lies on the Hanson Creek Formation, but rapidly grades into lime mudstone over a span of a few feet above the contact. The Roberts Mountains Formation in the area of this study appears to have been deposited on the tidal shelf and or on a very gentle foreslope (figs. 2 and 3). Cook (1972) and Cook and Mullins (1983) proposed a low-relief platform-margin model that appears consistent with facies of the Roberts Mountain Formation.

Bootstrap Limestone Unit, Carbonate Shelf Facies

The study of the informally named Silurian and Devonian Bootstrap limestone is based on a series of cores, which drilled into the Bootstrap limestone. These are the Minorca (96-1C), Meikle Mineshaft (MP-1), Dee Mine (DC95-01) and Uranerz (RU-8) cores. The Minorca (96-1C) was collared near the southwest corner of the Santa Renia Fields quadrangle and cored 970 ft of the Bootstrap limestone unit. The drill hole at the shaft site of the Meikle Mine (MP-1) cored 919 ft, and the Uranerz cored 1,201 ft of the Bootstrap limestone unit. Similar thickness for the Bootstrap limestone are reported to be present in exposures at the Bootstrap window (fig. 1) roughly 2-1/2 miles northwest of the Meikle Mine, where the Bootstrap limestone has an approximate 900 ft thickness (Evans and Mullens, 1976). Outcrops of the Bootstrap limestone unit were not available for investigation. Our study of the cores DC95-01 and conodont study of Uranerz RU-8 (see below) demonstrates the Bootstrap limestone unit is structurally complex and, in places, may have been repeated by cryptic faulting along bedding planes. It is difficult to ascertain the true thickness of the Bootstrap limestone unit.

The Bootstrap limestone unit in the Meikle shaft MP-1, Minorca 96-1C, and the lower part of the Dee DC95-01 cores,

is typical of shallow marine carbonate shelf limestones that are dominated by multiple shoaling upward sequences (Wilson, 1975, Moore, 1989).

Bootstrap lime mudstone to ooid grainstone (fig. 5) contains many lithoclasts, which are subrounded to rounded, and are as large as 10 cm. They appear to be storm rip-up clasts. Parts of the cores display many shoaling upward successions of facies, each several to tens of feet thick, that grade from fossiliferous ooid grainstones to packstone and wackestone, into poorly laminated, lime mudstone with birdseye structure. The Bootstrap limestone unit generally is a well-cemented carbonate rock with little or no inherent permeability or porosity.

Environments of Deposition

Ooid packstone, grainstone, wackestone, and lime mudstone in the upper parts of the Bootstrap limestone unit were deposited on a wide shallow, shelf margin adjacent to a basin in which the Popovich Formation (see below) was deposited. Shallow shelf environments are marked by sedimentation ratios that can generally track or outstrip even the most rapid sea level rise (Wilson, 1975; Moore, 1989). Rapid sedimentation to or above base level is the norm for carbonate shelves, and the result is the ubiquitous, stacked upward shoaling sequence that gives carbonate shelves their typical internal cyclic architecture. The thickness of the total cycles is controlled by a combination of the rate of shelf subsidence and eustatic fluctuation (Moore, 1989).

The numerous upward shoaling shelf cycles within the Bootstrap limestone resulted in repeated seaward progradation over the shelf margin environment. The sedimentary cycles within the Bootstrap limestone indicates there were a series of relative rapid rises of sea level that occurred repeatedly on a steadily subsiding shelf. These rapid sea level rises were followed by sedimentary progradation and a carbonate sediment fill-in of the inundated area. On the outer edges of the shelf, subsidence is too continuous and water is too deep for the effects of relatively small cyclic sea level fluctuations to be reflected in the sedimentary record (Wilson, 1975; Wilkinson and others, 1997). The well-formed ooids that are the base of each Bootstrap cycle are, by analogy with Holocene sediments, indicative of strong and regular tidal currents. The ooid shoal of Joulter's Cay (Harris, 1979) and Cat Cay, Bahamas (Ball, 1967), are a reliable modern analog for the ooids in the Bootstrap limestone unit. The thickness of these shoaling cycles is controlled by the rate of shelf subsidence and carbonate sediment production (Read and others 1986; Moore, 1989).

In all the cores studied, well-defined coral reefs are absent. Ooid shoals do not form behind a well-developed barrier reef because the presence of the reef usually would restrict the flow of tidal currents—thick sequences of ooid sediments necessitate the presence of an unrestricted flow of tidal currents. Within each upward shoaling cycle the ooids grade up into

bioclastic wackestone and birdseye (fenestral fabric) lime mudstone. The Bootstrap limestone during a relative sea level fall would be emergent and would undergo extensive meteoric diagenesis, cementation and karstification. The Bootstrap limestone was repeatedly exposed to the atmosphere and meteoric waters prior to deposition of the overlying cycle. Some cores from the Bootstrap limestone display textures indicative of karst that developed prior to deposition of the overlying Popovich Formation. These textures include large cavities now filled by collapse breccia, zebra-like textures, and spar calcite. Furthermore, one of the cores examined shows breccia and a spar-calcite-filled cavity that is cut by a 2 inch-wide igneous dike. Only in areas of karst and collapse breccia development in the Bootstrap limestone are there likely to be porous environments well suited for subsequent hydrothermal fluids and mineralization.

Diagenetic History of the Oolite to Lime Mudstone

Davis (1996) found that, in less than 10 years, subaerially exposed oolitic sands on Eleuthera Island, Bahamas, was completely casehardened by freshwater vadose calcite cementation. This phenomenon demonstrates the rapidity of freshwater carbonate diagenesis and explains, in part, why carbonate platforms preferentially shed unconsolidated sediment during highstands and not during lowstands when they are subaerially exposed.

The Bootstrap fossiliferous oolitic packstone to lime mudstone was deposited in near-normal salinity on a shallow shelf, shoal water environment. Four distinct types of cement are present within the Bootstrap oolite. The first is a bladed to fibrous habit and lines the walls of pores and is on the surface of oolites, pellets and bioclasts. This was the first cement formed and these textures are generally interpreted to be of an early marine origin (James and Choquette, 1990b). Isopachous phreatic zone cement overlies the fibrous marine cement. Inter-ooid cements that indicate time within the vadose environment are meniscus and microstalactitic cements. A final phreatic event resulted in blocky, equant-grained cement that completely fills pores space. No other volumetrically significant types of cement have been observed in the oolitic grainstones. Pore-central ferroan calcite cement was not found. Ferroan calcite cement has been interpreted as late diagenetic and deep burial in origin in other limestones (Bathurst, 1975). This indicates that all porosity in the Bootstrap oolite packstone-grainstone was filled before deep burial. Choquette and James (1990, p. 65–66) stated shelf sediments "are varied and may include, in various combination limestones of mudstone to grainstone textures, peritidal limestones and dolomites and coastal plain evaporites. Because these shallow marine to coastal sediments are commonly exposed intermittently during accretion, they are periodically filled with meteoric ground water. Consequently, before they exit the meteoric environment they may have seen multiple generations of fresh to brackish to marine or even hypersaline water related

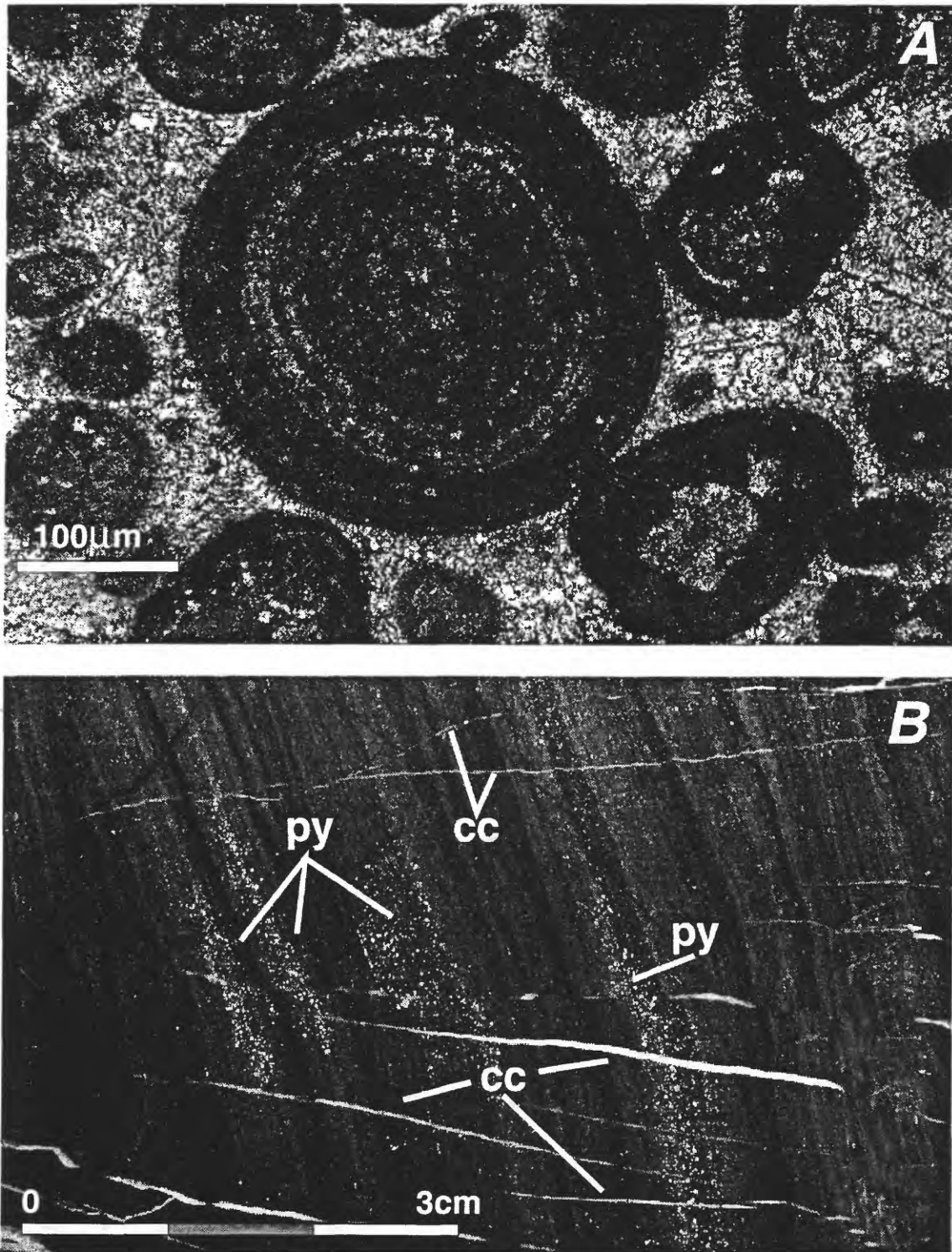


Figure 5. Photomicrographs of Devonian Bootstrap limestone and Devonian Popovich Formation. (A), Ooid grainstone in Bootstrap limestone. Variably sized, coated particles, some with broken fossils centers, all show dark micritic envelopes caused by boring algae and sponges into the surface of the particles. Spar calcite cement between particles. Sample no. 96-1C+4506. (B), Vertical cut core illustrating the mm-size laminations and graded bedding of the Popovich Formation and absence of bioturbation. py, fine-grained pyrite; cc, calcite along tension gashes, some of which show minor amounts of offsets of laminae. Sample no. 96-1C+3512.

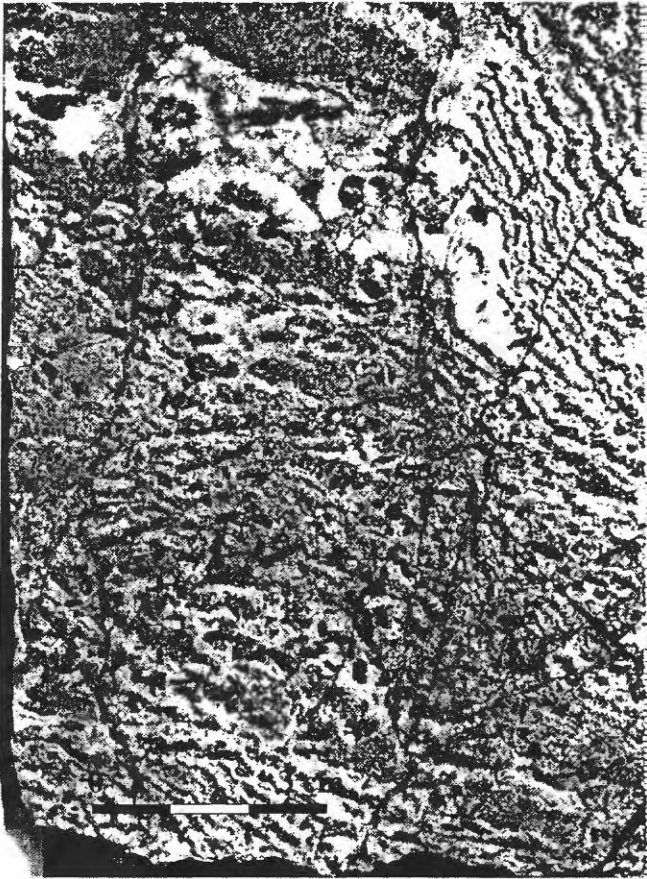


Figure 6. Zebra texture and structures from drill core within ore bodies of the Meikle Mine. The Bootstrap limestone has been altered hydrothermally. The zebra structures at the Meikle Mine are typically alternating 0.5 to 5 mm wide bands of dark gray and white dolomite.

to low and high stands of sea level.”

Some of the limestones have disseminated dolomite. The dolomite crystals are characteristically 10 to 80 μm in size, euhedral, although locally ragged in their detailed outlines. These dolomite rhombs are clear, and are replacive in nature crosscutting bioclasts, oolites and cements. Folk (1974), and Cantrell and Walker (1985) proposed that dolomites of this type were precipitated by meteoric water probably deep in the subsurface.

Analysis of Uranerz RU-8 Bootstrap Limestone Core

Conodont studies on the Uranerz RU-8 core reveal the section is faulted and repeated (figs. 7 and 8). Furthermore, petrographic studies show that above and below the fault two distinct carbonate facies are present with two distinct diagenetic histories. The higher fault block, from 3,025 to 3,630 ft, is

Lochkovian (Lower Devonian) to Wenlockian (Lower Silurian) in age. Within the lower fault block, this exact age distribution is repeated again from 3,630 to 4,226 ft. A fault is suggested at about 3,630 ft. The base of the upper block of Wenlockian (Silurian) age is faulted on Lochkovian (Early Devonian) dolostones of the lower block.

Environment of deposition and diagenesis, limestones, Upper Fault Block 3,025 to 3,500 ft.

The fossiliferous, oolitic to (micrite) lime mudstone in the upper block above the fault at 3,630 ft records periods of deposition in near-normal salinity on a shallow-shelf, shoaling water environment. This limestone is similar in its depositional and diagenetic history to the Bootstrap limestone from the Meikle Mine shaft and Minorca cores.

Analysis of Uranerz RU-8 Bootstrap Dolomite Core

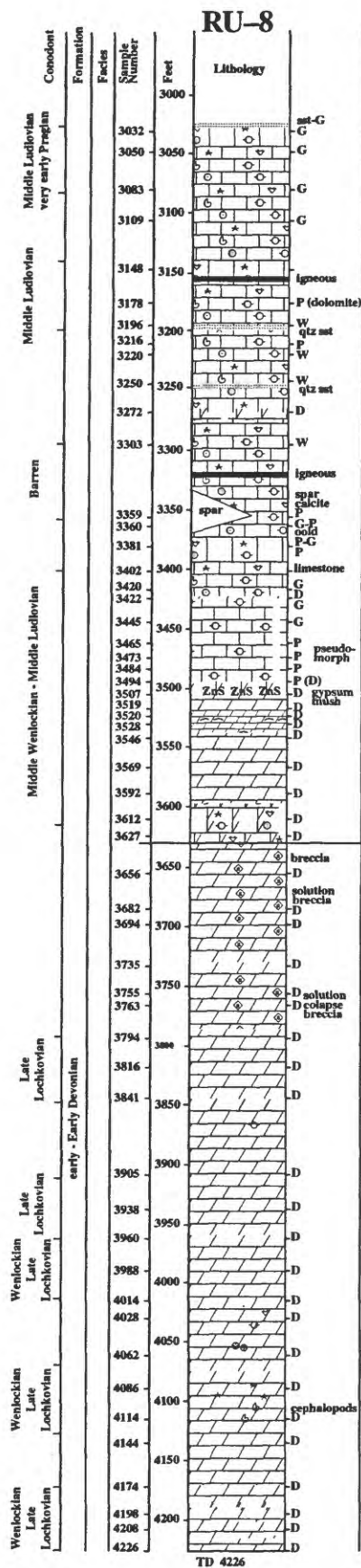
Petrology and Environment of Deposition, Dolomites

In the upper block, at the base of the section, from 3,510 to 3,630 ft, are dolostones. The dolostones contain algal mats (cyanobacteria microbialites at 3,510 to 3,530 ft), intraformational conglomerates, dolomite pseudomorphs of enterolithic fold structures, and gypsum mush and spar dolomite pseudomorphs of nodular anhydrite (see also, Schreiber, 1986; Demicco, and Hardie, 1994). The sedimentary structures and fabric indicate that this 130-ft interval of dolostones was deposited in subtidal, intertidal to supratidal sabkha environments (fig. 9).

Below the fault at 3,630 ft, the lower 599 feet of the Bootstrap limestone, in the lower block, is also Lochkovian (Lower Devonian) to Wenlockian (Lower Silurian) age. From 3,630 ft to the bottom of the hole at 4,226 ft is a complex suite of sedimentary structures and dolostones. Within the dolostones are abundant intercrystalline pores and large vugs. Although the dolostones are vuggy, very little to no permeability is present. With the exception of void-filling dolospar, the dolomite crystals are subhedral to anhedral. Essentially all the dolomite rhombs, whether matrix or void filling, are cloudy. Stylolites and microstylolites that postdate the dolomitization events are relatively common, as are healed fractures.

Solution breccias with rounded clasts and white dolomite spar cements are found from 3,727 to 3,790 ft. This solution breccia may be the result of early removal by meteoric waters of anhydrite and gypsum. The spaces between the breccia fragments are partially filled by spar dolomite. The sedimentary structures and fabric indicate that the dolostones were deposited in an intertidal to supratidal, sabkha environment.

The dolomites from 3,790 to 4,226 ft show evidence of deposition in shallow shelf marine environments. Polished

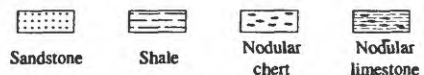
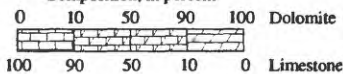


Explanation

Classification of carbonate particles other than fossils

	Size mm	Rounded mud	Any shape mud	Coated particles	
				one layer	two or more layers
Silt	.20	φ	∞		
	.063	φ	∞		
Sand	2.0	φ	◇	Superficial ooid	Oolite •
	4.0	φ	◇		Pisoid ○
Granule					
Pebble					

Composition, in percent



Symbols for fossil particles

- Algal mats
- Calcareous algae
- Foraminifers
- Molluscan in general
- Ostracodes
- Echinoderms
- Brachiopod
- Coral

Sedimentary structures

- x/n Crystallin calcite
- ◇ Solution breccia

Dunham's (1962) carbonate rock classification

- M Lime mudstone
- W Wackestone
- P Packstone
- G Grainstone
- D Dolomite

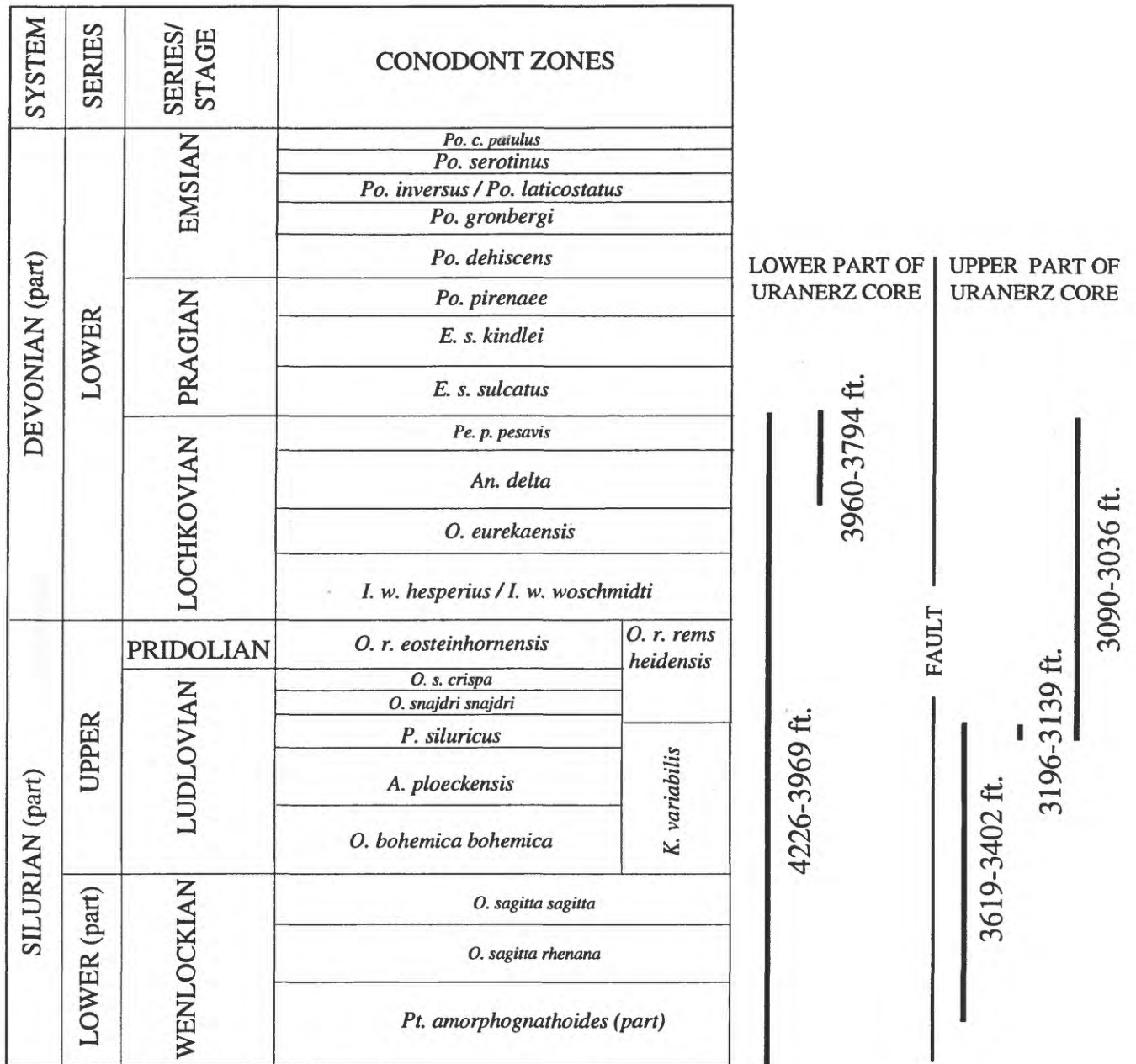


Figure 8. Conodont zonation for the two fault blocks in the Uranerz RU-8 Bootstrap limestone core. Both fault blocks have the same age from Wenlockian (Lower Silurian) to Lochkovian (lower Devonian). A full listing of the conodont paleontology and zonation is in Appendix A.

Figure 7. (Located on page 48) Stratigraphic section of the Uranerz core RU-8. The lower fault block is almost pure dolomite. The higher fault block, from 3,025 to 3,630 ft, is Lochkovian (Lower Devonian) to Wenlockian (Lower Silurian) in age. Within the lower fault block this exact age distribution is repeated again from 3,630 to 4,226 ft. A fault is suggested at about 3,630 ft. The base of the upper block of Wenlockian, Silurian age is faulted on early Devonian, Lochkovian dolostones of the lower block.

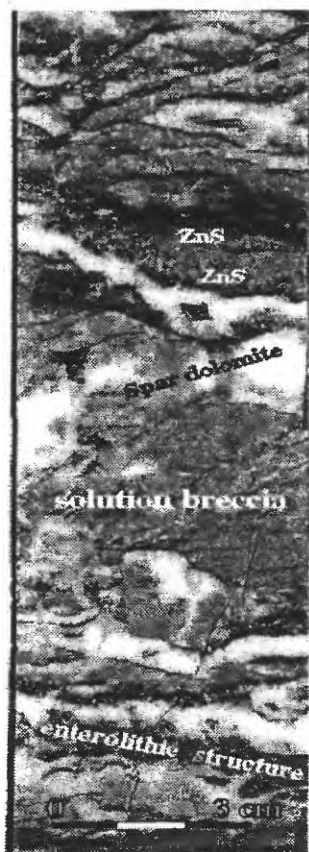


Figure 9. Dolostones at 3,519 ft has intraformational conglomerates, dolomite pseudomorphs of enterolithic fold structures, and gypsum mush and spar dolomite pseudomorphs of nodular anhydrite. The sedimentary structures and fabric indicate the dolostones were deposited in supratidal sabkha environments. Sphalerite (ZnS) mineralization appears to be associated with geopetal, crystal silts.

core samples have fragments of echinoderms, crinoids, brachiopods, rugosa and tabulate corals, stromatoporoids and numerous nautiloid cephalopods. These beds represent dolomitized open shelf carbonate strata. Intertidal to supratidal sedimentation is indicated at 4,170 to 4,180 ft by algal mats (cyanobacteria microbialites).

Diagenetic History of the Dolostones

Morse and Mackenzie (1990) have shown that the transformation of aragonite and high magnesium calcite to low magnesium calcite and the dolomitization of carbonate sediments and rocks are among the most important processes in the diagenesis of carbonate sediments, but major aspects of these processes are still poorly understood. One of the primary reasons for this is that although reactions may occur over geologically short times, their kinetics are too slow to be studied in the laboratory under conditions closely approaching those in natural systems. Consequently, our

understanding of the chemical processes and mechanisms that are reliably applicable to these major phase transformations is relatively limited. Morrow (1990a) also states the inability to precipitate dolomite under controlled laboratory conditions constitutes the essence of the problem of the origin of dolomite.

Three models for the dolomitization of this thick sequence of shelf limestone are presented. The dolostones result from mesogenetic replacement of early dolomitization followed by neomorphism in the burial environment, or some combination of these two end member models.

- (1) *Sabkha Reflux Model.* A close association of supratidal sabkha sedimentary features and dolomitization apparently exists with dolostone in the lowest 130 ft of the upper block and also all the dolostone of the lower block. The well-documented setting for penecontemporaneous dolomite is the sabkha environment (Beales and Hardy, 1980; Morrow, 1990a, b). It is restricted to those dolomites with accompanying evaporite minerals. Dolomites in the sabkhas of the Persian Gulf are most abundant as 1 to 5 μm euhedral crystals in the high intertidal zone close to the strandline and are strongly controlled by the network flood channels across the sabkha. Storm driven tides reach furthest inland along these channel courses. The frequency of flooding decreases landward across the sabkha but the Mg/Ca ratio of floodwaters rises uniformly landward by means of gypsum precipitation so that the zone of optimum dolomite formation is less than a half a mile wide straddling the boundary between high intertidal and supratidal areas (Morrow, 1990b). The presence in the upper block of the Uranerz core at 3,500 to 3,600 ft of sabkha sedimentary structures such as algal mat laminations, rip-up clasts, and intraformational conglomerates indicates this part of the Bootstrap dolostone was deposited at times in subtidal to supratidal environments. Intertidal to supratidal sedimentary structures also are present in the lower block of dolostones at 3,630 to 3,790 ft and again at 4,170 to 4,180 ft. Dolomite pseudomorphs of gypsum and anhydrite indicate the existence during deposition of laterally adjacent or overlying evaporites that could have provided sources of Mg-bearing hypersaline solutions capable of dolomitizing by seepage-refluxion this sequence of dolostones.

- (2) *Burial Compaction Model.* The petrographic textures of the Bootstrap dolostones are similar to those described by Gregg (1988) for the Cambrian Bonnetterre Formation, Viburnum trend, southeast Missouri. The dolostones in the Bonnetterre were

formed by late diagenetic events that were warm basinal waters circulating through the carbonate strata. A similar origin for the Bootstrap dolomite is not unreasonable. This would explain the appearance of the iron free, honey colored, late pore filling sphalerite in the dolostones at 3,507 to 3,519 ft. A possible weak Mississippi Valley type of mineralization may be responsible for the sphalerite mineralization.

- (3). *Hydrothermal Convection Model.* In this model, brines probably have interacted with crustal rocks (Morrow, 1990b). Dense hypersaline brines migrate to great depths in the earth's crust and are recirculated to shallow depths by thermal convection where they can dolomitize porous limestone. The dolomites in the Meikle Mine ore bodies that are associated with the gold-mineralized rocks and massive amounts of pyrite clearly belong to the hydrothermal convection model. The dolomites in the Uranerz core were extensively studied with the SEM and EDAX and were found to be essentially devoid of any minerals except dolomite, rare calcite and quartz, and exceptionally rare pyrite. No barite or other sulfide minerals were found. The absence of any minerals except the sphalerite at 3,507 to 3,519 ft suggests the dolomitizing fluids were not hydrothermal. The sphalerite crystals (figs. 9 and 10) are associated with geopetal dolomite crystal silts. It is possible that the crystal silt was deposited in the vadose environment from meteoric water. If this is truly geopetal silt, then their environment of deposition fits the vadose environment as defined by Dunham (1969).

Comparison of the Uranerz RU-8 Dolostone

The dolostones in the base of the upper block from 3,500 to 3,630 ft and the massive coarse crystalline dolomite in the lower block from 3,630 to 4,226 ft have not been recognized in other drill cores from this part of the district. Zenger and Dunham (1988) describe a similar suite of shelf carbonate rocks (limestone overlying dolomite) and diagenetic history for the subsurface Silurian-Devonian rocks of southeastern Mexico.

Hydrothermal Alteration of Bootstrap Limestone

The Bootstrap limestone unit in the Meikle Mine has been altered into coarse dolomite. Dolostone samples from Meikle Mine drill hole MS-19, for example, are so altered to

clay and silica mineral assemblages that there is not the faintest suggestion as to their original microfabric or microfacies.

Zebra Spar at the Meikle Mine

The Bootstrap limestone unit in the area of the Meikle ore bodies has been subjected to strong hydrothermal alteration. The zebra structures at the Meikle Mine comprise alternating 0.5 to 5 mm wide bands of dark gray and white dolomite (fig. 6). The altered Bootstrap dolostones are remarkably similar to those from the Mississippian Leadville Dolostone of the Colorado mineral belt. In that area, the zebra structures of the Leadville Dolostone have been interpreted differently by a number of authors. The zebra rocks from the Meikle Mine also are similar to zebra rock in the Metaline Mining District, Washington, (Fischer, 1988) as well as the Mississippi Valley, the East Tennessee mining areas, and the Devonian Presqu'île Dolostone, Pine Point Mines, Canada (Beales and Hardy, 1980). Whatever the inherent cause of dolomitization and recrystallization in these areas, the dolomites of the Carlin trend share the riddle of zebra structure development with them.

Beales and Hardy (1980) suggested that zebra dolomite is the product of precipitation of white sparry dolomite in vugs formed by the dissolution of primary evaporite nodules. Horton and DeVoto (1990) found that zebra dolostones at Leadville, Colorado, are intimately associated with karst breccia bodies. Incipient zebra dolostones are found in Uranerz core RU-8 in association with sabkha sedimentary structures and karsting, as well as carbonate collapse structure. Elsewhere, areas of intense zebra development commonly are adjacent to well-developed breccia bodies, and, at the Meikle Mine, they are proximal to north-northwest striking fault zones that apparently acted as feeder zones for gold-bearing fluids. In some cases, zebra spar is present as isopachous rims on karst breccia. This relation indicates that the cavities into which zebra spar dolomite precipitated formed after regional dolomitization was essentially completed and suggests that the cavities formed during karst development. Studies of particular interest in understanding and deciphering the Meikle Mine zebra and dolomite beds are Horton (1985a, b) and Horton and Geisman (1990), which focused on zebra textures in the Leadville Dolostone. Their research demonstrated that during an Early Pennsylvanian marine transgression, zebra spar precipitated into open spaces that had been created during karst erosion. The solutions from which zebra spar precipitated were hotter and more saline than those from which sucrose or coarsely crystalline dolomites had formed. They further stated that, in the Leadville dolomites, hydrothermal fluids associated with Laramide and Tertiary igneous activity caused dedolomitization in places, and minor dolomite recrystallization and deposition of pyrite as open-space fill, as well as some replacement dolomite elsewhere.



Figure 10. Photomicrograph of thin section RU-8+3519 that contains dolomite, quartz and sphalerite. Dolomite rhombs are 0.2 to 1 mm in size and are pure $\text{CaMg}(\text{CO}_3)_2$. The sphalerite is pure ZnS devoid of Fe in its lattice. The photograph shows large sphalerite crystals filling intercrystalline pore space in dolomite and illustrates sphalerite as the final pore space fill on silica. This illustration graphically shows the sequence of dolomite, then silica pore fill and final filling by sphalerite.

Popovich Formation

Four units have been delineated within the Popovich Formation in the area of the Meikle and Betze-Post deposits (fig. 2; see also Volk and others, 1996). From bottom to top, they are: a sedimentary breccia/wispy unit; a fossil hash/planar unit; a soft-sediment-deformation (SSD) unit; and an upper lime mud to mud lime unit.

The **sedimentary breccia/wispy unit** is an overall fining upward sequence of rocks. Thick debris-flow beds (megabreccia) are formed of various clast sizes and are composed of peloid, bioclastic, wackestones (biomicrites). Cook and others (1972) define megabreccia as a deposit in which angular clasts larger than 1-m across are conspicuous components. Many clasts of these deposits are smaller than 1 meter and may be rounded rather than angular. Spencer and

Tucker (1997) define megabreccias as all the products of major catastrophic gravitational instability events. Megabreccias may contain slides and slumps (fig. 11) of lithified or semi-lithified seafloor sediment. They are involved in either sliding as large coherent blocks (megablocks), reflecting elastic behavior, or as debris flows with large boulders freighted along in a disaggregated matrix of greatly reduced shear strength, reflecting plastic behavior, or a composite of both styles (Schatzinder, 1985). Megabreccias are distinct from carbonate grain flows and turbidity currents, both of which are flows of loose particulate sediment. Megabreccia flows may develop into turbidity currents through sediment disaggregation and increased incorporation of water during transport (Cook and Mullins, 1983).

The lime mud matrix-supported fossiliferous debris flows, and sparse intraformational debris flows have interbeds of

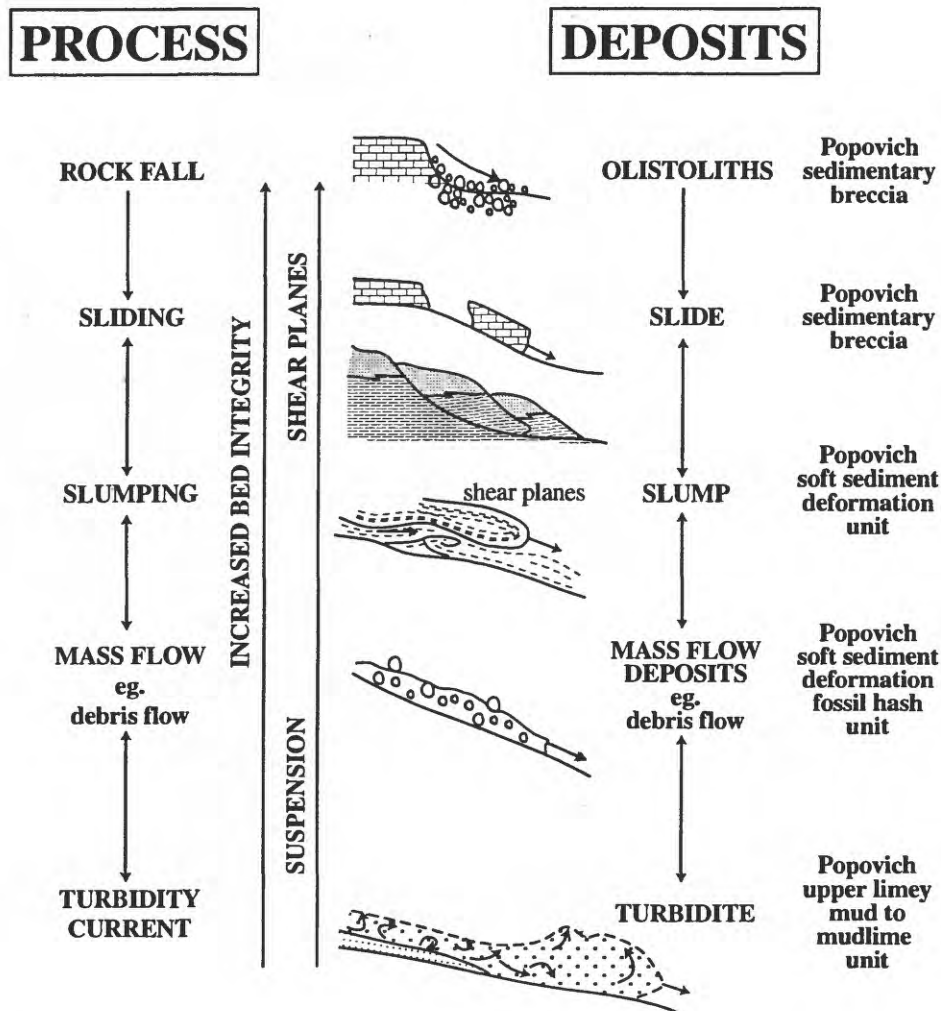


Figure 11. The relationship between mass-gravity processes including slides, slumps, debris-flows and turbidity flows. Modified from Schatzinger, and others (1985).

“wispy” laminated muddy limestone. Wispy laminations are interpreted as burrowed-bioturbated lime mudstones. Ichnofossils are rare to common in the unit. The unit contains foreslope carbonate breccia or oolite shelf talus with inclined beds and with boulders and redeposited fossils. Fine-grained beds are lithoclasts of redeposited fossiliferous wackestone. A significant part of these talus deposits is believed to form during sea level low stands by erosion of the shelf margin. Talus and rock-fall deposits are believed to form the major part of coarse, steeply deeply dipping deposits on the forereef of the Permian Capitan Formation (Melim and Scholle, 1995), Triassic Latemar buildup (Harris, 1994); and the Quaternary foreslope of the Tongue of the Ocean (Grammer and Ginsburg, 1992). The contact with the overlying fossil bioclastic/planar unit is gradational and conformable. The “wispy” beds grade upward into planar laminated arenaceous limestone and thin fossiliferous debris flows. These are replaced by thin to medium beds of fine-to-coarse fragment bioclasts in

wackestone allodapic beds. The latter are sediments transported into the basin by turbidity currents (Flügel, 1982).

Fossil hash/planar unit contains rare slump features. They also are rare in the underlying sedimentary breccia/wispy unit. A nearly ubiquitous horizon that contains abundant well-preserved graptolites is present just below the contact with the overlying SSD unit. The most abundant graptolite is *Monograptus* sp., but dendroidal graptolites also are common. The presence of pelagic *Monograptus* sp. as well as neritic dendroidal varieties, literally within the same bedding-plane parting surface, indicates that an anoxic environment was in close proximity to a shallow oxygenated environment from whence the dendroid graptolites were transported. The fossil hash/planar unit is conformable with the underlying sedimentary breccia/wispy unit and apparently marks the transition from oxygenated to anoxic deep-water conditions. This change to a starved basin environment of deposition occurs in the upper one-third of the unit. The contact with the

overlying SSD unit is abrupt and commonly occupied by an intraformational slump with sparse fossil bioclasts. Some workers who studied drill cores in the district interpret the contact between the fossil hash/planar unit and the SSD unit as marking a surface of nondeposition. The graptolite zone near the contact with the SSD represents a "condensed time zone" related to a maxima flooding of the shoaling sequence resulting in a very slow to nondeposition environment.

Soft-sediment-deformation (SSD) unit is a sequence of thin- to thick-bedded (micritic) lime mudstone turbidites. This unit contains thick intervals of slump and (or) slide deformational features. Near to and adjacent to the Meikle Mine, the SSD unit contains rare lime mud, matrix-supported, sparsely fossiliferous wackestone debris flows. These debris flows indicate a juxtaposed upper slope and shelf facies with high carbonate sediment production. An alternative interpretation would be a relative lowering of the sea level that would result in transportation of bioclastic sediments from the shelf edge into the upper slope, toe-of-slope and silled basin environments (fig. 3). Near and adjacent to the Meikle mine the SSD unit is composed of a lime mud matrix limestone with numerous ooid, peloid, fossiliferous wackestone and packstone interbeds. These are formed by coarse debris flows up to boulder size. This indicates that much of the SSD in the area of the Meikle mine was deposited as part of the inner shelf to upper slope.

Upper limey mud to mud lime unit is variable in its lithology and sedimentary structures. Primarily the sedimentary structures are plane-laminated carbonate mud to dolomitic lime mudstone. The sediments are dark gray carbon rich, lime mudstone with numerous distal debris beds of small bioclasts and mud lumps and rare ooids. Sedimentary structures include inclined foresets, abundant slump structures (or, soft sediment deformation), carbonate mud lumps, and boulder beds. However, some beds of this unit have fossiliferous debris flows, moderately developed wispy laminations, and even rare micritic turbidites. The "pinstripe beds", characteristic of the top of the unit consist of laminated dolomitic lime mudstone with thin millimeter thick, discontinuous laminations of brass colored pyrite. Carbonate lime mud and quartz silt carried by distal turbidity currents and finally by contour currents (bottom currents) probably account for most of the sediments in the submillimeter laminations seen in this and the above units. The environment of deposition was anoxic. The contact with the overlying Rodeo Creek unit apparently is conformable, but, on the basis of preliminary ages from conodonts, it may be a hiatus or diastem.

Petrography

Petrographic microscope and SEM studies reveal that the matrix of the units in the Popovich Formation is composed of detrital silt size, angular to subrounded quartz, with minor amounts of feldspar, and some clay minerals. The carbonate

minerals make up various percentages of the rock (approximately 15 to 40 volume percent), and include 30 to 100 μm rhombs of calcite and euhedral dolomite. The rock is typically a calcitic dolostone with some intercrystalline vug porosity. Petrographic microscope studies reveal the rocks have micromillimeter, micrograded laminations that formed by variable amounts of detrital quartz, clays and carbonate minerals (fig. 12). Within the Popovich Formation are fine, millimeter thick, laminae of bioclastic debris including some derived from the Bootstrap oolitic shelf. These interbeds include micritic mud lumps, ooids and oolites, and fragments of shallow water marine organisms (brachiopod, crinoid, gastropod) that lived on the shelf.

The Popovich Formation shows a wide range of mineralogy. Samples from Minorca's 96-1C hole are calcitic dolomicrite composed, in part, of bimodal dolomite rhombs. The large rhombs are 30 to 50 μm wide and they float in a matrix of 2 to 20 μm subhedral dolomite and calcite rhombs. SEM studies reveal the presence of clay minerals in the matrix with minor amounts of quartz silt. Framboidal pyrite grains, 2 to 10 μm wide, are common in the dolomite matrix. Also present are abundant intercrystalline vugs and pore spaces that are filled by sulfur-rich carbon. The carbon is composed of extremely fine-grained aggregates with individual crystals approximately 10⁻³ mm wide of graphite as revealed by Raman spectroscopic studies (Leventhal and Hofstra, 1991). This carbon in pore spaces of the Popovich Formation has been shown to be sulfur rich by our SEM studies. It was derived from thermally altered petroleum.

Environments of Deposition

The Popovich Formation was deposited in a progressively deepening basin that developed over the drowned Bootstrap oolitic shoaling shelf. The base of the Popovich Formation was deposited on a fore slope and the basal deposits contain debris, which were derived from the oolitic shelf. They represent olistholiths, slide and slump transported ooid-shelf sediments that are mixed and interbedded with basinal silty dolostones and lime mud. These include slump blocks of fossiliferous ooid grainstones in wedge-shaped foresets. This shallow-shelf ooid and bioclastic debris was mixed and interbedded with lime mud, dolomicrite, and silt during downslope transport. The fossiliferous ooid grainstones and wedge-shaped foresets grade upward to the deeper water toe-of-slope carbonate facies of the Popovich Formation which contain abundant soft sediment slump structures (SSD unit, see above) and minor amounts of distal interbedded debris bioclasts derived from the shelf. Thick intervals of SSD are not a single genetic package but rather they are complex accumulations of multiple slumps of soft sediments. The Minorca core and the cores from the Meikle Mine shaft, however, indicate that the stratigraphically higher beds of the Popovich Formation (upper limey mud to mud lime unit, see above) were deposited in deep shelf margin to basin or starved

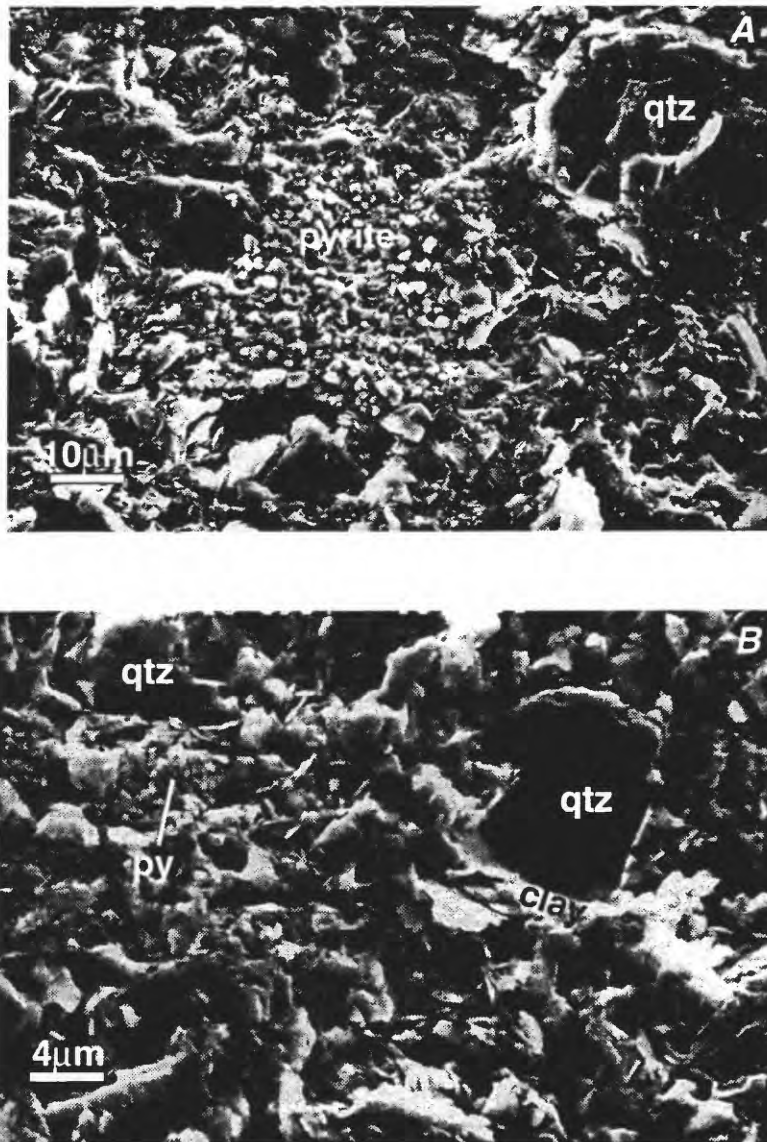


Figure 12. Scanning electron micrographs of Devonian Popovich Formation. (A), Calcitic-dolostone composed of very fine grained, intimate mixture of calcite, dolomite, and detrital quartz. Rare apatite crystals and a rare-earth phosphate with La and Ce are accessory minerals. Framboidal pyrite in center of photograph. Sample 96-1C+3269. (B), Silica and clay replacement of typical calcitic dolostone fabric showing framboidal pyrite, hydrothermal silica, clay minerals, and detrital quartz.

basin environments. The sediments are framboidal pyrite rich, contain detrital quartz silt and white mica, and are well-bedded, platy, and laminated micrograded. The partly siliceous upper limey mud to mud lime unit of the Popovich Formation, which includes some argillite and cherty material, appears to have been deposited in an euxinic (starved) environment. Sparse fossil bioclasts in the upper limey mud to mud lime unit are fossil debris derived from higher up the slope or from the oolite shelf. The well-preserved micro-laminations and micrograded laminations reflect an absence of burrowing organisms because

the water generally was poorly oxygenated or anoxic. Farther to the south near the Carlin Mine, the basal parts of the Popovich Formation reflect a much more shallow environment that was closer to a carbonate sediment source (fig. 13) and contain massive biomicrites made up of ostracods, trilobites, and ichnofossils (Ettner, 1989). An anoxia environment in the northern part of Carlin trend also is indicated by an abundance of framboidal pyrite and rare hematite (Yukio, 1997). The terrigenous sediment admixture in the Popovich Formation includes highly angular fragments of quartz,

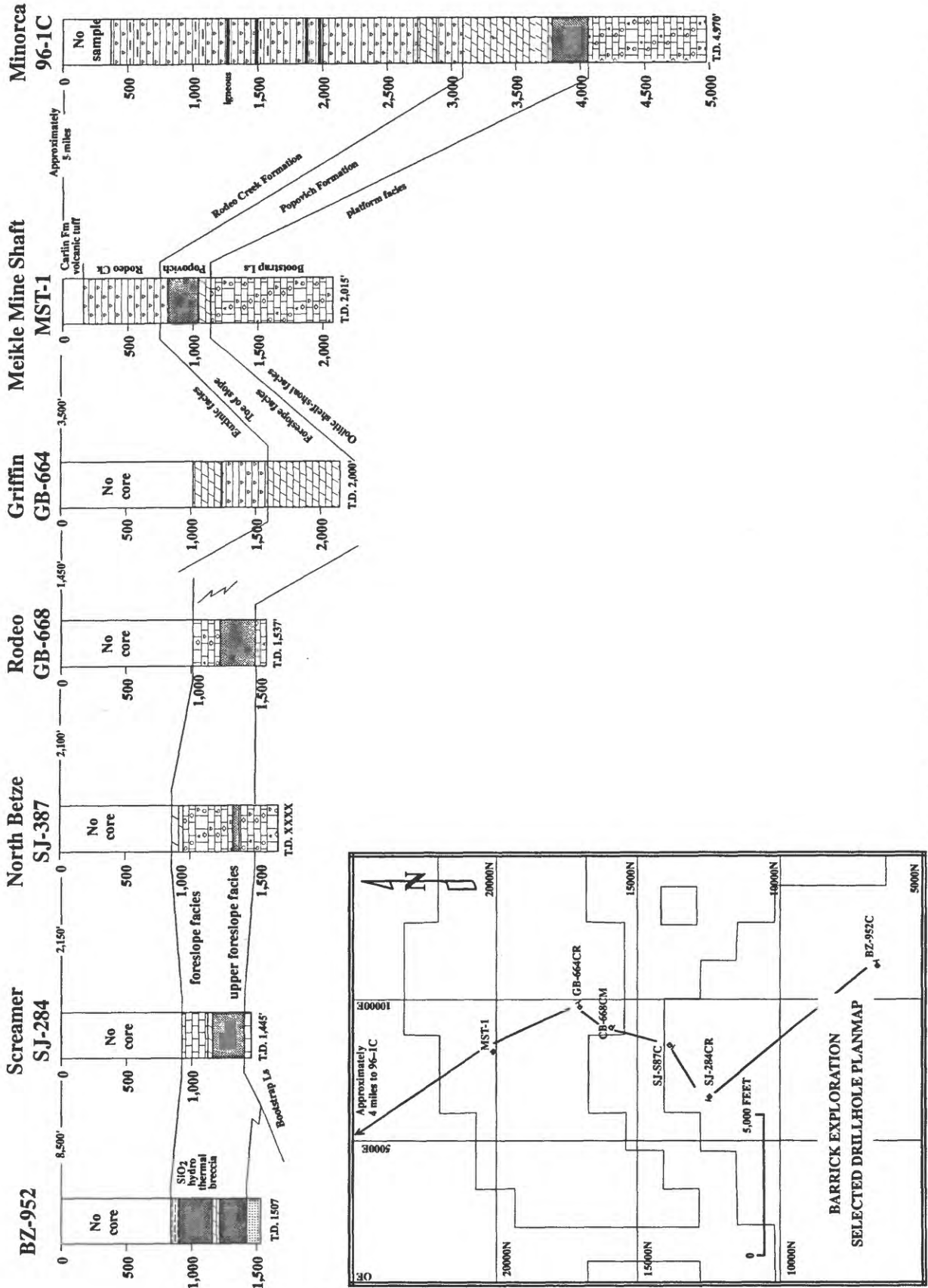


Figure 13. Stratigraphic north-south section of the Popovich Formation from the Minorca core hole 96-1C to the Meikle Mine shaft MST-1, Griffin GB-664, Rodeo GB-668, North Betze SJ-387, Screamer SJ-284, and SJ-952. Above the Bootstrap limestone, the Popovich Formation thins to the south and changes facies to more shallow water with more abundant debris beds and interbeds of crinoid, brachiopod, mollusk and corals. Local mine coordinates are shown.

feldspar, white mica, and rare zircon, as well as clay minerals which are silt sized or smaller and are the results of turbidity currents and eolian transport.

The deep water or starved basin lime mudstone possibly are the result of redistribution of distal axial turbidity currents and bottom currents (contour currents) and the slow rain of pelagic skeleton and of eolian quartz and clay to the sea floor (Galloway and McGilveray, 1995). The cores also show a spectrum of resedimentation features interpreted as the product of distal slump, debris flow and turbidity currents (Shanmugan and others, 1995).

Diagenesis

The Popovich is silty, dolomitic limestone (micrite) to calcitic dolostone (dolomicrite). The dolomitization process within the Popovich Formation is incomplete. Sperber and others (1984) examined Paleozoic dolomites from North America that provide insight into how different types of dolomitization processes may be reflected in carbonate rocks. Their data indicates that two separate processes may lead to two distinct populations of sedimentary dolomites. The processes are divided into closed and open systems. Closed system dolomitization is associated with micrites that contained initially substantial amounts of magnesium calcite and resulted in dolomitic limestone. Dolomites in these limestones are generally calcium-rich if they have undergone only shallow burial. Open system dolostones, where most of the carbonate minerals have been converted to nearly stoichiometric dolomite, are believed to be the result of large-scale circulation of fluids capable of providing the Mg necessary for dolomitization.

The Popovich Formation contains abundant pyrite with the dolomite and this suggests that sulfate reduction was an important process. Baker and Kastner (1981) also emphasize the importance of dolomite in the geologic record and suggest that reduction of marine sulfate have a causative relationship to the formation of dolomite. Studies by Vasconcelos and others (1997) indicate that when dolomite is associated with sediments rich in organic carbon, biologic parameters must be considered as an important influence on the process of dolomitization. Mullins and others (1988) demonstrated in their study of Florida-Bahamas Neogene deep-water (475 to 2,767 m) carbonate strata that relatively small concentrations of dolomite are a natural consequence of early submarine, shallow-burial diagenesis of deep-water periplatform carbonate minerals originally rich in metastable components. Their conclusions are: (1) calcium-rich dolomite is a common (<20 percent) but rarely abundant authigenetic component of deep water periplatform carbonate that contains metastable aragonite and magnesium calcite; (2) deep-water dolomite is present mostly as scattered euhedral rhombs 5 to 20 μm wide, precipitated as pore fillings; and (3) along discontinuities, deep-water dolomites can constitute as much as 86 percent of the carbonate fraction in hardgrounds, occurring as both pore fill

and as calcite replacement.

Morrow (1990b) describes the organogenic sea floor penecontemporaneous to the early dolomitization model. The dolomite beds form by precipitation from marine-derived fluids only a few meters beneath the sediment-water interface in offshore deeper marine continental margin settings. The intrasediment diagenetic environment is strongly reducing, leading to sulfate depletion by sulfate reduction and the oxidation of organic material. Both the reduction in sulfate concentration and the generation of carbon alkalinity are thought to enhance dolomitization (Baker and Burns, 1985).

Hydrothermal Alteration

Pervasive hydrothermal replacement of the Popovich Formation is present primarily in the foreslope facies. The Popovich Formation had an inherent porosity due to primary early crystallization of dolomite in the lime mud (micrite) and the development of intercrystalline porosity (figs. 4A-C). The porous foreslope facies of the Popovich Formation was deposited on the well-cemented ooid facies of the Bootstrap limestone, which probably was well cemented prior to deposition of the Popovich Formation as described above. Relations in some cores of the Bootstrap limestone indicate that parts of the Bootstrap limestone shelf were subjected to meteoric water and karsting. The debris flows of the foreslope facies of the Popovich Formation contained particularly well developed primary vuggy porosity. Furthermore, this porous calcite fossil debris was subject to reaction with ascending hydrothermal fluids which occurred much later during Cretaceous (Arehart and others, 1993b) or Tertiary (Seedorff, 1991) time. Initial stages of hydrothermal alteration associated with mineralization in the foreslope facies were the dissolution and removal of calcite minerals and bioclasts that greatly increased its porosity.

Hydrothermal replacement is, moreover, manifested by the introduction of hydrothermal dolomite and an increased crystal size of the dolomite rhombs, which further increases overall porosity of the rocks. It is because of the multiple generations of dolomite that plots of molar ratios of Ca/Ti versus Mg/Ti for gold-bearing and altered carbonate rocks in many Carlin-type deposits show a clustering of data points largely along the model line for dolomite (Madeisky, 1996). Introduction of microcrystalline silica, in places, gave rise to a near perfect silica pseudomorphic replacement of the original rock fabric. Pore space is infilled by coarse crystalline quartz, and silicified breccia contains irregular veins of white silica, residual carbon, pyrite, and bands of orange-brown sphalerite. Some relict dolomite and late vein calcite also are present. Examination of a limited number of these silicified samples by SEM reveals those relatively large anhedral masses of apatite, locally hundreds of mm wide, are concentrated on the leading edges of silica fronts that have developed in the Popovich Formation. In addition, in some samples, pyrite and brannerite (ideally $(\text{UO}, \text{TiO}, \text{UO}_2)\text{TiO}_3$), which typically are

approximately 5 to 10 mm wide, also are present along the apatite-hydrothermal silica contacts. The textural relations and crystal habits of the brannerite strongly suggest that it was completely recrystallized or reconstituted during the hydrothermal event associated with introduction of silica, pyrite, and gold.

At the Meikle Mine, the Popovich Formation is altered completely by hydrothermal fluids, and now is predominantly silica, hydrothermal collapse breccia, including variable amounts of clay minerals. In the Genesis and Blue Star gold deposits (fig. 1), most gold is hosted by silicic-argillic altered rocks, decalcified and containing approximately 10 to 35 volume percent mostly 1M illite (Drews-Armitage and others, 1996).

Rodeo Creek Unit

Cored sections of the Rodeo Creek unit are available for study from the Minorca (1,800 ft? thick) and Meikle Mine shaft drill holes (554 ft thick). At the latter locality, the Rodeo Creek unit is tectonically overlain along the Roberts Mountains thrust by rocks of the Ordovician Vinini Formation, Silurian Elder Formation (Merriam and Anderson, 1942; Smith and Ketner, 1975; Clure, 1997) and Devonian Slaven Chert (E.A. Lauha, written commun., 1997), all of which are, in turn, unconformably overlain by the Miocene Carlin Formation. The Rodeo Creek unit includes some quartz silt-dolostone and quartz silt-dolomite-argillaceous chert. The hand-specimen scale porosity of these rocks is similar to that described above in the Popovich Formation, but the overall extent of the sequences of carbonate rocks in the Rodeo Creek unit is relatively limited. Widespread chert in the Rodeo Creek unit is gray to black, distinctly thin bedded, rich in carbon, and rich in framboidal pyrite (fig. 14C). The rocks of this unit are essentially devoid of fossils except for radiolarians and sparse conodonts in some of the calcareous siltstone interbeds near the West Bazza pit. Rare sedimentary structures include slump structures, abundant siliceous mud lumps, and pervasive millimeter-size laminations, as well as medium-scale cross beds in silt-size beds. The Rodeo Creek unit, as recorded in these drill holes, is a monotonous sequence of chert with variations in percentages of clay minerals, silt, dolomite, and calcite content.

The Rodeo Creek unit exposed in the Betze-Post pit, two miles south of the Meikle shaft, is composed of three lithologic packages. They are: (1) a lower 200 ft of thin-bedded chert and argillite with minor siltstone, sandstone, and quartzite; (2) a middle 250 ft of interbedded chert, siltstone, and sandstone; and (3) an upper 150 ft of limy siltstone, micritic limestone, and minor chert (Bettles and Lauha, 1991; Leonardson and Rahn, 1996).

Environment of Deposition

The Rodeo Creek unit was deposited in a silled starved basin, anoxic environment as was previously described by Ettner (1989). The chert may be the result of pelagic radiolarian sedimentation—sponge spicules are quite rare. The terrestrial sediment in the unit is silt size quartz, clay, white micas, and rare feldspars, all of probable eolian origin. The absence of bioturbation and presence of well preserved and persistent millimeter laminations indicate no infauna in the sedimentary rocks and support deposition under anoxic conditions (see also, Ettner, 1989). The carbonate materials may have been carried in suspension by seawater from the oolitic shelf and, in part, derived from pelagic organisms that settled to the sea floor (fig. 14).

Mineralization

Many of the original oxide-zone gold deposits in the area that predated large-scale mining in the northern part of the Carlin trend were confined to rocks of the Rodeo Creek unit. This unit is present in the Minorca hole and the Meikle Mine shaft, and mineralized rocks in the unit appear to be quite limited and confined to favorable structural settings or traps associated with fractures and faults. In the Betze-Post pit area, the Rodeo Creek unit was the primary host for the Post Oxide portion of the pit, as well as the open pits (Long Lac, Bazza, and West Bazza) mined by previous owner Western States Minerals Corporation (WSMC) in the early to middle 1980s. Approximately 1.5 million oz Au were mined from the Post Oxide deposit by Barrick, and 300,000 oz Au were mined by WSMC in the other oxide pits. When compared to Carlin-type deposits away from the Carlin trend and other types of gold deposits elsewhere in Nevada, gold deposits that formed in the Rodeo Creek unit are nonetheless quite substantial. In all, oxidized and highly fractured gold deposits in the Rodeo Creek unit have yielded approximately 2 million oz Au from the general area of the northern Carlin trend (fig. 2; see also, Volk and others, 1996).

Environment of Deposition

An idealized sequence of standard facies belts for the depositional environments of the Bootstrap limestone, Popovich Formation and Rodeo Creek unit is shown in figures 2 and 3. The concept for this model is from Wilson (1975). The Bootstrap limestone was deposited as ooid, grapestone, and bioclastic sands to lime mudstones on a shoaling shallow shelf environment. A modern analog for the Bootstrap carbonate sand is the Holocene ooid sediments of Joulter's Cay, Bahamas (Harris 1979). The schematic block diagram of Ball (1967) that illustrates the sedimentary structures and grain types that typify marine sand belts of the western Great Bahama Banks, at Cat Cay also is an analog for the Devonian Bootstrap ooid depositional environments (fig. 3). As described above,

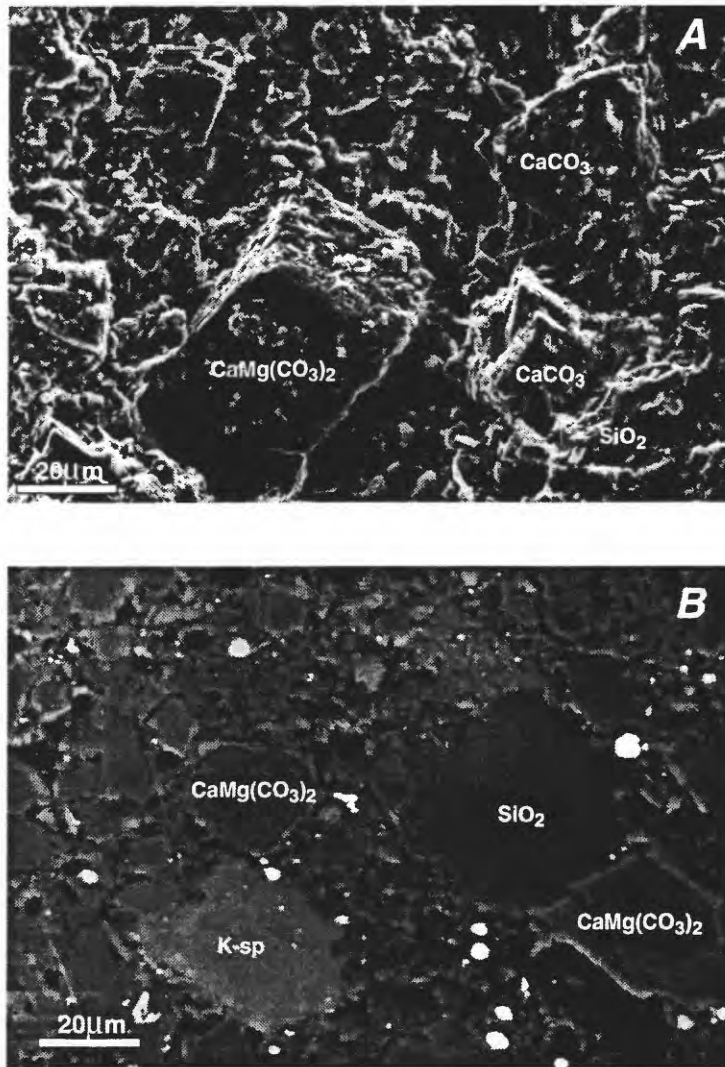


Figure 14. Scanning electron micrographs of Devonian Rodeo Creek unit. (A), Calcite and dolomite crystals and detrital quartz. Intercrystalline and interparticle porosity is well developed and pore space is filled by sulfur-rich carbon determined by SEM. Sample no. GB664-1047. (B), Polished section of rock showing an admixture of dolomite, calcite, detrital K-feldspar (K-sp), quartz, and framboidal pyrite. Pore space is black. Sample no. GB664+1150. (C), Mixture of calcite and dolomite rhombs with round framboidal pyrite crystal (py) in center of electron photomicrograph. Sample no. GB664+1031. (on page 60)

cores studied from the Bootstrap limestone provide no evidence for the presence of a coral barrier reef. The presence in the lower part of the Uranerz core at 3,500 to 3,600 ft of sabkha sedimentary structures such as algal mat laminations, rip-up clasts, and intraformational conglomerates indicates this part of the Bootstrap dolostone was deposited at times in subtidal to supratidal sabkha environments. Intertidal to supratidal sedimentary structures also are present in the lower part of the core. Dolostones at 3,630 to 3,790 ft and again 4,170 to 4,180 ft have pseudomorphs of gypsum and anhydrite, which indicate

existence during deposition of laterally adjacent or overlying evaporites that could have provided sources of Mg-bearing hypersaline solutions capable of dolomitizing, by seepage-refluxion, this sequence of dolostones.

The base of the Popovich Formation represents drowning of the Bootstrap shelf, possibly because of downwarping and (or) faulting. The three upper units of the Popovich Formation represent foreslope deposits in an oxygenated to anoxic environment at the edge of the Bootstrap ooid shoals. They represent slide- and slump-transported ooid-shelf sediments

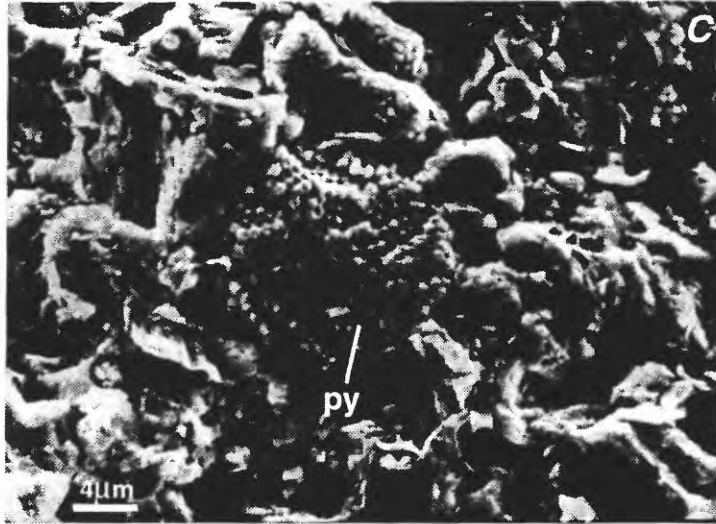


Figure 14. (C), Mixture of calcite and dolomite rhombs with round framboidal pyrite crystal (py) in center of electron photomicrograph. Sample no. GB664+1031

that are mixed and interbedded with basal silty dolostones and lime mud. The rocks included are talus blocks, slump deposits, debris-flows, and turbidites. Features indicative of slope deposits in the Popovich Formation are: (1) syndimentary folds formed by slump or creep; (2) low-angle truncation surfaces; and (3) slump scars (Emos and Moore, 1983). The middle and upper parts of the Popovich Formation were deposited in the toe-of-slope and deep shelf environments. The rocks are carbonate turbidites and distal base-of-slope sediments similar to those described elegantly by Ettner (1989) farther to the south along the Carlin trend.

The petrology, diagenesis, and depositional environments of the Rodeo Creek unit currently are under further study. The sediments represented by this unit, however, appear to have been deposited in the toe-of-slope, deep shelf, and euxinic basin environments. The rocks generally are quite siliceous with quartz silt and clays suggesting, in part, an eolian and pelagic (radiolarian) source for them.

CONCLUSION

Of the five Silurian-Devonian host-rock units below the Roberts Mountain thrust in the Carlin trend, the Hanson Creek Formation, Roberts Mountains Formation, Bootstrap Limestone, Popovich Formation, and the Rodeo Creek unit, only the Roberts Mountains and Popovich Formation have the mineralogy and porosity which favors gold mineralization. In both the Roberts Mountains and the Popovich Formations, sediments are typically calcitic dolostones with primary intercrystalline vug porosity resulting essentially from diagenetic crystallization of dolomite. The Roberts Mountains and Popovich Formations thus had an inherent porosity due

to primary early crystallization of dolomite in lime mud (micrite) and abundance of intercrystalline sulfur rich carbon has subsequently enhanced its reactivity to gold-bearing fluids that circulated there during the Cretaceous and (or) Tertiary.

REFERENCES CITED

- Arehart, G. B., Chryssoulis, S. L., and Kesler, S. E., 1993a, Gold and arsenic in iron sulfides from sediment-hosted disseminated gold deposits: Implications for depositional processes: *Economic Geology*, v. 88, p. 171-185.
- Arehart, G. B., Foland, K. A., Naeser, C.W., and Kesler, S.E., 1993b, $^{40}\text{Ar}/^{39}\text{Ar}$, K/Ar, and fission track geochronology of sediment-hosted disseminated gold deposits at Post-Betze, Carlin trend, northeastern Nevada: *Economic Geology*, v. 88, p. 622-646.
- Armstrong, A. K., Bagby, W. C., Eklburg, C., and Repetski, J., 1987, Petrographic and scanning electron microscope studies of samples from the Roberts Mountains and Popovich Formations, Carlin Mine area, Eureka County, Nevada: U. S. Geological Survey Bulletin 1684, 23 p.
- Baker, P. A., and Kastner, M., 1981, Constraints on the formation of sedimentary dolomites: *Science*, v. 213, p. 214-216.
- Baker, P. A., and Burns, S. J., 1985, Occurrence and formation of dolomite in organic-rich continental margin sediments: *American Association of Petroleum Geologists, Bulletin*, v. 69, p. 1917-1930.
- Ball, M. M., 1967, Carbonate sand bodies of Florida and the Bahamas: *Journal of Sedimentary Petrology*, v. 37, p. 556-591.
- Bathurst, R. G. C., 1975, Carbonate Sediments and Their Diagenesis, *Developments in Sedimentology*, no. 12: New York, Elsevier, 658 p.
- Beales, F. W., and Hardy J. L., 1980, Criteria for the recognition of diverse dolomite types with an emphasis on studies on host rocks for Mississippi Valley-type ore deposits: *Society of Economic Paleontologists and Mineralogists Special Publication* 28, p.197-213.

- Bettles, K. H., and Lauha, E. A., 1991, Gold deposits of the Carlin Trend, Nevada: World '91, Forum on Technology and Practice: Second Australian Institute of Mining and Metallurgy-Society of Mining and Metallurgy Joint Conference, 21-26 April, Cairns, Australia, p. 251-257.
- Cantrell, D. L., and Walker, K. R., 1985, Depositional and diagenetic patterns, ancient oolites Middle Ordovician, Eastern Tennessee: *Journal of Sedimentary Petrology*, v. 54, p.518-531.
- Choquette, P. W., and James, N. P., 1990, Limestones-The burial diagenetic environment, in McIlreath, I. A., and Morrow, D. W., eds., *Diagenesis: Geoscience Canada reprint series no. 4*, p. 75-111.
- Christensen, O. D., 1996, Carlin trend geologic overview, in Peters, S.G., Williams, C. L., and Volk, Jeff, Field trip guidebook for Trip B—Structural geology of the Carlin trend, in Green, S.M., and Struhsacker, Eric, eds., *Field Trip Guidebook Compendium: Reno, Nevada*, Geological Society of Nevada, p. 147-156.
- Cluer, J. Kelly, Cellura, B. R., Keith, S. B., Finney, S. C., and Bellert, S. J., 1997, Stratigraphy and structure of the Bell Creek nappe (Antler orogen), Ren Property, northern Carlin trend, Nevada, in Perry, A. J., and Abbott, E. A., eds., 1997 Fieldtrip Guidebook: Nevada Petroleum Society, p. 41-53.
- Cook, H. E., 1972, Miette platform evolution and relation to overlying bank (reef) localization, Upper Devonian, Alberta: *Bulletin Canadian Petroleum Geology*, v. 20, no. 3, p. 375-411.
- 1993, Submarine carbonate breccias: Criteria for their recognition, depositional models, and their role in petroleum and hydrothermal mineral exploration, in William C. L., ed., *Northeastern Nevada breccia bodies: Geological Society of Nevada Symposium Proceedings*, p. 1-7.
- Cook, H. E., McDaniel, P. N., Mountjoy, E. W., and Prey, L. C., 1972, Allochthonous carbonate debris flow at Devonian bank wall (reef) margins, Alberta, Canada: *Bulletin of Canadian Petroleum Geology*: v. 20, no. 3, p. 439-497.
- Cook, H. E., Mullins, H. T., 1983, Basin margins, in Scholle, P.A., Bebout, D.G., and Moore, C.H. eds., *Carbonate depositional environments: American Association of Petroleum Geologists, Memoir 33*, p. 539-618.
- Cox, D. P., and Singer, D.A., 1986, Mineral deposit models: U.S. Geological Survey Bulletin 1693, 379 p.
- Davis, J. J., 1996, Rapidity of freshwater calcite cementation-implications for carbonate diagenesis and sequence stratigraphy: *Sedimentary Geology*, v. 107, p. 1-10.
- Demico, R. V., and Hardie, L.W., 1994, Sedimentary structure and early diagenetic features of shallow marine carbonate deposits: *Society of Economic Paleontologists and Mineralogists Atlas Series no. 1*, Tulsa Oklahoma, 265 p.
- Dobra, J.L., 1997, The U.S. gold industry 1996: Nevada Bureau of Mines and Geology, Special Publication 21, 32 p.
- Drews-Armitage, S. P., Romberger, S. B., Whitney, C. G., 1996, Clay alteration and gold deposition in the Genesis and Blue Star deposits, Eureka County, Nevada: *Economic Geology*, v. 91, p. 1,383-1,393.
- Dunham, J.B., and Olson, E. R., 1980, Shallow subsurface dolomitization of subtidally deposited carbonate sediments in the Hanson Creek Formation (Ordovician-Silurian) of central Nevada: *Society of Economic Paleontologist and Mineralogist, Special Publication no. 28*, p. 139-161.
- Dunham, R. J., 1962, Classification of carbonate rocks according to depositional texture, in Ham, W. E., ed., *Classification of carbonate rocks: American Association of Petroleum Geologists, Memoir 1*, p. 108-121.
- Dunham, R. J., 1969, Early vadose silt in Townsend mound (reef), New Mexico, in G. M. Friedman, ed., *Depositional Environments in Carbonate Rocks: a Symposium: Society of Economic Paleontologist and Mineralogist, Special Publication 14*, p. 182-191.
- Emos, P., and Moore, C. H., 1983, Fore-reef slope environments, in Scholle, P. A., Bebout, D. G., and Moore, C. H., eds., *Carbonate depositional environments: American Association Petroleum Geologist, Memoir 33*, p. 508-537.
- Ettner, D. C., 1989, Stratigraphy and structure of the Devonian autochthonous rocks, north-central Carlin trend of the southern Tuscarora Mountains, northern Eureka County, Nevada: Pocatello, Idaho, Idaho State University, M.Sc. thesis, 177 p.
- Ettner, D. C., Snyder, W. S., and Zimmerman, C., 1989, Roberts Mountains thrust: Reevaluation in the Carlin trend, southern Tuscarora Mountains, Nevada: *Geological Society of America, Abstracts with Programs*, v. 21, p. 76-77.
- Evans, J. G., 1974, Geologic map of the Welches Canyon quadrangle, Eureka County, Nevada: U. S. Geological Survey Geological Quadrangle Map GQ-1117 [scale 1:24,000].
- Evans, J. G., and Mullens, T. E., 1976, Bootstrap window, Elko and Eureka Counties: U.S. Geological Survey, *Journal of Research*, v. 4, p. 119-125.
- Fischer, H. J., 1988, Dolomite diagenesis in the Metaline Formation, northeastern Washington state, in Shukla, V., and Baker, P. A., eds., *Sedimentology and geochemistry of dolostone: Society of Economic Paleontologists and Mineralogists Special Publication*, no. 43, p. 209-219.
- Folk, R. L., 1974, The natural history of crystalline calcium carbonate: effects of magnesium content and salinity: *Journal of Sedimentary Petrology*, v. 44, p. 40-53.
- Flügel, E., 1982, *Microfacies analysis of limestones: Springer-Verlag, New York*, 633 p.
- Hardie, B. S., 1966, Carlin gold mine, Lynn District, in AIME Pacific Southwest Mineral Industry Conference, Sparks, Nevada: Nevada Bureau of Mines Report 13, Part A, p. 73-83.
- Galloway, W. F., and McGilvery, T. A., 1995, Facies of a submarine canyon fill reservoir complex, lower Wilcox Group, (Paleocene), central Texas coastal plain, in Winn, R. D. Jr. and Armentrout, J. M., eds., *Turbidites and associated deep-water facies: Society of Economic Paleontologists and Mineralogists, core workshop no. 20*, p. 1-23.
- Gilluly, James, and Gates, O., 1965, Tectonic and igneous geology of the northern Shoshone Range, Nevada: U. S. Geological Survey Professional Paper 465, 153 p.
- Grammer, G. M., and Ginsburg, R. N., 1992, Highstand versus lowstand deposition on carbonate margins; insight from Quaternary foreslope in the Bahamas: *Marine Geology*, v. 103, p. 125-136.
- Gregg, J. M., 1988, Origin of the dolomites in the offshore facies in the Bonnetterre Formation (Cambrian), southeast Missouri, in Shukla, V., and Baker, P. A., eds., *Sedimentology and Geochemistry of Dolostones: Society of Economic Paleontologists and Mineralogists, Special Publication no. 43*, p. 67-83.
- Harris, M. T., 1994, The foreslope and toe of the slope facies of the middle Triassic Latemar buildup (Dolomite, northern Italy): *Journal of Sedimentary Research*, v. B64, p. 132-145.

- Harris, P. M., 1979, Facies anatomy and diagenesis of a Bahamian ooid shoal, in Ginsburg, R. N., ed., *Sedimenta VII, The comparative sedimentology laboratory*: University of Miami, Florida, 163 p.
- Horton, R. A., 1985a, Dolomitization and diagenesis of the Leadville Limestone (Mississippian), central Colorado: Ph.D. Dissertation, Colorado School of Mines, 178 p.
- Horton, R. A., 1985b, Dolomitization of the Leadville Limestone: Rocky Mountain section, Society of Economic Paleontologists and Mineralogists, 1985 SEPM midyear meeting field guide no. 2, p. 6-57 to 6-69.
- Horton, R. A., Jr., and DeVoto, R. H., 1990, Dolomitization and diagenesis of the Leadville Limestone (Mississippian) central Colorado, in Beaty, D.W., Landis, G. P. and Thompson, T. B., eds., *Carbonate-hosted sulfide deposits of the central Colorado Mineral Belt: Economic Geology Monograph 7*, p. 86-107.
- Horton, R. A., Jr., and Geisman, J. W., 1990, Geochemistry of the Leadville Dolomite (Mississippian), central Colorado, in Beaty, D.W., Landis, G. P. and Thompson, T. B., eds., *Carbonate-hosted sulfide deposits of the central Colorado Mineral Belt: Economic Geology Monograph 7*, p. 66-85.
- James, N. P., and Choquette, P. W., 1990a, Limestones—The sea-floor diagenetic environment., *Geoscience Canada, Reprint Series 4*, p. 13-29.
- James, N. P., and Choquette, P. W., 1990b, Diagenesis-Limestones—The meteoric diagenetic environment, *Geoscience Canada, Reprint Series 4*, P.35-73.
- Jones, D. L., Wrucke, C. T., Holdsworth, Brian, and Sucek, C. A., 1978, Revised ages of chert in the Roberts Mountains allochthon, northern Nevada: *Geological Society of America Abstracts with Programs*, v. 10., no. 3, p. 111.
- Leonardson, R. W., and Rahn, J. E., 1996, Geology of the Betze-Post gold deposits, Eureka County, Nevada, in Coyner, A. R., and Fahey, P. L., eds., *Geology and ore deposits of the American Cordillera: Geological Society of Nevada Symposium Proceedings, Reno/Sparks, Nevada, April 1995*, v. 2, p. 61-94.
- Leventhal, J. S., and Hofstra, A. H., 1991, Characterization of carbon in sediment hosted disseminated gold deposits, north-central Nevada, in Hausen, D.M., and others, eds., *Gold'90: Denver, Society for Mining, Metallurgy, and Exploration*, p. 365-368.
- Madeisi, H. E., 1996, Application of Pearce element analysis to lithochemical exploration of Carlin-type carbonate-hosted gold deposits, in Coyner, A. R., and Fahey, P. L., eds., *Geology and ore deposits of the American Cordillera: Geological Society of Nevada Symposium Proceedings, Reno/Sparks, Nevada, April, 1995*, v. 2, p. 709-732.
- Madrid, R. J., 1987, Stratigraphy of the Roberts Mountains allochthon in north-central Nevada: Stanford, California, Stanford University, Ph.D. dissertation, 341 p.
- Melim, L. A., and Scholle, P. A., 1995, The foreereef facies of the Permian Capitan Formation: the role of sediment supply versus sea-level changes: *Journal of Sedimentary Research*, v. B65, p. 107-118.
- Merriam, C. W., 1940, Devonian stratigraphy and paleontology of the Roberts Mountains region, Nevada: *Geological Society of America Special Paper 25*, 114 p.
- Merriam, C. W., 1963, Paleozoic rocks of Antelope Valley Eureka and Nye Counties Nevada: U. S. Geological Survey Professional Paper 423, 67 p.
- Merriam, C. W., and Anderson, C. A., 1942, Reconnaissance survey of the Roberts Mountains, Nevada: *Geological Society of America Bulletin*, v. 53, p. 1,675-1,728.
- Moore, C. H., 1989, Carbonate diagenesis and porosity: *Developments in Sedimentology 46*, Elsevier, Amsterdam, 338 p.
- Morrow, D. W., 1990a, Dolomite-part 1: the chemistry of dolomitization and dolomite precipitation, in McIlreath, I. A., and Morrow, D. W., eds., *Digenesis: Geoscience Canada, Reprint Series 4*, p. 113-123.
- Morrow, D. W., 1990b, Dolomite part 2: dolomitization models and ancient dolomites, in McIlreath, I. A., and Morrow, D. W., eds., *Digenesis: Geoscience Canada, Reprint Series 4*, p.125-139.
- Morse, J. W., and Mackenzie, J. A., 1990, *Geochemistry of sedimentary carbonates*: Elsevier, Amsterdam, 707 p.
- Mullens, T. E., 1980, Stratigraphy, petrology, and some fossil data of the Roberts Mountains Formation, north-central Nevada: U. S. Geological Survey Professional Paper 1063, 67 p.
- Mullins, H. T., Dix, G. R., Gardulski, G., and Land, L. S., 1988, Neogene deep-water dolomite from the Florida-Bahamas platform, in Shukla, V., and Baker, P. A., eds., *Sedimentology and geochemistry of dolostones: Society of Economic Paleontologists and Mineralogists, Special Publication no. 43*, p. 236-243.
- Nolan, T. B., Merriam, C. W., and Williams, J. S., 1956, The stratigraphic section in the vicinity of Eureka Nevada: U. S. Geological Survey Professional Paper 276, 77 p.
- Read, J. F., Grotzinger, J. B., Bova, J. A., and Koerschner, W. F., 1986, Model for generation of carbonate cycles: *Geology*, v. 14, p. 107-110.
- Roberts, R. J., 1964, Stratigraphy and structure of the Antler Peak quadrangle, Humboldt and Lander Counties, Nevada: U.S. Geological Survey Professional Paper 459-A, 93 p.
- Roberts, R. J., 1966, Metallogenic provinces and mineral belts in Nevada: Nevada Bureau of Mines Report 13, part A, p. 47-72.
- Roberts, R. J., Hotz, P. E., Gilluly, James, and Ferguson, H. G., 1958, Paleozoic rocks in north-central Nevada: *American Association of Petroleum Geologists Bulletin*, v. 42, no. 12, p. 2,813-2,857.
- Roberts, R. J., Montgomery, K. M., and Lehner, R. E., 1967, Geology and mineral resources of Eureka County, Nevada: Nevada Bureau of Mines and Geology Bulletin 64, 152 p.
- Schatzinger, R. A., Feazel, C. T., and Henry, W. E., 1985, Evidence of resedimentation in chalk from the central graben, North Sea, in Crevello, P. D. and Harris, P. M., eds., *Deep water carbonates: buildup, turbidites, debris flow and chalk, a core workshop: Society of Economic Paleontologist and Mineralogist workshop no. 6*, p.342-385.
- Schreiber, B. C., 1986, Arid shorelines and evaporites, in Reading, H. G., ed., second edition, *Sedimentary environments and facies: Blackwell Scientific Publications*, p. 189-228.
- Seedorff, Eric, 1991, Magmatism, extension, and ore deposits of Eocene to Holocene age in the Great Basin—mutual effects and preliminary proposed genetic relationships, in Raines, G. L., Lisle, R. E., Schafer, R. W., and Wilkinson, W. H., eds., *Geology and ore deposits of the Great Basin, Symposium Proceedings: Reno, Nevada, Geological Society of Nevada*, p. 133-178.
- Shanmugam, G., Salding, T. D., and Rofheart, D. H., 1995, Deep-marine bottom reworked sands (Pliocene and Pleistocene), Ewing bank 826, field, Gulf of Mexico, in Winn, R. D. Jr. and Armentrout, J. M., eds., *Turbidites and associated deep-water facies: Society of Economic Paleontologist and Mineralogist*,

- core workshop no. 20, p. 25- 54.
- Smith, J. F., Jr., and Ketner, K. B., 1968, Devonian and Mississippian rocks and the date of the Roberts Mountains thrust in the Carlin-Piñon area, Nevada: U.S. Geological Survey Bulletin 1251-I, 18 p.
- Smith, J. F., Jr., and Ketner, K. B., 1975, Stratigraphy of the Paleozoic rocks in the Carlin-Piñon area, Nevada: U.S. Geological Survey Professional Paper 867-A, 87 p.
- Stewart, J. H., and McKee, E. H., 1977, Geology of Lander County Nevada: Nevada Bureau of Mines and Geology Bulletin 88, 106 p.
- Stewart, J. H., and Poole, F. G., 1974, Upper Precambrian and Lower Paleozoic miogeoscline, Great Basin, western United States: Society of Economic Paleontologists and Mineralogists Special Paper 22, p. 28-57.
- Spencer, G. H., and Tucker, M. E., 1997, Genesis of limestone megabreccias and their significance in carbonate sequence stratigraphic models: a review: *Sedimentary Geology*, V. 112, p.163-193.
- Sperber, C. M., Wilkinson, B. H., and Peacor, D. R., 1984, Rock composition, dolomite stoichiometry and rock/water reaction in dolomite carbonate rocks: *Journal of Geology*, v. 92, p. 609-622.
- Vasconcelos, C., and McKenzie, J., A., 1997, Microbia mediation of modern dolomite precipitation and diagenesis under anoxic conditions (Largo Vermelha Rio de Janerio, Brazil): *Journal of Sedimentary Research*, v. 67, p. 378-390.
- Volk, J. A., Lauha, Eric, Leonardson, R. W., and Rahn, J. E., 1996, Structural geology of the Betze-Post and Meikle deposits, Elko and Eureka Counties, in Peters, S.G., Williams, C. L., and Volk, Jeff, Field trip guidebook for Trip B—Structural geology of the Carlin trend, in Green, S. M., and Struhsacker, Eric, eds., *Field Trip Guidebook Compendium*: Reno, Nevada, Geological Society of Nevada, p. 180–194.
- Whitebread, D. H., 1994, Geologic map of the Dun Glenn quadrangle, Pershing County, Nevada: U. S. Geological Survey Miscellaneous Investigations Series Map I-1209, 1 sheet, scale 1:48,000.
- Wilkinson, B., H., Diedrick, N., W., and Drummond, C., N., 1997, Facies successions in peritidal carbonate sequences: *Journal of Sedimentary Research*, v. 66, p. 1065- 1078.
- Wilson, J. L., 1975, Carbonate facies in geologic history: New York, Springer-Verlag, 471 p.
- Yukio, I., 1997, Permo-Triassic boundary superanoxia and stratified superocean: records from lost deep seas: *Science*, v. 276, p. 235-238.
- Zenger, D. H., and Dunham, J. B., 1988, Dolomitization of Siluro-Devonian limestones in a deep core (5350 m), southeastern New Mexico, in Shukla, V., and Baker, P. A., eds., *Sedimentology and geochemistry of dolostones*: Society of Economic Paleontologists and Mineralogists, Special Publication, No. 43, p. 161-173.

Appendix A. Summary of conodont paleontology and zonation from the Bootstrap limestone recovered from Uranerz RU-8 drill hole.

Field no. (USGS col. no.)	LITHOLOGY & STRATIGRAPHIC UNIT	CONODONT FAUNA	AGE	CAI	CONODONT BIOFACIES & DEPOSITIONAL ENVIRONMENT	REMARKS
Ru-8-3036- 3090' (12780-SD)	Light-gray lime mudstone containing bryozoans, gastropods (<0.5 cm in diameter), and small pelmatozoan plates.	1 Pa element <i>Ozarkodina remscheidensis remscheidensis</i> (Ziegler) 1 indet. bar, blade, or platform fragment	middle Ludlovian- very earliest Pragian (middle early Late Silurian-early Early Devonian).	4	Indeterminate (too few conodonts); probably shallow- water near restricted depositional setting.	3.3 kg of rock processed (160 g +20 and 10 g 20- 200 mesh insoluble residue). Heavy-mineral concentrate: chiefly dolomite, phosphatic argillaceous flakes containing fine pyrite and minor argillaceous composite flakes and pyrite.
Ru-8-3139- 3196' (12779-SD)	Light-gray lime mudstone/wackestone containing abundant small pelmatozoan plates and sparse calcite-filled vugs.	1 Pa element fragment <i>Ozarkodina douroensis Uyeno</i> 1 Pa element <i>Ozarkodina excavata</i> <i>excavata</i> (Branson & Mehl) 5 <i>Panderodus unicosstatus</i> Branson & Mehl 2 indet. coniform and blade fragment	middle Ludfordian (=middle Ludlovian (early Late Silurian); thus far only found in the very lowermost <i>O.</i> <i>remscheidensis</i> Zone (known from the Canadian Arctic Islands, Great Basin, and Appalachian basin).	4.5-5	Indeterminate (too few conodonts); probably shallow- water depositional setting.	4.3 kg of rock processed (180 g +20 and 20 g 20- 200 mesh insoluble residue). Heavy-mineral concentrate: chiefly fine euhedral and anhedral pyrite and composite anhedral dolomite with and without pyrite, and very rare euhedral biotite.
Ru-8-3305- 3359'	Medium-light- to medium-gray lime mudstone/wackestone containing common small pelmatozoan plates and white calcite fracture fills.	Barren.				6.2 kg of rock processed (220 g +20 and 16 g 20- 200 mesh insoluble residue). Heavy-mineral concentrate: chiefly phosphatized carbonaceous and argillaceous very fine pyrite-bearing flakes and minor barite.

Appendix A. (continued)

Field no. (USGS colln. no.)	LITHOLOGY & STRATIGRAPHIC UNIT	CONODONT FAUNA	AGE	CAI	CONODONT BIOFACIES & DEPOSITIONAL ENVIRONMENT	REMARKS
Ru-8-3402-3466' (12778-SD)	Light-gray lime mudstone containing rare pelmatozoan plates and white calcite vein fillings.	1 Pa element <i>Ozarkodina confluenta</i> (Branson & Mehl)? 1 <i>Panderodus</i> sp. element 1 unassigned Melement	middle Wenlockian-middle Ludlovian (late Early-middle early Late Silurian)	4	Indeterminate (too few conodonts); probably shallow-water depositional setting.	6.0 kg of rock processed (310 g +20 and 60 g 20-200 mesh insoluble residue). Heavy-mineral concentrate: chiefly anhedral and lesser rhombohedral dolomite, common euhedral pyrite and pyritic dolomite, and minor to rare composite ferruginous and (or) pyritic grains.
Ru-8-3574-3619' (12777-SD)	Core interval contains three lithologies: 1) Light- to very light-gray, stylonitic, brecciated dolomite to limestone containing vugs. 2) Light- to medium-gray, fossiliferous (including echinoderm columnals and moldic brachiopods) packstone/wackestone. Most of core has mottled bioturbated texture. 3) Light-gray, vuggy dolomite to lime micrite with no visible fossils or bedding.	1 incomplete Pa element <i>Ozarkodina confluenta</i> (Branson & Mehl)?		~4.5-5	Indeterminate (too few conodonts); probably shallow-water depositional setting.	5.3 kg of rock processed (380 g +20 and 569 g 20-200 mesh insoluble residue). Heavy-mineral concentrate: chiefly composite dolomitic and (or) pyritic argillaceous grains, relatively rare composite ferruginous flakes, and rare euhedral pyrite.

Appendix A. (continued)

Field no. (USGS colln. no.)	LITHOLOGY & STRATIGRAPHIC UNIT	CONODONT FAUNA	AGE	CAI	CONODONT BIOFACIES & DEPOSITIONAL ENVIRONMENT	REMARKS
RU-8-3794-3849 (12776-SD)	Core interval contains two lithologies: 1) majority of core is light-gray, mottled/bioturbated, vuggy porosity, no visible fossils or bedding, few stylonolites, some possible muddy intraclasts. 2) Dark-gray, pyritic, stylolitic mudstone with no visible bedding.	1 Pa element fragment <i>Ozarkodina excavata excavata</i> (Branson & Mehl)	<i>A. n. delta</i> Zone through succeeding <i>P. e. pesavis</i> Zone (=late Lochkovian; =early Early Devonian)	~4.5-5	Indeterminate (too few conodonts).	5.4 kg of rock processed (240 g +20 and 508 g 20-200 mesh insoluble residue). Heavy-mineral concentrate: chiefly rhombohedral and anhedral dolomite and lesser euhedral pyrite, composite fine-grained pyrite, composite ferruginous flakes, and minor siltstone.
RU-8-3906-3960 (12775-SD)	Core interval has two lithologies: 1) light- to medium-gray, burrow-mottled, dolomitized, vuggy micrite (vugs 1-3 cm) containing a few calcite veins (mainly 2-3 mm that are vertical to subvertical); no visible fossils or bedding; 2) light- to dark-gray, brecciated dolomite with many fractures, a few vugs and many calcite veins with random orientation. Remnant mm-scale bedding in clasts within breccia.	4 <i>Belo della</i> sp. elements <i>Icriodus</i> sp. indet. of Lochkovian morphotype 1 juvenile P & 4 M & S coniform elements 2 icritodontid P element fragments 1 Pa(?) <i>Oulodus?</i> sp. indet. element <i>Ozarkodina excavata excavata</i> (Branson & Mehl) 6 Pa, 4 Pb, 6 M, 2 Sa, 6 Sb & 10 Sc elements (mostly incomplete) 5 Pa (chiefly incomplete) elements <i>Ozarkodina pandora</i> Murphy, Matti & Walliser - morphotype 4 <i>Panderodus unicosotatus</i> (Branson & Mehl) elements 3 M & S coniform elements <i>Pedavis</i> sp. indet.		4.5-5 & minor 5.5 & 5.5-6	Ozarkodinid biofacies, normal-marine middle shelf or deeper water depositional setting.	6.1 kg of rock processed (520 g +20 and 495 g 20-200 mesh insoluble residue). Heavy-mineral concentrate: chiefly composite anhedral dolomite grains, composite dolomite and carbonaceous grains with and without pyrite, and lesser euhedral and anhedral pyrite.

Appendix A. (continued)

Field no. (USGS colln. no.)	LITHOLOGY & STRATIGRAPHIC UNIT	CONODONT FAUNA	AGE	CAI	CONODONT BIOFACIES & DEPOSITIONAL ENVIRONMENT	REMARKS
RU-8-3969'- 4014' (12774-SD)	Core interval has three lithologies: two are like those in previous core interval and C is a medium-gray, vuggy, dolomitized dolomitic. Vugs small (4 cm), no visible bedding or fossils.	1 Pb? element fragment <i>Oulodus?</i> sp. indet. <i>Ozarkodina excavata excavata</i> (Branson & Mehl) 2 Pa, 2 Pb, 1 M, 4 Sb & 1 Sc elements 4 <i>Panderodus</i> sp. elements 6 indet. bar, blade, and platform fragments	Wenlockian-late Lochkovian (no younger than <i>Pe. pedavis</i> Zone)	4.5 and minor 5.5 & 6	Indeterminate (too few conodonts); presence of <i>O. excavata</i> indicates normal-marine depositional setting.	4.7 kg of rock processed (140 g +20 and 385 g 20-200 mesh insoluble residue). Heavy-mineral concentrate: chiefly anhedral dolomite, anhedral pyrite, dolomitized bioclasts (brachiopods), and composite pyritiferous and carbonaceous grains.
RU-8-4014'- 4069' (12773-SD)	Two major lithologies: 1) Medium-light- to light-gray, bioturbated, dense limestone to dolostone (wackestone/mudstone) containing large bioclasts (>5 cm) of ramose bryozoans, favositid? corals, calcite veins, vuggy porosity locally, moldic porosity (after fossil fragments) in other places, locally stylonitic, and some quartz filled vugs. 2) Medium-dark-gray limestone containing calcite veins, abundant stylonites (no apparent bedding).	1 adenticulate <i>Belodella?</i> sp. indet. element		5-6	Indeterminate (too few conodonts).	5.5 kg of rock processed (200 g +20 and 448 g 20-200 mesh insoluble residue). Heavy-mineral concentrate: chiefly composite carbonaceous, slight pyritiferous argillaceous flakes, anhedral and minor rhomboidal dolomite, lesser euhedral pyrite.

Appendix A. (continued)

Field no. (USGS colln. no.)	LITHOLOGY & STRATIGRAPHIC UNIT	CONODONT FAUNA	AGE	CAI	CONODONT BIOFACIES & DEPOSITIONAL ENVIRONMENT	REMARKS
RU-8-4069'-4124' (12772-SD)	Same as lithofacies (1) above but including wispy stylolites, possible intraclasts of mudstone, and a few pelmatozoan ossicles. Minor amounts of breccia occur in this core interval; breccia is light-gray limestone with extensive calcite veins and angular clasts.	1 coniform Sc element of an icriodontid(?) <i>Ozarkodina excavata excavata</i> (Branson & Mehl) 11 Pa, 7 Pb, 1 M, 1 Sb & 6 Sc elements 3 <i>Panderodus unicosatus</i> (Branson & Mehl) elements 20 indet. bar, blade, and platform fragments	Wenlockian-late Lochkovian (no younger than <i>Pe. pedavis</i> Zone)	4.5 and rare 5.5 and 5.5-6	<i>O. excavata</i> biofacies: middle shelf or deeper water depositional setting.	6.0 kg of rock processed (80 g +20 and 494 g 20-200 mesh insoluble residue). Heavy-mineral concentrate: chiefly anhedral and rhombohedral dolomite, minor euhedral pyrite, and rare chalcopyrite?
RU-8-4132'-4176' (12571-SD)	Light- and medium-gray burrow-mottled dense lime mudstone containing a abundant, tight fractures (mostly subvertical). Some beds are graded where burrowing is absent. Parts of the core are vuggy (as much as 0.3 cm) and contain quartz crystal (as much as ~3 mm in size).	2 Pa elements <i>Ozarkodina excavata excavata</i> (Branson & Mehl) 3 <i>Panderodus unicosatus</i> (Branson & Mehl) elements		5-7	Indeterminate (too few conodonts); presence of <i>O. excavata</i> indicates normal-marine depositional setting.	4.4 kg of rock processed (160 g +20 and 502 g 20-200 mesh insoluble residue). Heavy-mineral concentrate: chiefly composite dolomitized grains, rhombohedral dolomite, composite pyritized grains, and lesser composite ferruginous flakes.
RU-8-4176'-4226' (12570-SD)	Three lithologies noted: A) medium-gray, bioturbated, dolomitized wackestone with no apparent bedding and containing echinoderm and other shell fragments (some appear coated), small vugs, and calcite veins; B) light-gray, burrow-mottled, dolomitized micrite with small vugs and fractures; C) brecciated, light- to dark-gray, burrow-mottled, dolomitized micrite that is abundantly fractured.	1 <i>Belodella</i> sp. indet. element 1 dapsilodid(?) element <i>Ozarkodina excavata excavata</i> (Branson & Mehl) 12 Pa, 6 Pb, 2 M, 4 Sb & 1 Sc elements 14 <i>Panderodus unicosatus</i> (Branson & Mehl) elements 11 indet. bar, blade, and platform fragments		5-5.5 and rare 6	<i>O. excavata</i> biofacies: normal-marine middle shelf or deeper water depositional setting.	5.0 kg of rock processed (140 g +20 and 511 g 20-200 mesh insoluble residue). Heavy-mineral concentrate: chiefly rhombohedral and lesser anhedral dolomite, composite carbonaceous dolomite-pyrite grains, and lesser euhedral pyrite and pyritic flakes.

GEOLOGY OF THE NORTHERN TERMINUS OF THE CARLIN TREND, NEVADA: LINKS BETWEEN CRUSTAL SHORTENING DURING THE LATE PALEOZOIC HUMBOLDT OROGENY AND NORTHEAST-STRIKING FAULTS

By Ted G. Theodore, Augustus K. Armstrong, Anita G. Harris,
Calvin H. Stevens, and Richard M. Tosdal

ABSTRACT

Dating of depositional and structural events of Late Pennsylvanian to Miocene age in the Santa Renia Fields and Beaver Peak 7-1/2 minute quadrangles has allowed development of a more complete geologic history of northeastern Nevada. Upper Pennsylvanian and Lower Permian foreland clastic rocks of the Strathearn Formation extend into the area, and these rocks have been involved in what appears to be regionally extensive north-south shortening associated with the late Paleozoic Humboldt orogeny. A major thrust in the area, the Coyote thrust, places Ordovician rocks of the Vinini Formation on top of lower strata of the Strathearn Formation probably sometime in the late Paleozoic, because the Vinini Formation also is overlain depositionally by upper strata of the Strathearn Formation. The upper plate of the Coyote thrust includes a number of generally north-dipping, imbricate thrust surfaces—its lower plate includes structurally related south-verging tightly overturned folds. Similar styles of deformation with similar folds and thrust-surface orientations are present elsewhere in many northeastern Nevada mountain ranges, where they may have continued to form as late as the Jurassic Elko orogeny. North-south late Paleozoic shortening also may have been directly associated with development of transcurrent sinistral shear along a northeast-trending deformation zone, in places as much as 20-km-wide. This feature, which has three major fault segments along its outcrop in the quadrangles, has been termed the Crescent Valley-Independence Lineament. A major strand of the Crescent Valley-Independence Lineament in the Beaver Peak quadrangle coincides with the northeast-striking Boulder Creek fault, which shows approximately 0.8 km sinistral offset of the Strathearn Formation, but only about 0.2 km sinistral separation of the Coyote thrust. This suggests some movements of the high-angle sinistral faults may predate final emplacement of the upper plate of the Coyote thrust.

Early deformation in lower Paleozoic strata along the site of the future Carlin trend of gold deposits is inferred to include a dilational jog between two of the major fault strands that

constitute the Crescent Valley-Independence Lineament. If a companion northwest-striking shear that is conjugate to the Crescent Valley-Independence Lineament is present somewhere in northern Nevada, a likely site for it is the present trace of the Miocene northern Nevada rift. We suggest that a "proto" northern Nevada rift during the late Paleozoic may have concentrated right lateral shear along its trace, largely in deeply buried lower Paleozoic rocks. Thus, a favorable environment for a "new" Carlin trend might be east-northeast-trending dilational jogs now reflected as horsts in Miocene rocks near the northern Nevada rift. Subsequent to late Paleozoic events, Paleozoic rocks in the northern Carlin trend were subjected to Mesozoic generally east-west shortening and emplacement of Jurassic and later plutons and dikes into the dilational jog, as well as Tertiary east-west extension. Tertiary extension is manifested by large numbers of faults of various orientations, and by largely unconsolidated deposits of the Miocene Carlin Formation, including widespread air-fall tuff, which has partly filled narrow pull-apart basins as much as 800 m deep.

INTRODUCTION

The purpose of this preliminary report is (1) to summarize recent geologic investigations in the Santa Renia Fields and Beaver Peak 7-1/2 minute quadrangles, (2) to integrate these investigations with others currently being completed along the trend (Peters, this volume; Fleck and others, this volume; Wallace and John, this volume; Rodriguez, this volume), and (3) to suggest, thereby, that a northwesterly zone of crustal weakness along the northern part of the Carlin trend, near which gold deposits eventually concentrated during Mesozoic and (or) Tertiary time, may be much older than previously envisaged. The northwest-trending zone of weakness along the Carlin trend may be a northwesterly-trending dilational jog across a northeast-trending, regional sinistral shear couple that initially formed during largely north-south shortening associated with the late Paleozoic Humboldt orogeny of Ketner (1977).

The northern part of the Carlin trend of gold deposits in northern Nevada—extending northwesterly from the Gold Quarry Mine to the Dee Mine (figs. 1 and 2)—is one of the richest and economically most important gold mining districts in the world since large-scale gold mining began in 1965 (Christensen, 1996; Teal and Jackson, 1997). These deposits collectively are referred to as Carlin-type systems, or sedimentary rock-hosted disseminated gold (Arehart's (1996) SHGD), which generally consist of submicron-sized gold, commonly within the crystal structure of pyrite that is disseminated in silicified, argillized, and decalcified sedimentary rocks and, to a lesser extent, in volcanic and other rocks (Tooker, 1985; Berger, 1986). Many of these deposits also are associated spatially either with syngenetic bedded barite occurrences or epigenetic vein occurrences, and recent investigations suggest that some of the Carlin-type deposits may have originated from CO₂-rich, Cl-poor, gold-bearing fluids separated from relatively deep-seated plutons (Ressel, 1998). Currently (1998), production from the State of Nevada is at the rate of approximately 7 million oz Au per year, roughly 9 percent of world gold production (Dobra, 1997), and most of the gold is being extracted from the northern part of the Carlin trend where 56 individual gold deposits are known (fig. 3). As noted by Christensen (1997), one of the crucial enigmatic questions still concerning Carlin-type deposits regards the geologic reasons that the deposits commonly are clustered in linear arrays as along the Carlin trend and elsewhere in Nevada. In order to address this question in the southern Tuscarora Mountains near the northern terminus of the Carlin trend, systematic 1:24,000 collaborative geologic mapping of the Santa Renia Fields and Beaver Peak quadrangles currently is underway by the U.S. Geological Survey and private industry (figs. 2, 4 and 5). The Santa Renia Fields quadrangle includes at least seven areas where epigenetic gold-mineralized rocks are prevalent and two areas where syngenetic bedded barite deposits have been exploited (fig. 4). The inactive (1997) Coyote bedded barite mine also is located in the southern part of the Beaver Peak quadrangle (Lapointe and others, 1991).

PREVIOUS WORK

Previous geologic investigations in the two quadrangles studied have spanned a period of approximately 130 years. The first systematic geologic observations recorded in the southern Tuscarora Mountains, then referred to as the Northern Cortez Range, were outlined by Emmons (1877, p. 608) who described "quartzites, and siliceous shales....[as well as] peculiar greenish quartzitic conglomerates" cropping out at Dalton Peaks. These peaks are now known as Beaver Peak and the ridgeline immediately to its west. These carbonate-rich and conglomeratic rocks today are recognized

as belonging to the Pennsylvanian and Permian Strathearn Formation, one of the formations that make up the largely clastic foreland of the late Paleozoic Humboldt orogeny (fig. 5; see below). Emmons (1877) also reported an approximately 200- to 250-m-thick sequence of thin-bedded limestone at Bootstrap Hill, from which a megafaunal assemblage then was assigned to an Early Devonian age (fig. 4). Middle Paleozoic juxtaposition of lower Paleozoic eastern carbonate (platform) rocks and western siliceous (basin) rocks along the regionally extensive Roberts Mountains thrust was not recognized until Merriam and Anderson's (1942) study in the Roberts Mountains (fig. 1). The thrust, as well as unconformably overlying Mississippian through Permian clastic rocks, subsequently were amalgamated conceptually into the Antler orogeny (Roberts and others, 1958; Roberts, 1964; and many others). In the part of the southern Tuscarora Mountains currently under study, the Roberts Mountains thrust crops out only in the general area of the Dee Mine and Bootstrap Hill (fig. 4).

A number of previous investigations bear directly on various aspects of the geology of the Santa Renia Fields and Beaver Peak quadrangles. The reconnaissance geologic map of Elko County (Coats, 1987) shows an undivided Ordovician, Silurian, and Devonian siliceous western assemblage unit, the Silurian and Devonian eastern assemblage limestones at Bootstrap Hill (fig. 4), and the much more areally restricted carbonate-rich rocks at Beaver Peak (fig. 5), which were assigned to the Permian Edna Mountain Formation. However, Evans and Mullens (1976) and Mullens (1980) mapped and described the eastern assemblage carbonate rocks at Bootstrap Hill as Silurian and Devonian Roberts Mountains Formation and an unnamed Devonian unit informally referred to as the Bootstrap limestone (see also, Armstrong and others, 1997). Coats and Riva (1983) assigned rocks at Beaver Peak to the Pennsylvanian and Permian Antler Peak Limestone of Roberts (1964) and attempted to explain a variability of dips in these rocks to an inferred Mesozoic thrust which they believed had since been removed by erosion. As will be described below, we find no evidence for such a thrust.

Various other aspects of the geology of the quadrangles also have been examined in a number of theses and published reports. The theses primarily have focused on mineralized areas, including both gold and barite (Greybeck, 1985; Ettner, 1989; Snyder, 1989). Snyder (1989) correctly assigned the chert-pebble conglomerate north of the Rossi barite mine (fig. 3) to the late Paleozoic overlap assemblage. A number of reports focused on the geology and mineralized rocks of the gold deposits in the Santa Renia Fields quadrangle (Wallace and Bergwall, 1984; Baker, 1991; Albino, 1994). Recently, an elegant evaluation of the stratigraphy and structure of rocks in the upper plate of the Roberts Mountains thrust in the Ren Mine area (fig. 4) was completed by Cluer and others (1997). In addition to all of the above investigations, the geology of

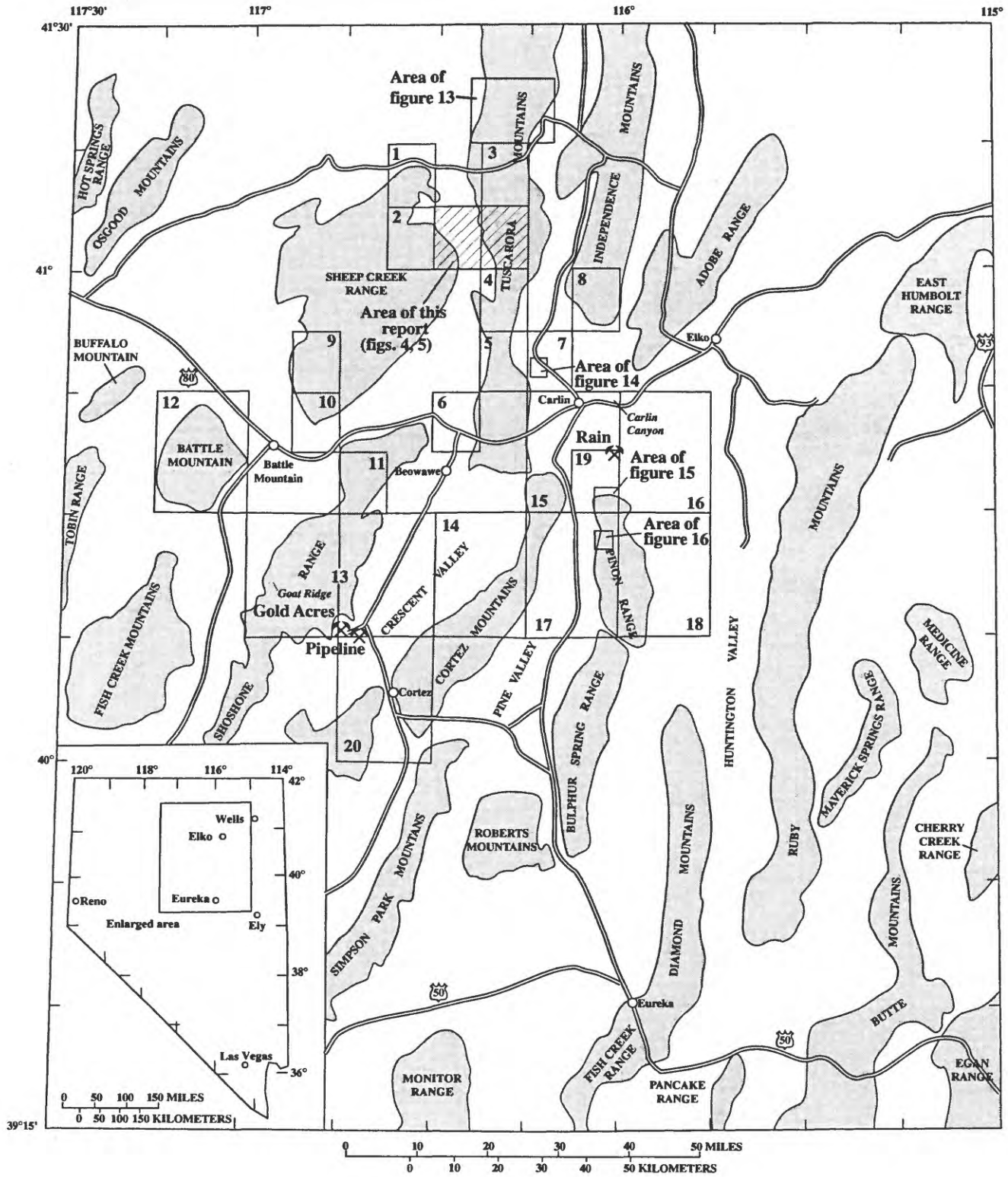


Figure 1. Index map showing location of major mountain ranges and areas discussed in northeast Nevada.

EXPLANATION

QT
Quaternary alluvial and playa deposits and Tertiary, mostly Miocene, sedimentary, tuffaceous, and lacustrine rocks (Tertiary and Quaternary)

VOLCANIC AND SHALLOW INTRUSIVE ROCKS
Tertiary volcanic rocks: andesite flows and breccias, rhyolite flows, shallow intrusive rocks, and ash-flow tuffs. Miocene rhyolite flows in Santa Renia Fields quadrangle (Tertiary)

INTRUSIVE ROCKS
Intrusive rocks of granitic to dioritic composition (Jurassic and Cretaceous)

SEDIMENTARY ROCKS
Mostly Devonian Woodruff and Ordovician Vinini Formations: shale, chert, siliceous argillite, limestone, quartzite, and greenstone. Ordovician quartzarenite widespread in Beaver Peak quadrangle. Also includes Pennsylvanian and Permian Strathern Formation and Silurian Elder Sandstone (see text) in Santa Renia Fields and Beaver Peak quadrangles (Ordovician, Silurian, Devonian, Pennsylvanian, and Permian)

Devonian limestone and Silurian and Devonian Roberts Mountains Formation: limestone, dolomite, and calcareous siltstone. Locally includes Devonian Popovich Formation, as well as several other Silurian and Devonian carbonate platformal units (Silurian and Devonian)

Contact

Fault

Gold deposit

Crescent Valley Independence Lineament (CVIL) of Peters (this volume), approximately located

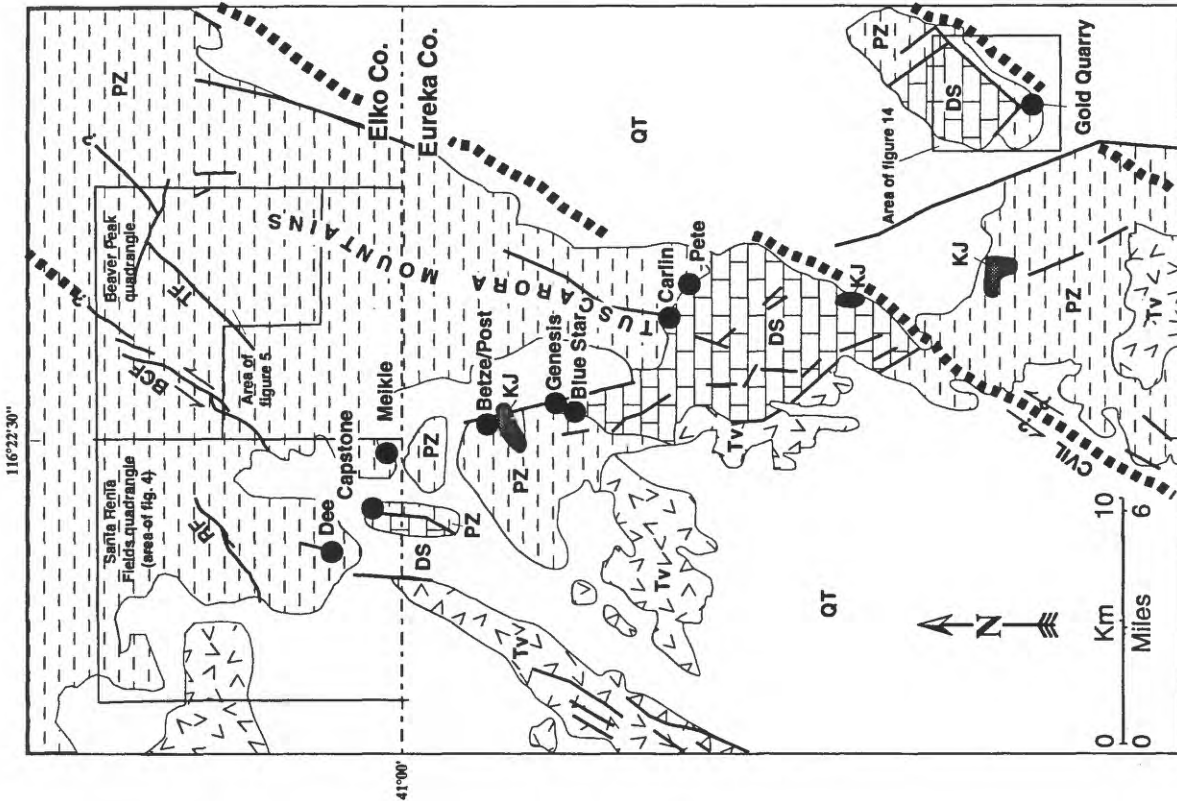


Figure 2. Generalized geology of the northern part of the Carlin trend showing location of Santa Renia Fields and Beaver Peak 7-1/2 minute quadrangles, Nev. Modified from Christensen (1996). Major faults with northeast strikes only shown in the two quadrangles. RF, Rossi fault; BCF, Boulder Creek fault; TF, Toro fault; CVIL, Crescent Valley Independence Lineament (modified from Peters, this volume).

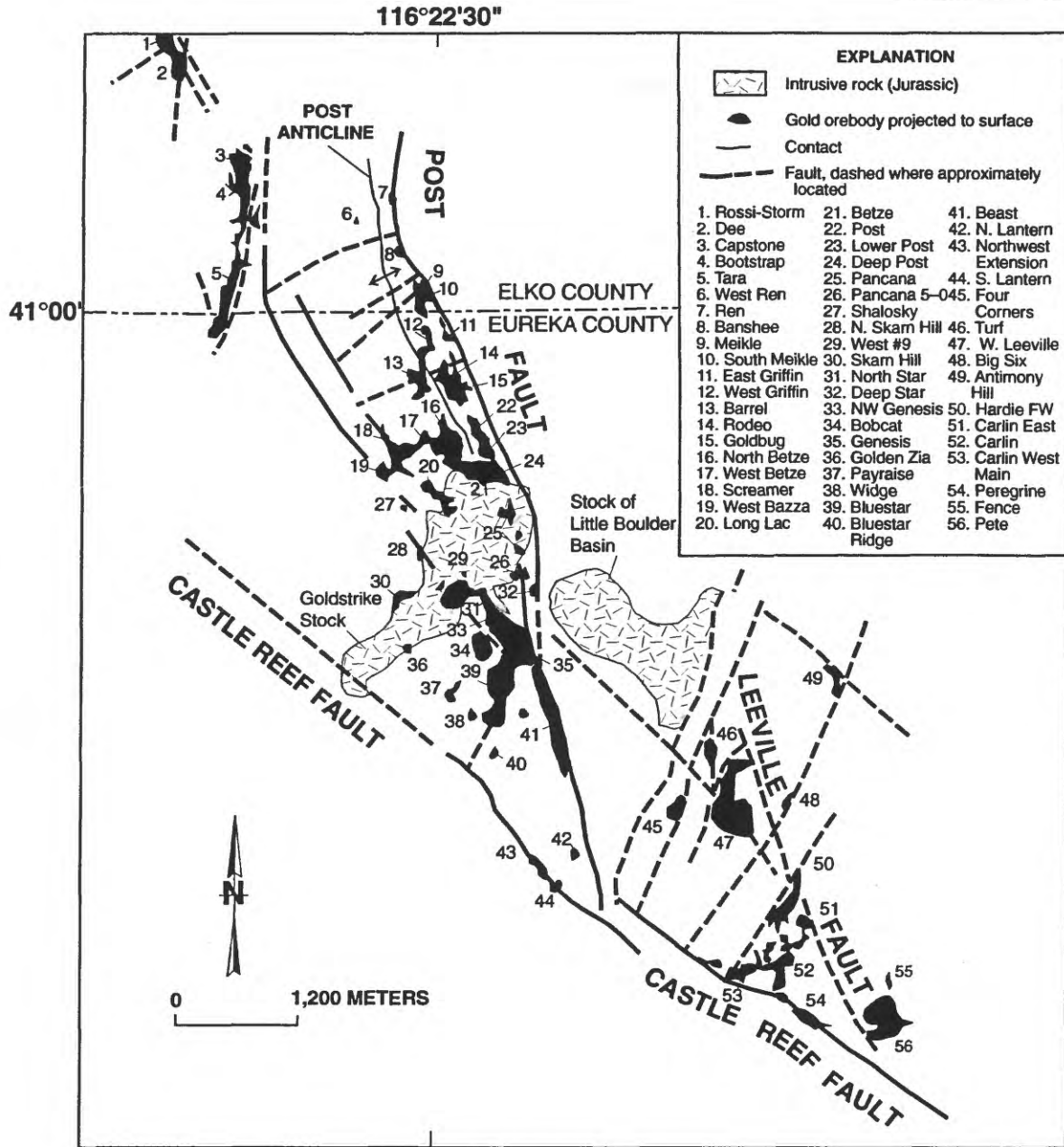


Figure 3. Sketch map showing gold deposits, major faults, and major intrusive bodies along the northern Carlin trend, Nev. Fifty-six deposits are aligned roughly along a N. 40° W., 12-km-long segment of the trend. Modified from Teal and Jackson (1997).

both quadrangles, but particularly that of the Santa Renia Fields quadrangle, has been the subject of a large number of unpublished proprietary company reports. Most of these reports describe exploration drilling projects that mainly have tested gold targets. Lastly, we would like to acknowledge the continuing positive impact on the regional geologic framework of the Carlin trend of the reports by Evans (1974a; 1974b) which concern the two quadrangles immediately south of the Beaver Peak quadrangle (fig. 1).

TECTONOSTRATIGRAPHIC RELATIONS IN THE SANTA RENIA FIELDS AND BEAVER PEAK QUADRANGLES

Structurally, from lowest to uppermost position, rocks in the stratigraphic column of the Santa Renia Fields and Beaver Peak quadrangles comprise a number of tectonostratigraphic packages (fig. 6). From the base, these include (1) sparse outcrops of autochthonous lower Paleozoic eastern assemblage

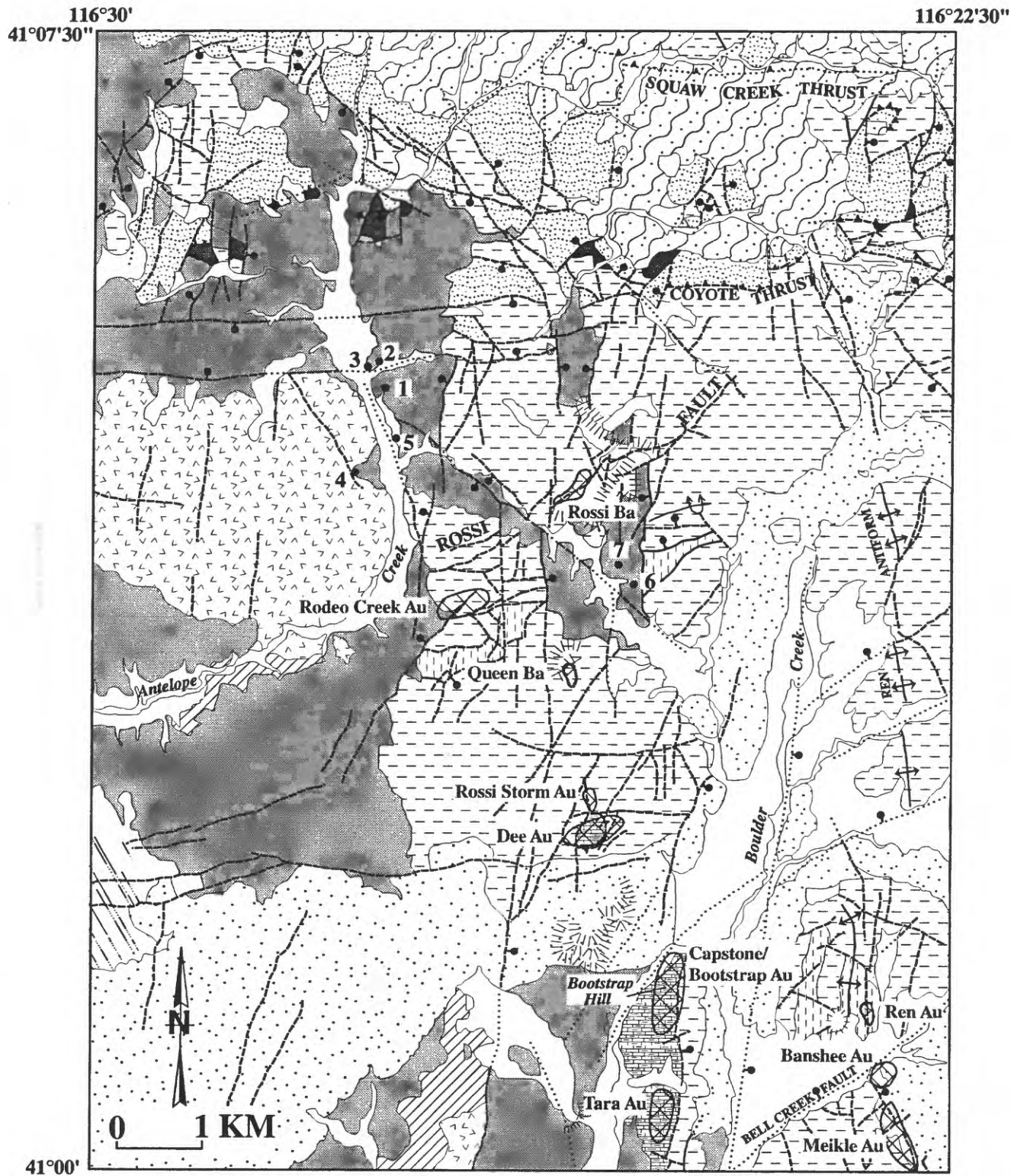


Figure 4. Geologic sketch map of the Santa Renia Fields quadrangle, Nev. Modified from T. G. Theodore, J.K. Cluer, and S.C. Finney (unpub. data, 1998). Includes area near Ren Mine modified from Cluer and others (1997); area near northwest corner modified from Rio Algom (unpub. data, 1998); area near Rossi Mine modified from Snyder (1989); area near Rodeo Creek Au modified from F.J. Menzer (written commun., 1996).

Figure 4 Explanation

CORRELATION OF MAP UNITS

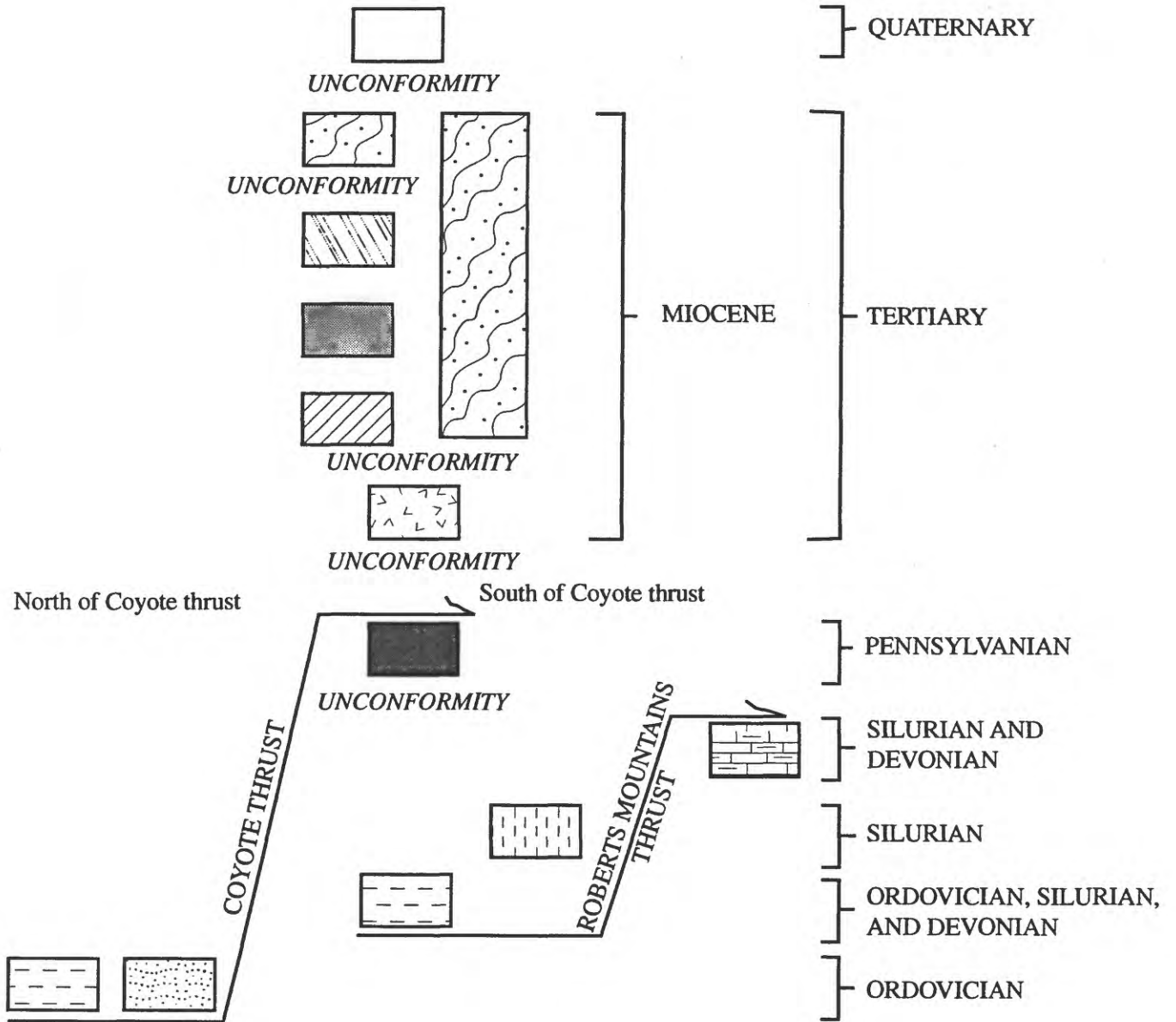


Figure 4 Explanation (continued)

DESCRIPTION OF MAP UNITS

	Alluvium and other unconsolidated deposits (Quaternary)		Contact
	Carlin Formation—Fanglomerate deposits, unconsolidated (Miocene)		Thrust fault—Sawteeth on upper plate. Dashed where approximately located; dotted where concealed
	Carlin Formation—Silt and sands, mostly unconsolidated (Miocene)		Fault—Dashed where approximately located; dotted where concealed; bar and ball on down-dropped side
	Carlin Formation—Silt and sands, mostly unconsolidated, sedimentary breccias, and abundant air-fall tuff (15.1 to 14.4 Ma, Miocene)		Mine dump
	Carlin Formation—Tuff, partly welded, and minor silt and sands, mostly unconsolidated (Miocene)		Fossil locality described in text; locality 4 same as table 1
	Carlin Formation—Undivided (Miocene)		Diamond drill hole Baxter no. 1 (see text)
	Porphyritic rhyolite vitrophyre (north of Antelope Creek) and peralkaline rhyolite (west of Boulder Creek). Same as informally named Craig rhyolite of Bartlett and others (1991) (Miocene)		
	Strathearn Formation—Chert-pebble conglomerate (Pennsylvanian and Permian)		
	Undivided autochthonous carbonate rocks below Roberts Mountains thrust—Includes laminated and shaly limestone of Silurian and Devonian Roberts Mountains Formation, ooid packstone of the informally named Devonian Bootstrap limestone, and laminated limey mudstone of the Devonian Popovich Formation		
	Elder Sandstone in upper plate Roberts Mountains thrust—Mostly siltstone and minor chert (Silurian)		
	Undivided siliceous sedimentary rocks in upper plate of Roberts Mountains thrust south of Coyote thrust—Mostly chert and argillite of Ordovician Vinini Formation, chert and argillite of probable Devonian Slaven Chert, and minor siltstone of Silurian Elder Sandstone. May include small areas of outcrop of cherty rocks belonging to Devonian Rodeo Creek unit (see text) (Ordovician, Silurian, and Devonian)		
	Undivided siliceous sedimentary rocks in upper plate of Coyote thrust—Siltstone, mostly, and some chert, probably belonging to Ordovician Vinini Formation (Ordovician)		
	Vinini Formation—Quartzarenite, mostly (Ordovician)		

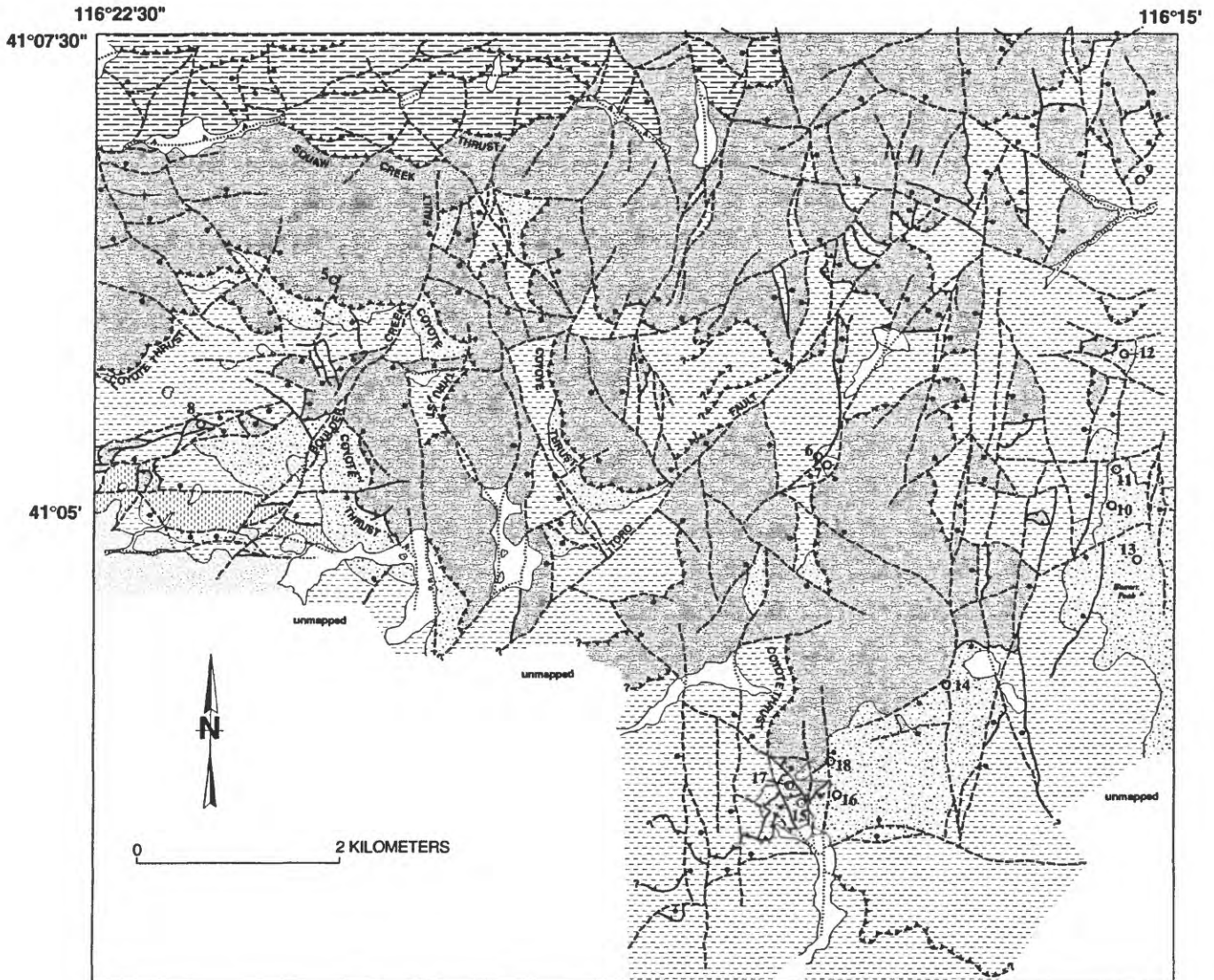


Figure 5. Geologic sketch map of northern part of Beaver Peak quadrangle, Nev. Modified from T.G. Theodore (unpub. data, 1998). See following pages for explanation of map units and symbols.

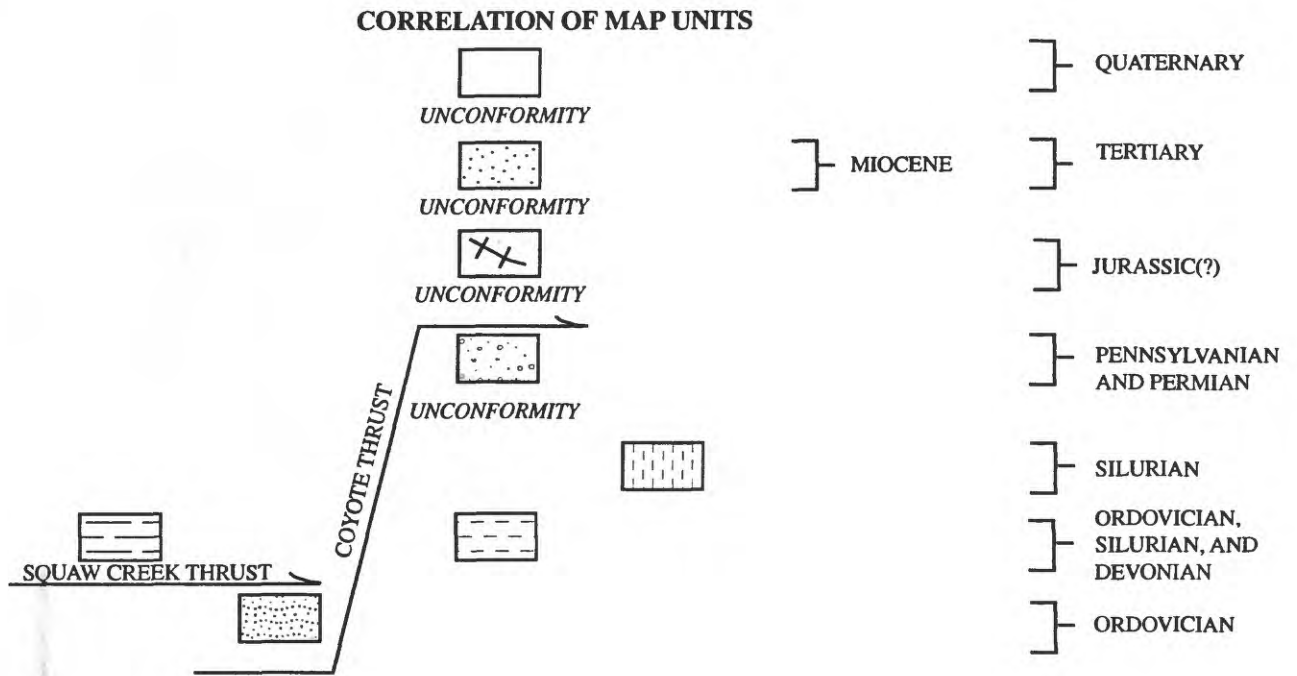
rocks; (2) widespread allochthonous lower Paleozoic western assemblage rocks in the upper plate of the Roberts Mountains thrust; (3) autochthonous upper Paleozoic overlap rocks belonging to a clastic foreland wedge of the Humboldt orogeny; (4) allochthonous lower Paleozoic rocks in the upper plate of the late Paleozoic Coyote thrust which has been emplaced above the overlap rocks; and, finally, (5) Miocene volcanic rocks as well as overlying unconsolidated deposits of the Miocene Carlin Formation (figs. 4 and 5). In addition, some major throughgoing northeast-striking faults—probably, in part, late Paleozoic in age—are present in the quadrangles, and their geology provides important information for our

interpretation of regional tectonism of the northern Carlin trend. Furthermore, the Paleozoic rocks have been intruded locally by Jurassic(?) dikes.

Autochthonous Eastern Assemblage Rocks

Autochthonous eastern assemblage carbonate rocks crop out in the open pit of the Dee Mine and in an approximately 3-km-long, north-south-oriented horst at Bootstrap Hill where the rocks dip largely to the east (fig. 4). The sequence of carbonate rocks at Bootstrap Hill has been described by

Figure 5. Explanation



DESCRIPTION OF MAP UNITS

- Alluvium and other unconsolidated deposits (Quaternary)
- Carlin Formation of Regnier (1960)—Fanglomerate deposits, unconsolidated (Miocene)
- Altered dike—Monzonite and alkali granite dikes comprised either of stubby intergrown laths of clay-clouded plagioclase and K-feldspar or mostly K-feldspar. Abundant iron oxide minerals, native sulfur, and secondary iron-arsenate minerals in surrounding wallrocks, primarily along microcracks (Jurassic?)
- Strathearn Formation of Dott (1955)—Chert-pebble conglomerate, mostly. Contains sparse quartzarenite fragments. Generally highly resistant ledges of drab gray brown to reddish brown, rubble strewn outcrops. Locally includes fossiliferous interbedded sandy micrite (as much as 30 m thick) containing abundant echinoderm spines, crinoids, brachiopods, and colonial rugose corals, as well as large concentrations of fusulinids (see text). Fusulinids concentrated in lower parts of micrite interbeds. Includes approximately 200-m-thick buff-weathering dolomitic siltstone near Beaver Peak (Pennsylvanian and Permian)
- Elder Sandstone of Gilluly and Gates (1965)—Feldspathic siltstone, gray to greenish gray weathering rusty brick red. Includes approximately 1-m-thick gray micrite beds which typically crop out no more than 5 m along strike. Unit generally poorly exposed; forms gently rounded slopes (Silurian)
- Allochthon of Squaw Creek thrust. Includes Ordovician and (or) Devonian mostly chert sequences as well as Elder Sandstone. Undivided (Ordovician, Silurian, and Devonian)

Figure 5. Explanation

DESCRIPTION OF MAP UNITS (*Continued*)

Chert and interbedded shaly argillite. Mostly gray to black, well-exposed, ridge-forming sequences in southern part of quadrangle where total exposed thickness is roughly 300 to 400 m. Basal parts of unit made up of relatively thin-bedded, rhythmically-bedded chert, mostly 2 to 4 cm between parting surfaces, whereas upper parts of unit include abundant thick-bedded sequences, mostly more than 4 cm between parting surfaces. Many sequences in upper part of unit severely tectonized. Unit probably includes sequences correlative with Ordovician Vinini Formation and Devonian Slaven Chert of Gilluly and Gates (1965). Unit also hosts a number of sedimentary exhalative barite occurrences and the inactive Coyote barite mine (Lapointe and others, 1991) located roughly 1.5 km south of south edge of map area (Ordovician, Silurian, and Devonian)



Vinini Formation. Generally orange-brown- to ochre-brown-weathering quartzarenite forming resistant, moderately rounded ridges. Includes green and black, thin discontinuous beds of chert that apparently increase in overall abundance downsection and to northwest in the northwest part of area. Includes sedimentary breccia and tectonic breccia, latter commonly shows recrystallization of angular quartz matrix among well-rounded monocrystalline detrital quartz grains. Commonly intensely recrystallized to white sucrose hornfels near Coyote thrust. Hornfels near thrust locally contains abundant brick-red iron-oxide minerals and breccia. Quartzarenite intensely lineated, in places including widespread slickensides, within 10 m of trace of Coyote thrust (Ordovician)



Contact



Fault—Dashed where approximately located; dotted where concealed; queried where uncertain; bar and ball on downdropped side



Thrust fault—Sawteeth on upper plate. Dashed where approximately located; dotted where concealed



Syncline



Fossil locality (locality number same as table 1 except locality 5, see text)

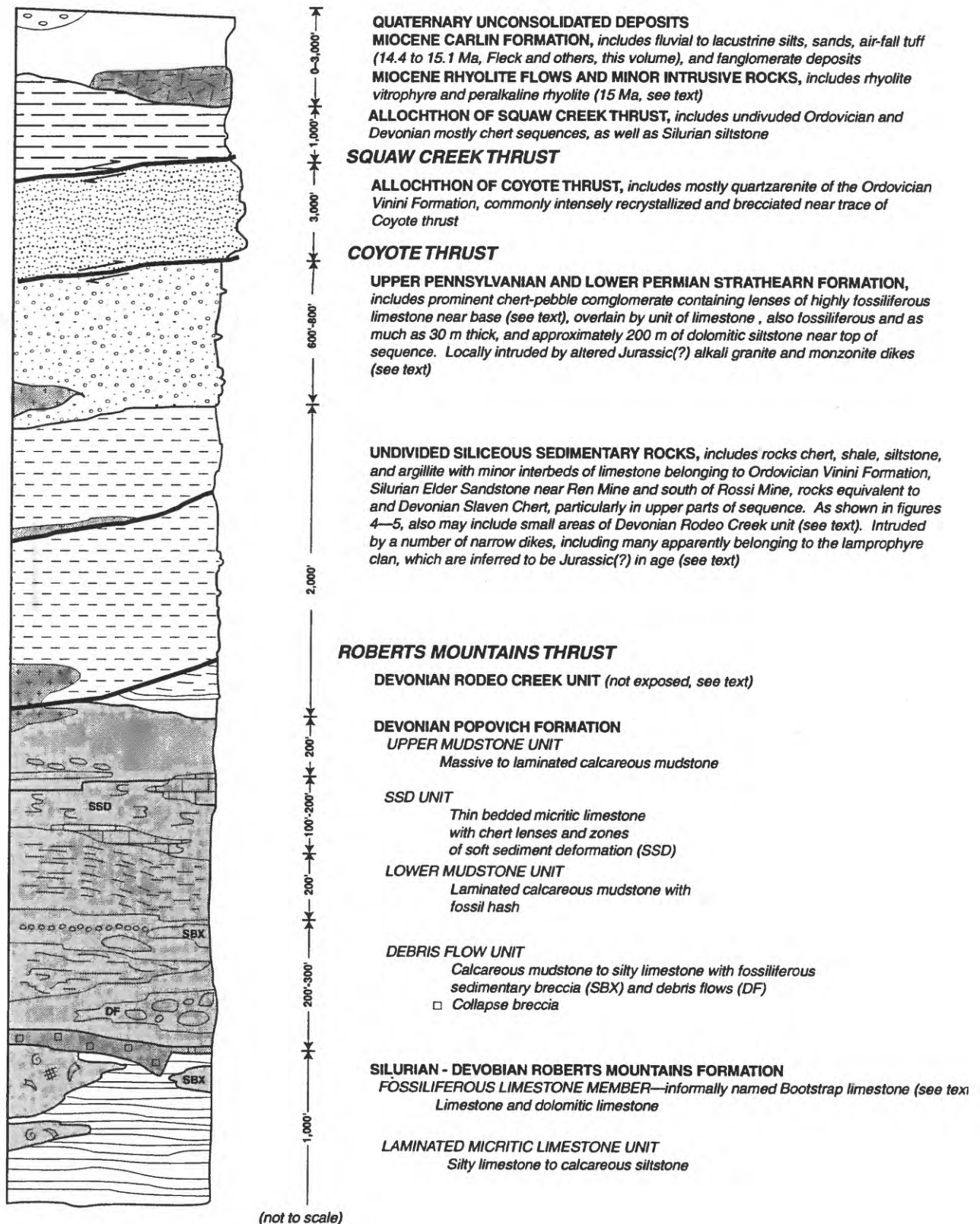


Figure 6. Schematic tectonostratigraphic column in general area of the Santa Renia Fields and Beaver Peak quadrangles, Nev. Modified from Armstrong and others (1997).

Evans and Mullens (1976) and Mullens (1980) as constituting a basal 180-m-thick section of mainly laminated limestone, which they assigned to the Silurian and Devonian Roberts Mountains Formation of Merriam (1940), and to an unnamed upper 280-m-thick section of Devonian coarse-grained limestone (fig. 6). This unnamed unit, which is primarily a peloid-oid packstone to grainstone with rounded and broken bioclasts of brachiopods, bryozoans, mollusks, echinoderms, tabulate and rugose corals, and calcareous algae, is now referred to informally as the Bootstrap limestone (Armstrong and others, 1997). A deep drill hole at the Rodeo Creek gold resource area (fig. 4) cored approximately 320 m of peloid-oid packstone belonging to the Bootstrap limestone, as well as an approximately 300-m-thick overlying section of dark-gray to black, fine-grained quartz silt, dolomicrite to lime mudstone characterized by millimeter-size laminations and soft sediment deformation (Armstrong and others, 1997). The latter unit is part of the Devonian Popovich Formation (Hardie, 1966; Evans, 1974b; Ettner, 1989), which elsewhere along the Carlin trend is overlain by cherty shale of the Devonian Rodeo Creek unit of Ettner (1989), also part of the eastern assemblage. Detailed petrographic examination at the Dee Mine of a cored sequence of carbonate rocks to depths as much as 700 m revealed that most carbonate rocks are Bootstrap limestone facies wackestones and packstones, as are the rocks as much as approximately 1,000 m below the Ren Mine as known from drill cores (see also, Armstrong and others, this volume). The Devonian rocks—including Bootstrap limestone, Popovich Formation, and Rodeo Creek unit—probably formed during drowning of a shallow carbonate platform (Armstrong and others, 1997; Armstrong and others, this volume). Some other deep drill holes near the southeast corner of the Santa Renia Fields quadrangle have penetrated strata belonging to the Ordovician and Silurian Hanson Creek Formation, which is present below the Roberts Mountains Formation (Armstrong and others, this volume).

Allochthonous Western Assemblage Rocks

In the Santa Renia Fields quadrangle, a wide expanse of generally north-dipping and broadly folded lower Paleozoic siliceous rocks—mostly chert, argillite, shale, and siltstone—make up the allochthonous western assemblage in the upper plate of the Roberts Mountains thrust (fig. 4). This sequence is shown as an undivided siliceous sedimentary rock unit, and includes tectonically interleaved rocks belonging to the Ordovician Vinini Formation of Merriam and Anderson (1942), Silurian Elder Sandstone of Gilluly and Gates (1965), and Devonian Slaven Chert of Gilluly and Gates (1965), as determined from a number of fossil collections (Snyder, 1989; Cluer and others, 1997; and many others). The undivided siliceous sedimentary rock unit also may include small areas of the eastern assemblage Rodeo Creek unit not separated

because of the difficulty of distinguishing it from other siliceous rocks. The Roberts Mountains thrust crops out in the open pit of the Dee Mine and shows evidence of reactivation a number of times since the siliceous allochthonous rocks were first emplaced during Devonian and Mississippian tectonism (Roberts and others, 1958) associated with the Antler orogeny (see also, Greybeck, 1985).

Undivided siliceous sedimentary rocks near the top of the unit in the upper plate of the Roberts Mountains thrust, although assigned to an undivided Ordovician, Silurian, and Devonian unit (figs. 4 and 5), probably are Devonian in age and most likely belong to the Devonian Slaven Chert. A thin bed of silty light-bluish-gray limestone in chert in the Santa Renia Fields quadrangle (fig. 4, loc. 1) produced abundant conodonts of Lochkovian to early Emsian age (Early Devonian), and a few redeposited conodonts of Middle Ordovician age (N.R. Stamm and A.G. Harris, written commun., 1994, to J. Zimmerman and G.L. Griffin; S.B. Keith, written commun., 1996). Locality 1 is approximately 0.2 km south of the trace of the Coyote thrust and is in a sequence of chert the strike of which is at a moderately high angle to the trace of the thrust (Theodore and others, unpub. data, 1998). The thicknesses, tectonic and stratigraphic, of the chert are estimated conservatively to reach at least approximately 800 m (fig. 4). Substantial subsurface relief on the surface of the Roberts Mountains thrust probably has been accentuated locally by the large number of subsequent structural events associated with Mesozoic shortening and Tertiary extension described below. For example, near the Rodeo Creek gold resource area (fig. 4, loc. 3), roughly 3 km northwest of the Dee Mine, Ordovician rocks are present to as much as approximately 500 m below the surface on the basis of age diagnostic, late Middle to Late Ordovician marine palynomorphs in carbonaceous siliceous rocks (Rosemary Askin-Jacobson, written commun., 1997; see also, Armstrong and others, 1997). In the north-central part of the quadrangle, similar siliceous rocks continue to as much as 800 m below the surface in the BX-1 drill hole (E.A. Lauha, written commun., 1996).

The undivided siliceous sedimentary rock unit locally shows evidence of multiple deformations that probably spanned a relatively long period of time. In the southeast part of the Santa Renia Fields quadrangle near the Ren Mine, a north-northwest-trending and north-plunging hingeline of an east-verging overturned anticline—not shown on figure 4 and referred to as the Bell Creek nappe by Cluer and others (1997)—is present in siliceous rocks of the Vinini Formation, Elder Sandstone, and Slaven Chert in the upper plate of the Roberts Mountains thrust. The nappe is inferred to have formed syntectonically with Devonian and (or) Mississippian emplacement of the Roberts Mountains allochthon (Cluer and others, 1997). Somewhat farther to the northwest, roughly 1 km southeast of the Rossi barite mine (fig. 4), an approximately 1-km-long hinge of a south-verging, overturned anticline (see

also, Snyder, 1989) has an east-west trend roughly parallel to the trace of the late Paleozoic Coyote thrust which crops out several km to the north. The east-west anticline, approximately at right angles to the probable middle Paleozoic Bell Creek nappe, is inferred to have formed during emplacement of the late Paleozoic Coyote thrust. Evans and Theodore (1978) determined that the trend of the Antler orogenic belt in the southern Tuscarora Mountains is approximately N 20°E on the basis of the orientation of small-scale folds in the siliceous sedimentary rocks. Moreover, the Bell Creek nappe and its surrounding rocks have been further uplifted by development of the Ren antiform, possibly during Mesozoic shortening (fig. 4). The hingeline of the Ren antiform can be followed approximately 6 km to the north beyond the Ren Mine, even though it has been systematically stepped to the east by a number of northeast-striking faults which parallel the Bell Creek fault (fig. 4). As will be described below, these dextral separations are inferred to reflect post-Mesozoic reactivation along fault zones that are believed to have formed originally in late Paleozoic time. The Ren antiform also can be traced 4 km to the southeast into the Post anticline by Peters and others (1996). This structure hosts the giant Betze-Post Carlin-type gold system (fig. 3), which may contain as much as approximately 50 M oz Au as a geologic resource. Farther to the south, the structure has been referred to as the Tuscarora Spur anticline (Orobona, 1996).

Autochthonous Clastic Foreland Rocks

Chert-pebble conglomerate and interbedded limestone, as well as a relatively thick sequence of dolomitic siltstone and some shale near Beaver Peak (fig. 6) are part of an autochthonous clastic foreland of the Humboldt orogeny (Ketner, 1977)—they are assigned to the Upper Pennsylvanian and Lower Permian Strathearn Formation of Dott (1955). These rocks rest unconformably on the lower Paleozoic undivided siliceous sedimentary rock unit of the upper plate of the Roberts Mountains thrust (figs. 4 and 5)—the upper contact of the Strathearn Formation throughout much of the area is the Coyote thrust. Where rocks of the Strathearn Formation are well exposed close to the Coyote thrust, they have been severely brecciated or tectonized and show variably developed ductile fabrics locally including strongly lineated surfaces, and, in places, rodded mylonite. Presence of clastic foreland deposits throughout much of the northern part of the Beaver Peak quadrangle is critical from a structural standpoint because of the excellent marker and time-stratigraphic horizons that they provide. The type section of the Strathearn Formation is in Carlin Canyon (fig. 1), approximately 40 km southeast (Dott, 1955). However, rocks assigned to this formation in the Santa Renia Fields and Beaver Peak quadrangles also include Early Permian strata that are lithologically and stratigraphically similar to an undivided sequence of rocks

described by Dott (1955) to lie conformably above the Strathearn Formation at its type section at Carlin Canyon (see below). Although Permian strata, conformably above the Strathearn Formation at Carlin Canyon, subsequently were divided by Fails (1960) into three formations—sequentially from base to top, Buckskin Mountain, Beacon Flat, and Carlin Canyon Formations. Smith and Ketner (1978) included these Permian strata as two undivided Upper and Lower Permian and Upper Pennsylvanian units in their map of the Carlin-Piñon Range area. Although Snyder (1989) and some later reconnaissance investigators in the quadrangles during the early 1990s recognized that chert-pebble conglomerate in the northern part of the Santa Renia Fields quadrangle were clastic foreland deposits (R.J. Roberts and R.J. Madrid, oral commun., 1996), many other geologists continued to believe that these rocks were an integral part of lower Paleozoic sequences because the strata were not shown separately on the regional map of Coats (1987). Nonetheless, where upper Paleozoic rocks provide a geologic record in the region, the Late Pennsylvanian and Early Permian apparently was a time of significant tectonism (see also, Marcantel, 1973).

A small number of isolated exposures of chert-pebble conglomerate assigned to the Strathearn Formation in the northern part of the Santa Renia Fields quadrangle overlie the lower Paleozoic undivided siliceous sedimentary rock unit that makes up the upper plate of the Roberts Mountains thrust (fig. 4). However, contact relations with surrounding rocks are obscure at best in this area because of generally poor exposures. Although samples from each exposure were thin sectioned, no fusulinids were found.

Rocks of the Strathearn Formation significantly expand eastwards into the Beaver Peak quadrangle in amount of areal exposure, thickness, and types of interbedded lithologies. The unit typically includes chert-pebble conglomerate near its base as well as interbedded limestone where best exposed near Beaver Peak (figs. 5 and 7A-B). The thickest sequence of the Strathearn Formation crops out on the western slopes of Beaver Peak where it includes a basal chert-pebble conglomerate, as much as 30 m thick, overlain by limestone as much as 100 m thick, and then a 200-m-thick sequence of buff to drab orange-buff, calcareous and (or) dolomitic siltstone interbedded with dolostone. Conodonts obtained from near the base of the limestone (fig. 5, loc. 10), where it is no more than 10 to 15 m thick, have an age range of Late Pennsylvanian to early Early Permian (table 1; fig. 8). The presence of a streptognathoid-hindeoid conodont biofacies indicates at least a middle shelf or deeper water depositional setting for the immediately surrounding rocks in this part of the stratigraphic section. Conodonts obtained from near the top of the sequence (fig. 5, loc. 13, 8,645-ft elevation) are latest Sakmarian-earliest Artinskian (middle Early Permian) in age (table 1; fig. 8), and represent a mesogondolellid biofacies indicative of a normal-marine, middle shelf or deeper water depositional setting, somewhat similar to locality 10 approximately 200 m lower

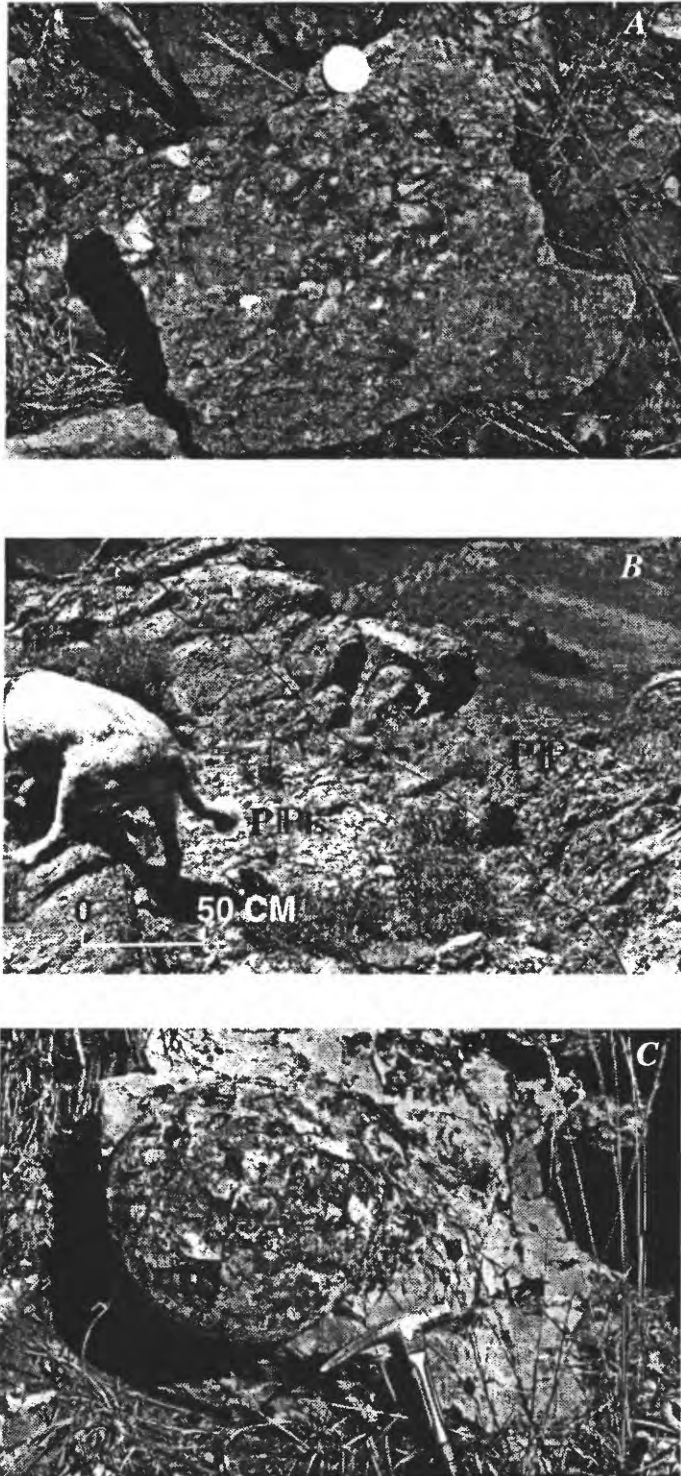


Figure 7. Photographs of Pennsylvanian and Permian Strathearn Formation. *A*, Chert-pebble conglomerate in west central part of quadrangle. Note quarter at top of photograph for scale; *B*, Lens of highly fossiliferous limestone (Pdl, loc. 6, fig. 5) interbedded with chert-pebble conglomerate (Pdc) near unconformity at base of unit; *C*, closeup view of round chert nodule in dolomitic micrite (loc. 15, fig. 5).

Table 1. Description of selected conodont samples from the Santa Renia Fields and Beaver Peak quadrangles, Nevada.

[Conodont samples collected by T.G. Theodore; conodont analyses by A.G. Harris. Map locality number keyed to figures 4 and 5; all samples from Beaver Peak quadrangle except locality 4 from Santa Renia Fields quadrangle. CAI, conodont color alteration index]

MAP LOC. NO. (FIELD NO.; USGS COLLN. NO.) LAT. N./LONG. W.	STRATIGRAPHIC UNIT AND LITHOLOGY	CONODONT FAUNA	AGE AND CAI	CONODONT BIOFACIES AND DEPOSITIONAL ENVIRONMENT	SAMPLE WEIGHT AND COMPOSITION OF HEAVY-MINERAL CONCENTRATE (HMC)
4 (97TT-28) 41°01'38"/ 116°23'14"	Vinini Formation. Blackish-gray micrite, approximately 20 cm thick, interbedded in chert sequence. Sample also contains some quartz-calcite veins.	BARREN.			1.5 kg of rock proces- sed (50 g +20 and 129 g 20- 200 mesh insoluble residue). HMC: chiefly ferruginous quartz and lesser rhombohedral dolomite.
6 (97TT-51; 33385-PC) 41°05'15"/ 116°17'25"	Strathearn Formation. Approximately 1-m-thick bed near base of chert- pebble conglomerate sequence resting on lower Paleozoic chert. Thin section contains abundant fusulinids.	<i>Streptognathodus</i> sp. 10 Pa and 3 Pb elements (small juveniles, subadults, and a few adults) (figs. 8A, B) 19 indet. bar, blade, and platform fragments	Desmoinesian-Sakmarian (Late Pennsylvanian-early Early Permian); fusulinids from same locality indicate a late Missourian age (late Late, but not latest, Pennsylvanian). 1.5-2	Indeterminate (too few generically identifiable conodonts); normal- marine depositional setting.	1.5 kg of rock proces- sed (80 g +20 and 74 g 20-200 mesh insoluble residue). HMC: chiefly anhedral and euhedral barite and lesser ferroan dolomite and composite ferruginous flakes.
7 97TT-52 41°05'11"/ 116°17'21"	Strathearn Formation. Buff-weathering dolomitic siltstone containing angular fragments of quartz and abundant Kfeldspar.	1 indet. bar or blade fragment	Ordovician-Triassic. 1.5 or 2	Indeterminate (too few conodonts).	0.5 kg of rock proces- sed (380 g +20 and 30 g 20- 200 mesh insoluble residue). HMC: composition not recorded.
8 97TT-53; 11517-CO) 41°05'29"/ 116°21'46"	Vinini Formation. Gray- brown micrite. Approximately 1 m thick, interbedded with relatively thick siltstone sequence.	Virtually all conodonts are fragments of juveniles. <i>Amorphognathus</i> sp. indet. 2 Pa (small fragments), 1 Pb, 2 Sb, and 8 bar element fragments (figs. 8O-Q) 7 <i>Panderodus</i> sp. indet. elements 1 S element <i>Paroistodus mutatus</i> (Rhodes)? <i>Periodon</i> sp. indet. 2 S element fragments (fig. 8S) 2 <i>Protopanderodus liripipus</i> Kennedy, Barnes, and Uyeno? (fig. 8R) 5 <i>Protopanderodus</i> sp. indet.	Caradocian (= middle Middle-middle Late Ordovician; = Blackriveran- middle Maysvillian). 3	Indeterminate; the taphonomy of the fauna indicates a postmortem hydraulic winnow and the species association indicates derivation from at least a middle shelf or deeper water setting.	1.5 kg of rock proces- sed (0 g +20 and 11 g 20-200 mesh insoluble residue). HMC: chiefly phosphatized composite grains and composite phosphatic ferruginous grains and flakes.
9 97TT-59 41°06'43"/ 116°15'12"	Slaven Chert(?). Brown- black micrite with abundant carbonaceous material along seams. Interbedded with thick chert sequence below tectonically overthrust package of quartzarenite.	BARREN.			1.6 kg of rock proces- sed (480 g +20 and 116 g 20- 200 mesh insoluble residue). HMC: chiefly composite ferruginous flakes and rare phosphatized composite grains and phosphatized spine steinkerns.
10 (97TT-63; 33386-PC) 41°04'58"/ 116°15'25"	Strathearn Formation. Buff-gray micrite, approximately 10-15 m thick, above basal chert- pebble conglomerate. Thin section contains abundant fusulinids.	<i>Hindeodus minutus</i> (Ellison)? 4 Pa, 2 Pb, 1 Sa, and 1 Sc elements (figs. 8E-G) <i>Streptognathodus</i> sp. 12 Pa and 1 M elements (fig. 8D) 19 indet. bar, blade, and platform fragments	Late Pennsylvanian- early Early Permian. 2	<i>Streptognathodid</i> - <i>hindeodid</i> biofacies; at least middle shelf or deeper water depositional setting.	1.2 kg of rock proces- sed (20 g +20 and 28 g 20-200 mesh insoluble residue). HMC: chiefly phosphatic brachiopod fragments and composite ferruginous flakes and grains, and minor ichthyoliths.
11 (97TT-64; 33387-PC) 41°05'11"/ 116°15'21"	Strathearn Formation. Same stratigraphic position as 97TT-63 but approximately 30 m thick at this locality. Buff-gray micrite with calcareous mud lumps and shell fragments.	<i>Streptognathodus</i> sp. indet. 4 juvenile Pa elements 1 unassigned Sc element 17 indet. bar, blade, and platform fragments	Late Pennsylvanian- early Early Permian. 1.5	Indeterminate (too few conodonts); the conodonts indicate a normal-marine depositional setting.	1.6 kg of rock proces- sed (15 g +20 and 77 g 20-200 mesh insoluble residue). HMC: chiefly phosphatic brachiopod fragments and composite dolomitic ferruginous grains.

Table 1. (continued)

MAP LOC. NO. (FIELD NO.; USGS COLLN. NO.) LAT. N./LONG. W.	STRATIGRAPHIC UNIT AND LITHOLOGY	CONODONT FAUNA	AGE AND CAI	CONODONT BIOFACIES AND DEPOSITIONAL ENVIRONMENT	SAMPLE WEIGHT AND COMPOSITION OF HEAVY-MINERAL CONCENTRATE (HMC)
12 (97TT-65) 41°05'48"/ 116°15'10"	Strathearn Formation. Dolomitic limestone with abundant angular silt- sized fragments of monocrystalline quartz. On strike with 97TT-63 and -64.	1 unassigned Sc element fragment 5 indet. bar, blade, and platform fragments	Silurian-Triassic, most probably Late Pennsylvanian-early Early Permian. 1.5-2	Indeterminate (too few conodonts).	1.8 kg of rock proces-sed (1.0 kg +20 and 85 g 20- 200 mesh insoluble residue). HMC: chiefly dolomitic and baritic composite grains and minor weathered euhedral pyrite and composite ferruginous flakes.
13 (97TT-67; 33388-PC) 41°04'40"/ 116°15'12"	Strathearn Formation. Silty to sandy sparry limestone near top of Beaver Peak and approximately 200 m stratigraphically above samples 97TT-63 to -65.	<i>Mesogondolella bisselli</i> (Clark and Behnken) 2 Pa elements (figs. 8H-J) <i>Mesogondolella</i> sp. indet. 25 Pa element fragments <i>Streptognathodus</i> sp. indet. 6 Pa element fragments <i>Sweetognathus whitei</i> (Rhodes) 4 Pa element fragments (figs. 8K-N) 1 unassigned M element 30 indet. bar, blade, and platform fragments	latest Sakmarian-earliest Artinskian (late Wolfcampian; middle Early Permian). 2.5	Mesogondolellid; normal-marine, middle shelf or deeper water depositional setting.	1.8 kg of rock proces-sed (100 g +20 and 82 g 20- 200 mesh insoluble residue). HMC: chiefly weathered pyrite euhedra, phosphatized bioclasts, phosphatic brachiopod fragments, and minor composite ferruginous grains and ichthyoliths.
14 (97TT-80) 41°04'02"/ 116°16'35"	Strathearn Formation. Drab light-gray to buff 2-m-thick sequence of silty limestone including abundant angular fragments of monocrystalline quartz.	3 indet. bar fragments	Silurian-Triassic. 1-1.5	Indeterminate (too few conodonts).	2.2 kg of rock proces-sed (1.46 kg +20 and 52 g 20- 200 mesh insoluble residue). HMC: composition not recorded.
15 (97TT-82; 33389-PC) 41°03'27"/ 116°17'31"	Strathearn Formation. Dolomitic siltstone.	<i>Streptognathodus</i> sp. indet. 1 juvenile Pa element fragment	late Morrowan-earliest Artinskian, most probably no older than Missourian (Middle Pennsylvanian- middle Early Permian, most probably no older than middle Late Pennsylvanian). 1.5-2	Indeterminate (too few conodonts).	2.7 kg of rock proces-sed (180 g +20 and 132 g 20- 200 mesh insoluble residue). HMC: chiefly barite and lesser ferruginous barite and baritized composite grains and minor dolomite.
16 (97TT-83; 33390-PC) 41°03'27"/ 116°17'20"	Strathearn Formation. Dolomitic siltstone including some rounded monocrystalline quartz sand grains. Sparry matrix partly replaced by barite.	<i>Polygnathus</i> sp. indet. 1 incomplete Pa element of Middle- Late Devonian morphotype (upper surface mostly covered by adventitious quartz grains) 1 juvenile Pa element fragment of Carboniferous-Permian morphotype 4 indet. bar, blade, and platform fragments	late Paleozoic (Late Mississippian-Early Permian) with redeposited Middle-Late Devonian conodonts. 1.5-2	Indeterminate (too few conodonts).	2.7 kg of rock proces-sed (120 g +20 and 363 g 20- 200 mesh insoluble residue). HMC: chiefly baritized composite grains and minor dolomite.
17 (97TT-84; 33391-PC) 41°03'34"/ 116°17'34"	Strathearn Formation. Sparry dolomitic siltstone rests unconformably above tectonically emplaced quartzarenite of Vinini Formation.	<i>Streptognathodus</i> sp. indet. 16 Pa element fragments (chiefly juveniles and subadults) (fig. 8C) 1 digyrate Sa element fragment 11 indet. bar, blade, and platform fragments	late Morrowan-Sakmarian, probably Missourian- Sakmarian (probably Late Pennsylvanian-early Early Permian). 1.5-2	Postmortem transport from or within the streptognathodid biofacies suggesting middle shelf or deeper water depositional setting.	4.2 kg of rock proces-sed (300 g +20 and 337 g 20- 200 mesh insoluble residue). HMC: chiefly barite and lesser phosphatic composite grains and minor dolomite.
18 (97TT-85) 41°03'39"/ 116°17'21"	Strathearn Formation. Flaggy, brown-gray dolomitic siltstone.	BARREN.			3.0 kg of rock proces-sed (2.5 kg +20 and 24 g 20- 200 mesh insoluble residue). HMC: chiefly barite, rock fragments and minor ferruginous rock fragments and composite ferruginous flakes.

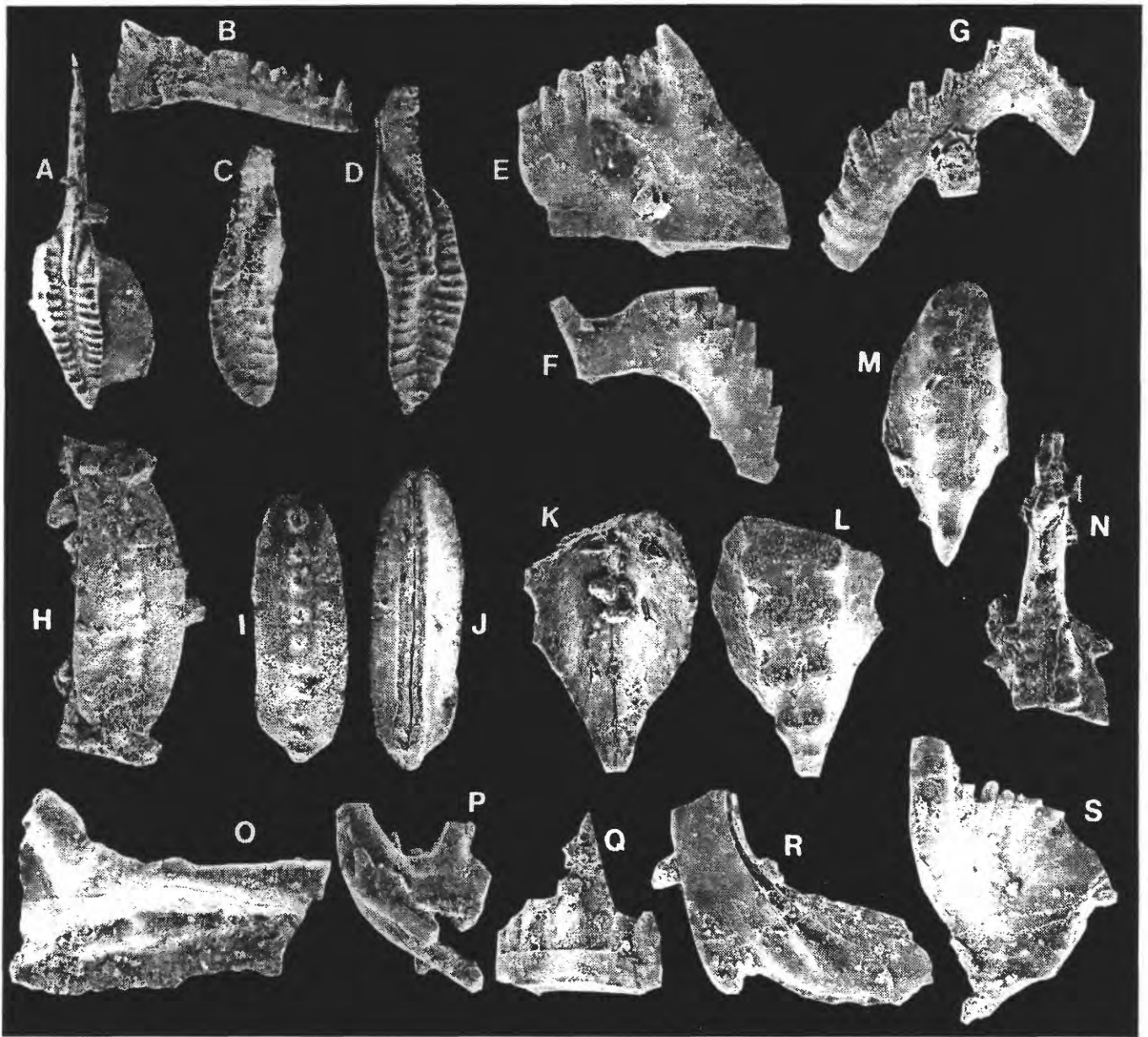


Figure 8. Scanning electron micrographs of conodonts from selected collections from the Strathearn (A-N) and Vinini (O-S) Formations (locality numbers keyed to table 1 and figs. 4 and 5). **A, B**, *Streptognathodus* sp., Pa (x35) and Pb (x50) elements, upper and inner lateral views, loc. 6 (same locality that produced late Missourian fusulinids). **C, D**, *Streptognathodus* sp., Pa elements, upper views, x50, locs. 17 and 10, respectively. **E-G**, *Hindeodus minutus* (Ellison)?, Pa, Pb, and Sa elements, two lateral and one posterior views, x75, loc. 10. **H-J**, *Mesogondolella bisselli* (Clark and Behnken), upper view of Pa element, (x50) and upper and lower views of another Pa element (x75), loc. 13. **K-N**, *Sweetognathus whitei* (Rhodes), three Pa element fragments, upper and lower views of posterior platform fragment (x100), upper view of posterior platform fragment (x100), and upper view of anterior platform fragment and free blade (x75); the presence of *M. bisselli* and *S. whitei* restrict the age of this collection to a narrow interval that straddles the Sakmarian-Artinskian boundary (late Wolfcampian of western North America). **O-Q**, *Amorphognathus* sp. indet., Pa (x75) and Sb and bar (x100) fragments, loc. 8. **R**, *Protopanderodus liripipus* Kennedy, Barnes, and Uyeno?, lateral view, x100, loc. 8. **S**, *Periodon* sp. indet., Sc element, inner lateral view, x100, loc. 8. The conodont faunule from loc. 8 is a cosmopolitan cool-water species association typical of the middle Middle to middle Late Ordovician part of the Vinini Formation.

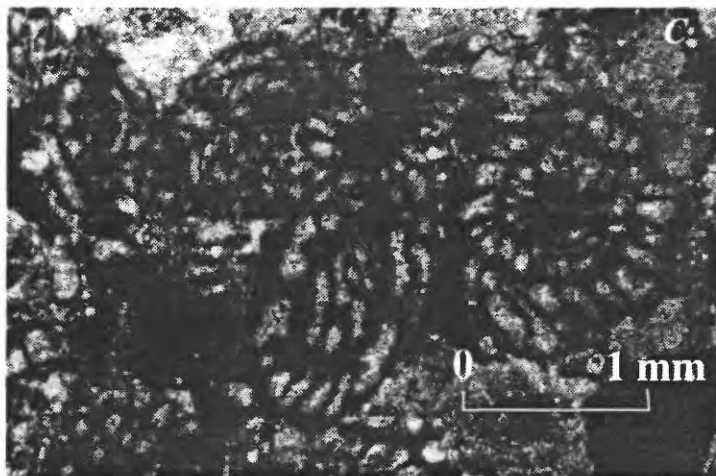
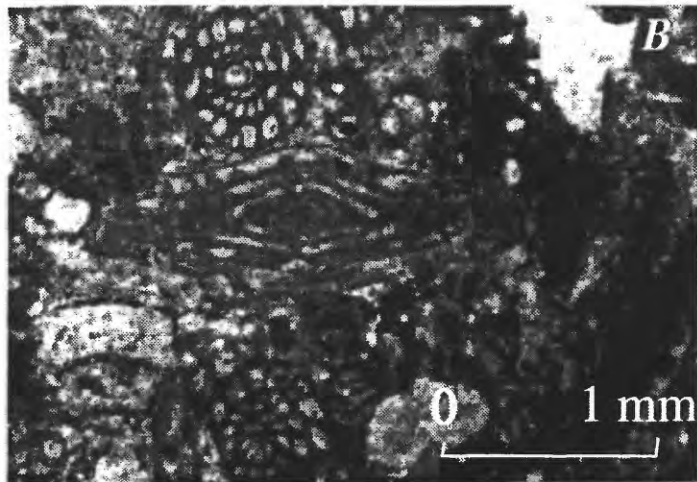
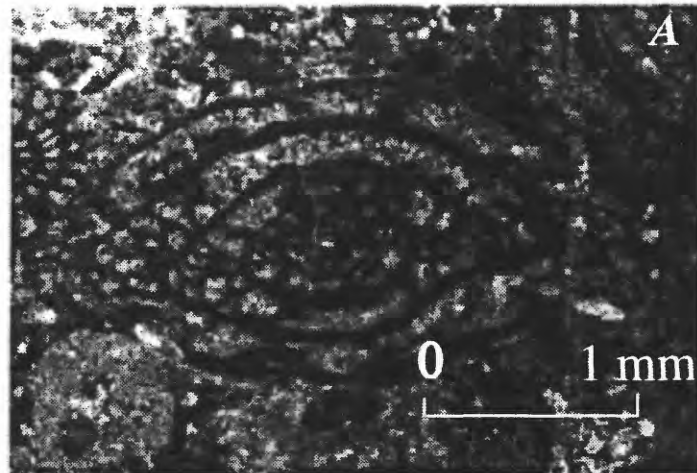


Figure 9. Photomicrographs of fusulinids from limestone lens shown in figure 7B near base of Pennsylvanian and Permian Strathearn Formation (loc. 6, fig. 5). Plane polarized light. *A*, *Triticites newelli* Burma; *B*, *Pseudofusinella* sp. cf *Pseudofusinella utahensis* Thompson; *C*, probably *Triticites newelli* Burma.

in the sequence of the Strathearn Formation near Beaver Peak. A conodont collection from dolomitic siltstone of the Strathearn Formation at locality 16 (fig. 5) includes redeposited Middle or Late Devonian conodonts together with younger conodonts. Further, rocks at locality 13 contain sparse infilling of their open spaces by low temperature, crossfiber-textured chalcedonic quartz. The conodont color alteration index (CAI) at this locality is 2.5 suggesting these rocks reached at least 100 to 125 °C (Epstein and others, 1977).

In addition, a narrow exposure of the Strathearn Formation near Hill 8026, approximately 3.5 km northwest of Beaver Peak (fig. 5, loc. 6; closeup of locality shown in fig. 7B), contains an approximately 1.5-m-thick limestone lens in a sequence of largely chert-pebble conglomerate no more than 5 m above the base of the unit. This conglomerate also contains small amounts of quartzarenite fragments. The limestone lens hosts a phenomenal concentration of fusulinids near its base in a zone of carbonate sand the upper and lower contacts of which grade into surrounding bioclastic sands that contain abundant fragments of echinoderm spines, crinoids, brachiopods, and the colonial rugose coral *Durhamina*. The latter are quite rare in Pennsylvanian sequences in the western United States. The presence of *Triticites newelli* Burma and *Pseudofusinella* cf. *P. utahensis* Thompson (fig. 9) suggests a late Missourian age (late Late, but not latest Pennsylvanian). Overall depositional environment of the limestone lens is that of a shallow shoal, and, when compared to the middle shelf environments determined for most of the overlying sequence of the Strathearn Formation, suggests a progressive deepening or drowning with time.

Petrographic examination of the dolomitic siltstone facies that makes up much of the upper part of the Strathearn Formation reveals a number of additional striking features. First, presence of low temperature silica that partly fills voids in otherwise fresh-appearing rocks, as described above, is quite unexpected. Second, buff-weathering, dark-gray dolomitic siltstone near locality 13 (fig. 5) contains roughly 10 to 15 volume percent K-feldspar as angular framework grains, together with angular quartz fragments and much less abundant detrital white mica. A source for the detritus that makes up these rocks might be an uplifted granitic terrane that is pre-Late Pennsylvanian in age. However, another possible source is the Silurian Elder Sandstone in the nearby Roberts Mountains allochthon. Near the Ren Mine, these rocks contain abundant detrital grains of white mica and some K-feldspar.

Stratigraphic relations of the Late Pennsylvanian and Early Permian (Missourian to Wolfcampian) Strathearn Formation in Carlin Canyon provide important controls on late Paleozoic history of the region that impact our interpretations of geologic relations of the formation in the Santa Renia Fields and Beaver Peak quadrangles. The strata

of the Strathearn Formation are as much as 300 m thick in Carlin Canyon and rest on a spectacularly exposed 15°– to 30°-angular unconformity developed on underlying Late Mississippian through Middle Pennsylvanian (Meramecian through Desmoinesian) rocks belonging to the Tonka, Moleen, and Tomera Formations of Dott (1955). Most of the Tonka Formation is considered to be part of the Mississippian Newark Valley sequence of Trexler and Nichtman (1990) and Trexler and Cashman (1991), who found an important unconformity in the Mississippian Diamond Peak Formation in the Diamond Mountains (fig. 1; see also, Silberling and others, 1997). The Strathearn Formation in Carlin Canyon mostly includes “quartz-silty limestones, and thin commonly cross-bedded, chert granule and pebble conglomerate,” which are notably rich in fusulinids in the lower and upper sequences of the formation (Dott, 1955, p. 2,248). The lower strata of the formation contain several species of *Triticites*. On top of the Strathearn Formation near Carlin Canyon, Dott (1955, p. 2,256) described the undivided, conformably overlying, approximately 300-m-thick Permian sequence as “grayish yellow-weathering, calcareous siltstones, and fine sandstone, generally very poorly exposed in grassy slopes.” This sequence of Permian rocks is lithologically similar to the upper part of the clastic foreland sequence included with the Strathearn Formation in the Beaver Peak quadrangle, and is best exposed on the west slopes of Beaver Peak (see above).

Jansma and Speed (1990) questioned the presence of an unconformity at the base of the Strathearn Formation in Carlin Canyon (fig. 1), and others, as described below, have shown that the rocks are variably deformed below the Strathearn Formation, suggesting that the base of the Strathearn Formation is a low-angle fault of probable Mesozoic age, and that the Humboldt orogeny of Ketner (1977) primarily involved vertical tectonics. We will present evidence in the next section that widespread largely horizontal tectonism in the Santa Renia Fields and Beaver Peak quadrangles is indeed associated with the Humboldt orogeny. Ketner (1998) further points out that faults are ubiquitous in the region and that the unconformity at the base of the Strathearn Formation in Carlin Canyon may in fact be faulted locally. It would not be surprising that some minor shearing may have occurred along the unconformity in response to north-south shortening associated with the Coyote thrust (see below), or with any other subsequent structural event. Snyder and others (1997) recorded low-angle thrust faults and map-scale fault propagation folds at Carlin Canyon to be especially concentrated in middle Paleozoic rocks and that strata younger than Middle Pennsylvanian are less deformed. Peters and others (1996) and Peters (1997) described similar styles of deformation in the same general area—northeast-striking fault zones with chaotic geometries and truncated northeast-trending monoclines—as being concentrated in the Middle Pennsylvanian Tomera Formation and the Middle and Lower Pennsylvanian Moleen Formation of Dott (1955). These

deformation events appear to have predated emplacement of the Coyote thrust in the Santa Renia Fields and Beaver Peak quadrangles because the dislocations are present only in rocks beneath the pre-Strathearn unconformity.

Allochthonous Rocks above the Coyote Thrust

Ordovician rocks belonging to the Vinini Formation as well as Silurian rocks apparently comprise an allochthonous package of rocks that was emplaced tectonically along the Coyote thrust onto rocks of the Strathearn Formation and its underlying undivided siliceous sedimentary rock unit (figs. 4–6). The Coyote thrust is a generally east-west-striking structure that is highly disrupted by later high-angle faults in the Santa Renia Fields quadrangle, where much of its trace has been covered by Tertiary and Quaternary unconsolidated deposits. The upper plate of the Coyote thrust actually comprises two major structural packages that apparently were coevally emplaced into the area—a lower one made up mostly of quartzarenite belonging to the Vinini Formation and marked by the Coyote thrust as its sole, and an upper one which has the Squaw Creek thrust at its base (figs. 4 and 5). The Coyote thrust is envisioned as forming the master dislocation surface along which regional (see below) horizontal dislocations occurred. Rocks in the upper plate of the Coyote thrust are referred to as the Coyote nappe by Cluer and others (1997).

Confirmation of presence of a major thrust fault in the area involving late Paleozoic rocks of the clastic foreland resulted from a number of investigations. First documented occurrence of an older-over-younger sequence in western facies siliceous units in this general area was verified in conodont collections obtained from Barrick's diamond drill hole BX-1 which was collared near the northwest corner of the Santa Renia Fields quadrangle (fig. 4; E.A. Lauha, oral commun., 1994). In this hole, an age reversal between 300– and 800–m depths places rocks containing conodonts of latest Llandoveryan age (middle Early Silurian) on top of rocks containing early Late Devonian conodonts (N.R. Stamm and A.G. Harris, written commun., 1994, to J. Zimmerman and G.L. Griffin). Subsequently, large-scale mapping by S.B. Keith (written commun., 1997) in the northern part of the quadrangle confirmed that the Coyote thrust can be recognized in outcrop. Concurrently, mapping by the senior author (Theodore and others, unpub. data, 1998) verified that Ordovician rocks unquestionably are structurally above chert-pebble conglomerate of the Strathearn Formation near the east edge of the Santa Renia Fields quadrangle where a narrow sliver of the conglomerate crops out low on a hillside beneath quartzarenite of the Vinini Formation. Moreover, continued mapping farther to the east-southeast across much of the northern half of the Beaver Peak quadrangle during 1997 revealed numerous unequivocal, probably even more convincing geologic relations wherein the Ordovician

quartzarenite unit has been emplaced structurally along a relatively shallow-dipping surface above conglomerate of the Strathearn Formation (fig. 10A–B). This fault, in places, also is well exposed in the northeast part of the Beaver Peak quadrangle where it crops out as a planar, shallow-dipping fault between Ordovician quartzarenite and the underlying Ordovician, Silurian, and Devonian undivided siliceous sedimentary rock unit (fig. 10C).

Rocks in the upper plate of the Coyote thrust are largely Ordovician in age. The Ordovician age of quartzarenite structurally widespread above conglomerate of the Strathearn Formation is confidently assigned on the basis of Middle Ordovician graptolites identified by S.C. Finney (written commun. to J.K. Cluer, 1997) including *Cryptograptus schaeferi*, *Glossograptus* sp., *Nemagraptus* sp., (?)*Leptograptus*, and *Pseudoclimacograptus* sp. at locality 5 (fig. 5) in shale interbedded in green chert and quartzarenite in allochthonous rocks about 30 m above the trace of the Coyote thrust. In addition, at locality 8 (fig. 5), an approximately 1–m-thick limestone bed, which is present in a fault sliver of siltstone apparently dropped into the surrounding Ordovician, Silurian, and Devonian undivided siliceous sedimentary rock unit, contains a Caradocian (middle Middle to middle Late Ordovician) conodont faunal assemblage (table 1 and figs. 8O–S).

The Coyote thrust is a regional tectonic feature. To the west-northwest, quartzarenite in the upper plate of the Coyote thrust may comprise the paleotopographic high beneath Tertiary volcanic rocks at the Hollister Mine in the Ivanhoe Mining District described by Bartlett and others (1991) (see also, Wallace and John, this volume). To the east, the Coyote thrust extends across the entire Beaver Peak quadrangle as a relatively gently north-dipping surface that has been variably offset along a number of high-angle late Paleozoic, Mesozoic(?), and Tertiary normal faults. The southernmost leading edge of the thrust crops out approximately 4 km southwest of Beaver Peak (fig. 5). To the north of Tuscarora, Nev., the Coyote thrust probably also is present in a block of Paleozoic rocks largely surrounded by middle Tertiary volcanic rocks (see below).

Ordovician quartzarenite in the upper plate of the Coyote thrust may have been emplaced into the basin where Upper Pennsylvanian and Lower Permian rocks of the Strathearn Formation were being deposited on the basis of relations at localities 15 and 17 (fig. 5). Rocks of the Strathearn Formation are present tectonically below a thin sheet of Ordovician quartzarenite (loc. 15) as well as being present positionally on the quartzarenite (loc. 17). This relation tightly constrains emplacement of allochthonous rocks in the upper plate of the Coyote thrust to sometime during deposition of rocks of the Strathearn Formation in this area—Upper Pennsylvanian and Early Permian (fig. 8; see map locality nos. 15 and 17, table 1, for specific conodont descriptions and ages at these localities). According to the geologic time scale of Harland and others

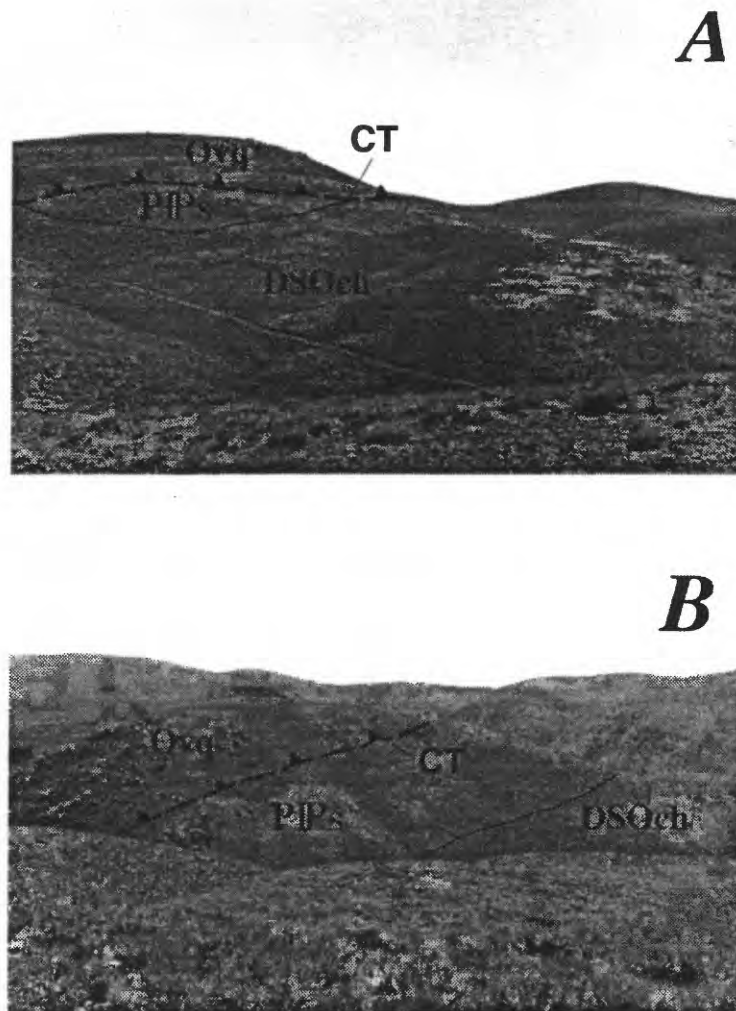


Figure 10. Photographs showing geologic relations in Beaver Peak quadrangle, Nev. *A*, View to north near east edge of quadrangle showing trace of Coyote thrust. Quartzarenite (Ovq) of the Ordovician Vinini Formation makes up upper plate and Pennsylvanian and Permian Strathearn Formation (Pds) as well as undivided Ordovician, Silurian, and Devonian chert and shale unit (DSOch) make up lower plate; *B*, view to southeast near south-central part of figure 5 showing trace of Coyote thrust between upper plate quartzarenite of Vinini Formation (Ovq) and lower plate Strathearn Formation (Pds) which, in turn, rests unconformably on undivided chert and shale unit (DSOch).

(1989), this allows an interval of approximately 18 m.y. during deposition of the Strathearn Formation in this area. In addition, Smith and Ketner (1977) postulated that the unconformity at the base of the Strathearn Formation in Carlin Canyon represents a time interval of about 6 m.y. Thus, tectonism during development of the unconformity and thrusting has a maximum time interval of about 24 m.y. to have occurred, which we believe is more than sufficient. Kerr

(1962) and Coats and Riva (1983) also described a number of east-west thrusts that involve overlap assemblage rocks farther to the north. However, Coats (1987) had suggested that the Humboldt orogeny be downgraded to a "disturbance" on the basis of relatively minimal volumes of Upper Pennsylvanian and Permian clastic rocks present in the region, but structural and depositional relations described herein provide further evidence that crustal shortening involved significant horizontal

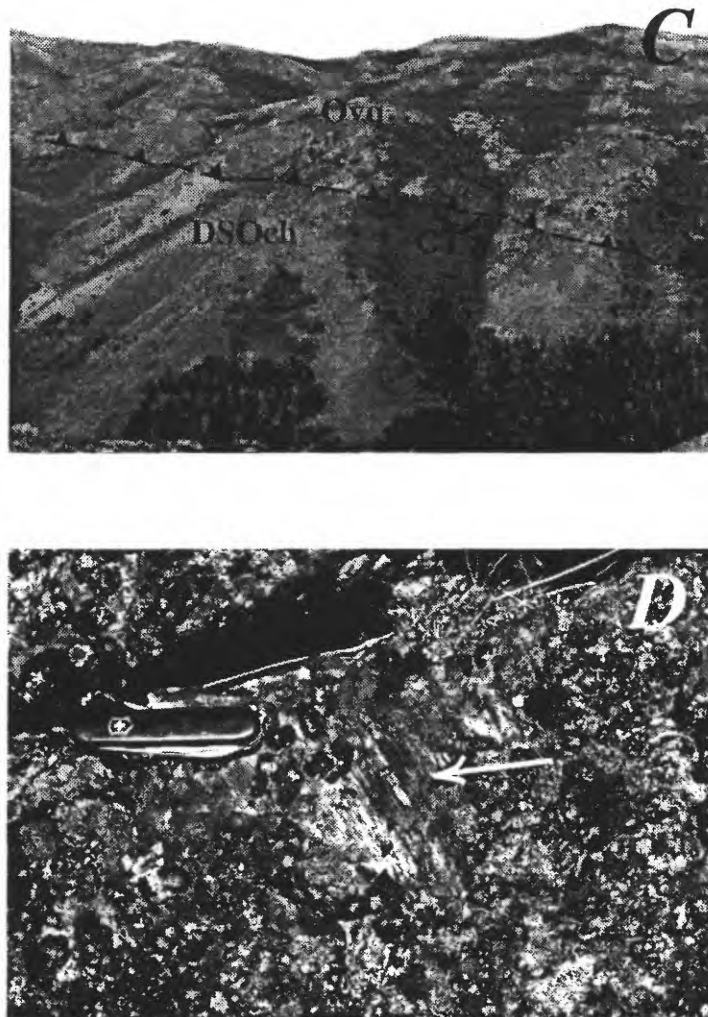


Figure 10 (cont'd)—*C*, view to southwest near the northeast corner of quadrangle showing trace of Coyote thrust (CT) between upper plate quartzarenite of Vinini Formation (Ovq) and undivided chert and shale unit (DSOch); *D*, Close up view of stickensides (at head of arrow) near trace of Coyote thrust near west edge of quadrangle.

transport during the late Paleozoic Humboldt orogeny of Ketner (1977).

The Squaw Creek thrust, the trace of which is inferred to be about 2 km north of the Coyote thrust in the Santa Renia Fields quadrangle, is an east-west-striking imbricate thrust structurally higher than, but temporally related to the late Paleozoic Coyote thrust (fig. 4). As shown in the Beaver Peak quadrangle, the undivided allochthon of the Squaw Creek thrust includes a structurally complex package of Ordovician and

(or) Devonian mostly undivided siliceous rocks as well as probable Silurian Elder Sandstone (fig. 5). Many of these rocks are present in the upper plate of the Squaw Creek thrust in blocks of rock bounded by high-angle normal faults. Reconnaissance excursions north into the Sugarloaf Butte quadrangle (fig. 1) suggest that the upper plate of the Squaw Creek thrust contains a number of quartzarenite- and chert-rich packages bounded by additional imbricate thrust faults associated with the Squaw Creek and the Coyote thrusts.

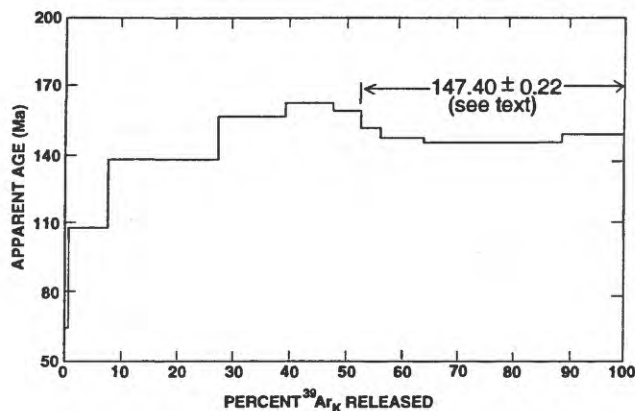


Figure 11. $^{40}\text{Ar}/^{39}\text{Ar}$ age spectrum for biotite from informally named Arturo dike at Dee Mine. Sample no. 94B50/49/DD58. Modified from L.W. Snee (written commun., 1997).

Jurassic(?) Dikes

A number of igneous dikes, inferred to be Jurassic(?) on the basis of lithologic similarities with other radiometrically dated igneous rocks along the Carlin trend, crop out in the Santa Renia Fields and Beaver Peak quadrangles, but most are too small to show at the scale of our maps (figs. 4 and 5). Many dikes of various composition and texture also have been encountered in drill holes during exploration programs in the quadrangles. Although in places intensely altered, many dikes have fabrics with common euhedral aligned biotite or amphibole phenocrysts. This suggests that the dikes are varieties of lamprophyres, or lamprophyric microdiorites in the terminology of Orobona (1996), which are quite common in the northern Carlin trend (M.W. Ressel and D.C. Noble, written commun., 1998). Arehart and others (1993) established a Jurassic age (157.2 to 158.1 Ma) for emplacement of the Goldstrike stock (fig. 3), and its roughly coeval lamprophyre dikes also are Jurassic (157 to 165.7 Ma) (M.W. Ressel and D.C. Noble, written commun., 1998). During the Jurassic magmatic event, dikes were intruded parallel to the trend, and several large Jurassic plutons have been emplaced into it south of the Betze gold orebody (fig. 3). On the basis of granodiorite sills of the Goldstrike pluton that have been folded along with the Tuscarora Spur anticline in the Genesis deposit, Orobona (1996) concluded that development of major northwest-trending folds in the Carlin trend resulted from Mesozoic compression. A prominent dike is present in the open pit of the Dee Mine and has been informally referred to as the Arturo dike—biotite yielded an apparent 132 ± 5 -Ma age by the K-Ar method (A. Lande, written commun., 1994). Another biotite sample from this dike examined by $^{40}\text{Ar}/^{39}\text{Ar}$ techniques yields a highly disturbed age spectrum that has a maximum plateau at an apparent age of 162 Ma on a percent ^{39}ArK released versus apparent age diagram (fig. 11; L.W. Snee, written commun., 1997 to W.E. Brooks). The apparent

age calculated from the last six heating steps is 147.40 ± 0.22 Ma. Thus, the dike is apparently Jurassic in age, similar to ages of some other igneous rocks elsewhere along the trend.

Cursory petrographic studies were conducted on igneous rocks from below the Dee Mine, below the Ren Mine, and two dikes southeast of Boulder Creek (fig. 5). Four of five intensely clay-altered narrow dikes from a drill hole between 330- and 510-m-depths collared in the Dee Mine were examined, and they show a variety of poorly preserved textures suggestive of emplacement either as porphyritic lamprophyres or as felsic granite (*sensu lato*). The dikes are extremely porous and contain abundant secondary calcite—only vague shadows remain in thin section indicative of the former presence of primary biotite. Some also are intensely silicated. Sparse pyrite is present as fine-grained crystals locally concentrated in clots. Those dikes assumed to be some type of felsic granite probably are variants of the somewhat fresher alkali granite or monzonite dikes in the Beaver Peak quadrangle (see below). Six porphyritic dikes encountered below the Ren Mine between depths of 370 and 570 m in one drill hole and two dikes at 1,050-m and 1,110-m depths in another—although generally altered intensely to carbonate mineral(s), low-temperature quartz, clay, and pyrite, as well as sparse white mica and barite assemblages—show diagnostic fabrics that suggest all the dikes originally were emplaced as part of the clinopyroxene-biotite lamprophyre clan described elsewhere along the Carlin trend (M.W. Ressel and D.C. Noble, written commun., 1998). Phenocrystic quartz is absent from the dikes examined below the Ren Mine. However, because of widespread presence of secondary carbonate mineral(s), it is impossible to ascertain former presence of olivine, primary carbonate minerals, plagioclase, or K-feldspar, if any, whereby proper assignment of the dikes within the lamprophyre clan of Rock (1991) might be made. In the classification scheme of Mitchell and Bergman (1991), they would be termed minettes. However, most phenocrystic clinopyroxene has been altered to carbonate mineral(s). Where unaltered, aligned brown-to-red brown small biotite grains are quite abundant and impart a felted aspect to the groundmass; clinopyroxene is best preserved just interior to chilled margins of narrow dikes. Contacts with surrounding wallrocks are either intensely brecciated and partly filled by small sparse clots of pyrite, or they form knife-edge contacts with marble which contains much less than 1 volume percent pyrite near the dikes.

Two dikes exposed in the Beaver Peak quadrangle, southeast of Boulder Creek (fig. 5), also are presumed to be Jurassic(?)—they apparently are petrographically similar to some of the dikes observed at the Dee Mine (see above). These dikes are present in an approximately 1.5-km-long, S 20° E-trending zone of altered and fractured rocks of the Strathearn Formation, which also apparently contain some secondary arsenate minerals. Mineralogically, these medium-grained dikes show highly variable compositions, ranging from K-feldspar-rich alkali granite to monzonite containing clouded

and crowded laths of oligoclase and K-feldspar. Narrow seams of yellow limonite±iron-oxide mineral(s) as well as white mica are common. The dikes are inferred to have been emplaced along a zone of weakness developed subparallel to the main Carlin trend.

The Jurassic emplacement age for the dike at the Dee Mine should not be assumed necessarily to be the age of the mineralizing event there. Circulation of fluids associated with introduction of gold may have occurred long after intrusion of the dike. Two altered dikes encountered near mineralized zones deep in the Rodeo Creek gold-mineralized area, approximately 3 km northwest of the Dee Mine (fig. 4), have yielded 30-Ma and 40-Ma fission-track ages on apatite grains (A.M. Grist and M. Zentilli, written commun., 1998).

Northeast-striking Sinistral Faults

Three major sets of northeast-striking faults are present in the Santa Renia Fields and Beaver Peak quadrangles (figs. 4 and 5). One has significant sinistral separations along its trace, and the others are inferred to have initially broken with similar senses of displacement. The faults comprise a southwesterly-stepped en echelon fault set that, from west to east, include the Rossi fault, the Boulder Creek fault, and the Toro fault, the latter deriving its name from its fault segment along Toro Canyon near the northeast corner of the Beaver Peak quadrangle. The northeast-striking faults have a distinct geomorphic expression (fig. 12), and appear to parallel three major strands of a 20-km-wide set of linear features recognized by Peters (this volume) on Landsat imagery and called the Crescent Valley-Independence Lineament (CVIL). This feature extends northeast from the general area of the Pipeline gold deposits near Gold Acres (fig. 1), passes through the Carlin trend south of the Pete deposit, and finally reaches the gold deposits near Jerritt Canyon in the Independence Mountains, a distance of roughly 90 km. In addition, a large number of northeast-striking faults are present throughout the northern Carlin trend (fig. 3), many of which were instrumental in localizing gold-mineralized rocks either along their traces or in the immediately adjoining wallrocks.

The Boulder Creek fault, whose geomorphic expression defines the northwesternmost strand of the Crescent Valley-Independence Lineament (fig. 2), is a prominent northeast-striking fault close to the west edge of the Beaver Peak quadrangle. It has an approximate 0.8 km sinistral separation of the unconformity at the base of the Strathearn Formation (fig. 5). The magnitude of this separation cannot be accounted for by reasonable separations associated with normal displacements along west-dipping segments of the fault. Near the west edge of the quadrangle, northeast-striking zones of cataclastically brecciated rocks as much as 30 m wide are present along the trace of the Boulder Creek fault. Farther to the northeast, the Boulder Creek fault shows a sinistral

separation of the trace of the Coyote thrust of only roughly 0.2 km. These relations suggest that horizontal displacements along northeast-striking faults in the area may be quite old, and may be related to the Humboldt orogeny. They may even predate final emplacement of the Coyote allochthon, which is inferred to have been active some time during the Late Pennsylvanian and Early Permian (see above). Near the Dee Mine, Greybeck (1985) suggested that the northeast-striking faults are the oldest of the various fault sets that he recognized, whereas Snyder (1989) believed that northeast-striking faults near the Rossi Mine are the youngest. Displacements also probably occurred repeatedly along the northeast-striking faults and many other faults in the area in response to regional shortening during the Mesozoic and recurrent extension during the Tertiary. For instance, the dextral separations of the Ren antiform along northeast-striking faults near the southeast corner of the Santa Renia Fields quadrangle may be due to a regional stress regime related to Tertiary extension. The dextral separations may have focused along zones of weakness developed previously under an entirely different regional stress regime.

Miocene Rocks and Miocene Unconsolidated Deposits

Miocene rocks and Miocene unconsolidated deposits in the Santa Renia Fields quadrangle include several varieties of mostly rhyolite flows and minor intrusive rhyolite, as well as the overlying largely unconsolidated Carlin Formation—much of this section is modified from Fleck and others (this volume) (fig. 4). Although these rocks and unconsolidated deposits generally are considered to post-date mineralized rocks along the Carlin trend, their geology, nonetheless, is important because of what might be inferred about underlying strata. Miocene rhyolite porphyry that was informally named the Craig rhyolite by Bartlett and others (1991) in the Ivanhoe Mining District, 5 km to the northwest, extends into the west part of the Santa Renia Fields quadrangle where it is overlain by a 30-m- to 50-m-thick basal tuff unit of the Carlin Formation that includes thin beds of partly welded tuff and lesser amounts of siltstone, mudstone, and gravel. W.E. Brooks (written commun., 1997) reports an $^{40}\text{Ar}/^{39}\text{Ar}$ incremental-heating plateau age of 15.03 ± 0.05 Ma for rhyolite porphyry from a locality just to the west in the adjacent Willow Creek Reservoir SE quadrangle near Antelope Creek.

The Carlin Formation crops out widely in the west and north parts of the Santa Renia Fields quadrangle where moderately good exposures have allowed determination of the stratigraphy of these largely unconsolidated deposits. The Carlin Formation originally was defined by Regnier (1960) for a sequence of mostly unconsolidated silts, sands, fanglomerate, and pyroclastic rocks that overlie Ordovician to Miocene(?) strata in the vicinity of Carlin, Nev. In that area

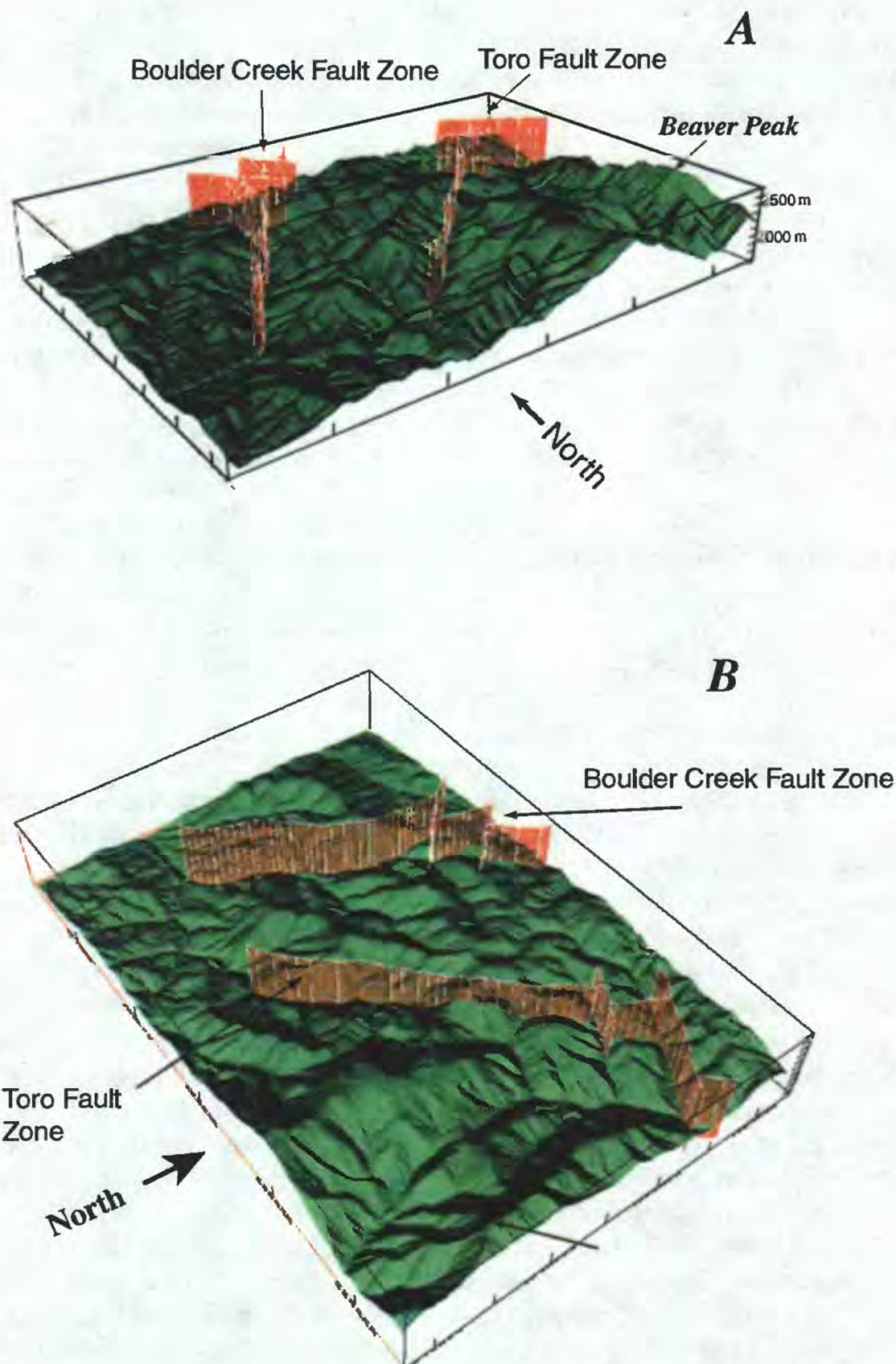


Figure 12. Oblique block diagram showing topographic expression of the Boulder Creek and Toro faults in the Beaver Peak quadrangle, Nev. Digital geomorphometric analysis prepared by R.J. Miller and B.C. Moring.

the Carlin Formation is approximately 130–200 m thick (Regnier, 1960). Originally thought to be entirely Pliocene in age (Regnier, 1960), on the basis of vertebrate fossils collected approximately 5 km northeast of Carlin, the strata were assigned a late Miocene and (or) Pliocene age by Evans and Cress (1972), a Pliocene age by Evans (1974a), and a Miocene and Pliocene age by Evans (1974b). In the west part of the Santa Renia Fields quadrangle, the Carlin Formation has been divided into four units, but, in the northeast part of the

quadrangle, the formation also includes an undivided unit (fig. 4). The basal tuff unit of the formation in the west part of the quadrangle is overlain by as much as 400 m of mostly unconsolidated silts, sands, and sedimentary breccia, as well as abundant volcanic ash and air-fall tuff (see also, Fleck and others, this volume). Bedded air-fall tuff crops out prominently throughout the quadrangle as either horizontal or gently dipping sequences; most exposed sequences are horizontal and ample evidence is present in the form of pisolites and abundant

worm burrows to indicate subaqueous deposition, probably lacustrine. Roadcuts through the formation reveal that many well-layered sequences of air-fall tuff are broken by high-angle normal faults that have separations of as much as 1 to 1.5 m. Where the air-fall-tuff-rich unit laps unconformably onto lower Paleozoic rocks, an underlying, thin, yellow-brown, sandy silt or massive olive-brown mudstone is present. In places, the underlying units form mud lumps in beds of gray-white, air-fall tuff. Thin beds of granitic debris, possibly derived from the Jurassic Goldstrike stock (fig. 3), also are present locally in the air-fall-rich sequence. The tuff-bearing unit is overlain, in turn, by poorly exposed mostly unconsolidated silts and sands that are conspicuously free of air-fall tuff. All of these units are overlain with a slight angular discordance by unconsolidated fanglomerate deposits, typically as much as 130 m thick and locally as much as 600 m thick. They appear to have been derived principally from Paleozoic rocks in the area of Beaver Peak. Twelve $^{40}\text{Ar}/^{39}\text{Ar}$ laser-fusion ages, obtained from alkali-feldspar-bearing air-fall tuffs in the formation, range from 14.4 to 15.1 Ma (Fleck and others, this volume).

Near the Ren Mine, two elongate areas of outcrop of an extremely thick fanglomeratic facies of the Carlin Formation, the uppermost unit of the four units recognized in the area, show apparent partial closure around the Ren antiform (fig. 4). The fanglomerate roughly follows bedding in the unconformably underlying Vinini Formation giving the appearance that the fanglomerate deposits were folded along with the underlying rocks. However, actually the fanglomerate deposits apparently were deposited in narrow channels that partly followed zones of weakness and faulting in the previously folded underlying rocks, which channels then acted as foci for debris being shed from the east during uplift of the entire Ren-Beaver Peak tectonic block. These channels were the conduits for a wide area of thick fanglomerate deposits that extend southwest into the northern parts of the Sheep Creek Range (Wallace and John, this volume). Some faults probably were active during deposition of the fanglomerate deposits, as well as possibly during uplift of the Ren antiform, indicated by locally extreme thickness of fanglomerate relative to its narrow width of outcrop; in places the fanglomerate is reported to be as much as 600 m thick. Indeed, many normal faults in the area now bounding unconsolidated deposits of the Carlin Formation and Paleozoic bedrock must have had senses of early displacement different from the last major movements recorded along them. Lastly, as described in Fleck and others (this volume) quartz adularia veins locally cut some sequences of the Carlin Formation, mostly along joints and fractures, suggesting that circulation of potentially gold-bearing fluids continued during the Miocene.

HUMBOLDT OROGENY AND NORTHEAST-STRIKING FAULTS IN THE CARLIN TREND

Geometric relations suggest a direct genetic link among

three major structural phenomena in the quadrangles: (1) north-south shortening associated with south-directed thrust faults of the late Paleozoic Humboldt orogeny, (2) northeast-striking sinistral shear faults along the Crescent Valley-Independence Lineament zone, and (3) a roughly N 40° W-trending dilational zone of crustal weakness along the Carlin trend of gold deposits. These three phenomena are consistent with a regional shortening or compressive tectonic regime the maximum principal paleostress direction of which was oriented roughly north-south and near horizontal during the late Paleozoic Humboldt orogeny (fig. 2). Although a sense of displacement has not been determined for the southern part of the Crescent Valley-Independence Lineament zone south of the Carlin Mine (Peters, this volume), if we assume that this segment of the zone also was due to sinistral shear, then the most logical interpretation for the Carlin trend is that it represents a dilational jog between two major strands of the zone (fig. 2). We do not suggest that the Carlin trend entirely represents only a dilational jog caused by northeast-southwest extension without any accompanying shear. Rather, the northwest orientation is envisioned as representing an ancestral zone of weakness that subsequently focused shear strains at various times as orientation of prevailing regional stress directions shifted periodically during subsequent Mesozoic and Tertiary events. These events converged along the northern Carlin trend primarily because it had earlier become a zone of crustal weakness.

Yet, why did the jog occur where it did? The answer to this perplexing question may lie in deep crustal structures that reside in crystalline basement. Rodriguez (1997) has shown from magnetotelluric soundings that a deep structure may underlie the lower Paleozoic miogeocline along the Carlin trend. The presence of such a structure also is suggested by the lead-isotope data of Wooden and others (this volume). Thus, regional sinistral shear along the northernmost strand of the Crescent Valley-Independence Lineament may have stepped to the southeast when it encountered a preexisting structural break in crystalline basement near the present trace of the Carlin trend. Indeed, part of the northwest orientation of outcrop-scale fold axes along the Carlin trend (Peters, 1996) may have resulted from a counterclockwise sense of rotation along the Carlin trend during development of the regional sinistral shear couple that involved reactivated parts of the northeast-trending Crescent Valley-Independence Lineament (fig. 2). Left-lateral sense of shear along northwest-striking axial planes of mesoscopic folds that plunge shallowly to the northwest and southeast along the Carlin trend (Peters, 1996) also is compatible with such a regional interpretation. Further, presence of Jurassic plutons and dikes parallel to the Carlin trend suggests that it existed as a dilational zone at the time of their emplacement. Previously, Gillett and Karlin (1996) speculated that many structures along the Carlin trend may be late Paleozoic, and Dean (1991) proposed, on the basis of fracture-pattern distribution in the southern part of the Carlin trend, that divergent dextral wrench faulting might account for the linearity of distribution of gold

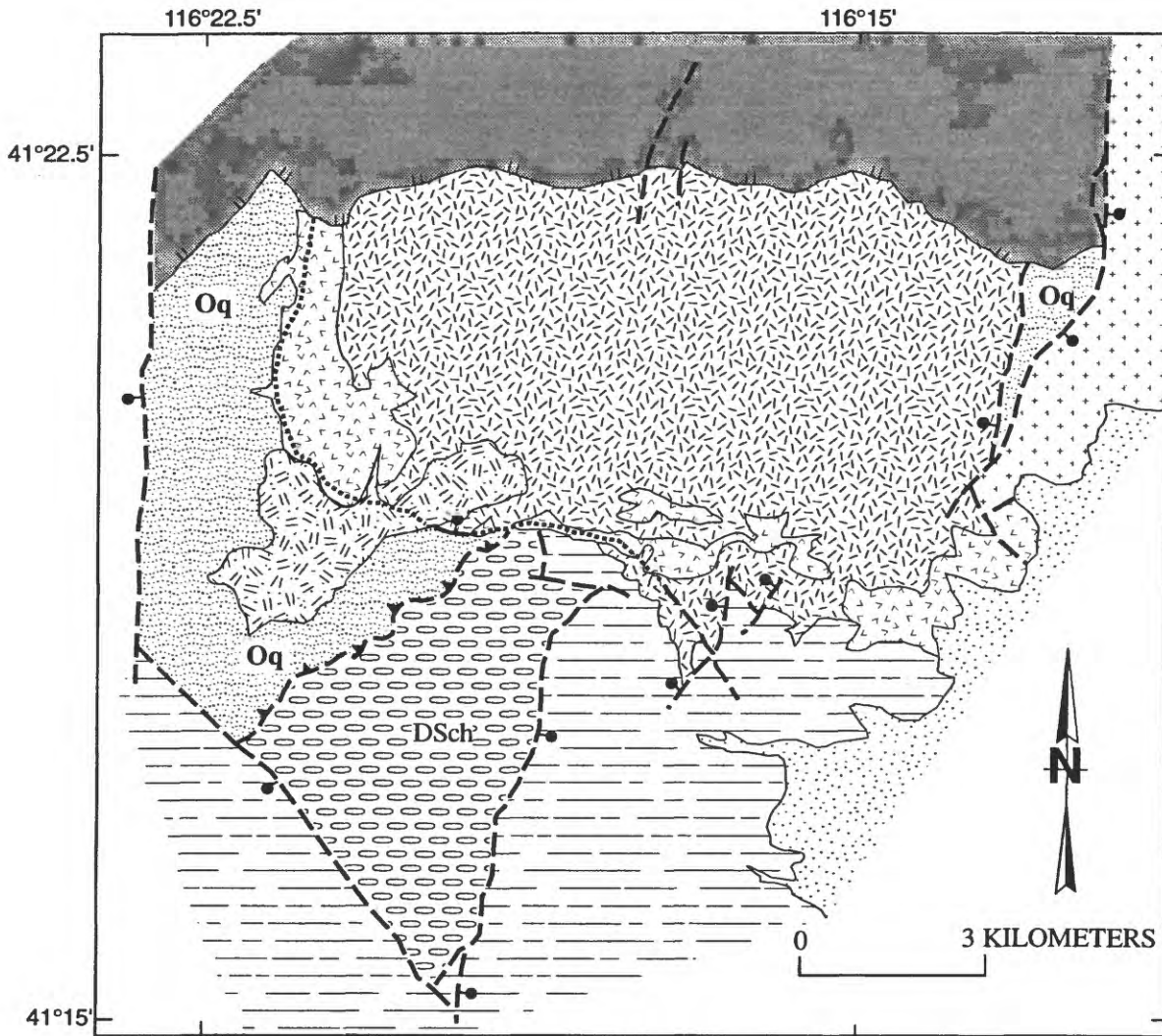
deposits along the entire trend.

Geologic relations are prevalent throughout many mountain ranges in northeastern Nevada that north-south shortening may have begun during the late Paleozoic Humboldt orogeny and may have continued into the Jurassic. As we described above, late Paleozoic rocks of the clastic foreland in the Santa Renia Fields and Beaver Peak quadrangles are overlain structurally by siliceous western assemblage Ordovician rocks of the Vinini Formation, which make up the lowermost structural package in the Coyote thrust, as well as additional structurally higher imbricate packages of rock such as above the Squaw Creek thrust (see above). Generally south-directed thrusting associated with the Humboldt orogeny was completed in this area during Late Pennsylvanian and Early Permian time. In addition, south-verging tightly overturned folds well away from the trace of the Coyote thrust attest to the district-scale pervasive character of deformation associated with north-south shortening (see above).

Evidence is widespread in northeastern Nevada for generally north-south shortening from the Independence Mountains in the north to the Piñon Range in the south (fig. 1). In the Independence Mountains, as well as in the Adobe Range east of the northern Carlin trend (fig. 1), rocks as young as Early Triassic were involved in north-south shortening (Ketner, 1987; Ketner and Smith, 1982; Ketner and Alpha, 1992; Ketner and others, 1993; Ketner, 1998), possibly at the time of the Jurassic Elko orogeny of Thorman and others (1990). In the Mount Blitzen area, approximately 35 km to the north in the Tuscarora Mountains, a major thrust fault between Ordovician quartzarenite and lower plate Silurian and Devonian chert and siltstone sequence mapped by Henry and Boden (1997; see also, this volume) may be a correlative with the Coyote thrust (fig. 13). These relations were interpreted as showing "outcrop-scale thrust faults, all in the southern package, [which] dip gently to the northwest, and slickenlines on striated surfaces on the quartzite pods trend mostly northwest or southeast. All these data are consistent with major shortening with transport toward the southeast" (C.D. Henry, written commun., 1997). Near the Gold Quarry Mine (fig. 2), Cole (1995) determined that the principal compressive stress had a near-horizontal, north-northeast orientation during generation of the northeast-striking Gold Quarry fault, which apparently is a fault segment coplanar with one of the major strands of the Crescent Valley-Independence Lineament (fig. 14). In addition, the Gold Quarry fault has a sinistral sense of displacement (Cole, 1995), which is compatible with the sinistral sense of displacements that we infer dominated the early tectonic history of the Crescent Valley-Independence Lineament. In the area of Carlin Canyon, Jansma and Speed (1990) describe the presence of an isoclinal recumbent fold in Pennsylvanian limestone and conglomerate below the Strathearn Formation that they believe is related to shear faulting toward the southeast. At the Rain gold deposit, approximately 30 km south of Carlin, Nev. (fig. 1), north-

dipping low-angle thrust faults are present in the Devonian Woodruff Formation, and they apparently show vergence to the south (J. Schilling, L. Shallow, and T. Thompson, written commun., 1998). However, the Rain fault—a N 60° W-striking structure that dips 50–70° southwest (Longo and Williams, 1997)—also may have formed during the Humboldt orogeny on the basis of two lines of evidence. First, its fault geometry is identical to other high-angle reverse faults of late Paleozoic age in the Piñon Range, being the youngest shortening structure in the area that cuts rocks of the Mississippian Newark Valley sequence. The only difference is that the dip of the Rain fault is to the southwest rather than to the northeast, or it is more like a back thrust. Second, bedding attitudes are reoriented near the fault from their generally regional northward strikes. This characterizes bedding as it approaches all other late Paleozoic faults and folds in the Ferdelford Creek area of the Piñon Range, Nev., approximately 60 km southeast of the Santa Renia Fields and Beaver Peak quadrangles (fig. 15). In this area, the Mississippian Newark Valley sequence also is cut by east-northwest, north-dipping thrust faults that must have a component of north-south shortening. These faults also cut rocks correlative with the Strathearn Formation. Silberling and others (1997) described roughly north-south shortening that is reflected in a broad open syncline that involves undivided Pennsylvanian and Permian rocks belonging to the foreland sequence in the Papoose Canyon area of the Piñon Range (fig. 16). Also in the northern Piñon Range, Smith and Ketner (1977) described a number of late Middle to early Late Pennsylvanian anticlines, synclines, and thrust faults, some of the folds showing a significant north-south component of shortening.

Direct linkage during tectonism between regional-scale low-angle thrust faults and high-angle strike-slip faults has been reported elsewhere in the Great Basin. Morris (1983) showed that the northeast-striking Leamington transcurrent fault in the central Sevier orogenic belt of west-central Utah is directly related to a number of thrust lobes. As pointed out by Morris (1983), wrench faults or strike-slip faults (see also, Wilcox and others, 1973) that result primarily from horizontal compression or shortening should develop as conjugate pairs. We do not know of a readily identifiable companion to the Crescent Valley-Independence Lineament. However, a throughgoing northwest-trending linear feature, the northern Nevada rift (NNR) (Zoback and others, 1994; Wallace and John, this volume), passes along the west edge of the Sheep Creek Range approximately 40 km west of the Crescent Valley-Independence Lineament at a latitude of 40°45' (fig. 16). Although it is widely known that the NNR is related primarily to Miocene extension (Zoback and others, 1994), deformation along a "proto" NNR may be much older. On the basis of admittedly somewhat tenuous evidence, including its geometric relation with the Crescent Valley-Independence Lineament and the presence of ductile-style northwest shear zones in lower Paleozoic rocks parallel to its trace in the Shoshone Range,



- | | | | |
|--|--|---------------------|--|
| | Gravel, unconsolidated (Quaternary) | | Mostly quartzite (Ordovician) |
| | Lavas of Sixmile Canyon (Eocene) | THRUST FAULT | |
| | Granodiorite of Mount Neva (Eocene) | | Mostly chert (Devonian and Silurian) |
| | Early dacite of Mount Neva intrusive episode (Eocene) | | Contact |
| | Tuff of Big Cottonwood Canyon (Eocene) | | High-angle fault—Dashed where approximately located; dotted where concealed. Bar and ball on downthrown side |
| | Tuff of Mount Blitzen, including dacite domes (Eocene) | | Thrust fault—sawteeth on upper plate. Dashed where approximately located |
| | Dacite and andesite of Pleasant Valley volcanic complex (Eocene) | | Caldera margin |

Figure 13. Simplified geologic sketch map of southeastern part of Tuscarora, Nev., volcanic field showing northeast-striking trace of thrust fault between upper plate Ordovician mostly quartzarenite unit (cq) and lower plate Silurian and Devonian mostly chert unit (cch). Modified from Henry and Boden (1997) and C.D. Henry (unpub. data, 1998).

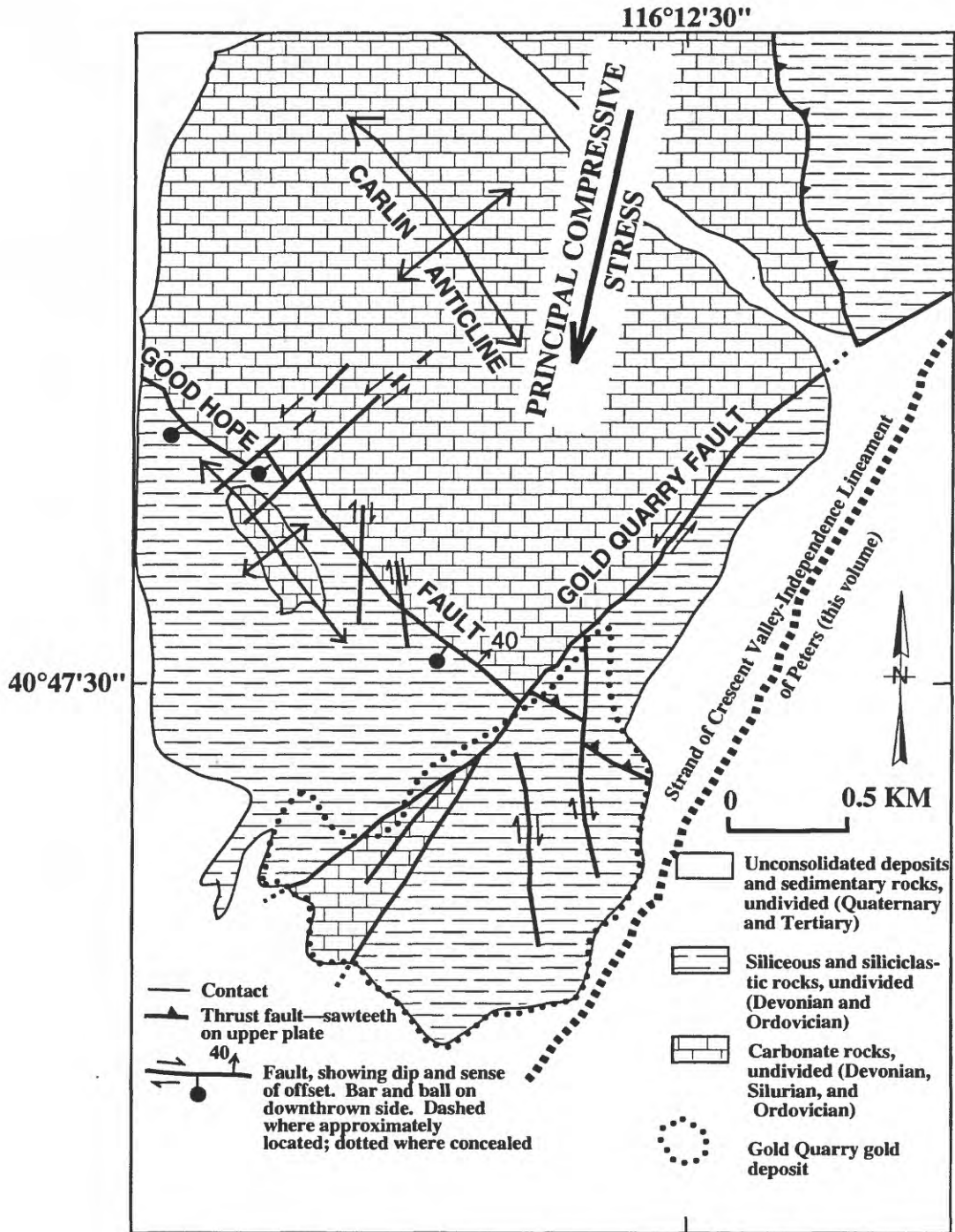


Figure 14. Inferred structural model for area around Gold Quarry gold deposit, Nev. Modified from Cole (1995).

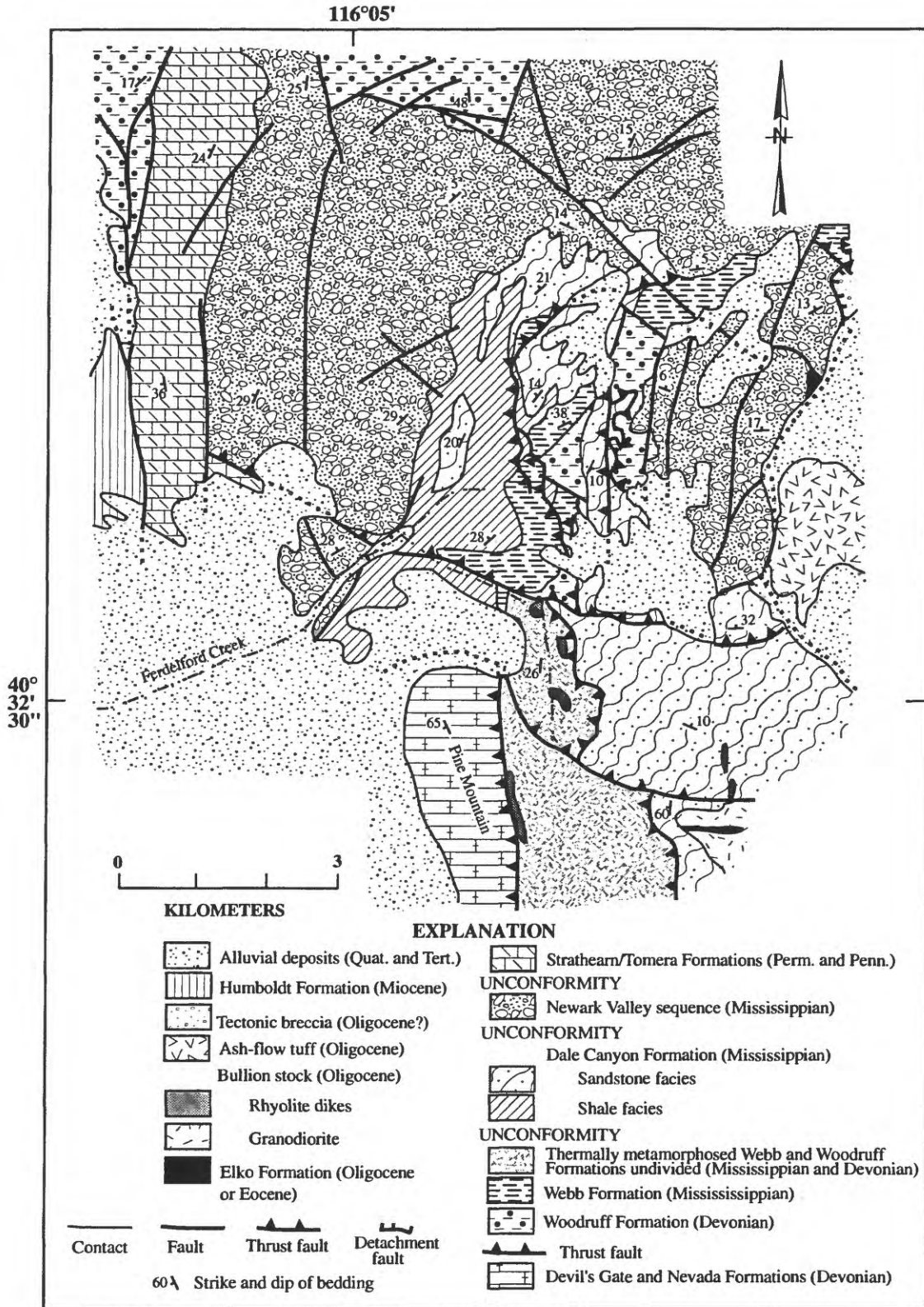


Figure 15. Geologic sketch map of the Ferdelford Creek area, Piñon Range, Nev., showing east-southeast striking thrust faults that cut the Mississippian and Pennsylvanian Newark Valley sequence. Modified from R.M. Tosdal (unpub. data, 1998).

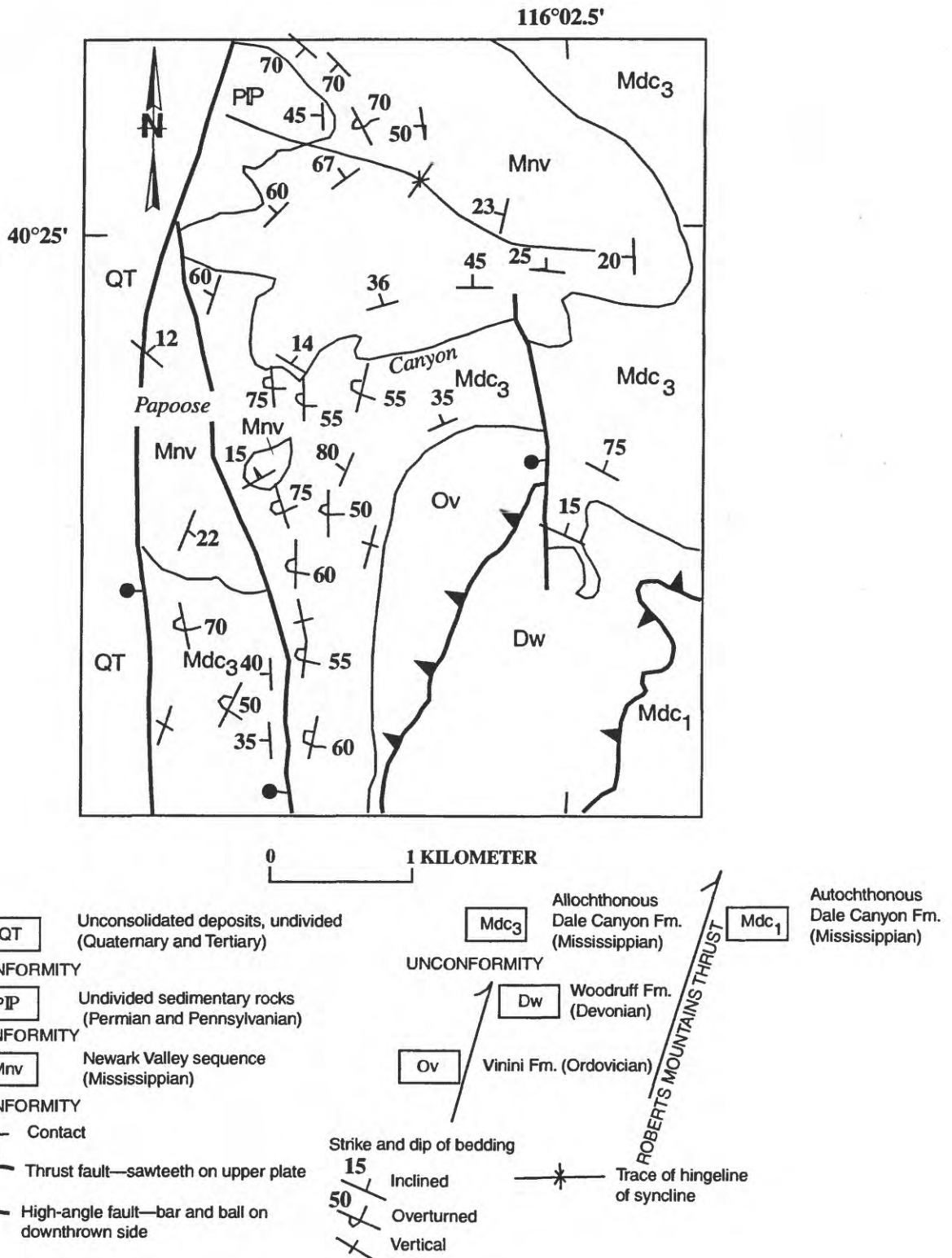


Figure 16. Simplified geologic sketch map of area around Papoose Canyon near west flank of Piñon Range, Nev., showing roughly east-west trending hingeline for fold involving rocks as young as Pennsylvanian and Permian (unit Pd). Modified from Silberling and others (1997).

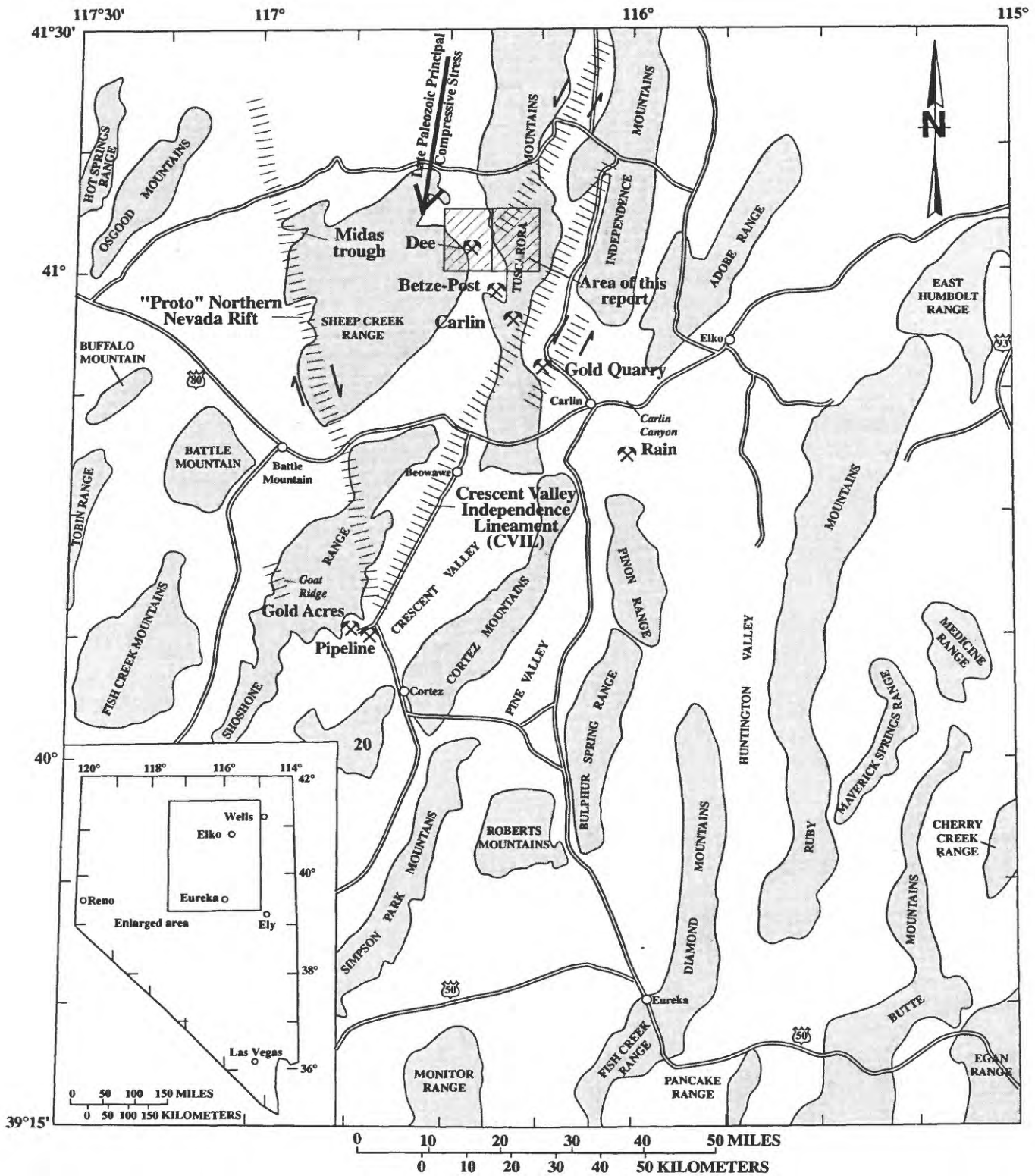


Figure 17. Summary diagram showing location of Crescent Valley Independence-Lineament (CVIL) of Peters (this volume), "proto" northern Nevada rift ("proto" NNR), and inferred senses of transcurrent dislocations. Locations of major mines discussed in text also shown, as is the inferred orientation of late Paleozoic, regional principal paleostress associated with formation of the CVIL and the "proto" NNR.

we suggest that orientation of the NNR is compatible with its including late Paleozoic right-lateral shear as a conjugate to the Crescent Valley-Independence Lineament.

In places, quite intense deformation occurred along both the NNR and the Crescent Valley-Independence Lineament. Gravity variations produced by pre-Tertiary basement show a prominent gravity gradient, a deep crustal fault zone, that coincides with the trace of the NNR—they do not show, however, a comparable gradient along the Crescent Valley-Independence Lineament (Jachens and Moring, 1990; Grauch and others, 1995; Ponce, 1997). Paleozoic rocks in the Tenabo area of the northern Shoshone Range have a strong north-northwest structural grain (Wrucke, 1974; C.T. Wrucke, unpub. data, 1998). Miogeoclinal rocks exposed in the lower plate of the Roberts Mountains allochthon at Goat Ridge in the Shoshone Range, albeit approximately 20 km from the trace the NNR (fig. 1), also include prominent northwest-striking shear fabrics that parallel the NNR (Prihar and others, 1996). Where the Crescent Valley-Independence Lineament and the NNR are projected to intersect near the Gold Acres and Pipeline gold deposits in the Shoshone Range (fig. 17), structural fabric of the rocks is dominated by northwest- and northeast-striking fault sets parallel to the trends of the NNR and the Crescent Valley-Independence Lineament (Foo and others, 1996). With regards to magnitude of overall shear along the major faults that comprise these inferred conjugate shear zones along the “proto” NNR and Crescent Valley-Independence Lineament, we speculate that it probably measures at most several km, and that it is highly unlikely to amount to as much as tens of km. Other geological evidence in the Cortez, Nev., area (fig. 17) indicates as much as approximately 5 km of right-lateral separation along the trace of the present-day NNR (J.K. Cluer, written commun., 1998; see also, McCormack and Hays, 1996). In the Cortez area, McCormack and Hays (1996) determined that the Cortez-Pipeline fault, which parallels the NNR, apparently shows approximately 5 km dextral offset of lower Paleozoic carbonate rocks and Jurassic igneous rocks after closure of Miocene extension across Crescent Valley. Rocks broken along the “proto” NNR undoubtedly ruptured subsequently again mostly in the Miocene as extension culminated during the time interval 14 to 17 Ma.

If these speculations concerning direct linkages between the Crescent Valley-Independence Lineament and a “proto” NNR have any merit, then it is appropriate for us to speculate further that a companion to the Carlin trend may be present somewhere along the NNR. However, because of inferred dextral shear along the “proto” NNR (see above), an analogous dilation jog there should have an orientation of about N. 40° E. prior to late Miocene extension, as opposed to the N. 40° W. trend of the Carlin trend (fig. 17). The Midas trough, a

zone of east-northeast trending late Tertiary grabens in Tertiary volcanic rocks (Wallace, 1991; Wallace and John, this volume), is present along the NNR at the latitude of the presently known northwest terminus of the Carlin trend (fig. 17). If the “proto” NNR involved dextral shear, the Midas trough may be a preferred site for prior development of a dilation jog in underlying pre-Tertiary basement, in particular where horsts are present in Miocene volcanic rocks near east-northeast grabens.

CONCLUSIONS

Critical to our structural syntheses in the Santa Renia Fields and Beaver Peak quadrangles has been documentation that Upper Pennsylvanian and Lower Permian rocks of the Strathearn Formation extend into the area, and that these rocks have been involved in what appears to be regionally extensive north-south shortening associated with the late Paleozoic Humboldt orogeny. A major thrust in the area, the Coyote thrust, places Ordovician rocks of the Vinini Formation on top of the Strathearn Formation, and the upper plate of the Coyote thrust includes a number of north-dipping imbricate thrust surfaces. Some south-verging tightly overturned folds also are present in deformed rocks in the lower plate of the Coyote thrust. Similar styles of deformation with similar orientations of their folds and thrust surfaces are present elsewhere in many northeastern Nevada mountain ranges, and the structures may have continued to form as late as the Jurassic Elko orogeny. North-south shortening also may have been directly associated with development of transcurrent sinistral shear along the northeast-trending Crescent Valley-Independence Lineament deformation zone. Early deformation of lower Paleozoic strata along the site of the future Carlin trend of gold deposits is inferred to include a dilational jog between two major fault strands that constitute the Crescent Valley-Independence Lineament. Finally, if a companion northwest-striking shear conjugate to the Crescent Valley-Independence Lineament is present in northern Nevada, then a likely site is the present trace of the northern Nevada rift, which we suggest may have included right-lateral shear also during the late Paleozoic. Subsequent to all these events, Paleozoic rocks in the northern Carlin trend show evidence of Mesozoic east-west shortening and emplacement of Jurassic and later plutons and dikes into the dilational jog, and Tertiary east-west extension. Tertiary extension is manifest by large numbers of faults of various orientations, and by largely unconsolidated deposits of the Miocene Carlin Formation, including widespread air-fall tuff that is 15 to 14 Ma and that partly fills narrow pull-apart basins as much as 800 m deep.

REFERENCES CITED

- Albino, G.V., 1994, Geology and litho-geochemistry of the Ren gold prospect, Elko County, Nevada—the role of rock sampling in exploration for deep Carlin-type deposits: *Journal of Geochemical Exploration*, v. 51, p. 37–58.
- Arehart, G.B., 1996, Characteristics and origin of sediment-hosted disseminated gold deposits: a review: *Ore Geology Reviews*, v. 11, no. 6, p. 383–403.
- Arehart, G.B., Foland, K.A., Naeser, C.W., and Kesler, S.E., 1993, $^{40}\text{Ar}/^{39}\text{Ar}$, K/Ar, and fission track geochronology of sediment-hosted disseminated gold deposits at Post-Betze, Carlin trend, northeastern Nevada: *Economic Geology*, v. 88, p. 622–646.
- Armstrong, A.K., Theodore, T.G., Kotlyar, B.B., Lauha, E.A., Griffin, G.L., Lorge, D.L., and Abbott, E.W., 1997, Preliminary facies analysis of Devonian autochthonous rocks that host gold along the Carlin trend, Nevada, in Vikre, Peter, Thompson, T.B., Bettles, Keith, Christensen, Odin, and Parratt, Ron, eds., Carlin-type gold deposits field conference: Society of Economic Geology Guidebook Series, v. 28, p. 53–73.
- Armstrong, A.K., Theodore, T.G., Oscarson, R.L., Kotlyar, B.B., Harris, Anita, Bettles, K.H., Lauha, E.G., Hipsley, R.A., Griffin, G.L., Abbott, E.W., and Cluer, J.K., (this volume), Preliminary facies analysis of Silurian and Devonian autochthonous rocks that host gold along the Carlin trend, Nevada, in Tosdal, R.M., ed., Contributions to the gold metallogeny of northern Nevada: U.S. Geological Survey Open-File Report.
- Baker, E.D., 1991, Geology and ore deposits of the Bootstrap subdistrict, Elko County, Nevada, in Raines, G.L., Lisle, R.E., Schafer, R.W., and Wilkinson, W.H., eds., Geology and ore deposits of the Great Basin, Symposium Proceedings: Reno, Nevada, Geological Society of Nevada, p. 619–623.
- Bartlett, M.W., Enders, M.S., and Hruska, D.C., 1991, Geology of the Hollister gold deposit, Ivanhoe district, Elko County, Nevada, in Raines, G.L., Lisle, R.E., Schafer, R.W., and Wilkinson, W.H., eds., Geology and ore deposits of the Great Basin, Symposium Proceedings: Reno, Nevada, Geological Society of Nevada, p. 957–978.
- Berger, B.R., 1986, Descriptive model of carbonate-hosted Au–Ag, in Cox, D.P. and Singer, D.A., eds., Mineral deposit models: U.S. Geological Survey Bulletin 1693, p. 175.
- Christensen, O.D., 1996, Carlin trend geologic overview, in Peters, S.G., Williams, C.L., and Volk, Jeff, Field trip guidebook for Trip B—Structural geology of the Carlin trend, in Green, S.M., and Struhsacker, Eric, eds., Field Trip Guidebook Compendium: Reno, Nevada, Geological Society of Nevada, Geology and ore deposits of the American Cordillera, p. 147–156.
- 1997, Western region gold deposits project evaluation, in Theodore, T.G., ed., 1997, Annual report of the Western Region Gold Project for fiscal year 1997: U.S. Geological Survey Administrative Report, Appendix 1, p. 69–74.
- Cluer, J.K., Cellura, B.R., Keith, S.B., Finney, S.C., and Bellert, S.J., 1997, Stratigraphy and structure of the Bell Creek nappe (Antler orogen), Ren property, northern Carlin trend, Nevada: Reno, Nevada, Nevada Petroleum Society, 1997 Fall Field Trip Guide, p. 41–54.
- Coats, R.R., 1987, Geology of Elko County: Nevada Bureau of Mines and Geology Bulletin 101, 112 p.
- Coats, R.R., and Riva, J.F., 1983, Overlapping overthrust belts of late Paleozoic and Mesozoic ages, northern Elko County, Nevada, in Miller, D.M., Todd, V.R., and Howard, K.A., eds., Tectonic and stratigraphic studies in the eastern Great Basin: Geological Society of America Memoir 157, p. 305–327.
- Cole, D.M., 1995, Structural evolution of the Gold Quarry deposit and implications for development, Eureka County, Nevada: Fort Collins, Colorado, Colorado State University, M.S. thesis, 79 p.
- Dean, D.A., 1991, Geologic overview of the southern extension of the Carlin trend, in Buffa, R.H., and Coyner, A.R., eds., Geology and ore deposits of the Great Basin: Reno, Nevada, Geological Society of Nevada, Field Trip Guidebook Compendium, v. 1, p. 85–93.
- Dobra, J.L., 1997, The U.S. gold industry 1996: Nevada Bureau of Mines and Geology, Special Publication 21, 32 p.
- Dott, R.H., Jr., 1955, Pennsylvanian stratigraphy of Elko and northern Diamond Ranges, northeastern Nevada: American Association Petroleum Geologists Bulletin, v. 39, no. 11, p. 2,211–2,305.
- Emmons, S.F., 1877, Region north of the Humboldt River, in King, Clarence, Report of the U.S. Geological Exploration of the Fortieth Parallel: U.S. Army Engineer Department Professional Paper 18, Descriptive Geology v. 2, p. 590–617.
- Epstein, A.G., Epstein, J.B., and Harris, L.D., 1977, Conodont color alteration—an index to organic metamorphism: U.S. Geological Survey Professional Paper 995, 27 p.
- Ettner, D.C., 1989, Stratigraphy and structure of the Devonian autochthonous rocks, north-central Carlin trend of the southern Tuscarora Mountains, northern Eureka County, Nevada: Pocatello, Idaho, Idaho State University, M.S. thesis, 177 p.
- Evans, J.G., 1974a, Geologic map of the Welches Canyon quadrangle, Eureka County, Nevada: U.S. Geological Survey Geological Quadrangle Map GQ-1117 [scale 1:24,000].
- 1974b, Geologic map of the Rodeo Creek NE quadrangle, Eureka County, Nevada: U.S. Geological Survey Geological Quadrangle Map GQ-1116 [scale 1:24,000].
- Evans, J.G., and Cress, L.D., 1972, Preliminary geologic map of the Schroeder Mountain quadrangle, Nevada: U.S. Geological Survey Miscellaneous Field Studies Map MF-324, 1 sheet [scale 1:24,000].
- Evans, J.G., and Ketner, K.B., 1971, Geologic map of the Swales Mountain quadrangle and part of the Adobe Summit quadrangle, Elko County, Nevada: U.S. Geological Survey Miscellaneous Geologic Investigations MF-324 [scale 1:24,000].
- Evans, J.G., and Mullens, T.E., 1976, Bootstrap window, Elko and Eureka Counties: U.S. Geological Survey, Journal of Research, v. 4, p. 119–125.
- Evans, J. G., and Theodore, T.G., 1978, Deformation of the Roberts Mountains allochthon in north-central Nevada: U.S. Geological Survey Professional Paper 1060, 18 p.
- Fails, T.G., 1960, Permian stratigraphy at Carlin Canyon, Nevada: American Association of Petroleum Geologists Bulletin, v. 44, no. 10, p. 1,692–1,703.
- Fleck, R.J., Theodore, T.G., Sarna-Wojcicki, Andrei, and Meyer, C.E., (this volume), Age an possible source of air-fall tuffs of the Miocene Carlin Formation, northern Carlin trend, in Tosdal, R.M., ed., Contributions to the gold metallogeny of northern Nevada: U.S. Geological Survey Open-File Report.
- Foo, S.T., Hays, R.C., Jr., and McCormack, J.K., 1996, Geology and mineralization of the Pipeline gold deposit, Lander County, Nevada, in Coyner, A.R., and Fahey, P.L., eds., Geology and ore deposits of the American Cordillera: Geological Society of Nevada Symposium Proceedings, Reno/Sparks, Nevada, April,

- 1995, v. 1, p. 111–121.
- Gillett, S.L., and Karlin, R.E., 1996, Possible implications of regional late Paleozoic chemical remagnetization for mineralization in the Great Basin and vicinity, *in* Coyner, A.R., and Fahey, P.L., eds., *Geology and ore deposits of the American Cordillera: Geological Society of Nevada Symposium Proceedings*, Reno/Sparks, Nevada, April, 1995, v. 1, p. 679–686.
- Gilluly, James, and Gates, Olcott, 1965, Tectonic and igneous geology of the northern Shoshone Range, Nevada: U.S. Geological Survey Professional Paper 465, 153 p.
- Gilluly, James, and Masursky, Harold, 1965, Geology of the Cortez quadrangle, Nevada: U.S. Geological Survey Bulletin 1175, 117 p.
- Grauch, V.J.S., Jachens, R.C., and Blakely, R.J., 1995, Evidence for a basement feature related to the Cortez disseminated gold trend and implications for regional exploration in Nevada: *Economic Geology*, v. 90, no. 1, p. 203–207.
- Greybeck, J.D., 1985, Geology of the Dee Mine area, Elko County, Nevada: Moscow, Idaho, University of Idaho, M.S. thesis, 101 p.
- Hardie, B.S., 1966, Carlin gold mine, Lynn District, in AIME Pacific Southwest Mineral Industry Conference, Sparks, Nevada, Papers: Nevada Bureau of Mines Report 13, Part A, p. 73–83.
- Harland, W.B., Armstrong, R.L., Cox, A.V., Craig, L.E., Smith, A.G., and Smith, D.G., 1989, *A geologic time scale 1989*: New York, Cambridge University Press, 263 p.
- Henry, C.D., and Boden, D.R., 1997, Eocene magmatism of the Tuscarora volcanic field, Elko County, Nevada, and implications for Carlin-type mineralization, *in* Vikre, Peter, Thompson, T.B., Bettles, Keith, Christensen, Odin, and Parratt, Ron, eds., *Carlin-type gold deposits field conference: Society of Economic Geology Guidebook Series*, v. 28, p. 193–202.
- Jachens, R.C., and Moring, B.C., 1990, Maps of the thickness of Cenozoic deposits and the isostatic residual gravity over basement for Nevada: U.S. Geological Survey Open-File Report 90–404, 15 p.
- Jansma, P.E., and Speed, R.C., 1990, Omissional faulting during Mesozoic regional contraction at Carlin Canyon, Nevada: *Geological Society of America Bulletin*, v. 102, no. 4, p. 417–427.
- Kerr, J.W., 1962, Paleozoic sequences and thrust slices of the Seetoya Mountains, Independence Range, Elko County, Nevada: *Geological Society of America Bulletin*, v. 73, p. 439–460.
- Ketner, K.B., 1977, Deposition and deformation of lower Paleozoic western facies rocks, northern Nevada, *in* Stewart, J.H., Stevens, C.H., and Fritsche, A.E., eds., *Paleozoic paleogeography of the western United States: Pacific Coast Paleogeography Symposium 1*: Los Angeles, Society of Economic Paleontologists and Mineralogists, Pacific Section, p. 251–258.
- , 1987, Post-Early Triassic, pre-middle Eocene folds and thrust faults, northern Adobe Range, Nevada: *Geological Society of America Centennial Field Conference, Cordilleran Section*, no. 21, p. 91–94.
- , 1998, The nature and timing of tectonism in the western facies terrane of Nevada and California—an outline of evidence and interpretations derived from geologic maps of key areas: U.S. Geological Survey Professional Paper 1592, 19 p.
- Ketner, K.B., and Alpha, A.G., 1992, Mesozoic and Tertiary rocks near Elko, Nevada—evidence for Jurassic to Eocene folding and low-angle faulting: U.S. Geological Survey Bulletin 1988–C, 13 p.
- Ketner, K.B., Murchey, B.L., Stamm, R.G., and Wardlaw, B.R., 1993, Paleozoic and Mesozoic rocks of Mount Ichabod and Dorsey Canyon, Elko County, Nevada—evidence for post Early Triassic emplacement of the Roberts Mountains and Golconda allochthons: U.S. Geological Survey Bulletin 1988–D, 12 p.
- Ketner, K.B., and Smith, J.F., Jr., 1982, Mid-Paleozoic age of the Roberts thrust unsettled by new data from northern Nevada: *Geology*, v. 10, p. 298–303.
- Lapointe, D.D., Tingley, J.V., and Jones, R.B., 1991, Mineral resources of Elko County, Nevada: Nevada Bureau of Mines and Geology Bulletin 106, 236 p.
- Longo, A., and Williams, C., 1997, Rain underground deposit, *in* Teal, Lewis, and Jackson, Mac, *Geologic overview of the Carlin trend gold deposits and descriptions of recent deep discoveries*, *in* Vikre, Peter, Thompson, T.B., Bettles, Keith, Christensen, Odin, and Parratt, Ron, eds., *Carlin-type gold deposits field conference: Society of Economic Geology Guidebook Series*, v. 28, p. 30–32.
- Marcantel, J.B., 1973, Upper Pennsylvanian and Lower Permian sedimentation in northeast Nevada: Columbus, Ohio, Ohio State University, Ph.D. dissertation, 112 p.
- McCormack, J.K., and Hays, R.C., Jr., 1996, Crescent Valley: A model for reconstruction of district mineralization in the Basin and Range, *in* Coyner, A.R., and Fahey, P.L., eds., *Geology and ore deposits of the American Cordillera: Geological Society of Nevada Symposium Proceedings*, Reno/Sparks, Nevada, April, 1995, v. 2, p. 635–646.
- Merriam, C.W., 1940, Devonian stratigraphy and paleontology of the Roberts Mountains region, Nevada: *Geological Society of America Special Paper* 25, 114 p.
- Merriam, C.W., and Anderson, C.A., 1942, Reconnaissance survey of the Roberts Mountains, Nevada: *Geological Society of America Bulletin*, v. 53, p. 1,675–1,728.
- Mitchell, R.H., and Bergman, S.C., 1991, *Petrology of lamproites*: New York, Plenum Press, 447 p.
- Morris, H.T., 1983, Interrelations of thrusts and transcurrent faults in the central Sevier orogenic belt near Leamington, Utah, *in* Miller, D.M., Todd, V.R., and Howard, K.A., eds., *Tectonic and stratigraphic studies in the eastern Great Basin: Geological Society of America Memoir* 157, p. 75–81.
- Muffler, L.J.P., 1964, Geology of the Frenchie Creek quadrangle, north-central Nevada: U.S. Geological Survey Bulletin 1179, 99 p.
- Mullens, T.E., 1980, Stratigraphy, petrology, and some fossil data of the Roberts Mountains Formation, north-central Nevada: U.S. Geological Survey Professional Paper 1063, 67 p.
- Orobona, M.J.T., 1996, Structural setting of the Bluestar Subdistrict: Implications for origin of the Carlin trend, Eureka County, Nevada: Kingston, Ontario, Canada, Queen's University, M.S. thesis, 152 p.
- Peters, S.G., 1996, Definition of the Carlin trend using orientation of fold axes and applications to ore control and zoning in the central Betze orebody, Betze-Post Mine, *in* Green, S.M., and Struhsacker, Eric, eds., *Geology and ore deposits of the American Cordillera: Reno/Sparks, Nevada, Geological Society of Nevada Field Trip Guidebook Compendium*, p. 59–95.
- , 1997, Structural transect across the southern Carlin trend, Elko and Eureka Counties, Nevada: U.S. Geological Survey Open-File Report 97–347, 27 p.
- Peters, S.G., (this volume), Regional implications of the Crescent Valley-Independence Lineament, north-central Nevada, *in*

- Tosdal, R.M., ed., Contributions to the gold metallogeny of northern Nevada: U.S. Geological Survey Open-File Report.
- Peters, S.G., Williams, C.L., and Volk, Jeff, 1996, Roadlog for Trip B—Structural geology of the Carlin trend, *in* Green, S.M., and Struhsacker, Eric, eds., *Geology and ore deposits of the American Cordillera: Reno/Sparks, Nevada*, Geological Society of Nevada Field Trip Guidebook Compendium, p. 137–239.
- Ponce, D.A., 1997, Mapping the Humboldt River basin using gravity and magnetic methods, Winnemucca 1–by 2-degree quadrangle, northern Nevada: Geological Society of America, Abstracts with Programs, v. 29, no. 6, p. 304.
- Prihar, D.W., Peters, S.G., Bourns, F.T., and McKee, E.H., 1996, Geology and gold potential of the Goat Ridge window, Shoshone Range, Lander County, Nevada, *in* Coyner, A.R., and Fahey, P.L., eds., *Geology and ore deposits of the American Cordillera: Geological Society of Nevada Symposium Proceedings, Reno/Sparks, Nevada, April, 1995*, v. 1, p. 485–504.
- Regnier, Jerome, 1960, Cenozoic geology in the vicinity of Carlin, Nevada: Geological Society of America Bulletin, v. 71, no. 8, p. 1,191–1,199.
- Ressel, M.W., 1998, Mineralogical and chemical characterizations of intrusive rocks of the Carlin trend, with implications for the possible role of volatile-rich magmas [abs.]: Geological Society of Nevada, Elko Chapter, February 1998 Meeting Announcement, 1 p.
- Roberts, R.J., 1964, Stratigraphy and structure of the Antler Peak quadrangle, Humboldt and Lander Counties, Nevada: U.S. Geological Survey Professional Paper 459–A, 93 p.
- Roberts, R.J., Hotz, P.E., Gilluly, James, and Ferguson, H.G., 1958, Paleozoic rocks in north-central Nevada: American Association of Petroleum Geologists Bulletin, v. 42, no. 12, p. 2,813–2,857.
- Rock, N.M.S., 1991, *Lamprophyres: Glasgow, Blackie; New York, Van Nostrand Reinhold*, 285 p.
- Rodriguez, B.D., 1997, Deep regional resistivity structure across the Carlin trend, *in* Vikre, Peter, Thompson, T.B., Bettles, Keith, Christensen, Odin, and Parratt, Ron, eds., *Carlin-type gold deposits field conference: Society of Economic Geology Guidebook Series*, v. 28, p. 39–45.
- Silberling, N.J., Nichols, K.M., Trexler, J.H., Jr., Jewell, P.W., and Crosbie, R.A., 1997, Overview of Mississippian depositional and paleotectonic history of the Antler foreland, eastern Nevada and western Utah, *in* Link, P.K., and Kowallis, B.J., eds., *Proterozoic to Recent stratigraphy, tectonism, and volcanology, Utah, Nevada, southern Idaho, and central Mexico: Brigham Young University, Geology Studies 1997*, v. 42, part 1, p. 161–196.
- Smith, J.K., Jr., and Ketner, K.B., 1968, Devonian and Mississippian rocks and the date of the Roberts Mountains thrust in the Carlin-Piñon area, Nevada: U.S. Geological Survey Bulletin 1251–I, 18 p.
- 1975, Stratigraphy of the Paleozoic rocks in the Carlin-Piñon area, Nevada: U.S. Geological Survey Professional Paper 867–A, 87 p.
- 1977, Tectonic events since early Paleozoic in the Carlin-Piñon Range area, Nevada: U.S. Geological Survey Professional Paper 867–C, 18 p.
- 1978, Geologic map of the Carlin-Piñon range area, Elko and Eureka Counties, Nevada: U.S. Geological Survey Miscellaneous Series Investigations Map I–1028, 2 sheets [scale 1:62,500].
- Snyder, K.D., 1989, *Geology and mineral deposits of the Rossi Mine area, Elko County, Nevada: Reno, Nevada, University of Nevada, Ph.D. dissertation*, 198 p.
- Snyder, W.S., Trexler, J.H., Jr., Cashman, P.H., and Ritter, S., 1997, A newly recognized, important tectonic event in north-central Nevada [abs.]: Geological Society of America Annual Meeting, Salt Lake City, Late-breaking Research in Earth Science I, Handout, [p. 2].
- Teal, Lewis, and Jackson, Mac, 1997, Geologic overview of the Carlin trend gold deposits and descriptions of recent deep discoveries, *in* Vikre, Peter, Thompson, T.B., Bettles, Keith, Christensen, Odin, and Parratt, Ron, eds., *Carlin-type gold deposits field conference: Society of Economic Geology Guidebook Series*, v. 28, p. 3–37.
- Thorman, C.H., Ketner, K.B., and Peterson, Fred, 1990, The Elko orogeny—Late Jurassic orogenesis in the Cordilleran miogeocline [abs.]: Geological Society of America, Abstracts with Programs, v. 22, no. 3, p. 88.
- Tooker, E.W., ed., 1985, *Geologic characteristics of sediment and volcanic-hosted disseminated gold deposits—search for an occurrence model: U.S. Geological Survey Bulletin 1646*, 150 p.
- Trexler, J.H., Jr., and Cashman, P.H., 1991, Mississippian stratigraphy and tectonics of east-central Nevada: post-Antler orogenesis, *in* Cooper, J.D., and Stevens, C.H., eds., *Paleozoic paleogeography of the Western United States—II: Pacific Section Society of Economic Paleontologists and Mineralogists*, v. 67, p. 331–342.
- Trexler, J.H., Jr., and Nichtman, S.P., 1990, Sequence stratigraphy and evolution of the Antler foreland basin, east-central Nevada: *Geology*, v. 18, p. 422–425.
- Wallace, A.B., and Bergwall, F.W., 1984, Geology and gold mineralization at the Dee Mine, Elko County, Nevada [abs.]: Geological Society of America, Abstracts with Programs, v. 16, no. 6, p. 686.
- Wallace, A.R., 1991, Effect of late Miocene extension on the exposure of gold deposits in north-central Nevada, *in* Raines, G.L., Lisle, R.E., Schafer, R.W., and Wilkinson, W.H., eds., *Geology and ore deposits of the Great Basin, Symposium Proceedings: Reno, Nevada, Geological Society of Nevada*, p. 179–183.
- Wallace, A.R., and John, D.A., (this volume), New studies on Tertiary volcanic rocks and mineral deposits, northern Nevada rift *in* Tosdal, R.M., ed., *Contributions to the gold metallogeny of northern Nevada: U.S. Geological Survey Open-File Report*.
- Wilcox, R.E., Harding, T.P., and Seeley, D.R., 1973, Basic wrench tectonics: American Association Petroleum Geologists Bulletin, v. 57, no. 1, p. 74–96.
- Wooden, J.L., Tosdal, R.M., and Kistler, R.W., this volume, Pb isotopic mapping of crustal structure in the northern Great Basin and relationships to Au deposit trends, *in* Tosdal, R.M., ed., *Contributions to the gold metallogeny of northern Nevada: U.S. Geological Survey Open-File Report*.
- Wrucke, C.T., 1974, Geologic map of the Gold Acres-Tenabo area, Shoshone Range, Lander County, Nevada: U.S. Geological Survey Miscellaneous Field Studies Map MF–647, 2 sheets [1:15,840].
- Zoback, M.L., McKee, E.H., Blakely, R.J., and Thompson, G.A., 1994, The northern Nevada rift: Regional tectono-magmatic relations and middle Miocene stress direction: Geological Society of America Bulletin, v. 106, no. 3, p. 371–382.

EVIDENCE FOR THE CRESCENT VALLEY- INDEPENDENCE LINEAMENT, NORTH-CENTRAL NEVADA

By Stephen G. Peters

ABSTRACT

The Crescent Valley-Independence lineament (CVIL) in north-central Nevada is defined by deformation, igneous intrusions, and hydrothermal activity of several ages along a N20E- to N30E-striking zone. This zone extends for about 90 km from near the Independence Mining District in the north to near the Cortez Mine in the south. The center parts the CVIL mark the southeastern edge of the Tuscarora Mountains near the gold deposits along the Carlin trend. The southwestern part extends through Crescent Valley and the Cortez-Pipeline Mining District.

The CVIL is well exposed along its center segment in the Bob's Flat, Richmond, and the Carlin Mine areas where it contains intensely tectonized rock of the upper-plate of the Roberts Mountains allochthon, probably Ordovician Vinini Formation, northeast-striking faults, or Cretaceous or Tertiary northeast-striking dikes. Fabrics in deformed zones have characteristics of *mélange* that also exhibit fabric orientation parallel to fold orientations that result from deformation between the late Permian and late Jurassic (Sonoma and Elko orogenies). In addition, Tertiary-age jasperoid, breccia, calcite veins, and decalcification locally are present along the CVIL. Clusters of sedimentary rock-hosted gold deposits in the north and south ends of the CVIL contain several mineralogical features common to deposits in the Carlin trend area. All the districts contain northeast-striking faults that cross cut tectonic windows and structural highs through the upper-plate of the Roberts Mountains allochthon. The CVIL may be a major fluid conduit that was instrumental in formation of some of the gold deposits.

INTRODUCTION

This paper presents geologic and geomorphologic evidence for the Crescent Valley-Independence lineament (CVIL) in north-central Nevada, a 90-km-long tectonic feature that intersects three major sedimentary rock-hosted gold districts, the Cortez-Pipeline, Carlin, and Independence Mining Districts (fig. 1). Geologic features recognized in the center part of the CVIL, near the Carlin trend, suggest that

deformation, igneous intrusion, and hydrothermal activity were focused along the lineament periodically between the late Paleozoic and middle Tertiary.

Many sedimentary rock-hosted gold deposits in north-central Nevada cluster in mining districts that lie along northwest-trending belts (Roberts, 1960, 1966; Thorman and Christensen, 1991), or are associated with regional-scale lineaments (see Shawe, 1991). Belts and lineaments are compatible with genetic theories of sedimentary-rock-hosted gold deposit ore formation, which call for deep-seated, over-pressured fluids and associated conduits (Kuehn and Rose, 1995; Lamb and Cline, 1997). Alignment of these and other gold ore bodies has been suggested by Shawe (1991) to be an important factor in producing the large crustal endowment of gold in Nevada. Lineaments have been postulated to be the main conduits for deep-sourced metal-bearing fluids (Kerrich, 1986; Kerrich and Kyser, 1994) and may interact with these fluids near or in the ore depositional environment (Phillips, 1986; Henley and Ethridge, 1994; Hickman and others, 1994).

GENERAL GEOLOGY

Reconstructions of the tectonic history of north-central Nevada indicate that early and middle Paleozoic, deep-water sedimentary and igneous rocks were thrust eastward approximately 75 to 200 km during the Late Devonian to Early Mississippian Antler orogeny (Roberts, 1958; Roberts, 1964). These rocks compose the Roberts Mountains allochthon, which lies upon coeval shallow-water rocks of the continental platform. The two packages of rocks, the upper and lower-plates, are separated by the Roberts Mountains thrust (Merriam and Anderson, 1942; Roberts and others, 1958). Emplacement of the allochthon produced a topographic high, which shed sediments, that constitute the overlap assemblage of rocks, to the east and west in the late Paleozoic (Roberts, 1960; Madrid and others, 1992), and were followed by local volcanism in the early Mesozoic (fig. 1). Other tectonic reconstructions suggest that some geologic relations in the region also may be due to: (1) local Early Triassic remobilization of the Roberts Mountains allochthon (Ketner and Alpha, 1992; Ketner and others, 1993); (2) significant tectonism in the region during

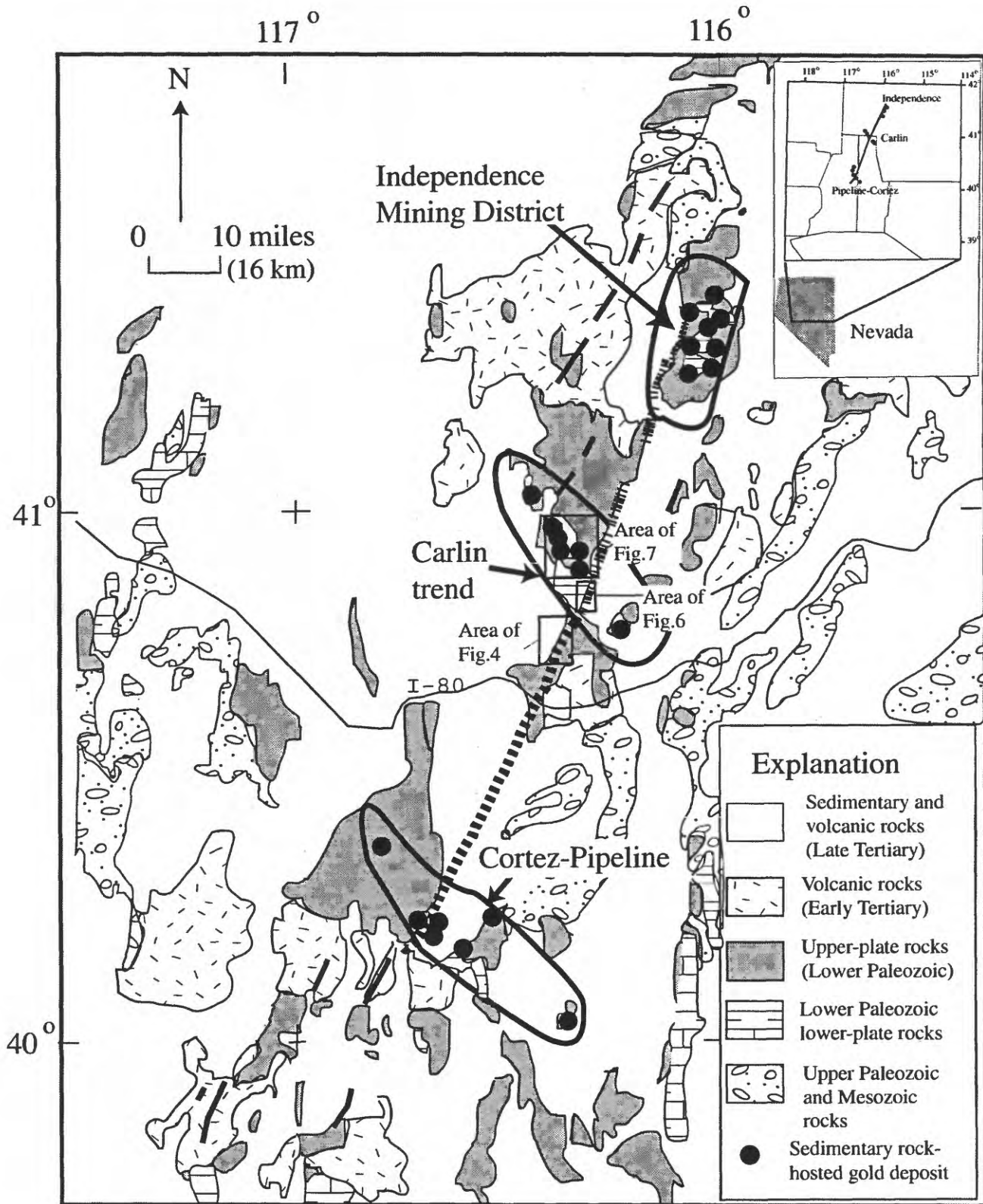


Figure 1. Location of the Crescent Valley-Independence lineament (CVIL) in north-central Nevada. The main focus of the lineament is indicated by the northeast-trending, partially dashed, black line that intersects the Independence, Carlin and Cortez-Pipeline Mining Districts. Note location of figures referred to in text, Bob's Flat, Richmond, and Carlin Mine. (Geology simplified from Stewart and Carlson, 1976).

the Late Jurassic Elko orogeny; (3) the Cretaceous to Early Tertiary Sevier orogeny; and (4) large-scale extensional detachment faulting in the late Eocene to early Oligocene (Thorman and others, 1991a, b; Seedorff, 1991; Wallace, 1991).

Orientation, nature, and geometric relations among tectonic fabrics in and near the CVIL may constrain the timing of events along it. Most fold axes in Paleozoic rocks in north-central Nevada plunge at low angles to the northeast and southwest (Evans and Theodore, 1978; Oldow, 1984; Peters and Evans, 1996). These folds have axial planes and fold axes that are roughly parallel to the CVIL; however, fold axes near major mineralized trends plunge at shallow angles to the northwest (Madrid, 1987; Madrid and Bagby, 1986; Peters, 1996, 1997a). The northwest-trending fold axes along the Carlin trend were postulated by Evans and Theodore (1978) to be due to Jurassic tectonism, which apparently is synchronous with some tectonic events recognized by Ketner and Smith (1982), Ketner (1987) and Thorman and others (1991a) in northeastern Nevada. This implies that much of the northeast-trending tectonic fabric in the CVIL predates the Jurassic; however, as detailed below, younger geologic events may also have northeast orientations in the CVIL.

The CVIL is defined by a N20E- to N30E-striking zone of linear geologic and geomorphologic features. As defined here, the lineament is present in the north on the west side of the Independence Mountains, on the east side of Independence Valley, and may include parts of the Independence Mining District (fig. 1). Farther to the southwest it marks the southeast edge of the Tuscarora Mountains near the Carlin trend. In its central parts, the CVIL passes through rocks of the Ordovician Vinini Formation in the southern Tuscarora Mountains near Boulder Valley and Bob's Flat. It then continues south through Beowawe on the northeast side of Crescent Valley and may extend into Carico Lake Valley and farther to the southwest.

The central parts of the CVIL constitute a 3- to 5-km-wide zone that may, in part, be part of a much larger, composite 20-km-wide zone containing additional northeast-trending linear features (fig. 2). The CVIL also roughly marks the western edge of a 80-km-wide Tertiary basin lying between the Independence and Ruby Mountains (see Regina, 1960; Stewart and Carlson, 1976; Solomon and others, 1979; Mueller, 1992). The northern projection of CVIL marks the eastern edge of the Boulder batholith (see Muehlberger, 1992), suggesting that it may be part of a larger crustal-scale feature. The importance of the CVIL for gold ore genesis is that it traverses or is adjacent to three major sedimentary-rock-hosted gold mining districts that have deposit styles and mineralogic characteristics of sedimentary-rock-hosted gold ("Carlin-type") deposits (Kuehn and Rose, 1995; Arehart, 1996; see also Peters and others, 1996). These characteristics are arsenian rims on older pyrite, presence of late orpiment, realgar, and stibnite, and alteration minerals assemblages formed during decalcification, carbonation and argillitization

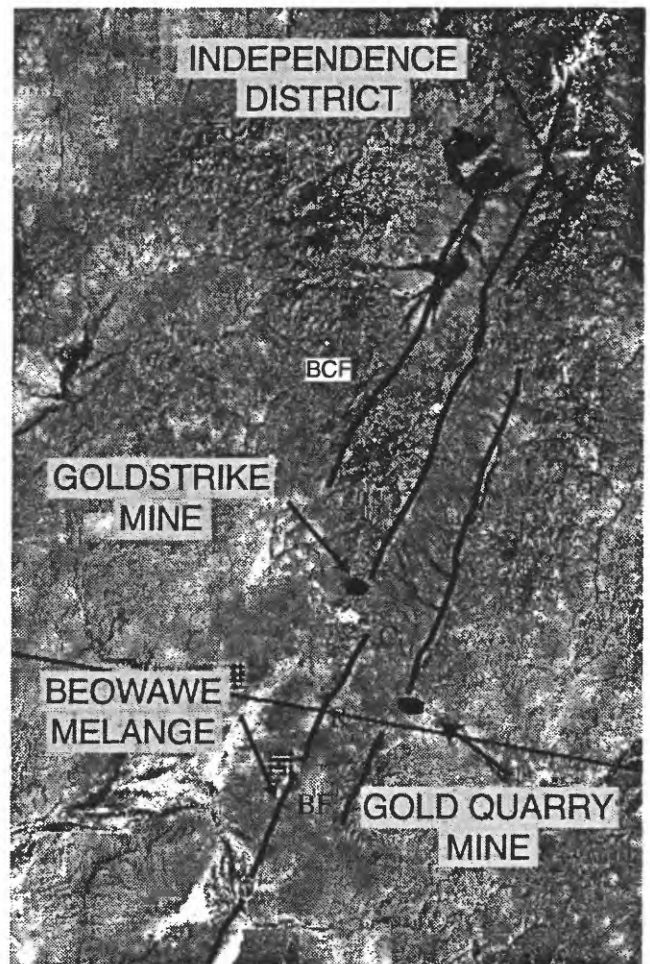


Figure 2. Annotated Landsat image of the northern part of the Crescent Valley-Independence lineament. Topographic features have been highlighted with dark lines. Using this image, the composite lineament zone is approximately 20 km wide, and contains three strands each of which may be 2 to 3 km wide. Large mines shown for location. BF, Bob's Flat; R, Richmond, C, Carlin Mine. BCF, Boulder Creek fault segment (from Theodore and others, this volume) of larger photo-lineament. Field of view approximately 77 by 144 km

of calcareous host rocks, typify. Because of the spatial and temporal relation to the three mining districts, it is possible that some geologic features present in the CVIL could have formed synchronous with the deposits.

CHARACTER, TERMS, AND GENESIS OF MÉLANGE ROCKS ALONG THE CVIL

Rock types near and in the CVIL contain fabrics that are typical of mélanges (see Peters, 1996, 1997a). Mélanges are mappable bodies of fragmented and mixed rock, with phacoidal shapes, in a scaly, shaly matrix, commonly called *clast-in-matrix rock* or *brokenite* (Raymond, 1984a, b; Peters,

1993). The chaotic nature of *mélange* is caused by either sedimentary or tectonic processes that produce fragmentation, mixing, disruption, and dismemberment. Although the laws of lateral continuity and superposition are not generally applicable in *mélange* (Hsu, 1968), the *mélange* outcrops near or in the CVIL retain symmetrical linear fabrics that trend northeast, parallel to fold axes in the region, which is compatible with formation under tectonic, uniform stress.

Generation of clast-in-matrix rock may be due to progressive bulk inhomogeneous shortening (Bell, 1981), where deformation and dissolution are concentrated at the margins of lesser deformed phacoids (fig. 3A). These

margins commonly are anastomosing or conjugate shear zones where strain and fluid has been partitioned around the undeformed phacoidal-shaped rocks, although they commonly retain internal symmetry (fig. 3B). This boudinage-style of deformation is important at all scales along the CVIL, particularly near the boundary of the upper and lower-plate rocks. Deformation of upper-plate rocks may have been the result of the Antler orogeny, and directly related to the emplacement of the Roberts Mountains allochthon, or could have been produced during, but also before or after allochthon emplacement. Similar *mélange*-type fabrics also characterize some ores of sedimentary rock-hosted gold deposits (Peters, 1997b; Lou Xiaohuan, 1993) (fig. 3C).

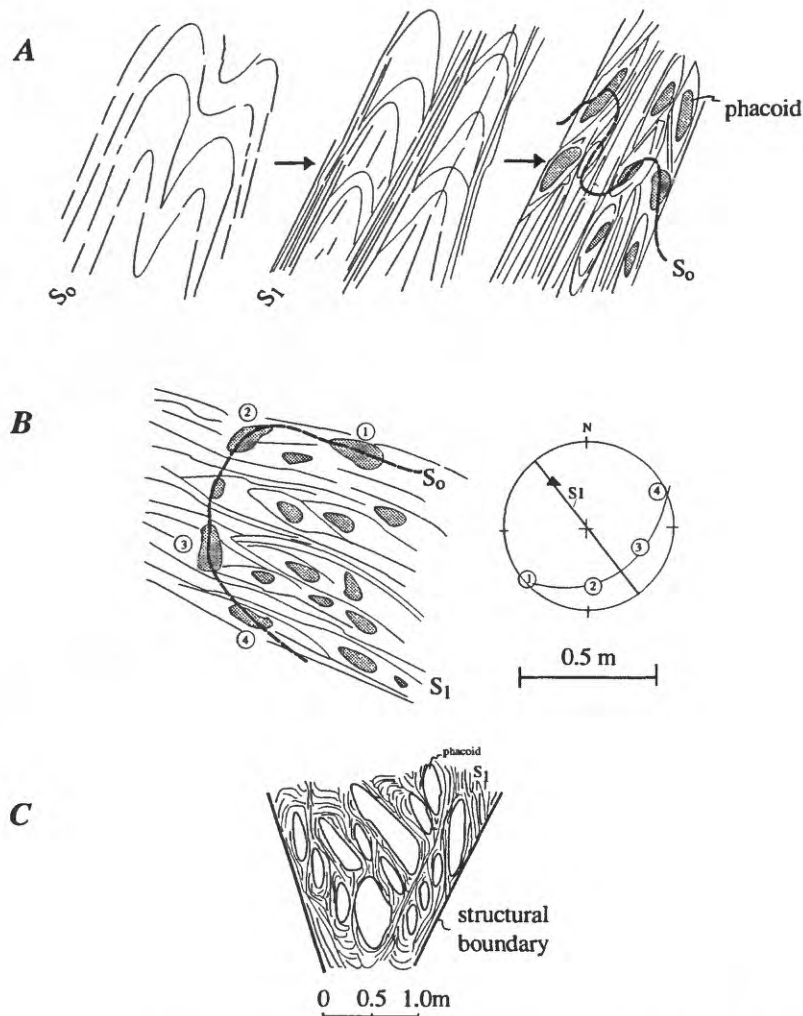


Figure 3. Sketches showing relict folds and symmetry preserved inside zones of intense deformation in clast-in-matrix rock (S_0 = bedding, S_1 = axial plane cleavage): (A) Domainal cleavage formation on fold limbs preserves competent fold hinges as phacoids; (B) Limbs and hinges are preserved and S_0 measurements in clasts define a fold with an axial plane that is coincident with cleavage in clast-in-matrix rocks. Solid triangle represents fold axis. Remnant folds from flexural slip transposition may also be preserved (Peters, 1993, 1996). (C) Clast-in-matrix zone in ore zone of Lannigou sedimentary rock-hosted gold deposit, Guizhou Province, P.R. China, (Lou Xiaohuan, 1993) showing that deformation resulting in phacoidal-shaped wallrock in a sheared matrix. This is a common texture in many structural-type sedimentary rock-hosted gold deposits (see Peters, 1996, 1997c).

DESCRIPTION OF STUDY AREAS ALONG THE CVIL

Along the CVIL, examples of mélangé-type deformation in upper-plate rocks are present in the Bob's Flat and the Carlin Mine areas discussed below. The Richmond area lies between these two areas along the CVIL lower-plate rocks, and contains no mélangé-type deformation. Additional evidence of the CVIL is also present in the Independence and Cortez-Pipeline Mining Districts.

Area of Bob's Flat

In the area of Bob's Flat, about 40 km west of the town of Carlin, evidence for the CVIL consists of northeast-

elongated ridges of intensely tectonized rock of the upper-plate, assigned by Stewart and Carlson (1976) to the Ordovician Vinini Formation, and by adjacent northeast-trending valleys (fig. 1). Tectonized fabrics and foliation strike northeast. A northeast-striking dacite dike of probable Tertiary age, on the basis of its association with volcanic rocks, also lies along the CVIL zone (fig. 4). Detailed exposure of intensely tectonized rocks in the CVIL zone is present at the Beowawe turnoff (fig. 5), a 500-m-long road cut along the west-bound lane of Interstate Highway I-80. Deformed rocks include laminated pelitic chert, massive chert, silty and calcareous sandstone, and massive dolomitic, fine-grained sandstone. Bedding has been dismembered and transposed such that competent layers, which are 1- to 100-cm-thick, have been broken or deformed into phacoids in a matrix of irregularly cleaved shale or clast-in-matrix rock.

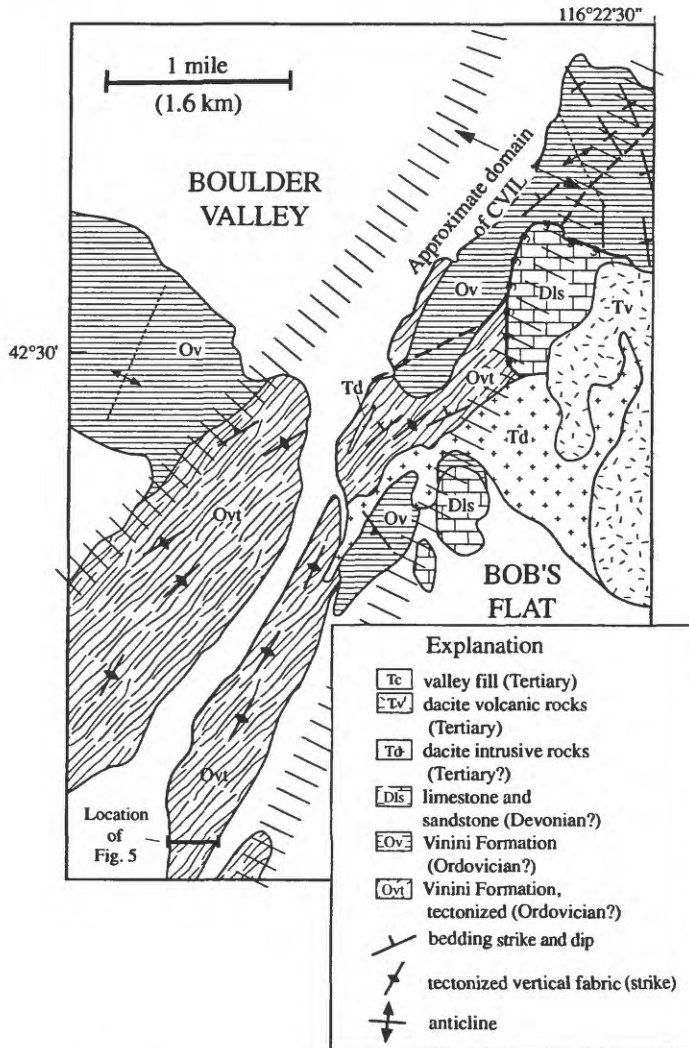


Figure 4. Geologic sketch map of the CVIL zone in the area of Bob's Flat (see fig. 1 for location). Evidence of the lineament is shown in the intensely deformed zones, defined by planar foliation and northeast-striking fabric and by northeast-striking dacite dikes. See fig. 1 for location (note location of Beowawe turnoff sketch—fig. 5).

Strain in the tectonized rocks is concentrated in the incompetent, pelitic matrix of the clast-in-matrix rock, which contains blocks of undeformed, thick-bedded locally deformed chert and massive dolomitic sandstone as much as 2-m-long (fig. 5). Although the deformed bedding, form line patterns, and broken appearance suggest chaotic, random symmetry, a consistent northeast, shallow-plunging, linear fabric has been documented by Peters (1996, 1997a).

The northeast-striking linear and planar fabrics in the *mélange* zones in the central part of the CVIL near Bob's Flat are parallel to fold axial planes and fold axes formed during deformation between the Late Permian and Late Jurassic, during the Sonoma and Elko deformation events, according to Peters (1997c). Folding and transposition of bedding and shearing in the tectonized zones imply local northwest-southeast shortening, internal strain, and possible dissolution along cleavage planes in the zone of the CVIL during that time. Early Tertiary(?) dacite emplacement along the CVIL zone also suggests that the lineament contained linear dilational segments during this later time, which were injected by the dikes.

Richmond Area

The CVIL in the Richmond area, along the Carlin trend, is present on the eastern margin of the Tuscarora Mountains range front (figs. 1 and 6). Here the northeast-striking Richmond Summit fault cuts Tertiary rocks along the main drainage (Evans, 1980). In addition, a northeast-trending zone of jasperoid, breccia, calcite veining, and decalcification crops out along the range front. Further, apophyses and dikes of the Cretaceous Richmond granite stock extend northeast-southwest. Finally, northeast-striking thrust faults interleave rocks belonging to the Ordovician Eureka Quartzite and the Silurian Hanson Creek Formation (fig. 6). Foliation and other deformation fabrics are not pronounced in the igneous

or contact metamorphosed sedimentary rocks. Hydrothermal alteration along the range front and displacement along the Richmond Summit fault indicate both hot-spring and tectonic activity along the CVIL in the Tertiary. Injection of the Richmond dike and Richmond stock also suggest that the CVIL had dilational segments during the middle Cretaceous.

Carlin Mine Area

The CVIL has an expression in the Carlin Mine area, in the Carlin trend, as an east-bounding edge to the range front, and as a series of parallel, northeast-striking faults (fig. 7). The Carlin trend contains over 100 million oz Au. Many northeast-striking faults lie along ore bodies or have jasperoid in outcrop (Peters, 1997d), and provided local structural controls for many of the orebodies (Teal and Jackson, 1997). There is a tendency for there to be more of these northeast-striking faults in a 3-km-wide zone adjacent to the projected center of the CVIL (fig. 7), indicating that hydrothermal fluids used faults in the CVIL zone as conduits.

The CVIL may also have an expression in the upper-plate rocks in *mélange* zones that contain northeast-trending fabrics in the Carlin Mine area. For example, on the east side of the Leeville fault zone (fig. 7), upper-plate rocks contain low-angle shear zones, which separate several 4- to 20-m-thick slabs of deformed rocks that are similar to *mélange* (fig. 8). The juxtaposition of distinctly different deformation styles and rock types on either side of the shear zones indicates that significant transport is likely to have taken place in the rock mass. Axes of folds in all rocks in the outcrop, regardless of slab position, plunge at low angles to the southwest and are parallel to fold axes in deformed rocks of the Vinini Formation north of the Carlin Mine (Peters, 1996, 1997d). This linear fabric is parallel to the linear and planar tectonized fabric in the area of Bob's Flat and may have predated the northeast-striking faults.

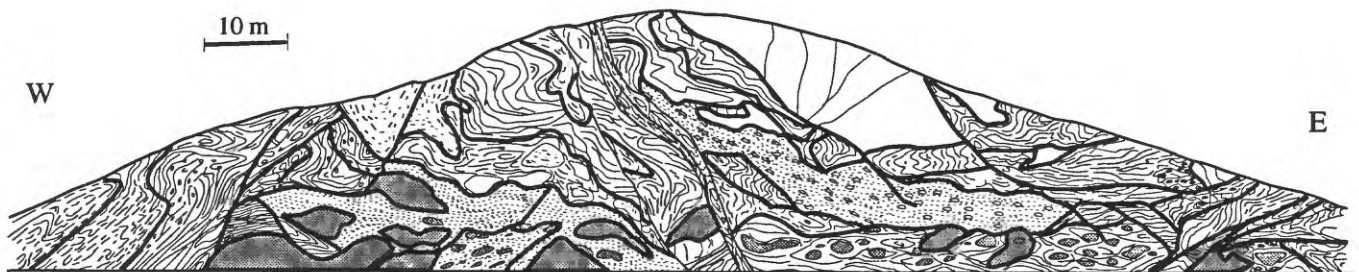


Figure 5. Sketch of exposed geology from the Beowawe turnoff road cut. Solid lines in sketch represent form lines of undifferentiated bedding (S_0). Dashed, dash-dot lines either bedding or foliation (S_1); Patterned or plain areas represent phacoids of competent rocks in sheared rock or clast-in-matrix rock (lensoid pattern). Rock types include laminated pelitic chert, massive chert, silty and calcareous sandstone, and massive dolomitic, fine-grained sandstone. See fig. 4 for location in area of Bob's Flat. See Peters (1996, 1997a) for detailed geologic legend and rock types.

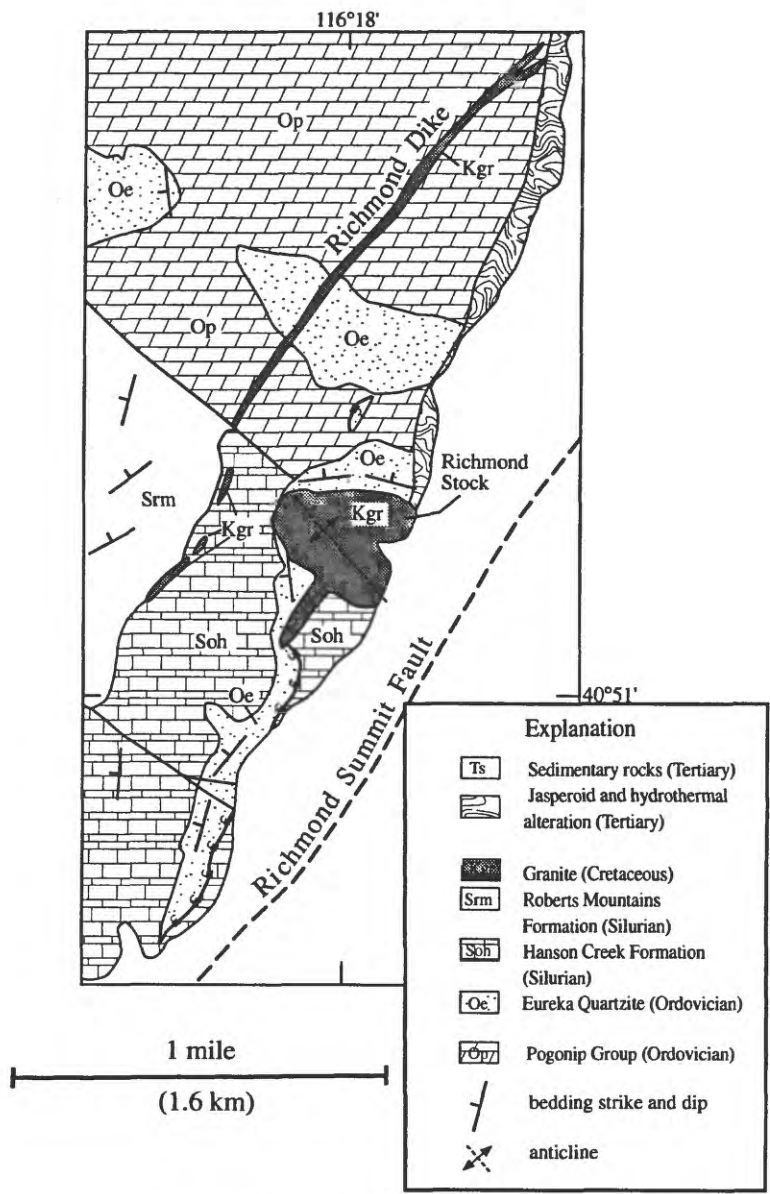


Figure 6. Geologic map of Richmond area in the central part of the CVIL. See fig. 1 for location. Modified from Evans (1980).

Independence and Cortez-Pipeline Mining Districts

Clusters of sedimentary rock-hosted gold deposits at the north and south ends of the CVIL contain structural features common to gold deposits in the Carlin trend area, specifically northeast-striking faults that cross cut tectonic windows through the upper-plate of the Roberts Mountains allochthon or associated structural highs below the allochthon. The gold deposits in the Independence, Carlin and Cortez-Pipeline Mining Districts also share similar mineralogic and geochemical signatures, such as elevated As, Sb, Tl, and Hg contents.

The Cortez-Pipeline Mining District lies along the Battle Mountain-Eureka trend and contains about 10 million oz Au in sedimentary rock-hosted gold orebodies (Bonham and Hess, 1996). The orebodies are mainly hosted in lower-plate rocks to the Roberts Mountain allochthon (Radtke and others, 1987; Foo and others, 1996a; McCormack and Hays, 1996). Northeast-striking faults have significant ore control, particularly the Fence fault in the Pipeline deposit (not shown on fig. 1; see Foo and others, 1996b) and the Gold Acres and Island faults in the Gold Acres deposit (Hays and others, 1991) (fig. 9A). These faults are interpreted here as expressions of the CVIL.

The Independence Mining District has produced

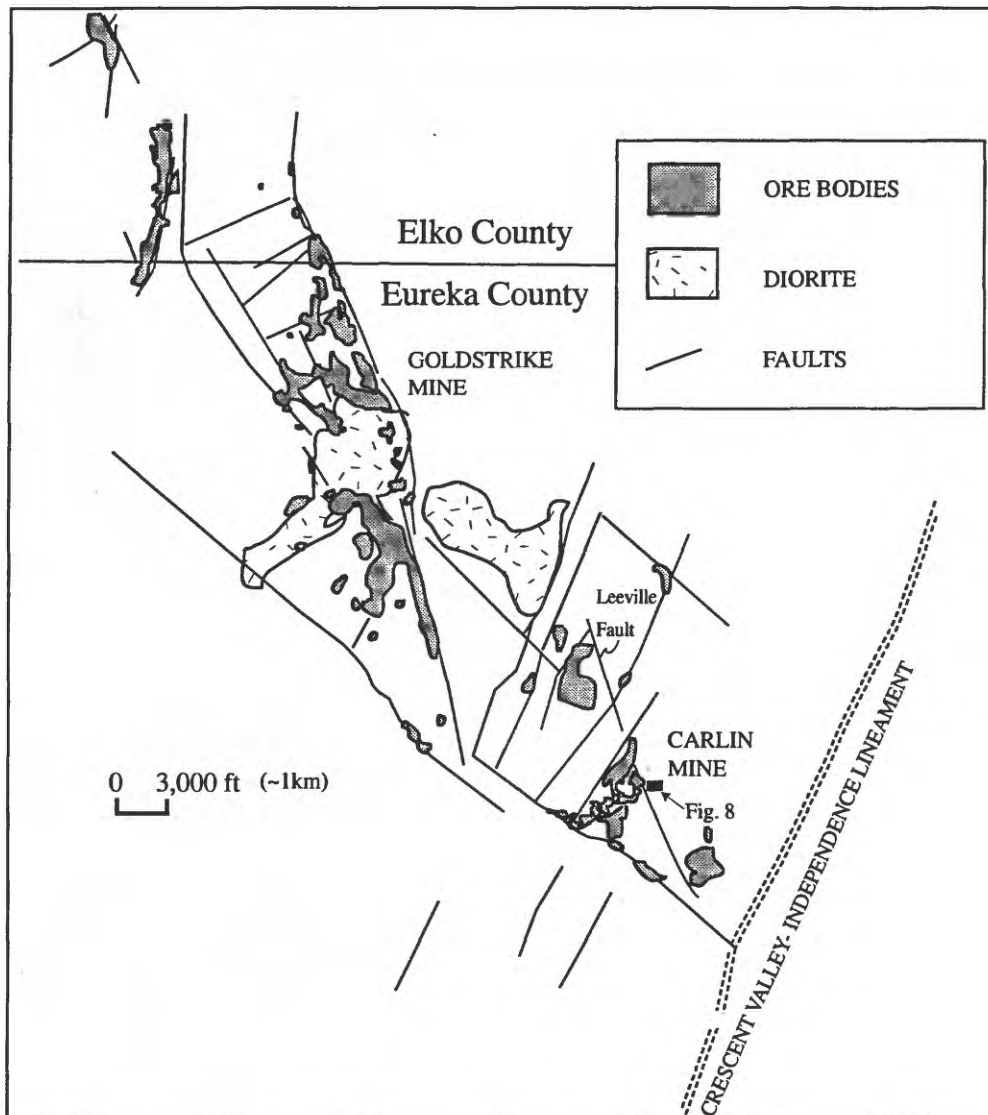


Figure 7. Orebody outlines, main intrusive bodies and faults in the north-central Carlin trend area. Note location of fig. 8. (Adapted from Teal and Jackson, 1997).

approximately 6 million oz Au from sedimentary rock-hosted gold deposits (Bonham and Hess, 1996). The outline of the district-scale orebody cluster defines a 6.5- to 8-km-wide northeast-trending zone containing tectonic windows through the upper-plate rocks of the Roberts Mountains allochthon (fig. 9B). The ore deposits mainly are hosted in lower Paleozoic carbonate rocks of the lower-plate, particularly in the Jerritt Canyon and Big Springs (not shown on fig. 9B) areas. Fold axial planes in the windows trend east or west-northwest and are cut by a set of northeast-striking faults, which outline the general trend of the gold deposits. The orebodies are structurally controlled, many by northeast-striking faults (Birak and Hawkins, 1985; Coats, 1987; Bratland, 1991; Daly and others, 1991; Lapointe and others, 1991), or have associations with early Tertiary dikes (Phinisey

and others, 1996). This northeastern elongation of faults, orebodies and windows is interpreted here as the expression of the CVIL.

DISCUSSION

Geologic features along the CVIL indicate deformation may have taken place repeatedly within the zone during late Paleozoic to early Mesozoic, Cretaceous, and Tertiary times. The post-Paleozoic time span coincidentally overlaps the most probable, but controversial, time interval of sedimentary rock-hosted gold deposits formation (Christensen, 1993). Such a temporal association would be consistent with the CVIL providing a high permeability conduit for a common ore fluid

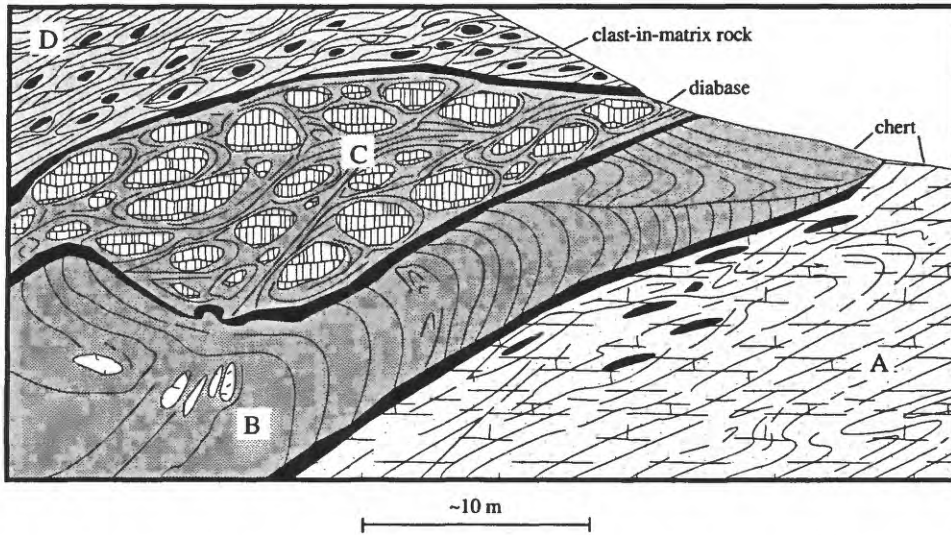


Figure 8. Sketch of Carlin Mine mélange, Carlin Mine area. Four rock packages are: (A) lower laminated isoclinally folded siliciclastic (chert); (B) cylindrically folded siliciclastic (chert); (C) latitic dacite (dolerite) deformed into phacoids; and, (D) black carbonaceous clast-in-matrix rock, containing <20% white, siliceous, 10 cm-scale phacoids in a planar phyllonitic matrix. Each package is separated by shallow-dipping shear zone (dark heavy lines). Fold orientations in each package are northeast-southwest, shallow-plunging (see text and Peters, 1996, 1997d).

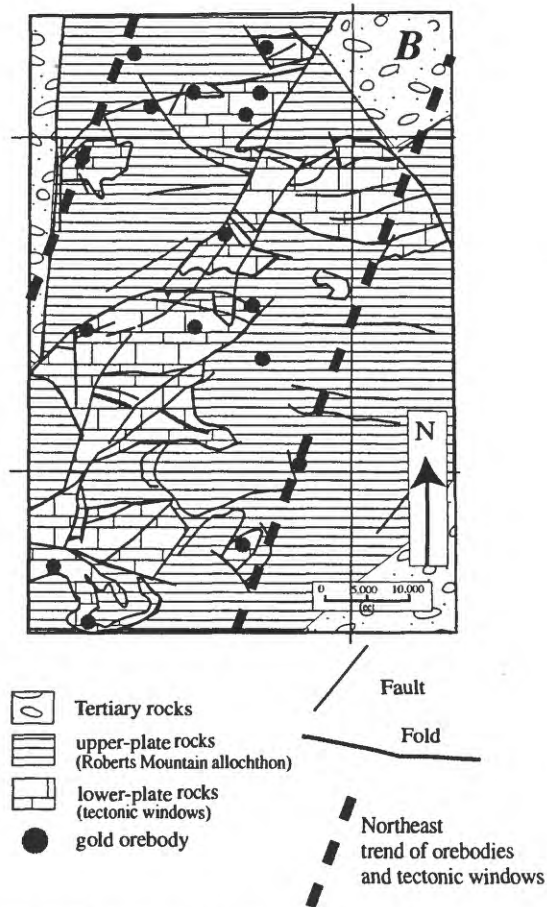
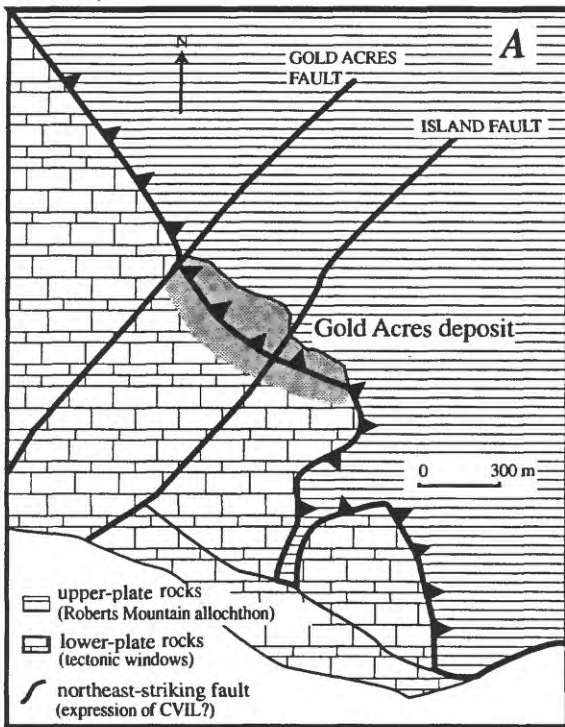


Figure 9. Examples of northeast-striking faults and trends in the northern and southern parts of the CVIL. (A) Gold Acres sedimentary rock-hosted gold deposit in the Cortez-Pipeline Mining District, showing control of northeast-striking Gold Acres and Island faults (adapted from Hays and Foo, 1991). (B) Independence Mining District, showing northeast-trend of windows and associated faults and orebodies (adapted from Daly and others, 1991, and Lapointe and others, 1991).

that could have produced all three major gold districts (see Scholz and Anders, 1994). In order to be related in a common way to ore genesis in all three mining districts, several mechanisms must have operated along CVIL. These are: (1) a single homogenous ore fluid may have traversed the entire lineament, producing clusters of ore deposits in the tectonic windows that served as permeable "traps" (see Hyndman, 1994); or (2) the intersection of the CVIL and northwest-striking structural trends and windows may have provided permeable foci to deep-seated ore; or (3) tectonism, crustal-scale hydrologic flow, and heat flow provided unique settings at different times in each mining district (see Logan and Decker, 1994). The CVIL, thus, could have provided a coincidental and local enhancement at these times and places to the ore-forming processes.

The three sedimentary rock-hosted gold districts along the CVIL are associated closely with tectonic windows through or structural highs beneath the Roberts Mountains allochthon. Polyphase deformation of the upper-plate rocks near the tectonic windows and the Roberts Mountains thrust partially may be the result of regional allochthon emplacement (D_1) and subsequent regional tectonic events, or may be attributable to local tectonism associated with development of the tectonic windows or structural highs (fig. 10). The geometric relations and relative ages of folds, faults, and lineaments in the Roberts Mountains allochthon and in the lower-plate rocks facilitate interpretation of how the gold deposits are related to deformation styles in and near the structural highs.

Deformation in upper-plate rocks, similar to intensely deformed mélangé rocks at Bob's Flat and the Carlin Mine areas, is commonly interpreted to be the result of the Antler orogeny (D_1), and therefore directly related to the emplacement of the Roberts Mountains allochthon (see deformation nomenclature in fig. 10). Folding and transposition of bedding and shearing along cleavage of the clast-in-matrix rock reflect local northwest-southeast shortening, internal strain, and bulk transport within the allochthon. These fabrics parallel folding that is superimposed on the allochthon after emplacement. However, mélangé zones that are part of the CVIL could also have formed after allochthon emplacement (D_{2-3}). Although the fold axes, fold axial planes, shear zones, and tectonized zones in the Bob's Flat and East Carlin Mine areas parallel late Paleozoic to early Mesozoic folds, the dissolution and intense deformation indicated in these rocks may have occurred later and could have been superimposed on the earlier northeast-trending fabric. This would be compatible with high rates of fluid flow in the CVIL in late Mesozoic or early Tertiary times that would be necessary for the formation of the gold ore bodies.

Mélangé development is commonly associated with dissolution, progressive bulk shortening of the rock mass, and local fluid flow (Bell, 1981). Upper-plate mélangé zones and northeast-striking tectonite fabrics, such as in the Bob's Flat (Beowawe turnoff) and the Carlin Mine areas, most likely predated gold mineralization (D_{1-2} ?). However, several mélangé-

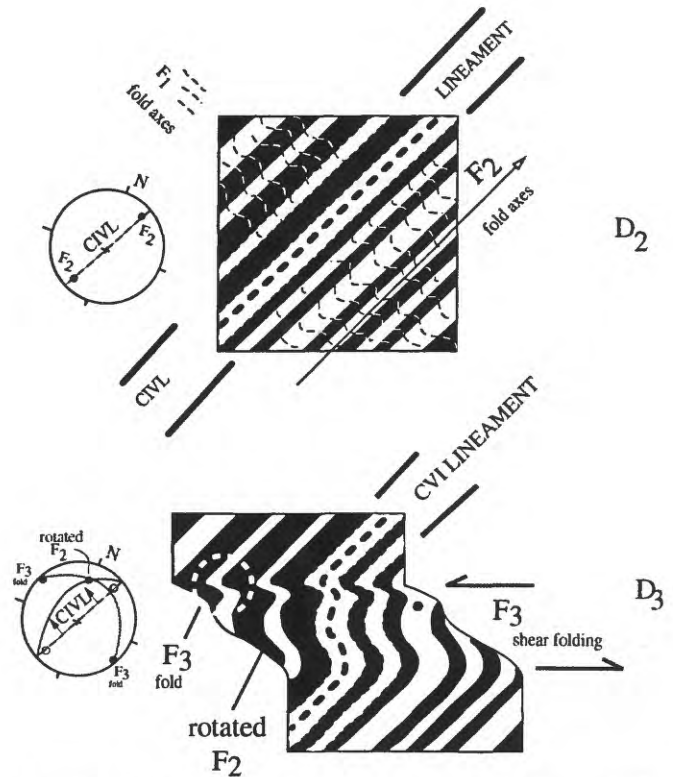


Figure 10. Shear fold model for deformation near the CVIL. The numerous deformations affecting rocks in Carlin trend area, including CVIL, between Paleozoic and middle Tertiary time are generalized by Peters (1997) as a three-phase (D_1 to D_3) sequence of tectonic events. These events are: (1) Late Devonian and Late Pennsylvanian Antler and Humboldt orogeny (Peters, 1997) (D_1 , F_1 folds) synchronous with and following emplacement of the Roberts Mountains allochthon; (2) Late Permian and Late Jurassic Sonoma and Elko deformation (Peters, 1997) (D_2 , F_2 folds), which was characterized by penetrative, shallow northeast- and southwest-plunging fold axes, local intrusions, and northwest-striking faults; and (3) Late Jurassic and Early Eocene Sevier deformation (D_3 , F_3 folds) which rotated or refolded many F_2 folds to north- and northwest-trends and produced local west northwest-trending F_3 shear folds. Pre-deformation events are designated as D_0 . Stereo nets show fold axes as circles. Of specific interest are the D_2 , F_2 folds, which parallel the CVIL. The examples of shear zones and shear folds illustrate the deformation style that may have been present in north-central Nevada near the CVIL. The west northwest-striking shear zones produced shear (F_3) folds by refolding original F_2 folds from northeast-southwest to northwest orientations (adapted from Ramsey, 1980). This may also have resulted in refolding of northeastern planar fabric in the CVIL, resulting in westerly dips (see second stereonet). Early events along the CVIL may have been coeval with the F_2 folds and therefore would also be folded or diluted, particularly near the northwest-trending gold belts.

like fabrics in the D_3 shear folds, such as the Dillon deformation zone in the Goldstrike Mine (Peters, 1997c), have spatial associations with mineralization that suggest that they were active during the gold mineralizing event. Syn-deformational

ore deposition has been proposed for some sedimentary rock-hosted gold deposits by Peters and others (1997) in Nevada and by Lou Xiaohuan (1993; 1996) for some Carlin-type gold deposits in China. The host structural zones in the syn-deformational gold deposits are interpreted in the Carlin trend area by Peters (1996, 1997d) to act like F_3 shear folds that may have folded F_2 folds in a right lateral sense (fig. 10). These D_3 shear zones are deformed, broad, 200-m-thick zones with multiple, sheared strands, breccia bodies, and phacoidal-shaped blocks and slabs (Peters, 1997c).

Although relative ages of mineralization have not been resolved or are enigmatic in north-central Nevada, the formation of sedimentary rock-hosted gold deposits, deformation in the CVIL and the crosscutting northwest-striking deformation zones, may have been synchronous during the time of gold transport and deposition.

Hot saline ore fluids capable of traveling distances of over 100 km with metals have been described by Sverjensky (1984) in sedimentary basin settings similar to those in north-central Nevada. Much of the rock traversed by such fluids would be through the porous, calcareous lower-plate rocks below the Roberts Mountains allochthon. If the ore fluid had a composition similar to that described by Voitsekhowskaya and Peters (this volume) capable of producing sedimentary rock-hosted gold deposits, it could retain metals in solution and be able to transport metals over regional-scale distances within these rocks, due to the large buffering capacity of the carbonate in the rocks (see Crerar and others, 1985). Such fluid flow could have been channeled into high permeability conduits (see also Rodriguez, 1997), such as the CVIL, and may have been accompanied by deformation, coeval dissolution, magmatism, and crustal heat flow.

Fabrics related to emplacement of the Roberts Mountains allochthon (D_1) were overprinted by subsequent penetrative deformation events that most likely also penetrated the lower-plate rocks. One or more of these deformation events may have been synchronous with gold mineralization. Because there are similarities between deformation styles in each of the three generalized deformation events, it is possible that a number of unrecognized D_3 deformation zones may be present in the CVIL as northeast-trending masses that served as regional-scale conduits for fluids that formed sedimentary rock-hosted gold deposits.

REFERENCES CITED

- Arehart, G. B., 1996, Characteristics and origin of sediment-hosted gold deposits: a review: *Ore Geology Reviews*, v. 11, p. 383–403.
- Bell, T.H., 1981, Foliation development—The contribution, geometry and significance of progressive, bulk, inhomogeneous shortening: *Tectonophysics*, v. 75, p. 273–296.
- Birak, D.J., and Hawkins, R.B., 1985, The geology of the Enfield Bell Mine and the Jerritt Canyon District, Elko County, Nevada, in Tooker, E.W., ed., *Geologic characteristics of sediment- and volcanic-hosted disseminated gold deposits— search for an occurrence model*: U.S. Geological Survey Bulletin 1646, p. 95–105.
- Bonham, H.F., Jr., and Hess, R.H., 1996, Major precious-metal deposits, in the Nevada Mining Industry—1995: Nevada Bureau of Mines and Geology Special Publication MI-1995, p. 21–34.
- Bratland, C.T., 1991, Geology of the Winters Creek gold deposit, Independence Mountains, Elko County, Nevada, in Raines G.L., Lisle, R.E., Schafer, R.W., and Wilkinson, W.H., eds., *Geology and Ore Deposits of the Great Basin*, Geologic Society of Nevada Symposium Proceedings, Reno/Sparks, Nevada, April, 1990, v. 1, p. 607–618.
- Christensen, O.D., 1993, Carlin trend geologic overview, in Christensen, O.D., ed., *Gold Deposits of the Carlin Trend, Nevada*: Society of Economic Geologists Guidebook Series, v. 18, p. 12–26.
- Coats, R.R., 1987, Geology of Elko County, Nevada: Nevada Bureau of Mines and Geology Bulletin 101, 112 p., 1 plate [scale 1:250,000].
- Crerar, D., Scott, W., and Brantley, S., 1985, Chemical controls on solubility of ore-forming minerals in hydrothermal solutions: *Canadian Mineralogist*, v. 23, p. 333–352.
- Daly, W.E., Doe, T.C., and Lavanger, R.J., 1991, Geology of the Northern Independence Mountains, Elko County, Nevada, in Raines, G.L., Lisle, R.E., Schafer, R.W., and Wilkinson, W.H., eds., *Geology and Ore Deposits of the Great Basin*, Geologic Society of Nevada Symposium Proceedings, Reno/Sparks, Nevada, April, 1990, p. 583–602.
- Evans, J.G., 1980, Geology of the Rodeo Creek northeast and Welches Canyon quadrangles, Eureka County, Nevada: U.S. Geological Survey Bulletin 1473, 81 p.
- Evans, J.G., and Theodore, T.G., 1978, Deformation of the Roberts Mountains allochthon in north-central Nevada: U.S. Geological Survey Professional Paper 1060, 18 p.
- Foo, S.T., Hays, R.C., Jr., and McCormack, J.K., 1996a, Geology and mineralization of the South Pipeline gold deposit, Lander County, Nevada, in Coyner, A.R., and Fahey, P.L., eds., *Geology and Ore Deposits of the American Cordillera*: Geological Society of Nevada Symposium Proceedings, Reno/Sparks, Nevada, April, 1995, p. 111–121.
- Foo, S.T., Hays, Jr., R.C., and McCormack, J.K., 1996b, Geology and mineralization of the Pipeline gold deposit, Lander County, Nevada, in Coyner, A.R., and Fahey, P.L., eds., *Geology and Ore Deposits of the American Cordillera*: Geological Society of Nevada Symposium Proceedings, Reno/Sparks, Nevada, April, 1995, p. 95–109.
- Hays, R.C., Jr., and Foo, S.T., 1991, Geology and mineralization of the Gold Acres deposit, Lander County, Nevada, in Raines, G.L., Lisle, R.E., Schafer, R.W., and Wilkinson, W.H., eds., *Geology and Ore Deposits of the Great Basin*: Geological Society of Nevada Symposium Proceedings, Reno/Sparks, Nevada, April, 1990, p. 677–685.
- Henley, R.W., and Ethridge, M.A., 1994, Syn-deformational gold transport and deposition in brittle-ductile shear zones - some chaotic thoughts, in Hickman, Stephen, Sibson, Richard, and Bruhn, Ronald, eds., 1994, *Proceedings of Workshop LXIII The Mechanical Involvement of Fluids in Faulting*, 6-10 June, 1993: U.S. Geological Survey Open-File Report 94-228, p. 204–215.

- Hickman, Stephen, Sibson, Richard, and Bruhn, Ronald, eds., 1994, Proceedings of Workshop LXIII The Mechanical Involvement of Fluids in Faulting, 6-10 June, 1993: U.S. Geological Survey Open-File Report 94-228, 615p.
- Hsu, K.J., 1968, Mélanges and their distinction from olistostromes: Society of Economic Paleontologists and Mineralogists, Special Paper 19, p. 321-333.
- Hyndman, R.D., 1994, Widespread fluids in the lower crust: a source to crustal penetrating faults, *in* Hickman, Stephen, Sibson, Richard, and Bruhn, Ronald, eds., Proceedings of Workshop LXIII The Mechanical Involvement of Fluids in Faulting, 6-10 June, 1993: U.S. Geological Survey Open-File Report 94-228, p. 178-189.
- Kerrick, Robert, 1986, Fluid transport in lineaments: Philosophical Transactions Royal Society London, v. A317, p. 216-251.
- Kerrick, Robert, and Kyser, T.K., 1994, The geochemistry and role of fluids in large continental structures: an overview, *in* Hickman, Stephen, Sibson, Richard, and Bruhn, Ronald, eds., 1994, Proceedings of Workshop LXIII The Mechanical Involvement of Fluids in Faulting, 6-10 June, 1993: U.S. Geological Survey Open-File Report 94-228, p. 349-389.
- Ketner, K.B., 1987, Post-Early Triassic, pre-middle Eocene folds and thrust faults, northern Adobe Range, Nevada: Geological Society of America Centennial Field Conference-Cordilleran Section, no. 21, p. 91-94.
- Ketner, K.B., and Alpha, A.G., 1992, Mesozoic and Tertiary rocks near Elko, Nevada—evidence for Jurassic to Eocene folding and low-angle faulting: U.S. Geological Survey Bulletin 1988-C, 13 p.
- Ketner, K.B., Murchey, B.L., Stamm, R.G., and Wardlaw, B.R., 1993, Paleozoic and Mesozoic rocks of Mount Icabod and Dorsey Canyon, Elko County, Nevada—evidence for Post-early Triassic emplacement of the Roberts Mountains and Golconda allochthons: U.S. Geological Survey Bulletin 1988-D, 12 p.
- Ketner, K.B., and Smith, J.F., Jr., 1982, Mid-Paleozoic age of the Roberts thrust unsettled by new data from northern Nevada: *Geology*, v. 10, p. 298-303.
- Kuehn, C.A., and Rose, A.W., 1995, Carlin gold deposits, Nevada: Origin in a deep zone of mixing between normally pressured and over pressured fluids: *Economic Geology*, v. 90, p. 17-36.
- Lamb, J.B., and Cline, J.M., 1997, Depths of formation of the Meikle and Betze/Post deposits, *in* Vikre, P., Thompson, T.B., Bettles, K., Christensen, O., and Parratt, R., eds., Carlin-type Gold Deposits Field Conference: Society of Economic Geologists Guidebook Series, v. 28, p. 101-108.
- Lapointe, D.D., Tingley, J.V., and Jones, R.B., 1991, Mineral resources of Elko County, Nevada: Nevada Bureau of Mines and Geology Bulletin 106, 236p., 1 plate [scale 1: 250,000].
- Logan, J.M., and Decker, C.L., 1994, Cyclic fluid flow along faults, *in* Hickman, Stephen, Sibson, Richard, and Bruhn, Ronald eds., 1994, Proceedings of Workshop LXIII The Mechanical Involvement of Fluids in Faulting, 6-10 June, 1993: U.S. Geological Survey Open-File Report 94-228, p. 190-203.
- Lou Xiaohuan, 1993, Exploration of the mechanisms and features of ore-control faults (F₃) and structural metallogenic processes at the Lannigou gold deposit: *Guizhou Geology*, v. 1, no. 1, p. 26-40 (in Chinese).
- 1996, A study on the control of geometric and kinetic features of fault structures on the location of gold deposits—example from Carlin-type gold deposits of southwest Guizhou: *Guizhou Geology*, v. 14, no. 1, p. 46-54 (in Chinese).
- Madrid, R.J., 1987, Stratigraphy of the Roberts Mountains allochthon in north-central Nevada: Stanford University, Ph.D. dissertation, 341 p.
- Madrid, R.J., and Bagby, W.C., 1986, Structural alignment of sediment-hosted gold deposits in north central Nevada: An example of inherited fabric: *Geological Society of America Abstracts with Programs*, v. 18, p. 393.
- Madrid, R.J., Poole, F.G., and Wrucke, C.T., 1992, Rocks of the Antler orogen—The Roberts Mountain allochthon, *in* Burchfiel, B.C., Lipman, P.W., and Zoback, M.L., eds., The Cordilleran Orogen: Conterminous U.S.: Geological Society of America, The Geology of North America, Volume G—3, p. 28-34.
- Merriam, C.W., and Anderson, C.A., 1942, Reconnaissance survey of the Roberts Mountains, Nevada: *Geological Society America Bulletin*, v. 53, no. 12, p. 1675-1727.
- McCormack, J.K., and Hays, R.C. Jr., 1996, Crescent Valley: a model for reconstruction of district mineralization in Basin and Range, *in* Coyner, A.R., and Fahey, P.L., eds., *Geology and Ore Deposits of the American Cordillera: Geological Society of Nevada Symposium Proceedings*, Reno/Spark, Nevada, April, 1995, p. 635-646.
- Muehlberger, W.R., 1992, Tectonic Map of North America: Association of Petroleum Geologists, Tulsa, 2 sheets, [scale 1:5,000,000].
- Mueller, K.J., 1992, Tertiary basin development and exhumation of the northern East Humboldt-Wood Hills metamorphic complex, Elko County, Nevada: Ph.D. dissertation, Laramie, University of Wyoming, 205p.
- Oldow, J.S., 1984, Spatial variability in the structure of the Roberts Mountains allochthon, western Nevada: *Geological Society of America Bulletin*, v. 95, p. 174-185.
- Peters, S.G., 1993, Polygenetic mélange in the Hodgkinson goldfield, Northern Tasman orogenic zone: *Australian Journal of Earth Sciences*, v. 40, p. 115-129.
- 1996, Definition of the Carlin trend using orientation of fold axes and applications to ore control and zoning in the central Betze orebody, Betze-Post Mine, *in* Green, Steve ed., Trip B, Structural Geology of the Carlin Trend, *Geology and Ore Deposits of the American Cordillera—A Symposium, Field Guide Compendium: Geological Society of Nevada, Reno, Nevada*, p. 59-95.
- 1997a, Structural transect across the southern Carlin trend, Eureka County, Nevada: U.S. Geological Survey Open-File Report 97-0347, 27 p. 2 sheets, [scale 1:500].
- 1997b, Structural transect across the north-central Carlin trend, Eureka County, Nevada: U.S. Geological Survey Open-File Report 97-83, 41 p., 6 sheets, [scale 1:500].
- 1997c, The nature of some upper- and lower-plate rocks near the Roberts Mountains thrust, Carlin trend, *in* Perry, A.J., and Abbot, E.W., 1997, The Roberts Mountains Thrust, Elko and Eureka Counties, Nevada: Nevada Petroleum Society, 1997 Field Trip Guidebook, Reno, Nevada, p. 35-40.
- 1997d, Structural transect across the central Carlin trend, Eureka County, Nevada: U.S. Geological Survey Open-File Report 97-55, 40 p., 2 sheets, [scale 1:6,000].
- Peters, S.G., and Evans J.G., 1995, Mesoscopic and Megascopic fabric geometries in parts of the Carlin trend, Eureka and Elko Counties, Nevada *in* Symposium, *Geology and Ore Deposits of the American Cordillera*, April 1995, Program with Abstracts:

- Geological Society of Nevada, Reno/Sparks, Nevada p. 61–62.
- Peters, S. G., Nash, J.T., John, D.A., Spanski, G.T., King, H. D., Connors, K.A., Moring, B.C., Doeblich, J. L., McGuire, D.J., Albino, G.V., Dunn, V.C., Theodore, T.G., and Ludington, Steve, 1996, Metallic mineral resources in the U.S. Bureau of Land Management's Winnemucca District and Surprise Resource Area, northwest Nevada and northeast California: U.S. Geological Survey Open-File Report 96–712, 147 p., 11 sheets, [scale 1:100,000].
- Peters, S.G., Leonardson, R.W., Ferdock, G.C., and Lauha, E.A., 1997a, Breccia types in the Betze orebody, Goldstrike Mine, Eureka County, Nevada, *in* Vikre, P., Thompson, T.B., Bettles, K., Christensen, O, and Parrat, R., eds., Carlin-type Gold Deposits Field Conference: Society of Economic Geologists Guidebook Series, vol. 28, p. 87–107.
- Phillips, J.W., 1986, Hydraulic fracturing effects in the formation of mineral deposits: Transactions Institute Mining and Metallurgy, v. 95, p. B17–24.
- Phinisey, J.D., Hofstra, A.H., Snee, L.W., Roberts, T.T., Dahl, A.R., and Loranger, R.J., 1996, Evidence for multiple episodes of igneous and hydrothermal activity and constraints on the timing of gold mineralization, Jerritt Canyon District, Elko County, Nevada, *in* Coyner, A.R., and Fahey, P.L., eds., Geology and Ore Deposits of the American: Geological Society of Nevada Symposium Proceedings, Reno/Sparks, Nevada, April, 1995, p. 15–39.
- Radtke, A.S., Foo, S.T., and Percival, T.J., 1987, Geologic and chemical features of the Cortez gold deposit, Lander County, Nevada, *in* Johnson, J.L., ed., Bulk Mineable Precious Metal Deposits of the Western United States, Guidebook for Field Trips: Geological Society of Nevada, Reno, Nevada, p. 319–325.
- Ramsay, J.G., 1980, Shear zone geometry: a review: *Journal of Structural Geology*, v. 2, no. 1/2, p. 83–99.
- Raymond, L.A., 1984a, Classification of mélanges: Geological Society of America Special Paper 198, p. 7–20.
- ed., 1984b, Mélanges, their nature, origin and significance: Geological Society of America Special Paper 198, 170 p.
- Regnier, J., 1960, Cenozoic geology in the vicinity of Carlin, Nevada: Geological Society America Bulletin, v. 71, p. 1189–1210.
- Roberts, R.J., 1960, Alignment of mining districts in north-central Nevada: U.S. Geological Survey Professional Paper 400–B, p. 17–19.
- 1966, Metallogenic provinces and mineral belts in Nevada: Nevada Bureau of Mines Report 13, pt. A, p. 47–72.
- Roberts, R.J., Hotz, P.E., Gilluly, J., and Ferguson, H.G., 1958, Paleozoic rocks of north-central Nevada: American Association of Petroleum Geologists Bulletin, v. 42, no. 12, p. 2813–2857.
- Rodriguez, B.D., 1997, Deep resistivity structure across the Carlin trend, *in* Vikre, P., Thompson, T.B., Bettles, K., Christensen, O, and Parrat, R., eds., Carlin-type Gold Deposits Field Conference: Society of Economic Geologists Guidebook Series, v. 28, p. 39–46.
- Seedorff, Eric, 1991, Magmatism, extension, and ore deposits of Eocene to Holocene age in the Great Basin—mutual effects and preliminary proposed genetic relationships, *in* Raines, G.L., Lisle, R.E., Schafer, R.W., and Wilkinson, W.H., eds., Geology and Ore Deposits of the Great Basin, Geologic Society of Nevada Symposium Proceedings, Reno/Sparks, Nevada, April, 1990, p. 133–178.
- Scholtz, C.H., and Anders, M.H., 1994, The permeability of faults, *in* Hickman, Stephen, Sibson, Richard, and Bruhn, Ronald, eds., 1994, Proceedings of Workshop LXIII The Mechanical Involvement of Fluids in Faulting, 6–10 June, 1993: U.S. Geological Survey Open-File Report 94–228, p. 247–253.
- Shawe, D.R., 1991, Structurally controlled gold trends imply large gold resources in Nevada, *in* Raines, G.L., Lisle, R.E., Schafer, R.W., and Wilkinson, W.H., eds., Geology and Ore Deposits of the Great Basin: Geologic Society of Nevada Symposium Proceedings, Reno/Sparks, Nevada, April, 1990, p. 193–212.
- Solomon, B.J., McKee, E.H., and Anderson, D.W., 1979, Paleogene rocks near Elko, Nevada, *in* Armentrout, J.M., Cole, M.R., and TerBest, H. Jr., eds., Cenozoic Paleogeography of the western United States: Society of Economic Paleontologists and Mineralogists, Pacific Section III, p. 75–79.
- Stewart, J.H., and Carlson, J.E., 1976, Geologic map of north-central Nevada: Nevada Bureau of Mines and Geology, Map 50, 1 sheet, [scale 1:250,000].
- Sverjensky, D.A., 1984, Oil field brines as ore-forming solutions: *Economic Geology*, v. 79, p. 38–49.
- Teal, Lewis, and Jackson, Mac, 1997, Geologic overview of the Carlin trend gold deposits and descriptions of recent deep discoveries, *in* Vikre, P., Thompson, T.B., Bettles, K., Christensen, O, and Parrat, R., eds., Carlin-type Gold Deposits Field Conference: Society of Economic Geologists Guidebook Series, v. 28, p. 3–38.
- Theodore, T.G., Armstrong, A.K., Harris, A.G., Stevens, C.H., and Tosdal, R.M., this volume, Geology of the northern terminus of the Carlin trend, Nevada: links between crustal shortening during the Late Paleozoic Humboldt orogeny and northeast-striking faults, *in* Tosdal, R.M., ed., Contributions to the Au metallogeny of northern Nevada: U.S. Geological Survey Open-File Report.
- Thorman, C.H., and Christensen, Odin, 1991, Geologic settings of gold deposits in the Great Basin, western United States, *in* Ladeira, E.R., ed., Proceedings of Brazil Gold '91, An international symposium on geology of gold: Belo Horizonte, 1991, A.A. Balkema, Rotterdam, p. 65–76.
- Thorman, C.H., Ketner, K.B., Brooks, W.E., Snee, L.W., and Zimmerman, R.A., 1991a, Late Mesozoic-Cenozoic tectonics in northeastern Nevada, *in* Raines, G.I., Lisle, R.W., Schafer, R.W., and Wilkinson, W.H., eds., Geology and Ore Deposits of the Great Basin, Symposium Proceedings: The Geological Society of Nevada, p. 25–45.
- Thorman, C.H., Ketner, K.B., Snoko, A.W., Brooks, W.E., and Mueller, K.J., 1991b, Evidence for the involvement of the Roberts Mountains allochthon in Mesozoic tectonics and its effect on mineral deposit and petroleum accumulation models in northeast Nevada, Field Trip 13, *in* Buffa, R.H., and Coyner, A.R., eds., Geology and Ore Deposits of the Great Basin—Field Trip Guidebook Compendium—Great Basin Symposium, April, 1990: Geological Society of Nevada, Reno/Sparks, p. 869–905.
- Wallace, A. R., 1991, Effect of Late Miocene extension on the exposures of gold deposits in north-central Nevada, *in* Raines, G.L., Lisle, R.E., Schafer, R.W., and Wilkinson, W.H., eds., Geology and Ore Deposits of the Great Basin: Geologic Society of Nevada Symposium Proceedings, Reno/Sparks, Nevada, April, 1990, p. 179–184.
- Woitsekhowskaya, M., and Peters, S.G., this volume, Geochemical modeling of alteration and gold deposition in the Betze deposit, *in* Tosdal, R.M., ed., Contributions to the Au metallogeny of northern Nevada: U.S. Geological Survey Open-File Report.

INITIAL RESULTS OF STRATIGRAPHIC AND STRUCTURAL FRAMEWORK STUDIES IN THE CEDARS QUADRANGLE, SOUTHERN SHOSHONE RANGE

By Thomas E. Moore and Benita L. Murchey

ABSTRACT

Stratigraphic, structural, and paleontological studies in The Cedars quadrangle in the southern Shoshone Range show that its geology is analogous to that of the Battle Mountain area. The structurally lowest units consist of deformed chert and quartzite of the Roberts Mountains allochthon. These rocks are unconformably overlain by a shoaling upward sequence, part of the overlap assemblage of Roberts (1964), composed of conglomeratic turbidites and overlying shelfal siltstone, shale, and sandstone that are correlative with the Pennsylvanian and Permian Antler sequence of the Battle Mountain area. A thin limestone at the base of the shelf deposits has yielded Late Pennsylvanian conodonts that are coeval in part with the Pennsylvanian and Permian Antler Peak Limestone, middle formation of the overlap sequence. Sedimentary features suggest that the overlap sequence in The Cedars quadrangle may comprise fan-delta deposits that were deposited in a more basinward position relative to the rocks of the Antler sequence in the Battle Mountain area.

The overlap sequence in The Cedars quadrangle is overlain on a structural contact by the Mississippian, Pennsylvanian, and Permian Havallah sequence of the Golconda allochthon. New radiolarian and conodont collections show that the Havallah consists of distinct lithological packages of Late Pennsylvanian and Permian siltstone and argillite and Middle and Late Pennsylvanian and Permian argillite and chert that probably once were deposited along the eastern, proximal margin of the Havallah basin. The structural contact between the overlap sequence and the Golconda allochthon suggest that it is correlative with the Golconda thrust. Our new paleontologic and structural data, however, do not support a thrust relation across the fault and instead suggest only stratal disruption in a homoclinal succession of strata. Several explanations are possible, including (1) the base of the Havallah sequence in The Cedars quadrangle is an extensional fault, possibly developed by submarine landsliding in the Permian, (2) the Golconda thrust is located higher in Havallah strata, requiring that Havallah strata compose part of the footwall as well as the hangingwall of the thrust, and (3) the uppermost, undated part of the overlap sequence in the footwall includes rocks that are younger (Permian?) than the dated Late Pennsylvanian limestone in the middle of the overlap sequence.

The Paleozoic rocks are overlain by a succession of Tertiary volcanic rocks including ash flow tuff and are cut by systems of generally north- and east-trending high-angle faults of Tertiary age. An episode of alteration marked by extensive silicification and liesegang banding is developed in the coarse-grained, lower part of the overlap sequence and is associated with north-striking faults.

The Cedars quadrangle is located along the western margin of the Battle Mountain-Eureka mineral trend and south of the southward projection of the pluton-related Ag-Au mineral deposits in the Battle Mountain area. The geology of The Cedars quadrangle displays many characteristics that mark mineral deposits in the Battle Mountain district, including (1) intersection of structural trends; (2) presence of north-striking normal faults, (3) presence or suspected presence of magmatic-hydrothermal systems, (4) presence of rocks of the Antler sequence as a receptive host; and (5) the presence of a fault similar to the Golconda thrust for sealing ascending hydrothermal fluids. These features suggest that The Cedars quadrangle provides an opportunity to test predictive models for distal disseminated gold-silver deposits in a region that is highly prospective for these types of deposits.

INTRODUCTION

The Cedars 7.5' quadrangle, located in the southern Shoshone Range about 60 km south of Battle Mountain in north-central Nevada (fig. 1), lies along the southwestern margin of the Battle Mountain-Eureka mineral trend (Roberts, 1966; Shawe, 1991). The quadrangle is located south of the south-striking porphyry-related and distal disseminated Ag-Au deposits in the Battle Mountain area (Doebrich and Theodore, 1996) and the Cove and McCoy deposits (Brooks and others, 1991), and it is west of the sediment-hosted Carlin-type Pipeline and Cortez deposits (Foo and others, 1996). Structurally-controlled zones of hydrothermal alteration are present in the The Cedars quadrangle and indicate a potential for presence of widespread mineralized rocks. The quadrangle has been actively explored by mining companies since the 1970's as evidenced by numerous exploration roads, pits, drillpads, and other excavations, although no mines are located within its boundaries. Nonetheless, published geologic map

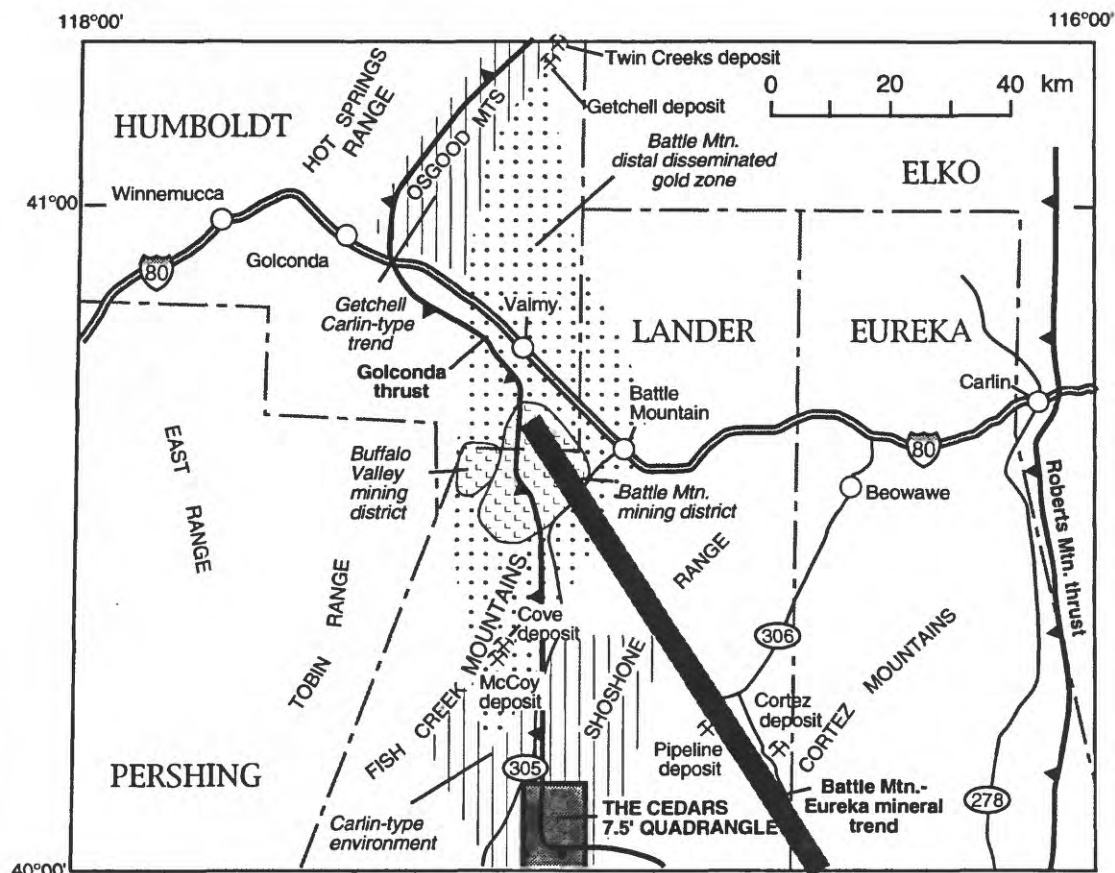


Figure 1. Index map for north-central Nevada showing the location of The Cedars quadrangle, the Battle Mountain mining district, the Battle Mountain-Eureka mineral trend, and locations mentioned in the text. Also shown is an inferred north-striking zone of distal disseminated gold deposits in the Battle Mountain area and the zone of Carlin-type deposits in the Osgood Mountains. A similar zone of Carlin-type deposits may be hypothesized to adjoin the southern margin of the Battle Mountain distal disseminated gold zone in the area of The Cedars quadrangle.

and other information from The Cedars quadrangle are sparse and limited to a reconnaissance 1:63,360-scale geologic map (McKee and Stewart, 1969) and smaller scale (1:250,000) regional geologic maps (Stewart and Carlson, 1976; Stewart and McKee, 1977). These maps indicate the stratigraphy of the Battle Mountain Mining District (Doeblich and Theodore, 1996), especially the Pennsylvanian and Permian Antler sequence, may be present in The Cedars quadrangle. Because rocks of the Antler sequence are the most favorable host for hydrothermal ore deposits in the Battle Mountain Mining District (Doeblich and Theodore, 1996), their presence would suggest potential for distal disseminated Ag-Au deposits. Alternatively, Carlin-type deposits may be present in The Cedars quadrangle if alteration is not associated with plutonic rocks.

This report presents stratigraphic and structural results of an ongoing geologic investigation in The Cedars quadrangle begun in the fall of 1996. Initial work is concentrated in the

north-central part of the quadrangle, with geologic reconnaissance elsewhere in the quadrangle (fig. 2). This report includes new paleontologic data and stratigraphic observations that provide a basis for comparison with the stratigraphy of the Battle Mountain Mining District and other parts of north-central Nevada. These results and associated structural observations suggest that the framework geology of The Cedars quadrangle shares several key characteristics with the geology of the Battle Mountain Mining District.

GEOLOGIC SETTING

The northeast-trending ranges of north-central Nevada contain a structural stratigraphy that is regionally extensive in the western U.S. (Roberts and others, 1958; Silberling and Roberts, 1962; Roberts, 1964) (fig. 1). The uppermost structural unit is the Golconda allochthon, which consists of

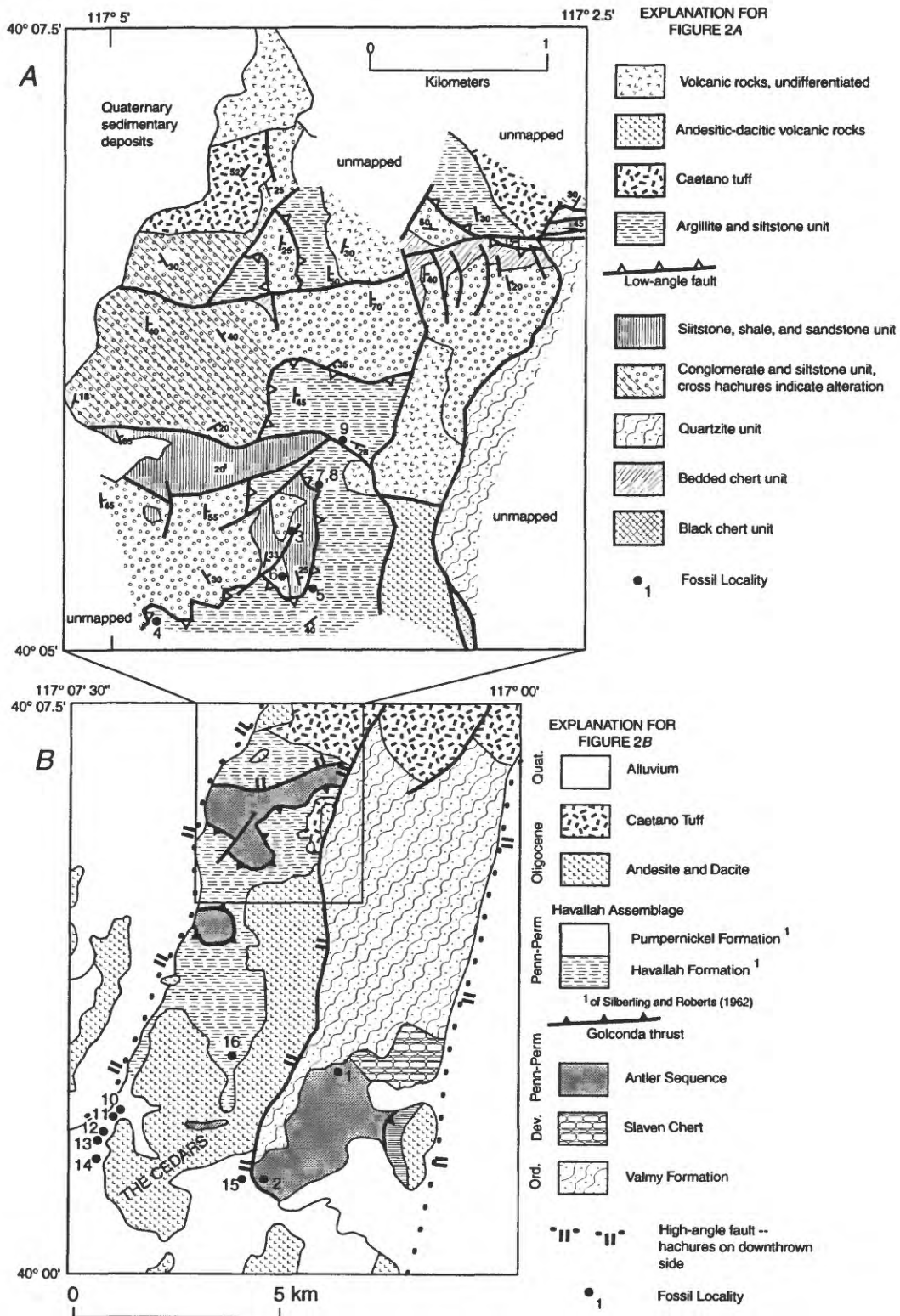


Figure 2. Geologic maps of The Cedars quadrangle. A., Simplified geologic map of the north-central part of The Cedars quadrangle; B., Generalized geologic map of The Cedars quadrangle modified from McKee and Stewart (1969), Stewart and Carlson (1976), and Stewart and McKee (1977).

deformed upper Paleozoic basal rocks, including radiolarian chert, argillite, lithic sandstone, and mafic volcanic rocks. These rocks represent the deformed fill of a marginal basin that was thrust eastward on the Golconda thrust during the Permo-Triassic Sonoman orogeny (Silberling and Roberts, 1962; Burchfiel and Davis, 1972; Speed, 1979; Miller and others, 1992). The Golconda allochthon was emplaced onto an older allochthonous basal assemblage, the Roberts Mountains allochthon, which consists of lower and middle Paleozoic quartz-rich sandstone, black shale, radiolarian chert, and mafic volcanic rocks. The Roberts Mountains allochthon was thrust eastward at least 100 km onto autochthonous lower and middle Paleozoic continental-shelf carbonate and clastic rocks of the miogeocline of the western North America during the mid-Paleozoic Antler orogeny. Following the Antler event, but prior to the emplacement of the Golconda allochthon, an overlapping succession of Upper Paleozoic coarse-grained clastic rocks, limestone, and fine-grained calcareous clastic rocks were deposited in angular unconformity on deformed rocks of the Roberts Mountains allochthon. The overlap sequence, thought to have been deposited in multiple local basins, was derived from local sources in highlands that developed during the Antler orogeny (Roberts and others, 1958). Stratigraphic relations of the overlap sequence are significant because they confirm that at least two contractional deformational episodes are represented in this part of north-central Nevada. These rocks are covered by Tertiary ash-flow tuffs and other volcanic rocks and cut by numerous high-angle faults related to Cenozoic extension in the Great Basin.

The Cedars quadrangle is located at the eastern margin of the Golconda allochthon in central Nevada (fig. 1). McKee and Stewart (1969) showed that the eastern limit of the allochthon in The Cedars quadrangle is delineated by a prominent north-striking high-angle fault (fig. 2). To the east of this fault are chert, shale, and quartzite of the Roberts Mountains allochthon, which they assigned to the Ordovician Valmy Formation and Devonian Slaven Chert. West and south of the fault, McKee and Stewart (1969) assigned rocks of the Golconda allochthon to the Pennsylvanian(?) Pumpnickel Formation and the Pennsylvanian and Permian Havallah Formation of Roberts (1964). Paleontological data from outside the quadrangle, however, have shown that the Pumpnickel and Havallah Formations are tectonic rather than lithostratigraphic units (Stewart and others, 1977; Murchey, 1990) and these formational assignments are now thought to have little or no stratigraphic significance. In contrast to McKee and Stewart (1969), the regional maps of Stewart and Carlson (1976) and Stewart and McKee (1977) showed areas of exposure of the overlap sequence in structural windows through the Golconda allochthon. This relation is of interest because one exploration model in the Battle Mountain Mining District suggests that coarse-grained deposits of the overlap sequence form host rocks for ore-bearing fluids that were trapped beneath the finer grained deposits of the Golconda

allochthon (Doebrich and Theodore, 1990). Stewart and Carlson (1976) and Stewart and McKee (1977) also showed overlap sequence rocks in depositional contact on rocks of the Roberts Mountains allochthon east of the prominent north-trending high-angle fault. Thick ash flow tuffs of the Oligocene Caetano Tuff overlie Paleozoic rocks in the northern part of the quadrangle and volcanic rocks of unknown affinity overlie Paleozoic rocks in the southern part of the quadrangle.

LOCAL STRATIGRAPHY Roberts Mountains allochthon

Rocks of the Roberts Mountains allochthon in The Cedars quadrangle were described by McKee and Stewart (1969) as "black chert, dark shale, and light and dark gray quartzite". They assigned most of these rocks to the Ordovician Valmy Formation but tentatively assigned thin-bedded black chert to the Devonian Slaven Chert in the southeastern part of the quadrangle (fig. 2B). No fossil localities have been reported from rocks of the Roberts Mountains allochthon in The Cedars quadrangle to confirm these lithologic correlations.

In the north-central part of The Cedars quadrangle (fig. 2A), we tentatively divide the Roberts Mountains allochthon

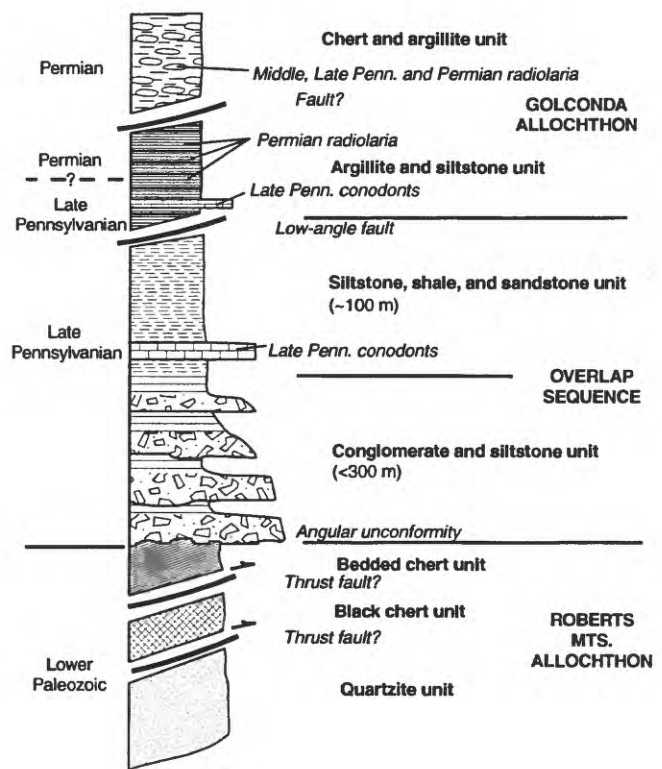


Figure 3. Generalized stratigraphic section for Paleozoic rocks of The Cedars quadrangle and known age relations.

into three units, which from base to top are quartzite, black chert, and bedded chert (fig. 3). These units are presumed to be structural units, although depositional relations may be revealed as more detailed mapping and paleontologic information become available.

The quartzite unit consists of massive medium gray to bluish gray fine-grained quartzite. Layering is commonly visible from a distance, but sedimentary structures, including bedding, are difficult to identify in outcrop-scale exposures. The quartzite unit has a structural thickness of several hundred meters, but may be repeated by folding and (or) faulting.

The black chert unit is thick bedded (5–20 cm thick) to massive, radiolarian-bearing, and displays few or no argillitic interbeds, lending a massive appearance to the unit. Bedding in the black chert unit is generally concordant to undulose and is only deformed locally into outcrop-scale folds. Local units of white and gray chert are associated with the black chert and display bedding characteristics similar to the black chert and thus are included in this unit. The stratigraphic thickness of the unit is uncertain but it has a structural thickness of about 100 m as presently mapped.

The bedded chert unit is conspicuously bedded in layers 2 to 5 cm thick and consists of gray and greenish-gray partially recrystallized chert which contains abundant radiolarians. Interbedded light to medium gray fissile argillite beds comprise 2 to 50 percent of the unit (fig. 4A). The bedded chert unit typically displays complex outcrop-scale folds that distinguish it from the black chert unit (fig. 4B). The difference in structural style may result from the presence of relatively less competent interlayered argillite in the bedded chert unit. The structural thickness of the unit is about 300 m, although the stratigraphic thickness of the unit is likely much less because of structural thickening caused by contractional deformation.

Overlap sequence

The overlap sequence rests in angular unconformity on rocks of the bedded chert unit of the Roberts Mountains allochthon in the north-central part of The Cedars quadrangle (figs. 2A and 5) and on quartzite and black argillite in at least two localities in the southern part of the quadrangle, east of the prominent north-striking high-angle fault in the middle of the quadrangle (Stewart and Carlson, 1976; Stewart and McKee, 1977) (fig. 2B). We have divided the overlap sequence into two units in the north-central part of the quadrangle (fig. 3). The lower unit consists of thick, massive intervals of gray chert-pebble conglomerate with interbedded intervals of thin-bedded quartz-rich siltstone (fig. 6). The upper unit consists of yellow brown siltstone, brown shale, and very fine-grained sandstone. A thin unit of fossiliferous limestone is locally present near the base of the upper unit.

Conglomerate in the conglomerate and siltstone unit

contains abundant angular and subangular chert clasts and sparse quartzite clasts. Clasts in the conglomerate are locally as large as 6 cm, although clast sizes are less than 3 cm in most exposures. Bedding in the conglomerate is commonly massive or obscured by alteration, a common feature of the conglomerate and siltstone unit, but displays sharp, erosional bases and normal grading at the tops of beds where bedding is visible (fig. 7A). Conglomerate beds are 50 to 200 cm thick and commonly form amalgamated units as much as 20 m thick, particularly near the base of the unit. The conglomerate is typically framework supported, channelized, and cross bedding is rare or absent. Thin-bedded intervals of quartz siltstone as thick as 10 m thick are interbedded with the conglomerate and are apparently more common, thicker, and finer grained higher in the section. The thin-bedded intervals consist of light gray, laterally continuous beds of quartz siltstone and very fine-grained sandstone and sparse graded beds of conglomerate as thick as 1 m (fig. 7B). Ripple cross lamination is locally present in the siltstone. The consistent east dip of the conglomerate and siltstone unit coupled with its map distribution suggest that it has a thickness of over 1,200 m. However, as discussed in more detail below, the stratigraphic thickness of the unit is likely less than about 300 m because numerous west-dipping normal faults drop the section incrementally down to the west.

The overlying siltstone, shale and sandstone unit is typically poorly exposed, consisting of platy, chippy slightly calcareous sandstone and siltstone float. Thickness of the unit is uncertain because of poor exposure and structural control, but may be as much as 100 m. Outcrops of this unit consist of 1- to 2-m-thick intervals of parallel laminated to flaggy very fine-grained micaceous sandstone in thin-bedded to massive gray argillite. The sandstone intervals consist of thickening upward cycles composed of sandstone beds (fig. 8). Bioturbation is very abundant and commonly obscures sedimentary structures. Where visible, sandstone beds are laterally continuous and display erosional bases, slight normal grading, and current and wave rippled tops (fig. 8). In a few places just above the base of the siltstone, shale, and sandstone unit is a distinctive interval of calcareous siltstone, sandstone, and sandy limestone as much as 10 m thick. The sandy limestone beds, as much as 1 m thick, consist of normally graded fossiliferous grainstone with an abundant and diverse megafaunal and trace fossil assemblages (figs. 3). In one location (map locality 3, table 1, fig. 2A), the limestone yielded a diverse conodont assemblage, including indigenous Late Missourian conodonts and redeposited middle Osagean and Atokan conodonts (A. Harris, written comm., 1996).

Sedimentary structures in the overlap sequence suggest deposition in a marine setting. Beds in the thin-bedded intervals in the conglomerate and siltstone unit consistently have erosional bases, lateral continuity, and sedimentary structures indicative of deposition by turbidity currents and other sediment-gravity flows. Sponge spicules in siltstone

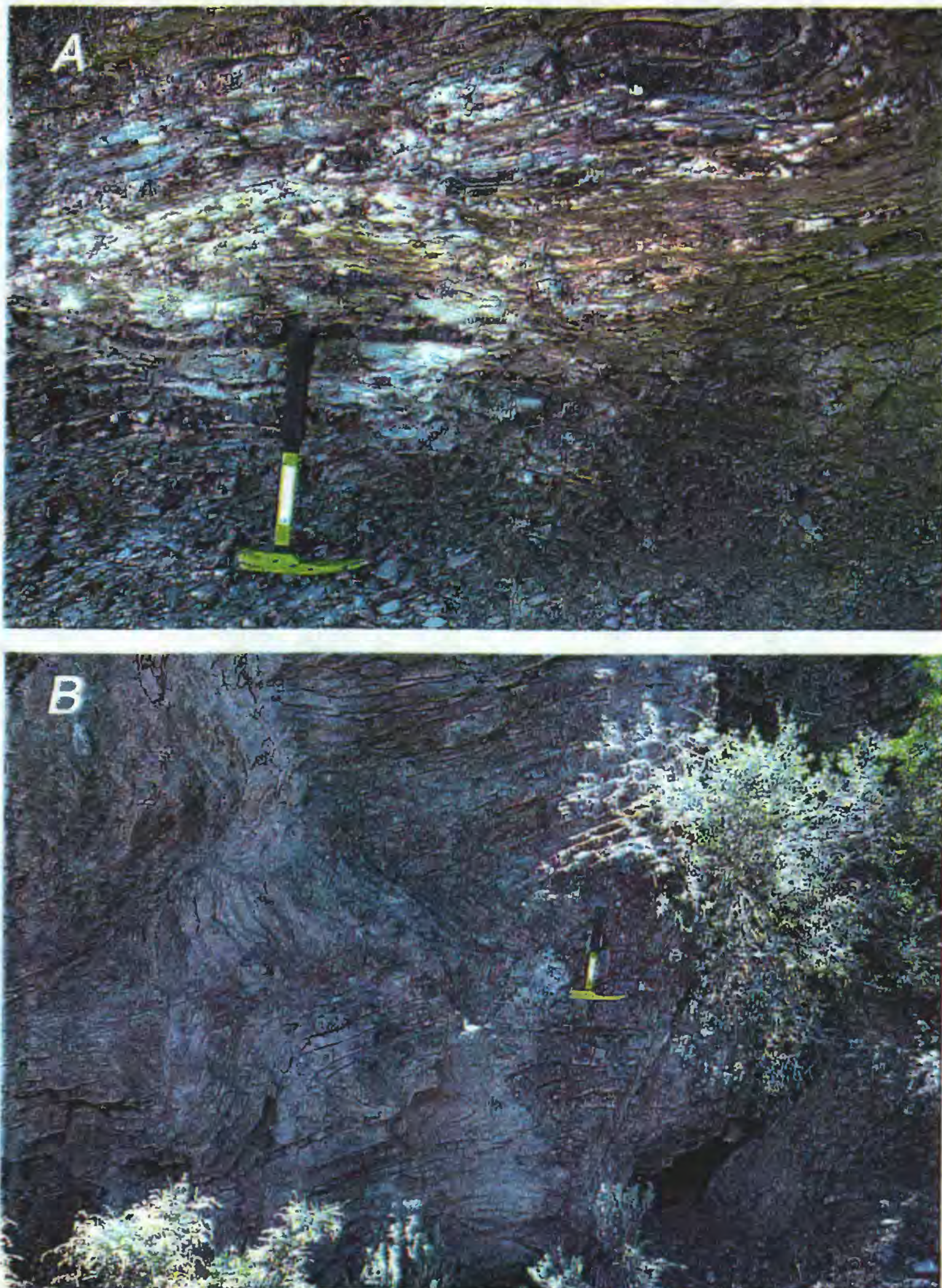


Figure 4. Photographs of bedded chert unit of bedded chert unit in the Roberts Mountains allochthon. A., interbedded chert and argillite; B., disharmonic folds, suggesting structural transport to left (northward)



Figure 5. Photograph of conglomerate in conglomerate and siltstone unit resting in angular unconformity on chert of the bedded chert unit (contact at hammer).



Figure 6. Northeastward view of contact between conglomerate and siltstone and siltstone, shale, and sandstone units of overlap sequence. Bold outcrops in conglomerate and siltstone unit are conglomeratic intervals. White arrow, for example, indicates part of a conglomerate interval that can be traced discontinuously up hill to left toward higher geologist. Light-colored areas of float are siltstone intervals (for example, at black arrows). Fossiliferous limestone is present at top of hill in siltstone, shale, and sandstone unit. Circles indicate geologists for scale.

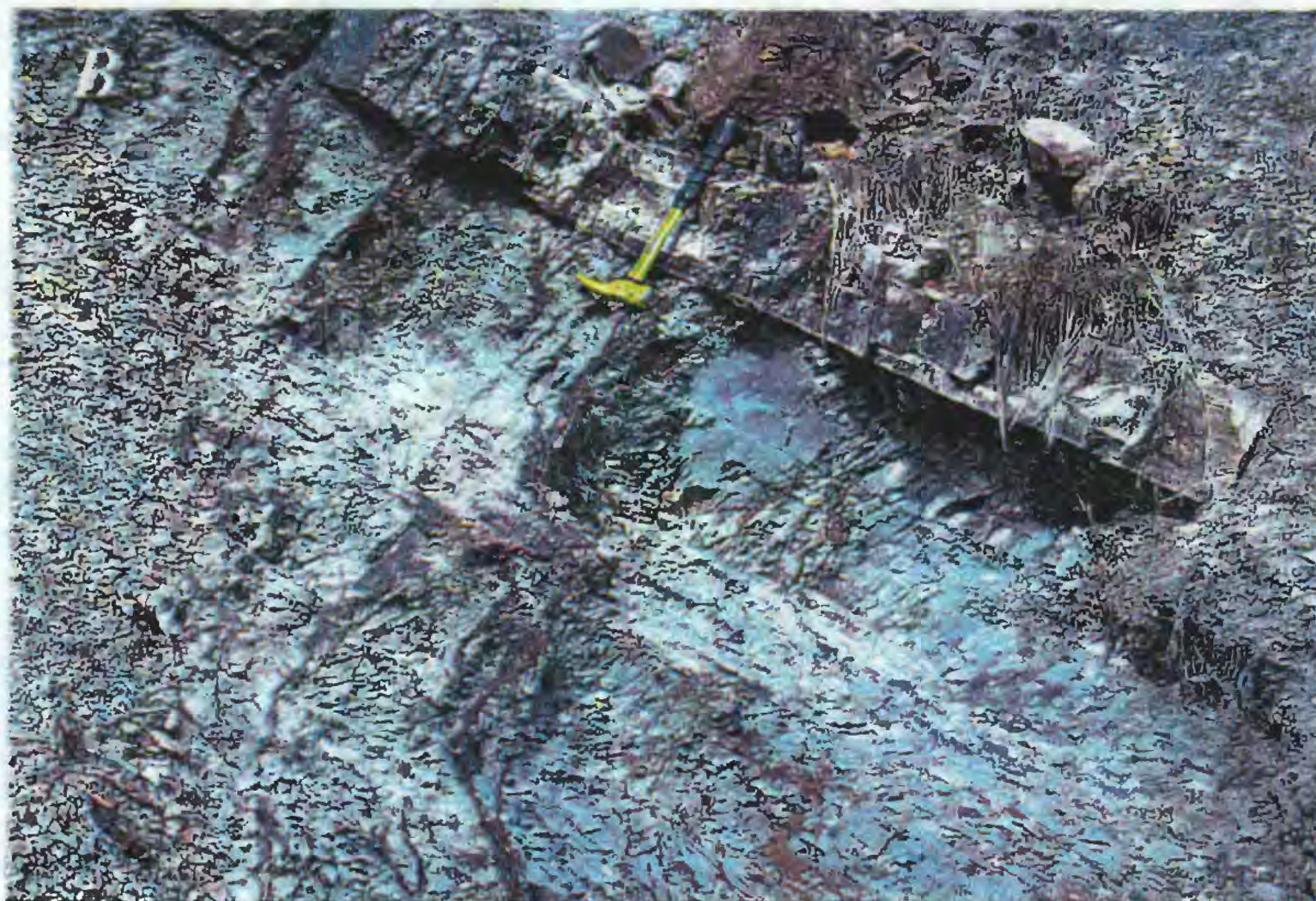


Figure 7. Photographs of conglomerate and siltstone unit of overlap sequence. *A.*, Thin zone of normal grading (at hammar head) at top of conglomerate bed; *B.*, Thin-bedded siltstone and fine-grained sandstone of siltstone interval. Note sharp, planar bases of beds.

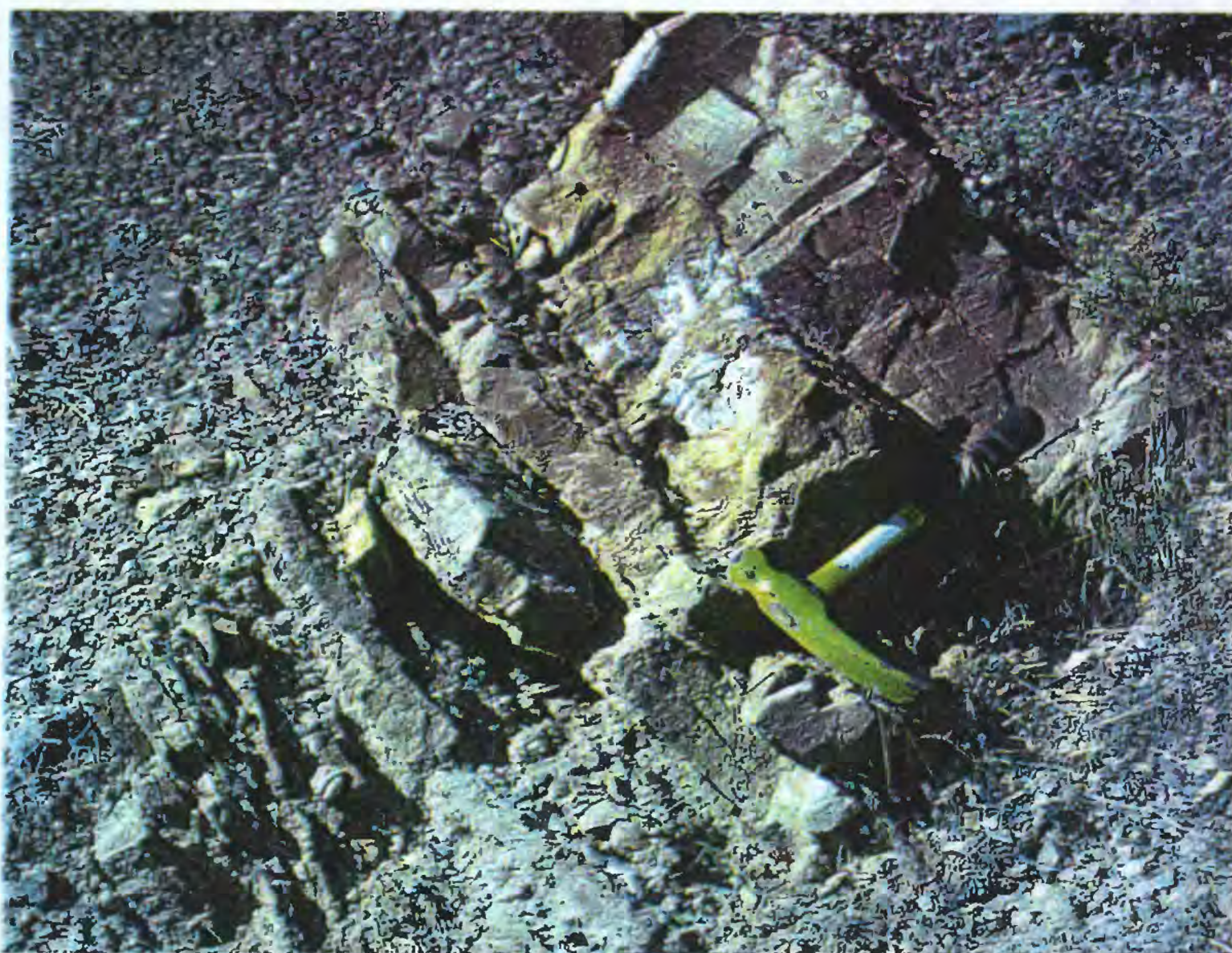


Figure 8. Photograph of thickening upward sequence of calcareous sandstone in siltstone, shale, and sandstone unit of overlap sequence. Uppermost bed displays wave ripples indicative of deposition above wave base.

(map locality 6, table 1, fig. 2) of the conglomerate and siltstone unit also indicate a marine origin. The dominantly coarse-grained amalgamated and channelized deposits of angular debris at the base of the succession suggest deposition as coarse grained turbidites or other sediment-gravity flow deposits on a submarine fan of unknown extent. The change upward in the sequence to the overlying siltstone, shale and sandstone unit indicates waning sedimentation under marine conditions. The ubiquitous bioturbation, calcareous composition, and presence of wave ripples in the upper unit suggest deposition above wave base in a shelf setting. Sedimentary structures observed in sandstone in the upper unit are similar to tempestite deposits, which result from wind and wave-induced storm flow, whereas the argillite records suspension sedimentation between storm events. These preliminary observations suggest that the overlap sequence in The Cedars quadrangle records shoaling conditions.

Golconda allochthon

The Golconda allochthon in The Cedars quadrangle rests in structural contact on rocks of the overlap sequence on a prominent fault that is analogous in its structural position to

the Golconda thrust (Stewart and Carlson, 1976; Stewart and McKee, 1977). Rocks of the allochthon consist dominantly of poorly exposed thin-bedded argillite and siltstone with local interleaved lenticular bodies of chert. We tentatively subdivide these rocks into two principal lithologic associations, including (1) an argillite and siltstone unit and (2) chert and argillite unit (fig. 3). These units correspond in general to the rocks previously assigned to the Havallah and Pumpnickel Formations, respectively, (McKee and Stewart, 1969; Stewart and Carlson, 1976; Stewart and McKee, 1977) but the units are likely structural rather than stratigraphic units as interpreted by earlier workers. For this reason, we refer to the upper Paleozoic strata of the Golconda allochthon as the Havallah sequence following the usage of Murchey (1990) rather than using the older formal stratigraphic nomenclature for these rocks.

All rocks of the Golconda allochthon in the north-central part of The Cedars quadrangle are included in the argillite and siltstone unit. This unit consists of even, graded beds of light to dark gray siliceous argillite, silty argillite, siltstone, shale, and very fine-grained quartz-rich sandstone (fig. 9). In outcrop, these strata are laterally continuous with beds typically less than 10 cm thick. Coarse-grained sandstone and granule conglomerate are present locally as sparse, isolated 5- to 10-

Table 1. Fossil locality information for the Cedars quadrangle.

Map location	Sample number	Field locality number	Latitude	Longitude	Unit	Fossil type	Age
1	96TM-155A	96TM-155A	40° 02.71'	117° 03.20'	Overlap sequence	Conodonts ¹	Redeposited? Llandoveryan (Early Silurian) to late Emsian (Early Devonian)
2	16039-49J	16039-49J	40° 01'	117° 05.'	Overlap sequence or Havallah sequence ²	Conodonts ³	late early Desmoinesian (late Middle Pennsylvanian)
3	96MY-4	96MY-4	40° 05.53'	117° 04.19'	Siltstone, shale, and sandstone unit, overlap sequence	Conodonts ⁴	Indigenous late Missourian (middle Late Pennsylvanian); includes redeposited middle Osagean (Lower Mississippian) and Atokan (Middle Pennsylvanian)
4	97TM-262D2	97TM-262	40° 05.06'	117° 04.90'	Argillite and siltstone unit, Havallah sequence	Conodonts ⁴	Indigenous late Missourian to early Virgilian (middle Late Pennsylvanian); includes redeposited Early Mississippian
5	96MY-009	96TM-115	40° 05.25'	117° 04.06'	Argillite and siltstone unit, Havallah sequence	Radiolarians	Leonardian or Guadalupian (late Early or early Late Permian)
6	96MY-010	96TM-118	40° 05.30'	117° 04.15'	Conglomerate and siltstone unit ⁶ , overlap sequence	Sponge spicules	Phanerozoic
7	96MY-011	96TM-120	40° 05.63'	117° 03.97'	Argillite and siltstone unit, Havallah sequence	Radiolarians	late Leonardian (late Early Permian)
8	96MY-012	96TM-121	40° 05.70'	117° 04.03'	Argillite and siltstone unit, Havallah sequence	Radiolarians, Sponge spicules	Phanerozoic
9	96MY-016A	96TM-125	40° 05.82'	117° 03.71'--	Argillite and siltstone unit, Havallah sequence	Radiolarians	late Leonardian (late Early Permian)
10	96MY-020	96TM-137	40° 01.01'	117° 06.80'	Chert and argillite unit, Havallah sequence	Radiolarians	Atokan? or Desmoinesian (Middle Pennsylvanian)
11	96MY-021	96TM-138	40° 02.29'	117° 07.09'	Chert and argillite unit, Havallah sequence	Radiolarians	Atokan? or Desmoinesian (Middle Pennsylvanian)
12	96MY-023	96TM-141	40° 01.99'	117° 06.94'	Chert and argillite unit, Havallah sequence	Radiolarians	Missourian to Wolfcampian (Late Pennsylvanian to early Early Permian)
13	96MY-024	96TM-142	40° 01.75'	117° 06.99'	Chert and argillite unit, Havallah sequence	Sponge spicules	Probable Guadalupian (early Late Permian)
14	96MY-028	96TM-146	40° 01.54'	117° 07.12'	Chert and argillite unit, Havallah sequence	Radiolarians	Leonardian (late Early Permian)
15	96MY-031	96MY-031	40° 01.61'	117° 04.56'	Chert and argillite unit, Havallah sequence	Radiolarians	late Leonardian to Guadalupian (late Early Permian to early Late Permian)
16	96MY-032	96TM-154A	40° 02.63'	117° 04.62'	Chert and argillite unit, Havallah sequence	Radiolarians	Leonardian (late Early Permian)

¹Identified by A.G. Harris, U.S. Geological Survey, report WMRT-97-1

²Reported as Havallah Formation or Antler sequence (Overlap sequence) by Stewart and McKee (1977), p. 27.

³Originally identified by J.W. Huddle in report SW-69-3; Updated by A.G. Harris and B.R. Wardlaw, U.S. Geological Survey, report WMRT-96-3

⁴Identified by A.G. Harris and B.R. Wardlaw, U.S. Geological Survey, report WMRT-97-2

⁵Identified by A.G. Harris and B.R. Wardlaw, U.S. Geological Survey, report WMRT-96-4

⁶Sample collected from siltstone interval

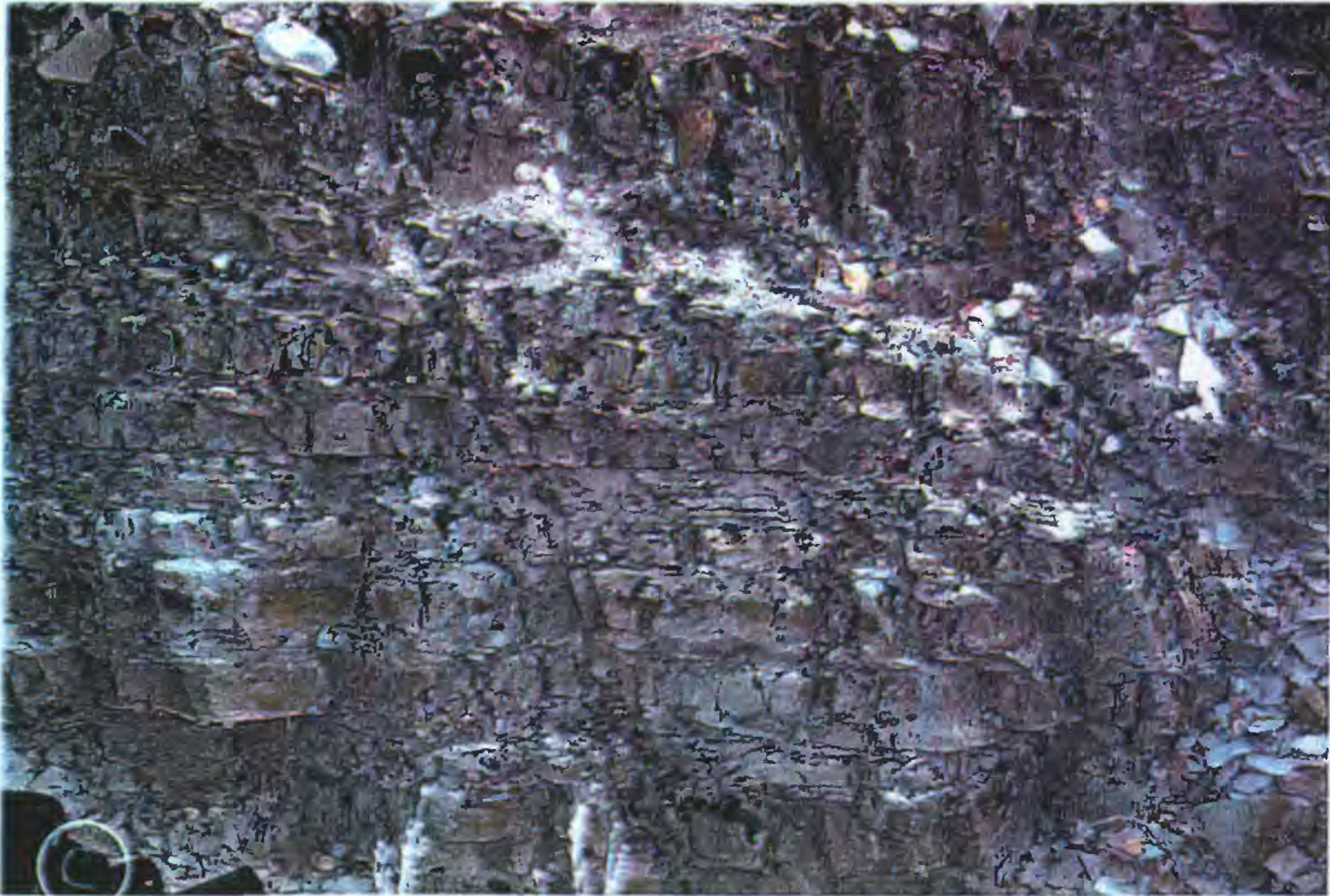


Figure 9. Photograph of thin-bedded siltstone in siltstone and argillite unit of Golconda allochthon. Note sharp bases and normal grading of beds. Buckle on back pack at extreme lower left (circle) is 5 cm in length.

cm-thick beds. The sandstone beds consist principally of chert, quartzite, and argillite grains. Rare beds of bioclastic limestone and calcareous siltstone also are present. One limestone bed consists of sandy packstone that has yielded a diverse conodont assemblage, including apparently indigenous late Missourian or early Virgilian conodonts and redeposited Early Mississippian conodonts (A. Harris, written comm., 1997) (map locality 4, table 1 and figs. 2, 10).

Like the argillite and siltstone unit, the chert and argillite unit contains abundant argillite, but is more siliceous than the argillite and siltstone unit. Stewart and McKee (1977) considered it a different map unit (their Pumpnickel Formation (fig. 2B)), although they showed the nature of the contact between the siltstone and argillite unit (Havallah Formation of Stewart and McKee (1977)) as uncertain. A reconnaissance examination of the chert and argillite unit in the southwestern part of The Cedars quadrangle indicates that it consists dominantly of thin-bedded siliceous argillite with subordinate packages of red-brown siltstone and very fine sandstone, pink claystone, radiolarian chert that is red, green, or black, and greenish gray sponge-spicule chert. Chert bodies commonly are 2- to 10-m thick and compose about 20 percent of the unit. Quartz-rich sandstone beds, as thick as 10 cm, are locally present in the argillite and display sharp basal contacts,

lateral continuity, graded bedding, current ripple cross lamination and other features typical of thin-bedded turbidites.

Radiolarians are the most common index fossils in the argillite and siltstone unit as well as the chert and argillite unit. They are found in bedded chert, siliceous argillite, and siliceous mudstone. Studies of radiolarians in the Golconda allochthon in the Battle Mountain area and in the eastern Tobin Range have determined the stratigraphic ranges of nine Early Mississippian (middle Osagean) to early Late Permian (early Guadalupian) radiolarian assemblages (Murchey, 1989; 1990). The radiolarian faunas of our study area have not been previously studied but systematic high-density radiolarian-dating in other map areas has proven that the Golconda allochthon is characteristically imbricated by multiple thrust faults at all scales (Miller and others, 1982, 1984; Snyder and Brueckner, 1983; Brueckner and Snyder, 1985; Stewart and others, 1986; Murchey, 1990; Tomlinson, 1990).

The location of twelve new microfossil localities from the Havallah sequence in The Cedars quadrangle are shown in table 1 and figure 2. Also shown in table 1 and figure 2 is a previously collected conodont sample (map locality 2) taken from what may be Havallah or possibly the overlap sequence (Stewart and McKee, 1977, p. 27). We tentatively assign this sample to the overlap sequence. Of these localities, ten

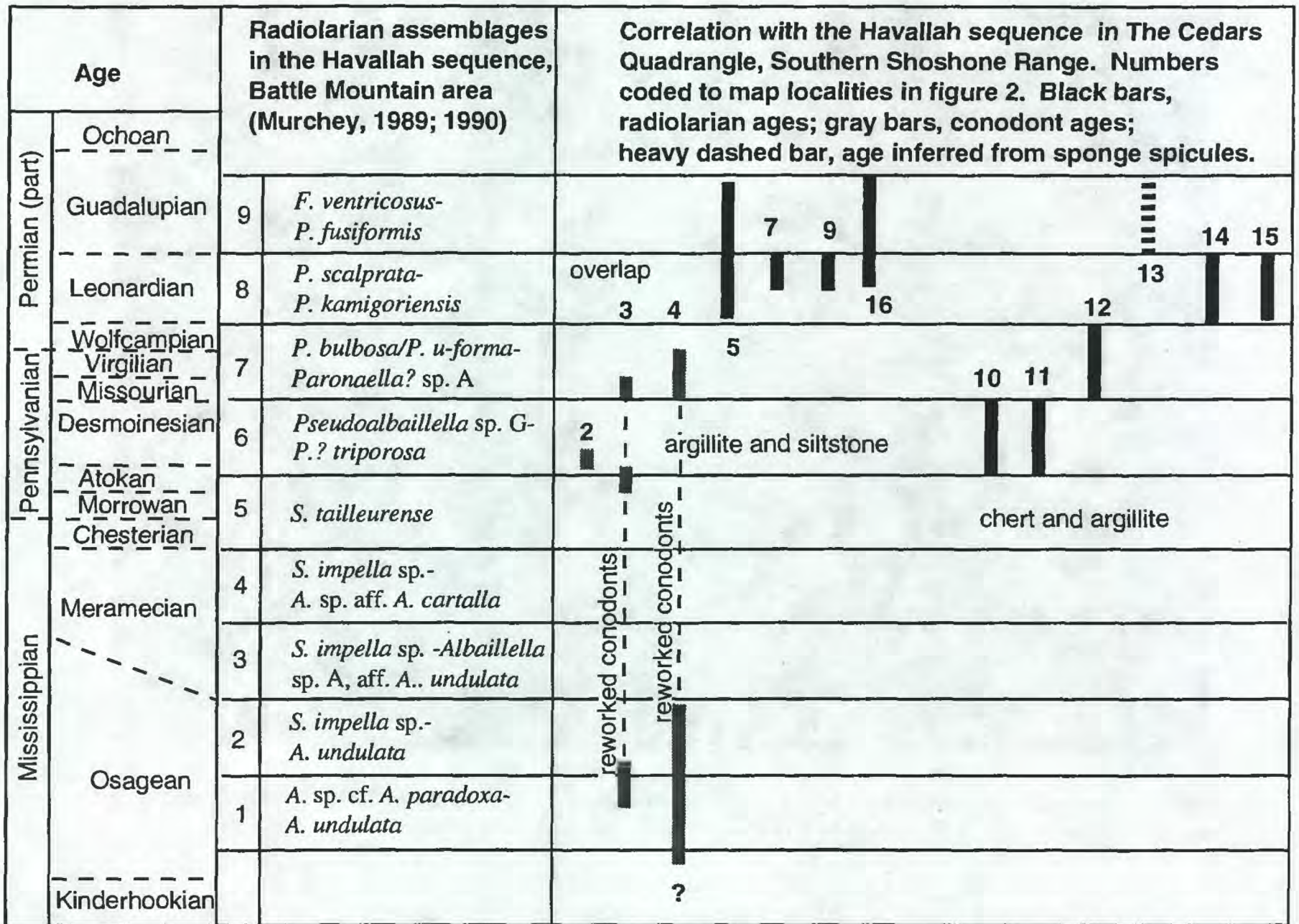


Figure 10. Age ranges of conodont and radiolarian assemblages from the Golconda allochthon in The Cedars quadrangle. Note that dated samples from the argillite and siltstone unit are younger than overlap sequence samples, suggesting that low-angle fault between these units may not have thrust relations. Chert and argillite unit of Golconda allochthon, however, contains assemblages that are older than overlap sequence and the argillite and siltstone unit suggesting that it could have been thrust onto these units.

contained radiolarian assemblages, two contained conodonts, and one contains only sponge spicules. The radiolarian faunas in these samples are correlated in figure 10 with the nine Early Mississippian (middle Osagean) to early Late Permian (early Guadalupian) radiolarian assemblages established in the Havallah sequence in the Battle Mountain area and the Tobin Range by Murcheý (1989; 1990). The conodont samples from the Havallah sequence and overlap sequence also are shown for comparison on figure 10. Of the 11 samples of siliceous fauna from the Havallah, four were collected from the argillite and siltstone unit, whereas seven were collected from the chert and argillite unit. The details of these samples are as follows:

The argillite and siltstone unit in the north-central part of the quadrangle (fig. 2A) contains radiolarians as well as delicate sponge spicules. Map localities 7 (tan and green, chippy siliceous mudstone), 9 (alternating bedded siliceous argillite,

siltstone, and shale; see fig. 9), and 16 (green siliceous mudstone beds to as much as 2 cm thick within a predominantly shale and argillite section) contain radiolarian faunas with elements characteristic of the younger part of the Leonardian *Pseudoalbaillella scalprata*-*Pseudotormentus kamigoriensis* assemblage of Murcheý (1989, 1990). Map locality 5 (green siliceous argillite) has elements of the Leonardian *P. scalprata*-*P. kamigoriensis* or early Guadalupian *Follicucullus ventricosus*-*Pseudoalbaillella fusiformis* assemblages. Map locality 15 (float collection of green siliceous argillite, laminated black chert; tentatively included in the "Pumpnickel Formation" in map figure 2B) is on strike with the samples above and contains the early Guadalupian radiolarian *P. fusiformis*. The Permian radiolarian faunas recovered thus far from the argillite and siltstone unit postdate the youngest conodonts ages, Late Pennsylvanian, obtained

from the quadrangle from either the argillite and siltstone unit (sample 4) or the structurally underlying overlap sequence (map locality 3 in the siltstone, shale, and sandstone unit).

Based on preliminary examinations of the Permian faunas, the relative abundance patterns of sponge spicule and radiolarian faunal groups are similar to those found in faunas from siliceous argillite and mudstone in the structurally lowest thrust-bounded package of the Havallah sequence in the Battle Mountain area (Lithotectonic Unit 1 of Murchey (1990)). *Stauraxon* radiolarians are more abundant than *Albaillellaria* in all samples and delicate sponge spicules are more abundant than radiolarians in some sieve residues. A high ratio of stauraxon radiolarians to *Albaillellaria* is characteristic of relatively deep marginal marine basins in the arc and back arc regions of the Permian Cordillera, but not of the open ocean region to the west (Murchey and Jones, 1993). For similar sponge spicule faunas in the Battle Mountain area, based on spicule morphotypes, relative abundance, and hemipelagic character of host strata, Murchey (1989, 1990) inferred a basin depth between 150 m and 1,000 m.

Samples from the chert and argillite unit were collected from the southern part of The Cedars quadrangle. Localities 10 to 14, collected on a north-south traverse south of Wood Canyon, yielded radiolarian and sponge spicule faunas ranging in age from Middle Pennsylvanian (Desmoinesian) to probable early Late Permian (early Guadalupian?). Localities 10 (green siliceous argillite) and 11 (black chert float) contain faunal elements of the late Middle Pennsylvanian *Pseudoalbaillella* sp. *G - Paronaella? triporosa* fauna of Murchey (1990). Significantly, these faunas are older than the Late Pennsylvanian conodonts in sample 3 of the overlap sequence. Locality 12 (green and maroon siliceous mudstone interbedded with maroon argillite) contains *Pseudoalbaillella bulbosa* and has a possible range from Missourian to Wolfcampian. Sample 14 (bedded green-gray chert with 1- to 2-cm thick beds) contains faunal elements characteristic of the Leonardian *P. scalprata - P. kamigoriensis* assemblage of Murchey (1990). Delicate but fairly diverse sponge spicule assemblages are present with the radiolarian faunas. Based on the paleobathymetric model of Murchey (1989, 1990), the radiolarian-bearing samples were deposited at depths between 150 m and 1,000 m, in a setting possibly deeper and (or) more distal than the depositional site of the argillite and siltstone unit.

Map locality 13 (2 cm bed of black chert) is a sponge spiculite with no radiolarians. The fauna is distinctive for its large monaxons, bean-like rhaxes, strongyles, and round sterrasters. Rhax-bearing spicule faunas appear to be confined to an early Guadalupian depositional belt extending from the Permian Phosphoria basin in Idaho southward down the trend of the Antler Highlands and eastern Golconda allochthon. The faunas are found in autochthonous shallow marine siltstones of the Permian Edna Mountain Formation near Battle Mountain (Murchey and others, 1995) and black bedded chert

of the coeval Phosphoria Formation of southern Idaho (Murchey, 1989). These types of spicule faunas are present in black chert and cherty limestone turbidites of the eastern part of the Havallah sequence elsewhere from northern Nevada (Murchey, 1989, 1990) to at least as far south as the Reese River area in the southern Shoshone Range (Tomlinson, 1990). In the autochthonous rocks of the Phosphoria basin and Antler Highlands and the allochthonous rocks of the Golconda allochthon, the rhax-bearing faunas are spatially associated with phosphatic sandstone or siltstone and the large monaxon spicules are commonly infilled with phosphatic material. We interpret the spicule faunas of locality 13 as a redeposited assemblage probably derived from the lower Guadalupian Edna Mountain Formation or equivalent unit somewhere along the trend of the Antler Highlands. In the north-central part of The Cedars quadrangle, however, we have not recognized overlap sequence rocks that are as young as Guadalupian or that contain rhax spicule faunas.

Tertiary rocks

Tertiary rocks in The Cedars quadrangle consist entirely of intermediate and felsic volcanic rocks. In the northern part of the quadrangle, the volcanic rocks consist of a thick sequence of light gray ash-flow tuff that has been mapped as the Oligocene Caetano Tuff (McKee and Stewart, 1969; Stewart and Carlson, 1976; Stewart and McKee, 1977). These rocks are at least 250 m thick and, at their base, consist of crystal-poor tuff with well developed eutaxitic texture. To the south, these tuffs thin dramatically, possibly due to faulting or irregular topography beneath the tuff. In the southern part of the quadrangle, volcanic rocks consist of red-brown-weathering, porphyritic plagioclase-biotite andesitic or dacitic flows that display a characteristic flaggy planar fabric. The porphyritic volcanic rocks are at least 400 m thick and are exposed over a broad area but are undated. The relation between the Caetano ash-flow tuff and the porphyritic volcanic rocks in the southern part of The Cedars quadrangle is presently unknown. Outcrops of black vitrophyre, crystal-rich tuff and pink weathering densely welded tuff are present in the intervening area. Some of these rocks have been correlated with the Miocene Bates Mountain tuff; others with the Caetano Tuff (Stewart and McKee, 1977). Stratigraphic studies, geochemical analysis, and Ar-Ar age dating of these volcanic units currently are in progress.

STRUCTURAL RELATIONS

The structural geology of The Cedars quadrangle is complex in detail and the observations reported here represent only initial results. Nonetheless, our studies to date allow classification of structures into several categories and

determination of a few preliminary conclusions. We discuss separately below structures in The Cedars quadrangle associated with (1), the Roberts Mountains allochthon; (2) the Golconda "thrust" and allochthon; and (3) high-angle faults.

Roberts Mountains allochthon

Rocks of the Roberts Mountains allochthon display contractional structures at both outcrop and map scale. Outcrop-scale structures are well developed in the bedded chert unit, which exhibits abundant disharmonic folds (fig. 4B). Folds are open to tight and vary in style from chevron to strongly asymmetric. Small-displacement thrust faults and zones of brecciation disrupt the folds. Asymmetric folds at one locality indicate northward structural transport, with axial planes that strike N65°E and dip to the south. In contrast to the bedded chert unit, the black chert unit displays few outcrop-scale folds. This unit lacks argillite interbeds which allow disharmonic folding in the bedded chert unit and instead appears to have deformed as a rigid beam by faulting.

At map scale, the lithologic units that comprise the Roberts Mountains allochthon in the north-central part of The Cedars quadrangle dip moderately to the west. Contacts between these units are thought to be thrust faults, although critical evidence that demonstrate these relations have not yet been established. Radiolarian fauna in the chert are currently being processed to test this hypothesis.

Golconda thrust and allochthon

Rocks of the Golconda allochthon in the north-central part of The Cedars quadrangle are separated from overlap sequence rocks by a poorly exposed, yet prominent fault that dips about 30° to the east (figs. 2 and 11). This fault, which has been correlated with the Golconda thrust (Stewart and Carlson, 1976; Stewart and McKee, 1977), is located at a stratigraphic position that is near the base or within the upper, siltstone, shale and sandstone unit of the overlap sequence. The fault is commonly marked by a 10-m-thick zone of dark scaly argillite and, where the conglomerate and siltstone unit is in the footwall, by sheared and brecciated rocks in the footwall. Thin sections of the scaly argillite indicates that grain-scale deformation is absent or poorly developed at this contact, suggesting that deformation may have occurred at relatively high hydrostatic pressures. Tectonic slivers of the siltstone, shale, and sandstone unit of the overlap sequence are locally incorporated in the fault. These slivers, coupled with varying stratigraphic sections adjacent to the contact in the footwall and hanging wall units, show that the contact is a fault. Nonetheless, bedding in rocks above and below the fault generally are concordant with the fault. In the few significant outcrops of hanging wall rocks (Golconda allochthon)

examined, strata dip consistently eastward and do not display folds or other evidence of contractional deformation.

Available age data indicate that strata in the footwall are at least as young as Late Pennsylvanian (late Missourian), whereas strata in the hanging wall are no older than Late Pennsylvanian (late Missourian or early Virgilian) (table 1). These relations allow two possibilities. The first possibility is that the fault is a thrust fault that duplicates Upper Pennsylvanian strata, placing basal strata onto shelfal strata. This interpretation would require that the fault is essentially a footwall flat that outside our study area has ramped upward from a position below Upper Pennsylvanian strata. This hypothesis implies that shortening was significant because the fault places basal facies onto shelfal facies. A thrust model could be confirmed if Permian strata are eventually found to be present in the undated uppermost part of the siltstone, shale and sandstone unit in the footwall of the fault. The second possibility is that the fault is fundamentally a depositional contact modified by small displacement faults that may be of extensional character. In this case, small displacement faults form a zone of stratal disruption in Upper Pennsylvanian strata, perhaps in an interval of incompetent shale. This hypothesis requires the rocks of the overlap sequence and the Golconda allochthon at one time formed a continuous depositional succession that recorded basin subsidence in the late Paleozoic. This hypothesis satisfies our present observations and data, but it is not supported by regional relations of the Golconda allochthon, which exhibits older-on-younger relations indicative of contractional deformation (for example, Miller and others, 1982). Our studies to date cannot distinguish between these two possibilities. Continuing paleontological analysis of footwall and hangingwall rocks coupled with structural studies may help resolve this question.

High-angle faults

Ubiquitous high-angle normal faults in the north-central part of The Cedars quadrangle greatly complicate its geology. Most high-angle faults are small displacement, north-trending structures. The most significant of these are portrayed in figure 2 and include range-bounding west-dipping structures along the western Shoshone Range as well the north-striking fault that marks the eastern extent of the Golconda allochthon in the interior of Cedars quadrangle. Using the basal contact of the overlap sequence as a datum, the latter fault drops rocks down to the west a minimum of 300 m, whereas the distribution of Tertiary volcanic rocks suggest a minimum displacement of about 500 m, assuming they were once present east of the fault as well as to the west. These faults truncate the Tertiary volcanic rocks, indicating that they were active in post-Oligocene time.

Not shown in figure 2 are numerous very small displacement brittle faults that appear to be related to the more

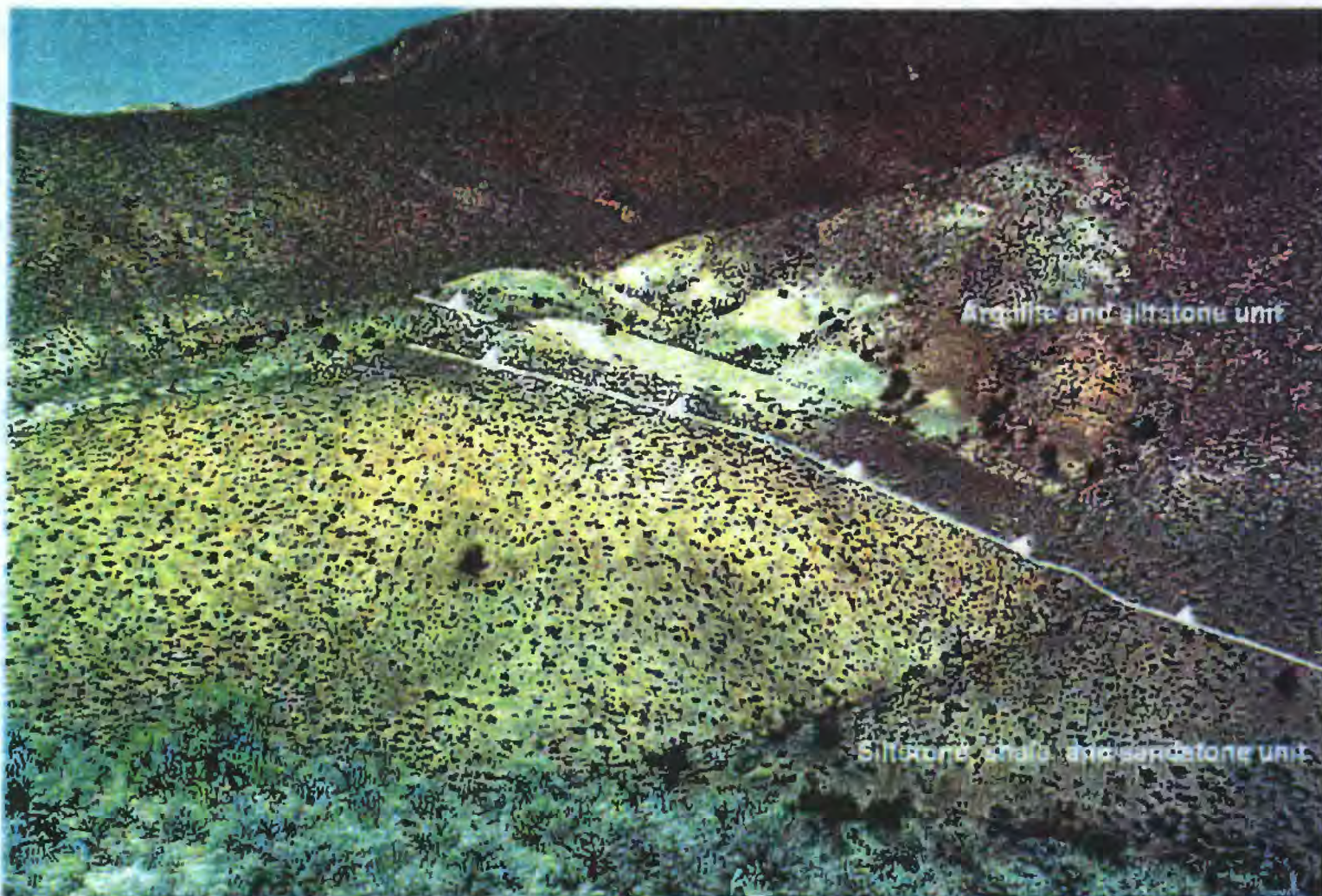


Figure 11. Northward view of low-angle fault contact between argillite and siltstone unit of Golconda allochthon and siltstone, shale, and sandstone unit of overlap sequence. Contact is marked by dark, scaly shale.

prominent north-striking faults and cause much of the structural complexity in the north-central part of the quadrangle. These faults commonly are difficult to locate in the field because of poor exposure, superimposed alteration, and because they commonly juxtapose similar rocks. Marker beds, however, for example the basal unconformity of the overlap sequence, indicate that incremental amounts of down-to-the-west displacement has resulted in more than 500 m of cumulative displacement on these faults (fig. 12). These relations show that the Battle Formation, a common host rock in the Battle Mountain Mining District, is significantly thinner than is apparent from the map pattern shown in figure 2A.

A second set of widely spaced high angle normal faults intersects the north-striking faults in the north-central part of the quadrangle (fig. 2). These faults are east-striking and appear to control positions of some major canyons. Over 200 m of displacement can be demonstrated on these faults, although they have an inconsistent sense of displacement. The southernmost faults of this type in the north-central part of The Cedars quadrangle form a trough that drops the siltstone, shale, and sandstone unit down against the conglomerate and siltstone unit. The northernmost east-striking faults may form the southern margin of a second east-striking trough whose axis lies to the north. These structural troughs seem to be part of a large, east-striking extensional depression in the central Shoshone Range defined by the distribution of the Caetano Tuff (Stewart and Carlson, 1976; Stewart and McKee, 1977).

The relative ages of the north and east-striking fault systems are presently unclear. Map patterns suggest that the north-striking faults displace the east-striking ones and thus are younger, although alternatively both systems may have developed concurrently.

ALTERATION

A zone of alteration is present in the north-central part of The Cedars quadrangle, along the western margin of the Shoshone Range (fig. 2). Host rocks of the alteration are the conglomerate and siltstone unit of the overlap sequence. The alteration is characterized by widespread silicification that is coupled with local development of wispy, red halos marking sites of oxidized disseminated pyrite (fig. 13). Workings excavated for mercury are present in the most intense areas of alteration and the large number of recent prospect pits indicate that gold exploration also has been focused on this zone. The alteration is concentrated along north-striking zones that are most likely controlled by the north-striking faults discussed above. Alteration appears to diminish eastward in the conglomerate and siltstone unit, does not affect the overlying siltstone, shale, and sandstone unit of the overlap sequence, and only locally affects the rocks of the Golconda allochthon. No igneous rocks have been found to be associated with the altered rocks.

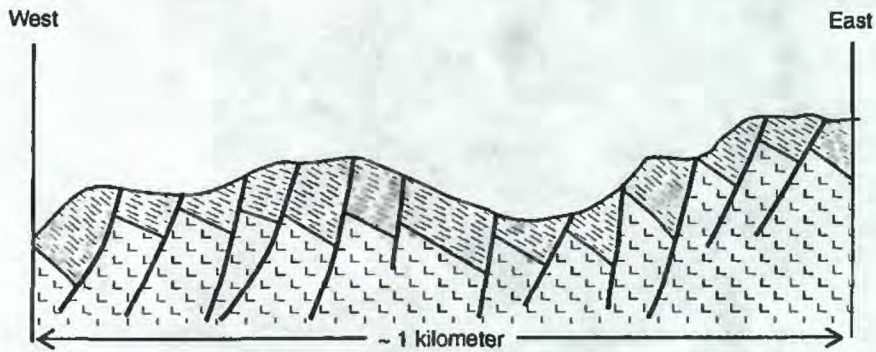


Figure 12. Conceptual structural section illustrating the apparent paradox of eastward bedding attitudes and westward regional dip. Numerous west-dipping normal faults drop section down to the west in incremental fashion. Poor exposure, massive lithologic units, and alteration obscure normal faults in the field so that stratigraphic section

REGIONAL CORRELATION OF THE OVERLAP SEQUENCE

Two units are recognized in the overlap sequence in the area of figure 2A: (1) an undated lower unit of conglomerate and siltstone and (2) an upper unit of siltstone, shale, and sandstone that contains a sandy limestone with Late Pennsylvanian (Missourian) conodonts and reworked Osagean and Atokan conodonts. These strata form a marine sequence deposited on deformed strata of the Roberts Mountains allochthon.

The "classic" Antler overlap sequence of Roberts (1964) is present in the Battle Mountain area to the north of The Cedars quadrangle (fig. 1). From oldest to youngest, the overlap sequence in the Battle Mountain area includes the Middle Pennsylvanian (Atokan, Desmoinesian?) Battle Formation, Pennsylvanian and Permian Antler Peak Limestone, and Permian Edna Mountain Formation (fig. 14). The Battle Formation and limestone units correlative with the Antler Peak Limestone have been mapped as far north as the Osgood Mountains (e. g. Saller, 1980) (fig. 1).

From the northern Shoshone Range north to the Osgood Mountains, deposition on the Antler orogenic highlands occurred during regional subsidence in the Pennsylvanian and early Permian (Roberts, 1964; Saller, 1980; Madrid, 1987; Miller and others, 1992). Topographic irregularities are reflected in the wide variability in thickness of the Battle Formation: 240 m thick at Battle Mountain; 40 to 130 m thick in the Osgood Mountains (Saller, 1980), 30 to 200 m thick in the northern Shoshone Range (Madrid, 1987), suggesting that sandstone and conglomerate of the Battle Formation accumulated in valleys of the foundering highlands. Saller (1980) described a transgressive sequence of environments and lithofacies within the Battle Formation beginning with conglomeratic proximal braided stream deposits and culminating with calcareous sandstone, mudstone, and conglomerate of tidal and deltaic origin. In the northern Shoshone Range, the sequence consists of undated fluvial strata

and interbedded talus deposits that transition upward to marine strata (limestone) with conodonts having a possible range from Middle Pennsylvanian to Early Permian (Madrid, 1987).

The conglomerate and siltstone unit in The Cedars quadrangle is likely coeval with the Battle Formation in its type area. It has not been dated directly but is depositionally overlain by Missourian strata. We interpret the unit as a marine turbidite sequence whose coarse-grained detritus may have been carried to the shores of the Antler highlands by high energy fluvial systems similar to those which deposited non-marine strata of the type Battle Formation. These gravels were subsequently redeposited into an extensional marine basin, possibly in a fan-delta along a faulted margin. The submarine basement of the Antler islands and, possibly, the easternmost margin of the Havallah depositional basin must have been composed of deformed strata of the Roberts Mountains allochthon.

The conglomerate and siltstone unit consists of thick, coarse-grained poorly-sorted clastic deposits that may represent a transitional facies between nonmarine deposits of the classic Battle Formation and clastic marine units in the Havallah basin, which was located to the west prior to thrusting. Coeval units in the Havallah basin consist of submarine conglomeratic debris flows with clasts of Devonian and older radiolarian chert that were deposited above latest Devonian (locally) and Mississippian pillow basalt and pelagic radiolarian chert (Murchey, 1990). Alternatively, the conglomerate and siltstone unit may represent an eastward transition from the Battle Formation to coeval and (or) older Mississippian and Lower Pennsylvanian marine conglomerate and quartzite (e.g., the Diamond Peak Formation in eastern Nevada) that were deposited in the foreland of the Antler orogenic belt.

Shallow seas transgressed most of the Antler highlands by the Late Pennsylvanian, creating a variety of shallow marine environments favorable for the deposition of the Missourian or Virgilian to Wolfcampian Antler Peak Limestone and the Atokan to Wolfcampian Etchart Limestone (Saller, 1980). In the north-central part of The Cedars quadrangle, the lower part of the siltstone, shale, and sandstone unit contains a thin interval of limestone that yields conodonts as young as Missourian. These data indicate that this part of the siltstone, shale, and sandstone unit is coeval with at least part of the Antler Peak Limestone. The siltstone, shale, and sandstone unit displays sedimentary structures that indicate deposition above wave base. The upper part of the siltstone, shale, and sandstone unit above the limestone-bearing interval is undated but is lithologically similar to the early Guadalupian Edna Mountain Formation and thus may include Permian strata.

As previously mentioned, map locality 3 in the sandy limestone of the siltstone, shale, and sandstone unit contains a conodont fauna with Missourian conodonts and older reworked Atokan and Osagean conodonts. The Atokan conodonts were reworked from marine strata coeval with parts of the Battle

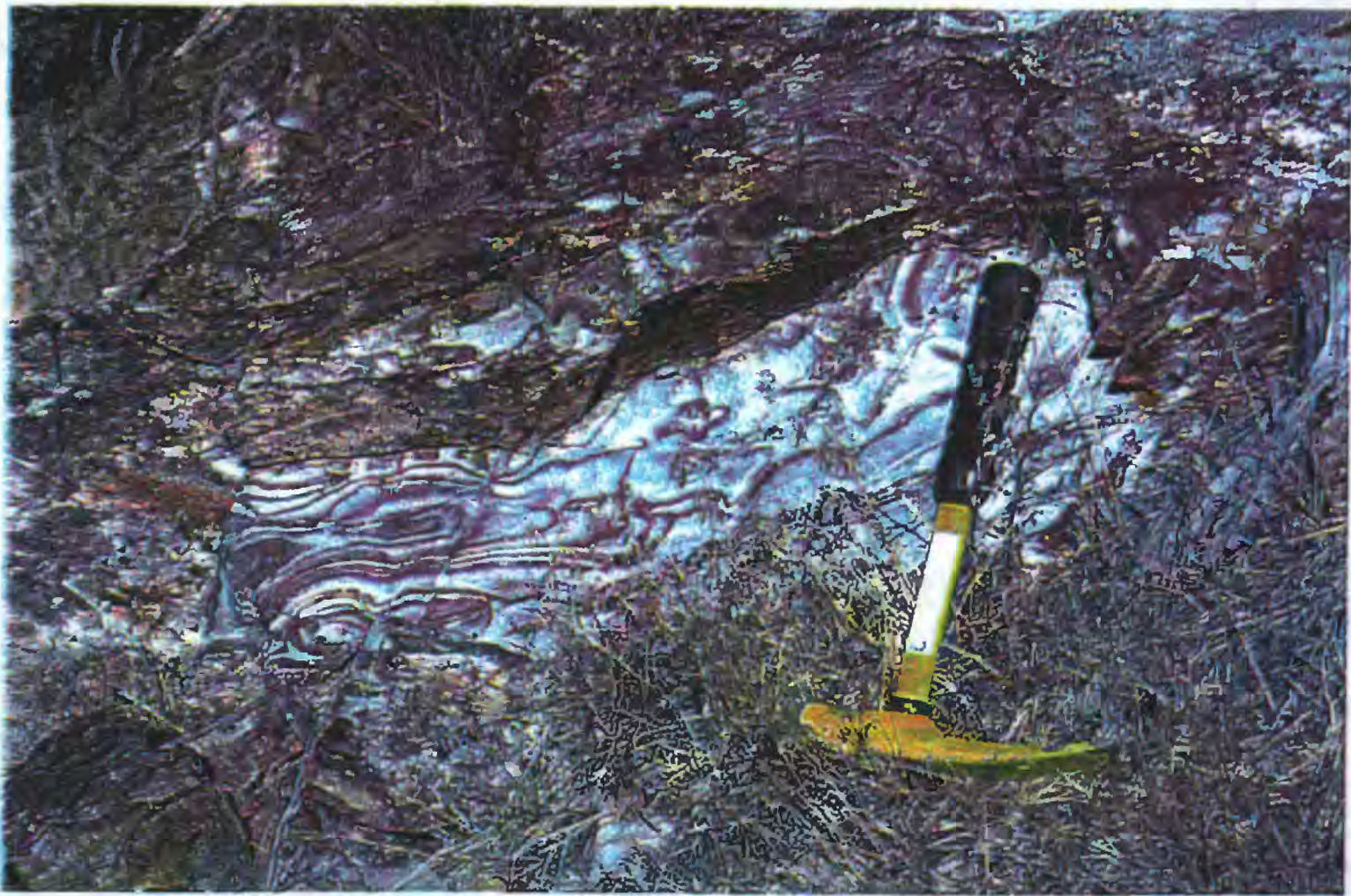


Figure 13. Photograph of liesegang banding in alteration zone near small, abandoned mercury mine. Alteration developed in siltstone of conglomerate and siltstone unit of overlap sequence.

Formation, Highway Limestone, and the Etchart Limestone. The presence of the middle Osagean reworked conodonts is intriguing because Mississippian strata are not preserved in the classic Antler sequence. The conodonts indicate that Osagean marine strata were deposited locally in the Antler highlands and subsequently eroded, or that Early Mississippian conodonts from the foreland or shelf region to the east were transported westward to the site of the former Antler orogenic belt, probably in the Pennsylvanian.

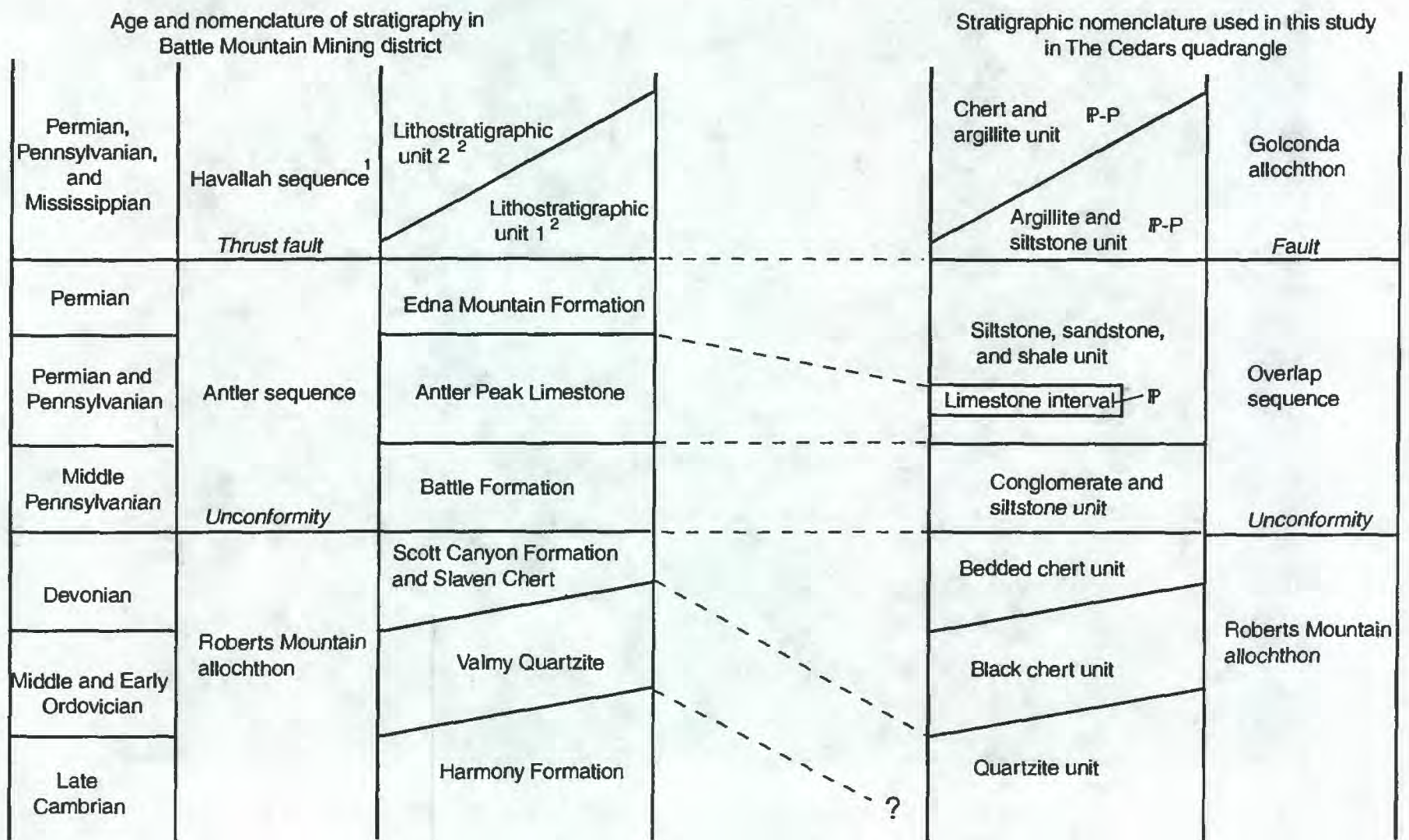
REGIONAL CORRELATION OF THE GOLCONDA ALLOCHTHON

The argillite and siltstone unit of figure 2A, and the more siliceous and partly older chert and argillite unit to the south in figure 2B, are generally similar in age, lithology, and faunal assemblages to the structurally lowest, thrust-bounded lithotectonic units of the Havallah sequence lying along the eastern edge of the Golconda allochthon in the Battle Mountain area, southernmost Shoshone Range, and the northern Toiyabe Range (Murchey, 1990; Tomlinson, 1990) (lithostratigraphic unit I, figs. 14 and 15). All of these exposures of the Havallah sequence are dominated by hemipelagic strata (argillite, siltstone, mudstone) deposited in a relatively deep marine environment. Structurally higher lithotectonic units of the Golconda allochthon are characterized by less argillite, more bedded chert, pillow basalt, and in some structural units, a

higher proportion of turbidite and debris-flow sequences (Stewart and others, 1986; Murchey, 1990; Tomlinson, 1990).

The argillite and siltstone unit undoubtedly was deposited in a relatively deep, hemipelagic setting similar to that of the Havallah strata, which elsewhere are demonstrably allochthonous. We insert a word of caution, however, regarding the correlation of the low-angle fault separating the argillite and siltstone unit from the underlying units of the overlap sequence in The Cedars quadrangle with the Golconda thrust fault. We have not proven an older-over-younger relation between these units, nor eastward vergence on the fault. It remains possible that the fault is an extensional fault and(or) that the Pennsylvanian overlap sequence (fig. 2A) foundered and was subsequently covered by deeper marine hemipelagic facies of the argillite and siltstone unit. If so, the "real" Golconda thrust may be present at a structurally higher position in The Cedars quadrangle. One possibility is that it lies beneath the more siliceous chert and argillite unit in the southern part of the quadrangle, which our age data indicates predates part of the overlap sequence. If so, the siltstone and argillite unit might lie in the footwall of the Golconda thrust as a preserved, autochthonous part of the Havallah basin, a relation not previously observed in north-central Nevada.

Figure 15 is a schematic north-south cross section of the Golconda allochthon showing inferred age, lithologic, and structural relations along the Golconda thrust from the Osgood Mountains to the southern Shoshone Range and northern Toiyabe Range along the Battle Mountain-Eureka trend. This



¹ Silberling and Roberts (1962)

² Murchey (1990)

Figure 14. Proposed stratigraphic correlation, shown with dashed lines, rocks in The Cedars quadrangle with rocks in the Battle Mountain area. Solid diagonal lines indicate structural contacts between units. Ages and stratigraphy of Battle Mountain area from Doebrich and Theodore (1996).

diagram, modified from Tomlinson's (1990) schematic east-west cross section, illustrates that more distal, basal parts of the Havallah basin lie above the Golconda thrust in the north, whereas more proximal parts of the basin lie above the thrust to the south. This relation suggests that the Battle Mountain-Eureka trend crosses the structural strike of the Golconda allochthon.

IMPLICATIONS TO MINERALIZATION

The Cedars quadrangle is located about 20 km west of the main axis of the Battle Mountain-Eureka trend, in about the same position in relation to that trend as the Cove and McCoy deposits (Shawe, 1991). The deposits of the Battle Mountain Mining District and associated deposits form the northern end of the Battle Mountain-Eureka trend and delineate a subtrend that extends southward over 100 km from the Getchell and Twin Creeks deposits to the Cove and McCoy deposits (fig. 1). Location of The Cedars quadrangle adjacent to the Battle

Mountain Eureka-trend and on the southward projection of the deposits of the Battle Mountain area suggests that the quadrangle may be prospective for gold deposits that are pluton-related.

Doebrich and Theodore (1996) presented a model for gold mineralization in the Battle Mountain district and identified several characteristics that are common denominators to its major deposits. These are: (1) intersection of regional structural features such as faults; (2) presence of pre-late Eocene north-striking normal faults; (3) the presence of late Eocene or early Oligocene magmatically related hydrothermal systems; (4) the presence of rocks of the Antler sequence as a receptive host, and (5) the presence of the Golconda thrust, which acted as a seal for hydrothermal fluid flow.

Our initial stratigraphic and structural framework studies suggest that many of these common denominators also are present in The Cedars quadrangle. The stratigraphic relations in the quadrangle compare favorably with those in the Battle Mountain area in that correlatives of the Antler sequence are present and are sufficiently thick and coarse-grained to provide

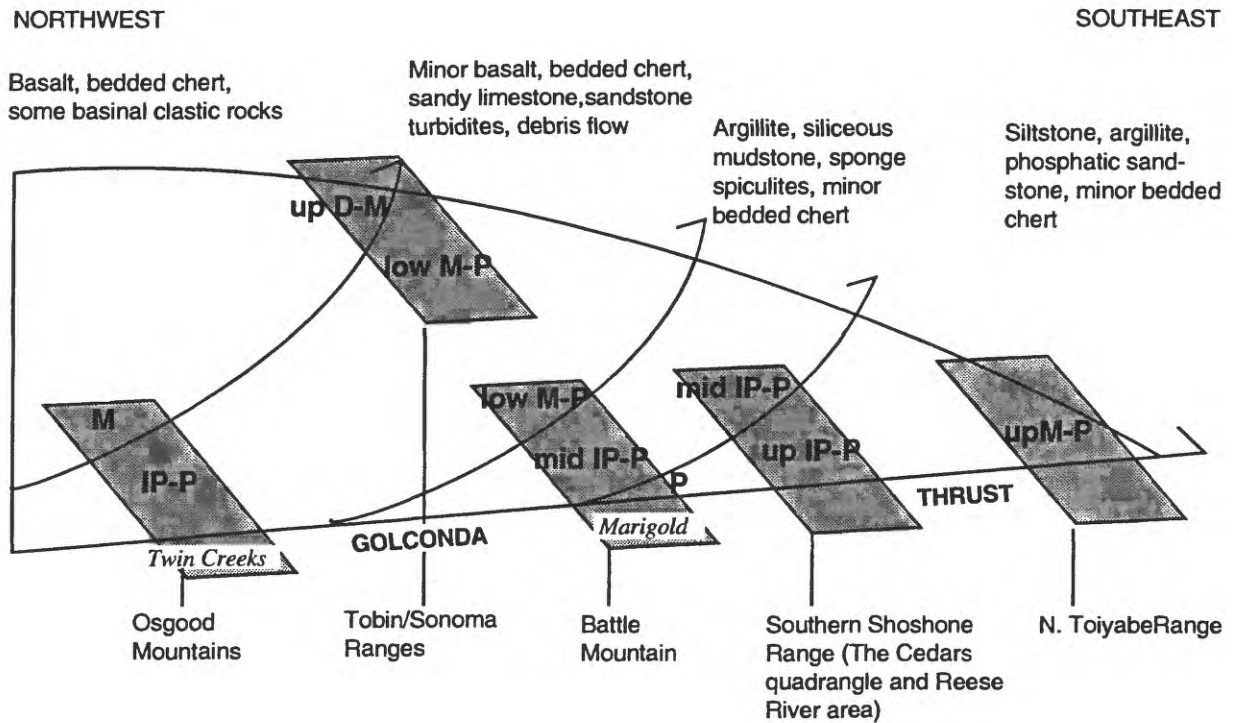


Figure 15. Conceptual model for the Golconda allochthon along a profile along Battle Mountain-Eureka trend (fig. 1) from the Osgood Mountains to the northern Toiyabe Range. Diagram illustrates relative structural positions and ages (Devonian to Permian) of major lithostratigraphic units of the Golconda allochthon. No attempt has been made to illustrate internal structural complexities within individual lithostratigraphic units. The structural position of the Twin Creeks and Marigold deposits are shown for reference.

a receptive host for subsequent hydrothermal ore deposition. Widespread alteration is present in these rocks in The Cedars quadrangle. Thin-bedded and fine-grained rocks similar to those of the Golconda allochthon overlie the Antler sequence on a low-angle structural contact analogous to the Golconda thrust. The restriction of hydrothermal alteration to coarse-grained rocks below this low-angle fault, despite our uncertainty about its correlation, indicates that it may have played a role similar to that of the Golconda thrust in controlling the channeling and ponding of ascending hydrothermal fluids. Our identification of north-striking and east-striking faults in The Cedars quadrangle allows the possibility that mineralization may be present in the areas where these faults intersect. Alteration zones are visibly related to north-striking faults, indicating that hydrothermal fluid flow was structurally controlled. The absence of outcrops of intrusive rocks associated with the hydrothermal system and the silica + pyrite alteration products prevent confirmation of a magmatic origin for the system but it may reasonably be hypothesized to have originated from a magmatic body at depth. At present, we do not know the precise age of the hydrothermal system nor the age of the structural zones that controlled its distribution, but both are likely of Tertiary age.

The presence of hydrothermal alteration in The Cedars

quadrangle without associated magmatic rocks suggests that sediment-hosted Carlin-type gold occurrences also must be considered. Although The Cedars quadrangle is located to the west of the Carlin trend, Carlin-type deposits are located at the Pipeline and Cortez deposits about 30 km to the northeast of The Cedars quadrangle and at the Getchell and Twin Creeks deposits, about 75 km north of Battle Mountain. The Pipeline and Cortez deposits are located in carbonate rocks in the footwall of the Roberts Mountains allochthon, a relation not exposed in The Cedars quadrangle. Rytuba (1985), however, suggested that the heat that drove hydrothermal systems at the Cortez and nearby deposits was provided by the waning stage of the magmatic system that produced the Caetano Tuff. The source of the heat that produced the hydrothermal alteration in The Cedars quadrangle is unknown, but could have been related to the Caetano Tuff magmatic system through a hydrothermal system developed in the east-striking extensional trough. The Twin Creek and Getchell deposits are structurally controlled deposits hosted in part by rocks of the Roberts Mountains allochthon and carbonate rocks of the overlap sequence that unconformably overlie the Roberts Mountains allochthon. The Twin Creeks and Getchell deposits are located about the same distance to the north of the porphyry-related and distal disseminated silver-gold deposits in the Battle

Mountain Mining District as The Cedars quadrangle is to the south of the Battle Mountain Mining District. This distribution suggests an alternative possibility that the hydrothermal systems that led to mineralization of the Carlin-type deposits at Twin Creeks and Getchell could be mineralized systems distal to magmatic centers in the Battle Mountain Mining District (T. G. Theodore, oral comm., 1997). This model suggests that Carlin-type deposits analogous to those at Twin Creeks and Getchell also might be possible in The Cedars quadrangle.

CONCLUSION

Initial results in The Cedars quadrangle show that the Paleozoic rocks of the area can be divided into three major lithostratigraphic units: the Roberts Mountains allochthon, overlap sequence, and Golconda allochthon. The Roberts Mountains allochthon consists of contractionally deformed black chert, bedded chert, and fine-grained quartzite. The age of these units has not been established in The Cedars quadrangle but probably is correlative with the Ordovician Valmy Formation and the Devonian Slaven Chert or Devonian Scott Canyon Formation.

In The Cedars quadrangle, the overlap sequence consists of two parts, in aggregate measuring about 400 m in thickness. The lower part consists of interbedded chert-pebble conglomerate and thin-bedded siltstone that comprise sedimentary-gravity flows including turbidites. These rocks appear to be correlative with the Battle Formation in the Battle Mountain area. The upper part of the overlap sequence consists of heavily bioturbated thin-bedded siltstone, shale, and sandstone, which near its base includes a thin interval of interbedded calcareous sandstone and sandy limestone. The limestone has yielded Late Pennsylvanian conodonts that indicate it may be correlative with at least part of the Antler Peak Limestone of the Battle Mountain area. The remainder of the upper part of the overlap sequence in The Cedars quadrangle displays lithologic affinities to the Permian Edna Mountain Formation of the Battle Mountain area, although we have not recovered any fossils that might confirm this correlation. The entire overlap succession appears to compose a shoaling sequence that progressed from deposition of turbidites at the base to shelfal clastics and limestone at the top. The marine character of the overlap sequence in The Cedars quadrangle suggests that it may have been deposited in a location more basinward than the dominantly fluvial and shallow-marine overlap sequence deposits in the Battle Mountain area. Considering the thickness of the Battle Formation and its correlatives (generally < 300 m), the preponderance of fluvial deposits, and the extensional tectonic environment of its deposition (Saller, 1980; Miller and others, 1992), we suggest that the overlap sequence may comprise fan-delta deposits that prograded southwestward from the

Antler highlands.

Overlying the overlap sequence in The Cedars quadrangle is the Golconda allochthon, whose rocks are assigned to the Havallah sequence of Murchey (1990) and which contains two distinct lithologic assemblages. The northern assemblage consists of thin-bedded siltstone and argillite that yields Late Pennsylvanian conodonts and Permian radiolarian faunas, whereas the southern assemblage consists of argillite and chert that yield Middle Pennsylvanian to Permian radiolarian assemblages. Both lithologic assemblages are most similar to hemipelagic deposits that are the most proximal of the structural-stratigraphic packages recognized by Murchey (1990) in the Golconda allochthon. We suggest that both lithologic assemblages of the Havallah in The Cedars quadrangle were probably deposited along the eastern margin of the Havallah basin and now comprise some of the structurally lowest rocks of the Golconda allochthon.

Separating the overlap sequence and the Golconda allochthon in The Cedars quadrangle is a low-angle fault that is located at the position of the Golconda thrust in the Battle Mountain area. Our paleontologic data and structural observations, however, at present do not confirm older-on-younger relations on this fault. Instead, the fault could represent a zone of stratal disruption in an otherwise homoclinal sequence. The stratal disruption could have been caused by extensional deformation, perhaps by submarine landsliding in the Permian. Alternatively, it is possible that the undated siltstone, shale, and sandstone unit in the upper part of the overlap sequence may prove to contain Permian fossils, thus requiring a thrust relation along the low-angle fault. A third possibility is that the Golconda thrust may be located at the contact between the siliceous, southern lithologic assemblage of the Havallah sequence in The Cedars quadrangle and the siltstone and argillite of the northern assemblage of the Havallah. This relation would require that the most proximal part of the Havallah basin (i.e., the siltstone and argillite unit) be present in the footwall of the Golconda thrust, a relation that has not been previously recognized.

Our studies in The Cedars quadrangle provide an opportunity to test and refine the model developed by Doebrich and Theodore (1996) for ore genesis in the Battle Mountain Mining District. They suggested that fluids emanating from porphyritic intrusions resulted in the distal disseminated silver-gold mineralization both near the magmatic bodies and in adjacent or structurally higher areas that lack magmatic bodies. The Cedars quadrangle contains most of the elements critical for ore deposition, including (1) the chemically receptive Antler sequence, (2) an overlying low-angle fault, and (3) hydrothermal alteration possibly related to a buried magmatic system at the intersection of generally north and east-striking high-angle fault systems. These findings suggest that the conditions suitable for distal disseminated silver-gold occurrences are present in The Cedars quadrangle.

Acknowledgments

We gratefully acknowledge Anita Harris and Bruce Wardlaw for their expert analysis of conodont assemblages collected from The Cedars quadrangle. We also thank Dave Blake for helpful discussions of the alteration and exploration history of the area and Ivano Aiello for support in the field. Constructive reviews of the manuscript were provided by Ted Theodore and Dick Tosdal. We are especially grateful to Theodore for introducing us to the geology of The Cedars quadrangle and providing advice and encouragement during the course of the project.

REFERENCES CITED

- Brueckner, H. K., and Snyder, W. S., 1985. Structure of the Havallah sequence, Golconda allochthon, Nevada; Evidence for prolonged evolution in an accretionary prism: *Geological Society of America Bulletin*, v. 96, p. 1113-1130.
- Burchfiel, B.C., and Davis, G.A., 1972, Structural framework and evolution of the southern part of the Cordilleran orogeny, western United States: *American Journal of Science*, v. 272, p. 97-118.
- Brooks, J.W., Meinert, L.D., Kuyper, B.A., and Lane, M.L., 1991, Petrology and geochemistry of the McCoy gold skarn, Lander County, Nevada, *in* Raines, G.L., Lisle, G.E., Schafer, R.W., and Wilkinson, W.H., *Geology and ore deposits of the Great Basin: Reno, Nevada*, Geological Society of Nevada, p. 419-442.
- Doeblich, J.J., and Theodore, T.G., 1996, Geologic history of the Battle Mountain mining district, Nevada, and regional controls on the distribution of mineral systems, *in* Coyner, A.R., and Fahey, P.L., eds., *Geology and Ore Deposits of the American Cordillera: Geological Society of Nevada Symposium Proceedings, Reno/Sparks, Nevada, April 1995*, p. 453-483.
- Foo, S.T., Hays, Jr., R.C., and McCormack, J.K., 1996, Geology and mineralization of the Pipeline gold deposit, Lander County, Nevada, *in* Coyner, A.R., and Fahey, P.L., eds., *Geology and ore deposits of the American Cordillera: Geological Society of Nevada Symposium Proceedings, Reno/Sparks, Nevada, April 1995*, p. 95-109.
- Gilluly, J. and Gates, O., 1965, Tectonic and igneous geology of the northern Shoshone Range, Nevada: *U.S. Geological Survey Professional Paper 465*, 147 p.
- Hotz, P. E. and Willden, R., 1964, Geology and mineral deposits of the Osgood Mountains quadrangle, Humboldt County, Nevada: *U.S. Geological Survey Professional Paper 431*, 128 p.
- Madrid, R., 1987, Stratigraphy of the Roberts Mountains allochthon in north-central Nevada [Ph.D. thesis]: Stanford, California, Stanford University, 336 p.
- McKee, E.H., and Stewart, J.H., 1969, Geologic map of The Cedars 15' quadrangle, Lander County, Nevada: *U.S. Geological Survey Open-File Report 69-158*, 1 sheet, scale 1:62,500.
- Miller, E.L., Holdsworth, B.K., Whiteford, W.B., and Rodgers, D., 1984, Stratigraphy and structure of the Schoonover sequence, northeastern Nevada; implications for Paleozoic plate-margin tectonics: *Geological Society of America Bulletin*, v. 95, p. 1063-1076.
- Miller, E.L., Kanter, L.R., Larue, D.K., Turner, R.J., Murchey, B., and Jones, D.L., 1982, Structural fabric of the Paleozoic Golconda allochthon, Antler Peak quadrangle, Nevada: progressive deformation of an oceanic sedimentary assemblage: *Journal of Geophysical Research*, v. 87, no. B5, p. 3795-3804.
- Miller, E.L., Miller, M.M., Stevens, C.H., Wright, J.E., and Madrid, R., 1992, Late Paleozoic paleogeographic and tectonic evolution of the western U.S. Cordillera, *in* Burchfiel, B.C., Lipman, P.W., and Zoback, M.L., eds., *The Cordilleran orogen: conterminous U.S.: Boulder, Colorado*, Geological Society of America, *The Geology of North America*, v. G-3, p. 57-106.
- Murchey, B. L., 1989, Late Paleozoic siliceous basins of the western Cordillera of North America (Nevada, California, Mexico, and Alaska); three studies using radiolarians and sponge spicules for biostratigraphic, paleobathymetric, and tectonic analyses [Ph.D. thesis]: Santa Cruz, University of California, 188 p.
- Murchey, B.L., 1990, Age and depositional setting of siliceous sediments in the upper Paleozoic Havallah sequence near Battle Mountain, Nevada: implications for the paleogeography and structural evolution of the western margin of North America, *in* Harwood, D.S., and Miller, M.M., eds. *Paleozoic and early Mesozoic paleogeographic relations; Sierra Nevada, Klamath Mountains, and related terranes: Geological Society of America Special Paper 255*, p. 137-155.
- Murchey, B. L., and Jones, D. L., 1992, A mid-Permian chert event: widespread deposition of biogenic siliceous sediments in coastal, island arc and oceanic basins: *Palaeogeography, Palaeoclimatology, Palaeoecology*, v. 96, p. 161-174.
- Murchey, B. L., and Jones, D. L., 1993, Two coeval radiolarian-sponge associations in eastern Oregon: environmental and tectonic significance, *in* Vallier, T. and Brooks, H. (eds.): *U.S. Geological Survey Professional Paper 1439*, Chapter 9, p. 183-198.
- Murchey, B. L., Theodore, T. G., and McGibbon, D. H., 1995, Regional implications of newly discovered relations of the Permian Edna Mountain Formation, North-central Nevada: *Geology and Ore Deposits of the American Cordillera: Symposium, Reno-Sparks, Nevada, April 10-13, 1995, Program with Abstracts*, p. A57-A58.
- Roberts, R.J., 1964, Stratigraphy and structure of the Antler Peak quadrangle, Humboldt and Lander Counties, Nevada: *U.S. Geological Survey Professional Paper 459-A*, 93 p.
- Roberts, R.J., 1966, Metallogenic provinces and mineral belts in Nevada: *Nevada Bureau of Mines Report 13*, p. 47-72.
- Roberts, R.J., Hotz, P.E., Gilluly, J., and Ferguson, H.G., 1958, Paleozoic rocks of north-central Nevada: *American Association of Petroleum Geologists Bulletin*, v. 42, no. 12, p. 2813-2857.
- Rytuba, J.J., 1985, Development of disseminated gold deposits of Cortez, Horse Canyon, and Gold Acres, Nevada at the end stage of caldera-related volcanism: *U.S. Geological Survey Circular 949*, p. 47.
- Saller, A. H., 1980, Depositional setting of post-Antler Pennsylvanian strata in north-central Nevada [M.A.thesis]: Stanford, California, Stanford University, 118 p.
- Shawe, D.R., 1991, Structurally controlled gold trends imply large gold resources in Nevada, *in* Raines, G.L., Lisle, R.E., Schafer, R.W., and Wilkinson, W.H., eds., *Geology and ore deposits of the Great Basin symposium proceedings: Geological Society*

- of Nevada, Reno, p. 199-212.
- Silberling, N.J., and Roberts, R.J., 1962, Pre-Tertiary stratigraphy and structure of northwestern Nevada: Geological Society of America Special Paper 72, 58 p.
- Snyder, W.S., and Brueckner, H.K., 1983. Tectonic evolution of the Golconda allochthon, Nevada: problems and perspectives, *in* Stevens, C.H., ed., Pre-Jurassic rocks in western North America suspect terranes: Society of Economic Paleontologists and Mineralogists, Pacific Section, Special Publication, p. 103-123.
- Speed, R.C., 1979, Collided Paleozoic microplate in the western United States: *Journal of Geology*, 1979, v. 87, p. 279-292.
- Stewart, J. H., and Carlson, J.E., 1976, Geologic map of north-central Nevada: Nevada Bureau of Mines and Geology, Map 50, 1 sheet, scale 1:250,000.
- Stewart, J.H., MacMillan, J.R., Nichols, K.M., and Stevens, C.H., 1977, Deep-water Upper Paleozoic rocks in north-central Nevada—a study of the type area of the Havallah Formation, *in* Stewart, J.H., Stevens, C.H., and Fritsche, A.E., Paleozoic paleogeography of the western United States: Pacific Section, Society of Economic Paleontologist and Mineralogists Symposium 1, p. 337-347.
- Stewart, J. H., Murchey, B. L., Jones, D. L., and Wardlaw, B. R., 1986, Paleontologic evidence for complex tectonic interlayering of Mississippian to Permian deep-water rocks of the Golconda allochthon in Tobin Range, north-central Nevada: Geological Society of America Bulletin, v. 97, p. 1122-1132.
- Stewart, J.H., and McKee, E.H., 1977, Geology, pt. 1 of Geology and Mineral deposits of Lander County, Nevada: Nevada Bureau of Mines and Geology Bulletin 88, p. 1-59.
- Tomlinson, A. J., 1990, Biostratigraphy, stratigraphy, sedimentary petrology, and structural geology of the Upper Paleozoic Golconda allochthon, north-central Nevada [Ph.D. thesis]: Stanford, California, Stanford University, 492 p.

RECOGNITION AND SIGNIFICANCE OF EOCENE DEFORMATION IN THE ALLIGATOR RIDGE AREA, CENTRAL NEVADA

By C.J. Nutt and S.C. Good

ABSTRACT

The Alligator Ridge area, which is at the southern end of the Carlin Trend in central Nevada, includes scattered outcrops of Tertiary sedimentary rocks that are folded about northwest-trending axes. Lacustrine limestone from the sedimentary sequence yielded gastropod ages of latest Early to early Middle Eocene. The Eocene sedimentary rocks are unconformably overlain by undeformed, about 35-Ma volcanic rocks. This relationship indicates a period of Eocene deformation that is interpreted as transpressive and includes strike-slip movement on west- to northwest-trending faults. Transpressive deformation probably occurred along accommodation faults related to the Eocene extension occurring in the Ruby Mountain-East Humboldt Range core complex. Eocene deformation, including uplift and local transpression, is widespread in the eastern Great Basin and may extend into the Carlin trend.

INTRODUCTION

The Alligator Ridge area, which hosts disseminated gold deposits in Devonian and Mississippian rocks, is in central Nevada, about 70 miles northwest of Ely, Nevada, and along the southern extension of the Carlin trend (fig. 1). The disseminated character, geochemistry, and lack of age constraints of the Alligator Ridge area are typical of Carlin-type deposits (Ilchik, 1990). The position of the Alligator Ridge deposits is atypical of the Carlin Trend as they are east of the Roberts Mountain thrust, the edge of the relatively intact Proterozoic continent (Wooden and others, 1997), and most of the known Carlin-type deposits. The age of the Alligator Ridge deposits is unknown: Ilchik (1990) suggests a Tertiary age whereas Hitchborn and others (1996) interpret a Jurassic age and mineralization associated with a pluton at Bald Mountain. This paper recognizes a previously undocumented Eocene deformation event, related to the initiation of extension in the Great Basin and encompassing both extension and compression, that was accompanied or soon followed by silicification. Recognition of this event is important because of its possible relation to mineralization, as either starting the

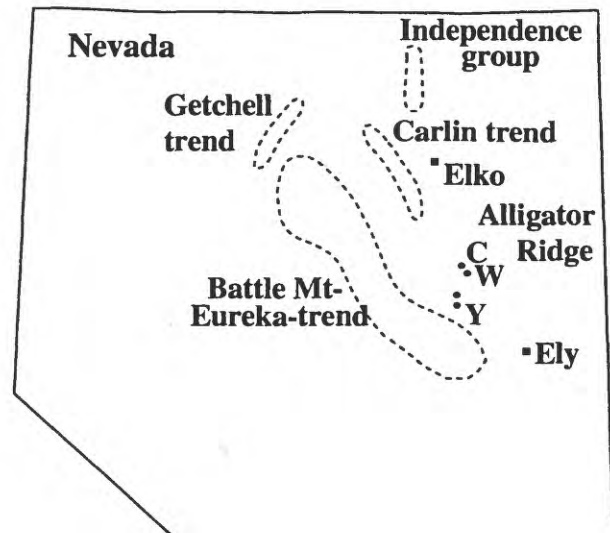


Figure 1: Location of Alligator Ridge in relation to the mineral belts of north-central Nevada. Other Carlin-type Au deposits in the Alligator Ridge-Bald Mountain area. C, Casino; Y, Yankee, W, Windrock.

process of fluid flow or opening structures for later mineralization, or by deforming or remobilizing earlier deposits.

Previously published geologic maps have depicted the Alligator Ridge-Bald Mountain area as an uplift that preserves relatively little pre-Basin and Range deformation located between the isoclinally folded and thrusts Diamond Mountains on the west side of Newark Valley and the broad syncline in the Butte Mountains on the east side of Long Valley (fig. 2) (Hose and Blake, 1976). Recent mapping at 1:24,000 scale (C.J. Nutt, unpublished mapping, 1994-1996) of the quadrangles encompassing the Alligator Ridge area reveals a more complex geology than implied on earlier maps (Rigby, 1960; Ilchik, 1990).

GEOLOGIC SETTING

Alligator Ridge is considered part of the Bald Mountain-

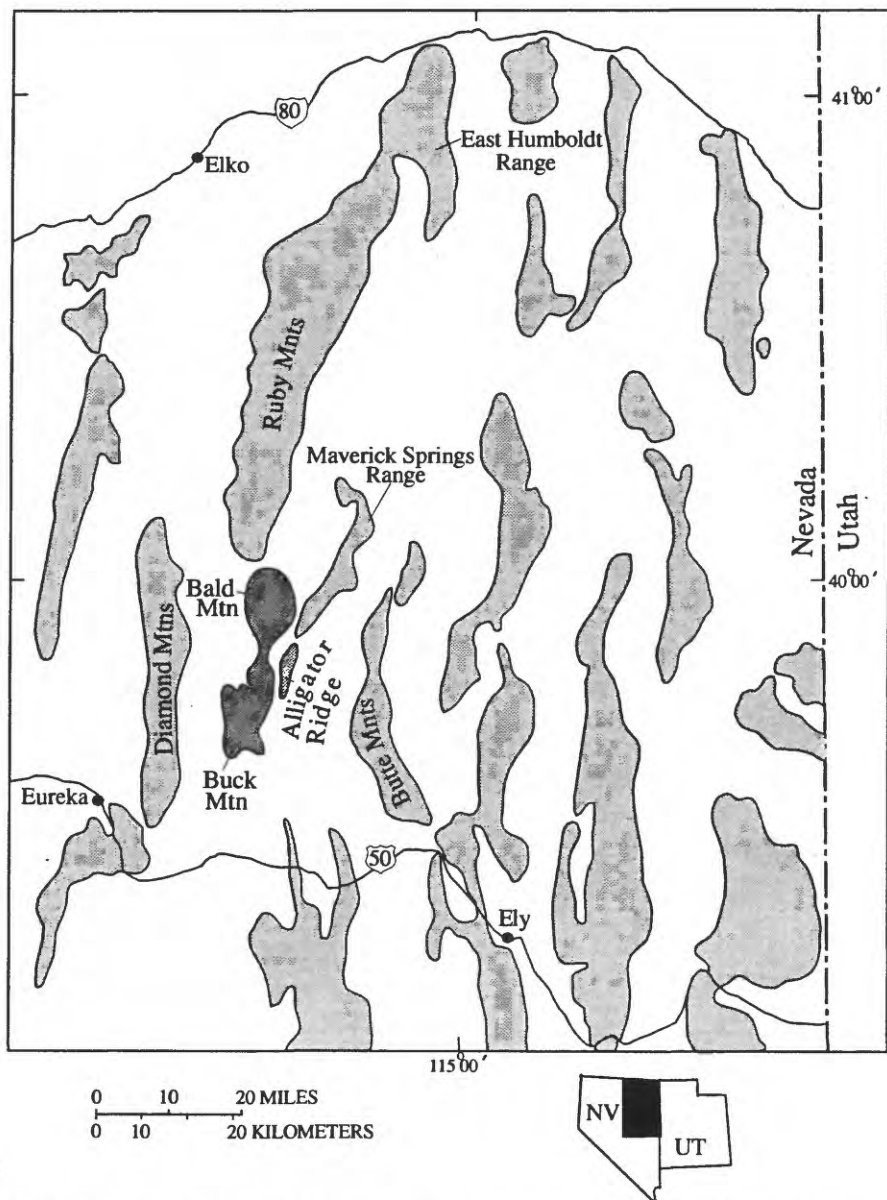


Figure 2. Location of Alligator Ridge and Bald Mountain in the eastern Great Basin, Nevada.

Buck Mountain region that is at the southern end of the Ruby Mountains (fig. 2). The Bald Mountain-Buck Mountain area, including Alligator Ridge, is underlain by Cambrian to Permian carbonate and clastic rocks, a Jurassic pluton, and Tertiary volcanic rocks (figs. 3 and 4). The Cambrian rocks and Jurassic pluton are restricted to the Bald Mountain area, and are on the upthrown side of a normal fault that cuts across the western edge of Bald Mountain. Middle and Lower Ordovician Poginip Group, Upper and Middle Ordovician Eureka Quartzite, and Upper Ordovician, Silurian and Devonian dolomites make up most of the western side of the range south of Bald Mountain and north of Buck Mountain. Upper and Middle Devonian Guilmette Formation, Lower Mississippian and Upper

Devonian Pilot Shale, Lower Mississippian Joana Limestone, Upper and Lower Mississippian Chainman Shale and Upper Mississippian Diamond Peak Formation crop out in the central part of Bald Mountain-Buck Mountain, and host the gold deposits in the Alligator Ridge area.

Lower Permian, Pennsylvanian, and Upper Mississippian Ely Limestone makes up the high ridge of Buck Mountain, and the more easily eroded Lower Permian Arcturus Formation and Rib Hill Sandstone underlie the flanks. Tertiary sedimentary rocks are only known in the Alligator Ridge area, whereas Tertiary volcanic rocks are widespread east and south of Bald Mountain.

The eastern Great Basin, including the Bald Mountain-

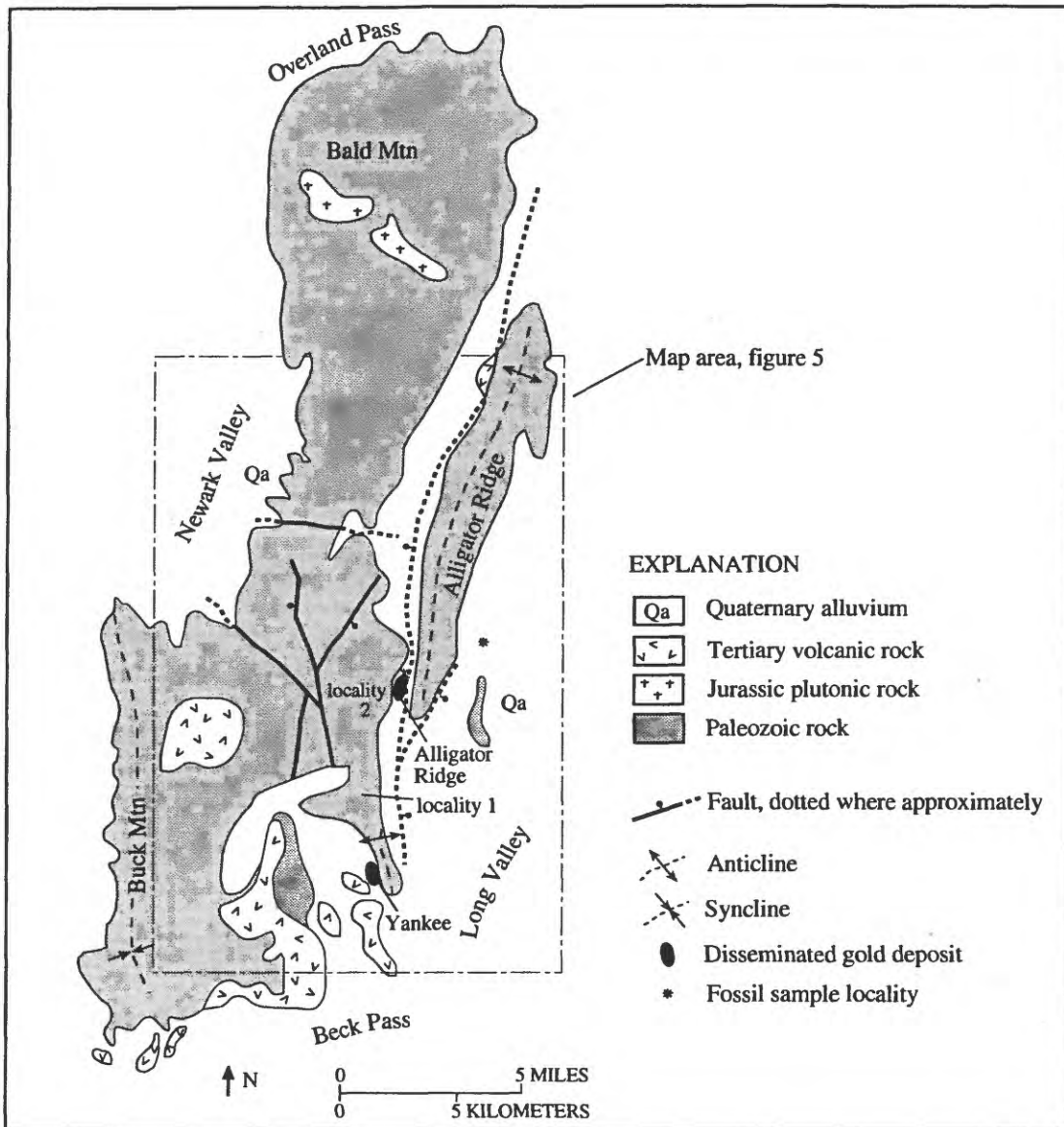


Figure 3. Simplified geologic map of the Bald Mountain-buck Mountain region, including the Alligator Ridge area. Modified from Rigby and Hose and Blake (1976).

Buck Mountain area, was affected by enigmatic Jurassic deformation, Cretaceous to early Tertiary contraction (the Sevier orogeny), and middle Tertiary extension. Mesozoic to early Tertiary structures in the Alligator Ridge area include regional north-trending gentle to overturned folds, younger-over-older low-angle faults (attenuation faults), reverse faults, and west- to northwest-striking strike-slip faults (Rigby, 1960; Nutt, 1997). Middle Tertiary and younger north-striking normal faults cut the area and in many places follow and disrupt earlier fold axes and reactivate earlier faults. The Ruby Mountain-East Humboldt Range core complex that is to the north of Alligator Ridge underwent rapid Oligocene and Miocene uplift (Wright and Snook, 1993); McGrew and Snee

(1994) interpret $^{40}\text{Ar}/^{39}\text{Ar}$ dates as also showing early Tertiary uplift.

Alligator Ridge area

The Alligator Ridge area, as used herein and coincident with the mapped area, is the central part of the Bald Mountain-Buck Mountain range, and hosts the Alligator and Yankee deposits (fig. 3). Devonian through Permian rocks dominate the outcrops, and jasperoid is common as a replacement of the Joana Limestone and as a replacement of massive to thin-bedded limestone at and near the contact between the Guilmette Formation and overlying Pilot Shale. Gold is in the Mississippian-Devonian Pilot Shale and in jasperoid at the top

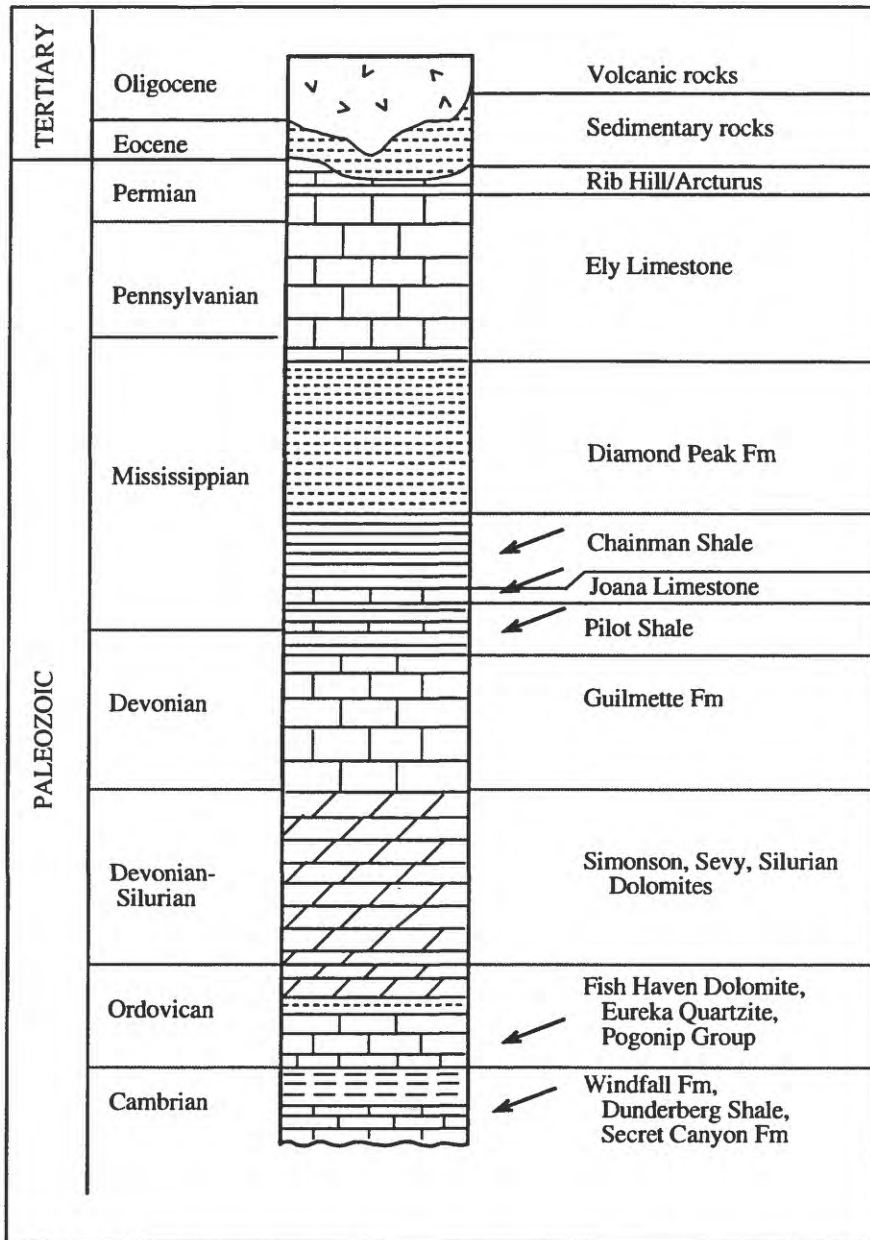


Figure 4. Stratigraphic section of Paleozoic and Tertiary rocks at Bald Mountain and Alligator Ridge. Arrow's point to hosts of disseminated gold ore: upper three are at Bald Mountain and in Alligator Ridge area, lower two are at Bald Mountain.

of the Devonian Guilmette Formation.

Structures in the Alligator Ridge area are shown on figure 5 (map area on fig. 3). Two sets of folds, north- and northwest-trending, deform the Alligator Ridge area. The north-trending folds are Mesozoic to early Tertiary in age and include a syncline at Buck Mountain, an anticline near Yankee, a steep to overturned anticline at Alligator Ridge, and anticline and syncline in the central part of the area that are disrupted by later faults (fig. 5). Shorter wave-length northwest-trending folds deform earlier north-trending folds (fig. 5). Almost all

faults show normal offset that reflects Miocene and younger extension of the area, but many faults are interpreted as having a pre-Miocene history.

EOCENE SEDIMENTARY ROCKS

Eocene sedimentary rocks crop out in the eastern part of the Alligator Ridge area, including at the Alligator Ridge deposits. The sequence consist of fluvial and lacustrine

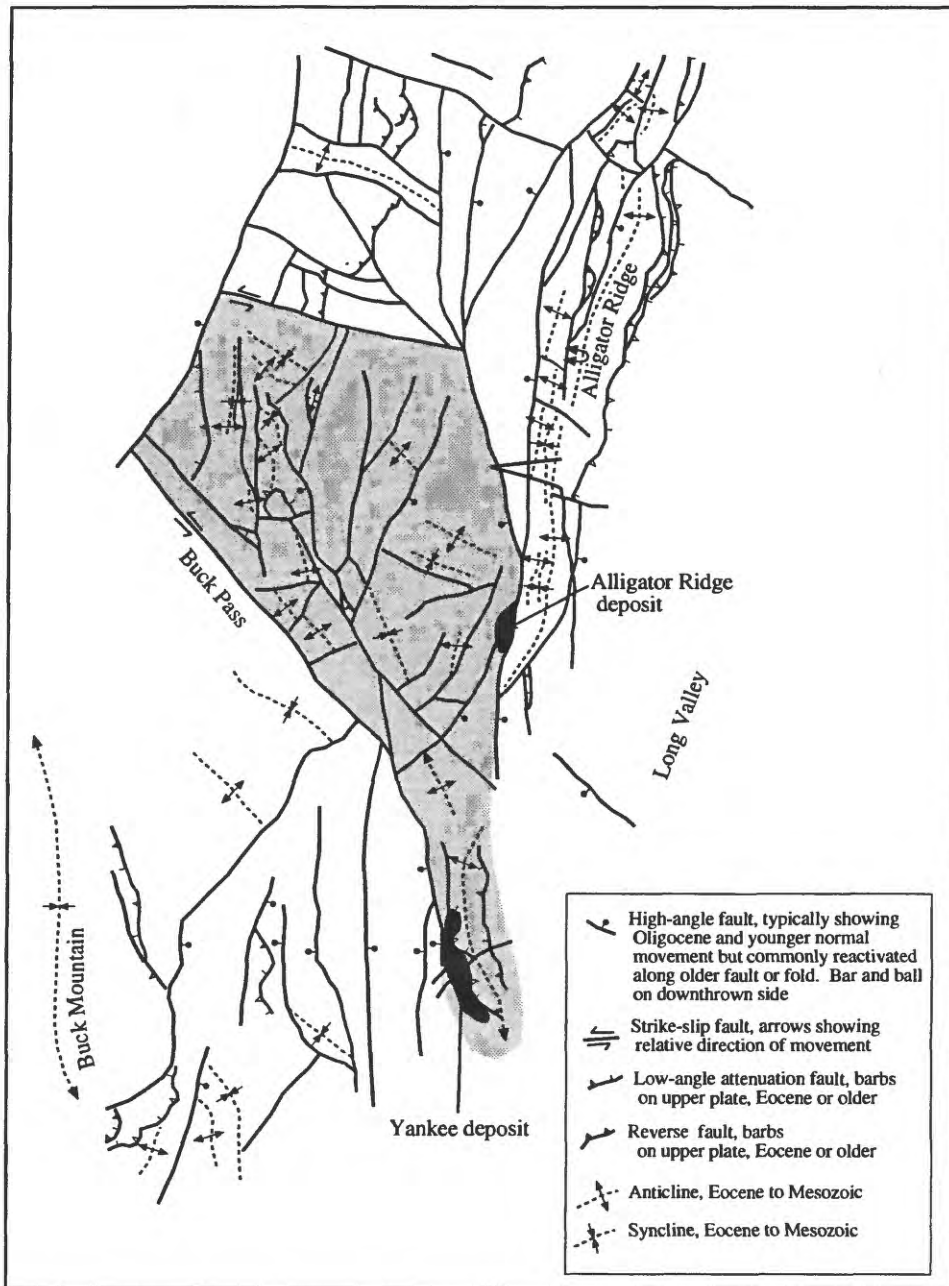


Figure 5. Structures from the map area on figure 3 (C.J. Nutt, unpublished mapping). Shaded area underlain by rotated fault blocks, as explained in text. Dark gray areas are Alligator Ridge and Yankee deposits.

sandstone, siltstone, and conglomerate, in part volcanoclastic or igneous-derived, and limestone. The clastic rocks contain chert clasts and quartz derived from the Diamond Peak Formation, and white, clay-altered fragments of an unknown igneous source. The Eocene rocks depositionally, and in places unconformably, overlie Upper and Lower Mississippian Chainman Shale, Lower Mississippian Joana Limestone, Lower Mississippian and Upper Devonian Pilot Shale, and Upper and Middle Devonian Guilmette Formation. They are

also unconformably overlain by biotite-quartz lithic tuff, in places reworked to a quartz-biotite sandstone, of about 35 Ma (Nutt, 1996).

Cretaceous, Paleocene, and Eocene sedimentary rocks are scattered throughout the eastern Great Basin (Fouch and others, 1979). Fouch and others (1979) and Soloman and others (1979) show that a volcanogenic component is in some places present in Eocene rocks, and as old as about 45 Ma.

An Eocene age for lacustrine limestone in the Alligator

Table 1. Fossil data from Alligator Ridge area

97ARlm1	
Phylum Mollusca	
Class Gastropoda	
Subclass Pulmonata	
Order Basommatophora	
Family Lymnaeidae	
<i>Pleurolimnaea tenuicosta</i> (Meek and Hayden, 1856)	Paleocene-Early Eocene
<i>Lymnaea</i> sp. Indet., resembles <i>L. similis</i> (Meek, 1860)	Bridgerian, latest Early to early Middle Eocene
97ARlm2	
<i>Lymnaea similis</i> Meek (1860)	Bridgerian, latest Early to early Middle Eocene
<i>Lymnaea</i> sp. C Good (1983, 1987)	upper Sheep Pass Formation, Bridgerian

Ridge area was determined by identification of gastropods from two localities: the Vantage pit at Alligator Ridge and from outcrop on the eastern side of Alligator Ridge (localities shown on fig. 3). The gastropods are recrystallized. However, excellent morphological details are available from external and internal molds. The sample from the Vantage pit at Alligator Ridge (ARlm1 on table 1) is from a limestone interbedded with volcanoclastic sandstones, siltstones, and mudstones. The gastropod fauna is *Pleurolimnaea tenuicosta* (Meek and Hayden, 1856) and *Lymnaea* sp. indeterminate, but resembles *L. similis* Meek (1860). The sample from the east side of Alligator Ridge (97ARlm2 on table 1) contains gastropods preserved in random orientations on bedding planes. The gastropod fauna consists of *Lymnaea similis* Meek (1860) and *Lymnaea* sp. C. Good (1983, 1987).

Age of the limestone can be inferred from the stratigraphic distribution of these gastropod species in the Rocky Mountain region where they are associated with ostracodes, charophytes and fossil mammals (Henderson, 1935; Hanley, 1974, 1976; Good, 1983, 1987). Both samples are interpreted as Bridgerian (latest Early to early Middle Eocene); see table 1 for the age ranges of each species. These mollusks indicate the limestone at Alligator Ridge is age correlative to the White Sage Formation in the Deep Creek Mountains, Nevada and Utah, (Potter and others, 1995) and the upper part of the Sheep Pass Formation (Good, 1987).

The depositional environment of the mollusk-bearing limestone is inferred from the paleoecological tolerances of the modern representatives (Dodd and Stanton, 1981). Paleoecological interpretations are drawn at the level of the Family Lymnaeidae. Lymnaeids are basommatophoran pulmonate gastropods (air-respiring gastropods that have returned to aquatic habitats). They can exchange gases through subcutaneous exchange or by bring the pneumostome to the air-water interface to intake air into the mantle cavity.

Lymnaeids prefer quiet-water habitats, live on aquatic-rooted, emergent vegetation, and are herbivorous (Good, 1987; Hanley, 1976). Lymnaeids are abundant in very small bodies of water with mud bottom and little aeration (Larocque, 1968). The mollusk assemblage indicates the depositional environment was a small, eutrophic, perhaps even ephemeral pond.

Geologic relationships support the proposal that the basins were small and derived sediment from local sources, and the variety of units that underlie Eocene rocks suggests that extensive tectonic denudation and/or erosion preceded deposition. The outcrops are scattered and small, and, even recognizing that they were in places eroded prior to Oligocene volcanism, most likely were never thick, widespread units. At locality 1 (fig. 3), Eocene rocks overlie Upper and Middle Devonian Guilmette Formation, Lower Mississippian and Upper Devonian Pilot Shale, Lower Mississippian Joana Limestone, and Upper and Lower Mississippian Chainman Shale, all within about a square mile. The range in rock units underlying the Eocene rocks implies significant uplift and erosion after deposition of Mississippian rocks and prior to deposition of the Eocene rocks.

EOCENE DEFORMATION

Eocene deformation in the Alligator Ridge area is evident by the presence of deformed Eocene rocks overlain by tilted, but not folded, 35 Ma volcanic rocks. At locality 1 (figs. 3 and 6), the Eocene rocks, along with the Paleozoic rocks, are folded about a northwest-trending axis. Involvement of the Eocene rocks suggests that all of the northwest-trending folds are of Eocene, and not of Mesozoic, age. Slightly less dips in the Eocene rocks than in the underlying Paleozoic rocks indicate deposition along a slight angular unconformity. This discordance is also visible at locality 2 on figure 3. Outcrops

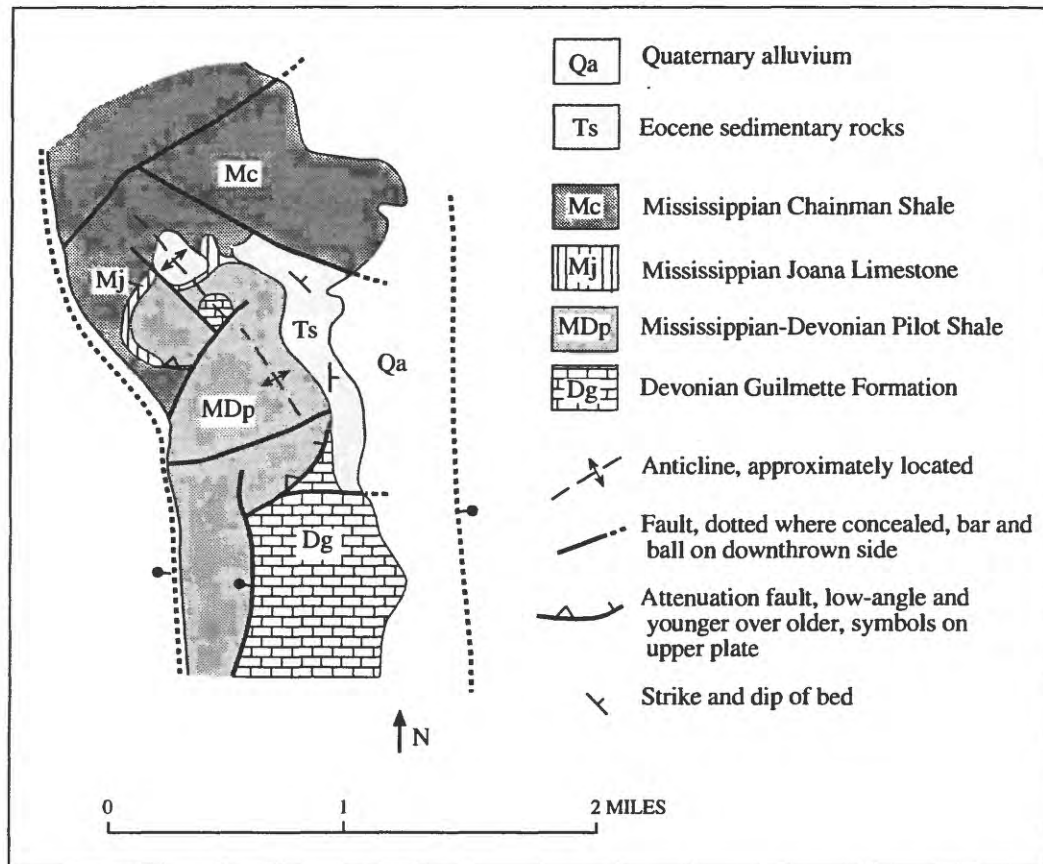


Figure 6. Geologic map of locality 1 (fig. 3) that shows Eocene sedimentary rocks folded northwest-trending fold axis.

at locality 2 and in the Vantage pit at Alligator Ridge show that the Eocene rocks are discordantly overlain by reworked 35 Ma tuff.

Eocene deformation is interpreted as primarily transpressional and expressed as strike-slip faults, with contemporaneous northwest-trending folding, and block rotation. Strike-slip movement along west- to northwest-striking faults is indicated by the presence of the northwest-trending folds, which are oriented near and at about an angle of 30 degrees or less to the faults (fig. 5). These domain-bounding west- to northwest-striking faults probably have a pre-Eocene history; the west to northwest elongation of the Jurassic pluton at Bald Mountain suggests west- to northwest-striking structures were active by the Jurassic. In addition, the faults were reactivated during younger Tertiary extension, and in most places now show normal offset. Block rotation in a left-lateral shear system is indicated by rotation of earlier Mesozoic to early Tertiary north-trending folds in the shaded area of figure 5. Rotation in this area is evident, in part, because of widespread outcrop of Pilot Shale that is easily deformed.

Quartz-flooding accompanied or soon followed deformation. At locality 1 (fig. 3), Joana Limestone and Eocene sedimentary rocks are silicified, whereas nowhere are

the 35-Ma volcanic rocks silicified. Eocene silicified rocks are not gold-bearing, although gold-bearing rocks are present in nearby Pilot Shale.

The silicified Joana limestone at locality 1 is aphanitic, gray green and contains relic bedding, characteristics typical of silicified Joana Limestone throughout the map area. This similarity strongly suggests that the widespread silicification of Joana Limestone in the Alligator Ridge area was likely an Eocene event.

Eocene deformation at Alligator Ridge is interpreted as related to uplift of the Ruby Mountain-East Humboldt Range core complex to the north. Using $^{40}\text{Ar}/^{39}\text{Ar}$ methods, McGrew and Snee (1994) documented Oligocene and Miocene uplift of the Ruby Mountain-East Humboldt Range core complex, and suggested that poorly constrained hornblende ages from rocks at high structural level indicate initial uplift was in the early Tertiary, estimated between 63–49 Ma. Our data constrain deformation to post-early Middle Eocene, indicate transpression along the southern edge of the uplifted complex, and demonstrate a distinct period of deformation. The Alligator Ridge area was near the terminus of uplift in the Ruby Mountains and East Humboldt Range, and was subjected to transpressive deformation. Earlier west- to northwest-striking

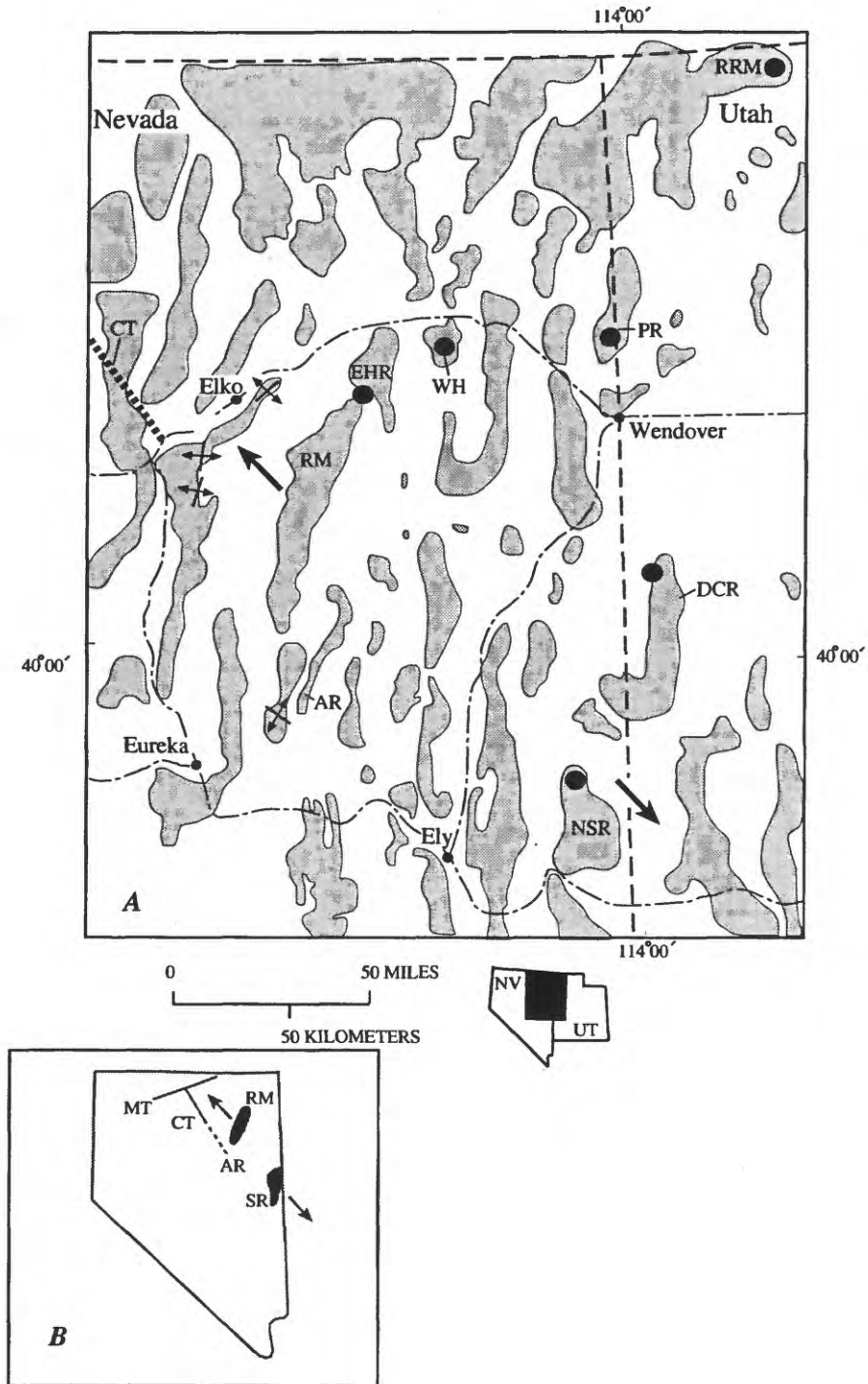


Figure 7. A. Locality map showing ranges in eastern Great Basin documented as having Eocene uplift (black circles) and folding (fold axes). Fold axis for Alligator Ridge is from this paper; fold axes in Eocene rocks in the Elko area are from Ketner and Alpha (1988). Approximate location of Carlin trend (CT) shown as dotted line. Bold arrows showing Tertiary extension direction from Wust (1986). AR, Alligator Ridge; DCR, Deep Creek Range; NSR, Northern Snake Range; PR, Pilot Range; RM, Ruby Mountains; RRM, Raft River Mountains; HER, East Humboldt Range, and WH, Wood Hills. **B.** Locality map showing the northwest striking Carlin trend (CT, dotted where extends to the south) and Midas trough (MT) in present-day Nevada in relationship to Tertiary extension. AR, Alligator Ridge; RM, Ruby Mountains, and SR, Snake Range.

faults were reactivated at this time, probably because of differential Tertiary extension manifested by strike-slip offset in cover rocks.

REGIONAL IMPLICATIONS

Evidence for widespread Eocene deformation in the central and eastern Great Basin is increasing. Localities where Eocene deformation, primarily extensional, has been documented are shown on figure 7A. Eocene uplift in the Ruby Mountain- East Humboldt Range is documented McGrew and Snee (1994). In the northern Deep Creek Range, northwest Utah, Potter and others (1995) mapped tilted early Eocene White Sage Formation overlain by flat-lying 39.6 Ma volcanic rocks. Miller and others (1987) inferred Eocene movement on a major detachment fault cut by 40 Ma dikes and sills in the Pilot Range, Utah and Nevada. Wells and others (in press) showed rapid cooling in the Raft River Mountains at 47-45 Ma. In the northern Snake Range, Nevada, Lee (1995) documented by $^{40}\text{Ar}/^{39}\text{Ar}$ methods that the earliest movement on the northern Snake Range detachment fault was middle Eocene (48-41 Ma). A probable middle Eocene age for displacement was interpreted along the Wood Hills detachment (Thorman and Snee, 1988; Hodges and others, 1992). In the Elko area and west and north of the Ruby Mountains, Ketner and Alpha (1988) documented Eocene-age folds in the Eocene Elko Formation. Extensional uplift was centered in the areas of core complexes in east-central Nevada; documented compressive structures are primarily located along the western edge of the area of core complexes (fig. 7A).

The age of uplift and related folding, based on the above geologic and isotopic data, was about 50 to 41 Ma. The presence of volcanic rocks in the folded Eocene rocks at Alligator Ridge suggest that at least in some areas the folding is 45-41 Ma. Stock and Molar's (1988) plate reconstructions indicate plate relations and movements in the time period of the Eocene deformation at about 50 Ma-42 Ma. Stock and Molar (1988) document that between 68 to 42 Ma, the Farallon plate approached the North American plate from the southwest and the boundary between the plates was a subduction zone. Between 56 and 42 Ma, the Vancouver plate broke from the Farallon plate and plate convergence of the Farallon/Vancouver and North America plates decreased. This decrease in convergence is about the same time as the Eocene deformation (Potter and others, 1995), and may coincide with initiation of extension in the area of core complexes in eastern Nevada.

The age of formation of Carlin deposits is controversial, but hypotheses include deposition related to fluid flow associated with Eocene volcanism (Hofstra, 1995) or extensional development of Tertiary core complexes (Ilchik and Barton, 1997). Gold deposition at Twin Creeks dated at about 42 Ma shows that at least some mineralization was during the Eocene (Hall and others, 1997). The Eocene

deformation in the Alligator Ridge area apparently occurred just prior to volcanism and possible mineralization. Because Eocene rocks are poorly documented in the Carlin trend, the extent and(or) type of Eocene deformation along the trend is unknown. If present, Eocene structures are likely be misinterpreted as Paleozoic or Mesozoic.

REFERENCES CITED

- Dodd, J.R., and Stanton, R.J., 1981, Paleocology, concepts and applications: John Wiley and Sons, New York, 559 p.
- Fouch, T.D., Hanley, J.H., and Forester, R.M., 1979, Preliminary correlation of Cretaceous and Paleogene lacustrine and related nonmarine sedimentary and volcanic rocks in parts of the Great Basin of Nevada and Utah, in Newman, G.W., and Goode, H.D., eds., Basin and Range symposium and Great Basin field conference: Rocky Mountain Association of Petroleum Geologists and Utah Geological Association, p. 305-312
- Good, S.C., 1983, Molluscan Paleobiology of the Sheep Pass Formation (Latest Cretaceous to Eocene) of East Central Nevada: M.S. Thesis, University of Colorado, Boulder, 142 p.
- Good, S.C., 1987, Mollusc-based interpretations of lacustrine paleoenvironments of the Sheep Pass Formation (Latest Cretaceous to Eocene) of east-central Nevada: *Palaios*, v. 2, p. 467-478.
- Hall, C.M, Simon, G., and Kesler, S.E., 1997, Age of mineralization at the Twin Creeks SHMG deposit, Nevada, in Vikre, P., Thompson, T.B., Bettles, K., Christensen, O., and Parratt, R., eds., Carlin-type Gold Deposits Field Conference: Society of Economic Geologists Guidebook Series v. 28, p. 151-153.
- Hanley, H.H., 1974, Systematics, paleocology, and biostratigraphy of nonmarine mollusca from the Green River and Wasatch Formations (Eocene), southwestern Wyoming and northwestern Colorado: PhD Dissertation, University of Wyoming, Laramie, 273 p.
- Hanley, J.H., 1976, Paleosynecology of nonmarine Mollusca from the Green River and Wasatch Formations (Eocene), southwestern Wyoming and northwestern Colorado, in Scott, R.W., and West, R.R., eds., Structure and Classification of Paleocommunities: Dowden, Hutchinson and Ross, p. 235-261.
- Henderson, J. 1935, Fossil nonmarine mollusca of North America: Geological Society of America Special Paper 3, 313 p.
- Hitchborn, A.D., Arbonies, D.G., Peters, S.G., Conners, K.A., Noble, D.C., Larson, L.T., Beebe, J.S., and McKee, E.H., 1996, Geology and gold deposits of the Bald Mountain mining district, White Pine County, Nevada, in Coyner, A.R., and Fahey, P.L., eds., Geology and Ore Deposits of the American Cordillera: Geological Society of Nevada Symposium Proceedings, Reno/ Sparks, Nevada, April 1995, p. 505-546.
- Hodges, K.V., Snoke, A.W., and Hurlow, H.A., 1992, Thermal evolution of a portion of the Sevier hinterland: the northern Ruby Mountains-East Humboldt Range and Wood Hills, Northeastern Nevada: *Tectonics*, v.2, p. 154-164.
- Hofstra, A., 1995, Timing and duration of Carlin-type gold mineralization in Nevada and Utah: Geological Society of America Abstracts with Programs, v. 27, no. 6, p. 329.
- Hose, R.K., and Blake, M.C., Jr., 1976, Geologic map of White Pine County, Nevada, scale: 1:250,000, in Geology and mineral

- resources of White Pine County, Nevada, Part I, Geology: Nevada Bureau of Mines and Geology Bulletin 85, p. 1-35.
- Ilchik, R.P., 1990, Geology and geochemistry of the Vantage gold deposits, Alligator Ridge-Bald Mountain mining district, Nevada: *Economic Geology* v. 85, p. 50-75.
- Ilchik, R.P., and Barton, M.D., 1997, An amagmatic origin of Carlin-type gold deposits: *Economic Geology*, v. 92, p. 269-288.
- Ketner, K.B., and Alpha, A.G., 1988, Mesozoic and Tertiary rocks near Elko, Nevada—evidence for Jurassic to Eocene folding and low-angle faulting: *U.S. Geological Survey Bulletin* 1988-C, p. C1-C13.
- Larocque, A., 1968, Pleistocene Mollusca of Ohio: *Geological Survey of Ohio, Bulletin* 62, Part 1, p. 357-553.
- Lee, Jeffrey, 1995, Rapid uplift and rotation of mylonitic rocks from beneath a detachment fault: insights from potassium feldspar $^{40}\text{Ar}/^{39}\text{Ar}$ thermochronology, northern Snake Range, Nevada: *Tectonics*, v. 14, p. 54-77.
- McGrew, A.J., and Snee, L.W., 1994, $^{40}\text{Ar}/^{39}\text{Ar}$ thermochronologic constraints on the tectono-thermal evolution of the northern East Humboldt Range metamorphic core complex, Nevada: *Tectonophysics*, v. 238, p. 425-450.
- Meek, F.B., 1860, Descriptions of new fossil remains collected in Nebraska and Utah, by the exploring expeditions under the command of Capt. J.H. Simpson, of the U.S. Topographical Engineers: *Philadelphia Academy of Natural Sciences, Proceedings*, v. 12, p. 308-315.
- Meek, F.B., and Hayden, F.V., 1856, A report on the invertebrate Cretaceous and Tertiary fossils of the upper Missouri country: *U.S. Geologic and Geographic Survey of Territories (Hayden Survey)*, v. 9, 629 p.
- Miller, D.M., Hillhouse, W.C., Zartman, R.E., and Lanphere, M.S., 1987, Geochronology of intrusive and metamorphic rocks in the Pilot Range, Utah and Nevada, and comparison with regional patterns: *Geological Society of America Bulletin*, v. 99, p. 866-879.
- Nutt, C.J., 1996, Cretaceous(?) to early Oligocene sedimentary and volcanic rocks at Alligator Ridge, Buck Mountain-Bald Mountain area, central Nevada, in Taylor, W.J., and Langrock, H., eds., *Cenozoic structure and stratigraphy in central Nevada: 1996 Field Conference Volume*, Nevada Petroleum Society Inc., Reno, p. 13-18.
- Nutt, C.J., 1997, Sequence of deformational events and the recognition of Eocene(?) deformation in the Alligator Ridge area, east-central Nevada, in Vikre, P., Thompson, T.B., Bettles, K., Christensen, O., and Parratt, R., eds., *Carlin-type Gold Deposits Field Conference Guidebook*, Elko, October 1997, Society of Economic Geologists Guidebook Series v. 28, p. 203-211.
- Potter, C.J., Dubiel, R.F., Snee, L.W., and Good, S.C., 1995, Eocene extension of early Eocene lacustrine strata in a complexly deformed Sevier-Laramide hinterland, northwest Utah and northeast Nevada: *Geology*, v. 23, p. 181-184.
- Rigby, J.K., 1960, Geology of the Buck Mountain-Bald Mountain area, southern Ruby Mountains, White Pine County, Nevada, in Boettcher, J.W., and Sloan, W.W., Jr., eds., *Guidebook to the geology of east-central Nevada: Intermountain Association of Petroleum Geologists and Eastern Nevada Geological Society Annual Field Conference*, 11th, 1960, Salt Lake City, Utah, p. 173-180.
- Solomon, B.J., McDee, E.H., and Andersen, D.W., 1979, Stratigraphy and depositional environments of Paleogene rocks near Elko, Nevada, in Armentrout, J.M., Cole, M.R., and TerBest, Harry, eds., *Cenozoic paleogeography of the western United States, Pacific Coast Paleogeography Symposium 3: Pacific Section, Society of Economic Paleontologists and Mineralogists*, p. 75-88.
- Stock, J., and Molnar, P., 1988, Uncertainties and implications of the Late Cretaceous and Tertiary position of North America relative to the Farallon, Kula, and Pacific plates: *Tectonics*, v. 7, no. 6, p. 1339-1384.
- Thorman, C.H., and Snee, L.W., 1988, Thermochronology of the metamorphic rocks in the Wood Hills and Pequop Mountains, northeastern Nevada: *Geological Society of America Abstracts and Program, Annual Meeting*, v. 20, p. A-18.
- Wells, M.L., Snee, L.W., and Blythe, in press, Dating of extensional shearing, an example from the Raft River Mountains, Basin and Range, western United States: *Tectonics*.
- Wooden, J.L., Tosdal, R.M., and Kistler, R.W., 1997, Pb and Sr isotopic mapping of crustal structure in the northern Great Basin, in Vikre, P., Thompson, T.B., Bettles, K., Christensen, O., and Parratt, R., eds., *Carlin-type Gold Deposits Field Conference Guidebook*, Elko, October 1997, Society of Economic Geologists Guidebook Series v. 28, p. 47-51.
- Wright, J.E., and Snoke, A.W., 1993, Tertiary magmatism and mylonitization in the Ruby-East Humboldt metamorphic core complex, northeastern Nevada: U-Pb geochronology and Sr, Nb, and Pb isotope geochemistry: *Geological Society of America Bulletin*, v. 105, p. 935-952.
- Wust, S.L., 1986, Regional correlation of extension directions in Cordilleran metamorphic core complexes: *Geology*, v. 14, p. 828-830.

TUNGSTEN-POLYMETALLIC-AND BARITE-MINERALIZED ROCKS IN THE RUBY MOUNTAINS, NEVADA

By Vladimir I. Berger *and* Robert L. Oscarson

ABSTRACT

Mineralized occurrences in the Ruby Mountains were examined for any inferred traces of gold-ore-forming fluids that might be connected to metamorphism and to formation of Carlin-type gold deposits at a higher structural level. Traverses across the metamorphic core complex of the Ruby Mountains and study of known tungsten-polymetallic and barite deposits revealed skarn as predominant type of mineralized rock. At least two phases of skarn formation are present: (1) an early phase connected with a Late Jurassic granitic intrusion, and (2) a later phase related to Oligocene granite-monzonite of the Harrison Pass pluton. Skarn deposits of both phases are present at generally the same stratigraphic level in Cambrian marble and recrystallized limestone and contain similar Pb, Zn, Cu, Ag, Ba \pm W mineralization. The main differences consist of variable compositions of the skarn assemblages: first, pyroxene-idocrase with minor garnet and a retrograde association of amphibole (actinolite-tremolite)-epidote-calcite accompanied by quartz-sulfide minerals; second, an amphibole-epidote-garnet skarn assemblage with a calcite-quartz retrograde association. This difference and varied ore textures, almost "epithermal" in the second case, have been probably caused by different depths of emplacement of the accompanying intrusions: deep Jurassic pegmatitic granite and shallow Tertiary pluton. Celsian, a barium plagioclase feldspar, was newly discovered in skarn deposits of both ages. Ore-host Cambrian carbonate rocks might have contained pre-metamorphic barite-bearing SEDEX(?) mineralization or the celsian might be a granite-generated component of the skarn-polymetallic-barite assemblage.

Combined vertical zoning of early first phase skarn can be traced for deposits of the Battle Creek Mine (2,220 m elevation), American Beauty Mine (2,460 m) and Knob Hill Mine (2,610 m), which are present in a roof pendant in a Jurassic pegmatitic granite. Tungsten and quartz-polymetallic mineralized rocks at the Battle Creek Mine are hosted by well-developed skarn. At the American Beauty Mine, at 240 m higher elevation, mineralized rock is characterized by a polymetallic sulfide assemblage without tungsten and is accompanied by quartz containing only fragments of skarn

that are almost entirely destroyed by retrograde processes. Approximately 150 m higher at the Knob Hill Mine, upper levels of the mineral zonation contain only quartz-polymetallic veins surrounded by a halo of hydrothermal silicified rocks and carbonate-altered rocks. Gold is not a significant component of skarn mineralization. Recognition of this vertical zonation of the skarn deposits seemingly does not allow space for any "skarn roots" for Carlin-type gold mineralization in the deeper crust represented by this migmatitic core.

Two types of barite mineralization are present in the Ruby Mountains: bedded barite at the Judy Mine which is present in Devonian dolomite in the southern part of the range, and vein and replacement barite mineralization which partially resulted from remobilization of earlier bedded barite during Tertiary extensional-related hydrothermal activity. The bedded barite might be roughly comparable to recently discovered minor barite-bearing SEDEX-type base and precious-metal mineralization in Devonian strata of the northern Carlin trend. However, an absence of base and precious metals in the bedded barite places limitations upon such comparisons. Barite is an insignificant but common component of many Carlin-type deposits. The same reasoning applies to comparison of vein-type barite occurrences in the Ruby Mountains with proximal minor barite-bearing Carlin-type deposits in the area of the Alligator Ridge and Yankee gold mines, south of the Ruby Mountains. These latter occurrences are commonly located in Mississippian strata.

Thus, this study did not demonstrate in Ruby Mountains any "roots", connections, or deeper analogs for Carlin-type gold deposits. However, the investigation did provide a clear understanding of the largely pluton-related mineral deposits of this prominent metamorphic terrane.

INTRODUCTION

Scattered ore deposits in the metamorphic core complex in the Ruby Mountains provide an opportunity to examine the potential association between gold-ore-forming fluids and metamorphism as well as any association with Carlin-type gold deposits, which would have formed at higher structural levels

in the crust. The work was initiated with the intention of either confirming or clarifying underlying assumption to the hypotheses of metamorphogenic (Seedorff, 1991) or amagmatic (Ilchik and Barton, 1997) origins of Carlin-type gold-forming fluids.

The Ruby Mountains are located in Basin and Range province of northeastern Nevada. The range formed as a late Cenozoic north-northeast-trending horst extending 115 kilometers at an angle of about 35° to the Carlin trend, whose southeastern extension crosses the southern end of the range (fig. 1). The metamorphic core complex exposed within the Ruby Mountains was the main object of field observations. Previous studies of the geologic, tectonic and magmatic history of this terrane by many others (Howard, 1966, 1971, 1980; Howard and others, 1979; Kistler and others, 1981; Snoke, 1980, 1997; Snoke and Miller, 1988) provided the framework for this mineral-resource investigation.

Fieldwork undertaken as part of this study examined the areal metasomatic events in metamorphic rocks that could be interpreted as evidence of widespread fluid activity, and documented the different types of mineralized rocks in the Ruby Mountains. The studies had two tasks: (1) to identify possible analogs to Carlin-type gold deposits, and (2) to determine spatial and temporal relationships of mineralized rocks to metamorphism. The first task was carried out by traverses across the Ruby Mountains. The second task required a first-hand acquaintance with deposits of the Ruby Mountains and Carlin-type gold deposits. The following accessible mineral deposits in the Ruby Mountains were examined: skarn-polymetallic±W deposits of the American Beauty Mine, Knob Hill Mine, Battle Creek Mine, Valley View Mine, and Summit View Mine; and barite deposits of the Judy Mine, B & P claims, and Dorsey Canyon prospect (fig. 2). Follow-up study included rock and ore microscopy, scanning electron microscope (SEM) and microprobe analysis, and preparation of samples for U–Pb age and Pb isotope determinations, and for sulfur-isotope analyses of barite. Preliminary results of the study are presented herein.

GEOLOGIC FRAMEWORK

Stratigraphic Units

The prominent deeply eroded Cenozoic horst of the Ruby Mountains is composed of different and contrasting rock complexes. According to Howard (1966, 1980); Howard and others (1979); Snoke (1980, 1997); Snoke and Miller, (1988); MacCready and others (1997), rocks in the range can be subdivided into two main units. A migmatitic core complex makes up the core of the Ruby Mountains. It consists of metaquartzite, pelitic schist, gneiss, and marble metamorphosed to upper amphibolite facies, with an indicator mineral association of sillimanite-muscovite-K-feldspar. Howard (1980) considered the protoliths of this complex as Early

Cambrian and Precambrian(?). Kistler and others (1981) argued that the metamorphic complex is chiefly Precambrian >1,450 Ma, and has been metamorphosed and intruded by granite-granodiorite gneisses at about 550 Ma. Lush and others (1988) reported a Late Archean age (2.5 ± 0.11 Ga) from a sample of orthogneiss in the adjoining East Humboldt Range. It seems noteworthy that the Precambrian part of this unit was not outlined on geologic maps of the Ruby Mountains. Old stratigraphic boundaries are obliterated by superposed polyphase magmatic and metamorphic events, and the possibility of delineating the Precambrian rocks within the core complex remains questionable. Thus, we focused our field observations generally on the entire migmatitic metamorphic sequence keeping in mind that it includes Paleozoic metasedimentary rocks, correlative with the miogeoclinal sequence of the eastern Great Basin (Howard, 1966, 1971).

Unmetamorphosed to low-metamorphic grade Cambrian to Triassic carbonate and clastic rocks compose the second main unit. These rocks are typical miogeoclinal sequences that continue southward into the southern part of the Ruby Mountains, south of granite exposures. Separate low-angle fault-bounded packages in the central and northern part of the range are made up of similar sedimentary rocks. Fossiliferous dolomite and limestone compose a substantial part of the unit. Tertiary clastic sedimentary rocks and rhyolitic volcanic rocks dated at approximately 15 Ma were involved in a low-angle fault complex and cut by detachment faults in the northern Ruby Mountain (Snoke, 1980; MacCready and others, 1997).

Magmatic Events

The horst in the Ruby Mountains appears to be a distinctive plutonic terrane (Howard, 1966, 1980; Kistler and others, 1981). Wide areal exposures of Mesozoic and Cenozoic granitic rocks in the central part of the range are surrounded northward by a migmatitic core complex. The latter appear like a roof pendant in a giant polyphase granitic intrusion that has been eroded and partially exhumed. Metasedimentary rocks are intercalated with numerous sills and cut by dikes of pegmatitic granite, the proportion of which increases downward. Phanerozoic magmatic successions of the Ruby Mountains include four main events.

(1) Pegmatitic granite predominates the Late Jurassic intrusive complex. It is accompanied by sparse gabbro and quartz diorite to trondjemite and biotite granodiorite. The presence of garnet in the metamorphic mineral assemblage and the gneissic texture are typical of these rocks. A Rb–Sr age for the pegmatitic granite is 159.7 ± 2.7 Ma (Kistler and others, 1981) whereas a U–Pb monazite age of 153 ± 1 Ma (Hudec and Wright, 1990) is slightly younger.

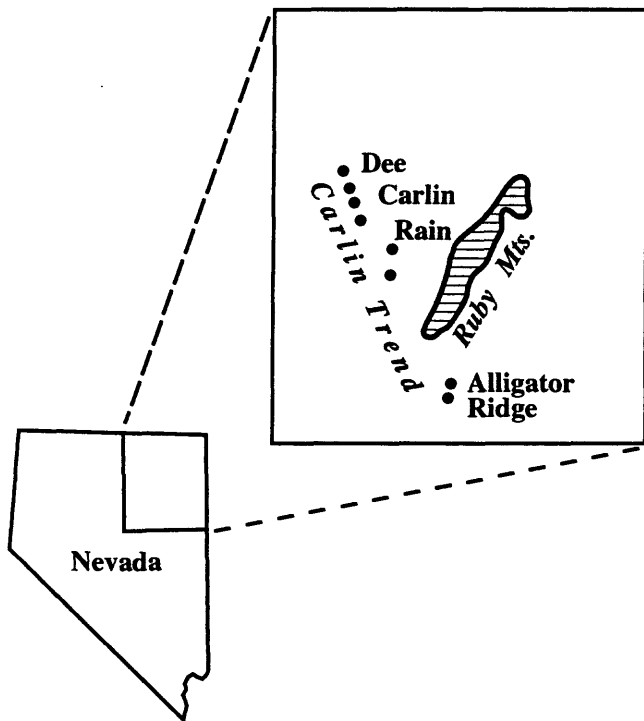


Figure 1 Location of the Ruby Mountains (hatched) in relation to the Carlin trend, Nevada.

(2) Cretaceous two-mica leucocratic granite has intruded the pegmatitic granite and is present as a subsidiary igneous phase mainly inside the Jurassic pluton in the central Ruby Mountains. A Rb–Sr age determined by Kistler and others (1981) is 83.9 ± 1.25 Ma.

(3) The Oligocene granite-monzonite of the Harrison Pass Pluton intrudes the older rocks. A Rb–Sr age of 31.9 ± 1.2 Ma has been determined by Kistler and others (1981) for these rocks. Cataclastic textures are characteristic for these rocks, and they are locally overlain by a klippe of unmetamorphosed Paleozoic sedimentary rocks. Wright and Snoke (1993) indicate that Tertiary intrusive rocks are widespread and make up a significant component of the metamorphic core complex in the northern Ruby Mountains. They report U–Pb ages between 40 to 29 Ma for 48 zircon and monazite fractions from granitic rocks, varying from quartz diorite to leucogranite in composition.

(4) Various other igneous rocks are assigned Late Tertiary ages (Snoke, 1980, MacCready and others, 1997). This group of rocks includes scattered basalt dikes with chilled margins that intruded mylonitic metamorphosed rocks at about 17–15 Ma, and felsic volcanic rocks in the northern Ruby Mountains, which were erupted about 15 Ma. The felsic volcanic rocks are similar in age to rhyolite flows near the northern terminus of the Carlin trend (Fleck and others, this volume).

In a road cut along Lamoille Canyon, dikes of granite porphyry that probably belong to the last magmatic event are well-exposed (fig. 3). The exposure is situated inside a transition mylonite zone, in the western edge of the Lamoille Canyon nappe outlined by Howard (1966, 1980) as a pre-metamorphic thrust structure. Flaggy micaceous quartzite interbedded with biotite schist contains a tectonic lens of contorted marble, partially replaced by diopside. Metasedimentary rocks dip gently 15° to $N10^\circ E$, and are intruded by boudinaged sills of pegmatitic granite. Overprinted blastomylonite fabric in pegmatitic granite is emphasized by foliated biotite (fig. 4A).

Wedge-like dikes of granite porphyry as much as 1.7 meters thick intersect the metasedimentary rocks and pegmatitic granite sills dipping 40° to $E30^\circ S$. The fine-grained quartz–K–feldspar matrix of the granite porphyry contains phenocrysts of zoned plagioclase and quartz (fig. 4B). The ductile flow fabric of the matrix is parallel to sharp margins of the dikes. The shape and fabric of the dikes indicate that they intruded brittle fissures formed during extension. They might be a subvolcanic analog of the Miocene rhyolite mapped farther northward (Snoke, 1980). The dikes have not been affected by metamorphism or mylonitization and are considered as post-metamorphic and post-deformational. They, thus provide constraints on the minimum age of important geologic events in the Ruby Mountains.

Metamorphic and Structural Features

Regional metamorphism of the sedimentary and igneous protoliths, their relation to the structural evolution of the Ruby Mountains, and the development and timing of a remarkable mylonitic transition zone are described by Coats (1987); Dallmeyer and others (1986); Dokka and others (1986); Howard (1966, 1980); Hudec (1992); Hudec and Wright (1990); Lush and others (1988); MacCready and others (1997); Snoke (1980, 1997); Snoke and Miller (1988); and Wright and Snoke (1993). The geologic sequence defined in these studies is summarized below. Chronologic data favor a Tertiary age of metamorphic and deformational events (MacCready and others, 1997).

Formation of structural and metamorphic patterns in the migmatitic core complex includes (1) large-scale recumbent folding and thrusting, (2) polyphase amphibolite-facies metamorphism and deformation, and (3) intrusion of pegmatitic granite and related migmatization in the late Jurassic around 160 Ma. The latter was a period of major crustal shortening and thickening in northeast Nevada. Details of the earlier events were strongly masked or even destroyed by a substantial Tertiary thermal and tectonic overprint.

The migmatitic core complex is overlain by a kilometer-scale mylonitic shear zone (the so-called “transition” zone of Howard, 1980) traced for >100 km along the west border of

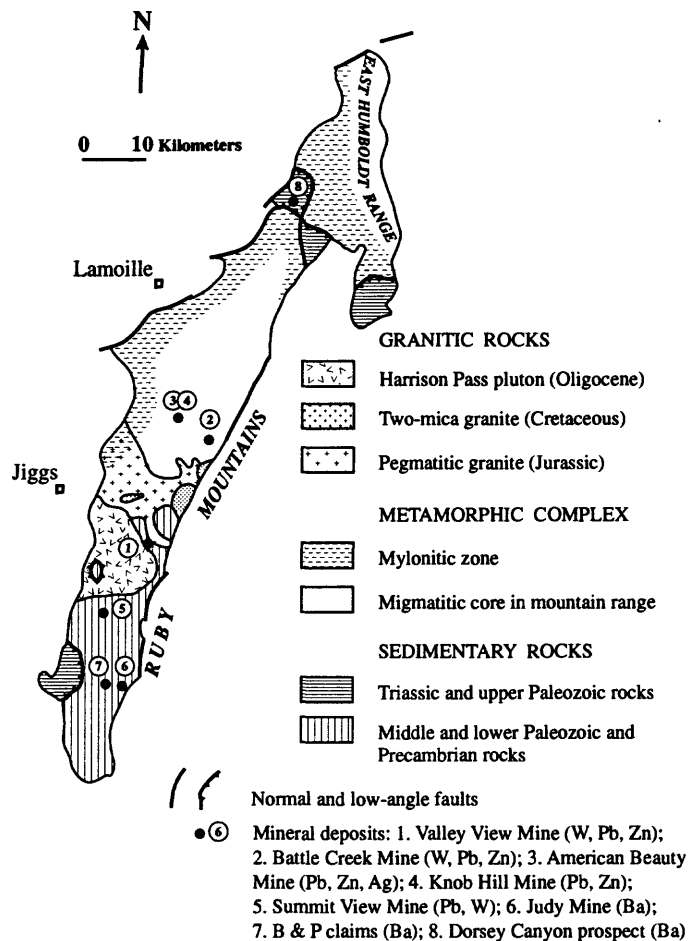


Figure 2 Distribution of mineral deposits studied in Ruby Mountains, Nevada. Geology simplified from Howard (1980); Howard and others (1979).

the Ruby Mountains. Intense ductile deformation, normal sliding and west-northwest trending streaky lineation of blastomylonitic fabric are characteristic of this zone. Variable mylonitic shear zones cutting metamorphic and granitic rocks beneath the main zone diminish with structural depth eastward. According to the geochronologic data, mylonitization developed mainly between 29 and 23 Ma and was superposed on 36–Ma Oligocene granitoids (Snoke, 1997; Wright and Snoke, 1993). In addition, 17- to 15-Ma Miocene basalt dikes cut the mylonite zone and were not affected by mylonitization. They constrain the minimum age of the ductile deformation.

Sheets of unmetamorphosed or low-grade Paleozoic and locally Tertiary rocks bounded by low-angle faults record late, post-mylonitic brittle detachment faulting. These structures are truncated by high-angle normal faults bordering the horst of the Ruby Mountains in some places.

In Search of Regional Metasomatic Events

During our traverses across the various structures that comprise the Ruby Mountains, we tried to find some traces of regional alteration that could be interpreted as a deep root for a Carlin-type fluid system. Decalcification, silicification, argillization, and at least sericitization are considered the main rock alteration around Carlin-type deposits (Bagby and Berger, 1985; Christensen, 1996; Cox and Singer, 1986; Theodore, 1997). Though these alteration types are typical of the structural level of Carlin-type gold ore deposition, we searched for any manifestations of the above-types of alteration as well as any other types of rock alteration.

Traverses across the metamorphic core complex demonstrate that two types of metamorphic rocks are regionally pervasive: (1) ubiquitous migmatitic granitic material composes

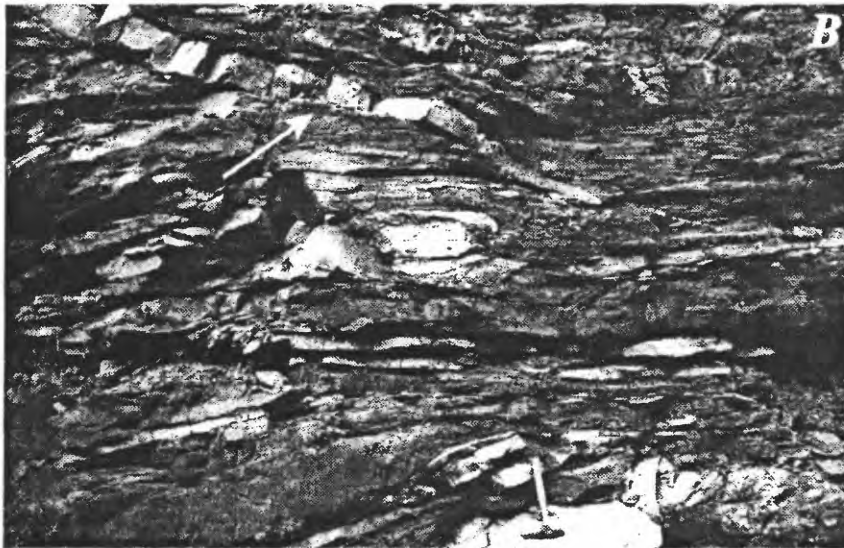
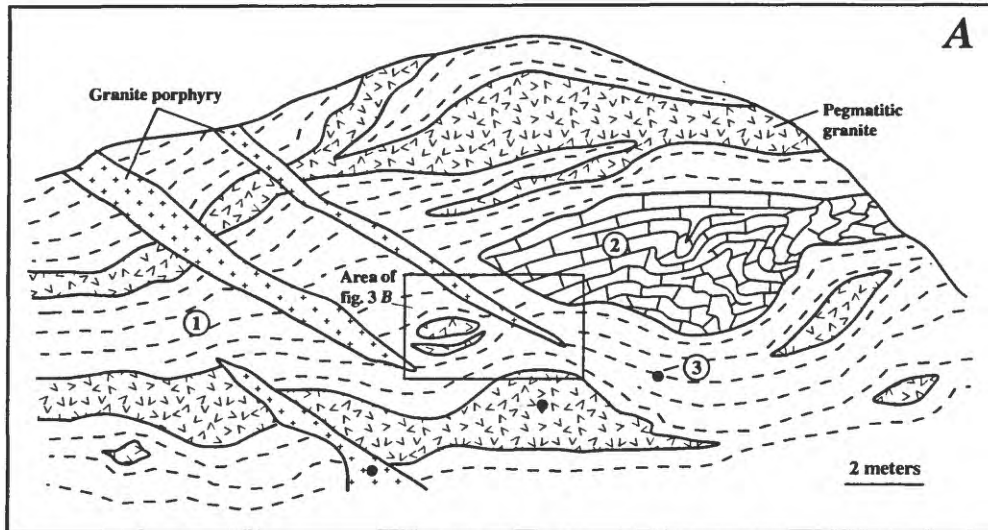


Figure 3 (A) Post-metamorphic and post-deformational wedge-like granite porphyry dikes in road cut in Lamoille Creek Canyon, 1 kilometer south of the Gaging Station, looking northeast. Sketch showing intersection with (1) schistose quartzite and metapelite; (2) marble; containing boudinaged sills of pegmatitic granite; (3) locality of samples for U-Pb age determination. (B) Photograph of area outlined in A.

no less than half of the exposed rock volume of the central and northern Ruby Mountains; and (2) local pyroxene skarn lenses are widespread in highly deformed beds of marble and crystallized limestone at contacts with sills and dikes derived from a pegmatitic granite. Skarn lenses underwent deformation and superposed boudinage, and subsequently cut by pegmatitic veinlets and accompanying quartz veins in some places. As a rule, these skarns are barren, but we have found sparse scheelite grains in alluvium-concentrate samples along creeks draining areas of skarn localities.

TUNGSTEN-POLYMETALLIC MINERALIZED ROCKS

The following accessible skarn-polymetallic \pm tungsten deposits in the Ruby Mountains were examined in detail: Valley View Mine, Battle Creek Mine, American Beauty Mine, Knob Hill Mine, and Summit View Mine, which are located in different parts of the range (fig. 2). All these deposits are small. They were explored and partially mined to varying degrees by open cuts, adits, and shafts during previous years, and the walls

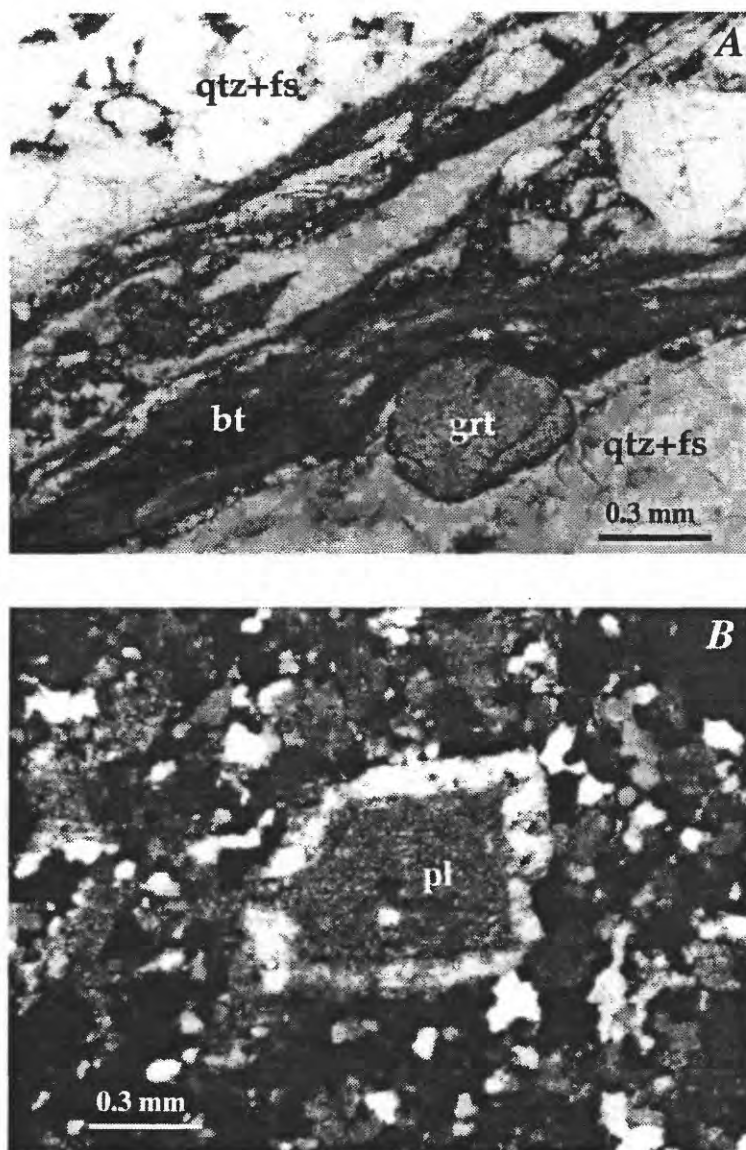


Figure 4 Photomicrographs of thin sections of samples from the outcrop shown on figure 3. (A) Mylonitic pegmatitic granite, plane-polarized light; (B) post-deformational granite porphyry, crossed nicols; qtz+fs, quartz and feldspar; bt, biotite; grt, garnet; pl, phenocryst of zoned plagioclase.

and faces of the old surface workings and dumps were generally accessible for examination.

The following general features characterize the deposits: (1) The deposits are present within Cambrian (and Ordovician in some places) marble, as much as 3,000 meters in tectonic thickness (Howard, 1980); (2) Exoskarn is predominant and present near or in the immediate contact with Late Jurassic and Tertiary granitic rocks; (3) The shape of the ore bodies varies from stratiform, and concordant to the marble bedding, to tabular to lensoid, and discordant to the bedding and

concordant to a granite contact; (4) Evidence of pre-ore brecciation and ore-accompanying retrograde alteration of skarn is common; and (5) Scheelite and polymetallic sulfide assemblages are close in time and spatially, but commonly, are present as separate ore bodies.

All information about exploration and mining activity, processing and production, as well as brief geologic data, especially about tungsten mineralization, is summarized from published descriptions of mineral deposits (Bentz and Tingley, 1983; Lapointe and others, 1991; Smith, 1976; Stager and

Tingley, 1988) and supplemented by our observations.

Valley View Mine

(Valley View district, Road Canyon area)

The Valley View deposit (fig. 2, location 1) was discovered in 1913. Tungsten and base-metal ores were explored by adit, open cut, and a vertical shaft. Small amounts of tungsten were produced intermittently in 1944, 1953–54, 1957 and 1978, totaling 263 units of WO_3 (a unit of WO_3 is equivalent to 1 percent of a short ton, or 20 pounds of WO_3) from ore that graded from 10 to 0.6 weight percent WO_3 .

The deposit is present inside a northwest trending 0.5–1.5-km strip of Cambrian crystalline limestone and quartzite dividing plutons of Jurassic pegmatitic granite and Tertiary Harrison Pass pluton of granite-quartz monzonite. A stratabound mineralized skarn zone 1–6 m in width is exposed intermittently over a strike length of approximately 150 m. Irregular skarn pods and seams are confined to a distinct bed of streaky carbonaceous siliceous marble and crystalline limestone, about 50 m wide striking west-northwest and dipping 75° N (figs. 5A and 6). Sills and dikes of granite, microdiorite, and quartz monzonite cut rocks in the general area of the deposit.

Most tungsten ore was mined from one mined-out skarn seam 1–6 inches wide and 48 feet in length along the contact between crystalline limestone and quartz monzonite sill. The scheelite ore of this seam was estimated to contain from 1 to 5 weight percent WO_3 and yielded 150 units of WO_3 . Scheelite is present in skarn consisting of diopside, epidote, calcite and quartz. Bismuthinite and native bismuth were found in the aggregate with pyrite and quartz in the centers of some granitic sills.

Stratabound skarn sulfide tabular bodies, exposed in the open cut (figs. 5A and 7A–B), consist mainly of oxidized ore. Disseminated sulfide grains and pods are present in siliceous crystallized biotitic limestone partially replaced by clinopyroxene and epidote. Grains of the earliest pyrrhotite, as much as 0.01 mm wide, are present along limestone bedding planes independent of any skarn minerals. Where minerals of the skarn assemblage accumulated, pyrrhotite is partially or entirely replaced by pyrite, chalcopyrite, sphalerite, and galena, in this succession. These sulfides are part of a retrograde skarn assemblage that is associated with epidote and quartz. They replaced the earlier and probably metamorphic pyrrhotite.

Quite distinctive of this sulfide skarn zone is a replacement of most widespread galena and sphalerite by late actinolite (fig. 8A–B). This substitution has led to drastic dilution of the sulfide ore. Quartz and epidote accompanied deposition of the major part of this sulfide assemblage. In addition, pre-sulfide pyroxene was replaced by an aggregate of lance-shaped crystals of amphibole. It looks like a superposition of a new hydrous amphibole skarn assemblage on an earlier skarn and retrograde

quartz-sulfide mineralization, which is interpreted to have been related to the Late Jurassic pegmatitic granite. The late amphibolization probably represents a second period of skarn formation associated with the nearby Tertiary Harrison Pass pluton, which is known elsewhere to have related amphibole-garnet-epidote skarns (fig. 2).

Battle Creek Mine

(Ruby Valley district)

The Battle Creek deposit (fig. 2, loc. 2) is located on the east side of the Ruby Mountains at an elevation of about 7,400 feet (2,220 meters). It includes several mineralized skarn zones spread over an area of about four square kilometers. The deposits were discovered in 1903; base metal and incidental silver and gold were produced during a period from 1908 until 1967, and since 1949 shipped ore averaged 55 weight percent Pb and 14.2 weight percent Zn. Tungsten had been detected in 1943 and produced intermittently from 1944 to 1977, the ore averaged 1.5 weight percent WO_3 during 1944–45. Exploration and mine workings consist of numerous trenches, an open cut, two shallow shafts, and four adits with a total 700 feet of underground workings. Total production from the Ruby Valley district is as follows: tungsten, 4,944 units; lead, 531,135 lbs; zinc, 250,300 lbs; copper, 24,413 lbs; silver, 11,332 ounces; gold, 56 ounces (Lapointe and others, 1991).

According to Stager and Tingley (1988), scheelite with little quartz and pyrite is present in several east-trending lenses of chlorite schist surrounded by granite and pegmatite. The largest vertical lens, 100-ft long and maximum 10-ft thick, strikes $N70^\circ E$. Unfortunately, chlorite schist was not found in the area, perhaps because this tungsten-bearing rock was completely mined out.

Mineralized skarn zones, as much as 4 m wide, dip at angles of 50° – 70° to the north or south depending on the attitude of the skarn-controlling contact between bleached Cambrian marble and dikes and sills of Jurassic pegmatitic granite. Granite is commonly gneissic and sheared along the contact. The main skarn zone exposed by an open cut is shown on figures 5B and 9. The zone consists of two bands parallel to the contact between white coarse-grained marble and medium-grained gneissic pegmatitic granite. The inner band is composed of exoskarn containing microscopic relicts of granite immediately adjacent to the contact. This skarn consists of a compact primary aggregate of pyroxene, mostly diopside, that is brecciated and cemented by quartz with disseminations and pods of galena, sphalerite, pyrite, pyrrhotite, chalcopyrite, and rare scheelite (see inset "b" on fig. 5B). Near quartz-sulfide veinlets, pyroxene is partially replaced by calcite and tremolite. The outer band consists entirely of a retrograde calcite-tremolite assemblage that replaces the adjoining marble. This band also is brecciated and cemented almost entirely by sulfide minerals with little quartz (see inset "a" on fig. 5B).

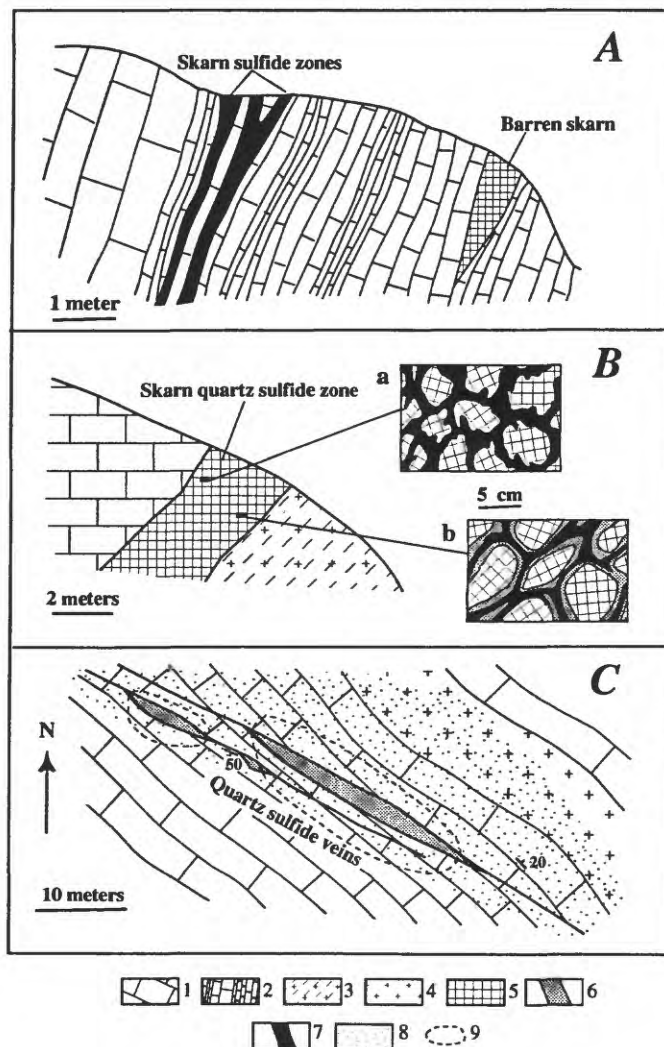


Figure 5 Sketches of polymetallic deposits of the Ruby Mountains: *A*, Valley View Mine, W-Pb-Zn skarn deposit, wall of the western open cut looking east; *B*, Battle Creek Mine, W-Pb-Zn skarn deposit, face of the main open cut looking northeast, (a) and (b), details of the ore breccia; *C*, reconstruction of quartz-sulfide veins on open cut floor in the Knob Hill Mine; 1, thick-bedded marble; 2, thin-layered streaky marble and crystallized limestone; 3, gneissic pegmatitic granite; 4, sill of pegmatitic granite; 5, skarn; 6, quartz with sulfide minerals; 7, veins and pods of sulfides; 8, quartz-sericite alteration; 9, outline

Mineralization in the deposit is divided into four stages: (1) pyroxene exoskarn formation; (2) shearing and gneissification of granite and brecciation of skarn along the contact; (3) overprint of skarn and adjoining marble by a retrograde tremolite-calcite association; and, finally, (4) brecciation within the whole skarn zone and precipitation of quartz and sulfide minerals. Clear textural evidence demonstrates some deposition of sulfide minerals after quartz. Within the sulfide assemblage, galena was consistently younger than sphalerite (fig. 10). Eventually, gangue and ore minerals were slightly deformed.

American Beauty Mine

(Lee district, northeastern side of the Long Canyon)

The American Beauty deposit (fig. 2, loc. 3) is on the western slope of the Ruby Mountains, about 6 kms northwest of the Battle Creek Mine, at an elevation of 8,200 feet (2,460 meters). It was discovered in 1869 with first recorded production in 1871, and then again in 1915–19, 1921–29, 1949–58. Production during the latter period came mainly from the nearby Knob Hill Mine. Total production includes: lead, 1,851,034 lbs; zinc, 123,148 lbs; copper, 24,413 lbs;



Figure 6 Crystallized streaky limestone containing pyrrhotite dissemination and carbon segregation along bedding planes; exposure nearby portal of the adit in the Valley View Mine.

silver, 11,332 ounces; gold, 56 ounces (Lapointe and others, 1991). Sorted ore during 1949 averaged 29 weight percent Pb and 2 oz Ag/t. The deposit was explored and mined by trenches, cuts, shaft and several east-trending adits.

In many previous descriptions, the deposit was described as "quartz-sulfide veins" present in massive gently east-dipping beds of marble invaded by pegmatitic granite, quartz monzonite, aplite and pegmatite (Lapointe and others, 1991). No vein was exposed in place but, according to Smith (1976), mineralized veins as much as 1.5-m wide strike northwest and dip southwest.

Our observations determined that this deposit originally formed as a typical skarn with intense superposition on the skarn assemblage by retrograde quartz-sulfide ore. Mineralized quartz-sulfide veins are located within an irregularly developed skarn zone in Cambrian marble near a contact with a sill of Jurassic pegmatitic granite; skarn also

persists as relicts completely surrounded by quartz.

In dumps from the deposit we found many fragments of skarn associated with quartz-sulfide material. Vitreous light gray to white recrystallized quartz is strongly metamorphosed to foliated mylonite containing rounded fragments of clinopyroxene, idocrase, and celsian from an earlier skarn-mineral assemblage (fig. 11). Quartz contains abundant disseminations, veinlets, and pods of sulfide minerals of two types: early pyrrhotite, chalcopyrite and pyrite; and late galena and sphalerite accompanied by rare tetrahedrite and barite. Galena shows ductile deformation textures (fig. 12). Bentz and Tingley (1983) noted late-stage quartz-pyrite veinlets in some samples of crudely banded quartz-sulfide veins.

The presence of celsian, a barium plagioclase feldspar, in a skarn assemblage is a particular feature of this deposit. We have checked numerous published sources and did not find any references to celsian in various well-described skarn deposits. This extraordinary fact attracted our attention and the celsian was studied in somewhat more detail. Celsian is represented by rounded fragments up to 0.3 mm in diameter within metamorphosed quartz. It is very abundant in some places, representing as much as 3 volume percent of the gangue mass. The mineral was identified and analyzed by Scanning Electron Microprobe (fig. 13A, table 1) and then compared with known mineralogical and analytical data (Deer and others, 1965). According to published mineralogical descriptions, celsian commonly is present as well-formed tabular crystals. In our case, however, the rounded fragments of celsian indicate that it underwent mylonitization along with pyroxene and other skarn minerals. In the same samples, fragments of pyroxene were found with fine barite and galena inclusions that exhibit a late barite-sulfide association (fig. 13A-B).

Three important features are emphasized about the deposit: (1) originally skarn-type, the deposit currently is represented mainly by superposed retrograde quartz-sulfide assemblages containing only relicts of skarn minerals including celsian; (2) the deposit contains no tungsten mineralization; (3) strong metamorphism and polyphase mylonitization of ore (pre- and post- quartz-sulfide mylonitization) are related to an offshoot of the regional "transition" mylonitic zone.

Knob Hill Mine

(Lee district, southwestern side of the Long Canyon)

The Knob Hill deposit (fig. 2, loc. 4) is located at elevation of 8,700 feet (2,610 meters) on the southwestern slope of the Long Canyon opposite the American Beauty Mine, by about 1 kilometer. Several open cuts were made in the vicinity of old underground workings, most likely during the 1970's.

Quartz-sulfide veins striking N40°W and dipping 50° SW and their surrounding geology have been reconstructed on a sketch of the upper open cut from fragments on the floor and small exposures on collapsed flanking walls (fig. 5C). Veins

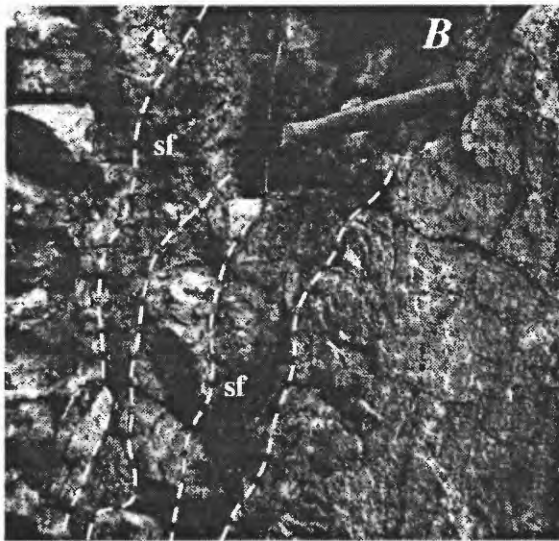
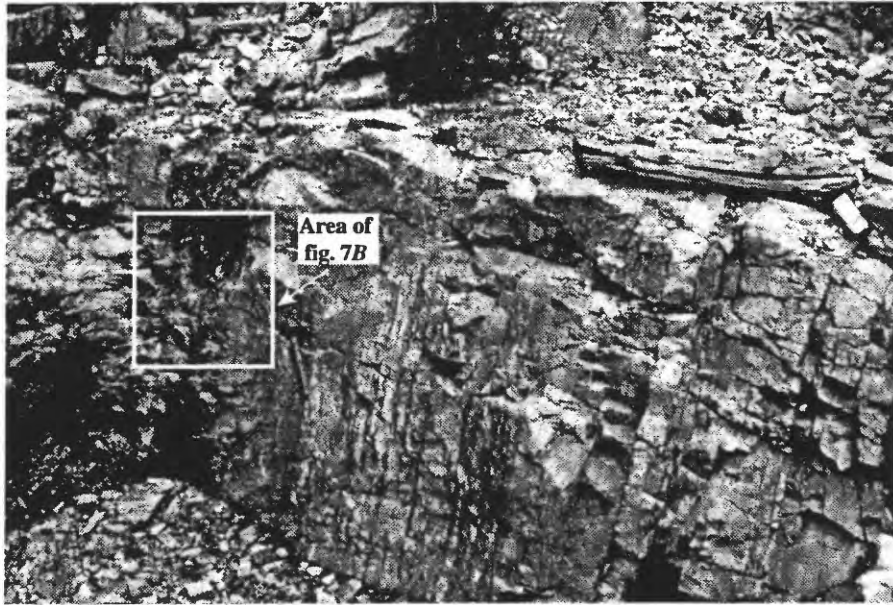


Figure 7 A, Stratabound skarn sulfide zones exposed on wall of the western open cut in the Valley View Mine, looking east. B, Photograph of area outline in A; sf, sulfide zone.

cut crystallized Cambrian limestone gently dipping to N20°E close to the pegmatitic granite sill. Both rock types are bleached, recrystallized, silicified, and cut by irregular thin quartz-calcite veinlets. The veins are composed of sugar-like quartz containing disseminations and pods of galena, sphalerite, and pyrite. All veins are deformed and recrystallized by strong metamorphism and mylonitization. Slickensides are traced on vein walls.

In this deposit located at a high elevation, no evidence of skarn was found around the quartz-sulfide veins or along the contact between limestone and pegmatitic granite. Instead,

hydrothermal silicification and veining by carbonate minerals are present. The deposit probably represents a “pure” end-member quartz-polymetallic vein type well known within skarn districts (Cox and Singer, 1986).

Summit View Mine (Corral Creek district)

The Summit View deposit (fig. 2, loc. 5) is on the south side of the Corral Creek valley, on the west slope of the Ruby

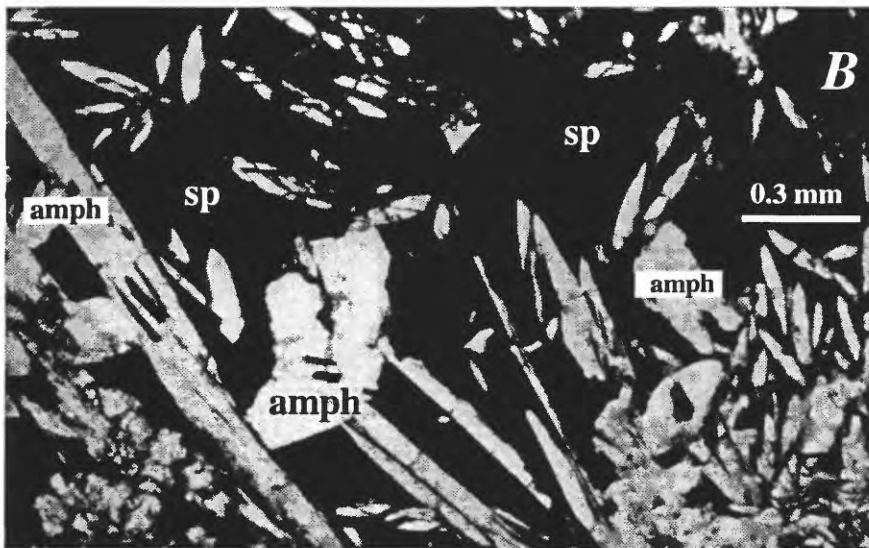
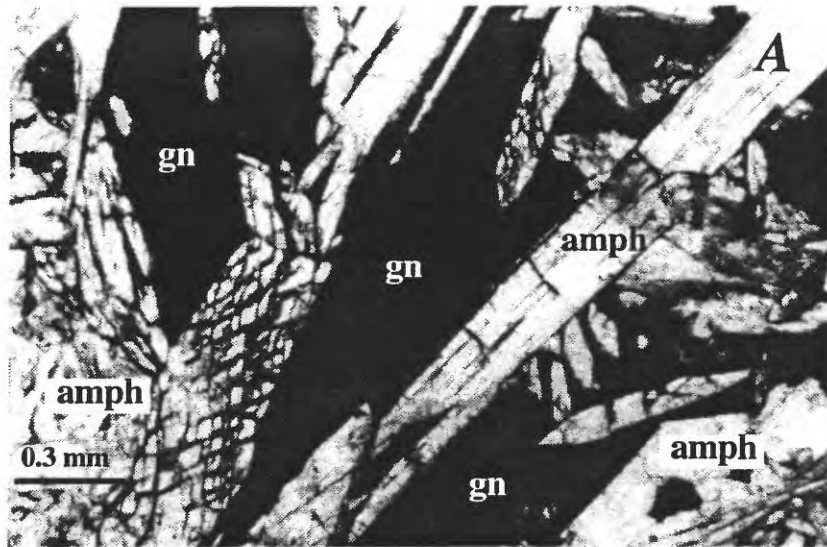


Figure 8 Photomicrographs of skarn sulfide ore from the Valley View Mine. Pods of (A) galena (gn) and (B) sphalerite (sp), partially replaced by late amphibole (amph).

Mountains, and southwest of Harrison Pass. The first known record of activity in the area was in 1925. Roughly 108 tons of sulfide ore that averaged 2.5 weight percent lead, 1.1 weight percent zinc, 0.15 weight percent copper, and 3.0 oz Ag/t were mined during 1948–1952. Three south-trending adits and relatively recent bulldozing are mentioned in the latest deposit description (Lapointe and others, 1991).

About 12 tons of tungsten ore averaged 0.6 weight percent WO_3 was mined from S. & L. Mother No 1 claim in 1979. This locality is about 3 km northeast of the Summit View Mine. A contact skarn zone between Cambrian limestone and Tertiary

Harrison Pass granitic pluton dips steeply at 70° to the northwest. Fine-grained laminated scheelite-bearing skarn consists of amphibole-garnet-epidote assemblages.

In the eastern part of the Summit View Mine, a quartz-sulfide vein was traced along the contact skarn zone between marble and leucocratic granite of the Harrison Pass pluton. A nearly horizontal mineralized zone 1-m thick is present. Disseminations and pods of galena, sphalerite, pyrite, chalcopyrite, and pyrrhotite are distributed in quartz with minor calcite. Quartz is distinguished by an original mosaic to crustified texture without any traces of metamorphism (fig.



Figure 9 Battle Creek Mine; face of the main open cut looking northeast; 1, Marble; 2, tremolite-actinolite skarn with sulfide minerals; 3, brecciated pyroxene skarn with quartz-sulfide veins; 4, gneissic pegmatitic granite.

14A). It contains fragments of garnet and amphibole from an older skarn assemblage. Sulfide minerals, representing mostly the latest portion of the mineralizing event, fill open spaces in quartz in association with well-shaped tabular crystals of celsian and aggregates of apatite, both as much as 0.2 mm wide (fig. 14B-C).

Grains of celsian are partially replaced with hyalophane (fig. 14D). Chemical compositions of the celsian, shown in the table 1, is nearly standard and close to samples from the American Beauty Mine. The principal difference is that celsian from that deposit is from a compound skarn assemblage that pre-dated quartz and sulfide minerals. In the Summit View Mine, celsian with sulfide minerals post-dates crystallization of quartz. Further study is needed to explain this difference.

BARITE DEPOSITS

During the 1997 field season, barite deposits of the Judy Mine, B & P claims, and Dorsey Canyon prospect, which are hosted by non-metamorphosed miogeoclinal sedimentary rocks, were also examined. The purpose of this investigation was to compare this barite mineralization with barite showings along the Carlin trend and around it. Data about the above listed barite deposits were gathered by Papke (1984), Bentz and Tingley (1983), Lapointe and others (1981), and Smith (1976).

Judy Mine (Cave Creek district)

The deposit at the Judy Mine (fig. 2, loc. 6) is situated in

southern part of the Ruby Mountains, immediately north of Elko-White Pine County line. Two claims were located in 1972; total past production was between 1,000 and 25,000 tons of barite from a 120-m-long open cut trending N25°E. The deposit area also was explored by shallow pits and drilling.

According to Papke (1984), a roughly stratiform zone of vein-replacement-type barite mineralization, 25 m of estimated stratigraphic thickness, is hosted by dark gray bituminous Devonian dolomite gently dipping southward at about 20°, and seldom exceeding 40°. At the south end of the area, mineralized dolomite is in steep fault contact with north-dipping, fossiliferous limestone. Downslope to the east, dolomite is underlain by sandstone.

During our visit to the deposit, the southern face of the open cut, about 9-m high, was partially accessible for detailed observations. High-grade stratiform barite >5 m thick is exposed in the lower part of the face. The lode consists of two bands with irregular outlines (fig. 15A). A footwall band 2–3 m thick is composed of gray massive bedded barite that follows the dolomite bedding. The upper band of the lode is made up of conformable barite-calcite-dolomite breccia superposed on an earlier massive bedded barite.

An east-west-striking high-angle (dipping 70° N) normal fault branches downward and terminates the massive barite ledge within the open cut. The massive barite reappears again at the north end of the open cut. The lode of similar “two-band” structure can be traced there, and is offset by a high-angle fault. Sparse coalescing calcite-barite veins as much as 5 cm thick and fragments of barite-calcite breccia with locally leached sandy dolomite are exposed within the central part of the open cut between the two ends of the pit.

Massive barite from the footwall ledge shows several particular features:

- it is fine- to medium-grained, slightly but clearly deformed and recrystallized;

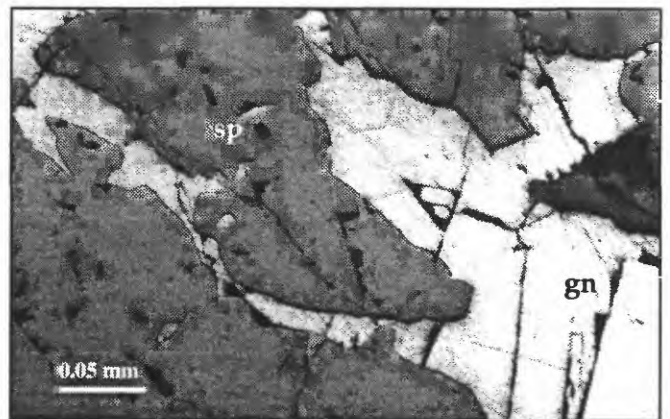


Figure 10 Photograph of galena (gn) in relation to sphalerite (sp) in quartz-sulfide vein in skarn zone of the Battle Creek Mine, reflected light.

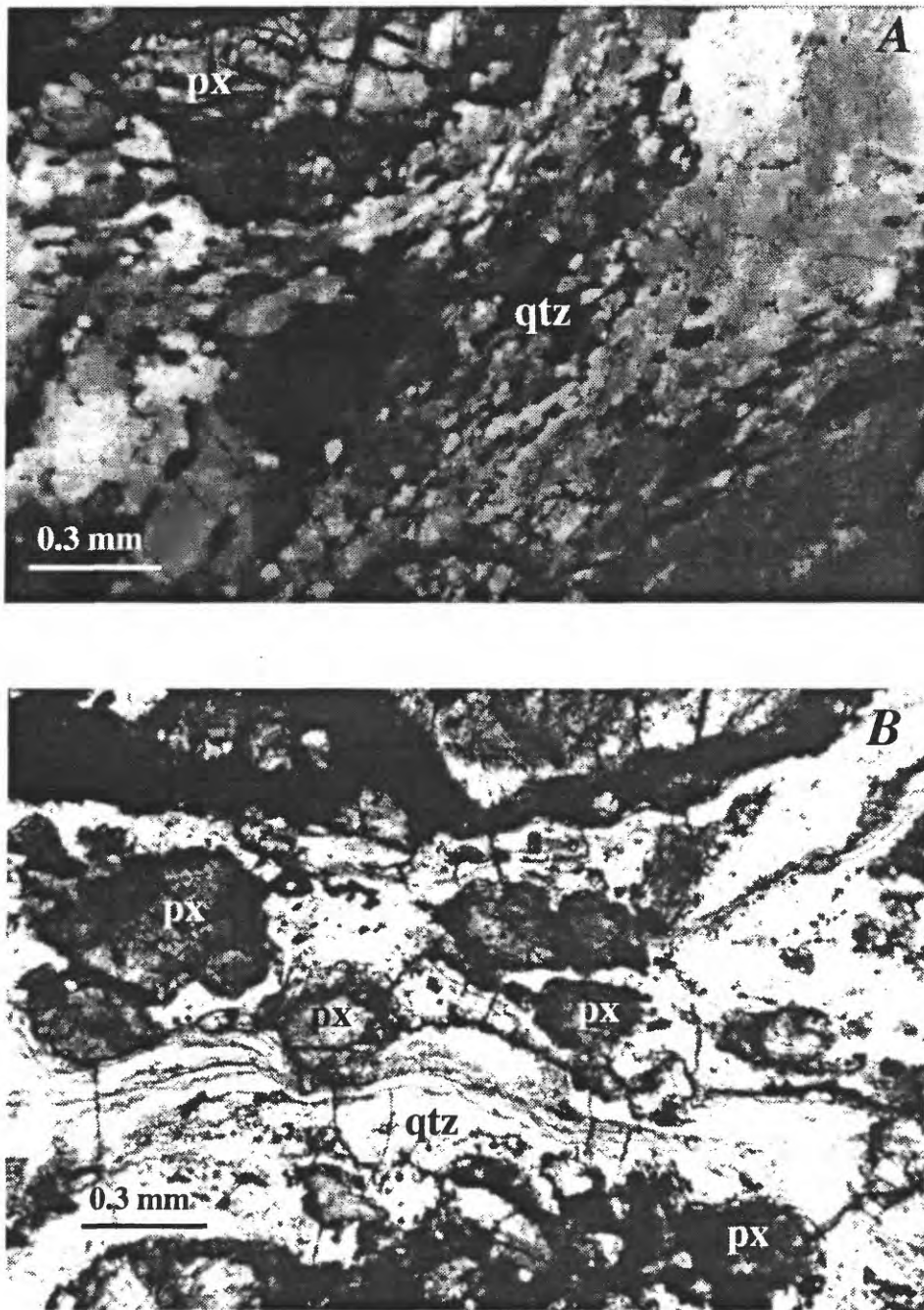


Figure 11 Photomicrographs of samples from quartz-skarn zone of the American Beauty Mine: *A*, cataclastic metamorphosed quartz (qtz) with fragment of pyroxene (px), crossed nicols; *B*, laminated mylonitic quartz containing rounded fragments of pyroxene, plane-polarized light.

- it contains relicts of original thin-lamination marked partially by bitumen inclusions along bedding planes (fig. 16A); the lamination are bent and rotated along microfaults that separate barite domains;
- it is partly replaced by newly grown rhomboids of calcite and dolomite (fig. 16B) accompanied by intergranular spheroid micropore resulting from barite dissolution;
- it is fetid when broken, which derives probably from unsealing of the micropores and H₂S-gas release during crushing.

The footwall stratiform ledge of early deformed massive barite obviously is of bedded barite-type. Such classification is supported by analogy to bedded barite deposits widespread throughout Nevada and well known in various stratigraphic

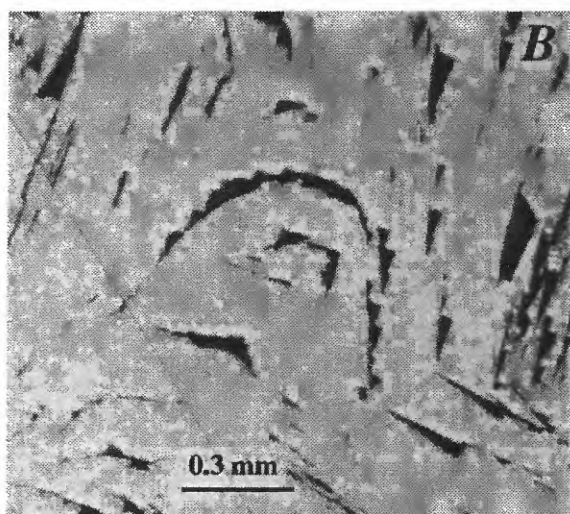
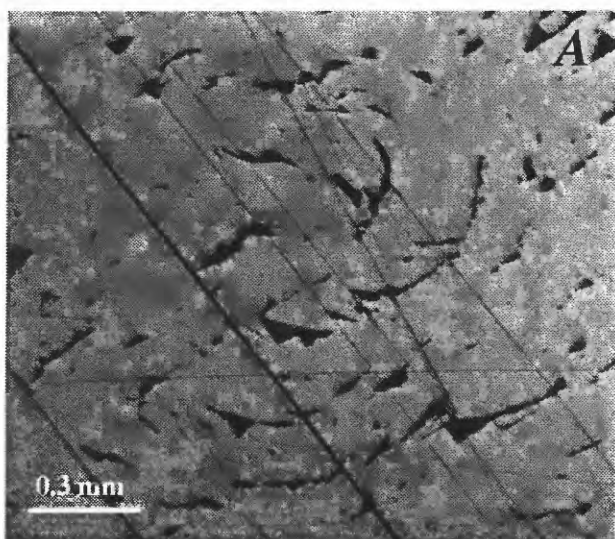


Figure 12 Photomicrographs of deformed galena in metamorphosed ore from the American Beauty Mine and Knob Hill Mine, reflected light: S-like (A) and dome-like (B) curved cleavage pits as a result of deformation.

units within Elko county (Zimmerman, 1969; Poole, 1975; Papke, 1984), including a Mississippian mudstone-chert sequence identified by conodonts in a bedded barite locality in the Snake Mountains (Poole and others, 1982).

The superposed barite-calcite-dolomite breccia conformably overlays bedded barite and include part of its upper part (fig. 15A-B). The breccia contains fragments of layers and angular blocks of dolomite-cemented bedded barite; these clasts are partially replaced by barite and calcite. White sugary veins of barite and calcite extend along bedding planes

and cut dolomite outside the breccia. The late barite is radically different from the earlier massive one. It is white and glassy, consisting of crustified and micro-drusy aggregates of tabular crystals without any signs of deformation (fig. 16C). It seems possible that this late barite is a product of late post-deformation, probably extensional, hydrothermal remobilization of older bedded barite that underwent partial dissolution and replacement by carbonate minerals during brecciation.

B & P Claims (Cave Creek district)

The B & P claims (fig. 2, loc. 7) were first located in 1972 as a barite prospect in the Mitchell Creek drainage area, 4 km northwest of the Judy Mine. The prospect was explored by trenches and drilling focused on an area of about 300 square meters. Papke (1984) described two barite-bearing zones exposed in a northeastward-trending face and separated by about 6 m of nearly barren dolomite.

Exposures of the main zone were in relatively good condition during our visit to the prospect. Barite-calcite breccia is present within a veined and fractured zone, as much as 5 m wide, striking N35-45°W and dipping 50-80° NE. The zone cuts medium- to dark-gray fine-grained Devonian dolomite. Nearby bedded fossiliferous limestone and dolomite striking north-south and dip 35° W.

An axial lens of pure barite, about 1 m thick and 6 m long, occupies the central part of the breccia zone. The barite lens is bordered by semiparallel shears zones. Sparse short barite and calcite veinlets and pods 5-10 cm thick are present along a 15-m strike length of the exposed zone. Calcite and minor quartz are also present in the zone. White sugary fine-grained barite is widespread. Glassy crystalline barite found in the main axial zone consists of microscopic aggregates of undeformed tabular crystals, similar to those in the breccia and veins of the Judy Mine.

Dorsey Canyon Prospect (Halleck district)

The Dorsey Canyon prospect (fig. 2, loc. 8) is located in the Secret Creek area within a low-angle fault sheet described by Snoke (1980) as a detachment slice of low-grade metasedimentary rocks structurally overlying the lower plate metamorphic complex. The mineralized zone at the prospect is exposed in several shallow pits. Calcite and quartz veinlets and local calcite-barite breccia cut bleached and silicified Permian limestone, striking N70°W, along a steep fault contact between limestone and siliceous conglomerate, striking N40°W. The angular mineralized breccia is obviously young.

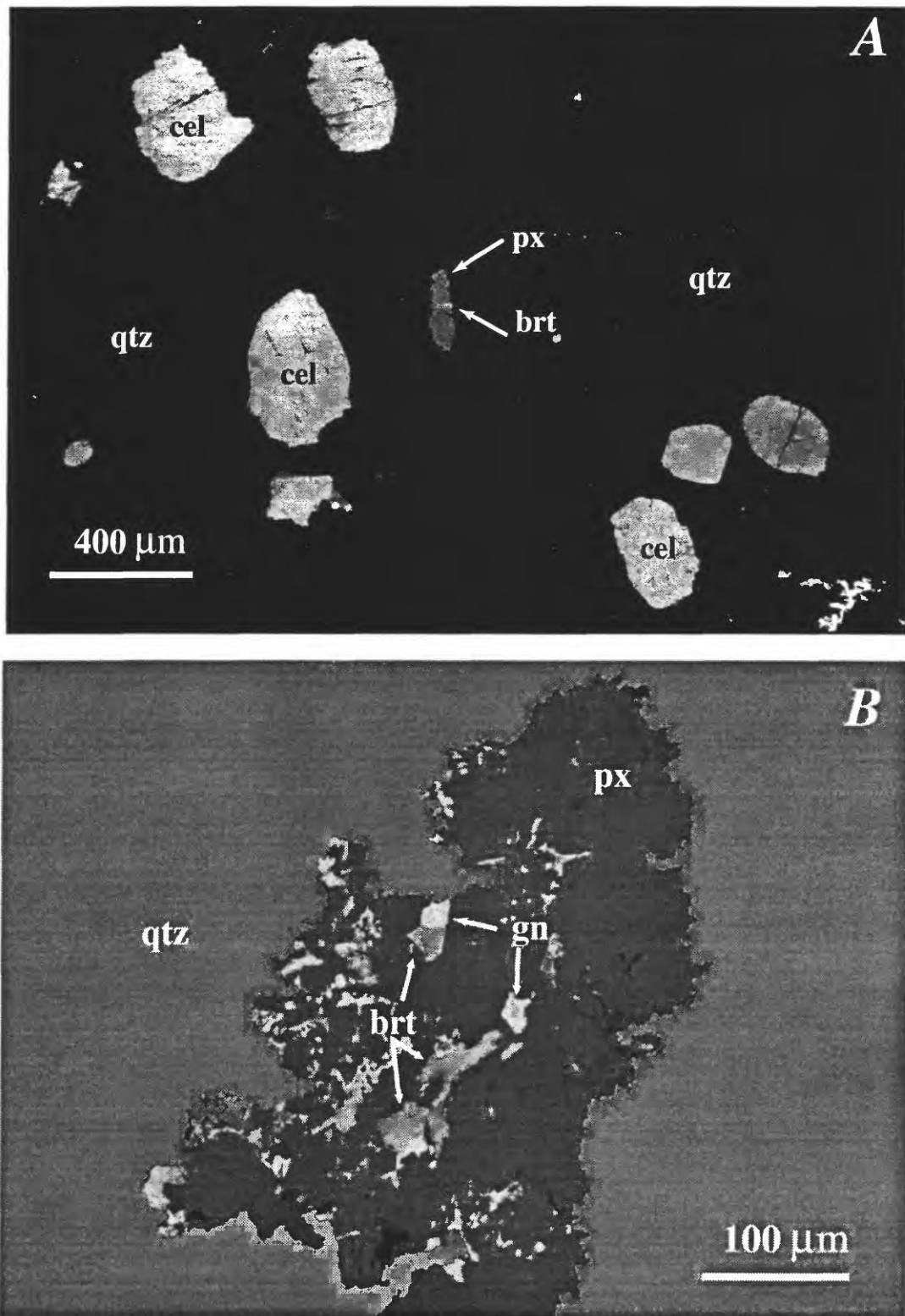


Figure 13 Back-scattered electron image (BSE) of ore from quartz skarn zone of the American Beauty Mine: *A*, rounded fragments of celsian (cel) in ore-host quartz (qtz) containing also single grain of pyroxene (px) with barite (brt) inclusion; *B*, fragment of pyroxene, surrounded by quartz, containing barite and galena (gn).

Table 1. Electron-microprobe analyses of celsian

No.	Deposit and sample No.	SiO ₂	Al ₂ O ₃	BaO	K ₂ O	Na ₂ O	Total
American Beauty Mine							
Sample B97-1							
1		34.44	27.84	38.92	0.39	0.15	101.73
2		34.04	28.02	39.57	0.35	0.16	102.14
3		34.07	28.23	39.58	0.34	0.13	102.34
4		33.96	28.02	40.29	0.20	0.15	102.61
5		34.04	28.25	39.37	0.27	0.14	102.07
6		34.64	28.28	39.37	0.46	0.16	102.92
7		34.16	28.32	39.32	0.29	0.15	102.24
8		34.17	27.95	39.25	0.38	0.13	101.89
9		34.07	28.08	39.83	0.34	0.20	102.52
10		34.17	27.92	38.89	0.41	0.13	101.52
Average		34.17	28.09	39.44	0.34	0.15	102.20
Sample B97-1B							
11		33.02	28.62	40.03	0.19	0.09	101.94
12		33.48	28.13	39.78	0.43	0.12	101.93
13		33.6	27.74	39.27	0.38	0.13	101.13
14		33.82	28.26	39.69	0.21	0.12	102.11
15		33.84	28.53	39.95	0.31	0.10	102.74
16		34.45	28.54	40.04	0.37	0.12	103.53
17		34.31	25.03	39.97	0.43	0.13	99.87
18		34.02	28.27	39.33	0.37	0.10	102.08
Average		33.82	27.89	39.76	0.34	0.11	101.92
Summit View Mine							
Sample B97-42E							
19		34.11	28.07	38.54	0.7	0.09	101.50
20		34.71	28.35	37.97	0.88	0.13	102.05
21		36.82	27.11	35.59	1.74	0.17	101.43
22		35.35	28.04	37.99	1.20	0.11	102.70
23		35.42	27.52	36.44	1.24	0.15	100.77
Average		35.28	27.82	37.31	1.15	0.13	101.69
Sample B97-42B							
24		35.04	27.96	37.56	0.69	0.20	101.45
25		35.82	27.90	36.82	1.07	0.23	101.85
26		35.88	28.08	37.11	1.10	0.25	102.42
27		34.97	28.13	39.28	0.72	0.24	103.34
28		36.53	28.00	38.02	0.89	0.20	103.63
29		37.6	27.25	35.89	1.55	0.29	102.58
30		36.68	27.97	36.61	1.34	0.30	102.90
31		34.89	26.63	36.06	0.95	0.27	98.80
32		47.85	24.45	31.20	2.52	0.41	106.43
33		36.22	24.77	36.37	1.12	0.22	98.71
34		35.66	27.71	37.47	0.97	0.21	102.02
35		34.18	28.28	39.48	0.35	0.11	102.39
36		43.41	24.22	34.32	0.73	0.17	102.84
37		36.81	27.78	37.02	1.43	0.30	103.34
38		38.36	27.20	37.44	0.65	0.18	103.83
39		42.98	25.03	34.55	0.71	0.21	103.47
40		35.52	28.25	38.11	0.81	0.26	102.95
41		44.87	24.77	34.62	0.88	0.21	105.35
Average		37.96	26.91	36.55	1.03	0.24	102.68

Table 1, continued. Atomic proportion

No	Deposit and sample No	Si	Al	Ba	K	Na	Total
	American Beauty Mine						
1	Sample B97-1	8.23	7.84	3.64	0.12	0.07	19.90
2		8.15	7.91	3.71	0.11	0.07	19.95
3		8.14	7.95	3.71	0.10	0.06	19.96
4		8.14	7.91	3.78	0.06	0.07	19.96
5		8.14	7.96	3.69	0.08	0.07	19.94
6		8.19	7.88	3.65	0.14	0.07	19.93
7		8.14	7.95	3.67	0.09	0.07	19.92
8		8.18	7.89	3.68	0.12	0.06	19.93
9		8.14	7.91	3.73	0.10	0.09	19.97
10		8.19	7.89	3.66	0.12	0.06	19.92
	Average	8.16	7.91	3.69	0.10	0.07	19.94
	B97 -1B						
11		7.96	8.14	3.78	0.06	0.04	19.98
12		8.07	7.99	3.75	0.13	0.05	19.99
13		8.04	7.82	3.68	0.12	0.06	19.72
14		8.10	7.98	3.73	0.06	0.06	19.93
15		8.07	8.02	3.73	0.09	0.05	19.96
16		8.13	7.94	3.70	0.11	0.06	19.94
17		8.50	7.31	3.88	0.14	0.06	19.89
18		8.13	7.97	3.69	0.11	0.05	19.95
	Average	8.13	7.90	3.74	0.10	0.05	19.92
	Summit View Mine						
	Sample B97-42E						
19		8.15	7.90	3.61	0.21	0.04	19.91
20		8.21	7.90	3.52	0.27	0.06	19.96
21		8.61	7.47	3.26	0.52	0.07	19.93
22		8.30	7.76	3.50	0.36	0.05	19.97
23		8.40	7.69	3.39	0.38	0.07	19.93
	Average	8.33	7.74	3.46	0.35	0.06	19.94
	Summit View Mine						
	Sample B97-42B						
24		8.31	7.81	3.49	0.21	0.09	19.91
25		8.40	7.72	3.39	0.32	0.11	19.94
26		8.38	7.73	3.40	0.33	0.11	19.95
27		8.23	7.81	3.62	0.22	0.11	19.99
28		8.45	7.64	3.45	0.26	0.09	19.89
29		8.67	7.41	3.24	0.46	0.13	19.91
30		8.48	7.62	3.32	0.40	0.13	19.95
31		8.44	7.59	3.42	0.29	0.13	19.87
32		9.99	6.02	2.55	0.67	0.17	19.40
33		8.81	7.10	3.47	0.35	0.10	19.83
34		8.39	7.69	3.46	0.29	0.10	19.93
35		8.14	7.94	3.69	0.11	0.05	19.93
36		9.65	6.35	2.99	0.21	0.07	19.27
37		8.50	7.56	3.35	0.42	0.13	19.96
38		8.76	7.32	3.35	0.19	0.08	19.70
39		9.52	6.53	3.00	0.20	0.09	19.34
40		8.31	7.79	3.49	0.24	0.12	19.95
41		9.70	6.31	2.93	0.24	0.09	19.27
	Average	8.67	7.39	3.33	0.30	0.11	19.81

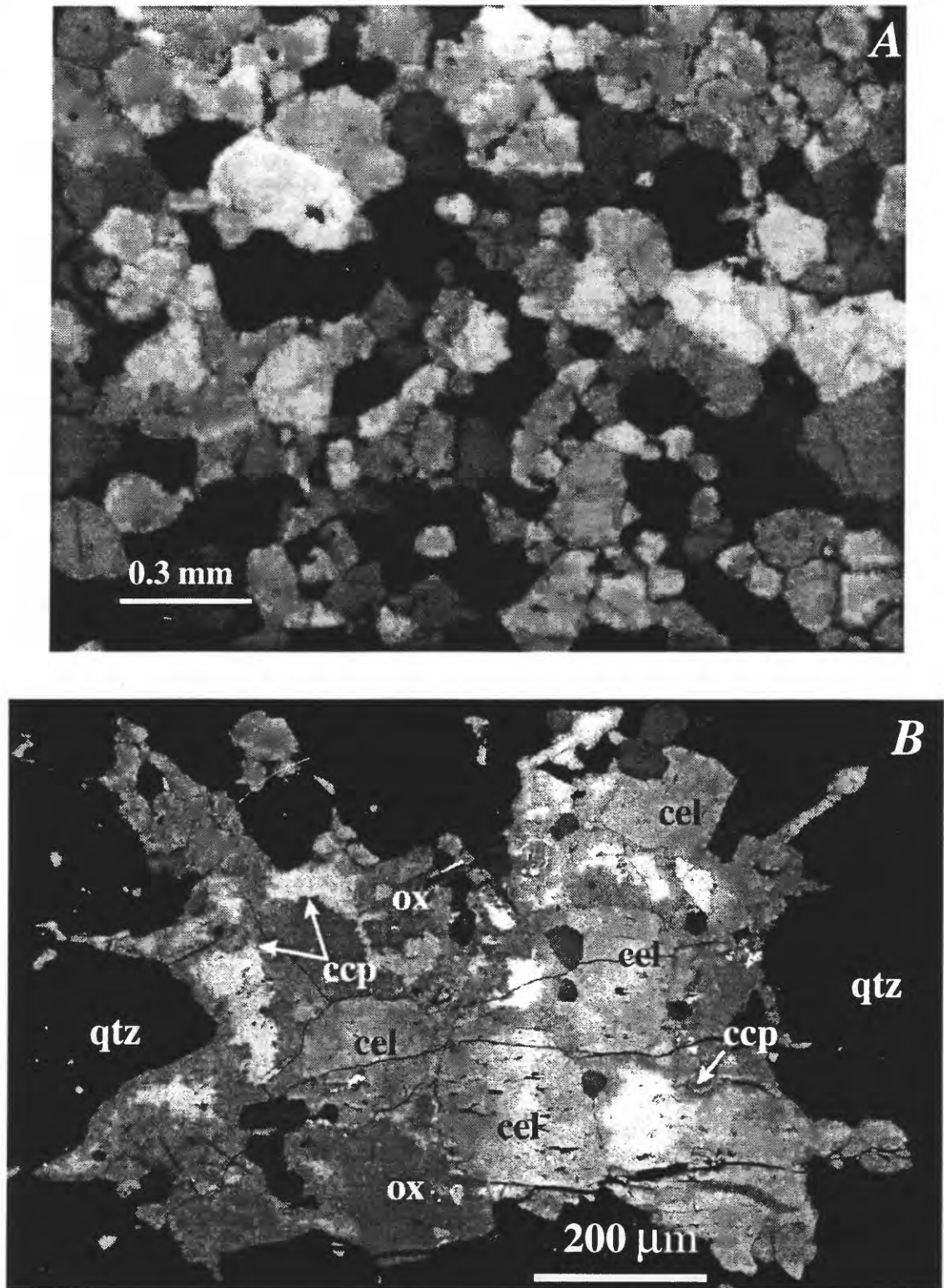


Figure 14 Photomicrograph and back-scattered electron images of samples from quartz skarn sulfide zone of the Summit View Mine. *A*, Photomicrograph of original mosaic texture of ore-host quartz, crossed nicols; BSE images; *B*, aggregate of celsian crystals (cel) with chalcopyrite (ccp) and Cu, Fe-oxides (ox) filling open space in quartz (qtz); *C* and *D* continued on next page.

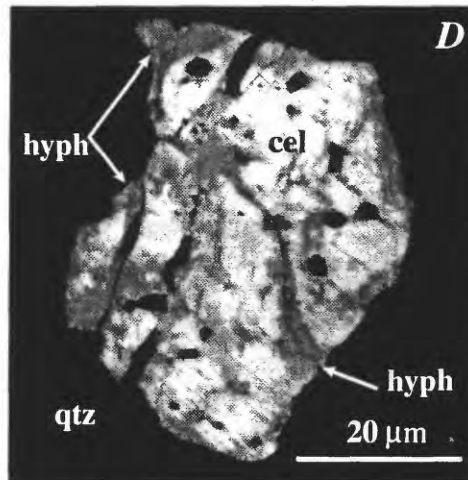
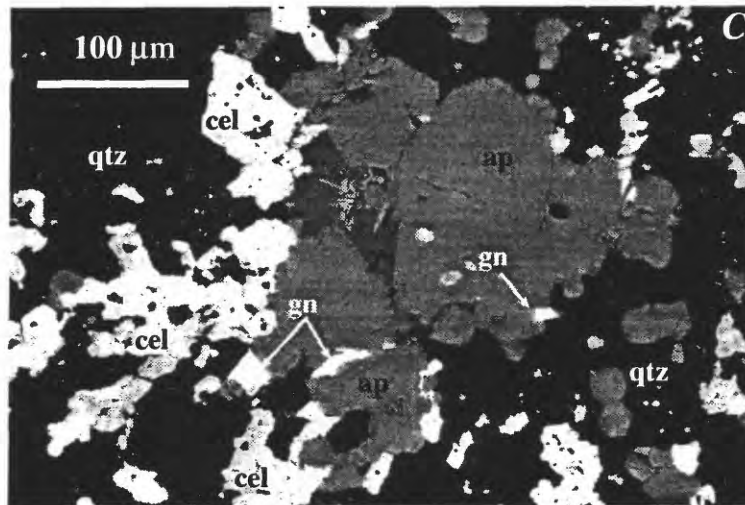


Figure 14 continued: *C*, aggregate of apatite (ap), celsian and galena (gn) filling open space in quartz; *D*, grain of celsian partially replaced (?) by hyalophane (hyph).

DISCUSSION AND CONCLUSIONS

Principal features of the mineral deposits and their geologic setting are shown on figure 17. Table 2 summarizes the general geologic and metallogenic succession within the Ruby Mountains.

Data obtained during this investigation allow us to conclude the following:

(1) At least two phases of skarn formation are evidenced in the Ruby Mountains: the first skarn phase is related to Late Jurassic magmatism and second to Oligocene granite-monzonite of the Harrison Pass pluton. Skarn deposits of both phases are present at the same stratigraphic level, which

is the Cambrian marble and limestone. They also contain mineralized rocks of very similar W + Pb, Zn, Cu, Ag, and Ba composition. The main difference includes the various compositions of the skarn-mineral assemblages themselves: first, pyroxene-idocrase with minor garnet and retrograde association of amphibole (actinolite-tremolite)-epidote-calcite accompanied by quartz-sulfide minerals; second, amphibole-epidote-garnet skarn assemblage with a calcite-quartz retrograde association. This difference and the varied ore textures, almost "epithermal" in the second case, probably result from different depths of the intrusion emplacement—deep Jurassic pegmatitic granite and shallow Tertiary pluton—and related differences in pressure and temperature during skarn formation. Einaudi and others (1981) and Meinert (1993)

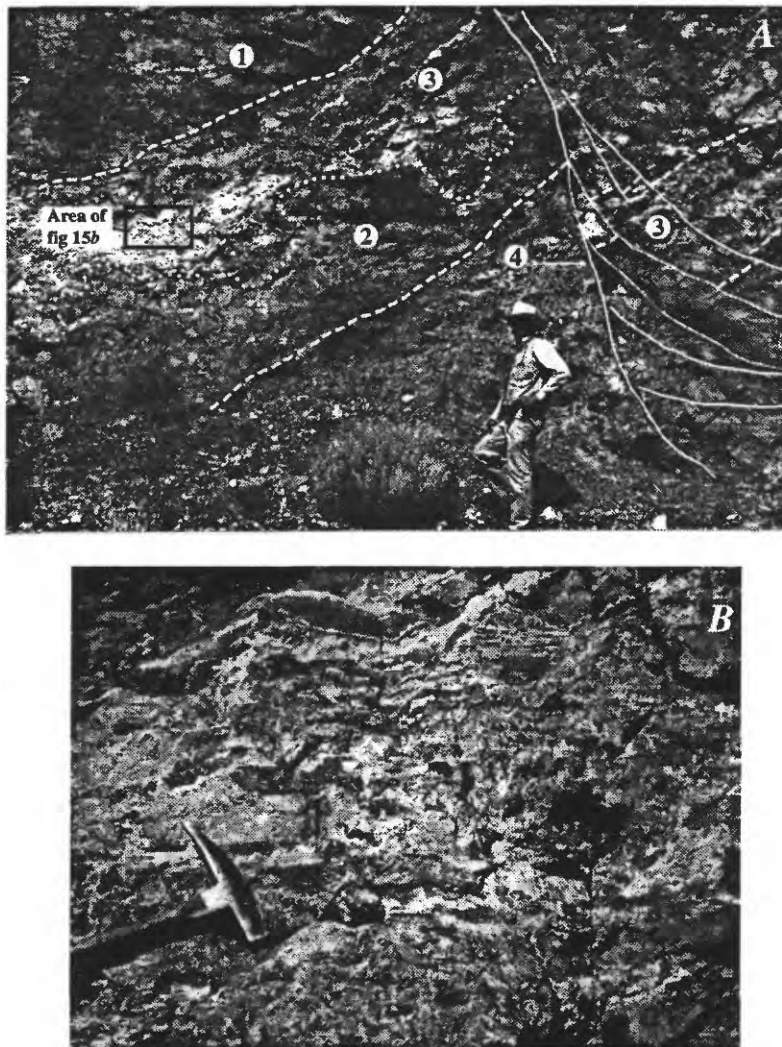


Figure 15 Face of the main open cut of the Judy barite mine looking northwest; **A**, Photograph of stratiform barite zone: 1, Devonian dolomite; 2, early bedded barite; 3, late barite-calcite-dolomite breccia; 4, post-mineral fault. **B**, Photograph of area outlined in **A** showing structure of the late breccia.

point out the importance of such depth factors during skarn genesis.

(2) Combined vertical zoning of skarn mineralization can be established for nearby deposits at the Battle Creek Mine (2,220 m elevation), American Beauty Mine (2,460 m) and Knob Hill Mine (2,610 m) which are present in the same area of a roof pendant of the Jurassic pegmatitic granite. At the lower elevations, tungsten and quartz-polymetallic mineralization is hosted by a well-developed skarn zone. Approximately 240 m higher, polymetallic sulfide mineralization without tungsten is hosted by quartz containing only fragments of skarn, that was almost completely destroyed during retrograde processes. About 150 m higher at the uppermost level of the hydrothermal

system, only quartz-polymetallic veins are present and surrounded by a hydrothermal halo of silicification and carbonate veinlets. No significant gold appears anywhere within this vertical zoning. Quartz-sulfide veins are located, as a rule, within skarn zones and rarely as individual occurrences in the upper part of the vertical zonation. They certainly are related to retrograde stages of skarn formation that had been initiated by granite intrusions. In places, the quartz-sulfide veins have been deformed cataclastically. The quartz-sulfide veins are post-regional metamorphism and late- or post-granitic and cannot be considered as an analog of low-sulfide gold-quartz vein type.

(3) Celsian (barium feldspar), discovered in skarn deposits of

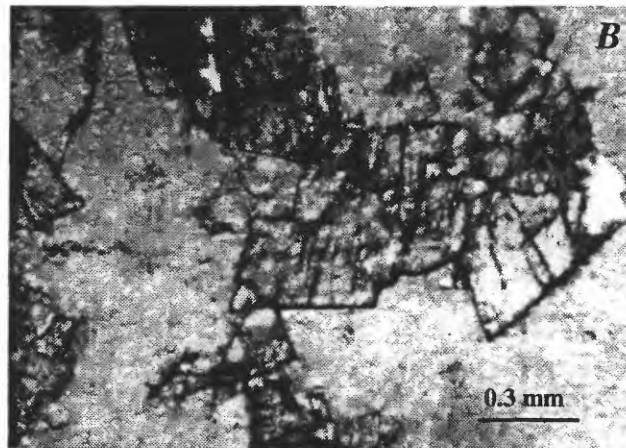
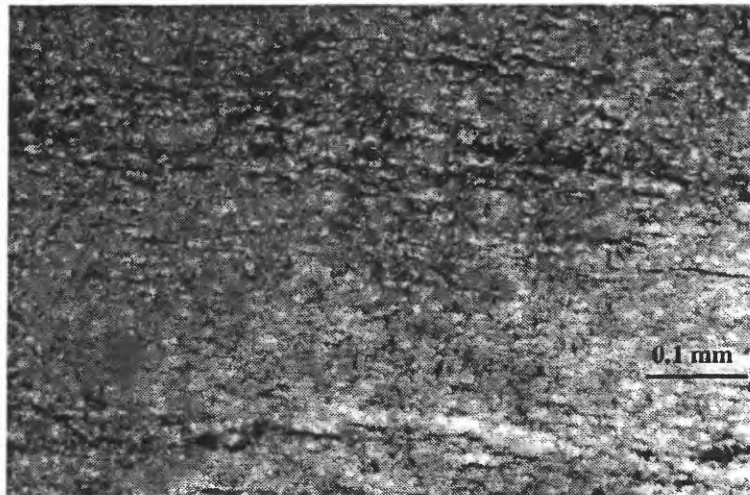


Figure 16 Photomicrographs of various types of barite from the Judy Mine, Nevada. *A*, early gray barite with parallel traces of probable original lamination, plane-polarized light; *B*, replacement of early barite by calcite rhomboids, plane-polarized light. (Figure *C* on the next page.)

the Ruby Mountains, is not reported as a component of skarn-mineral assemblages (Einaudi and others, 1981; Meinert, 1993; Singer and others, 1997). Theodore and Roberts (1971) first describe it from Nevada in deep drill holes at Iron Canyon in metamorphosed and altered chert, argillite and greenstone of the Devonian Scott Canyon Formation. Celsian was accompanied there by sphalerite. In many other cases, celsian was explained invariably as a result of metamorphism, commonly contact metamorphism, of barite-bearing VMS and SEDEX polymetallic deposits, and magnesium deposits (Segnite, 1946; Deer and others, 1965; Coats and others, 1980; Yudovskaya and others, 1997). In the Ruby Mountains, celsian is represented in ores of both major phases of skarn formation. Its appearance in a contact-metamorphic paragenesis needs

to be studied further. However, we can only speculate that the ore-host Cambrian carbonate rocks might have contained pre-metamorphic barite-bearing SEDEX mineralization (table 2). Unfortunately, we did not find any evidence of this precursor mineralization except for possibly the pyrrhotite disseminations in crystallized limestone at the Valley View Mine. An alternative possibility is to consider celsian as a granite-generated component of the skarn-polymetallic-barite assemblage.

(4) Skarn mineralization is not related commonly to Carlin-type gold deposits. But there is a case history at the Getchell deposit in the Osgood Mountains, Nevada, where granodiorite intrusion and associated tungsten skarns are located close to

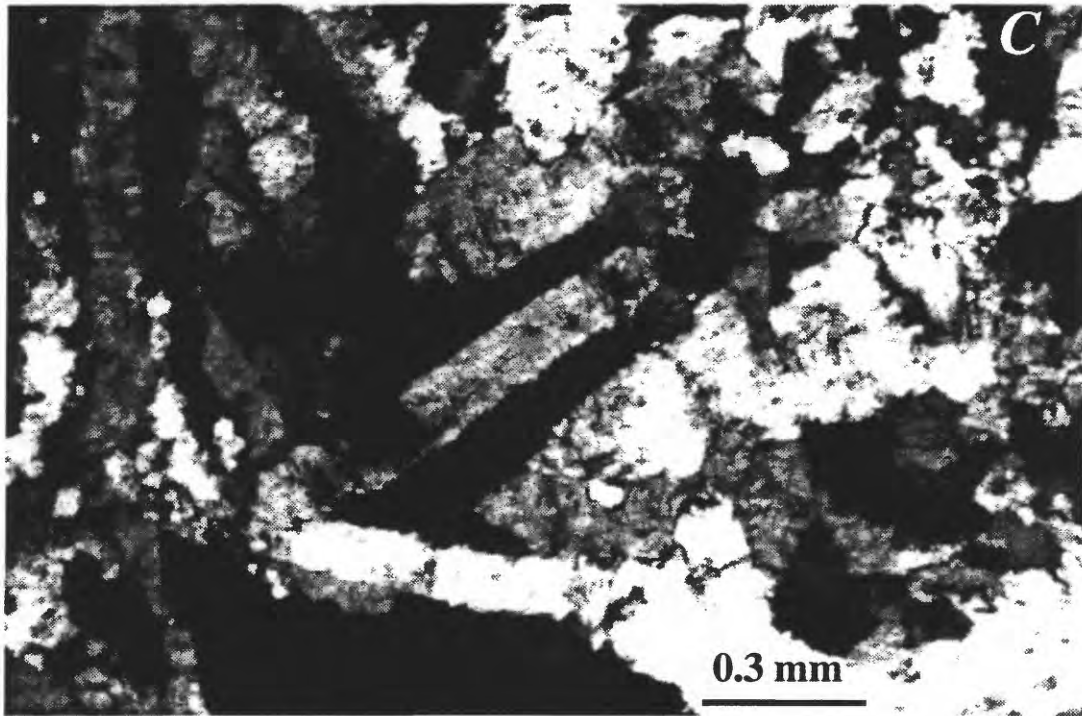


Figure 16 continued: C, aggregate of tabular crystals of late barite from veinlets, crossed nicols.

Carlin-type mineralization. Opposing opinions about their age and genetic ties have been discussed (Joralemon, 1975; Silberman and others, 1974). But true relationships of these two events are not clear still (Bagby and Cline, 1991), although many geologists believe the Carlin-type deposits at Getchell are much younger than the tungsten skarn (Groff and others, 1997). Gold is not a documented significant component of skarn mineralization in the Ruby Mountains. Furthermore, the existence of a complete combined vertical zoning of the skarn deposits probably does not allow space for any "skarn roots" of Carlin-type gold mineralization in the migmatitic core complex of this region.

(5) Bedded barite in Devonian dolomite of the southern Ruby Mountains could be roughly compared with the newly discovered barite-bearing SEDEX-type base- and precious-metal mineralized rocks of the northern Carlin trend (Emsbo and others, 1997). However, an absence of metallic associates in bedded barite of the Judy Mine places strong constraints upon such a comparison. Barite is an insignificant but common component of many Carlin-type deposits. But the same reasoning constrains comparisons of vein barite occurrences of the Ruby Mountains with Carlin-type deposits in the Alligator Ridge and Yankee Mine to the south of the Ruby Mountains (fig. 1). Those deposits are located in

Mississippian strata (Ilchik, 1991; Stout, 1997).

This study in the Ruby Mountains did not reveal any "roots", connections, or analogs for Carlin-type gold deposits. However, the investigation necessarily was of a short duration and should not be considered comprehensive.

ACKNOWLEDGMENTS

We would like to thank Ted G. Theodore for arranging this short study and for his effective support, permanent attention, and invaluable advice and guidance, and finally for rigorous reviewing of the report. Stephen G. Peters guided us by his leadership in that physically difficult first traverse to the American Beauty Mine, and brought out important ideas about the main features of the study. Connie Nutt helped to arrange our visit to the Bald Mountain Gold Mine, where Kerry Hart and Jeff Peterson were our elaborate and generous guides. Bill Stout showed us details of gold mineralized rocks in operating open pits of the Yankee Gold Mine and presented written description (Stout, 1997) of this southernmost deposit of the Carlin Trend. Many families around the Ruby Mountains cordially permitted us to overpass their properties and indicated appropriate ways to start our traverses. We are thankful to all of them.

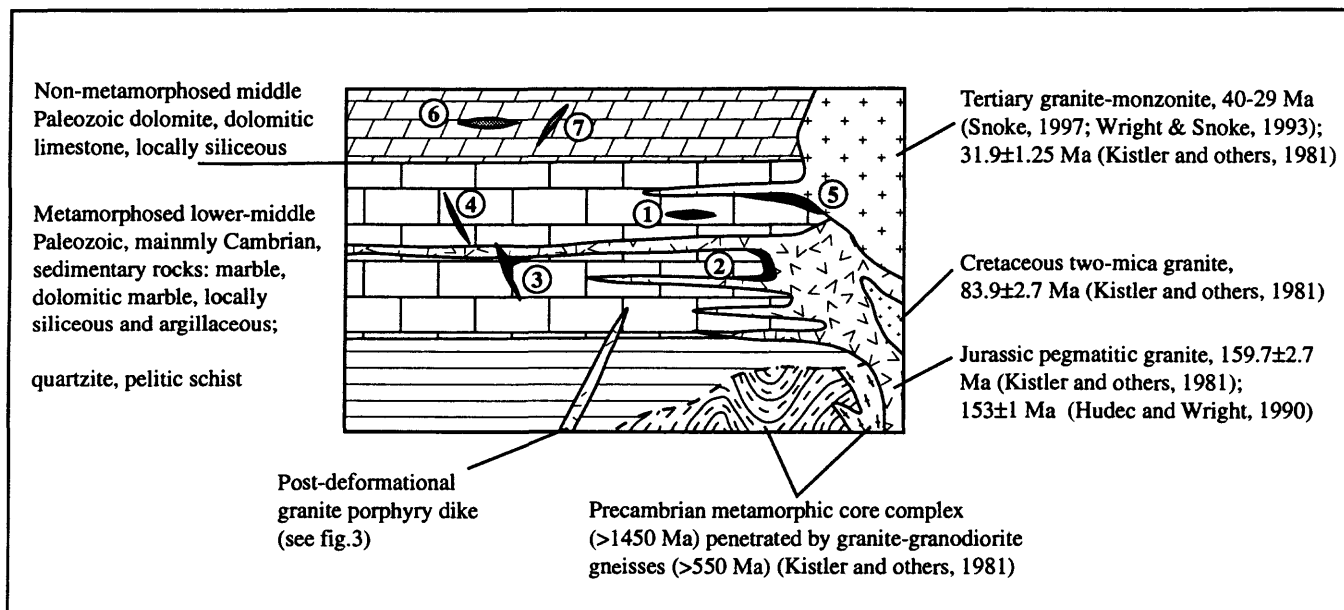


Figure 17. Mineral deposits in the Ruby Mountains, Nevada, shown in a schematic geologic setting simplified from Howard, 1966,1980; Kistler and others, 1981; Snoko, 1980, 1997; MacCready and others, 1997. Mineral deposits: (1) Valley View Mine, W, Pb, Zn skarn; (2) Battle Creek Mine, W, Pb, Zn skarn; (3) American Beauty Mine, Pb, Zn, Ag skarn; (4) Knob Hill Mine, Pb, Zn quartz vein; (5) Summit View Mine, Pb, W, Cu skarn; (6) Judy Mine, Ba, bedded barite; (7) B & P claims, Ba, vein .

Table 2. General geologic and metallogenic succession in the Ruby Mountains, Nevada

Period	Geologic events	Mineralization
Cenozoic	Faulting mylonitic transition zone granite-monzonite intrusion	Barite vein, replacement Amphibole-garnet-epidote skarn W+Pb, Zn, Cu, Ba (as late celsian)
Mesozoic	Granitic intrusion folding metamorphism	Pyroxene-idocrase skarn W+Pb, Zn, Cu, Ag, Ba (as earlier celsian and late barite)
Middle and Late Paleozoic	Epicratonic carbonate and clastic sedimentation	Bedded barite (SEDEX)
Early Paleozoic		Speculative barite-base metal SEDEX

REFERENCES CITED

- Bagby, W. C., and Berger, B. R., 1985, Geologic characteristics of sediment-hosted, disseminated precious-metal deposits in the western United States, *in* Berger, B. R., and Bethke, P. M., eds., *Geology and Geochemistry of Epithermal Systems: Reviews in Economic Geology*, Volume 2, Society of Economic Geologists, p. 169–202.
- Bagby, W. C., and Cline, J. S., 1991, Constraints on the pressure of formation of the Getchell gold deposit, Humboldt County, Nevada, as interpreted from secondary-fluid-inclusion data, *in* Raines, G. L., Lisle, R. E., Schafer, R. W., and Wilkinson, W. H., eds., *Geology and ore deposits of the Great Basin: Geological Society of Nevada*, p. 133–178.
- Bentz, J. L., and Tingley, L. V., 1983, A mineral inventory of the Elko resource area, Elko district, Nevada: Nevada Bureau of Mines and Geology Open-File Report 83–9, 212 p.
- Coats, J. S., Smith, C. G., Fortey, N. J., Gallagher, M. J., May, F., and McCourt, W. J., 1980, Stratabound barium-zinc mineralization in Dalradian schist near Aberfeldy, Scotland: *Transactions of the Institute of Mining and Metallurgy*, v. 89, p. B110–B121.
- Coats, R. R., 1987, *Geology of Elko County, Nevada: Nevada Bureau of Mines and Geology Bulletin 101*, 112 p.
- Cox, D. P., and Singer, D. A., eds., 1986, *Mineral deposit models*, U.S. Geological Survey Bulletin 1693, 379 p.
- Cristensen, O. D., 1996, Carlin trend geologic overview, *in* Green, S. M., and Struhsacker, E., eds., *Geology and ore deposits of the American Cordillera, Field Trip Guidebook Compendium: Geological Society of Nevada*, p. 147–156.
- Dallmeyer, R. D., Snoke, A. W., and McKee, E. H., 1986, The Mesozoic-Cenozoic tectonothermal evolution of the Ruby Mountains, East Humboldt Range, Nevada: *Tectonics*, v. 5, p. 931–954.
- Deer, W. A., Howie, R. A., and Zussman, J., 1965, Barium Feldspars, *in* *Rock-Forming Minerals, Volume 4, Framework Silicates*: London, Longmans, p. 166–178.
- Dokka, R. K., Mahaffic, M. J., and Snoke, A. W., 1986, Thermochronologic evidence of major tectonic denudation associated with detachment faulting, Northern Ruby Mountains-East Humboldt Range, Nevada: *Tectonics*, v. 5, no. 7, p. 995–1006.
- Einaudi, M. T., Meinert, L. D., and Newberry, R. J., 1981, Skarn deposits: *Economic Geology*, 75th Anniversary Volume, p. 317–391.
- Emsbo, P., Hutchinson, R. W., Hofstra, A. H., Volk, J. A., Bettles, K. H., Baschuk, G. J., Collins, T. M., Lauha, E. A., and Borhauer, J. L., 1997, Newly discovered Devonian Sedex-type base and precious metal mineralization, Northern Carlin Trend, *in* Vikre, P., Thompson, T. B., Bettles, K., Cristensen, O., and Parrat, R., eds., *Carlin-Type Gold Deposits, Field Conference: Society of Economic Geology Guidebook series*, v. 28, p. 109–117.
- Fleck, R.J., Theodore, T.G., Sarna-Wojcicki, Andrei, and Meyers, C.E., (this volume), Age and possible source of air-fall tuffs of the Miocene Carlin Formation, northern Nevada, *in* Tosdal, R.M., ed., *Contributions to the gold metallogeny of northern Nevada: U.S. Geological Survey Open-File Report*.
- Groff, J.A., Heizler, M.T., McIntosh, W.C., and Norman, D.I., 1997, $^{40}\text{Ar}/^{39}\text{Ar}$ dating and mineral paragenesis for Carlin-type gold deposits along the Getchell Trend, Nevada: Evidence for Cretaceous and Tertiary gold mineralization: *Economic Geology*, v. 92, p. 601–622.
- Howard, K. A., 1966, Structure of the metamorphic rocks of the northern Ruby Mountains, Nevada: New Haven, Conn., Yale University, Ph. D. dissertation, 170 p.
- 1971, Paleozoic metasediments in the northern Ruby Mountains, Nevada: *Geological Society of America Bulletin* 82, p. 259–264.
- 1980, Metamorphic infrastructure in the northern Ruby Mountains, Nevada, *in* Crittenden, M. D., Jr., Coney, P. J., and Davis, G. H., eds., *Cordilleran metamorphic core complexes: Geological Society of America Memoir 153*, p. 335–347.
- Howard, K. A., Kistler, R. W., Snoke, A. W., and Wilden, R., 1979, *Geologic Map of the Ruby Mountains: U.S. Geological Survey Map I-1136*, scale 1:125,000.
- Hudec, M. R., 1992, Mesozoic structural and metamorphic history of the central Ruby Mountains metamorphic core complex, Nevada: *Geological Society of America Bulletin*, v. 104, p. 1086–1100.
- Hudec, M. R., and Wright, J. E., 1990, Mesozoic history of the central part of the Ruby Mountains-East Humboldt Range metamorphic core complex, Nevada: *Geological Society of America, Abstracts with Program*, v. 22, no. 3, p. 30.
- Ilchik, R. P., 1991, Geology of the Vantage gold deposits, Alligator Ridge, Nevada, *in* Raines, G. L., Lisle, R. E., Schafer, R. W., and Wilkinson, W. H., eds., *Geology and ore deposits of the Great Basin: Geological Society of Nevada*, p. 645–663.
- Ilchik, R. P., and Barton, M. D., 1997, An amagmatic origin of Carlin-Type deposits: *Economic Geology*, v. 92, p. 269–288.
- Joralemon, P., 1975, K-Ar relations of granodiorite emplacement and tungsten and gold mineralization near the Getchell mine, Humboldt County, Nevada: *Economic Geology*, v. 70, p. 405–406.
- Kistler, R. W., Ghent, E. D., and O'Neil, J. R., 1981, Petrogenesis of garnet two-mica granites in the Ruby Mountains, Nevada: *Journal of Geophysical Research*, v. 86, p. 10,591–10,606.
- Lapointe, D. D., Tingley, J. V., and Jones, R. B., 1991, *Mineral Resources of Elko County, Nevada: Nevada Bureau of Mines Bulletin 106*, 236 p.
- Lush, A. P., McGrew, A. J., Snoke, A. W., and Wright, J. E., 1988, Allochthonous Archean basement in the northern East Humboldt Range, Nevada: *Geology*, v. 16, p. 349–353.
- MacCready, T., Snoke, A. W., Wright, J. E., and Howard, K. A., 1997, Mid-crustal flow during Tertiary extension in the Ruby Mountains core complex, Nevada: *Geological Society of America Bulletin*, v. 109, p. 1576–1594.
- Meinert, L. D., 1993, Igneous petrogenesis and skarn deposits, *in* Kirkham, R. V., Sinclair, W. D., Thorpe, R. I., and Duke, J. M., eds., *Mineral deposits modeling: Geological Association of Canada Special Paper 40*, p. 569–583.
- Papke, K. G., 1984, Barite in Nevada: *Nevada Bureau of Mines Bulletin 98*, 125 p.
- Poole, F. G., 1975, Bedded barite in southwestern Nevada, *in* *Geological Survey research 1975: U.S. Geological Survey Professional Paper 975*, p. 4.
- Poole, F. G., Ketner, K. B., and Smith, J. F., Jr., 1982, Bedded barite in Mississippian rocks of northeastern Nevada, *in* *Geological Survey research 1981: U.S. Geological Survey Professional Paper 1275*, p. 74.

- Seedorff, E., 1991, Magmatism, extension, and ore deposits of Eocene to Holocene age in the Great Basin - mutual effects and preliminary proposed genetic relationships, *in* Raines, G. L., Lisle, R. E., Schafer, R. W., and Wilkinson, W. H., eds., *Geology and ore deposits of the Great Basin: Geological Society of Nevada*, p. 133-178.
- Segnite, E. R., 1946, Barium-feldspars from Broken Hill, New South Wales: *Mineralogical Magazine*, vol. 27, p. 166-175.
- Silberman, M. L., Berger, B. R., and Koski, R. A., 1974, K-Ar age relations of granodiorite, tungsten, and gold mineralization near the Getchell mine, Humboldt County, Nevada: *Economic Geology*, v. 69, p. 646-656.
- Singer, D. A., Waller, N., Mosier, D. L., and Bliss, J. D., 1997, Digital mineralogy data for 55 types of mineral deposits; Macintosh version: U.S. Geological Survey Open-File Report 97-160, 8 p.
- Smith, R. M., 1976, Mineral resources of Elko County Nevada: U.S. Geological Survey Open-File Report 76-56, 201 p.
- Snoke, A. W., 1980, Transition from infrastructure to suprastructure in the northern Ruby Mountains, Nevada, *in* Crittenden, M. D., Jr., Coney, P. J., and Davis, G. H., eds., *Cordilleran metamorphic core complexes: Geological Society of America Memoir 153*, p. 287-333.
- 1997, Tectonic evolution of the Ruby-East Humboldt metamorphic core complex: *Geological Society of Nevada, Abstract of the January 30, 1997 Meeting*, 1 p.
- Snoke, A. W., and Miller, D. M., 1988, Metamorphic and tectonic history of the Northeastern Great Basin, *in* Ernst, W. G., ed., *Metamorphism and crustal evolution of the Western United States Ruby Volume VII: Englewood Cliffs, New Jersey, Prentice Hall*, p. 606-648.
- Stout, B., 1997, Geologic overview of the Yankee Mine, White Pine County, Nevada, Placer Dome US, Alligator Ridge Project, 7 p.
- Stager, H. K., and Tingley, J. V., 1988, Tungsten deposits in Nevada: Nevada Bureau of Mines and Geology Bulletin 105, 256 p.
- Theodore, T. G., ed., 1997, Annual Report of Western Region Gold Project for fiscal year 1997: U.S. Geological Survey, Menlo Park, 74 p.
- Theodore, T. G., and Roberts, R. J., 1971, Geochemistry and geology of deep drill holes at Iron Canyon, Lander County, Nevada: U.S. Geological Survey Bulletin 1318 32 p.
- Wright, J. E., and Snoke, A. W., 1993, Tertiary magmatism and mylonitization in the Ruby-East Humboldt metamorphic core complex, northeastern Nevada: U-Pb geochronology and Sr, Nd, and Pb isotope geochemistry: *Geological Society of America Bulletin*, v. 105, p. 935-952.
- Yudovskaya, M. A., Grinenko, L. N., and Eremin, N. I., 1997, Genesis of the Maleevskoe massive sulfide polymetallic deposit (Rudnyi Altai, Khazakhstan): *Geologiya Rudnykh Mestorozhdeni*, v. 39, No 2, p. 163-182 (in Russian).
- Zimmerman, R. A., 1969, Stratabound barite deposits in Nevada: *Mineralium Deposita*, v. 4, p. 401-409.

AGE AND POSSIBLE SOURCE OF AIR-FALL TUFFS OF THE MIOCENE CARLIN FORMATION, NORTHERN NEVADA

By Robert J. Fleck, Ted G. Theodore, Andrei Sarna-Wojcicki, and Charles E. Meyer

ABSTRACT

$^{40}\text{Ar}/^{39}\text{Ar}$ laser-fusion ages have been obtained from alkali-feldspar-bearing air-fall tuffs of the Carlin Formation, a Miocene clastic and volcanoclastic sedimentary unit of north-central Nevada. Ages of these tuffs are grouped tightly, ranging from 14.4 to 15.1 Ma, but even this limited range may be exaggerated by contamination during deposition with feldspar from underlying rhyolitic volcanic rocks. These tuffs and much of the Carlin Formation post-date at least some of the gold mineralization in the Midas and Ivanhoe mining districts, where ages of 15.3 and 15.1 Ma, respectively, are reported for vein adularia. Younger quartz-adularia veins in the Santa Renia Fields quadrangle cut detrital units of the Carlin Formation that overlie the air-fall tuff horizons northwest of the dated locations, suggesting that circulation of hydrothermal fluids probably continued during deposition of the formation.

The age, location, and major-element chemistry of the glass shards in the tuffs of the Carlin Formation are consistent with derivation from silicic volcanic centers associated with the Yellowstone hotspot and/or the northern Nevada rift. These parameters are most consistent with a subalkaline source in the Owyhee Plateau of Idaho, such as the Juniper Mountain volcanic center, but tuffs also could have been derived from local sources in the Snowstorm or Sheep Creek Mountains or from more distant calderas of the McDermitt or Lake Owyhee volcanic fields 50-60 km to the west or northwest. Additional studies of minor- and trace-element compositions of the tuffs and better age and chemical characterization of middle Miocene volcanic centers of the region are necessary for more precise tephrochronology of 14- to 16-Ma volcanism in northern Nevada and adjacent areas of Oregon and Idaho.

GEOLOGIC SETTING

The Carlin Formation was defined by Regnier (1960) for a sequence of largely unconsolidated silts, sands, fanglomerate, and pyroclastic rocks that overlie Ordovician to Miocene(?) strata in the vicinity of Carlin, Nev., approximately 50 km south-southeast of the Santa Renia Fields

quadrangle (fig. 1). In that area the Carlin Formation is approximately 130-200 m thick (Regnier, 1960). Originally thought to be entirely Pliocene in age (Regnier, 1960), based on the presence of vertebrate fossils approximately 5 km northeast of Carlin, the strata were assigned a Miocene and Pliocene age by Evans and Cress (1972) and Evans (1972, 1974). As mapped in the western part of the Santa Renia Fields quadrangle by T.G. Theodore, J. Kelly Cluer, and Stanley C. Finney (unpub. data, 1997), four units are identified, but these were not found to be mappable throughout the area (fig. 2). In the quadrangle, the 30 m-to-50 m-thick basal tuff unit includes thin beds of partly welded tuff and lesser amounts of siltstone, mudstone, and gravel. This unit rests on Miocene rhyolite porphyry informally named the Craig Rhyolite of Bartlett and others (1991). W.E. Brooks (written communication, 1997) reports an $^{40}\text{Ar}/^{39}\text{Ar}$ incremental-heating plateau age of 15.03 ± 0.05 Ma for similar rhyolite porphyry approximately 5 km southwest of location 4 (fig. 2) in the adjacent Willow Creek Reservoir SE quadrangle. The basal tuff unit is overlain by a unit, as much as 400 m thick, including mostly unconsolidated silts, sands, and sedimentary breccia, as well as abundant volcanic ash and air-fall tuff. Because the volcanic debris is present variously as unconsolidated and consolidated deposits, the terms, ash, tuff, and tephra are all correct and are used here depending upon the context. Bedded air-fall tuff crops out prominently throughout the quadrangle as nearly white bands across slopes (fig. 3). Beds in the various units of the Carlin Formation are either horizontal or gently dipping; most exposed sequences are horizontal and ample evidence is present in the form of pisolites and abundant worm burrows to indicate subaqueous deposition, probably lacustrine. The organisms commonly used brown mud or silt to fill their burrows through the air-fall tuff. Roadcuts through the formation reveal that many well-layered sequences of air-fall tuff are broken by high-angle normal faults that have separations of as much as 1 to 1.5 m. Where the air-fall-tuff-rich unit laps unconformably onto lower Paleozoic rocks, an underlying, thin, yellow-brown, sandy silt or massive olive-brown mudstone is present. In places the underlying units form mud lumps in beds of gray-white, air-fall tuff. Thin beds of granitic debris, possibly derived from the Jurassic Goldstrike

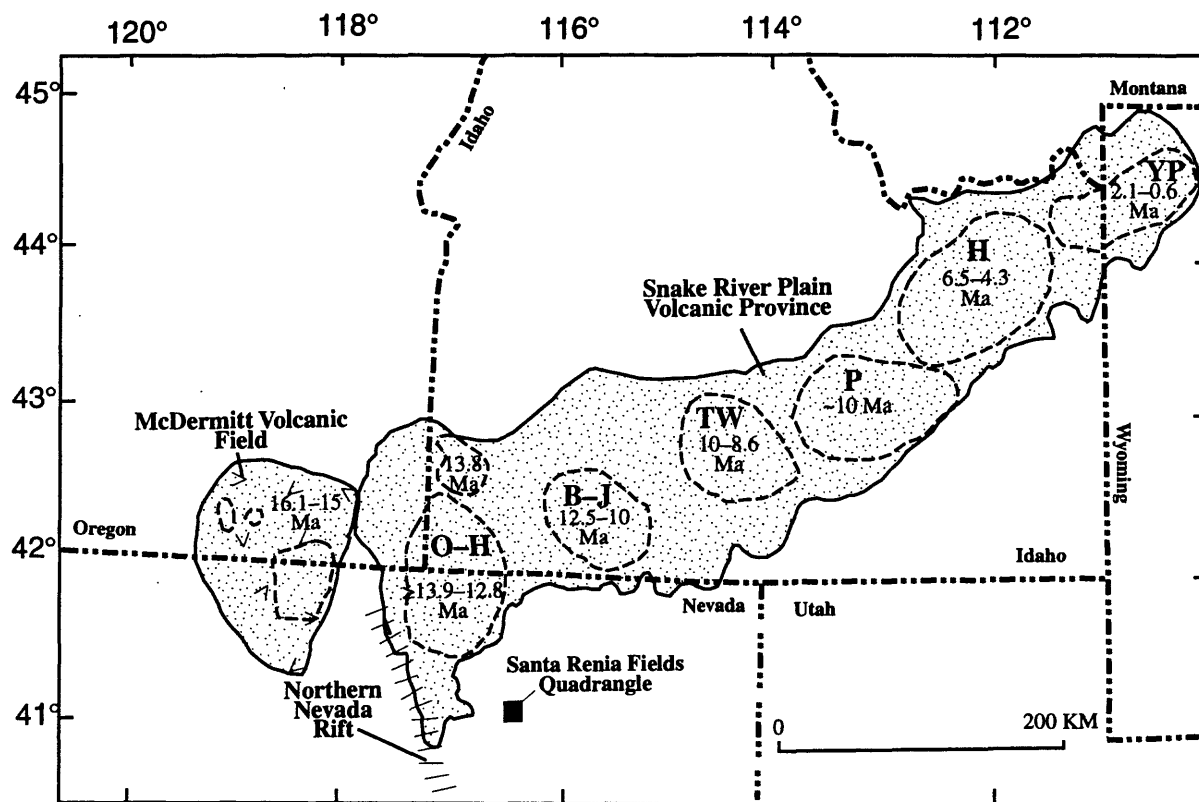


Figure 1. Index map showing location of the Santa Renia Fields quadrangle, Nev., the Snake River volcanic province (modified from Perkins and others, 1995), the McDermitt volcanic field (modified from Rytuba and McKee, 1984), and the northern Nevada rift (Zoback and Thompson, 1978; Zoback and others, 1994). Dashed lines within Snake River volcanic province approximate the major volcanic fields proposed by Perkins and others (1995): O-H, Owyhee-Humboldt volcanic field; B-J, Bruneau-Jarbidge volcanic field; TW, Twin Falls volcanic field; P, Picabo volcanic field; H, Heise volcanic field; YP, Yellowstone Plateau volcanic field. Age range of major explosive volcanic activity in Snake River volcanic province modified from Pierce and Morgan (1992) and Perkins and others (1995). Dashed lines within McDermitt volcanic field are locations of major calderas with age range modified from Rytuba and McKee (1984).

pluton approximately 10 km to the southeast, also are present locally in the air-fall-rich sequence. The tuff-bearing unit is overlain, in turn, by poorly exposed silts and sands, mostly unconsolidated, that are conspicuously free of air-fall tuff. All of these units are overlain by unconsolidated fanglomerate deposits — typically as much as 130 m thick and locally as much as 600 m thick — that appear to have been derived principally from Paleozoic rocks in the area of Beaver Peak, approximately 10 km to the east.

The spatial and temporal relationship of epithermal and hot-springs-generated ore deposits in the northern Great Basin to magmatic and hydrothermal activity has been documented by field and geochronologic studies of these deposits (McKee and others, 1974; Silberman and others, 1976; Noble and others, 1988; Wallace and others, 1990). Noble and others (1988) summarize evidence for mineralization throughout the 17- to 14-Ma period in this region. West of the Santa Renia Fields quadrangle, sedimentary strata correlated with the Carlin Formation overlie volcanic rocks thought to post-date mineralization in the Hollister mine in the Ivanhoe mining

district (McKee and others, 1974; Alan R. Wallace, written commun., 1997). Locally within the quadrangle, however, some sequences of the Carlin Formation are cut by low-temperature quartz-adularia veins. Roughly 4.8 km west of the Dee gold mine, near the west edge of the quadrangle, these veins are present as fracture and fragment coatings within fanglomerate of the formation (fig. 4). Rhyolite flows and hypabyssal domes that appear to postdate some of the Carlin sedimentary rocks show evidence of weak alteration (Alan R. Wallace, written commun., 1997), and support the continuation of mineralization during Carlin sedimentation.

SAMPLING AND ANALYTICAL TECHNIQUES

Sample Collection of Air-Fall Tuffs

Samples of bedded air-fall tuff were obtained from the Carlin Formation in the central part of the Santa Renia Fields

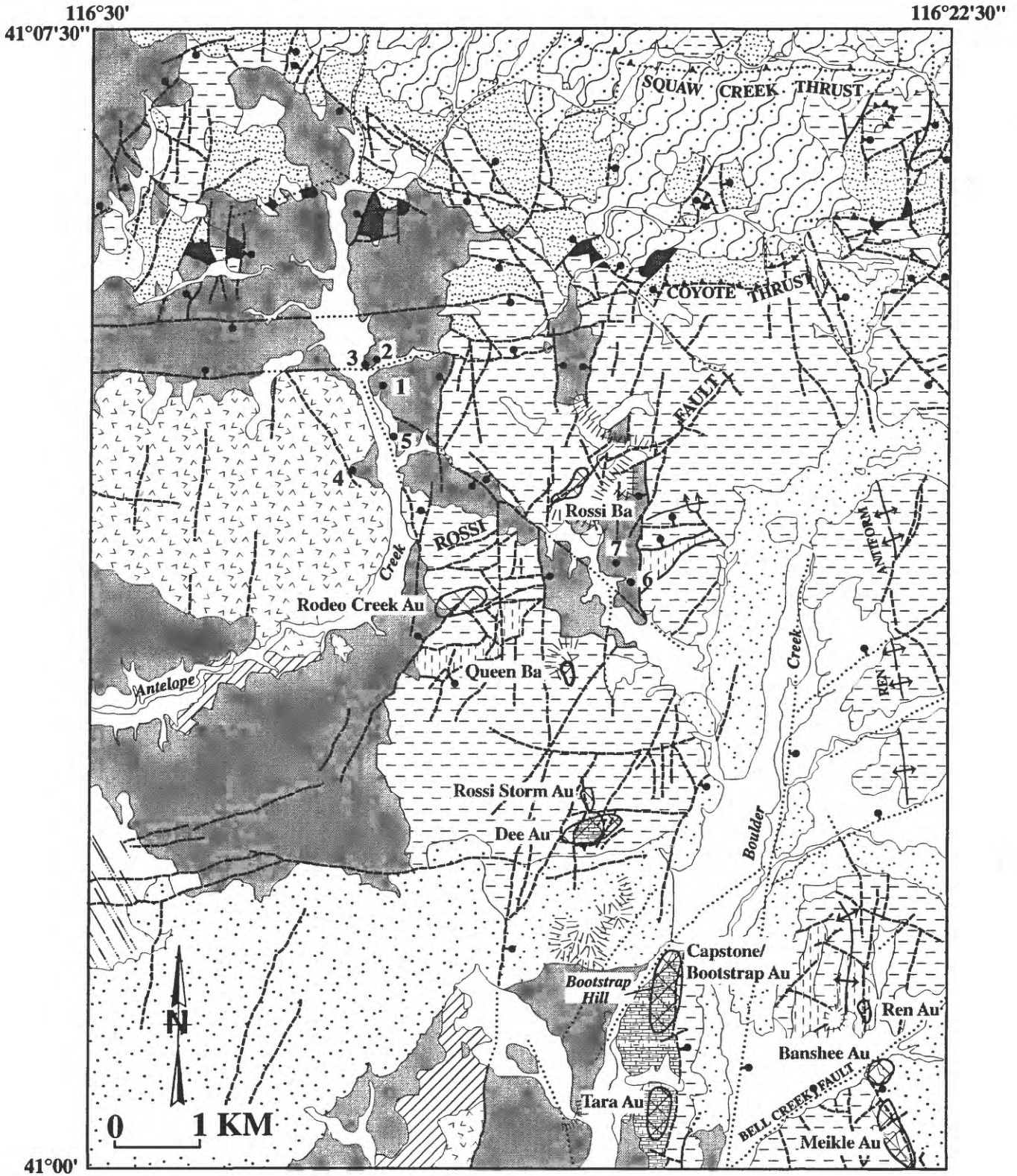
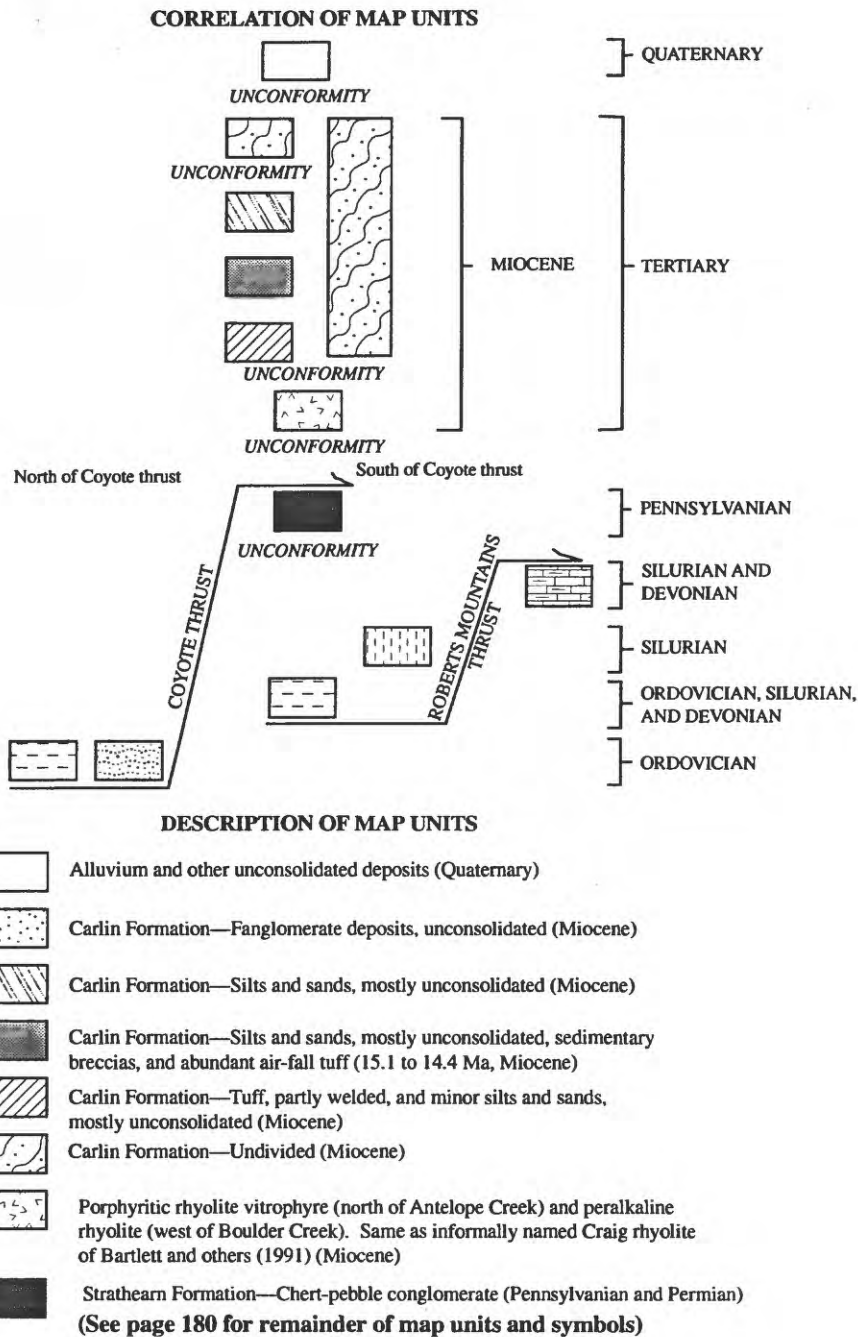


Figure 2. Geologic sketch map of the Santa Renia Fields quadrangle, Nev., showing locations of samples dated from the Miocene Carlin Formation. Modified from T.G. Theodore, J.K. Cluer, and S.C. Finney (unpub. data, 1997). Location numbers same as in tables 1-3.

Figure 2—Explanation



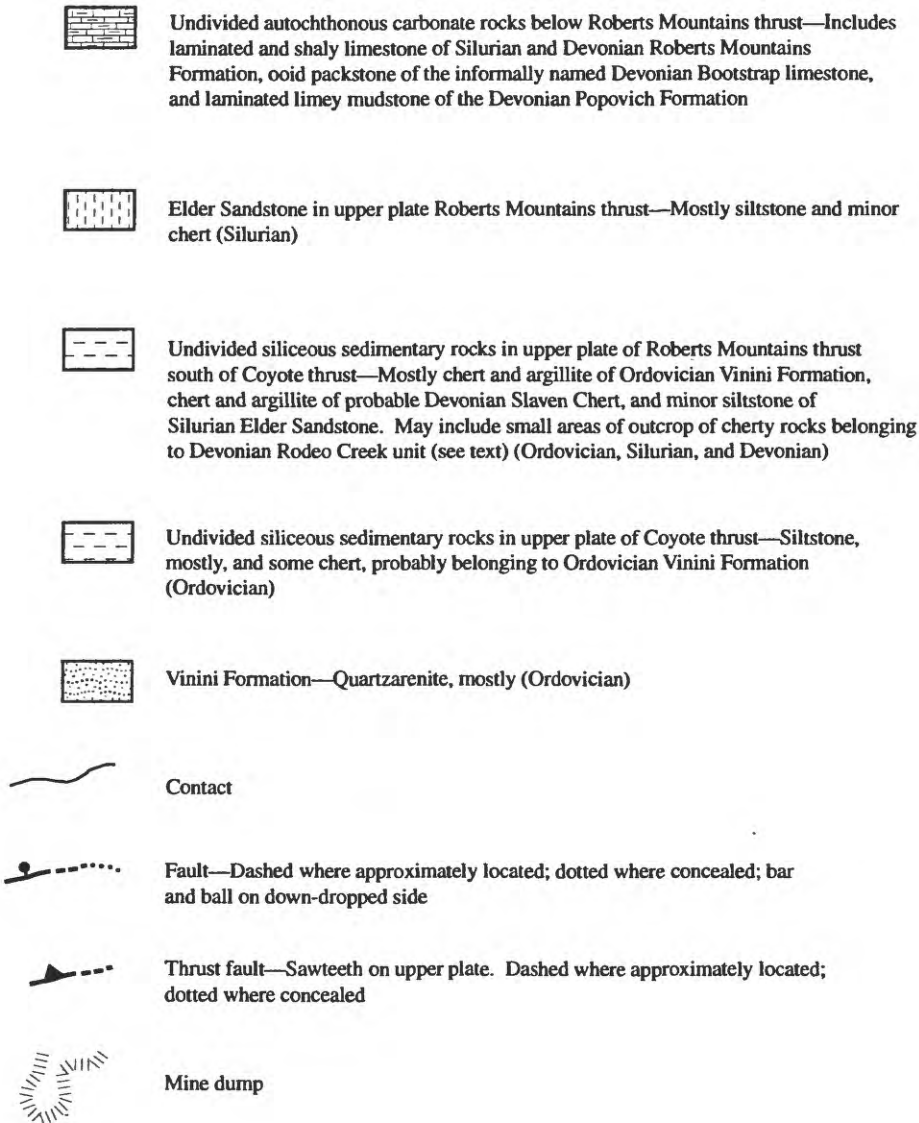
quadrangle after repeated visual examination to assure collection of the freshest and least contaminated material. Twelve of these samples from seven different localities (fig. 2) were selected for initial $^{40}\text{Ar}/^{39}\text{Ar}$ dating and several additional samples were used for tephrochronology. Many additional localities were examined but rejected because of inadequate exposures or alteration of the tuffs. Most samples represent material obtained from approximately 10-cm-thick, well-bedded stratigraphic intervals with minimal evidence of

reworking. Some outcrops of the tuff, however, are severely bioturbated such that only traces of bedding surfaces remain.

$^{40}\text{Ar}/^{39}\text{Ar}$ Laser-Fusion Dating

The $^{40}\text{Ar}/^{39}\text{Ar}$ dating technique was first utilized in its common form by Merrihue and Turner (1966) and has since become utilized more commonly than conventional K-Ar

Figure 2—Explanation cont'd.



dating because of its increased precision and utility (Dalrymple, 1989). Although the early advances with $^{40}\text{Ar}/^{39}\text{Ar}$ involved step-wise heating of samples and evolving the argon gas in multiple increments, total fusion of extremely small amounts of material through the use of a continuous laser (laser-fusion $^{40}\text{Ar}/^{39}\text{Ar}$) has become the technique of choice for mineral separates from thermally undisturbed samples (York and others, 1981; Dalrymple and Duffield, 1988). Laser-fusion $^{40}\text{Ar}/^{39}\text{Ar}$ dating has evolved to dating of single or small numbers of mineral grains and is especially useful to detect and overcome the effects of xenocrystic contamination (LoBello and others, 1987; Fleck and Carr, 1990) and incomplete extraction of radiogenic Ar from alkali

feldspar (McDowell, 1983).

The laser-fusion technique used in this study follows procedures described by Dalrymple and Duffield (1988), Dalrymple (1989), and Fleck and Carr (1990). These analyses were performed on the same mass spectrometer and using the same argon extraction-system described by Dalrymple (1989). Samples used in $^{40}\text{Ar}/^{39}\text{Ar}$ dating were irradiated for 16 hours in the U.S. Geological Survey TRIGA Reactor Facility in Denver, Colorado. An intralaboratory standard sanidine, 85G003, (Taylor Creek Rhyolite, 27.92 Ma) was used for calculation of the neutron flux in all irradiations. The age of this monitor mineral is as reported by Duffield and Dalrymple (1990), standardized to an age of 513.9 Ma for interlaboratory

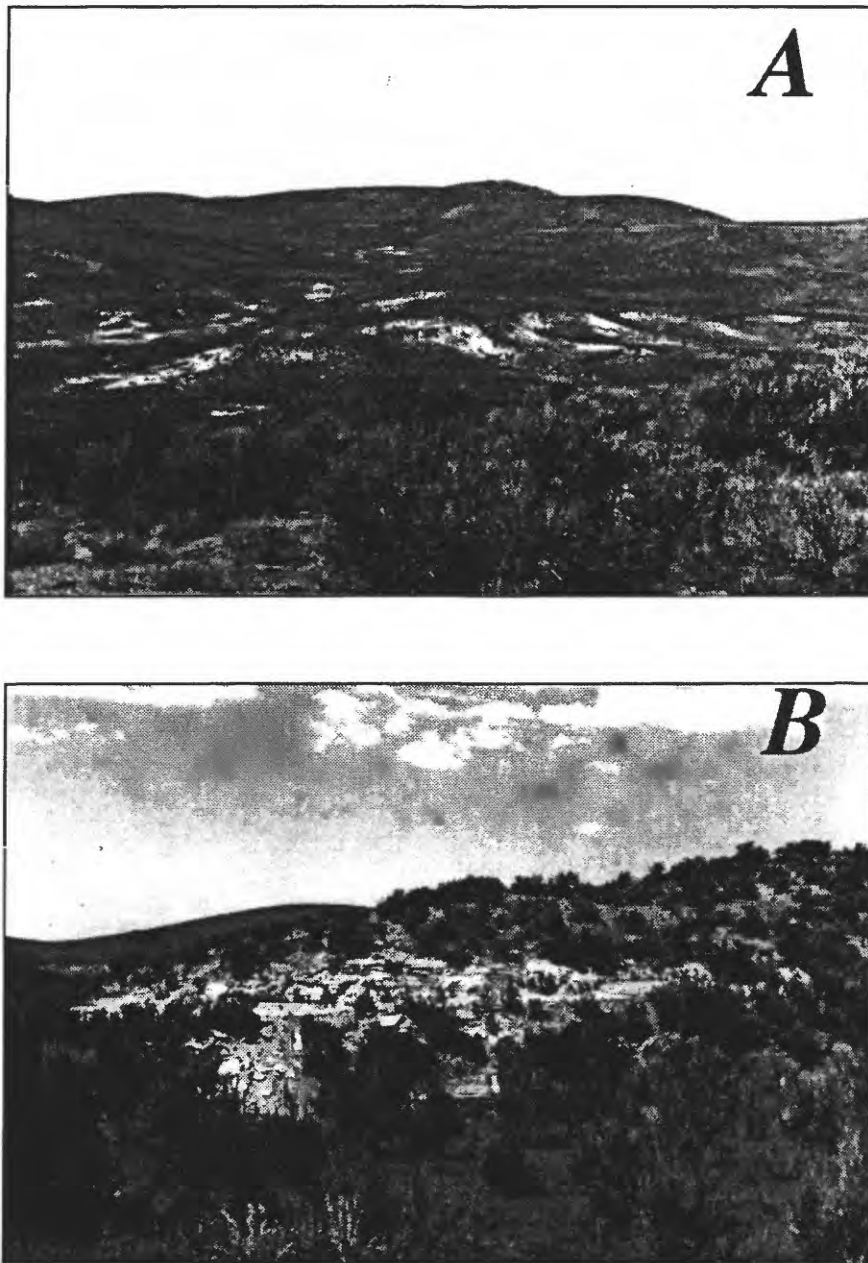


Figure 3. Photographs showing field relations of air-fall tuff-rich unit of Miocene Carlin Formation, Santa Renia Fields quadrangle, Nev. *A*, Distribution of air-fall tuff west of Santa Renia Springs near upper reaches of Antelope Creek, Santa Renia Fields quadrangle, Nevada; *B*, character of well exposed air fall tuff at map location 3 (fig. 2).

standard hornblende, MMhb-1 (Samson and Alexander, 1987) as measured in the Menlo Park laboratory and the intralaboratory standard biotite, SB-3 (Lanphere and others, 1990). Decay and abundance constants for all ages reported are those recommended by Steiger and Jager (1977).

Best-estimate ages for each sample are represented by the weighted means of replicate laser-fusion analyses, with

the inverse variance of propagated, within-run (*i.e.*, "internal") errors used as the weighting factors (Taylor, 1982). The goodness of fit parameter, MSWD or Mean-Square-of-Weighted-Deviates (McIntyre and others, 1966), is calculated for these means and is used to determine the presence of any error component in excess of estimated analytical error (an "external" error). Where the MSWD of a mean is greater than

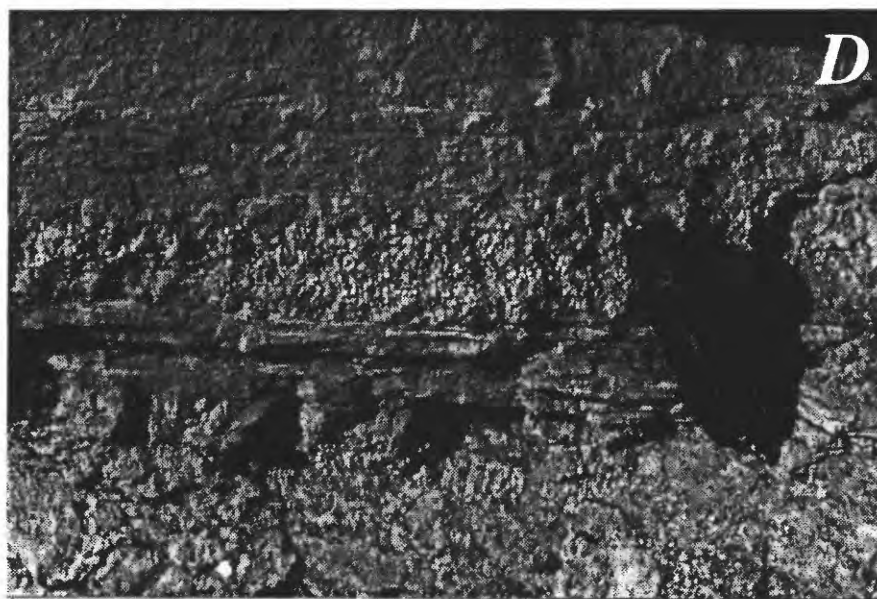
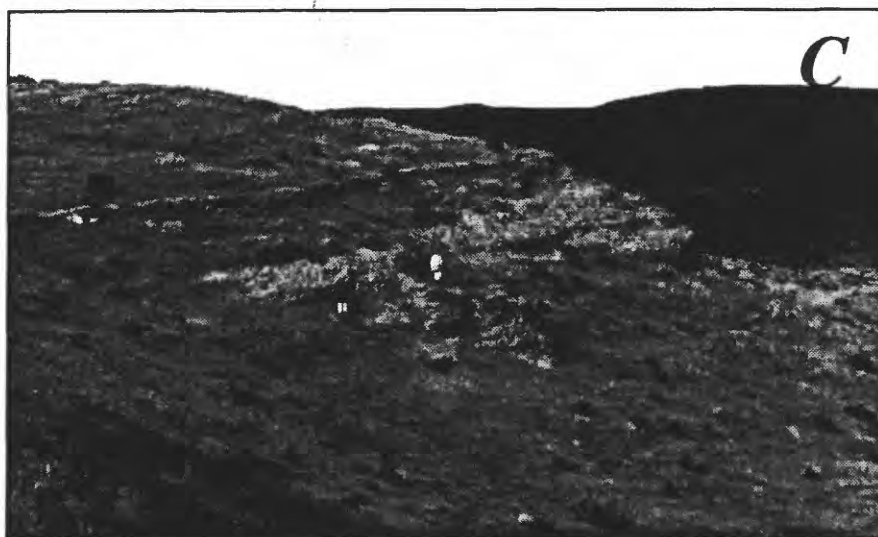


Figure 3. (cont'd) Photographs showing field relations of air-fall tuff-rich unit of Miocene Carlin Formation, Santa Renia Fields quadrangle, Nev. *C*, gently dipping beds of air-fall tuff near upper contact of unit in west-central part of quadrangle, Nev. *D*, close-up of thin layers of air-fall tuff and pisolites approximately 2-5 cm above sample 96TT134 (loc. 3, fig. 2)

1.0, analytical errors are multiplied by the square root of MSWD, as discussed by Ludwig (1988) and Fleck and others (1996), to incorporate this error.

Tephrochronologic Methods

Volcanic glass shards from samples of air-fall tuff (tephra

layers) of the Carlin Formation were separated and analyzed by electron microprobe using methods described by Sarna-Wojcicki and others (1984). Briefly, samples were wet-sieved with water in plastic sieves fitted with nylon screens, retaining the 200 to 100 mesh size fraction (about 80 to 150 microns, respectively) for separation of glass shards. This fraction was placed in water in an ultrasonic vibrator, treated with a 10 percent solution of HCl for a few minutes to remove authigenic

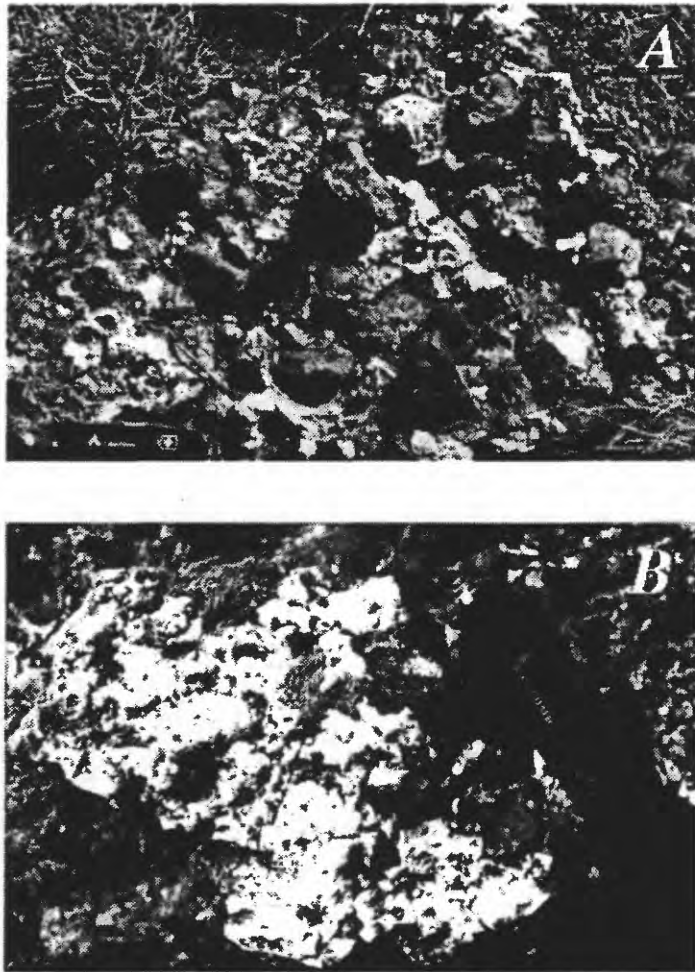


Figure 4. Photographs of quartz-adularia veins (white) in air-fall tuff-rich unit of Miocene Carlin Formation approximately 4.8 km west of Dee gold mine. *A*, Veins cementing largely unconsolidated fanglomerate deposits; *B*, veins along fracture surface in fanglomerate.

carbonate adhering to the glass particles, and leached with an 8 percent solution of HF acid for about 30 seconds to one minute to remove other coatings or altered rinds that may have been present on the glass shards. The glass shards were then separated from other components of each tephra sample using (1) a magnetic separator and (2) heavy liquids of variable density made from mixtures of methylene iodide and neothene or acetone. Most glass samples analyzed in the present study were already partly processed during separation of alkali feldspar (sized and most crystalline material was separated), and the volcanic glass was suitable for analysis.

Each glass separate was mounted in epoxy resin in shallow holes drilled into Plexiglas slides, and the slides were ground-down and polished with diamond paste to expose the shards and prepare a smooth, uniform surface for analysis. The polished sample was coated with carbon, and 15 to 25

individual glass shards were analyzed for Si, Al, Fe, Mg, Mn, Ca, Ti, Na, and K using a JEOL 8900 electron-microprobe. Details of the analytical techniques are reported by Sarna-Wojcicki and others (1984).

ANALYTICAL RESULTS

Results of individual laser-fusion $^{40}\text{Ar}/^{39}\text{Ar}$ experiments on samples from air-fall tuff or ash layers collected within the Santa Renia Fields quadrangle are shown in table 1 and summarized in table 2. Apparent ages range from 15.1 Ma to 14.4 Ma, but internal precision varies as shown by the MSWD. Values of MSWD greater than about 2.5 are commonly considered to reflect scatter beyond reasonable expectations of analytical error and are interpreted as indicating geologic

Table 1. $^{40}\text{Ar}/^{39}\text{Ar}$ Laser-Fusion Analyses of Alkali Feldspars from the Miocene Carlin Formation, Nevada

Sample #/Irrad #	Run #	J	$^{40}\text{Ar}^*$ (mol)	K/Ca	$^{40}\text{Ar}^*$ (%)	Age (Ma)
96TT129	252A	0.0037795	1.153E-15	9.88	93.4	14.87 ± 0.19
CXLIII-1	252B	"	9.202E-15	13.27	94.7	14.32 ± 0.12
Map location 1	252C	"	7.094E-15	6.37	92.7	14.28 ± 0.13
	252E	"	6.270E-15	2.56	90.5	14.43 ± 0.15
	252F	"	1.335E-14	7.29	95.3	14.49 ± 0.10
	Means		7.414E-15	7.88	93.35	
					Wtd. Mean MSWD	14.43 ± 0.08 1.92
96TT130	253A	0.0037761	5.317E-15	3.78	92.7	14.22 ± 0.16
CXLIII-2	253B	"	5.855E-15	6.78	93.8	14.71 ± 0.16
Map location 1	253C	"	7.036E-15	8.30	98.0	15.13 ± 0.14
	253D	"	4.207E-15	10.73	63.7	13.96 ± 0.20
	253E	"	4.511E-15	7.19	91.1	14.92 ± 0.19
	253F	"	5.217E-15	7.08	88.9	14.07 ± 0.16
	Means		5.365E-15	8.02	87.10	
					Wtd. Mean MSWD	14.55 ± 0.20 8.62
96TT131	254A	0.0037728	1.220E-14	10.35	91.5	14.47 ± 0.10
CXLIII-3	254B	"	1.569E-14	10.66	96.3	14.36 ± 0.09
Map location 1	254C	"	1.428E-14	13.41	96.3	14.39 ± 0.09
	254D	"	1.145E-14	7.93	60.7	14.43 ± 0.11
	254E	"	1.044E-14	8.33	95.6	14.42 ± 0.10
	Means		1.281E-14	10.14	88.08	
					Wtd. Mean MSWD	14.41 ± 0.04 0.19
96TT132	255A	0.0037695	8.288E-15	6.63	96.9	14.51 ± 0.11
CXLIII-4	255B	"	8.815E-15	6.08	95.1	14.43 ± 0.11
Map location 2	255C	"	4.188E-15	4.92	89.4	14.30 ± 0.17
	255D	"	1.088E-14	7.86	96.6	14.54 ± 0.10
	255E	"	5.036E-15	5.00	90.0	14.53 ± 0.15
	255F	"	9.042E-15	6.39	97.2	14.45 ± 0.11
	Means		7.592E-15	6.05	93.67	
					Wtd. Mean MSWD	14.48 ± 0.05 0.37

Table 1. $^{40}\text{Ar}/^{39}\text{Ar}$ Laser-Fusion Analyses of Alkali Feldspars from the Miocene Carlin Formation, Nevada—
Continued

Sample #/Irrad #	Run #	J	$^{40}\text{Ar}^*$ (mol)	K/Ca	$^{40}\text{Ar}^*$ (%)	Age (Ma)
96TT133	97Z0256A	0.0037624	8.010E-15	5.59	97.8	14.68 ± 0.12
CXLIII-5	97Z0256B	"	1.025E-14	6.15	98.0	14.68 ± 0.10
Map location 3	97Z0256C	"	1.038E-14	6.37	99.6	14.80 ± 0.11
	97Z0256E	"	7.492E-15	4.75	98.4	14.71 ± 0.12
	97Z0256F	"	1.200E-14	8.25	98.6	14.70 ± 0.10
	Means		9.627E-15	6.22	98.49	
					Wtd. Mean MSWD	14.72 ± 0.05 0.24
96TT134	97Z0257A	0.0037587	1.283E-14	9.23	99.4	14.86 ± 0.10
CXLIII-6	97Z0257B	"	1.095E-14	7.73	97.2	14.88 ± 0.10
Map location 3	97Z0257C	"	1.312E-14	9.65	98.6	14.62 ± 0.10
	97Z0257D	"	6.944E-15	8.74	95.1	14.47 ± 0.12
	97Z0257E	"	7.628E-15	12.88	96.2	14.29 ± 0.12
	97Z0257F	"	6.766E-15	6.91	95.1	14.30 ± 0.12
	Means		9.080E-15	9.18	96.46	
					Wtd. Mean MSWD	14.61 ± 0.10 5.58
96TT136	97Z0258A	0.0037550	7.386E-15	1.43	96.8	14.87 ± 0.12
CXLIII-7	97Z0258B	"	5.837E-15	1.16	96.5	14.78 ± 0.14
Map location 4	97Z0258C	"	5.563E-15	1.63	95.2	14.58 ± 0.14
	97Z0258D	"	6.084E-15	1.92	99.8	15.31 ± 0.14
	97Z0258E	"	7.100E-15	1.67	99.1	15.19 ± 0.13
	97Z0258F	"	7.793E-15	2.52	97.6	14.83 ± 0.12
	Means		6.476E-15	1.78	97.65	
					Wtd. Mean MSWD	14.93 ± 0.10 3.88
96TT137	97Z0263A	0.0037513	8.321E-15	1.62	95.0	14.76 ± 0.12
CXLIII-8	97Z0263B	"	1.086E-14	2.28	98.3	15.00 ± 0.10
Map location 4	97Z0263C	"	4.796E-15	2.46	86.0	14.65 ± 0.16
	97Z0263D	"	1.092E-14	1.75	98.6	15.20 ± 0.11
	97Z0263E	"	7.260E-15	2.02	97.8	15.07 ± 0.13
	97Z0263F	"	8.084E-15	1.20	86.7	14.97 ± 0.12
	Means		8.384E-15	1.94	93.46	
					Wtd. Mean MSWD	14.97 ± 0.08 2.59

Table 1. $^{40}\text{Ar}/^{39}\text{Ar}$ Laser-Fusion Analyses of Alkali Feldspars from the Miocene Carlin Formation, Nevada—
Continued

Sample #/Irrad #	Run #	J	$^{40}\text{Ar}^*$ (mol)	K/Ca	$^{40}\text{Ar}^*$ (%)	Age (Ma)
96TT138	97Z0267A	0.0037310	4.428E-14	4.40	97.7	14.73 ± 0.09
CXLIII-12	97Z0267B	"	2.873E-14	9.73	97.8	14.77 ± 0.09
Map location 4	97Z0267D	"	4.232E-14	1.58	97.9	14.95 ± 0.09
	97Z0267E	"	6.322E-14	7.81	98.4	14.87 ± 0.09
	97Z0267F	"	3.905E-14	4.20	96.8	14.91 ± 0.09
	Means		4.333E-14	5.83	97.75	
					Wtd. Mean	14.84 ± 0.04
					MSWD	1.12
96TT139	97Z0264A	0.0037434	1.856E-14	3.10	95.7	15.20 ± 0.09
CXLIII-9	97Z0264B	"	2.052E-14	10.45	98.1	15.07 ± 0.09
Map location 5	97Z0264C	"	2.942E-14	3.86	97.8	15.08 ± 0.09
	97Z0264D	"	2.687E-14	4.80	98.1	14.81 ± 0.09
	97Z0264E	"	1.473E-14	5.08	98.5	14.92 ± 0.10
	97Z0264F	"	2.262E-14	5.33	97.3	15.48 ± 0.09
	Means		2.283E-14	5.90	97.96	
					Wtd. Mean	15.09 ± 0.09
					MSWD	6.26
96TT151	97Z0265A	0.0037393	1.441E-14	1.63	90.3	15.15 ± 0.10
CXLIII-10	97Z0265B	"	7.263E-15	0.89	86.2	15.47 ± 0.13
Map location 6	97Z0265C	"	1.117E-14	1.21	90.5	14.95 ± 0.11
	97Z0265E	"	8.729E-15	1.41	91.1	14.99 ± 0.12
	97Z0265F	"	1.355E-14	1.23	97.0	15.07 ± 0.10
	Means		1.018E-14	1.19	91.19	
					Wtd. Mean	15.10 ± 0.08
					MSWD	2.80
96TT153	97Z0266A	0.0037352	1.288E-14	1.22	98.4	15.37 ± 0.10
CXLIII-11	97Z0266B	"	1.628E-14	0.90	98.6	15.33 ± 0.10
Map location 7	97Z0266C	"	1.802E-14	1.46	95.1	15.17 ± 0.10
	97Z0266D	"	2.007E-14	1.44	96.7	15.19 ± 0.09
	97Z0266E	"	1.214E-14	3.29	95.2	14.64 ± 0.10
	97Z0266F	"	3.294E-14	11.34	97.4	14.87 ± 0.09
	Means		1.989E-14	3.68	96.61	
					Wtd. Mean	15.09 ± 0.11
					MSWD	8.32

Table 2. Compilation of $^{40}\text{Ar}/^{39}\text{Ar}$ laser-fusion analyses of air-fall tuff units within the Carlin Formation, northern Nevada.

Location # (figure 1)	N Latitude	W Longitude	Sample #	Number of Analyses	J	Averages for Analyses			Wtd Mean	
						$^{40}\text{Ar}^*$ (mol)	K/Ca	$^{40}\text{Ar}^*$ (%)	Age (Ma)	MSWD
1	41° 05.182'	116° 27.545'	96TT129	5	0.0037795	7.414E-15	7.88	93.35	14.43 ± 0.08	1.925
	"	"	96TT130	6	0.0037761	5.365E-15	8.02	87.10	14.55 ± 0.20	8.625
	"	"	96TT131	5	0.0037728	1.281E-14	10.1	88.08	14.41 ± 0.04	0.185
4										
2	41° 05.24'	116° 27.462'	96TT132	6	0.0037695	7.592E-15	6.05	93.67	14.48 ± 0.05	0.374
3	41° 05.28'	116° 27.652'	96TT133	5	0.0037624	9.627E-15	6.22	98.49	14.72 ± 0.05	0.241
	"	"	96TT134	6	0.0037587	9.080E-15	9.18	96.46	14.61 ± 0.10	5.582
4	41° 04.589'	116° 27.724'	96TT136	6	0.0037550	6.476E-15	1.78	97.65	14.93 ± 0.10	3.876
	"	"	96TT137	6	0.0037513	8.384E-15	1.94	93.46	14.97 ± 0.08	2.588
	"	"	96TT138	5	0.0037310	4.333E-14	5.83	97.75	14.84 ± 0.04	1.123
5	41° 04.957'	116° 27.426'	96TT139	5	0.0037434	2.283E-14	5.90	97.96	15.01 ± 0.07	2.656
6	41° 03.84'	116° 25.285'	96TT151	5	0.0037393	1.018E-14	1.18	91.19	15.10 ± 0.08	2.804
7	41° 03.923'	116° 25.385'	96TT153	6	0.0037352	1.989E-14	3.68	96.61	15.09 ± 0.11	8.321

error. The most probable form of geologic error in age determinations of air-fall tuff is contamination of the ash by accidental material incorporated during eruption or by detrital grains mixed into the ash during post-depositional reworking. The ages of these samples fall into 3 general groupings. Those from locations 1 and 2 (fig. 2) indicate an age of about 14.45 Ma. Samples from locations 4-7 with an age of about 15.0 Ma are statistically different from the first group, but in moderate agreement with each other. Samples from location 3 yield ages between the other two groupings, but sample 96TT134 has a high MSWD and 3 of the 6 analyses agree well with the 14.45 Ma group (tables 1 and 2). Consideration of the depositional environment of these types of deposits may explain some of the age variation.

As discussed briefly above, air-fall tuffs and ash may incorporate xenocrysts or xenoliths from older units as accidental materials from the volcanic edifice during eruption or as detrital material incorporated during reworking of the ash by wind or water. Contamination is common in pyroclastic materials (*see also*: Dalrymple and others, 1965; LoBello and others, 1987; Fleck and Carr, 1990) and represents the most probable cause of geologic error in their $^{40}\text{Ar}/^{39}\text{Ar}$ ages. Where the contaminating grains are from much older rocks, the contamination is easily recognized in laser-fusion $^{40}\text{Ar}/^{39}\text{Ar}$ ages because large age variations will be found between replicate measurements. Where contaminants are only slightly older than the ash, however,

contamination may be difficult to identify unless single mineral grains can be analyzed. Because the Carlin Formation in the area of study is immediately underlain by the Craig Rhyolite containing alkali feldspar that has yielded an age of 15.03 ± 0.05 Ma (W.E. Brooks, written commun., 1997), the potential for contamination of the water-laid ashes is considerable and the small age difference further complicates interpretation. This may be especially true in distal ashes, where small grain-size requires fusion of many grains to produce reliably measurable signals. Grain sizes of the alkali feldspar utilized in this study required between 8 and 12 grains for high-precision analyses.

As mentioned earlier, statistical parameters such as MSWD, must be utilized to measure the dispersion of age data compared to estimates of analytical error, as a means to identify contamination. Sample 96TT153 (loc. 7, table 1; fig. 2) is an example of potential contamination because the age range of 14.6 to 15.4 Ma is well outside analytical error, as reflected by the MSWD of 8.32 (table 1). Age results for samples 96TT130 and 134 (table 1) also exhibit scatter outside analytical error, but the external agreement between the mean ages lends some confidence to those results. Although these ages may be accurate, their lower than expected precision leaves them suspect.

To provide additional information on the possible presence of contamination, independent chemical parameters were evaluated using tephrochronologic techniques. Average major element compositions were obtained for 15 to 20

individual glass shards from each tuff sample using the electron microprobe (table 3). Results indicate a high degree of similarity between all samples except 96TT154, for which no age results are available. Samples from locations 1-3 are nearly identical, whereas the remaining ashes have somewhat greater dispersion. Comparison of Al_2O_3 and SiO_2 contents in the glass shards (approximately 12 and 76 weight percent, respectively) suggests that the eruptive center from which these tuffs were derived has a distinctly peralkaline character (table 3). Returning to table 2, K/Ca ratios for the alkali feldspars are calculated from amounts of Ca-derived ^{37}Ar and K-derived ^{39}Ar produced during irradiation and measured during $^{40}\text{Ar}/^{39}\text{Ar}$ analyses. The most important information from the K/Ca values is that the alkali feldspars are not high-K sanidines, which yield K/Ca ratios of 30 to 60, but are either Na-rich sanidine or anorthoclase with K/Ca of 1 to 10, typical of alkaline magmas. The K/Ca values also indicate strong similarity between samples from locations 1-3, which may be chemically distinct from locations 4-7. Because the ages of location 3 samples and their MSWD are elevated at the 95-percent level of confidence relative to chemically indistinguishable tuffs from locations 1 and 2, location 3 samples are probably contaminated by xenocrystic alkali feldspar, possibly from the Craig Rhyolite. The minimal scatter and low MSWD of measurements on 96TT133 question this interpretation, but results for 96TT134 and the chemical similarity to younger samples support it (table 2).

Differences in glass chemistry between locations 1-3 and 4-7 support an interpretation of a true difference in age. Location 4 is immediately above the base of the Carlin Formation where it rests directly on the Craig Rhyolite (fig. 2). Locations 2 and 3, however, are located north of the east-west-trending fault bounding a graben containing as much as 400 m of Carlin sedimentary fill. This large variation in thickness of the Carlin Formation is documented by drilling northwest of location 3, demonstrating that the older apparent ages at location 4 are consistent with the observed stratigraphy. If the age of the Craig Rhyolite is 15.03 ± 0.05 Ma as reported (W.E. Brooks, written commun., 1997), the ages measured at locations 4-7 may be slightly contaminated, but this cannot be proven with available data. With the available age control, the best age estimates for the ash layers are about 14.4 and 15 Ma. Additional studies are underway to refine this chronology.

SOURCE OF AIR-FALL TUFFS OF THE CARLIN FORMATION

Age estimates of about 14.4 Ma to 15.1 Ma for air-fall tuffs of the Carlin Formation reported here permit a wide variety of potential source areas of silicic tuffs in northern Nevada, southeasternmost Oregon, and southwesternmost Idaho (Luedke and Smith, 1981; 1982; 1983; 1984). Volcanic rocks of the approximate age are abundant in the immediate

area of study, such as the Snowstorm or Sheep Creek Mountains (fig. 2; Luedke and Smith, 1984), but major calderas have yet to be identified there. Volcanic centers that represent known sources of pyroclastic materials and for that reason are targets for additional, more detailed study include the McDermitt, Lake Owyhee, and the Owyhee Plateau volcanic fields. Ages of 16.1 to 15.0 Ma are reported by Rytuba and McKee (1984) for the major ash-flow tuffs of the McDermitt center. The tuff of Whitehorse Creek, from the Whitehorse caldera, the youngest of the McDermitt calderas, yielded an age of 15.0 ± 0.3 Ma (Rytuba and McKee, 1984), similar to ages of the older group of Carlin tuffs. Rytuba and VanderMeulen (1991), however, report similar ages of 15.5 to 15.0 Ma for ash-flow tuffs of the Lake Owyhee volcanic field and ages from about 16 to 13.8 Ma are reported by Ekren and others (1984) for the older volcanic rocks of the Juniper Mountain volcanic center on the Owyhee Plateau, but younger ages are dominant to the east (fig. 1; Perkins and others, 1995).

Despite the limited chemical variation in volcanic glass of the tuffs of the Carlin Formation, correlation with other ashes and identification of their source requires study of the chemistry and age of more proximal ashes whose sources can be ascertained. Minor- and trace-element studies of the Carlin Formation air-fall tuffs are planned to extend coverage beyond the major element suite currently available. Current results permit some observations and interpretations, however. The low Mg and Ca contents of the glass and a paucity of mafic minerals in the tuffs are compatible with either peralkaline or subalkaline magmas. The low-K content of the alkali feldspars from the Carlin Formation tuffs is consistent with more alkalic sources rather than metaluminous sources. Total alkalis (Na_2O plus K_2O) and aluminum of glass shards of Carlin Formation tuffs indicate a generally subalkaline magmatic character (table 3), although the alkali contents in bedded ash layers may be subject to substantial diagenetic modification. The molecular $(\text{Na}_2\text{O} + \text{K}_2\text{O})/\text{Al}_2\text{O}_3$ of the tuffs is quite constant at about 0.90, however, suggesting that alteration has not produced significant effects. Figure 5 shows the distribution of alkalis versus alumina for the glass of the Carlin tuffs compared to rhyolites of the McDermitt (Rytuba and McKee, 1984) and Juniper Mountain (Owyhee Plateau, Ekren and others, 1984) volcanic fields. Compositions of glass from both groups of Carlin Formation tuffs (locations 1-3 and 4-7) plot entirely within the subalkaline field, although not far inside the alkaline/subalkaline boundary (fig. 5). The peralkaline character of the McDermitt and Lake Owyhee volcanic fields, however, makes those areas less attractive as possible sources of the Carlin Formation tuffs, although a substantial number of the analyses from the McDermitt field are subalkaline (fig. 5). The Lake Owyhee field contains both peralkaline and metaluminous tuffs, according to Rytuba and VanderMeulen (1991). Analyses of rhyolites of the Juniper Mountain volcanic center (Ekren and others, 1984) group tightly with those of the Carlin tuffs (fig. 5), providing the best fit with available

Table 3. Electron-microprobe analyses of volcanic glass shards from tuffs of the Miocene Carlin Formation, northern Nevada.

Sample#	SiO ₂	Al ₂ O ₃	Fe ₂ O ₃	MgO	MnO	CaO	TiO ₂	Na ₂ O	K ₂ O	Total(O)	Total(R)
96TT129	76.14	12.1	1.88	0.03	0.03	0.56	0.17	2.32	6.78	93.46	100.01
±s; n=20	0.51	0.13	0.09	0.01	0.03	0.03	0.04	0.14	0.17	0.52	
96TT130	76.17	12.06	1.91	0.04	0.03	0.58	0.14	2.29	6.78	93.69	100.00
±s; n=19	0.53	0.17	0.06	0.01	0.02	0.02	0.05	0.17	0.26	0.52	
96TT131	76.26	12.1	1.79	0.03	0.03	0.54	0.14	2.33	6.76	93.64	99.98
±s; n=18	0.4	0.17	0.08	0.01	0.03	0.03	0.04	0.12	0.17	0.49	
96TT132	76.06	12.08	1.88	0.04	0.03	0.57	0.17	2.27	6.91	93.53	100.01
±s; n=20	0.49	0.14	0.13	0.02	0.03	0.1	0.05	0.1	0.21	0.59	
96TT133	76	12.09	1.93	0.04	0.04	0.57	0.17	2.25	6.91	93.27	100.00
±s; n=19	0.34	0.12	0.09	0.01	0.03	0.03	0.04	0.12	0.19	0.46	
96TT134	76.36	12.08	1.81	0.03	0.03	0.55	0.16	2.26	6.72	93.42	100.00
±s; n=15	0.45	0.13	0.1	0.01	0.02	0.03	0.06	0.18	0.19	0.57	
96TT136	75.25	12.51	2.15	0.09	0.04	0.67	0.27	2.39	6.63	93.1	100.00
±s; n=19	0.54	0.22	0.12	0.02	0.02	0.05	0.05	0.21	0.25	0.55	
96TT137	75.5	12.40	2.03	0.08	0.04	0.62	0.24	2.30	6.78	93.04	99.99
±s; n=19	0.59	0.27	0.13	0.02	0.03	0.05	0.06	0.16	0.15	0.50	
96TT138	76.13	12.40	1.84	0.06	0.03	0.55	0.21	2.42	6.37	94.09	100.01
±s; n=20	0.61	0.20	0.14	0.02	0.02	0.05	0.04	0.21	0.16	0.47	
96TT139	76.30	12.20	1.78	0.06	0.03	0.53	0.22	2.28	6.61	94.19	100.01
±s; n=20	0.35	0.18	0.15	0.01	0.02	0.03	0.04	0.15	0.19	0.43	
96TT151	75.96	12.27	1.94	0.07	0.04	0.58	0.21	2.57	6.35	93.50	99.99
±s; n=18	0.83	0.24	0.17	0.02	0.04	0.07	0.04	0.21	0.36	0.63	
96TT153	75.65	12.62	2.04	0.08	0.03	0.61	0.26	2.60	6.11	93.53	100.00
±s; n=20	0.62	0.27	0.22	0.02	0.01	0.09	0.05	0.15	0.31	0.39	
96TT154	74.73	12.41	2.6	0.08	0.05	0.7	0.23	2.39	6.79	93.4	99.98
±s; n=15	0.55	0.15	0.18	0.01	0.03	0.05	0.05	0.17	0.24	0.4	

Shards were analyzed using the JEOL8900* instrument.

Standard deviation calculated from individual analyses of shards. Oxide values given are recalculated to a 100% fluid-free basis.

Total(O) - original total on analysis; Total (R) - total recalculated to a 100% fluid-free basis.

analyses. Silicic volcanic rocks of both the McDermitt and Juniper Mountain volcanic centers have low abundances of mafic minerals, but high Fe₂O₃ contents (McKee, 1976; Rytuba and McKee, 1984; Ekren and others, 1984). The mean Fe₂O₃ content of the glass shards of the Carlin tuffs of 1.99 percent is very high for rhyolite glasses at 76 percent SiO₂, such as those of the Owyhee Plateau region (Ekren and others, 1984), but slightly lower than the less silicic volcanic rocks of the McDermitt and Lake Owyhee fields. Based on the subalkaline character and range of ages extending to less than 14 Ma (Ekren and others, 1984), the Juniper Mountain tuffs of the Owyhee Plateau are a more favorable candidate as the source for the Carlin tuffs than the peralkaline centers of

McDermitt and Lake Owyhee. The oldest ages reported in tables 1 and 2 for Carlin tuffs are compatible with a 15-Ma source such as the McDermitt or Lake Owyhee fields, but rhyolitic volcanism younger than 15 Ma is more common in the Juniper Mountain tuffs (Ekren and others, 1984). Attributing the tuffs studied here to any of these identified calderas, however, is tentative without better chemical and age studies of the tuffs. In addition to more detailed study of glass chemistry of the larger volcanic fields of McDermitt, Lake Owyhee, and Juniper Mountain, the chemistry of sources more local to the Carlin area, such as in the Snowstorm and Sheep Creek Mountains, also needs evaluation.

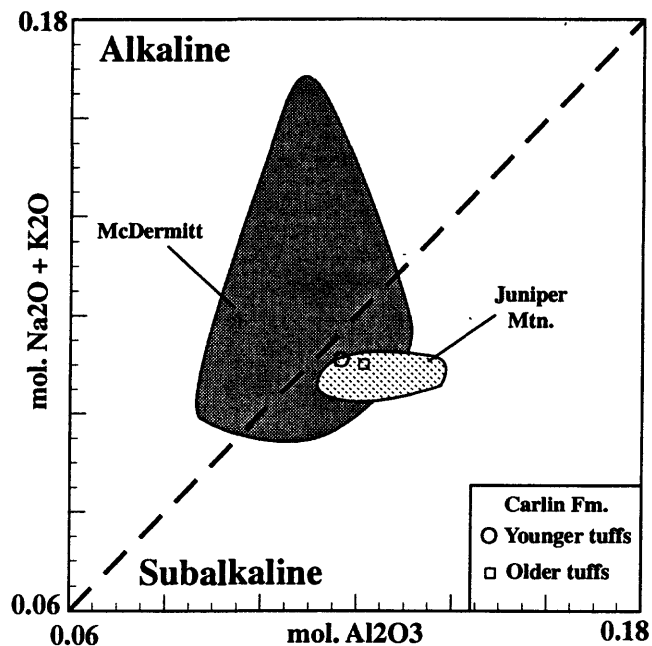


Figure 5. Al_2O_3 versus total alkalis diagram for glass shards from air-fall tuffs of the Miocene Carlin Formation, demonstrating the subalkaline character of these glasses. The younger group of tuffs of the Carlin Formation (locations 1-2 with an age of about 14.4 Ma) have slightly lower Al_2O_3 than the older group (locations 4-7 with ages between 14.8 and 15.1 Ma), but identical alkalis. Note the extremely-low compositional variation of the glass. Fields are shown for analyses reported by Rytuba and McKee (1984) for the McDermitt volcanic field and by Ekren and others (1984) for the Juniper Mountain volcanic field of the Owyhee Plateau. Both volcanic centers contain rocks of similar composition, but the Juniper Mountain field has a very restricted range of compositions, all within the field of subalkaline magmas.

DISCUSSION

North and east of Battle Mountain, Nev., the Carlin Formation post-dates 15- to 16-Ma volcanic rocks associated with the northern Nevada rift (NNR), an over 500-km long zone of north-northwest-trending dikes and lava flows that extends from near the Nevada-Oregon border to southeastern Nevada (Zoback and Thompson, 1978; McKee and Noble, 1986; Blakely and Jachens, 1991; Zoback and others, 1994). The NNR is well defined by both gravity and aeromagnetic anomalies and modeled as a swarm of near vertical mafic dikes (Philbin and others, 1963; Mabey, 1966; Zoback and Thompson, 1978; Blakely and Jachens, 1991). Basaltic flows and dikes, marking the surface expression of the rift between

the Roberts Mountains in the south to Midas, Nev. in the north, yield ages between 18.6 and 13.6 Ma with the majority between 17 and 14 Ma (Zoback and others, 1994). North of Midas, rhyolite dikes, flows, and domes belonging to two sequences of silicic volcanic rocks are present along the NNR (Wallace, 1993). The older group is interbedded and approximately coeval with basalts and basaltic andesite flows associated with the rift (Zoback and Thompson, 1978; Wallace, 1993; Zoback and others, 1994). Synchronous with magmatism along the NNR, eruption of the bulk of the voluminous flood basalts of the Columbia Plateau occurred between 16 and 15 Ma from north-northwest-trending feeder dikes aligned generally along the trend of the NNR (Bottomley and York, 1976; Pierce and Morgan, 1992; Zoback and others, 1994). Midway between the Columbia Plateau and the southern end of the NNR, the McDermitt and Owyhee volcanic centers are identified with the initial position of the Yellowstone hotspot (Pierce and Morgan, 1992; Zoback and others 1994). The Lake Owyhee volcanic field is 100-150 km north of the McDermitt volcanic field and the track of the Yellowstone hotspot. The spatial and temporal trace of the hotspot along the eastern Snake River Plain has been studied by numerous authors, who document the progress of volcanism, faulting, and crescent-shaped uplift from the McDermitt-Owyhee area at about 16 Ma to its present position at the Yellowstone Plateau (Armstrong and others, 1975; Pierce and Morgan, 1992; Anders and Sleep, 1992; Zoback and others, 1994; Perkins and others, 1995). These authors provide persuasive evidence of a common origin for the northern Nevada rift, the flood basalts of the Columbia Plateau, and the silicic and basaltic volcanism at the McDermitt and Owyhee volcanic centers as resulting from the interaction of the head of a mantle plume with the base of the lithosphere at about 16 Ma. Pierce and Morgan (1992) and Zoback and others (1994) present a model of rift formation north-northwest and south-southeast of the McDermitt volcanic center as the rift propagated rapidly away from the plume head normal to the direction of plate motion. That west-southwest motion of the North American plate corresponds precisely with the N70-75°E orientation of the hotspot track between 16 and 10 Ma (Pierce and Morgan, 1992). Based on the 14.4- to 15.1-Ma ages obtained from the tuffs of the Carlin Formation in the Santa Renia Fields quadrangle, an Owyhee Plateau source would be most consistent with the timing and location determined for the hotspot during that period. Although the hotspot model presents an internally consistent argument for the location of a currently-unknown source region for the tuffs, we recognize that the actual source might be either more distant, as in the volcanic centers of the western Snake River plain (e.g. McKee and Noble, 1986; Rytuba and VanderMeulen, 1991) or more local, related to volcanism responsible for the many silicic volcanic units of the northern Nevada area (e.g., McKee and others, 1974; Wallace and others, 1990).

REFERENCES CITED

- Anders, M.H. and Sleep, N.H., 1992, Magmatism and extension: The thermal and mechanical effects of the Yellowstone Hotspot: *Journal of Geophysical Research*, v. 97, p. 15,379-15,393.
- Armstrong, R.L., Leeman, W.P., and Malde, H.E., 1975, K-Ar dating, Quaternary and Neogene volcanic rocks of the Snake River Plain, Idaho: *American Journal of Science*, v. 275, p. 225-251.
- Bartlett, M.W., Enders, M.S., and Hruska, D.C., 1991, Geology of the Hollister gold deposit, Ivanhoe district, Elko County, Nevada, in Raines, G.L., Lisle, R.E., Schaefer, R.W., and Wilkinson, W.H., eds., *Geology and ore deposits of the Great Basin: Reno, Nevada*, Geological Society of Nevada, Symposium Proceedings, p. 957-978.
- Blakely, R.J. and Jachens, R.C., 1991, Regional study of mineral resources in Nevada: Insights from three-dimensional analysis of gravity and magnetic anomalies: *Geological Society America Bulletin*, v. 103, p. 795-803.
- Bottomley, R.J. and York, D., 1976, $^{40}\text{Ar}/^{39}\text{Ar}$ age determinations on the Owyhee Basalt of the Columbia Plateau: *Earth and Planetary Science Letters*, v. 31, p. 75-84.
- Dalrymple, G.B., 1989, The GLM continuous laser system for $^{40}\text{Ar}/^{39}\text{Ar}$ dating: Description and performance characteristics: *U.S. Geological Survey Bulletin* 1890, p. 89-96.
- Dalrymple, G.B. and Duffield, 1988, High precision $^{40}\text{Ar}/^{39}\text{Ar}$ dating of Oligocene rhyolites from the Mogollon-Datil volcanic field using a continuous laser system: *Geophysical Research Letters*, v. 15, no. 5, p. 463-466.
- Dalrymple, G.B. and Lanphere, M.A., 1969, Potassium-argon dating, W.H. Freeman, San Francisco, 258p.
- Dalrymple, G.B., Cox, A., and Doell, R.R., 1965, Potassium-argon age and paleomagnetism of the Bishop Tuff, California: *Geological Society America Bulletin*, v. 76, p. 665-674.
- Duffield, W.A. and Dalrymple, G.B., 1990, The Taylor Creek Rhyolite of New Mexico: a rapidly emplaced field of lava domes and flows: *Bulletin of Volcanology*, v. 52, p. 475-487.
- Ekren, E.B., McIntyre, D.H., and Bennett, E.H., 1984, High-temperature, large-volume, lavalike ash-flow tuffs without calderas in southwestern Idaho: *U.S. Geological Survey Professional Paper* 1272, 76 p.
- Evans, J.G., 1972, Preliminary geologic map of the Welches Canyon quadrangle, Nevada: *U.S. Geological Survey Miscellaneous Field Studies Map* MF-326.
- Evans, J.G., 1974, Geologic map of the Rodeo Creek NE quadrangle, Eureka County, Nevada: *U.S. Geological Survey Geological Quadrangle Map* GQ-1116.
- Evans, J.G. and Cress, L.D., 1972, Preliminary geologic map of the Schreoder Mountain quadrangle, Nevada: *U.S. Geological Survey Miscellaneous Field Studies Map* MF-324.
- Fleck, R.J. and Carr, M.D., 1990, The age of the Keystone Thrust: Laser-fusion $^{40}\text{Ar}/^{39}\text{Ar}$ dating of foreland basin deposits, southern Spring Mountains, Nevada: *Tectonics*, v. 9, no. 3, p. 467-476.
- Fleck, R.J., Turrin, B.D., Sawyer, D. A., Warren, R. G., Champion, D. E., Hudson, M. R., and Minor, S. A., 1996, Age and character of basaltic rocks of the Yucca Mountain region, southern Nevada: *Journal Geophysical Research*, v. 101, no. B4, p. 8205-8227.
- Lanphere, M.A., Dalrymple, G.B., Fleck, R.J., and Pringle, M.S., 1990, Intercalibration of mineral standards for K-Ar and $^{40}\text{Ar}/^{39}\text{Ar}$ Age measurements: *EOS, American Geophysical Union Transactions*, v. 71, no. 43, p. 1658.
- LoBello, P., Feraud, G., Hall, C.M., York, D., Lavina, P., and Bernat, M., 1987, $^{40}\text{Ar}/^{39}\text{Ar}$ step-heating and laser fusion dating of a Quaternary pumice from Neschers, Massif Central, France: The defeat of xenocrystic contamination: *Chemical Geology*, v. 66, p. 61-71.
- Ludwig, K.R., 1988, ISOPLOT Version 2: A plotting and regression program for isotope geochemists, for use with HP series 200/300 computers: *U.S. Geological Survey Open-File Report* 88-601, 49 p.
- Luedke, R.G. and Smith, R.L., 1981, Map showing the distribution, composition, and age of Late Cenozoic volcanic centers in California and Nevada: *U.S. Geological Survey Miscellaneous Investigations Series Map* I-1091-C.
- Luedke, R.G. and Smith, R.L., 1982, Map showing the distribution, composition, and age of Late Cenozoic volcanic centers in Oregon and Washington: *U.S. Geological Survey Miscellaneous Investigations Series Map* I-1091-D.
- Luedke, R.G. and Smith, R.L., 1983, Map showing the distribution, composition, and age of Late Cenozoic volcanic centers in Idaho, western Montana, western South Dakota, and northwestern Wyoming: *U.S. Geological Survey Miscellaneous Investigations Series Map* I-1091-E.
- Luedke, R.G. and Smith, R.L., 1984, Map showing the distribution, composition, and age of Late Cenozoic volcanic centers in the western conterminous United States: *U.S. Geological Survey Miscellaneous Investigations Series Map* I-1523.
- Mabey, D.R., 1966, Regional gravity and magnetic anomalies in part of Eureka County, Nevada, in Hansen, D.A., Heinrichs, W.E., Jr., Holmer, R.C., MacDougall, R.E., Rogers, G.R., Sumner, J.S., and Ward, S.H., eds., *Mining geophysics, Volume 1: Tulsa, Oklahoma, Society of Exploration Geophysicists*, p. 77-83.
- McDowell, F.W., 1983, K-Ar dating — Incomplete extraction of radiogenic argon from alkali feldspar: *Isotope Geoscience*, v.1, p. 119-126.
- McIntyre, G.A., Brooks, C., Compston, W., and Turek, A., 1966, The statistical assessment of Rb-Sr isochrons: *Journal Geophysical Research*, v. 71, no. 22, p. 5459-5468.
- McKee, E.H., 1976, Origin of the McDermitt caldera in Nevada and Oregon and related mercury deposits: *Transactions, American Institute of Mining, Metallurgy, and Petroleum Engineering*, v. 260, p. 196-199.
- McKee, E.H. and Noble, D.C., 1986, Tectonic and magmatic development of the Great Basin of western United States during late Cenozoic time: *Modern Geology*, v. 10, p. 39-49.
- McKee, E.H., Tarshis, A.L., and Marvin, R.F., 1974, Summary of radiometric ages of Tertiary volcanic and selected plutonic rocks in Nevada — Part V: Northeastern Nevada: *Isochron/West*, no. 16, p. 15.
- Merrihue, C. and Turner, G., 1966, Potassium-argon dating by activation with fast neutrons: *Journal Geophysical Research*, v. 71, p. 2852-2857.
- Noble, D.C., McCormack, J.K., McKee, E.H., Silberman, M.L., and Wallace, A.B., 1988, Time of mineralization in the evolution of the McDermitt caldera complex, Nevada-Oregon, and the relation of middle Miocene mineralization in the northern Great Basin to coeval regional basaltic magmatic activity: *Economic Geology*, v. 83, p. 859-863.
- Perkins, M.E., Nash, W.P., Brown, F.H., and Fleck, R.J., 1995, Fallout tuffs of Trapper Creek, Idaho — A record of Miocene explosive volcanism in the Snake River Plain volcanic Province: *Geological*

- Society America Bulletin, v. 107, p. 1484-1506.
- Philbin, F.W., Meuschke, J.L., and McCaslin, W.E., 1963, Aeromagnetic map of the Roberts Mountains, central Nevada: U.S. Geological Survey Open-File Map, March 7, 1963, scale 1:25,000.
- Pierce, K.L. and Morgan, L.A., 1992, The track of the Yellowstone Hot Spot: Volcanism, faulting, and uplift, *in* Link, P.K., Kuntz, M.A., and Platt, L.B., eds., Regional geology of eastern Idaho and western Wyoming: Geological Society America Memoir 179, p. 1-53.
- Regnier, Jerome, 1960, Cenozoic geology in the vicinity of Carlin, Nevada: Geological Society America Bulletin, v. 71, no. 8, p. 1191-1199.
- Rytuba, J.J. and McKee, E.H., 1984, Peralkaline ash flow tuffs and calderas of the McDermitt volcanic field, southeast Oregon and north central Nevada: Journal Geophysical Research, v. 89, p. 8616-8628.
- Samson, S.D. and Alexander, E.C., 1987, Calibration of the interlaboratory $^{40}\text{Ar}/^{39}\text{Ar}$ dating standard, MMhb-1: Chemical Geology (Isotope Geoscience Section), v. 66, p. 27-34.
- Sarna-Wojcicki, A., Bowman, H.R., Meyer, C.E., Russell, P.C., Woosward, M.J., McCoy, G., Rowe, J.J., Jr., Baedeker, P.A., Asaro, F. and Michael, H., 1984, Chemical analyses, correlations, and ages of upper Pliocene and Pleistocene ash layers of east-central and southern California: U.S. Geological Survey Professional Paper 1293, 40 p.
- Silberman, M.L., Stewart, J.H., and McKee, E.H., 1976, Igneous activity, tectonics, and hydrothermal precious-metal mineralization in the Great Basin during Cenozoic time: Society Mining Engineers AIME Transactions, v. 260, no. 3, p. 253-263.
- Steiger, R.H. and Jager, E., 1977, Subcommittee on geochronology: Convention on the use of decay constants in geo- and cosmochronology: Earth and Planetary Science Letters, v. 36, p. 359-362.
- Taylor, J.R., 1982, An Introduction to Error Analysis: The Study of Uncertainties in Physical Measurements: Mill Valley, California, University Science Books, 270 p.
- Wallace, A.R., 1993, Geologic map of the Snowstorm Mountains and vicinity, Elko and Humboldt Counties, Nevada: U.S. Geological Survey Miscellaneous Investigations Map I-2394, scale 1:50,000.
- Wallace, A.R., McKee, E.H., Zoback, M.L., and Zimmerman, R.A., 1990, New ages for volcanic rocks, western Elko County, Nevada: Isochron/West, no. 55, p. 3-5.
- York, D., Hall, C.M., Yanase, Y., Hanes, J.A., and Kenyon, M.J., 1981, $^{40}\text{Ar}/^{39}\text{Ar}$ dating of terrestrial minerals with a continuous laser: Geophysical Research Letters, v. 8, p. 1136-1138.
- Zoback, M.L., and Thompson, G.A., 1978, Basin and Range rifting in northern Nevada; clues from a mid-Miocene rift and its subsequent offsets: Geology, v. 6, p. 111-116.
- Zoback, M.L., McKee, E.H., Blakely, R.J., and Thompson, G.A., 1994, The northern Nevada rift: Regional tectono-magmatic relations and middle Miocene stress direction: Geological Society of America Bulletin, v. 106, no. 3, p. 371-382.

IMPORTANCE OF CLAY CHARACTERIZATION TO INTERPRETATION OF $^{40}\text{Ar}/^{39}\text{Ar}$ DATES ON ILLITE FROM CARLIN-TYPE GOLD DEPOSITS: INSIGHTS FROM JERRITT CANYON, NEVADA.

By H.W. Folger, A.H. Hofstra, D.D. Eberl, and L.W. Snee

ABSTRACT

Illite has been dated extensively in attempts to determine the age of Carlin-type gold deposits. Theoretical considerations and empirical results from the Jerritt Canyon Mining District show that a number of problems must be addressed to properly interpret $^{40}\text{Ar}/^{39}\text{Ar}$ or K-Ar dates on illite from Carlin-type gold deposits. By characterizing, dating, and evaluating the illitic clays by various methods we were able to identify the ore stage illite and determine the degree and mechanism(s) of illite recrystallization. We question whether the temperature and duration of hydrothermal activity at the Carlin-type deposits was sufficient for complete loss of argon from illite by diffusion such that the isotopic clock of illite is completely reset. Most geochronologic studies of illite in Carlin-type deposits have not adequately addressed these concerns and therefore the age interpretations are suspect. Although using illite to date Carlin-type deposits is problematic, meaningful age constraints can be obtained if each of these concerns is carefully evaluated.

INTRODUCTION

The age of Carlin-type gold deposits is controversial because of the difficulty in finding datable minerals that are clearly cogenetic with ore formation. Of the possible minerals present in these deposits, clay minerals have been dated extensively in attempts to determine the age of these large gold deposits. Reported ages based on isotopic dates on white mica or sericite range from Middle Jurassic to Middle Tertiary (Wilson and Parry, 1995; Arehart and others, 1993; Groff and others, 1997; Drewes-Armitage and others, 1996; Hall and others, 1997). In contrast, crosscutting relationships between gold-bearing rocks and dated igneous rocks constrain the age of several deposits to the mid-Tertiary (Hofstra, 1994, Maher and others, 1993, Emsbo and others, 1996). The geochronology of clay minerals from the Carlin-type deposits is therefore an area of importance for understanding their genesis as well as of considerable interest for geochronologists.

Critical questions include: (1) Did the clay minerals form

during gold mineralization?; and (2) Were the radiometric clocks of older clay minerals reset by the hydrothermal system? The Jerritt Canyon Mining District is an ideal place to evaluate the meaning of isotopic dates on clay minerals because gold mineralization is clearly younger than basalt dikes dated at 40.8 Ma (Hofstra, 1994). As part of our study to date gold mineralization at the Jerritt Canyon Mining District (fig. 1), we discovered that clay-size micas from high-grade-Au zones do not necessarily yield the age of mineralization. In fact, in the Jerritt Canyon Mining District the opposite is true. In the following sections, we discuss some of the reasons why careful characterization of clays for geochronology is essential for meaningful interpretations.

Using clays as geochronometers

The behavior of clay minerals and their use as geochronometers and geothermometers are topics of considerable research. Of particular importance to ore genesis studies are the evolutionary changes clay minerals undergo prior to, during, and subsequent to ore deposition. For sediment-hosted deposits, the clay cycle generally begins with weathering and transport of potassium-bearing minerals into a sedimentary basin. Upon burial in sedimentary basins, clay minerals undergo diagenesis and possibly isotopic resetting as temperature and depth increases. The chemical composition of pore fluids and amount of water-rock interaction between clay particles and fluids control changes in clay mineralogy. Complicating the evolutionary story, these sedimentary rocks may be altered by externally derived fluids such as 1) fluids migrating along faults and fracture zones, 2) fluids associated with igneous dikes and intrusions and 3) metamorphic fluids. In any given setting, there are likely to be multiple generations of clays depending on the history of the rocks.

Dating hydrothermal ore deposits by K/Ar or $^{40}\text{Ar}/^{39}\text{Ar}$ methods requires that a potassium (K)-bearing mineral be identified that records the hydrothermal event of interest. In many cases, K-bearing clay minerals can be isolated from detrital micas and other K-bearing minerals by preparing samples of different grain sizes. However, separating different

generations of the same clay mineral may be impossible. Therein lies the problem. K-bearing minerals from different origins will contribute their own isotopic histories to the total isotopic picture resulting in composite isotopic ages when multiple generations of clay minerals are analyzed as one sample.

Clay characterization is needed to determine what minerals are present, how they fit into the history of the rock, and what generation of clay should be dated. Therefore, careful sample handling is critical to insure that the clays do not suffer "investigator effects" (described by Clauer and others, 1992). Identification and separation (methods described by Moore and Reynolds, 1989) of the clays must be done using methods of disaggregation that do not impose artificial grain sizes on minerals or alter the isotopic ratios of the minerals being analyzed.

Identification of minerals and polytypes as well as measurements of illite crystallinity are made by x-ray diffraction and SEM analyses. Illite crystallinity can be used as a qualitative indicator of temperature and degree of diagenetic evolution. For instance, Kisch (1990) defined low temperature metamorphic zones in terms of changes in crystallinity and temperature. Fundamental particle thicknesses are modeled by *Mudmaster* software, which, allows for evaluation and comparison of changes in the illite crystallinity. Changes in crystallinity inferred by changes in mean particle thicknesses also afford insight into possible illitization mechanisms and the inherited crystallinity of older mica in unaltered fractions. Thus, the crystallinity of illite provides a framework on which changes caused by the hydrothermal system can be measured.

Fine-grained clay samples are prone to argon loss during irradiation by the $^{40}\text{Ar}/^{39}\text{Ar}$ method. In order to capture $^{39}\text{Ar}_K$ released during irradiation the prepared clay samples are encapsulated into glass vials or "breakseals", which are sealed under high vacuum prior to irradiation (Foland and others, 1992). The loss of $^{39}\text{Ar}_K$ can significantly affect the calculated apparent and total-gas ages. The K/Ar method of dating is based on the natural decay of ^{40}Ar to stable ^{40}Ar by electron capture and positron emission (McDougall and Harrison, 1988). The $^{40}\text{Ar}/^{39}\text{Ar}$ method is based on the formation of ^{39}Ar by irradiation of ^{39}K with thermal and fast neutrons. Several critical assumptions are made about the samples including that the mineral systems have been closed to loss or gain of potassium, and that no radiogenic ^{40}Ar escaped from the mineral during its life. If these assumptions are violated then the radiometric ages are meaningless.

Early works by Hamilton and others (1989) and Burley and Flisch (1989) showed a trend of decreasing ages with decreasing grain size in samples collected from petroleum reservoirs. The mechanism responsible for the age difference was thought to be due to the diminishing presence of contaminants such as old, detrital mica in the finest size fractions. The finest fractions contained the purest fraction of

diagenetic mica. Hunziker and others (1986) researching low grade metamorphic environments in the Glarus Alps, proposed that the K-Ar system of the less than 2 micron mica would be completely reset by diffusive loss of radiogenic argon at temperatures of about 260° C and duration of 10 million years. This model further predicts that even finer-grained micas could be reset at even lower temperatures. Yet, current studies of fine-grained mica suggest that argon loss by diffusion may not be significant in low-temperature metamorphic environments. Recently, Hassanipak and Wampler (1996) conducted experiments that showed that there was no preferential loss of radiogenic argon during step-heating in the finer grain sizes compared to the coarser grain sizes. Clauer and others (1997) found there was no notable diffusion from the cores of fine grained clays and that the decrease in isotopic ages associated with decreasing grain size of fine-grained illite particles is more commonly related to a decrease in the content of detrital contaminants than to diffusion. Because of the uncertainty associated with the degree to which clay minerals have undergone argon diffusion (ranging from none to complete diffusion), it is impossible to predict whether clay minerals from a particular deposit will record a mineralizing event or a composite date.

Clay minerals in Carlin-type deposits

Prior to gold mineralization, the sedimentary rocks that host the Carlin-type deposits contained a variety of K-silicate minerals such as detrital muscovite, K-feldspar, diagenetic illite, illite-smectite (I-S), or adularia (Mullens, 1980). Portions of many deposits (for example, Getchell and Gold Acres) are also hosted in Jurassic, Cretaceous, or Tertiary intrusive rocks or in their adjacent contact metamorphic rocks; each contains a variety of K-silicate minerals. The igneous intrusions and dikes are usually altered to some degree and commonly contain sericite and chlorite. Similarly, the contact metamorphic minerals are often altered to mica, chlorite, and a variety of clay minerals. K-metasomatism associated with many of these intrusions produced extensive areas of potassic or phyllic alteration unrelated to the Carlin-type hydrothermal system; examples included Getchell, Mike, and Bluestar/Genesis deposits. Some of the older K-silicate minerals provide opportunities for dating subsequent Carlin-type mineralization. For example, older K-feldspar and biotite are relatively unstable in Carlin-type fluids and are likely to be altered to clay minerals (Phinisey and others 1996). In contrast, older muscovite or illite are relatively stable and are less likely to be destroyed (Phinisey and others, 1996). The challenge then is to distinguish K-micas produced by the Carlin-type hydrothermal systems from older K-micas in the rocks. Alternatively, it is necessary to determine whether preexisting micas could have been completely reset via diffusive argon loss at the temperatures and duration of the hydrothermal system or by

recrystallization. An additional problem in some districts is that the hydrothermal event associated with a Carlin-type system may be overprinted by a younger hydrothermal event. For example, mercury mineralization is present in the Miocene Carlin Formation that unconformably overlies the Meikle deposit (P. Emsbo, 1998 oral commun.).

The clay minerals associated with gold ores in the Carlin-type deposits have been described in only a few deposits, and seldom have clays been described from barren host rocks. Drews-Armitage and others (1996) describe the clay mineralogy in rocks of the Devonian calcareous Popovich Formation, the siliciclastic Rodeo Creek unit, and siliciclastic Vinini Formation, which host the Bluestar/Genesis deposits. In the distal portions of the deposit, kaolinite and cryptocrystalline quartz replace the detrital quartz and feldspar in the Popovich Formation. In the most altered portions of the Popovich Formation proximal to the deposit, detrital minerals are replaced by kaolinite, quartz, and locally illite (mostly 1M). Altered siliciclastic rocks distal to the deposit contain quartz, kaolinite, and detrital illite (2M1). Altered siliciclastic rocks proximal to the deposit contain quartz, kaolinite, and detrital illite (2M1), with locally occurring quartz-illite (1M) veins. Bakken and others (1989) note that detrital feldspar at the Carlin deposit is present in minor amounts (up to a few percent) in unaltered Roberts Mountains Formation and is absent in altered rock. They also report an "abundance of smectite, illite, and kaolinite, and a trace of chlorite" in unaltered Roberts Mountains Formation. In altered Roberts Mountains Formation, the predominant clays are 1M and 2M illite with varying amounts of kaolinite. Smectite, chlorite, and feldspar were notably absent and detrital muscovite was present. Also at the Carlin deposit, Kuehn and Rose (1992) reported that barren Roberts Mountains Formation contains quartz, calcite, dolomite, K-feldspar, illite and pyrite which progressively changes to zones of quartz, kaolinite-dickite, and pyrite, but no feldspar, in the ore zone. They also determined that illite was destroyed at the expense of kaolinite-dickite formation in the ore zones. Ferdock and others (1997) suggest that illite formed during the early stages and was followed by kaolinite in the late stages of the gold mineralizing system at the Post-Betze deposit. In most of the deposits discussed above, there appears to be transitional zones of alteration mineralogy from the distal, barren host rocks to the fluid conduits and high-grade zones. However, not enough is known as to the effects a hydrothermal system may have played in resetting and (or) recrystallizing older illites, and thus changing their isotopic systems. More studies that characterize both the mineralogy and isotopic ages of barren and mineralized rocks are needed in order to determine what clays or generation of clays were formed by the gold system.

In summary, these studies suggest that: (1) The clay minerals formed by the hydrothermal fluids are dependent on the mineralogy of the host rock. (2) Illite, I-S (illite-smectite), and kaolinite are the main clay minerals produced by Carlin-

type hydrothermal systems. (3) Older illite of multiple origins may be present in high-Au-grade ores. Even though illite and I-S can be dated by K/Ar and $^{40}\text{Ar}/^{39}\text{Ar}$ isotopic methods, their behavior under hydrothermal conditions of low temperature and short duration have not been well studied. Although any new illite that formed during gold deposition would record the age of mineralization, the effect on the isotopic systems of older illite is not well known. It is important to learn whether argon loss by diffusion from the crystal lattices occurs and whether these losses significantly affect the isotopic dates recorded by the illite.

CLAY MINERALS IN THE JERRITT CANYON MINING DISTRICT

Introduction

The results of clay studies on the Carlin-type gold deposits in the Jerritt Canyon Mining District illustrate many of the concerns mentioned above. The approach used herein was to consider the isotopic dates within the context of the geology of the district and environment of ore deposition. The geochemistry of unaltered barren rocks are compared to those of altered mineralized rocks to evaluate mass transfer, particularly with respect to K. The mineralogy and crystallinity of the clay minerals were also compared and modeled to improve interpretation of the isotopic dates.

Geology

The Jerritt Canyon Mining District is located in the Independence Mountains approximately 62 kilometers north-northwest of Elko, Nevada and approximately 50 kilometers north-northeast of the Carlin Trend (fig. 1). The district has produced approximately 4 million ounces of gold and has an estimated 4 million ounces of gold resources (Nevada Bureau of Mines and Geology, 1996). The mines are owned and operated by Independence Mining Company. The district includes several sediment-hosted disseminated gold deposits hosted by Lower Silurian to Lower Devonian Roberts Mountains and Upper Ordovician to Lower Silurian Hanson Creek Formations. These rocks are exposed through windows in the Roberts Mountains Allochthon. The deposits are highly irregular but generally tabular in morphology. Their distribution is controlled by intersections of favorable lithologies with a complex array of faults. Most gold is produced from relatively unweathered black, carbonaceous, pyritic, refractory ores, with lesser production from weathered, tan and buff, oxidized ore, and from jasperoid ores. The refractory ores are often decalcified and locally contain realgar in open spaces. Silicification to produce jasperoid, and decalcification and sulfidation to produce refractory ore are

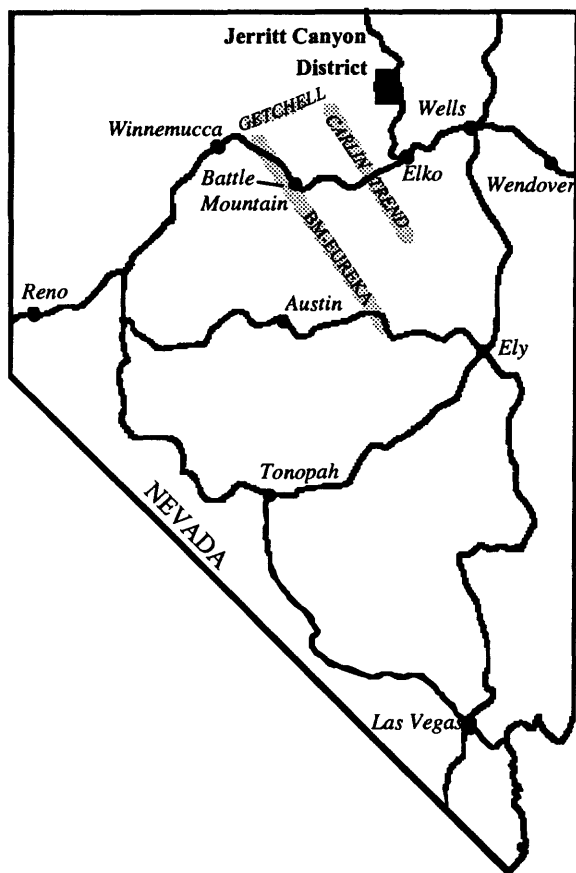


Figure 1. Location of the Jerritt Canyon Mining District in Elko County, Nevada. BM, Battle Mountain.

the major manifestations of the hydrothermal system that produced the gold deposits.

Environment of ore formation

Fluid inclusion data and mineral assemblages indicate that the hydrothermal fluids were not in excess of 260°C and generally much cooler. For example the presence of marcasite constrains the temperature to less than about 240°C (Murowchick, 1992). Fluid inclusion homogenization temperatures from quartz and calcite indicate trapping temperatures between about 120°C and 260°C (Hofstra, 1994). The duration of the hydrothermal system is unknown, but probably is in the range of 10,000 to 1 million years. It is also important to note that there are no Mesozoic intrusions exposed at the surface or in the mines in the mining district.

Mass Transfer

Geochemical analyses (Hofstra, 1994) of samples

collected from high-Au-grade zones and distal unaltered rocks indicate a relative enrichment in the ores of Au, As, Sb, Hg, and Tl, and strong depletion of calcium and strontium, whereas aluminum, potassium, iron, and titanium were relatively immobile. An important consideration for growth and crystallization of new mica is the source of potassium and when it became mobile in the system. In the Jerritt Canyon Mining District, the potassium content of ores remained nearly constant, indicating K-metasomatism was not an important factor in generating the mica that is present in the deposits.

Clay characterization

Rock samples were collected from an altered and mineralized zone and from an unaltered zone approximately 20 meters apart within the same stratigraphic interval of the Roberts Mountains Formation. These rocks were separated into seven different grain-sizes fractions and analyzed by x-ray diffraction to evaluate the effects of the gold-bearing hydrothermal system on the mica (Hofstra, 1994, Folger and others, 1996). The size-fractions are 40-20, 20-5, 5-2, 2-1, 1-0.5, 0.5-0.1, and <0.1 μm , and the dominant clay mineral is 2M1 illite with lesser amounts of kaolinite present in both the altered and unaltered samples. Minor amounts of illite-smectite (I-S), having less than 30% expandability, were present in the altered 0.5-0.1 μm and the <0.1 μm size fractions, the two smallest fractions analyzed.

Crystallinity studies

Several new software programs developed specifically for clay minerals were utilized to evaluate changes in illite morphology. Eberl and others (1997) developed a method that eliminates the effect of swelling clays on peak measurements in x-ray diffraction data. By eliminating peak broadening effects of interlayered smectite as well as shifts in d-spacing, more accurate measurement of the particle thickness and mineral strain are permitted. Samples were sodium saturated and suspended in a solution of PVP-10 (polyvinylpyrrolidone having a molecular weight of 10,000), then mounted on polished silicon wafers. The software programs *Mudmaster* (Eberl and others, 1997), *Overgrowth!* (Eberl and others, 1997) and *Galoper* (Eberl and others, 1997) utilize this special x-ray diffraction data to measure and calculate the mean particle thicknesses.

Subtle changes in mica crystallinity were detected in similar grain-size fractions in unaltered and altered fractions. Mica crystallinity, measured by Kübler indices, decreases with decreasing grain size for both the altered and unaltered size fractions indicating that the altered samples have greater crystallinity when compared to their unaltered counterparts. The exception is the smallest grain-size fractions. Figure 2

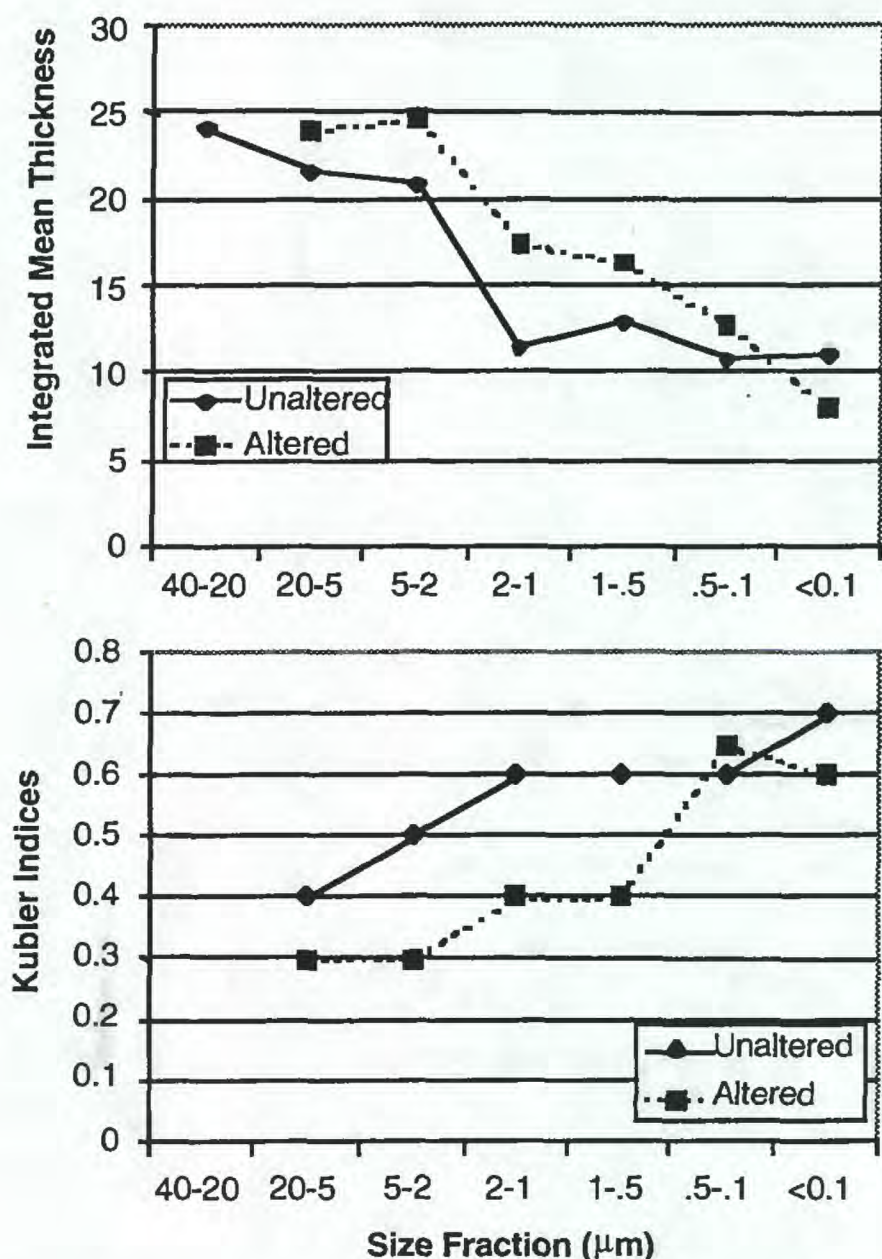


Figure 2. Comparison of crystallinity measured by the Kübler and integrated method peak methods.

shows a comparison of the Kübler indices measured from x-ray diffractograms and the integrated mean thickness calculated by *Mudmaster* for different grain size fractions. As the mica becomes more crystalline, the Kübler index (Kübler, 1964) decreases reflecting a sharper peak and a narrower peak width ($^{\circ}2\theta$). An increase in the integrated mean particle thickness is analogous to an increase in mica crystallinity. Only two coarse-grained fractions from the altered zone have crystallinities (Kübler index $<0.37^{\circ}2\theta$) that fall within the anchizone ($>200^{\circ}\text{C}$). All unaltered and the remaining fine-grained altered fractions had crystallinities (Kübler index $>0.37^{\circ}2\theta$) that fall within the diagenetic metamorphic zone ($<200^{\circ}\text{C}$). This implies that the rocks were not heated to high temperatures during their depth burial history prior to mineralization and that the hydrothermal fluids were not very hot.

To measure the fundamental particle size distributions and mean particle sizes in altered and unaltered size-fractions *Mudmaster* was used. Samples were prepared using the PVP-10 method (discussed above) and analyzed by XRD. Integrated

particle-size means were calculated from the particle-size distributions for each grain size fraction. The distribution curves for all size fractions are asymptotic rather than normal or log normal. Comparison of unaltered and altered mean values showed an increase in fundamental particle sizes in the altered size fractions. This reflects an increase in crystallinity for altered fractions similar to that observed by the Kübler method.

Galoper generated simulation of a distribution curve (fig. 3) that would resemble the original distribution curve of the unaltered fraction (green). Using an illitization mechanism of open system nucleation and growth, a distribution curve, which closely approximates the original unaltered fractions, was simulated (blue). The similarity between the original distribution curves and the simulated curve suggests that what we call "unaltered" mica formed by nucleation and growth processes. This simulated distribution curve was then used for further calculations using *Overgrowth!*. The resulting distribution curve remains asymptotic but with a greater proportion (frequency) of larger particle thicknesses.

Random ripening and Ostwald ripening (Eberl and others, 1997) are two possible illitization mechanisms for closed system growth. Here we mean the system was closed to potassium enrichment or depletion. When a particle is said to undergo a ripening process, one can imagine the addition of rims about a core particle.

If the original simulated particle size distribution undergoes random ripening, where the rate of crystal dissolution and growth is random with respect to specific surface area, then the particle distribution curve will remain asymptotic (orange line). If the original simulated particle size undergoes Ostwald ripening, then larger particles form at the expense of the smallest grain, and the original asymptotic curve takes on a log normal shape (brown line). Therefore, a random ripening model in which particles are randomly dissolved throughout the distribution and new particle material grow as overgrowths around rims of preexisting particles, most closely resemble the particle size distributions of the Jerritt Canyon samples. In this way the potassium is conserved, and the simulated particle size distribution increases only slightly mirroring a similar increase in illite crystallinity in the altered fraction. Assuming that the true age of the deposit is less than 40.8 Ma, just 15% of the illite present in the unaltered fraction would need to undergo random ripening to explain the changes in isotopic dates. This percentage works well for all grain sizes except the very smallest size fraction, where the presence of illite-smectite lowers the crystallinity and age even more.

K/Ar and $^{40}\text{Ar}/^{39}\text{Ar}$ dates

Age determinations were made of clay samples characterized by conventional K/Ar and step-heating $^{40}\text{Ar}/^{39}\text{Ar}$ methods. The diagram in figure 4 compares the total-gas ages (K/Ar and $^{40}\text{Ar}/^{39}\text{Ar}$) of the altered and unaltered size fractions.

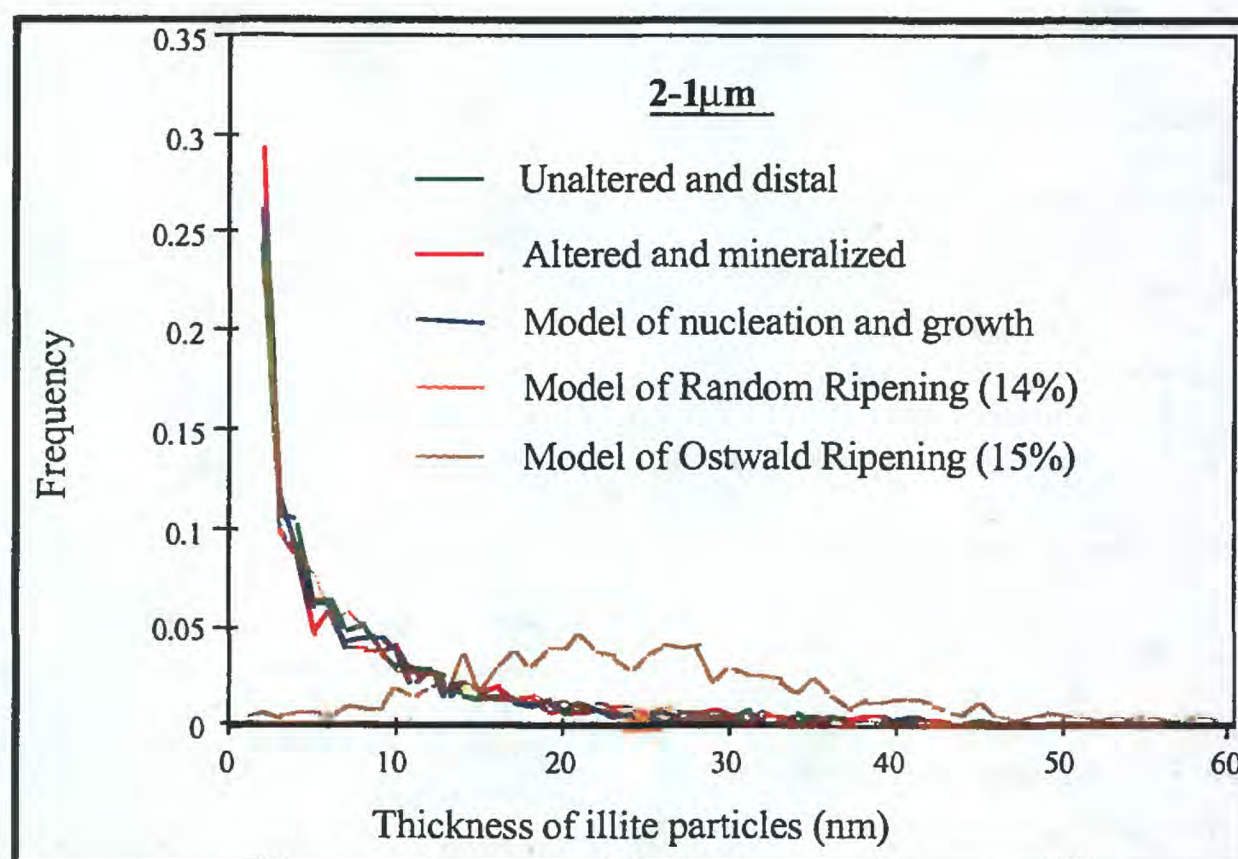


Figure 3. Original and simulated particle size distributions for the altered and unaltered mica. The green and magenta lines are the original particle size distributions curves for the unaltered and altered fractions respectively. In this fraction it can be seen that there is an increase in the frequency of the smallest particle sizes in the altered fraction as compared to unaltered. The blue line, representing the simulated model, nearly approximates these distribution curves.

The apparent age (y-axis) is plotted for each grain-size fraction (x-axis) where grain-size increases from right to left. What is striking and unexpected is that the altered fractions yield ages much older than the presumed <40 Ma age of the deposits. Also, the mineralized fractions have consistently younger ages than their unmineralized counterpart. This is seen in the nearly parallel downward shift in the trend of altered ages. The youngest total-gas age of 149 Ma was from the mineralized less than 0.1 micron size fraction.

The negative trend of total-gas ages for the size fractions could be a reflection of the evolution of mica through a random ripening process, a result of mixing of several different generations of illite within the sample, or both. The altered fractions have younger ages and greater crystallinity (smaller Kübler indices and larger particle thickness) compared to their unaltered counterparts. It can be seen that the effect of the hydrothermal system on the mica has been an almost uniform lowering of total-gas ages across all grain sizes except in the finest fraction (<0.1mm) which has been lowered even more significantly.

$^{40}\text{Ar}/^{39}\text{Ar}$ spectra of the altered and unaltered grain-size fractions show trends of decreasing apparent ages with decreasing grain-size (fig. 5). Several features are evident from the $^{40}\text{Ar}/^{39}\text{Ar}$ age spectra of samples.

First, the percentage of argon loss due to $^{39}\text{Ar}_K$ recoil is

progressively greater in the smallest size fractions. This phenomenon is related to the effective grain size and crystallinity of the sample; the finer grained and less crystalline a sample, the greater the amount of ^{39}Ar lost during irradiation. This process is relatively unimportant in the coarse grained samples such as the 40-20 mm fractions, but is quite significant in the finer size fractions. Because $^{39}\text{Ar}_K$ is present in the "breakseal" volumes and radiogenic ^{40}Ar is absent, the $^{39}\text{Ar}_K$ was recoiled during irradiation. This process effectively increases the $^{40}\text{Ar}/^{39}\text{Ar}$ ratio of the samples for some or all of the additional heating steps. Thus the apparent age, which is directly proportional to the $^{40}\text{Ar}/^{39}\text{Ar}$ ratio, is too high for some or all heating steps of the samples that exhibit $^{39}\text{Ar}_K$ recoil. In contrast, the total-gas date, which is analogous to a conventional K/Ar date, is calculated for each sample by adding the recoiled ^{39}Ar and non-recoiled ^{39}Ar ; thus a true measurement of the $^{39}\text{Ar}_K$ is used. Figure 6 compares the amount of $^{39}\text{Ar}_K$ recoil and crystallinity for both the altered and unaltered fractions.

Second, the altered and fine-grained fractions have strongly discordant and broader step-like spectra, indicating a more complex geologic history compared to unaltered and coarse-grained fractions (fig. 5). In the past there have been two widely accepted explanations for this type of spectral shift: a partial loss of radiogenic ^{40}Ar by volume diffusion due to a

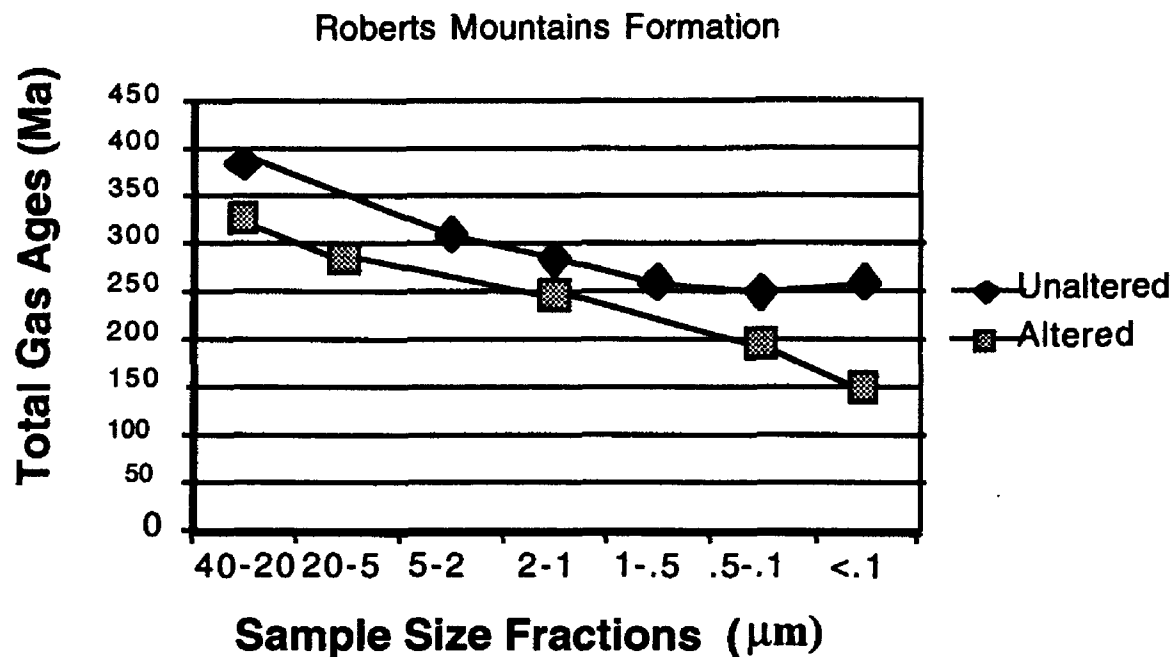


Figure 4. Comparison of total-gas ages for K/Ar and $^{40}\text{Ar}/^{39}\text{Ar}$ analysis of mica from the Roberts Mountains Formation. Isotopic ages for the altered and unaltered fractions are listed in table 1

thermal event or a mixing of different populations of mica with different argon retention characteristics. A convincing argument can be made that the changes in isotopic dates result from the addition of new illitic material as overgrowth formed by a ripening process or as very fine-grained illite-smectite formed by a later event such as the gold stage. These deductions are supported by the recent findings by Clauer and other researchers (discussed above) that show fine-grained illite is argon-retentive at temperatures similar to those at Jerritt Canyon and to the observed changes in illite crystallinity and morphology at Jerritt Canyon identified in XRD and SEM analysis and modeled by *Mudmaster, Galoper, and Overgrowth!*.

Discussion of Jerritt Canyon

The isotopic dates obtained from unaltered and altered size fractions represent composite ages because they are derived from samples having multiple populations of mica. The altered samples generally have lower ages and higher crystallinity than their unaltered counterparts. The smaller size fractions are less crystalline than the coarser sizes reflecting a population of less thermally mature mica in the smaller fractions. Yet the inverse relation of increased crystallinity and decreased apparent ages suggest that the hydrothermal system did have an effect on the crystallinity of the mica and also the total-gas ages. An illitization mechanism

Table 1. Total-gas ages, Kübler indices, integrated-mean thickness (IMT), and percentage of recoiled $^{39}\text{Ar}_K$ for each size fraction of the altered and unaltered samples.

Sample	Size	Ages	Kübler	IMT	^{39}Ar Recoil
Unaltered (J9054)	40-20	384.4		24.1	0
	20-5		0.4	21.5	
	5-2	307.5	0.5	20.8	15.9
	2-1	282.4	0.6	11.4	
	1-.5	258.6	0.6	12.9	
	.5-.1	248.2	0.6	10.7	19.7
	<0.1	257.4	0.7	11	22.3
Altered (J9051)	40-20	324.5			0
	20-5	283.7	0.3	24	
	5-2		0.3	24.7	8.3
	2-1	245.8	0.4	17.4	
	1-.5		0.4	16.3	20.3
	.5-.1	195.3	0.65	12.8	
	<0.1	149.1	0.6	8.1	28.2

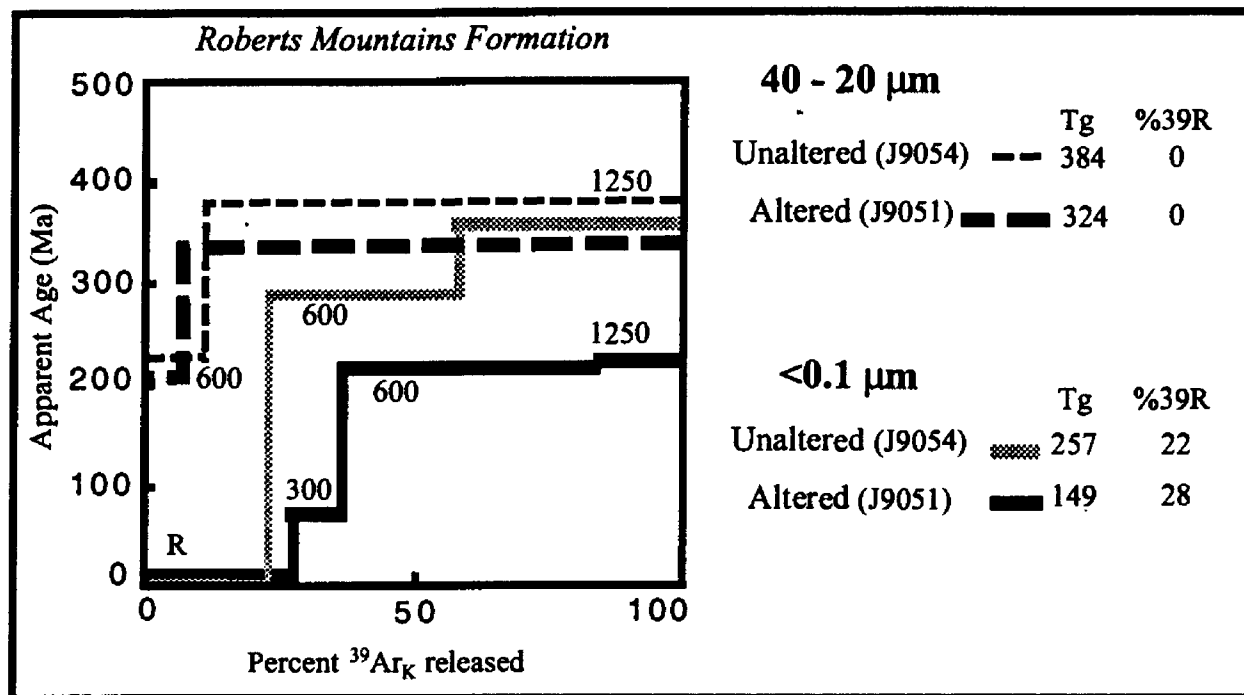


Figure 5. The argon spectra of altered and unaltered size-fractions from the Roberts Mountains samples. The amount of $^{39}\text{Ar}_K$ (potassium-derived argon) recoil has been included with the entire $^{39}\text{Ar}_K$ released and is designated by the letter "R". Also listed is the grain-size fraction analyzed (size) and the total-gas dates (Tg).

of random ripening best describes the changes seen in particle size distributions as well as the isotopic dates. This process incorporates new material as overgrowths on the older cores, thereby lowering the composite ages. Even though the greatest concentration of newly formed hydrothermal illite is found in the smallest size fraction, the effects of the older mica present in the sample is still reflected in the surprisingly old dates. The neof ormation and random ripening of illite appear to

explain changes observed in the isotopic ages and illite morphology.

CONCLUSIONS

The concerns described above and the empirical results from the Jerritt Canyon Mining District demonstrate that a number of problems must be addressed to properly interpret isotopic dates on illite from Carlin-type gold deposits. Most important to address are: 1. Identification of the mineralogical changes in the host rocks due solely to the mineralizing event. To do this requires comparative studies of both barren and mineralized rock. 2. Demonstrate that the mica being dated is ore stage and not contaminated by earlier generations of mica. This can be quite difficult if the mica has undergone ripening or partial dissolution. 3. Alternatively, prove that the temperature and duration of mineralization was sufficient for argon loss by diffusion to completely reset the isotopic clock of the micas. 4. The samples analyzed must be prepared and dated in a manner so as not to deleteriously influence the isotopic results.

Previous geochronologic studies of illite in Carlin-type deposits have not adequately addressed these concerns and therefore the age interpretations are suspect. Although using micas to date Carlin-type deposits can be problematic, meaningful results can be obtained if these concerns are addressed. With appropriate care, samples can be selected to increase the likelihood of finding ore stage micas that will yield the age of mineralization. This is the direction of our current research.

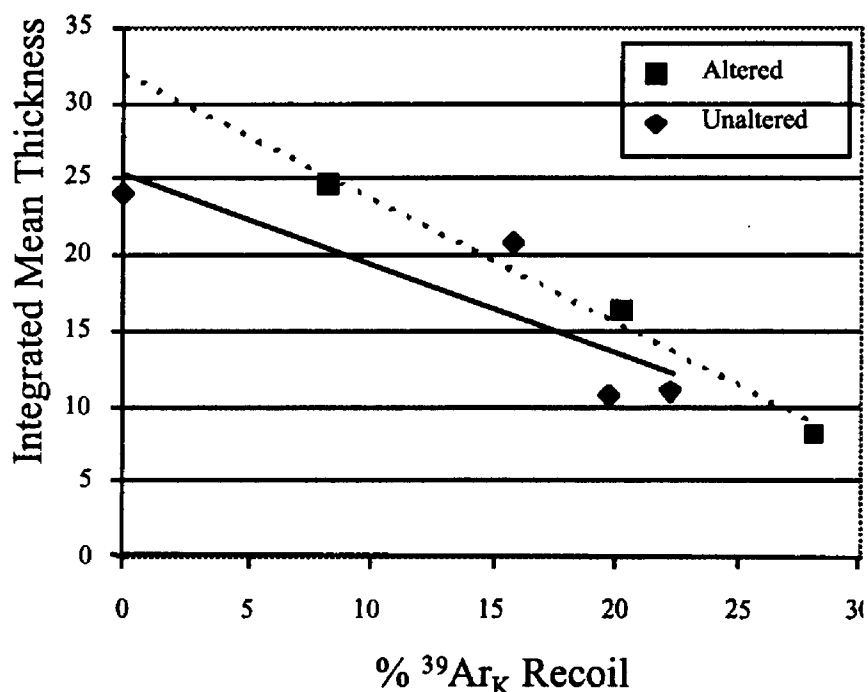


Figure 6. Integrated mean thicknesses calculated by *Mudmaster* reflect a trend similar to the Kübler Index where the less crystalline mica is more prone to argon recoil

REFERENCES CITED

- Arehart, G.B., Foland, K.A., Naeser, C.W., and Kesler, S.E., 1993, $^{40}\text{Ar}/^{39}\text{Ar}$, K/Ar, and fission track geochronology of sediment-hosted disseminated gold deposits at Post/Betze, Carlin Trend, northeastern Nevada: *Economic Geology*, v. 88, p. 622-646.
- Bakken, B.M., Hochella, M.F. Jr., Marshall, A.F., and Turner, A.M., 1989, High-resolution microscopy of gold in unoxidized ore from the Carlin Mine, Nevada: *Economic Geology*, v. 84, p. 171-179.
- Burley, S.D. and Flisch, M., 1989, K-Ar geochronology and the timing of detrital I/S clay illitization and authigenic illite precipitation in the Piper and Tartan fields, Outer Moray Firth, UK North Sea: *Clay Minerals*, no. 24, p. 285-315.
- Clauer, N., Cocker, J.D., and Chaudhuri, S., 1992, Isotopic dating of diagenetic illites in reservoir sandstones: Influence of the investigator effect: *Society of Economic Paleontologists and Mineralogists Special publication no. 47*, p. 4-12.
- Clauer, N., Srodon J., Francu, J., and Sucha, V., 1997, K-Ar dating of illite fundamental particles separated from illite-smectite: *Clay Minerals*, v. 32, p. 181-196.
- Drewes-Armitage, S., Romberger, S.B., and Whitney, C.G., 1996, Clay alteration and gold deposition in the Genesis and Blue Star deposits, Eureka County, Nevada: *Economic Geology*, v. 91, p. 1383-1393.
- Eberl, D.D., Drits, V.A., Srodon, J., 1998, Deducing growth mechanisms of minerals from the shapes of crystal size distributions: *American Journal of Science*, in press.
- Eberl, D.D., Drits, V.A., Srodon, J., and Kuesch, R., 1996, *Mudmaster*: A program for calculating crystallite size distributions and strain from the shapes of x-ray diffraction peaks: U.S. Geological Survey Open-File Report 96-171, 51 p.
- Eberl, D.D., Kuesch, R., Sucha, V., and Tsipursky, S., 1998, Measurement of fundamental illite particle thicknesses by x-ray diffraction using PVP-10 intercalation: *Clays and Clay Minerals*, in press.
- Emsbo, P., Hofstra, A.H., Park, D., Zimmerman, J.M., and Snee, L., 1996, A mid-Tertiary age constraint on alteration and mineralization in igneous dikes on the Goldstrike Property, Carlin Trend, Nevada: *Geological Society of America Abstracts with Programs*, v. 28, no. 7, p. A476.
- Ferdock, G.C., Castor, S.B., Leonardson, R.W., Collins T., 1997, Mineralization and paragenesis of ore stage mineralization in the Betze gold deposit, Goldstrike Mine, Eureka County, Nevada, in Vikre, P., Thompson, T.B., Bettles K., Christensen, O., Parratt, R., eds., *Carlin-type gold deposits field conference: Society of Economic Geologists Guidebook Series v. 28*, p. 75-86.
- Foland, K.A., Hubacher, F.A., and Arehart, G.B., 1992, $^{40}\text{Ar}/^{39}\text{Ar}$ dating of very fine-grained samples: An encapsulated-vial procedure to overcome the problem of ^{39}Ar recoil loss: *Chemical Geology*, v. 102, p. 269-276.
- Folger, H.W., Snee, L.W., Mehnert, H.H., and Hofstra, A.H., 1996, Significance of K-Ar and $^{40}\text{Ar}/^{39}\text{Ar}$ dates from mica in Carlin-type gold deposits: Evidence from the Jerritt Canyon District, Nevada, in Coyner, A.R., and Fahey, P.L., eds., *Geology and Ore Deposits of the American Cordillera: Geological Society of Nevada Symposium Proceedings, Reno/Sparks, Nevada, April 1995*, p. 41-60.
- Groff, J.A., Heizler, M.T., McIntosh, W.C., and Norman, D.I., 1997, $^{40}\text{Ar}/^{39}\text{Ar}$ dating and mineral paragenesis for Carlin-type gold deposits along the Getchell Trend, Nevada: Evidence for Cretaceous and Tertiary gold mineralization: *Economic Geology*, v. 92, p. 601-622.
- Hall, C.M., Kesler, S.E., Simon, G., 1997, Ar dating micro-sampling techniques applied to problems in economic geology: *Geological Society of America Abstracts with Programs*, v. 29, no. 6, p. 51.
- Hamilton, P.J., Kelley, S., and Fallick A.E., 1989, K-Ar dating in hydrocarbon reservoirs: *Clay Minerals*, no. 24, p. 215-231.
- Hassanipak, A.A. and Wampler, J.M., 1996, Radiogenic argon released by stepwise heating of glauconite and illite: The influence of composition and particle size: *Clays and Clay Minerals*, v. 44, no. 6, p. 717-726.
- Hofstra, A.H., 1994, *Geology and genesis of the Carlin-type gold deposits in the Jerritt Canyon district, Nevada: Boulder, Colorado, University of Colorado, Ph.D. dissertation*, 719 p.
- Hunziker, J.C., 1986, The evolution of illite to muscovite: An example of the behavior of isotopes in low-grade metamorphic terrains: *Chemical Geology*, v. 57, p. 31-40.
- Kisch, H.J., 1990, Calibration of the anchizone: A critical comparison of illite "crystallinity" scales used for definition: *Journal of Metamorphic Geology*, v. 8, p. 31-46.
- Kübler, B., 1964, Les argiles, indicateurs de metamorphisme: *Revue de l'Institut Français des Petroles*, v. 19, p. 1093-1112.
- Kuehn, C.A. and Rose, A.W., 1992, Geology and geochemistry of wall-rock alteration at the Carlin gold deposit, Nevada: *Economic Geology*, v. 87, no.7, p. 1697-1720.
- Maher, B. J., Browne, Q. J., and McKee, E. H., 1993, Constraints on the age of gold mineralization and metallogenesis in the Battle Mountain-Eureka mineral belt, Nevada: *Economic Geology*, v. 88, p. 469-478.
- McDougall, I., and Harrison, T.M., 1988, *Geochronology and thermochronology by the $^{40}\text{Ar}/^{39}\text{Ar}$ method: Oxford Monographs on Geology and Geophysics*, no. 9, 212 p.
- Moore, D.M. and Reynolds, R.C. Jr., 1989, *X-ray diffraction and the identification and analysis of clay minerals: Oxford University Press*, 332 p.
- Mullens, T.E., 1980, *Stratigraphy, petrology, and some fossil data of the Roberts Mountains Formation, north-central Nevada: U.S. Geological Survey Professional Paper 1063*, 67 p.
- Murochick, J.B., 1992, Marcasite inversion and petrographic determination of pyrite ancestry: *Economic Geology*, v. 87, p. 1141-1152.
- Nevada Bureau of Mines and Geology, 1996, *The Nevada Mineral Industry: Special Publication MI-1995*, 54 p.
- Phinisey, J.D., Hofstra, A.H., Snee, L.W., Roberts, T.T, Dahl, A.R., and Longanger, R.J., 1996, Evidence for multiple episodes of igneous and hydrothermal activity and constraints on the timing of gold mineralization, Jerritt Canyon district, Elko County, Nevada in Coyner, A.R., and Fahey, P.L., eds., *Geology and Ore Deposits of the American Cordillera: Geological Society of Nevada Symposium Proceedings, Reno/Sparks, Nevada, April 1995*, p. 15-39.
- Wilson, P.N., and Parry, W.T., 1995, Characterization and dating of argillic alteration in the Mercur gold district, Utah: *Economic Geology*, v. 90, p. 1197-1216.

δD and $\delta^{18}O$ DATA FROM CARLIN-TYPE GOLD DEPOSITS- IMPLICATIONS FOR GENETIC MODELS

By Albert H. Hofstra *and* Robert O. Rye

ABSTRACT

δD and $\delta^{18}O$ data from quartz, clays, and inclusion fluids were used to characterize the isotopic composition of water in ore fluids. The hydrothermal fluids that formed most Carlin-type gold deposits had low δD_{H_2O} values (-116 to -164‰) and a wide range of $\delta^{18}O_{H_2O}$ values (-20 to 15‰) suggesting that ore fluids consisted of variably exchanged meteoric water. In contrast, fluids from Carlin-type deposits in the Getchell Trend had a much wider range of δD_{H_2O} values (-153 to -44‰) but a similar range of $\delta^{18}O_{H_2O}$ values suggesting that ore fluids were magmatic or metamorphic in origin, although variably exchanged meteoric water was also present.

The δD_{H_2O} variation of meteoric water in this region over the past 170 Ma provides a means to discriminate between the various ages proposed for the deposits. The unusually low δD_{H_2O} values of the hydrothermal fluids agree with the δD_{H_2O} values of meteoric water in the mid-Tertiary (42 to 30 Ma) when the climate was cool, but are lower than those of meteoric water in the Late Jurassic and Cretaceous when the climate was warm.

The data suggest that Carlin-type deposits formed in the mid-Tertiary soon after the onset of extension and magmatism in northern Nevada and northwest Utah. The increased permeability and high heat flow in this setting may have provided the drive for deep circulation of meteoric water and development of Carlin-type deposits in fracture systems that focused fluid flow. In the Getchell Trend, these structures may have tapped metamorphic fluids generated in the middle crust or magmatic fluids released from deep intrusions or batholiths.

INTRODUCTION

This report is adapted from information in Hofstra and others (in review). The goal of this report is to use δD and $\delta^{18}O$ data from Carlin-type gold deposits to identify the source(s) of water in the ore fluids. This information is important because it can improve genetic models and constrain the age of the deposits. The age information results from temporal variations in the isotopic composition of meteoric water in response to changes in climate. Included in this report are new and previously published isotopic data from the Jerritt

Canyon, Post/Betze, Carlin, Cortez, Gold Pick, Getchell, Twin Creeks, Alligator Ridge, and Mercur mines (Appendix A). The isotopic data are from quartz, clays, and inclusion fluids extracted from a variety of ore stage minerals.

Three different models have been proposed for the deposits with ore fluids derived from different sources: (1) the magmatic or distal-disseminated model where the deposits form from magmatic fluids in the distal parts of porphyry systems; (2) the meteoric water circulation model where the deposits form from rain water that evolved to become an ore fluid by deep circulation through sedimentary rocks; and (3) the metamorphic or shallow mesothermal vein model where the deposits form from metamorphic fluids expelled from shear zones at depth. Combinations of these end member models are also possible. It is important to point out that in each of these models a fluid from deeper levels displaces the local meteoric ground water at the sites of mineral precipitation. Therefore some of the isotopic data from each deposit is likely to reflect the isotopic composition of meteoric water at the time of mineralization.

ISOTOPIC CONSTRAINTS ON FLUID SOURCES

Figure 1 shows the δD and $\delta^{18}O$ values of water in Carlin-type ore fluids relative to some traditional references (see fig. 1 and Appendix A for sources of data). Fluids from most Carlin-type deposits have low hydrogen isotope values (< -116‰) and a wide range of oxygen isotope values that extend well away from the meteoric water line (fig.1). Variations in the temperature of deposition can only account for part of this range. The water-rock exchange curve shows how the isotopic composition of meteoric water would vary by progressive exchange with shaley marine limestones at a temperature of 300°C. The jasperoids with high $\delta^{18}O$ values can be explained if they precipitated from exchanged meteoric water that evolved by deep circulation through sedimentary rocks at elevated temperatures and low water-rock ratios. Jasperoids with low $\delta^{18}O$ values are representative of the relatively unexchanged meteoric ground water in the host rocks. At Jerritt Canyon, the jasperoids with the highest oxygen isotope values contain the most gold (fig. 1) suggesting that

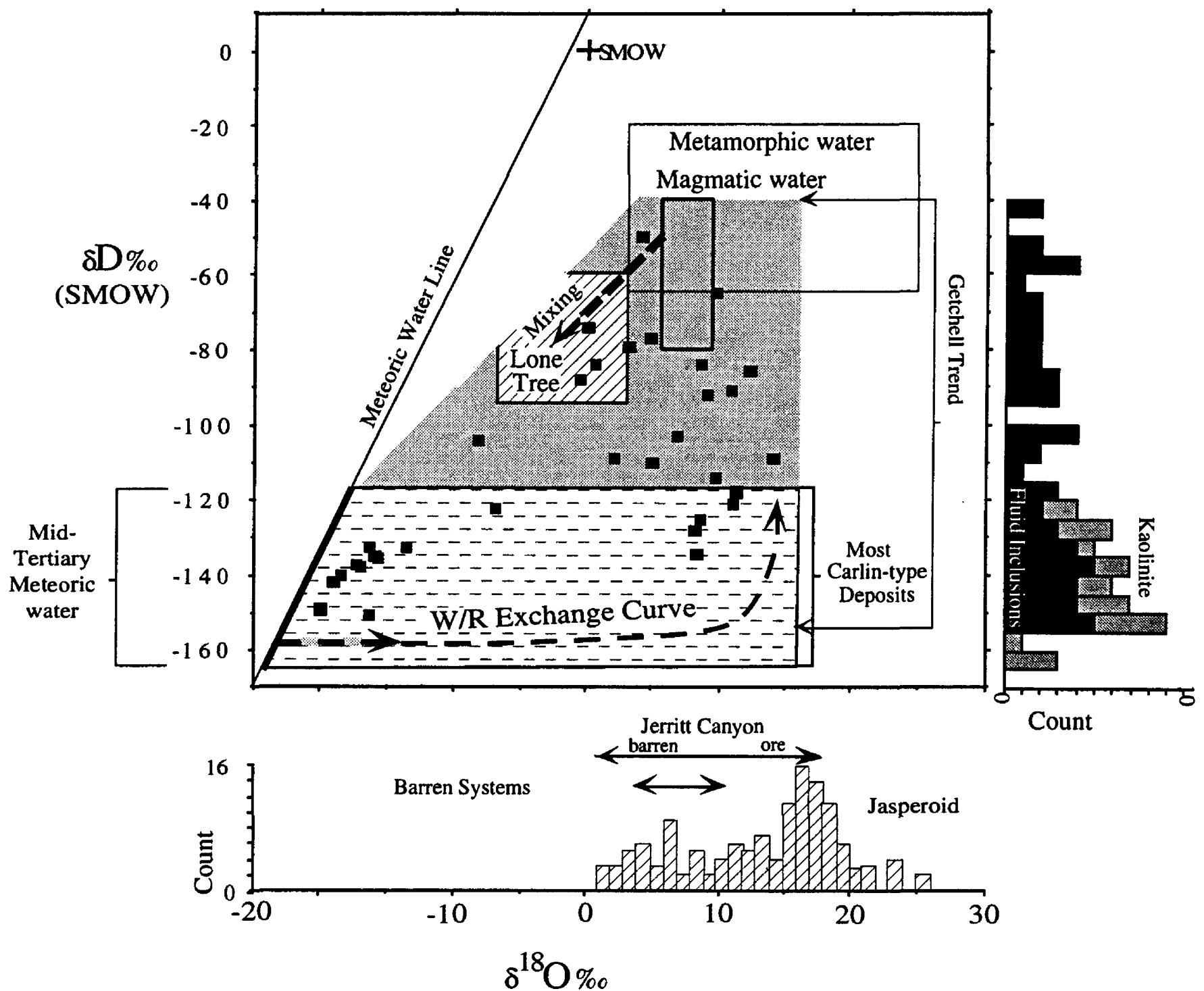


Figure 1. δD and $\delta^{18}O$ data from Carlin-type gold deposits. The black squares are samples for which there is both oxygen and hydrogen isotopic data. $\delta^{18}O$ data from jasperoids are shown on the x-axis (data from Hofstra, 1994; Ilchik, 1990; Holland and others, 1988; Radtke and others, 1980; Groff, 1996) and δD data from water in fluid inclusions and kaolinite are shown on the y-axis (see Appendix A for sources of data). The triangular field shows the calculated range of fluid compositions required by this data. Isotopic data from Lone Tree (diagonal rule pattern), a distal disseminated gold deposit, is shown for comparison (Howe and others, 1995; this study). See text for further description.

gold was transported by the isotopically exchanged fluid (Northrop and others, 1987; Hofstra and others, 1988). This observation is supported by evidence that jasperoids from barren systems (fig. 1) have low $\delta^{18}O$ compositions (Holland and others, 1988). Therefore, the large range of $\delta^{18}O$ values most likely reflects mixing between highly exchanged ore fluids and unexchanged meteoric ground water. Although it is possible that contributions from deep sources are present in these deposits and that the signal is masked by an overwhelming amount of meteoric water, there is a significant amount of data from Jerritt Canyon, Carlin, and Alligator Ridge that suggests the ore fluids consisted of exchanged meteoric water.

In contrast, samples from the Carlin-type deposits in the Gatchell Trend have a much wider range of δD values (fig. 1) that extend from -153 to -44 ‰ but a similar range of $\delta^{18}O$ values (Cline and others, 1996, 1997; Groff, 1996). Samples representative of the main stage of gold mineralization have the highest δD values suggesting that gold was introduced by a magmatic or metamorphic fluid. The triangular range of values suggests that the deep sourced ore fluid mixed with both unexchanged meteoric water and exchanged meteoric water. Despite the evidence for a deep fluid source, the mineralogy, alteration, and geochemical signature of the deposits in the Gatchell Trend are remarkably similar to Carlin-type deposits in the other districts. The most notable difference

is the presence of small amounts of fluorite and adularia.

The Lone Tree deposit has a number of features that distinguish it from classic Carlin-type gold deposits and it is considered to be a distal disseminated deposit (Doebrich and Theodore, 1996). For example, it is located about 10-15 km northwest of a group of mid-Tertiary porphyry systems in the Battle Mountain district and is younger than a 36.4 to 39.4 Ma rhyolite porphyry dike (Doebrich and others, 1995). It differs from most Carlin-type deposits in that most of the pyrite fills fractures rather than occurring as fine disseminations. It also contains traces of base metal sulfides and its Au/Ag ratios are lower than those in most Carlin type deposits. Mass transfer studies show that Fe was introduced rather than being immobile as in Carlin-types (this study). The introduction of iron suggests the presence of acidic, saline fluids and is consistent with the argillic alteration in the deposit and presence of halite daughter minerals in fluid inclusions (Kamali, 1996). The $\delta^{34}\text{S}$ systematics are also quite different from those typically found in Carlin-type deposits with bulk sulfur near 0‰ (Howe and others, 1995; Hofstra, 1997). The δD and $\delta^{18}\text{O}$ values of fluid inclusions in barite (Howe and others, 1995; this study) approach that of magmatic water (fig. 1). Collectively, this information suggests that gold was introduced by magmatic fluids.

In summary, the stable isotopic data from most Carlin-type deposits are consistent with the meteoric water circulation model, whereas, the data from the Getchell Trend are more consistent with the magmatic or metamorphic fluid models. The evidence from Lone Tree suggests that it formed from magmatic fluids, although it has a number of characteristics that distinguish it from most Carlin-type deposits. An important question then is whether deep sourced magmatic or metamorphic fluids are required to form Carlin-type deposits or whether the deposits in the Getchell Trend are unusual. Our current research is aimed at evaluating this possibility in other districts.

AGE CONTROVERSY

The age of Carlin-type deposits has been the subject of major debate and a variety of ages have been reported that range from the Late Jurassic to the Middle Tertiary (Emsbo and others, 1996; Hofstra, 1994, 1995; Hofstra and others, in review; Phinisey and others, 1996; Maher, and others, 1993; Silberman and others, 1974; Berger and others, 1975; Arehart and others, 1993; Wilson and Parry, 1995, 1991; Presnell and Parry 1992; Parry and others, 1997; and Drewes/Armitage and others, 1996). Figure 2 shows that the published ages for the deposits correspond to each of the major periods of magmatism in the region. The Late Jurassic and Cretaceous ages are based mainly on dates from white mica, or sericite, separated from mineralized sedimentary and igneous rocks and the mid-Tertiary ages are based mainly on cross-cutting relationships between gold ore and dated igneous rocks and a few dates on

hydrothermal adularia and apatite. The age controversy revolves around whether one accepts the cross-cutting relationships or the sericite dates. While interpretation of the mid-Tertiary dates is straight forward, the sericitic alteration that is present in the deposits has generally not been shown to be related to the gold systems and in many cases is clearly related to pre-ore events. This is not too surprising given that the gold deposits are located along structural zones that contain intrusive rocks with a variety of ages. Furthermore, Folger and others (1996; this volume) have shown that older fine grained sericite in the host rocks is unlikely to be reset by Carlin-type hydrothermal systems.

δD CONSTRAINTS ON THE AGE OF CARLIN-TYPE DEPOSITS

Several recent studies have shown that the isotopic composition of the oceans and meteoric water on the continents have varied dramatically through time in response to global changes in climate (e.g. Emiliani, 1954, 1966; Savin, 1977; Frakes and others, 1992; Francis and Frakes, 1993; Prothero, 1994; and references therein). The $\delta\text{D}_{\text{H}_2\text{O}}$ variation of meteoric water on the continent provides a means to discriminate between the Mesozoic and mid-Tertiary ages proposed for the deposits. Since the ore fluids in many Carlin-type deposits consist largely of meteoric water, comparisons of the $\delta\text{D}_{\text{H}_2\text{O}}$ values of the fluids with the δD -age record for

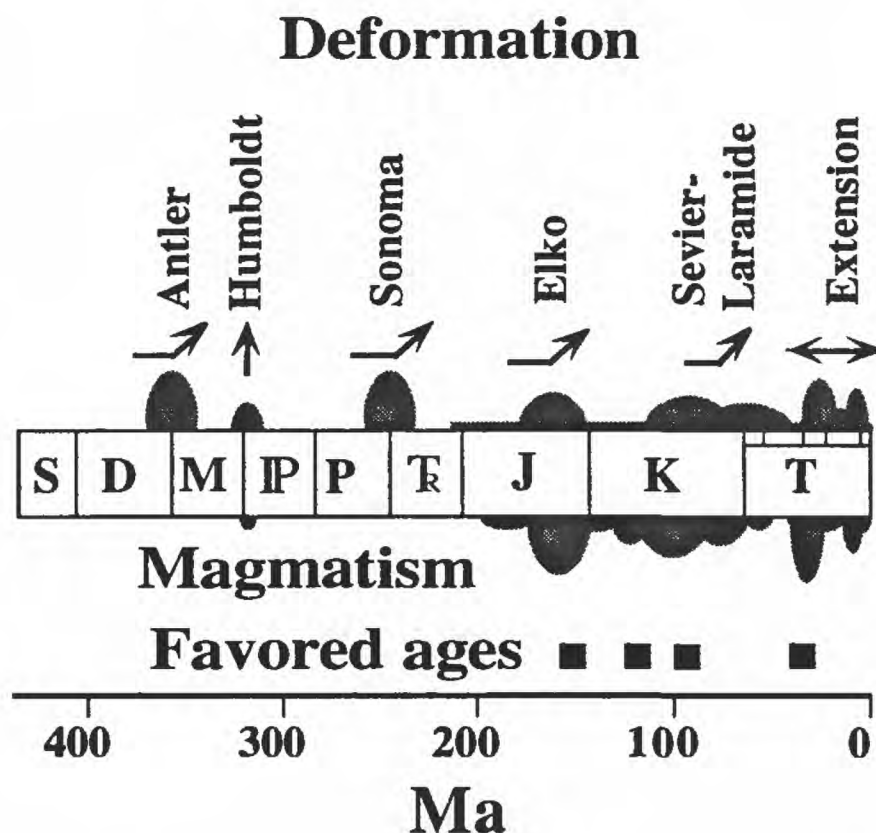


Figure 2. Major episodes of deformation and magmatism in the region and favored ages for Carlin-type gold deposits (Hofstra and others in review).

the region can be used to constrain the age of mineralization.

To date ore deposits from the δD_{H_2O} values of their ore fluids, it is necessary to construct a δD_{H_2O} versus age curve for meteoric water in the region (fig 3). Supergene alunites from the Great Basin provide a fairly continuous record of variations in the δD of meteoric water over the past 30 Ma (Arehart and O'Neil, 1993). Many of these supergene alunites are from Carlin-type gold deposits (Arehart and others, 1992). By combining the supergene alunite δD_{H_2O} -age curve with age and δD_{H_2O} data from older meteoric hydrothermal systems in the region (Appendix A), it is possible to construct a δD_{H_2O} -age curve for the past 170 million years as shown in figure 3. Prior to 170 Ma, this area was largely covered by sea water. The δD_{H_2O} -age curve constructed in this manner clearly shows that the δD of meteoric water in the region varied substantially over the past 170 Ma and that δD_{H_2O} values were lowest at about 30 Ma.

The δD_{H_2O} -age curve is consistent with the environmental factors that existed in the western U.S. over this time period and with global temperature curves. Isotopic patterns observed in continental precipitation today vary as a

function of latitude, elevation, surface air temperature, amount of precipitation, and distance from the coast (Dansgaard, 1964). Each of these parameters affects the average degree of rainout of moisture from a given air mass as it moves from the source regions (mainly subtropical oceans) to the site of precipitation. Although paleolatitudes were as much as 7 degrees further south 150-m.y.-ago, for the past 100 m.y., they have been within 1 or 2 degrees of the present latitude (Lawrence and Meaux, 1993). Atmospheric circulation patterns would therefore have been dominated, as today, by west to east flow. Elevations varied in space and time in response to episodes of orogenic activity (Elko, Sevier, Laramide orogenies) but have probably been highest since the Laramide orogeny. Fossil flora and fauna from the continent suggest that the climate was distinctly warmer in mid-Jurassic to mid-Eocene time (Hallam, 1994; Francis and Frakes, 1993) and that cooler climates have prevailed ever since (Prothero, 1994). Although the western Cordillera (in eastern California and westernmost Nevada) has been an important highland (rainout area) since the mid-Jurassic, the δD of meteoric water ($\delta D > -110$ ‰) in mid-Jurassic to mid Eocene time (fig. 3) is consistent with the

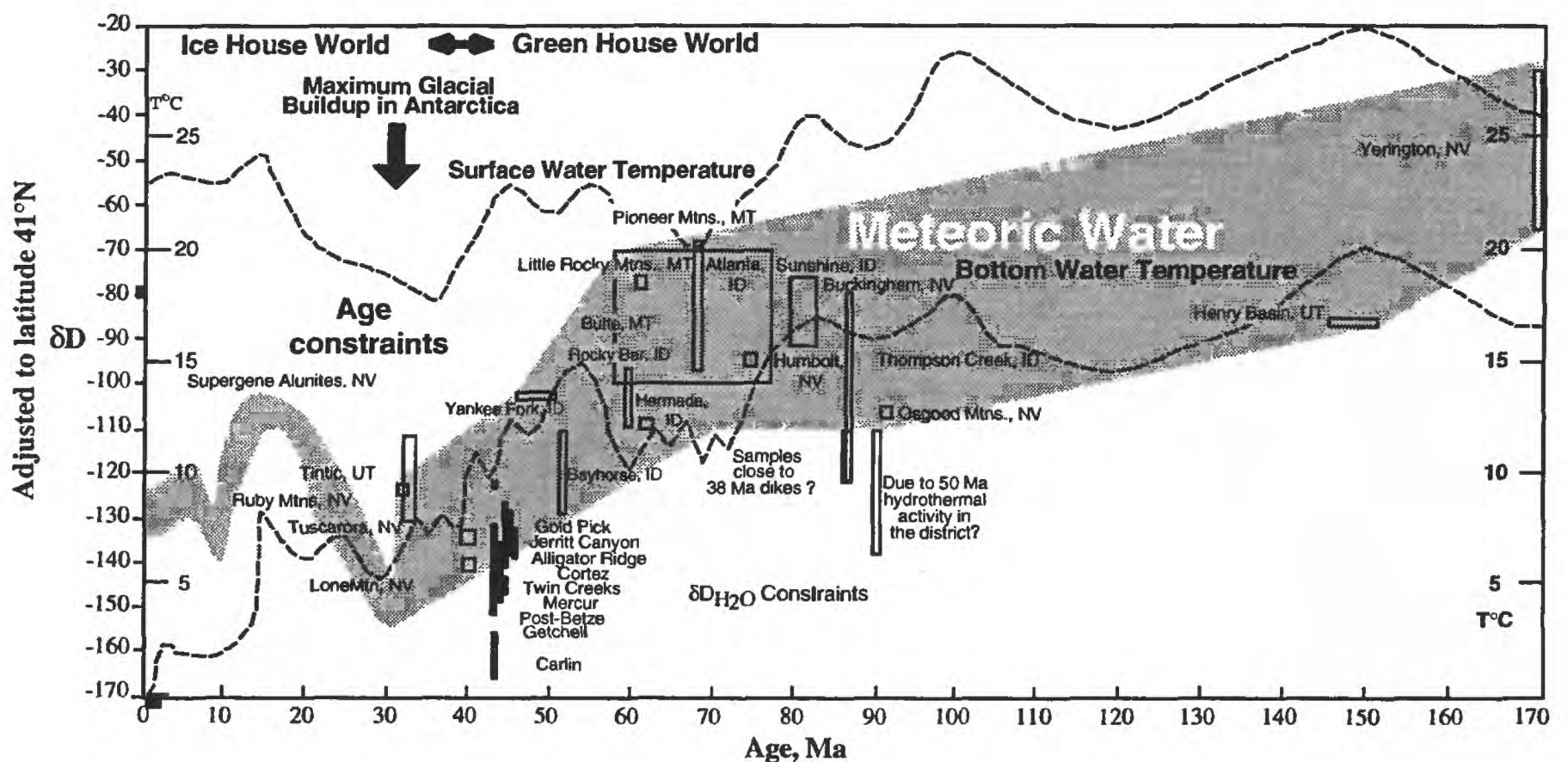


Figure 3. δD -Age curve showing variation in the isotopic composition of meteoric water over the past 170 Ma (constructed from information in Appendix A). The δD_{H_2O} values have been corrected to 41° North Latitude using a correction factor of 5 ‰ per degree latitude to be consistent with the alunite curve of Arehart and O'Neil (1993). In most respects the δD -Age curve agrees with knowledge of paleoclimates (see text). The δD -Age curve also corresponds well with paleotemperature curves for surface water and bottom water in the Pacific ocean (dashed lines) estimated from oxygen isotope analyses of calcareous microfossils (Douglas and Woodruff, 1981). The distinct minimum at about 30 Ma correlates with maximum glacial buildups in Antarctica and the maximum drop in sea level world wide. The unusually low δD_{H_2O} values from Carlin-type deposits (black bars) suggest that they formed near the low in curve when the climate was unusually cool. The δD_{H_2O} values agree well with the mid-Tertiary (42 to 30 Ma) age constraints on the deposits (bold rectangle) but are clearly at odds with the Jurassic and Cretaceous ages favored by some workers when the climate was much warmer. See text for further description. From Hofstra and others, in review.

relatively low elevation, warm climate, and close proximity to western (Pacific Ocean) and eastern (Carmel Sea-Cretaceous seaway) coastlines that characterized much of this period. The δD of meteoric water ($\delta D < -110\text{‰}$) since the mid Eocene is consistent with the higher elevations and cooler climatic conditions.

The δD_{H_2O} -age curve also mimics the global fossil foraminifera $\delta^{18}O$ pattern in the oceans (fig. 3), with relatively large δD_{H_2O} values greater than -110‰ in Jurassic, Cretaceous, and early Tertiary time, when the world was in a "green house" state, and low δD_{H_2O} values of less than -110 and often as low as -140 to -160 in late Eocene and Oligocene time, when the world was in an "ice house" state. Most importantly, the δD_{H_2O} minimum at ~ 30 Ma correlates with maximum glacial buildups in Antarctica and the maximum drop in sea level world wide (Prothero, 1994). Although there are many uncertainties in the data used to construct the δD_{H_2O} -age curve, in most respects the curve is consistent with our knowledge of global temperature variations and environmental factors in the western United States over this time period. It is therefore reasonable to use the curve to estimate the age of Carlin-type deposits.

The δD_{H_2O} values of ore fluids from nine Carlin-type

deposits range from -116 to -164‰ . These values are unusually low for the latitude of the deposits and are generally less than present day meteoric water (fig. 3). For such widely separated deposits to have such similar isotopically light fluids, suggests that they formed at about the same time, near the low in the δD_{H_2O} -age curve (fig. 3), when the climate was unusually cool. Most important, the age estimates obtained from comparison of the ore fluid δD_{H_2O} values with the δD_{H_2O} -age curve agree with the mid-Tertiary (42 to 30 Ma) age constraints on the deposits (Maher and others, 1993; Hofstra, 1994, 1995; Phinsey and others, 1996; Emsbo and others, 1996; Groff et al, 1996; Hall and others, 1997). The low δD_{H_2O} values are clearly at odds with the Cretaceous and Jurassic ages (based on mica dates) favored by many workers (Silberman and others, 1974; Berger and others, 1975; Arehart and others, 1993; Wilson and Parry, 1995, 1991; Presnell and Parry 1992; Drewes-Armitage, 1996; Groff et al, 1996; Parry and others, 1997) when the climate was much warmer.

The paleoclimate results provide compelling evidence that Carlin-type deposits in northern Nevada and northwestern Utah formed during a single metallogenic event in the mid-Tertiary. It is therefore important to consider the geologic setting at this time and the relation of mineralization to tectonics.

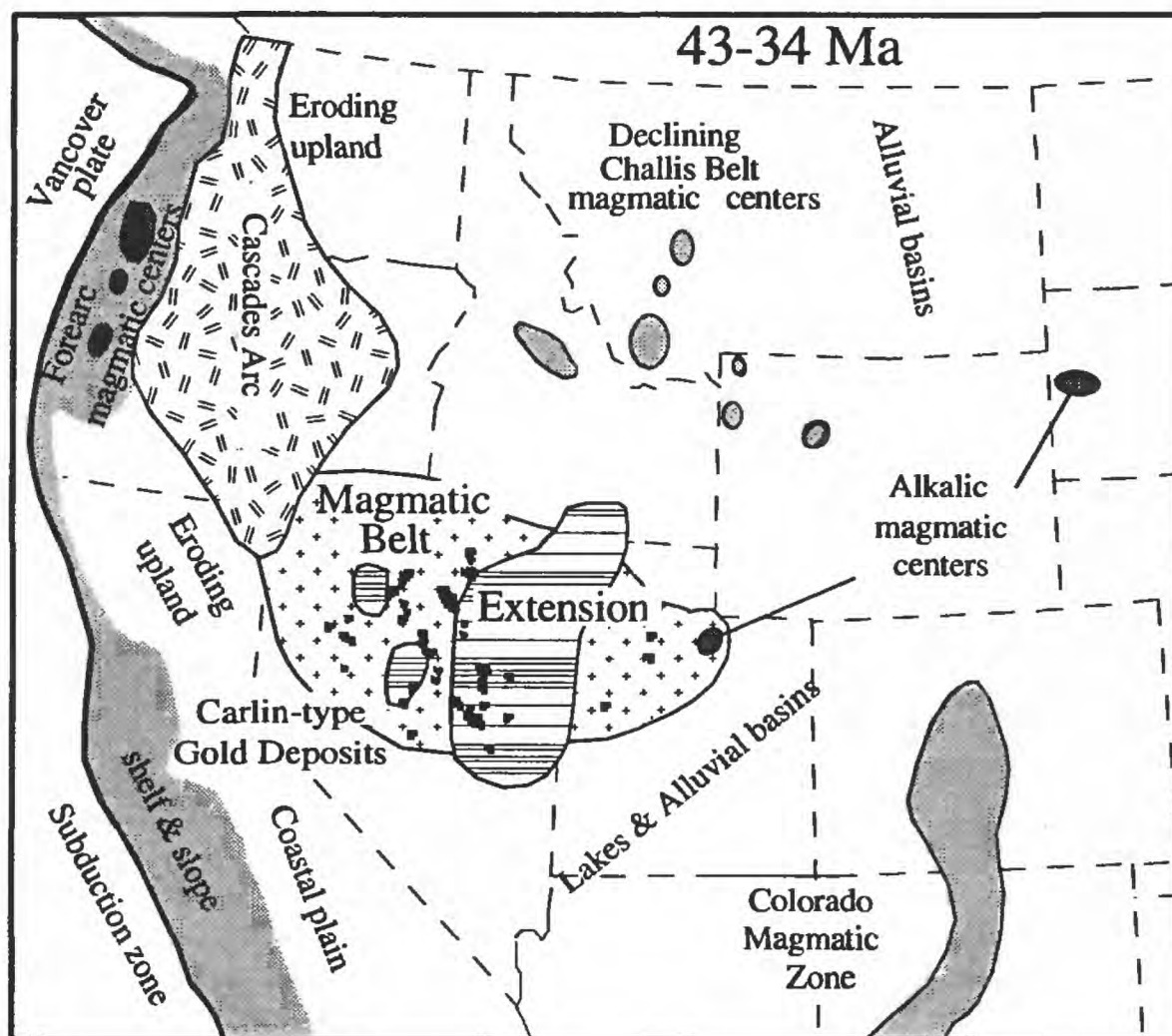


Figure 4. Paleogeography 43 to 34 million years ago showing the distribution of igneous activity, extensional tectonism (horizontal rule), and Carlin-type gold deposits (black dots). The increased permeability and high heat flow in this setting may have provided the drive for deep circulation of meteoric water and development of Carlin-type deposits in fracture systems that focused fluid flow. In the Getchell Trend, these structures may have tapped metamorphic fluids generated in the middle crust or magmatic fluids released from deep intrusions or batholiths. Modified from Christiansen and Yeats (1992).

GEOLOGIC SETTING IN THE MID-TERTIARY

Figure 4 shows the geologic setting in the western United States in the mid-Tertiary. The spatial correlation between Carlin-type deposits and areas undergoing magmatism and extension suggests that the deposits formed soon after the onset of this activity in northern Nevada and northwest Utah. The increased permeability and high heat flow in this setting may have provided the drive for deep circulation of meteoric water and development of Carlin-type deposits in fracture systems that focused fluid flow. In the Getchell Trend, these structures apparently tapped metamorphic fluids generated in the middle crust or magmatic fluids released from deep intrusions or batholiths. The results from Lone Tree indicate that distal disseminated deposits were forming at about the same time as classic Carlin-type deposits. Although gravity and magnetotelluric surveys (Grauch, and others, 1995; Rodriguez, 1997) suggest that deep penetrating structures and igneous intrusions are present below the Carlin Trend and Battle Mountain-Eureka Belt, thus far, there is no isotopic evidence for a deep fluid source in these districts. It is also important to note that Carlin-type deposits have not been recognized in similar tectonic settings to the north and south suggesting that additional factors were critical to their formation. This discussion points out the need for further studies to improve understanding of the source of ore fluid components, age of mineralization, and geologic framework of the deposits; information necessary to establish the relation between gold mineralization and tectonics.

REFERENCES CITED

- Arehart, G.B., Foland, K.A., Naeser, C.W., and Kesler, S.E., 1993, $^{40}\text{Ar}/^{39}\text{Ar}$, K/Ar, and fission track geochronology of sediment-hosted disseminated gold deposits at Post/Betze, Carlin Trend, northeastern Nevada: *Economic Geology*, v. 88, p. 622-646.
- Arehart, G.B. and O'Neil, J.R., 1993, D/H ratios of supergene alunite as an indicator of paleoclimate in continental settings: *Climate Change in Continental Isotopic Records*, Geophysical Monograph 78, p. 277-284.
- Arehart, G.B., Kesler, S.E., O'Neil, J.R., and Foland, K.A., 1992, Evidence for the supergene origin of alunite in sediment-hosted micron gold deposits, Nevada: *Economic Geology*, v. 87, p. 263-270.
- Berger, B.R., Silberman, M.B., and Koski, R.A., 1975, Discussion on K-Ar relations of granodiorite emplacement and tungsten and gold mineralization near the Getchell mine, Humboldt county, Nevada—A reply: *Economic Geology*, v.70, p. 1487-1491.
- Boden, D.R., Struhsacker, E.M., and Wright, W.A., 1993, Volcanism, extension, and contrasting types of mineralization, Tuscarora mining district and vicinity, Nevada: *Geological Society of Nevada*, November Newsletter, 2 pgs.
- Chesley, J.T., 1986, A combined $^{18}\text{O}/^{16}\text{O}$ and D/H isotopic study of molybdenite mineralization at Pear Lake and related areas in the Pioneer Mountains, southwest Montana: Corvallis, Oregon, Oregon State University, M.Sc. thesis, 91 p.
- Christiansen, R. L., and Yeats, R.S., 1992, Post-Laramide geology of the U.S. Cordilleran region, in Burchfiel, B.C., Lipman, P.W., and Zoback, M.L., eds., *The Cordilleran Orogen: Conterminous U.S.*: Boulder, Colorado, Geological Society of America, *The Geology of North America*, v. G-3, pp. 261-406.
- Cline, J.S., Hofstra, A.H., Landis, G.P., and Rye, R.O., 1997, Ore fluids at the Getchell Carlin-type gold deposit, northcentral Nevada, in *Carlin-Type Gold Deposits Field Conference*, Vikre, P., Thompson, T.B., Bettles, K., Christensen, O., and Parratt, R., eds., *Society of Economic Geologist Guidebook Series*, v 28, p. 155-166
- Coats, R.R., 1987, *Geology of Elko county, Nevada*: Nevada Bureau of Mines and Geology, Bulletin 101, 112 p., 1 pl.
- Criss, R.E., Fleck, R.J., and Taylor, H.P., Jr., 1991, Tertiary meteoric hydrothermal systems and their relation to ore deposition, northwestern United States and southern British Columbia: *Journal of Geophysical Research*, v. 96, no. B8, p. 13,335-13,356.
- Dansgaard, W., 1964, Stable isotopes in precipitation: *Tellus*, v 16, p. 436-468.
- Dilles, J.H., Solomon, G.C., Taylor, H.P., Jr., and Einaudi, M.T., 1992, Oxygen and hydrogen isotope characteristics of hydrothermal alteration at the Ann-Mason porphyry copper deposit, Yerington, Nevada: *Economic Geology*, v. 87, p. 44-63.
- Doebrich, J.L., Wotruba, P.R., Theodore, T.G., McGibbon, D.H., and Felder, R.P., 1996, Field Trip H: Geology and ore deposits of the Battle Mountain mining district, in *Geology and Ore Deposits of the American Cordillera Symposium, Field Trip Guidebook Compendium*: Geological Society of Nevada, p. 327-376.
- Doebrich, J.L., and Theodore, T.G., 1996, Geologic history of the Battle Mountain mining district, Nevada, and regional controls on the distribution of mineral systems, in Coyner, A.R and Fahey, P.L., eds., *Geology and Ore Deposits of the American Cordillera: Geological Society of Nevada Symposium proceedings*, Reno/Sparks, Nevada, April 1995, p. 453-483.
- Douglas, R.G., and Woodruff, F., 1981, Deep sea benthic foraminifera, in Emiliani, C., ed., *The Sea*: New York, Wiley Interscience, p.1233-1327.
- Drewes-Armitage, S.P., Romberger, S.B., Whitney, C.G., 1996, Clay alteration and gold deposition in the Genesis and Blue Star deposits, Eureka County, Nevada: *Economic Geology*, v. 91, p. 1383-1393.
- Emiliani, C., 1954, Depth habitats of some species of pelagic foraminifers as indicated by oxygen isotope ratios: *American Journal of Science*, v. 252, p. 149-158.
- Emiliani, C., 1966, Oxygen isotopes, oceanic sediments, and the ice ages: *Transactions-American Geophysical Union*, v. 47, no. 1, 44 p.
- Emsbo, P., Hofstra, A.H., Park, D., Zimmerman, J.M., and Snee, L., 1996, A mid-Tertiary age constraint on alteration and mineralization in igneous dikes on the Goldstrike Property, Carlin Trend, Nevada: *Geological Society of America Abstracts with Programs*, v. 28, no. 7, p. A476.
- Folger, H.W., Snee, L.W., Mehnert, H.H., Hofstra, A.H., and Dahl, A.R., 1996, Significance of K-Ar and $^{40}\text{Ar}/^{39}\text{Ar}$ dates from mica in Carlin-type gold deposits: Evidence from the Jerritt Canyon District, Nevada, in Coyner, A.R., and Fahey, P.L., eds., *Geology*

- and Ore Deposits of the American Cordillera: Geological Society of Nevada Symposium Proceedings, Reno/Sparks, Nevada, April 1995, p. 41-60.
- Folger, H.W., Hofstra, A.H., Snee, L.W., and Eberl, D.D., (this volume), K-Ar and $^{40}\text{Ar}/^{39}\text{Ar}$ dating of illites from Carlin-type gold deposits-Nature of the problem and guidelines for future studies, *in* Tosdal, R.M., ed., Contributions to the gold metallogeny of northern Nevada: U.S. Geological Survey Open-File Report.
- Frakes, L.A., Francis, J.E., and Syktus, J.I., 1992, Climate modes of the Phanerozoic: Cambridge University Press, 271 p.
- Francis, J.E., and Frakes, L.A., 1993, Cretaceous Climates, *in* Wright, V.P., ed., Sedimentology Review, 1: Blackwell Scientific Publications, Oxford, p. 17-30
- Grauch, V.J.S., Jachens, R.C., and Blakely, R.J., 1995, Evidence for a basement feature related to the Cortez disseminated gold trend and implication for regional exploration in Nevada: *Economic Geology*, v. 90, p.203-207.
- Groff, J., 1996, $^{40}\text{Ar}/^{39}\text{Ar}$ geochronology of gold mineralization and origin of auriferous fluids for the Getchell and Twin Creeks mines, Humboldt County, Nevada: Socorro, New Mexico, New Mexico Institute of Mining and Technology, Ph.D. Thesis, 291 p.
- Groff, J.A., Heizler, M.T., McIntosh, W.C., and Norman, D.I., 1996, $^{40}\text{Ar}/^{39}\text{Ar}$ dating and mineral paragenesis for Carlin-type gold deposits along the Getchell Trend, Nevada: Evidence for Cretaceous and Tertiary gold mineralization: *Economic Geology*, v. 92, p. 601-622.
- Hall, C.M., Simon, G., Kesler, S.E., 1997, Age of mineralization at the Twin Creeks SHMG Deposit, Nevada, *in* Vikre, P., Thompson, T.B., Bettles, K., Christensen, O., and Parratt, R., eds., Carlin-Type Gold Deposits Field Conference: Society of Economic Geologists Guidebook Series, v 28, p.151-154.
- Hall, W.E., Schmidt, E.A., Howe, S.S., and Broch, M.J., 1984, The Thompson Creek, Idaho, porphyry molybdenum deposit - An example of a fluorine-deficient molybdenum granodiorite system: Proceedings of the Sixth Quadrennial IAGOD Symposium, E. Schweizerbart'sche Verlagsbuchhandlung, Stuttgart, Germany, p. 349-357.
- Hallam, A., 1994, Jurassic climates as inferred from the sedimentary and fossil record, *in* Allen, J.R.L., Hoskins, B.J., Sellwood, B.W., Spicer, R.A., and Valdes, P.J., eds., Paleoclimates and Their Modeling with Special Reference to the Mesozoic Era: London, Allen, The Royal Society, Chapman and Hall, p. 79-88.
- Hofstra, A. H., Northrop, H.R., Rye, R.O., Landis, G.P., and Birak, D.J., 1988, Origin of sediment-hosted disseminated gold deposits by fluid mixing evidence from jasperoids in the Jerritt Canyon gold district, Nevada, U.S.A.: Bicentennial Gold '88, Oral Programme No. 22, Geological Society of Australia, p. 284-289.
- Hofstra, A.H., 1994, Geology and genesis of the Carlin-type gold deposits in the Jerritt Canyon district, Nevada: Boulder, University of Colorado, Ph.D. Dissertation, 719 p.
- Hofstra, A. H., 1995, Timing and duration of Carlin-type gold mineralization in Nevada and Utah—Relation to back-arc extension and magmatism: Geological Society of America Abstracts with programs, v. 27, no. 6, p. A-329.
- Hofstra, A. H., 1997, Isotopic composition of sulfur in Carlin-type gold deposits: Implications for genetic models, *in* Vikre, P., Thompson, T.B., Bettles, K., Christensen, O., and Parratt, R., eds., Carlin-Type Gold Deposits Field Conference: Society of Economic Geologists Guidebook Series, v 28, p. 119-129.
- Hofstra, A.H., Snee, L.W., Rye, R.O., Folger, H.W., Phinisey, J.D., Naeser, C.W., Stein, H.J., Loranger, R.J., Dahl, A.R., Lewchuk, M., in review, Age constraints on Jerritt Canyon and other Carlin-type gold deposits in the western United States — Relation to mid-Tertiary extension and magmatism: *Economic Geology*.
- Holland, P.T., Beatty, D.W., and Snow, G.G., 1988, Comparative elemental and oxygen isotope geochemistry of jasperoid in the northern Great Basin; evidence for distinctive fluid evolution in gold-producing hydrothermal systems: *Economic Geology*, v. 83, p. 1401-1423.
- Howe, S.S., Theodore, T.G., and Arehart, G.B., 1995, Sulfur and oxygen isotope composition of vein barite from the Marigold mine and surrounding area, north central Nevada: Application to gold exploration: *Geology and Ore Deposits of the American Cordillera, Abstracts with Programs*, p. A39.
- Ilchik, R.P., 1990, Geology and geochemistry of the Vantage gold deposits, Alligator Ridge-Bald Mountain mining district, Nevada: *Economic Geology*, v. 85, p. 50-75.
- Kamali, C., 1996, Characterization of ore fluids at the Lone Tree gold deposit, Humboldt County, Nevada: Socorro, New Mexico, New Mexico Institute of Mining and Technology, MSc. thesis, 137 p.
- Kuehn, C.A., 1989, Studies of disseminated gold deposits near Carlin, Nevada: Evidence for a deep geologic setting of ore formation: Pennsylvania State University, Ph.D Thesis, 395 p.
- Lawrence, J.R. and Meaux, J.R., 1993, The stable isotopic composition of ancient kaolinites in North America: Climate Change in Continental Isotopic Records: Geophysical Monograph 78, American Geophysical Union, p. 249-261.
- Lewis, R.S., 1990, Geology geochemistry and mineral potential of Cretaceous and Tertiary plutons in the eastern part of the Soldier Mountains, Idaho: Corvallis, Oregon, Oregon State University, Ph.D. thesis, 214 p.
- Maher, B. J., Browne, Q. J., and McKee, E. H., 1993, Constraints on the age of gold mineralization and metallogenesis in the Battle Mountain-Eureka mineral belt, Nevada: *Economic Geology*, v. 88, p. 469-478.
- Norman, D.K., Parry, W.T., and Bowman, J.R., 1991, Petrology and geochemistry of propylitic alteration at southwest Tintic, Utah: *Economic Geology*, v. 86, p. 13-228.
- Northrop, H.R., Rye, R.O., Landis, G.P., Lustwerk, R., Jones, M.B., and Daly, W.E., 1987, Sediment-hosted disseminated gold mineralization at Jerritt Canyon, Nevada, V-Stable isotope geochemistry and a model of ore deposition: Geological Society of America, Annual Meeting, Abstracts with programs, v.19, p. 791.
- Northrop, H.R. and Goldhaber, M.B., 1990, Genesis of the Tabular-type vanadium-uranium deposits of the Henry Basin, Utah: *Economic Geology*, v. 85, p. 215-269.
- Nutt, C., 1996, Cretaceous(?) to early Oligocene sedimentary and volcanic rocks at Alligator Ridge, Buck Mountain-Bald Mountain area, central Nevada, *in* Taylor, W.J. and Langrock, H., eds., Cenozoic structure and stratigraphy of central Nevada: 1996 Field Conference Volume, Nevada Petroleum Society Inc., Reno, Nevada, p. 13-18.
- Parry, W.T., Wilson, P.N., Presnell, R., 1997, Clay alteration and age of sediment-hosted disseminated gold deposits in the Fold and

- Thrust Belt, Utah, *in* Vikre, P., Thompson, T.B., Bettles, K., Christensen, O., and Parratt, R., eds., *Carlin-Type Gold Deposits Field Conference: Society of Economic Geologists Guidebook Series*, v 28, p. 185-192.
- Phinisey, J.D., Hofstra, A.H., Snee, L.W., Roberts, T.T., Dahl, A.R., Loranger, R.J., 1996, Evidence for multiple episodes of igneous and hydrothermal activity and constraints on the timing of gold mineralization, Jerritt Canyon District, Elko County, Nevada, *in* Coyner, A.R and Fahey, P.L., eds., *Geology and Ore Deposits of the American Cordillera: Geological Society of Nevada Symposium Proceedings*, Reno/Sparks, Nevada, April 1995, p. 15-39.
- Prothero, D.R., 1994, The Eocene-Oligocene Transition - Paradise Lost, Critical Moments, *in* Bottier, D.J. and Bambach, R.K., eds., *Paleobiology and Earth History Series: New York, Columbia University Press*, 291 p.
- Presnell, R.D., 1992, *Geology and geochemistry of the Barney's Canyon gold deposit, Salt Lake County, Utah*, Salt Lake City, Utah, University of Utah, Ph.D. thesis, 363 p.
- Presnell, R.D. and Parry, W.T., 1992, Argillic alteration at the Barney's Canyon gold deposit, *in* J.R. Wilson ed., *Field Guide to geologic excursions in Utah and adjacent areas of Nevada, Idaho, and Wyoming: Utah Geological Survey and Geological Society of America, Miscellaneous Publication 92-3*, p. 313-318.
- Radtke, A.S., Rye, R.O., and Dickson, F.W., 1980, *Geology and stable isotope studies of the Carlin gold deposit, Nevada: Economic Geology*, v. 75, p. 641-672.
- Rodriguez, B. D., 1997, Deep regional resistivity structure across the Carlin Trend, *in* Vikre, P., Thompson, T.B., Bettles, K., Christensen, O., and Parratt, R., eds., *Carlin-Type Gold Deposits Field Conference: Society of Economic Geologists Guidebook Series*, v. 28, p. 39-45.
- Rye, R.O., Doe, B.R., and Wells, J.D., 1974, Stable isotope and lead isotope study of the Cortez, Nevada, gold deposit and surrounding area: *U.S. Geological Survey Journal of Research*, v. 2, p. 13-23.
- Rytuba, J.J., 1985, Development of disseminated gold deposits of Cortez, Horse Canyon, and Gold Acres, Nevada, at the end stage of caldera-related volcanism: *U.S. Geological Survey Circular* 949, p. 47.
- Savin, S.M., 1977, The history of the Earth's surface temperature during the past 100 million years: *Annual Reviews of Earth and Planetary Science*, v. 5, p. 319-355.
- Seal, R.R., II, and Rye, R.O., 1993, Stable isotope study of fluid inclusions in fluorite from Idaho: Implication for continental climates during the Eocene: *Geology*, v. 21, p. 219-222.
- Shepard, S.M.F., and Taylor, H.P., Jr., 1974, Hydrogen and oxygen isotope evidence for the origins of water in the Boulder Batholith and the Butte ore deposits, Montana: *Economic Geology*, v. 69, p. 9226-946.
- Silberman, M.L., Berger, B.R., Koski, R.A., 1974, K-Ar age relations of granodiorite emplacement and tungsten and gold mineralization near the Getchell Mine, Humboldt county, Nevada: *Economic Geology*, v. 69, p. 646-656.
- Theodore, T.G., Blake, D.W., Loucks, T.A., and Johnson, C.A., 1992, *Geology of the Buckingham stockwork molybdenum deposit and surrounding area, Lander County, Nevada: U.S. Geological Survey Professional Paper 798-D*, 2 pls., 307 p.
- Tilling, R.I., 1973, Boulder Batholith, Montana: A product of two contemporaneous but chemically distinct magma series: *Geological Society of America Bulletin*, v. 84, p. 3879-3900.
- Wilson, M.R. and Kyser, Kurtis, 1988, *Geochemistry of porphyry-hosted Au-Ag deposits in the Little Rocky Mountains, Montana: Economic Geology*, v. 83, p 1329-1346.
- Wilson, P. N. and Parry, W.T., 1990, Mesozoic hydrothermal alteration associated with gold mineralization in the Mercur district, Utah: *Geology*, v. 18, p. 866-869.
- Wilson, P. N. and Parry, W.T., 1995, Characterization and dating of argillic alteration in the Mercur gold district, Utah: *Economic Geology*, v. 90, pp. 1197-1216.
- Wickham, S.M., Peters, M.T., Fricke, H.C., and O'Neil, J.R., 1993, Identification of magmatic and meteoric fluid sources and upward and downward-moving infiltration fronts in a metamorphic core complex: *Geology*, v. 21, p. 81-84.

Appendix A. Age and δD of meteoric water ore fluids in Carlin-type gold deposits and other ore deposit types in the western United States. From Hofstra and others, in review.

Location	Deposit Type	Mineral(s)	Lat.(DMS)	Long.(DMS)	δD H ₂ O, permil	δD H ₂ O, 41°N	AGE (Ma)	REFERENCE(S)
Jerritt Canyon, NV	Carlin-type	Orpiment, realgar, kaolinite	412500	1160000	-129 to -143	-127 to -141	<40.8	this study
Twin Creeks, NV	Carlin-type	realgar	411500	1171000	-145	-144	42.0	Groff, 1996
Getchell, NV	Carlin-type	realgar	411000	1171500	-153 to -129	-152 to -130	?	Cline and others, 1996; Groff, 1996; this study
Post-Betze, NV	Carlin-type	orpiment, realgar	405800	1162230	-135 to -149	-135 to -149	<38.6	Emsbo and others, 1996; Groff, 1996; this study
Carlin, NV	Carlin-type	qtz, cal, bar, kaol	402000	1161000	-139 to -164	-143 to -167	?	Radtke and others, 1980; Kuehn, 1989
Mercur, UT	Carlin-type	calcite	401830	1121215	-144	-147.5	>31.6	Wilson and Parry, 1995; this study
Cortez, NV	Carlin-type	qtz, kaol	401000	1163500	-128 to -135	-132 to -139	>34.8	Rye et al, 1974; Rytuba, 1985; this study
Alligator Ridge, NV	Carlin-type	kaolinite	395000	1153000	-132 to -122	-138 to -128	>35.3	Ilchik, 1990; Nurt, 1996
Gold Pick(Gold Bar), NV	Carlin-type	orp, real	394500	1162200	-116	-122	?	this study
Sunshine mine, ID	Ag vein	quartz	473000	1160400	-118	-86	~80	Hofstra and Snee unpublished data
Little Rocky Mtn mines, MT	Epithermal Au-Ag vein	fluorite	473000	1093000	-110	-77.5	60	Wilson and Kyser, 1988
Butte-Boulder Batholith, MT	Porphyry Cu	sericite, qtz	460000	1123000	-110+ -15	-85±15	57 to 78	Sheppard and Taylor, 1974; Tilling, 1973
Pioneer Mtns, MT	Porphyry Mo	quartz	452500	1130000	-120 to -90	-97.5 to -67.5	67	Chesley, 1986
Bayhorse district, ID	Epithermal F vein	fluorite	442730	1142000	-138±10	-121±10	51	Seal and Rye, 1993
Thompson Creek, Bayhorse dist., ID	Porphyry Mo	quartz	442000	1143500	-108 to -155	-91 to -138	89	Hall and others, 1984
Yankee Fork, So. Idaho Batholith, ID	Epithermal Au-Ag vein	quartz	442000	1144000	-120	-103	44 to 50	Criss and others, 1991; Lewis, 1990
Hermada, So. Idaho Batholith, ID	Epithermal Sb vein	sericite	440000	1150000	-124	-109	61	Criss and others, 1991; Snee unpublished data
Atlanta, So. Idaho Batholith, ID	Epithermal Au-Ag vein	sericite	434700	1150800	-123 to -87	-109 to -73	69	Criss and others, 1991; Snee unpublished data
Rocky Bar, So. Idaho Batholith, ID	Epithermal Au-Ag vein	qtz, sericite	434100	1151800	-124 to -114 qtz	-110 to -96	58	Criss and others, 1991; Snee unpublished data
Tuscarora, NV	Epithermal Au-Ag vein	quartz	411845	1161330	-134	-135.5	39	Snee unpublished data this study, Boden et al, 1993
Osgood Mtns, NV	Skarn and vein	quartz	411000	1171500	-107	-107	92	Taylor, 1976; Silberman and others, 1974
Lone Mountain, NV	Skarn and vein	quartz	410730	1165900	-140	-139	38	this study; Coats, 1987
Ruby Mtns, E Humboldt Range, NV	Core Complex	biotite	405000	1150500	-110 to -130	-111 to -131	> -32	Wickham and others, 1993 and refs. therein
Humbolt, NV	Epithermal Au-Ag	adularia	404000	1181500	-95	-97	73	O'Neil and Silberman, 1974
Buckingham, NV	Porphyry Mo	quartz	403615	1170300	-118 to -77	-120 to -79	86	Theodore and others, 1992
Tintic, UT	Epithermal Au-Ag vein	quartz	402000	1123500	-120	-123	~32	Norman and others, 1991
Yerington, NV	Porphyry Cu	sericite, chlorite	385800	1191500	-20 to -55	-30 to -65	169	Dilles and others, 1992
Henry Basin, UT	Sandstone U	chlorite, smectite	375500	1103000	-71	-86	150 to 144	

DMS-degrees, minutes, seconds

GEOCHEMICAL MODELING OF ALTERATION AND GOLD DEPOSITION AT THE BETZE DEPOSIT, EUREKA COUNTY, NEVADA

By M. B. Woitsekhovskaya and S. G. Peters

ABSTRACT

This study addresses ore-forming hydrothermal processes via geochemical modeling of the alteration and gold deposition in the Betze gold deposit. This deposit, located along the Carlin trend, is the largest of many Carlin-type deposits in Nevada.

The modeled ore-forming system is considered to be analogous to the natural depositional environment in the Betze gold deposit. This model was constrained by the results of geological, mineralogical, isotope and fluid inclusion studies of the deposit. Computer simulations include interaction of a CO₂-H₂S-NaCl ore fluid with the calcareous host rock, as the ore-forming system cools. The ore fluid transported gold, arsenic, antimony and other components from below the accessible Carlin system.

The major features of the alteration pattern observed in the deposit are produced from the model ore fluid by reaction with limestone of the Popovich Formation. Results indicated that the mineral stability relations in the CaO-MgO-CO₂-Al₂O₃-SiO₂-H₂O system are important and are reflected in the distribution of mineral phases in the alteration pattern. Mass transfer was accompanied by sulfidation of reactive iron in the system resulting in the higher hydrogen, lower aqueous sulfide activity, subsequent destabilization of H₃AsO₃ and Au(HS)₂⁻ complexes, and gold precipitation in association with As-rich pyrite.

The results of modeling provide data on the associated alteration patterns, geochemical controls and gold depositional mechanism in the Betze deposit. This study results in a better understanding of an evolving ore-forming system in the Betze deposit, and also broadens our knowledge of hydrothermal processes in other gold-producing terranes.

INTRODUCTION

Understanding the chemical evolution of metal-bearing hydrothermal fluids and metal-concentrating mechanisms is instrumental to our knowledge of ore formation. Much of the debate over the origin and character of sediment-hosted disseminated gold deposits centers on problems associated with the source(s) of the gold and other ore components, the chemistry of metal-bearing fluid(s) and the depositional mechanism(s), all of which are complicated by multiple

periods of tectonic, hydrothermal and metasomatic activities (Sillitoe and Bonham, 1990; Alvarez and Noble, 1988; Hofstra and others, 1988, 1991; Berry, 1992; Christensen, 1993; Volk and Lauha, 1993; Ilchick and Barton, 1996; Volk and others, 1996; Christensen, 1996). Descriptions can fuel speculation as to the genesis of ore deposits; however, descriptive models by themselves do not provide numerical insight into the geochemical processes that lead to the formation of ore deposits. Descriptive models are further limited because they cannot be tested, nor can they generate alternative models or utilize the nuances of alternative geological environments. The process models and mechanisms responsible for precipitation of gold and the chemical evolution of Carlin-type systems have been discussed by Hofstra and others (1991) and Ilchik and Barton (1996).

The purpose of our study was twofold: (1) to test, *via* numerical modeling, the generalized ore depositional processes outlined by previous researchers, and (2) to provide illustration of the computational methodology and its applications to understanding gold deposition in the Betze deposit. This study focuses on reconstruction of the chemical reactions associated with alteration and ore deposition. At present, our treatment is intended as an introduction to and an overview of the manifold ore depositional problems present in this large and complex deposit.

The modeling procedure presented in this paper represents an extension of the computational methodology developed in studies by Hemley and Woitsekhovskaya (1993), and Woitsekhovskaya and Hemley (1995). Preliminary geochemical modeling of the deposit is based on descriptive studies of the Betze deposit conducted by several workers (Bettles, 1991; Bettles and Lauha, 1991; Berry, 1992; Arehart and others, 1993a; Peters, 1996; Ferdock and others, 1997; Peters and others, 1997).

DESCRIPTION OF THE BETZE GOLD DEPOSIT

The Betze gold deposit is located along the Carlin trend in northeastern Nevada and exhibits mineralogical and alteration features typical for most Carlin-type gold deposits. The deposit is hosted in the upper units of the Devonian and Silurian Roberts Mountains Formation, the Devonian Popovich

Formation, and the lower parts of the Devonian Rodeo Creek unit, all of which are para-autochthonous, and are in contact with the northeast margin of the Jurassic Goldstrike diorite stock (Lauha and Bettles, 1993). The Betze deposit contains over 30 million oz Au representing the largest concentration of gold currently known in the Western Hemisphere (Leonardson and Rahn, 1996).

Previous workers documented the pre-ore and syn-ore stages of hydrothermal activity and the final post-ore and weathering stages that formed the Betze deposit (Arehart and others, 1993; Ferdock and others, 1997). The mineral paragenesis in Betze can be summarized as follows: (1) the main hydrothermal stage of gold mineralization is characterized by the formation of clay minerals (illite, kaolinite, and minor smectite), quartz, pyrite, gold, calcite, dolomite, As-rich pyrite, arsenopyrite and rare native arsenic, and (2) the late paragenetic sequence is characterized by formation of quartz, calcite, realgar, orpiment, stibnite, and barite.

Gold resides predominantly within As-rich overgrowths on pyrite (Arehart and others, 1993a). The intimate association of sub-micron size "invisible" gold with As-rich pyrite is a characteristic feature of Carlin-type deposits, and has been the subject of many studies (Bakken and Einaudi, 1986; Bakken and others, 1991; Arehart and others, 1993a; Sha, 1993; Fleet and Mumin, 1997). Several workers reported that gold in Carlin-type deposits might also be associated with other sulfide minerals including chalcopyrite, sphalerite and cinnabar (Wells and Mullens, 1973; Bakken and Einaudi, 1986), as well as with quartz, carbonate minerals, and clay minerals (Hausen and Kerr, 1968; Drews-Armitage and others, 1996). Understanding the mineral association of hypogene gold in ores in the Betze deposit is crucial, because it helps to constrain fluid chemistry and depositional mechanisms. The most common and economically important minerals in Betze are considered in modeling calculations, although there are many other minor minerals that are found only locally.

A complex interplay between: (1) proximity to the Jurassic Goldstrike stock; (2) degree of fracturing and brecciation that are related to Mesozoic and Tertiary high to low-angle faults; and (3) favorable permeable calcareous stratigraphic units in the Paleozoic host rocks results in variation in the type of gold occurrences, paragenetic interpretations, and alteration patterns in the Betze deposit (Bettles, 1989; Bettles and Lauha, 1991; Lauha and Bettles, 1993; Madeisky, 1993; Peters, 1996; Ferdock and others, 1997). Alteration is similar to that of other sediment-hosted disseminated gold deposits (Radtke, 1985; Bakken and Einaudi, 1986; Kuehn, 1989). It varies from negligible to intense in and between orebodies, and has resulted in decarbonatization, silicification and argillization of individual carbonate beds of the Popovich Formation and the upper Roberts Mountains Formation (Leonardson and Rahn, 1996; Arehart, 1996; Teal and Jackson, 1997).

Temporal and spatial relations between alteration types are poorly understood, although it is well documented that the majority of the ore is present in decarbonatized and weakly to moderately silicified rocks. Most of the gold ore is associated with the decarbonatized host rocks that constitute the most pervasive and intense alteration zones in the Betze deposit. The documented alteration assemblages that sequentially developed during decarbonatization are summarized in the following order (Leonardson and Rahn, 1996; Arehart, 1996; Teal and Jackson, 1997):

fresh carbonate rocks:

calcite+dolomite+kaolinite+pyrite±illite±quartz±carbon;

weak to moderate decalcification:

dolomite+quartz+kaolinite±As-rich

pyrite±illite±calcite±gold±carbon;

intensive decalcification:

kaolinite+pyrite±quartz±dolomite±carbon;

decarbonatization:

kaolinite+pyrite±quartz±carbon.

GEOCHEMICAL CONSTRAINTS ON FLUID CHEMISTRY

The geochemical constraints used herein were based on stable isotope, fluid inclusion, and field studies for Betze and other Carlin-type deposits as documented by previous researchers (Kuehn, 1989; Hofstra and others, 1991; Arehart and others (1993), Kuehn and Rose, 1995; Lamb, 1995; Arehart, 1996; Ilchik and Barton, 1997; Lamb and Cline, 1997). Available fluid inclusion data for the Betze deposit are summarized in table 1. These data suggest that the ore fluid associated with the main stage of gold mineralization contained high density CO₂ (0.86 to 0.78 gm/cm³) and was of moderate to low salinity (10 wt. percent NaCl equivalent). The trapping pressures of the fluid inclusions were 1,000 to 1,425 bars. This mineralization stage took place at minimum temperatures from 210° to 200° C. In contrast, the late stage mineralization resulted in silicification of host rocks and took place at lower temperatures (from 180° to 150° C) and lower salinity. Stable isotope studies by Hofstra and others (1991), and Arehart and others (1993) document a wide range of the stable isotope values [$\delta^{34}\text{S}$ = -30 to +20 per mil (sulfides); $\delta^{18}\text{O}$ values ranging from 0 to +5 per mil (altered rocks) and values of +18 to +24 per mil (unaltered rocks); δD values near -150 per mil; and $\delta^{13}\text{C}$ values -2 to +1 per mil], suggesting that two different fluids were involved in the gold ore-forming episode. The sulfur isotope data for sulfide minerals and barite are evidence for disequilibrium between reduced and oxidized sulfur species in solution. The wide range in sulfur isotopic composition also may reflect compositional variations of sources and variations due to isotopic exchange in the hydrothermal system.

MODELING APPROACH

The alteration mineral assemblages, their paragenetic sequence, and fluid inclusion data (table 1) indicate two major gold mineralization stages, and also indicate that each stage of mineralization took place under different geological conditions. Two sets of modeling calculations were, therefore, required. The first set of calculations involved reaction of ore fluid (table 2) with fresh rock (FR11 on table 3) at the higher temperature and pressure conditions representative of the decarbonation process and the main stage of mineralization (table 1). The second run of calculations involved reaction of the ore fluid with altered rocks at lower temperature and pressure conditions representative of the silicification process and the later event of hydrothermal activity (table 1). To model the later mineralization stage, the alteration mineral assemblages from the first run were used to simulate reaction with the ore fluid, which was similar to that indicated in table 2.

Field studies indicate that advective transport of chemical components by hydrothermal fluid(s) influenced the chemical processes of gold emplacement in the depositional environment. For example, higher gold grades are often associated with multi-increment deformation such as described by Bettles (1989), exhibiting the intense fluid-rock interactions that enhanced gold removal from the hydrothermal fluid. This study focused on modeling of these fluid-rock interactions as the system cooled, that resulted in mineral precipitation and development of alteration patterns in the Betze deposit. Boiling and fluid mixing were not modeled, because fluid inclusion and mineralogical studies do not provide significant evidence of the boiling process, and because fluid mixing alone cannot account for the observed mineral assemblages and alteration patterns.

The preliminary model of the fluid-rock interaction during cooling is discussed below and emphasizes three important controls on the mineral assemblages produced: (1) temperature, (2) pH, and (3) changes in aqueous silica activity. Although other controls also are important, such as the role of thermochemical sulfate reduction reactions, carbonate dissolution reactions, metal transport concentrations, salinity, and pressure or pH buffered conditions, the selected example

provides adequate illustration of the methodology and its application to understanding of gold deposition during alteration in the Betze deposit.

COMPUTATIONAL PROCEDURE

To model fluid-rock interaction in a geological and geochemical context, a polythermal-polybaric reaction path and thermodynamically open system was required. The modeled system was constructed utilizing a series of chemical "reactors" that simulate chemical mass transfer driven by successive interactions between "flowing" fluid and discrete increments of host rock under temperature gradients. Chemical reactors are the individual parts of the modeled system, which are linked by carrying the dissolved constituent materials from one reactor to each successive reactor with the deposited minerals left behind. Phase relations among hydrothermal minerals in the system are calculated on the basis of the change in the chemical potential of a component and its activity during a geochemical process where ξ is the progress variable for the process (De Donder, 1920; Helgeson, 1968). This methodology implies an examination of geochemical processes in a dynamic open hydrothermal system over a range of environmental constraints. It has been used to model different ore-forming processes (Woitsekhowskaya, 1992; Woitsekhowskaya and others, 1992; Woitsekhowskaya and others, unpublished data, 1997). Some aspects of the "flowing through reactors" computational methodology were developed by Krajnov and others (1988).

The computer software used was the HCh program of Shvarov (1976), which includes the GIBBS code and the UNITHERM database of thermodynamic properties of minerals, aqueous species and gases (see also Krajnov and others, 1988). The GIBBS code is based on the minimization of Gibbs free energy and has been developed for simulation of equilibrium states among gaseous-solid-aqueous phases in homogeneous or heterogeneous systems in the temperature range 0° to 1,000° C and pressure range 1 to 5,000 bars. The GIBBS program treats the overall water-rock-gas interaction as the summary of many simpler processes (dissolution of a single mineral, formation of a single aqueous complex, etc.).

Table 1. Summary of fluid characteristics of two successive stages of gold mineralization in the Betze deposit*

Fluid characteristics	Main gold event	Late gold event
Pressure total (bars)	1,425 - 1,000	1,235 - 750
Salinity (wt.% NaCl equivalent)	≤10.0	3.0 - 0.1
Temperature (°C)	210 - 200	180 - 150
Density of bulk CO ₂ (gm/cm ³)	0.86 - 0.78	0.86 - 0.78

*Value adapted from Lamb, 1995; Kuehn and Rose, 1995; Lamb and Cline, 1997.

The database UNITHERM (Shvarov and others, unpublished data, 1997) is substantially similar to SUPCRT92 (Johnson and others, 1992), but is not cited extensively outside the Russian literature.

Composition of the ore fluid used in simulation

The chemical composition of the ore fluid in the Betze deposit was simulated assuming mutual solubility of pyrite+realgar+stibnite+gold at $T = 250^{\circ}\text{C}$ and $P_{\text{tot}} = 1,200$ bars. The starting temperature used in the calculations was 250°C . This temperature is higher than indicated in table 1 because the fluid inclusion data refer only to a given point of observations and not to the hypothetical initial state of the fluid. Because of a lack of definitive initial state information, multiple calculations were conducted with variable salinity, total Cl was varied from 0.1 to 1.5 molar (maximum value was 7.5 wt. percent NaCl equivalent) and CO_2 at 0.78 g/cm^3 . The activities of O_2 and H_2S , as well as the pH values, were calculated as the functions of a mutual solubility reaction. These parameters are dependent variables in the hypothetical fluid that changed as the equilibrium between the mineral assemblage and fluid chemistry changed. For purposes of sensitivity analysis, several ore fluid compositions were used to react with limestone and altered rock to simulate decarbonatization and silicification processes in Betze. The calculated initial metal concentrations in the ore fluid that was considered to be responsible for formation of the Betze deposit are listed in table 2.

The speciation-solubility calculations demonstrate that

gold was transported mainly as a bisulfide complex $\text{Au}(\text{HS})_2^-$, antimony as a H_3SbO_3 complex, arsenic as a H_3AsO_3 complex, and iron as a dichloride complex. The calculated aqueous iron concentration was low, suggesting that the host rocks or underlying rocks, or both, buffered iron in the system. Similarly, sulfide sulfur was relatively low ($a_{\text{H}_2\text{S}}$ at 10^{-3}). A possible second source for sulfur from reduction of sulfate sulfur is suggested by isotope evidence.

Host rocks used in simulation

Ore in the Betze deposit is hosted, for the most part, by limestone of the Popovich Formation and, therefore, chemical analyses of these rocks were used in the mass transfer calculations. For purposes of sensitivity analysis, different rock types composing the Popovich Formation were utilized and the calculated mineral assemblages were compared. The results of these calculations revealed no significant differences in the calculated depositional patterns, although some deviations in mass abundance of the deposited minerals were considered to be significant. Chemical analyses of representative rocks used in the chemical reaction path calculations are listed in table 3.

RESULTS AND DISCUSSION

The calculations presented below refer to two successive evolutionary phases during alteration and ore deposition. The major compositional characteristics of a natural heterogeneous

Table 2. Initial fluid characteristics used in modeling.

Constituent/parameter	Concentration (in moles)	Source
As*	8.02E-03	calculated from realgar solubility
Au *	3.94E-07	calculated from gold solubility
Cl**	1.01	fluid inclusion (table 1)
Fe *	4.55E-07	calculated from pyrite solubility
K **	0.01	fluid inclusion (table 1)
Na**	1.0	fluid inclusion (table 1)
S *	8.06E-03	calculated from total sulfides solubility
Sb*	2.20E-05	calculated from stibnite solubility
T($^{\circ}\text{C}$)	250**	fluid inclusion (table 1)
pH	4.31*	calculated
log a_{O_2}	-40*	calculated
log a_{H_2}	-5*	calculated
CO_2 (gm/cm^3)	0.78**	fluid inclusion (table 1)
P total (bar)	1,200**	fluid inclusion (table 1)

Note: E is scientific notation = 10^x

*Concentrations determined by modeling mutual solubilities of gold, realgar, stibnite and pyrite in the solution that includes $\text{NaCl} = 1.0$ mole and $\text{KCl} = 0.01$ mole, and that was constrained to be in equilibrium with CO_2 (bulk density of 0.78 gm/cm^3).

** Values are adapted from the study by Lamb and Cline (1997).

Table 3. Host rock lithologies used in modeling.

Sample ID	SiO ₂	Al ₂ O ₃	Fe ₂ O ₃	FeO	MgO	CaO	Na ₂ O	K ₂ O	CO ₂	S
FR8 ¹ (wt. %)	13.79	2.89	2.89	0.54	1.52	42.55	0.01	0.49	34.79	0.02
FR11 ² (wt.%)	38.66	5.4	5.4	1.42	8.73	17.73	0.06	1.53	22.95	0.1

¹Dp, Ls, upper unit, limestone of the Popovich Formation ; ²Dp lower unit, limestone of the Popovich Formation (G. Ferdock, unpublished data). Data indicated in this table are those were used in the sets of calculations and, therefore, they do not represent all data in chemical analysis for these samples.

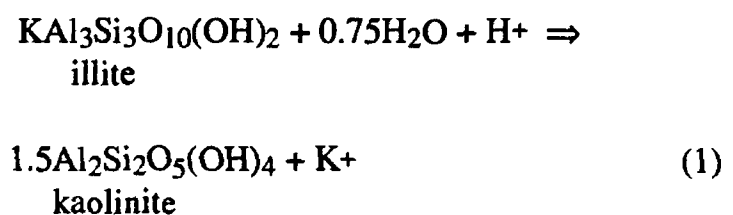
aqueous-solid-gaseous hydrothermal system in Betze is described in terms of 15 components (Al, As, Au, C, Ca, Cl, Fe, H, K, Mg, Na, O, S, Sb, and Si) comprising the modeling set. To mimic fluid-rock reactions during cooling, the solution was constrained to be in equilibrium with specified amounts of the host limestone at a specified temperature, total pressure and partial pressure CO₂. Therefore, each computational step was defined by the following parameters: (1) rock-fluid ratio, (2) temperature, and (3) total pressure. Selection of initial values of these specified parameters required a series of alternative calculations. Results were evaluated on the basis of geological and chemical criteria that included temperature and pressure ranges consistent with the geological context, the mineral phase rule, and the degree of consistency of the calculated mineral assemblage with field observations. Results of other alternative calculations indicated the values of temperature and rock-fluid ratio at each computational step. These values were carefully chosen to ensure the most adequate simulation of the mineral assemblages documented in the field.

Reaction of the ore fluid and limestone

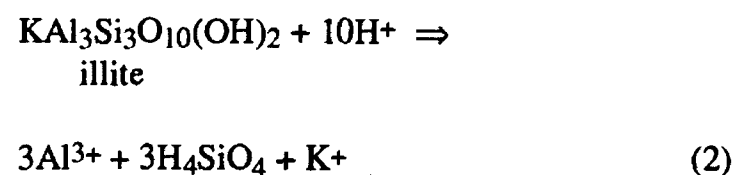
Gold deposition and decarbonatization of the host rock were simulated by a series of fluid-rock reactions between an ore fluid (table 2) and appropriate amounts of relatively fresh limestone (FR-11 from table 3). Small incremental changes of temperature and rock-fluid ratio were utilized while total pressure was maintained approximately at 1,200 bars throughout the entire reaction path. Calculated mineral assemblages, associated chemical reactions, mass transfer, gold deposition interval, pH, temperature, and pressure, corresponding to progressive fluid-rock interaction during decarbonatization, are shown in table 4, figures 1 through 3, and are discussed below.

Modeling results indicated that important chemical reactions occurred during interaction of the ore fluid with limestone and are as follows: (1) dissolution of the clay minerals, silica-leaching and silica-fixation reactions, and (2) carbonate dissolution. Fluid-rock interaction led first to the formation of a kaolinite+pyrite+graphite mineral assemblage, which was accompanied by a relatively low pH value, while the ratio between precipitated solids and dissolved constituents

was small (table 4, reaction step [a]). Overall, the clay minerals in the Betze deposit can be described in the system K₂O-Al₂O₃-SiO₂-H₂O by the general formula K_x(Al₂)(Al_xSi_{4-x})O₁₀(OH)₂ where x is the number of Al³⁺ and interlayer K⁺ ions. It is assumed that when x = 1 the simplified expression between reaction of clay minerals and ore fluid may be written such as follows:



The calculations show that over the first few reaction steps, dissolution reactions produced an aqueous phase in which the Si/Al ratios are higher than those in dissolved limestone (table 4, reaction steps from [a] through [f]). Aqueous silica concentration increased over the entire reaction path and was attributable to alteration of clay minerals in the host rock. Clay minerals (predominantly illite) dissolution (table 4, reaction steps from [a] through [c]) and concurrent precipitation of H₄SiO₄ as quartz (table 4, reactions steps from [d] through [f]), required a reaction such as follows:



Reaction 2 played an important role in the replacement process along the decarbonatization reaction path. In the intermediate zone of alteration, precipitation of quartz from H₄SiO₄ released by hydrolysis proceeded concurrently with clay mineral dissolution (table 4, reaction steps from [c] through [f]).

The pH value is important, but also of significance when the fact that H⁺ was continually consumed as the solution migrated and reacted with host rock as the system cooled. Dissolution of calcite occurred during the first computational steps (table 4, reaction steps from [a] through [c]) expressed by equation (3). Dolomite was stable at slightly higher pH (table 4, reaction step [b], equation (4)). These carbonate

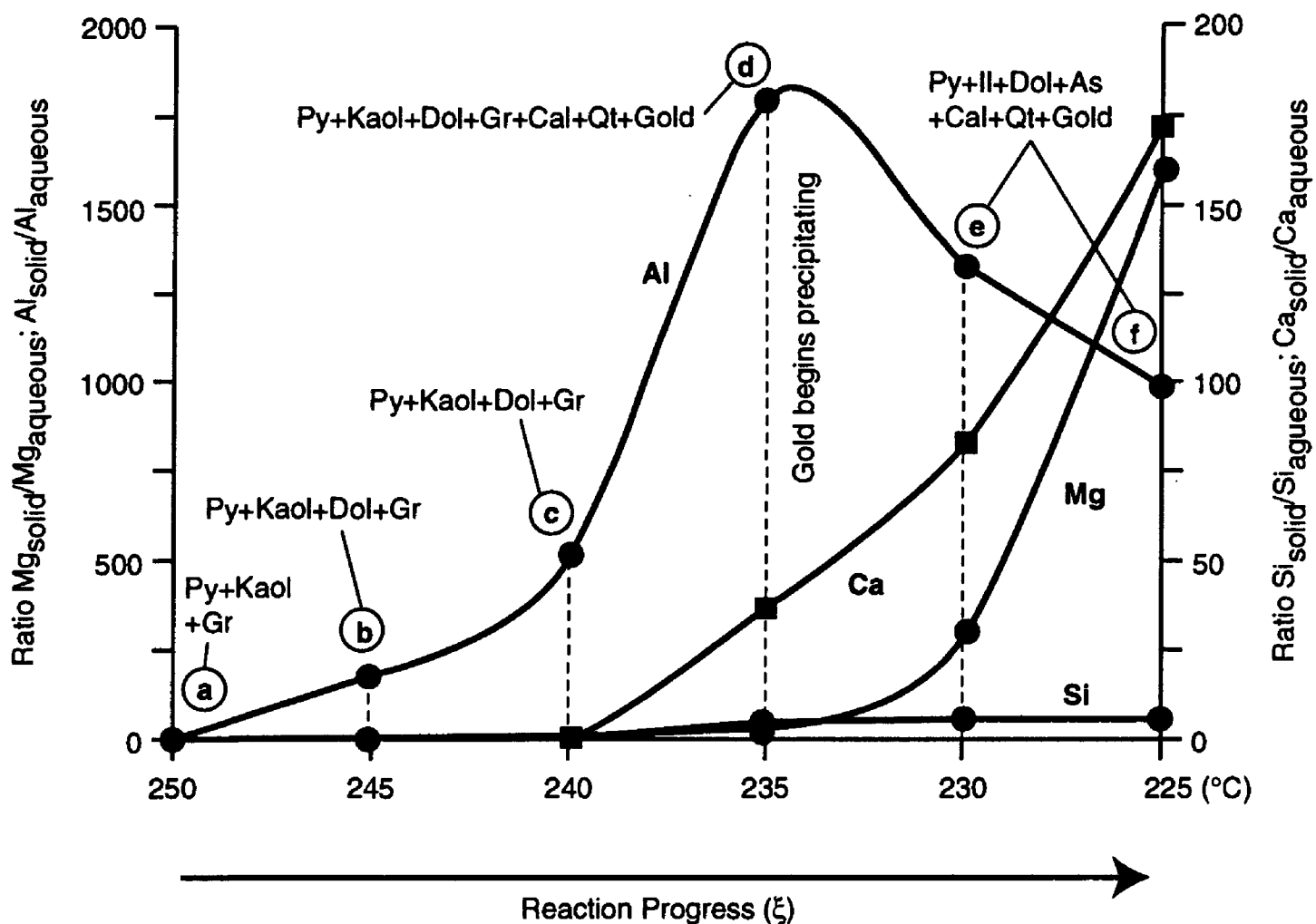
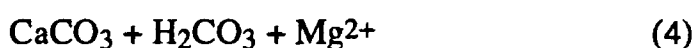
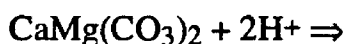
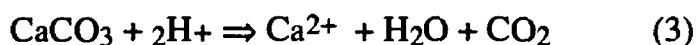


Figure 1. Diagram showing the modeled distribution between solid and aqueous phases for aluminum, magnesium, calcium and silica during main stage reaction steps and decarbonatization processes in the Betze deposit. Gold started to precipitate at 230°C, (1,200 bars, pH = 5.1, and log rock/fluid = -2.5 (reaction step [d], table 4). Note the difference in silica behavior that indicates a more complex control by the system. The letter annotations and dashed lines in the figure refer to sequential events of reaction progress steps (table 4).

dissolution reactions may have contributed to the high CO₂ contents measured in fluid inclusions from Carlin-type deposits.



A significant increase in the pH of the solution was accompanied by the formation of dolomite+calcite+kaolinite+pyrite+gold + quartz + graphite assemblage (reaction step [d], table 4). In this study, the As-rich pyrite formula was interpreted as the sum of native arsenic and pyrite, because of the lack of available petrographic and thermodynamic characteristics for this mineral found in the Betze deposit and other Carlin-type deposits. Arsenic in association with pyrite and gold precipitated in reaction step [e] (table 4). A subsequent reaction path moved along the kaolinite-illite phase

boundary until kaolinite completely gave way to illite (table 4, reaction steps [e] and [f]).

A series of alternative calculations did not reveal significant control by total pressure on the distribution of constituents and, therefore, on gold precipitation, which suggests that neither the stability of solid phases nor the stability of aqueous species varied strongly with pressure under the modeled conditions. In contrast, silica displayed a complex dependence on pressure, temperature, and pH changes in the system. No clear effect of Eh was observed over the pH range calculated in modeled system.

The compositional changes in the aqueous phase during decarbonatization can be outlined in terms of changes in aqueous silica, calcium, magnesium and aluminum activities that occurred in response to the fluid-rock interactions. Distribution of aqueous versus solid phases of the above components also is of interest. Figure 1 is a graphical representation of the distribution of calcium, magnesium, aluminum and silica between solid and aqueous phases during reaction progress in the modeled system (see also table 4 for

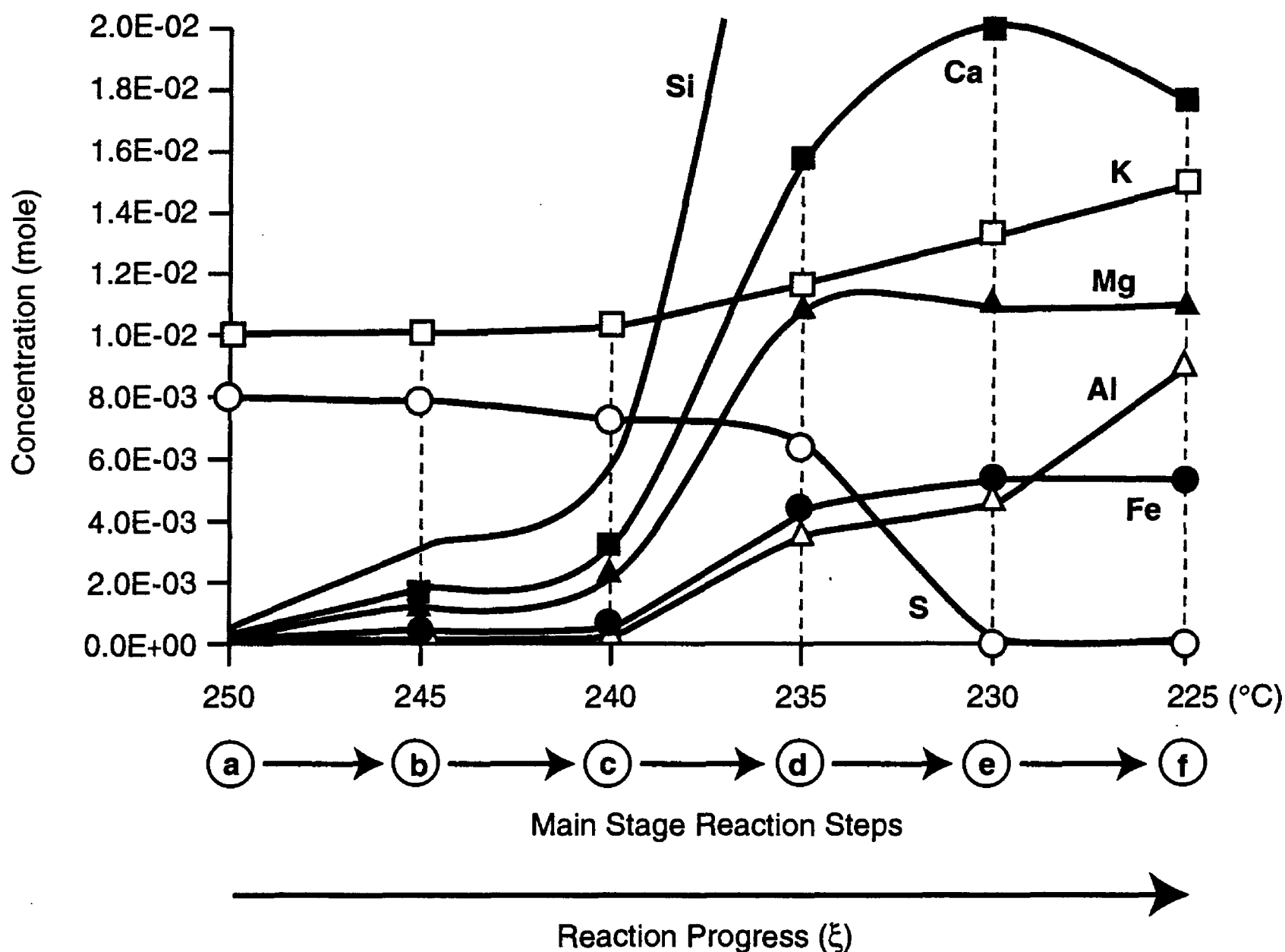


Figure 2. Schematic illustration of the calculated mass transfer of major constituents of the modeled system during the main stage of mineralization in the Betze gold deposit. Mass transfer reflects the mass of minerals produced and destroyed and appears to be a function of reaction progress in the reaction of the ore fluid and limestone. Note the changes in slope of the iron and sulfur curves that depict the calculated reaction path. Sulfur distribution relations demonstrate sulfidation in the modified flow with depletion model, where the total amount of sulfur was deposited and removed, as sulfide mineral precipitated. The letter annotations and dashed lines in the figure refer to sequential events of reaction progress steps (table 4).

more details). Lower ratios correspond to the loss of constituents to the aqueous phase from solid phases and, therefore, the earliest increments of the titrated limestone were almost dissolved. Further acid reduction toward neutral conditions in the system contributed to stabilization of carbonate minerals and illite. The distribution curves for aluminum, calcium and magnesium show that the starting point of gold precipitation corresponded to a degree of destruction of the constituent minerals of the host limestone during rock-fluid interaction. The mass transfer associated with the decarbonatization and hydrolysis reactions discussed above is shown graphically in figure 2. A decrease in the amount of destroyed limestone clearly corresponds to an increase in the

total concentrations of silica, calcium, magnesium, aluminum and potassium as the fluid-rock reaction progressed under cooling conditions. Note an increase in iron and depletion of sulfur that correlate with the onset of gold precipitation. The onset of gold precipitation also corresponds to a decrease in the activity of aqueous sulfur due to sulfidation of the reactive iron in the host rock. Mass transfer demonstrates that gold precipitation was a direct function of the reaction progress variable ξ .

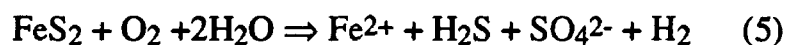
The results of modeling show that gold was complexed as a $\text{Au}(\text{HS})_2^-$ complex and transported in the +1 oxidation state, whereas the dominant arsenic complex was H_3AsO_3 with +3 oxidation state. The calculated association of gold and As-

Table 4. Computed mineral assemblages and associated variables corresponding to the main stage of gold mineralization and decarbonatization process (see text for further discussion).

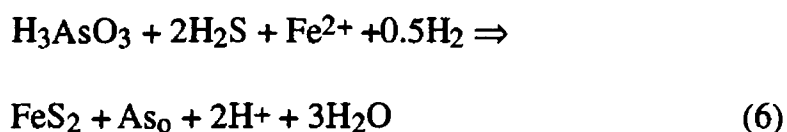
Reaction progress (ξ)	Lo r/f	T ($^{\circ}$ C)	Mineral assemblages (computed)	pH
[a]	-4.0	250	Py + Kaol + Gr	4.4
[b]	-3.5	245	Py + Kaol + Dol + Gr	4.7
[c]	-3.0	240	Py + Kaol + Dol + Gr	4.7
[d]	-2.5	235	Py + Kaol + Dol + Gr + Cal + Qt + Gold	5.1
[e]	-2.5	230	Py + Il + Dol + Cal + Qt + Gold + Arsenic	7.3
[f]	-2.0	225	Py + Il + Dol + Cal + Qt + Gold + Arsenic	7.5

Minerals computed given in order of reaction progress during interaction of the ore fluid (table 2) with a limestone (table 3). Abbreviations for table: Py = pyrite; Kaol = kaolinite; Gr = graphite; Dol = dolomite; Cal = calcite; Qt = quartz; Il = illite. Ratio r/f = rock-fluid ratio that was used in calculations.

rich pyrite (native arsenic + pyrite) could be attributable to simultaneous reactions that caused precipitation of arsenic, pyrite, a decrease in the sulfur activity, and co-fixation of gold (see equations from (5) through (9)). For example, the oxidation of part of a pyrite grain may lead to low a_{O_2} and high a_{H_2} expressed in the following equation:

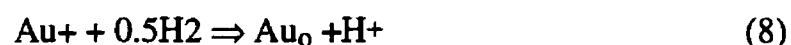


The reaction expressed in (5) is coupled with a reaction contributing to the precipitation of As-rich pyrite:

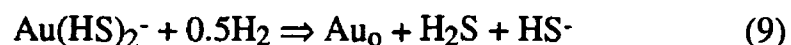


where association of pyrite and arsenic is interpreted as As-rich pyrite.

A decrease in sulfur activity and the presence of hydrogen in the solution, as referred by the following equations (from 7 to 9) contributed to the destabilization of the $Au(HS)_2^-$ complex and gold precipitation:



The resulting equation of the above reactions is as follows:



Reaction of the ore fluid and altered limestone

To model deposition of gold, iron, arsenic, and antimony minerals during the later stage of mineralization, a series of calculations were made between the ore fluid with the alteration mineral assemblages from the previous reaction path calculations (table 4). As before, the equilibrium solution chemistry after each computational step was used as the input ore fluid for the next step. Table 5 summarizes the changes in mineral assemblages deposited and the corresponding incremental changes in pH, temperature and rock-fluid ratio. An alternative series of calculations indicated that, in order to calculate mineral assemblages consistent with those

Table 5. Computed mineral assemblages and associated variables corresponding to the late stage of gold mineralization and silicification (see text for further discussion).

Reaction progress (ξ)	Lo r/f	T ($^{\circ}$ C)	Mineral assemblages (computed)	pH
[g]	-4.0	220	Py + Realg + Orpm + Kaol + Gold	4.7
[h]	-3.5	215	Py + Dol + Stib + Kaol + Gold + Qt + Gr	4.8
[i]	-3.5	200	Py + Dol + Stib + Kaol + Gold + Qt + Gr	4.7
[j]	-3.0	190	Py + Dol + Kaol + Gold + Qt + Gr	4.8

Minerals computed given in order of reaction progress during interaction of the ore fluid (table 2) with altered limestone (computed mineral assemblages of the altered limestone are listed in table 4, reaction steps from [a] through [c]). Abbreviations for table: Py = pyrite; Kaol = kaolinite; Gr = graphite; Dol = dolomite; Cal = calcite; Qt = quartz; Il = illite; Realg = realgar; Orpm = orpiment; Stib = stibnite. Ratio r/f = rock-fluid ratio that was used in calculations.

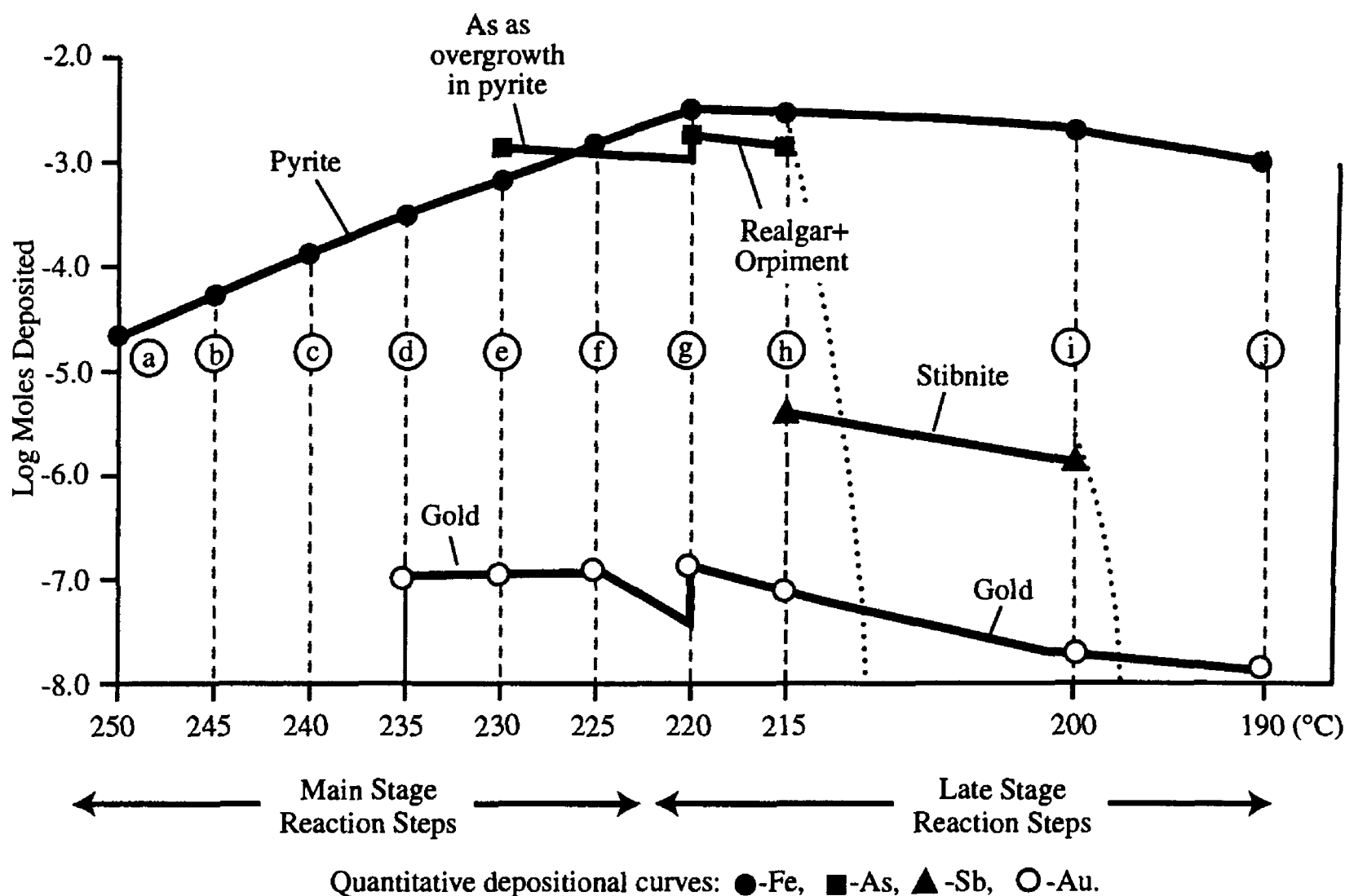


Figure 3. Quantitative depositional curves for sulfide minerals and gold corresponding to the main and late stage of mineralization events in the Betze deposit; quantity of minerals is shown in log moles/kg fluid for each temperature and pressure increment (with 5°C intervals for the main stage calculations; and from 5°C to 15°C intervals for the late stage calculations). Mass of minerals produced is a function of progress in the reaction of the ore fluid (table 2) with limestone (table 3) at temperature and pressure of the process (table 1). The letter annotations in the figure refer to sequential events of reaction progress steps during the main and late mineralization events (see table 4 and table 5).

documented, total pressure should be maintained at about 400 bars, which is relatively lower than indicated in table 1. In addition, relatively high aqueous silica values were assumed to model silicification. A series of alternative calculations also indicated that silica-leaching reactions did not result in saturation of the system with respect to quartz in the first reaction steps, because host limestone is relatively silica-poor (table 3).

As shown in table 5, gold precipitated over the entire reaction path indicating that cooling was important precipitation mechanism during the late gold event (table 5, reaction steps from [g] through [j]). The replacement of calcite by quartz occurred in reaction step [h]. The pH gradient is very small, indicating that leaching reactions were not important during the late stage, and that the mineralizing process was not chemically aggressive, enabling a preservation of textures during the course of replacement.

Calculated quantitative depositional curves for pyrite, native arsenic, realgar, orpiment, gold and stibnite during

alteration are depicted in figure 3. These curves show the relative amounts of minerals precipitated during the reaction steps from [a] through [f] (based on 5° C cooling steps), reaction steps from [h] through [i] (based on 15° C cooling steps), and a 10° C degree cooling increment between reaction steps [i] and [j]. Gold and arsenic were consistently depleted as the system followed the reaction path. Realgar and orpiment precipitated at the lower temperatures of the later stage, and eventually stibnite precipitated due to decrease in sulfur activity and temperature. The geologic expression of these relations is the interplay between changing mineral solubility and depletion of metal in the system.

CHEMICAL MODELING CONSTRAINTS ON BETZE ORE FORMATION

Geologically meaningful results have been obtained by computing reaction paths in the multicomponent and

multiphase system. The modeled system is considered to be analogous to the natural depositional environment in the Betze gold deposit. The modeling results suggest that gold was complexed as a $\text{Au}(\text{HS})_2^-$ whereas the dominant arsenic complex was H_3AsO_3 , and antimony was complexed as a $\text{Sb}(\text{OH})_3$. Gold, arsenic, antimony and other components were transported to the depositional site from below the accessible Carlin system. Geologic evidence suggests that the transported fluids were focused along permeable high- to low-angle faults into favorable conduits in the Popovich Formation.

The major features of the alteration zonation pattern observed in the deposit were simulated by the reaction of the ore fluid with limestone as the system cooled. The mineral stability relations in the $\text{CaO-MgO-CO}_2\text{-Al}_2\text{O}_3\text{-SiO}_2\text{-H}_2\text{O}$ system were reflected in the distribution of the mineral phases in the modeled and actual system. Dissolution-precipitation reactions, including carbonate destruction, silica-leaching, silica-fixation, and sulfide mineral precipitation controlled mass transfer in the Betze deposit.

Mass transfer calculations indicate that gold precipitation was associated with sulfidation of reactive iron in the system, and corresponded to a particular reaction progress variable ξ . Sulfidation resulted in higher hydrogen and lower sulfide sulfur activity in the system, which destabilized H_3AsO_3 and $\text{Au}(\text{HS})_2^-$ complexes, and resulted in gold precipitation in association with As-rich pyrite. The results of our modeling study are similar to those of Hofstra and others (1991), and confirm that sulfidation of host rock iron during reaction of the ore fluid with host rock was the primary gold precipitation mechanism in Carlin-type deposits.

The modeling results cannot provide an adequate answer to whether a fluid or a mixture of fluids of various origins entered the depositional environment. Although stable isotope data suggest that the ore fluids mixed with meteoric water, the modeling results indicate that interactions between a single fluid and the host rocks can account for the observed mineral assemblages, suggesting that fluid mixing was not an important depositional control in the Betze deposit.

Research efforts are in progress to better understand geochemical and geological processes controlling gold transport and deposition in Carlin-type gold deposits. Modeling of the origin and character of the ore-forming fluid(s) and its interactions with host rocks in conjunction with field, experimental and laboratory studies will help us to better understand the processes of ore formation in Carlin-type gold deposits.

ACKNOWLEDGMENTS

We are indebted to Dave John, Julian Hemley, Al Hofstra, Randy Koski and Dick Tosdal for their helpful suggestions and critical reviews of the manuscript.

Encouragement to conduct this work came from Ted Theodore, Eric Lauha and Keith Bettles. The geochemical modeling study of the Betze deposit was performed due to financial support received by senior author from U.S. Geological Survey and Barrick Goldstrike Mines Inc. Permission by Barrick Goldstrike Mines Inc. to publish the results of this study is greatly appreciated.

REFERENCES CITED

- Alvarez, A.A., and Noble, D.C., 1988, Sedimentary rock-hosted disseminated precious metal mineralization at Purisima Concepcion, Yauricocha District, central Peru: *Economic Geology*, v. 83, p. 1368–1378.
- Arehart, G.B., 1996, Characteristics and origin of sediment-hosted gold deposits: a review: *Ore Geology Reviews*, v. 11, p. 383–403.
- Arehart, G.B., Foland, K.A., Naeser, C.W., and Kesler, S.E., 1993a, $^{40}\text{Ar}/^{39}\text{Ar}$, K/Ar, and fission track geochronology of sediment-hosted disseminated gold deposits at Post Betze, Carlin trend, northeastern Nevada: *Economic Geology*, v. 88, p. 622–646.
- Arehart, G.B., Chryssoulis, S.L., and Kesler, S.E., 1993b, Gold and arsenic in iron sulfides from sediment-hosted disseminated gold deposits: Implications for depositional processes: *Economic Geology*, v. 88, p. 171–185.
- Arehart, G.B., Eldridge, C.S., Chryssoulis, S.L., and Kesler, S.E., 1993c, Ion microprobe determination of sulfur isotope variations in iron sulfides from the Post/Betze sediment-hosted disseminated gold deposit, Nevada, USA: *Geochimica et Cosmochimica Acta*, v. 57, p. 1505–1519.
- Bakken, B.M., and Einaudi, M.T., 1986, Spatial and temporal relations between wall-rock and gold mineralization, main pit, Carlin gold mine, Nevada, *in* MacDonald, A.J., *Gold '86: Willowdale, Ontario*, Konsult International Inc., p. 388–403.
- Bakken, B.M., Fleming R.H., and Hochella M.F., 1991, High-resolution microscopy of auriferous pyrite from the Post deposit, Carlin District, Nevada, *in* Hausen, D.M., Petruk, W., Hagni, R.D., and Vassiliou A., eds., *Process Mineralogy XI: Characterization of Metallurgical and Recyclable Products: The Minerals, Metals and Materials Society*, p. 13 - 23.
- Berry, A.R., 1992, A geological study of the Betze gold deposit, Eureka County, Nevada: University of Nevada, Reno, M.S. Thesis, 173 p.
- Bettles, K.H., 1989, Gold deposits of the Goldstrike Mine, Carlin Trend, Nevada: *Society of Mining Engineers Preprint*, 89–158, p. 14.
- Bettles, K.H., and Lauha, E.A., 1991, Gold deposits of the Carlin Trend, Nevada: *World Gold '91, Forum on Technology and Practice: Second Australian Institute of Mining and Metallurgy Society of Mining and Metallurgy Joint Conference*, 21–26 April, Cairns, Australia, p. 251–257.
- Christensen, O. D., 1993, Carlin trend geologic overview, *in* Christensen, O.D., ed., *Gold Deposits of the Carlin Trend, Nevada: Society of Economic Geologists Guidebook Series*, v. 18, p. 326.
- 1996, Carlin trend geologic overview, *in* Green, S.M., and

- Strusacker, E., eds., *Geology and ore deposits of the American Cordillera Road Trip B, Structural Geology of the Carlin Trend: Geological Society of Nevada Field Trip Guidebook Compendium*, 1995, Reno/Sparks, Nevada, p. 147–156.
- De Donder, T., 1920, *Leçons de Thermodynamique et de Chimie Physique*: Paris, Gauthier Villars, 210 p.
- Drews-Armitage, S.P., Romberger, S.B., and Whitney, C.G., 1996, Clay alteration and gold deposition in the Genesis and Blue Star deposits, Eureka County, Nevada: *Economic Geology*, v. 91, p. 1383–1393.
- Ferdock, G.C., Castor, S.B., Leonardson, R.W., and Collins, T., 1997, Mineralogy and paragenesis of ore stage mineralization in the Betze gold deposit, Goldstrike Mine, Eureka County, Nevada, *in* Vikre, P., Thompson, T.B., Bettles, K., Christensen, O., and Parratt, R., eds., *Carlin-type Gold Deposits Field Conference: Society of Economic Geologists Guidebook Series*, v. 28, p. 75–87.
- Fleet, M. E., and Mumin A. H., 1997, Gold-bearing arsenian pyrite and marcasite and arsenopyrite from Carlin Trend gold deposits and laboratory synthesis: *American Mineralogist*, v. 82, p. 182–193.
- Hausen, D. M., and Kerr, P. F., 1968, Fine gold occurrence at Carlin, Nevada, *in* Ridge, J.D., ed., *Ore Deposits of the United States: American Institute Mining Metallurgy and Petroleum Engineers*, New York, p. 908–940.
- Helgeson, H.C., 1979, Mass transfer among minerals and hydrothermal solutions, *in* Barnes, H.L., ed., *Geochemistry of Hydrothermal Ore Deposits*: New York, Holt, Rhinehart, and Winston, p. 568–610.
- , 1968, Evaluation of irreversible reactions in geochemical processes involving minerals and aqueous solutions: I. Thermodynamic relations: *Geochimica and Cosmochimica Acta*, v. 32, p. 853–877.
- Hemley, J.J., and Voitsekhovskaya, M., 1993, Modeling ore metal transport and deposition in hydrothermal systems: *Geological Society of America, Abstract with Programs*, v. 25, p. A401.
- Hofstra, A.H., Northrop, H.R., Rye, R.O., Landis, G.P., and Birak, D.J., 1988, Origin of sediment-hosted disseminated gold deposits by fluid mixing: Evidence from jasperoids in the Jerritt Canyon gold district, Nevada, USA, *in* Goode, A.D.T., and Bosma, L.I., eds., *Geological Society of Australia, Proceedings of Bicentennial Gold' 88: Economic Geology, Abstract Series no. 22*, p. 284–289.
- Hofstra, A.H., Leventhal, J.S., Northrop, H.R., Landis, G. P., Rye, R.O., Birak, D.J., and Dahl, A. R., 1991, Genesis of sediment-hosted disseminated gold deposits by fluid mixing and sulfidation: chemical reaction path modeling of ore depositional processes documented in the Jerritt Canyon District, Nevada: *Geology*, v. 19, no. 1, p. 36–40.
- Ilchik, R.P., and Barton, M.D., 1996, Physical and chemical constraints for an amagmatic origin of Carlin-type gold deposits, a source-sink approach, *in* Coyner, A.R., and Fahey, P.L., eds., *Geology and Ore deposits of the American Cordillera: Geological Society of Nevada Symposium Proceedings*, v. 2, p. 687–708.
- Johnson, J.W., Oelkers, E.H., and Helgeson, H.C., 1992, SUPCRT92: A software package for calculating the standard molal thermodynamic properties of minerals, gases, aqueous species and reactions from 1 to 5,000 bars and 0 to 1,000° C: *Computers and Geosciences*, v. 18, p. 899–947.
- Krajnov, S.R., Shvarov, Y.V., and Grichuk, D.V., 1988, *Methods of thermodynamic modeling and forecasting in hydrogeology*: Nedra Press, Moscow, 203 p., (in Russian).
- Kuehn, C.A., 1989, *Studies of disseminated gold deposits near Carlin, Nevada: Evidence for a deep geologic setting of ore formation*: Pennsylvania State University, Ph.D. dissertation, 395 p.
- Kuehn, C.A., and Rose, A.W., 1995, Carlin gold deposits, Nevada: Origin in a deep zone of mixing between normally pressured and over pressured fluids: *Economic Geology*, v. 90, p. 17–36.
- Lamb, J.B., 1995, *A petrographic and fluid inclusion study of the Purple Vein and Post-Betze orebodies, Carlin, Nevada*: University of Nevada, Las Vegas, M.S. Thesis, 161 p.
- Lamb, J.B., and Cline, J.M., 1997, Depth of formation of the Meikle and Betze/Post deposits, *in* Vikre, P., Thompson, T.B., Bettles, K., Christensen, O., and Parratt, R., eds., *Carlin-type Gold Deposits Field Conference: Society of Economic Geologists Guidebook Series*, v. 28, p. 101–108.
- Lauha, E.A., and Bettles, K.H., 1993, *A geologic comparison of the Post/Betze and Purple vein deposits of the Goldstrike and Meikle Mines, Nevada*: Society for Mining, Metallurgy, and Exploration, Preprint 93–170, 20 p.
- Leonardson, R.W., and Rahn, J.E., 1996, *Geology of the Betze-Post gold deposits, Eureka County, Nevada*, *in* Coyner, A.R., and Fahey, eds., *Geology and Ore Deposits of the American Cordillera: Geological Society of Nevada, Symposium Proceedings*, Reno/Sparks, Nevada, April, 1995, p. 61–94.
- Madeisky, H.E., 1993, Pearce element ratio analysis: applications in lithochemical exploration, *in* Coyner, A.R., and Fahey, P.L., *Geology and Ore Deposits of the American Cordillera: Geological Society of Nevada Symposium Proceedings*, Reno/Sparks, Nevada, April, 1995, p. 709–732.
- Peters, S.G., 1996, Definition of Carlin trend using orientation of fold axes and applications to ore control and zoning in the central Betze orebody, Betze/Post Mine, *in* Green, S.M., and Strusacker, E., eds., *Geology and Ore Deposits of the American Cordillera, Trip B-Structural Geology of the Carlin Trend, Field Trip Guidebook Compendium, 1995: Geological Society of Nevada, Reno/Sparks, Nevada*, p. 59–95.
- Peters, S.G., Leonardson, R.W., Ferdock, G.C., and Lauha, E.A., 1997, Breccia types in the Betze orebody, Goldstrike Mine, Eureka County, Nevada, *in* Vikre, P., Thompson, T.B., Bettles, K., Christensen, O., and Parratt, R., eds., *Carlin-type Gold Deposits Field Conference: Society of Economic Geologists Guidebook Series*, v. 28, p. 87–101.
- Radtke, A.S., 1985, *Geology of the Carlin gold deposit, Nevada*: U.S. Geological Survey Professional paper 1267, 124 p.
- Sillitoe, R.H., and Bonham, H.F., 1990, Sediment-hosted gold deposits: Distal products of magmatic-hydrothermal systems: *Geology*, 18, p. 157–161.
- Sha, P., 1993, *Geochemistry and genesis of sediment-hosted disseminated gold mineralization at the Gold Quarry Mine, Nevada*: Ph.D. Thesis, University of Alabama, 254 p.
- Shvarov, Y.V., 1976, Calculation of equilibrium composition in a multicomponent heterogeneous system: *Academia Nauk SSSR Doklady*, v. 229, no. 6, p. 223–225 (in Russian).
- Teal L., and Jackson M., 1997, *Geologic overview of the Carlin trend gold deposits and description of recent deep discoveries*, *in* Vikre, P., Thompson, T.B., Bettles, K., Christensen, O., and Parratt, R., eds., *Carlin-type Gold Deposits Field Conference*:

- Society of Economic Geologists Guidebook Series, v. 28 , p. 3-37.
- Volk, J.A., and Lauha, E.A., 1993, Structural controls on mineralization at the Goldstrike property, Elko and Eureka counties: Geological Society of America Abstracts with Programs, v. 23, no. 2, p. 106.
- Volk, J.A., Lauha, E., Leonardson, R.W., and Rahn, J.E., 1996, Structural geology of the Betze Post and Meikle deposits, Elko and Eureka Counties, *in* Green, S.M., and Struhsacker, E., eds., Geology and Ore Deposits of the American Cordillera, Trip B, Structural Geology of the Carlin Trend, Field Trip Guidebook Compendium, 1995: Geological Society of Nevada, Reno/Sparks, Nevada, p. 180-194.
- Wells, J.D., and Mullens, T.E., 1973, Gold-bearing arsenian pyrite determined in microprobe analysis, Cortez and Carlin gold mines, Nevada: Economic Geology, v. 65, p. 187-201.
- Woitsekhowskaya, M., 1992, A modeling study of alteration process sequences in response to Au-mineralization associated with volcanic rocks: International Conference on Mineral Deposit Modeling in Relation to Crustal Reservoirs of the Ore-forming Elements, Nottingham, United Kingdom, (unpaginated).
- Woitsekhowskaya, M. B., and Hemley, J.J., 1995, Modeling metal transport and deposition in Butte-type hydrothermal systems: Economic Geology, v. 90, p. 1329-1337.
- Woitsekhowskaya, M., McArdle, P., and O'Connor, P., 1992, Chemical modeling of the Au-Cu Avoca deposit, SE Ireland: 2nd Symposium on Thermodynamics of Natural Processes, Novosibirsk, Russia, (unpaginated).

MIXED SOURCES OF Pb IN SEDIMENTARY-ROCK-HOSTED Au DEPOSITS, NORTHERN NEVADA

By R. M. Tosdal, J. S. Cline, A.H. Hofstra, S. G. Peters, J.L. Wooden, and M.N. Young-Mitchell

ABSTRACT

Pb isotopic compositions for sulfide minerals (orpiment, realgar, stibnite, marcasite, pyrite and galena) in the sedimentary-rock-hosted, or Carlin-type, Au deposits at Getchell, Betze-Post, and in the Jerritt Canyon Mining District in northern Nevada suggest mixing of distinct Pb sources during their formation. Host rocks for the deposits are principally Paleozoic calcareous miogeoclinal rocks. They are commonly capped by siliciclastic eugeoclinal rocks along structural contacts that constitute the Roberts Mountains thrust system; the eugeoclinal rocks are not common host rocks to gold ore. Stocks of Jurassic, Cretaceous and Eocene age are spatially associated with many deposits but a genetic linkage is not established. In the Betze-Post deposit, pre-main gold ore stage base-metal veins contain Pb derived from the host late Middle Jurassic Goldstrike stock of granodioritic composition. Sulfides deposited during formation of a sedimentary-rock-hosted Au deposit do not show any obvious component of Pb from the host Paleozoic miogeoclinal rocks, but rather shows evidence of mixing of two Pb isotopically distinct fluids. One source is characterized by a large range of $^{206}\text{Pb}/^{204}\text{Pb}$ (18.5-25.3) with a limited range of $^{208}\text{Pb}/^{204}\text{Pb}$ (38.1-39.5) indicating low but variable Th/U values. This source resembles the Paleozoic siliciclastic eugeoclinal rocks. The second source was characterized by slightly elevated $^{207}\text{Pb}/^{204}\text{Pb}$ (>15.75) at relatively low $^{206}\text{Pb}/^{204}\text{Pb}$ (19-20), and by Th/U values close to 4. This source could have been (1) magmatic, or (2) Late Proterozoic and early Paleozoic sedimentary rocks that are generally unexposed in the vicinity of the deposits but must lie at deeper crustal levels, or (3) still deeper lower or middle crustal rocks. Regardless of the exact nature of this low $^{206}\text{Pb}/^{204}\text{Pb}$ source, mixing of Pb probably took place close to or at the site or ore deposition in order to maintain isotopic integrity of the two sources. The Pb isotopic evidence for fluid mixing is consistent with mineralogic and geochemical data for the sediment-hosted Au deposits.

INTRODUCTION

Establishing the source, or sources, of Au in sedimentary

rock-hosted, or Carlin-type, Au deposits is critical to genetic models proposed for their formation (Christensen, 1993). In models appealing to amagmatic sources for the deposits, Au is thought to have been derived from thick sequences of upper Proterozoic and early Paleozoic sedimentary rocks during deep circulation of meteoric water driven by elevated geothermal gradients during Eocene extension and accompanying magmatism (Hofstra, 1995, 1997; Ilchik and Barton, 1997), or as a result of regional metamorphism and dehydration of these same metasedimentary rocks (Seedorf, 1991; Phillips and Powell, 1993; Keuhn and Rose, 1995). Crustal-scale hydrothermal systems are required in these models. In models proposing a magmatic link, Au is derived from a stock, and the deposits are referred to as distal-disseminated Ag-Au deposits (e.g. Sillitoe and Bonham, 1990; Theodore, 1998). A variation on the magmatic model proposes that plutons simply provided the thermal energy necessary for focusing a hydrothermal system (Arehart and others, 1993a; Keuhn and Rose, 1995). In this case, Au was derived largely from sedimentary rocks with little or no contribution from the pluton.

That the sedimentary rock sequence is a reasonable source of Au is supported indirectly by the observation of Titley (1991), who noted an association on a worldwide basis of sedimentary rock-hosted Au deposits with rocks of early Paleozoic or Jurassic and Cretaceous age. Deposition in deep water during times of high sea level and widespread submarine volcanism and hydrothermal activity typify these clastic sequences. In the case of northern Nevada, Young-Mitchell and Titley (1996) further demonstrate a relative enrichment of Au in the early Paleozoic sedimentary rocks. They postulated that Au is detrital and derived from the Precambrian craton to the east. Of interest is their observation that deeper water eugeoclinal rocks deposited farther from the craton are more enriched in Au than carbonate-rich rocks deposited in the shallower water of the miogeocline closer to the craton. Poole and others (1992) also note that eugeoclinal rocks are commonly metalliferous. The relative Au and metal enrichment inherent in the eugeoclinal rocks logically leads to a hypothesis that Au and other metals in sedimentary rock-hosted Au deposits might have been leached out of siliciclastic rock sequences and transported unknown distances as part of large hydrothermal circulation systems (for example, Ilchik and Barton, 1997).

Pb isotopes measured in ore minerals can constrain Pb sources in many types of hydrothermal systems. However, their utility for determining the source of associated metals, such as Au, is also limited by the assumption that Pb was transported and deposited as part of the same hydrothermal fluid. If true, then Pb isotopes serve as a proxy for constraining the source of associated metals. Still another limiting factor is the Pb concentration of a hydrothermal fluid with respect to potential Pb sources during transport and subsequent deposition. If a low Pb concentration characterizes a hydrothermal fluid, then water-rock interactions can change the Pb isotopic compositions of the fluid, hence minerals deposited therefrom (Powell and others, 1991). Pb isotopic compositions of an ore mineral in this situation will reflect mixing of Pb sources along fluid pathways or at the site of ore deposition. Mixing of Pb sources in hydrothermal systems is a common phenomenon (Heyl and others, 1974; Richards and others, 1991; Foley and Ayuso, 1994; Kesler and others, 1994), and should be expected in the environments of sedimentary rock-hosted Au deposits of Nevada, an observation that has been confirmed by mineralogic and geochemical data (Arehart and others, 1993b; Arehart, 1996; Cline and others, 1997; Hofstra, 1997; Ilchik and Barton, 1997). The likelihood of recording fluid mixing in the sedimentary rock-hosted Au deposits using Pb isotopes is further enhanced by apparent low Pb concentrations in the hydrothermal fluids (e.g. Groff and others, 1997) and also the range of potential Pb isotopic compositions of possible igneous or sedimentary rock sources. However, unlike stable isotopic data for mixing of fluid, Pb isotopes provide an avenue to constrain which of the potential sources actually contributed Pb to the hydrothermal system, thus indirectly constraining potential sources of Au.

This paper presents initial efforts to constrain Pb sources in sedimentary rock-hosted Au deposits in northern Nevada (fig. 1). To this end, Pb isotopic compositions are reported for sulfides in sedimentary rock-hosted Au deposits at Getchell (Cline and others, 1997; stage 5 of Groff and others, 1997), Betze-Post (Ferdock and others, 1997), and in the Jerritt Canyon Mining District, which forms a part of the Independence Group (Hofstra and others, 1991). In addition, sulfides deposited during an earlier pluton-related event at the Betze-Post deposit were also analyzed (Ferdock and others, 1997) (fig. 1; table 1) in order to constrain the Pb isotopic composition of a source fluid of magmatic composition. Critical for interpreting these ore-related Pb isotopic values is the Pb isotopic compositions of potential Pb reservoirs that might have contributed Pb to a hydrothermal system. These reservoirs are: (1) Jurassic, Cretaceous, and Tertiary plutonic and volcanic rocks (Wooden and others, 1997, this volume), and (2) Early and Middle Paleozoic sedimentary rocks (table 2) that either host the deposits or are present at higher structural levels. Contributions from a third reservoir, the deeply buried Late Proterozoic and earliest Paleozoic clastic wedge not widely exposed across northern Nevada, is

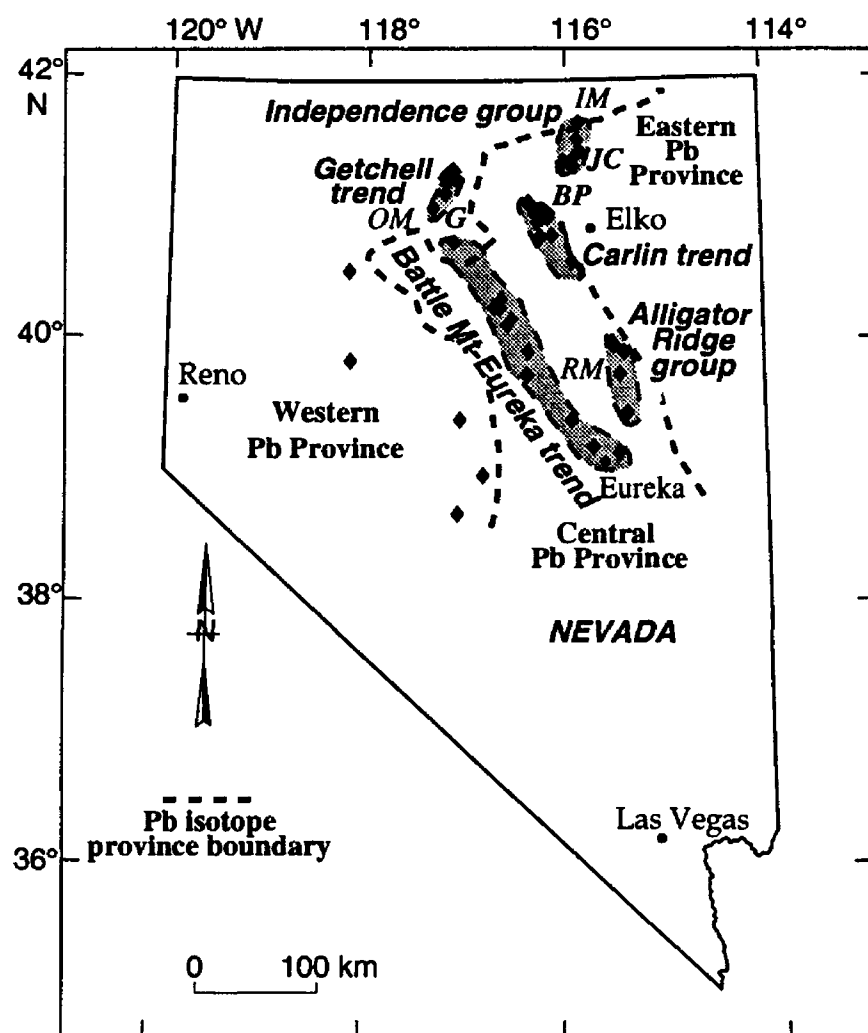


Figure 1: Location of sedimentary rock-hosted Au deposits (filled diamonds) in northern Nevada, showing major groups and trends of these deposits. B, Betze-Post; G, Getchell; JC, Jerritt Canyon District. Geographic localities are: IM, Independence Mountains; OM, Osgood Mountains; RM, Roberts Mountains.

predicted in amagmatic models (Ilchik and Barton, 1997). As yet, no Pb isotopic data is available for these rocks, and this lack needs to be rectified to fully understand the potential roles of various source terranes in contributing Pb, and by inference Au, to the sedimentary rock-hosted deposits. Continuing work using both conventional Pb isotopic methods and spot-analyses using the Sensitive High Resolution Ion-MicroProbe (SHRIMP) will provide additional information pertinent to this issue.

GEOLOGIC FRAMEWORK AND DEPOSIT SETTING

The geologic framework of sedimentary rock-hosted Au deposits in northern Nevada is well known (Stewart, 1980; Groff and others, 1997; Teal and Jackson, 1997). Principal host rocks for the deposits are Lower Cambrian through Devonian calcareous sedimentary rocks deposited on a westward prograding miogeoclinal shelf. The miogeoclinal rocks were tectonically buried beneath the Robert Mountains

Table 1: Present-day Pb isotopic compositions for sulfides from the Post-Betze, Getchell, and Jerritt Canyon sediment-hosted gold deposits, northern central Nevada.¹

Sample no.	Mineral or rock type	²⁰⁶ Pb/ ²⁰⁴ Pb	²⁰⁷ Pb/ ²⁰⁴ Pb	²⁰⁸ Pb/ ²⁰⁴ Pb
<i>Sediment-hosted Au deposit</i>				
<i>Betze-Post</i>				
BMV	Galena	19.635	15.753	39.287
	Pyrite	19.629	15.751	39.271
SP93-528	Pyrite	20.114	15.751	39.238
SP96-7033	Marcasite, "framboidal"	29.004	16.195	39.338
	replicate	28.872	16.186	39.354
<i>Getchell</i>				
G-7-15-3	Realgar	19.929	15.781	39.020
G92-205-1079	Orpiment	20.665	15.815	38.878
<i>Jerritt Canyon</i>				
J89-7	Orpiment	21.437	15.803	38.933
J89-8	Stibnite	19.653	15.737	39.225

¹ Sulfide dissolution techniques, column chromatography, and error analysis are described by Arribas and Tosdal (1994). Galena, pyrite, marcasite, and stibnite were dissolved using concentrated HNO₃. Orpiment and realgar were dissolved using concentrated aqua regia. Measured Pb isotopic compositions were corrected for 0.125 percent fractionation per atomic mass unit, based upon replicate analyses of the National Bureau of Standards 981 and 982. Laboratory procedural blanks were 1 ng Pb or less and the precision of the isotopic measurements was generally better than 0.05 percent at the 2 sigma confidence level. Lead isotope compositions are reproducible to the ±0.8, ±0.1, and ±0.14 percent (2 sigma), respectively, for ²⁰⁶Pb/²⁰⁴Pb, ²⁰⁷Pb/²⁰⁴Pb, and ²⁰⁸Pb/²⁰⁴Pb.

thrust system during the Devonian and early Mississippian Antler orogeny. Upper-plate rocks of the Antler allochthon consist of Ordovician eugeoclinal, fine-grained siliceous clastic rocks and chert deposited in deep water farther west from the craton. They represent the westward time-stratigraphic equivalents of the calcareous miogeoclinal rocks (Poole and others, 1992). The siliciclastic eugeoclinal rocks generally are not good hosts to ore, although some deposits are known in these rocks (Teal and Jackson, 1997). Less common host rocks in the sedimentary rock-hosted deposits are Mississippian carbonate-rich rocks deposited in the clastic wedge shed eastward as an overlap assemblage during and after emplacement of the Antler allochthon. Younger contractile deformation in the Pennsylvanian, early Triassic, and Early Cretaceous superposed additional structural and stratigraphic complexities to the vicinity of the deposits. Stocks and dikes were emplaced into structurally interleaved Paleozoic rocks in the Jurassic, Cretaceous, and Eocene, and several deposits are spatially related to their margins.

The Getchell deposit in the Osgood Mountains (fig. 1) is the westernmost sedimentary rock-hosted Au deposit from which Pb isotopic data are reported herein. This deposit is located along the flank of a Cretaceous granodioritic stock that intruded and thermally metamorphosed fine-grained calcareous rocks of the Lower Cambrian Preble and Ordovician Comus Formations (Cline and others, 1997; Groff and others,

1997). Gold ore is hosted principally in interbedded limestone and shale of the Preble Formation.

The Betze-Post deposit in the Carlin trend (fig. 1) is the largest Au deposit in Nevada (Leonardson and Rahn, 1996; Ferdock and others, 1997). Here, Au is hosted in altered miogeoclinal calcareous rocks of the Silurian and Devonian Roberts Mountains Formation, Devonian Popovich Formation, and overlying informally named Rodeo Creek unit. These rocks were structurally buried beneath eugeoclinal siliciclastic rocks and chert of the Ordovician Vinini Formation along the Roberts Mountains thrust. The structural sequence was intruded by the late Middle Jurassic Goldstrike granodioritic to dioritic stock and by Eocene and Oligocene quartz monzonite and monzonite dikes (Arehart and others, 1993a; Emsbo and others, 1996). Polyphase sulfide deposition characterizes the deposit. The oldest sulfide stage in the deposit is represented by quartz-sericite-pyrite-base metal veins associated with intrusion of the Middle Jurassic Goldstrike stock (Ferdock and others, 1997). These veins, from which galena and pyrite were analyzed, predate the main stage of gold deposition, although minor gold is associated with the veins. Pyrite also grew as part of the metamorphic minerals in thermally metamorphosed wall rocks surrounding the stock. Main stage gold deposition was superposed on the older sulfide depositional events.

The Jerritt Canyon Mining District in the Independence

Table 2: Present-day Pb isotopic compositions for lower and middle Paleozoic sedimentary rocks, north-central Nevada¹.

Sample no.	Formation	Rock type	²⁰⁶ Pb/ ²⁰⁴ Pb	²⁰⁷ Pb/ ²⁰⁴ Pb	²⁰⁸ Pb/ ²⁰⁴ Pb
<u>Eugeoclinal rocks</u>					
<i>Eureka Mining District</i>					
EU-2	Pogonip Group (Ordovician)	limestone with chert nodules	19.452	15.695	38.765
EU-4	Windfall Fm.(Cambrian)	limestone	19.604	15.686	38.797
<i>Roberts Mountains</i>					
RM-4	upper Vinini Fm. (Ordovician)	chert and shale sandy chert	19.680	15.668	38.571
RM-11			27.563	16.166	38.852
RM-24	upper Vinini (?) Fm.	shale	21.700	15.856	38.691
<i>Northern Independence Range</i>					
Valmy Group (late Cambrian to Middle Ordovician)					
NI-47	McAfee quartzite ²	shaley argillite	18.879	15.671	38.431
NI-17		shale/siltstone	19.734	15.714	39.323
NI-48	rocks of Jack's Peak ²	argillite, shale, chert	18.871	15.612	38.407
Snow Canyon Fm. (Ordovician)					
NI-3	Lower	shale	19.422	15.709	39.524
NI-6		claystone	21.473	15.833	38.568
NI-9		shaley mudstone	18.477	15.589	38.648
NI-10		sandstone	20.761	15.745	39.192
NI-12		shale	21.542	15.785	38.806
NI-15		shale and silstone	20.425	15.718	38.907
NI-54	Upper	siltstone	18.952	15.632	39.027
NI-55		shaley mudstone	25.321	16.019	38.618
NI-58		sandstone/shale	20.336	15.708	38.741
NI-61a		shale	18.386	15.569	38.470
NI-63		shale/siltstone	19.754	15.661	39.501
NI-71		shale/argillite	19.275	15.643	38.147
<u>Miogeoclinal rocks</u>					
NI-26	Roberts Mtn. Fm.	silty limestone	20.704	15.666	39.024
NI-27	(Silurian-Devonian)	limestone	19.794	15.651	39.033
NI-76	Hansen Creek Fm.	chert-limestone	22.743	15.780	38.654
NI-79	(Ordovician-Silurian)	limestone	18.130	15.571	37.560
NI-82		shaley limestone	20.015	15.715	38.956

¹ Whole-rock dissolution techniques, column chromatography, and error analysis are described by Arribas and Tosdal (1994). Measured Pb isotopic compositions were corrected for 0.125 percent fractionation per atomic mass unit, based upon replicate analyses of the National Bureau of Standards 981 and 982. Laboratory procedural blanks were 1 ng Pb or less and the precision of the isotopic measurements was generally better than 0.05 percent at the 2 sigma confidence level. Lead isotope compositions are reproducible to the ± 0.8 , ± 0.1 , and ± 0.14 percent (2 sigma), respectively, for ²⁰⁶Pb/²⁰⁴Pb, ²⁰⁷Pb/²⁰⁴Pb, and ²⁰⁸Pb/²⁰⁴Pb.

² The informal units, the McAfee quartzite and rocks of Jack's Peak, are stratigraphic designations restricted to the Independence Mountains. These units form part of the uppermost Ordovician Valmy Group at higher stratigraphic levels than the Snow Canyon Formation (D.T. Wilton, 1998, oral commun.)

Mountains (fig. 1) consists of several sedimentary rock-hosted Au deposits hosted in miogeoclinal calcareous rocks of the Ordovician and Silurian Hansen Creek Formation and overlying Silurian and Devonian Roberts Mountains Formation (Hofstra and others, 1991). Eugeoclinal siliciclastic rocks and chert of the Ordovician Valmy Group, including the Snow Canyon Formation and stratigraphically higher informal units known as the McAfee quartzite and rocks of Jack's Peak, structurally overlie the miogeoclinal calcareous rocks along the Roberts Mountains thrust system. Gold deposition is

interpreted to have occurred in the Eocene or early Oligocene (Hofstra, 1995).

Pb ISOTOPIC DATA FRAMEWORK IGNEOUS ROCKS

Pb isotopic compositions of intermediate and silicic plutonic and volcanic rocks emplaced through continental crust generally reflect the isotopic composition of crustal

environments (Davidson, 1996). Wooden and others (1997, this volume) noted large-scale geographic variations in Pb isotopic compositions of Mesozoic and Tertiary igneous rocks across northern Nevada and adjoining California and Utah. They, furthermore, argue that these Pb isotopic variations reflect compositional changes in the lower and middle crust and that they were established during continental rifting in the late Proterozoic and early Paleozoic (see also Tosdal and Wooden, 1997).

Three Pb isotopic provinces across northern Nevada were defined based on Pb isotopic compositions (fig. 1) (Wooden and others, 1997, this volume). These provinces, the western, central, and eastern Pb Provinces, form north-northwesterly trending crustal domains in central Nevada. The western Pb Province, unlike the other two, is more areally extensive, underlying most of western and northern Nevada where it cuts at high angles across the central and eastern Pb Provinces (fig. 1). Within the western and central Pb Province, Pb isotopic compositions of igneous rocks show regular eastward variations with geographic location (Wooden and others, this volume). The transition from the western to the central Pb Province is marked by a small but noticeable step increase in $^{208}\text{Pb}/^{204}\text{Pb}$ and $^{207}\text{Pb}/^{204}\text{Pb}$ at $^{206}\text{Pb}/^{204}\text{Pb}=19.1$. The eastward Pb isotopic variations across these province reflects increasing incorporation of crustal material in the igneous rocks, and the accompanying masking of any "mantle" signature in the magmas. This regular pattern changes at the boundary with the eastern Pb Province, or along the Carlin Trend, to the east of which no regular Pb isotopic pattern is discernible and there is a wide range of Pb isotopic compositions (Wooden and others, this volume). The most notable change here is the sudden increase in $^{208}\text{Pb}/^{204}\text{Pb}$ (>39.7) in Mesozoic plutons as well as a very large range in $^{206}\text{Pb}/^{204}\text{Pb}$ between 17 and 20 with a correspondingly high $^{208}\text{Pb}/^{204}\text{Pb}>37.5$ in Tertiary volcanic and plutonic rocks (fig. 2). These Pb isotopic compositions reflect the heterogeneous nature of the Archean crust, on the north, and Proterozoic crust, on the south (Zartman, 1974; Wright and Wooden, 1991; Wright and Snoke, 1993; Farmer and Ball, 1997; Wooden and others, 1997, this volume). Because of the regular Pb isotopic variations across the central Pb Province where most of the sedimentary rock-hosted Au deposits are located, the narrow Pb isotopic compositional range of any pluton that is potentially genetically related to a sedimentary rock-hosted Au deposit is predictable, if the data are not available.

Deposits for which sulfides were analyzed for their Pb isotopic compositions reported herein are scattered across northern Nevada. The westernmost is the Getchell deposit, which lies along the boundary between the western and central Pb Provinces (fig. 1), or at the edge of the thinned Precambrian crust. The Betze-Post deposit located along the Carlin trend lies along the boundary between the central and eastern Pb Provinces (fig. 1). The Jerritt Canyon Mining District lies close to the transition between the eastern or central Pb

Province and the western Pb Province (fig. 1). These deposits lie west of relatively intact Precambrian basement, as also suggested by Cunningham (1988).

SEDIMENTARY ROCKS

Present-day whole-rock Pb isotopic compositions are reported for twenty-seven Paleozoic sedimentary rocks from the Independence Mountains, Roberts Mountains, and from the Eureka area in northeastern Nevada (fig. 1; table 2). These samples include most major rock units and rock types present in the region of the sedimentary rock-hosted Au deposits along the Carlin trend and in the Independence Group (fig. 1). Notable exceptions are samples from the Popovich Formation and Rodeo Creek unit, which are the primary hosts for the deposits in the northern Carlin trend (Teal and Jackson, 1997). In addition, no Pb isotopic data are available for Cambrian and Ordovician sedimentary rocks hosting sedimentary-rock-hosted deposits in the Osgood Mountains in north-central Nevada. However, as Paleozoic detritus was derived principally from the east (Stewart, 1980; Poole and others, 1992; Gehrels and Dickinson, 1995), Pb isotopic compositions of Cambrian and Ordovician sedimentary rocks in the Osgood Mountains are likely to be similar to those determined for rocks farther east. A similar argument applies to the Popovich Formation and Rodeo Creek unit. Nonetheless, this assumption must be confirmed. Lastly, before a complete view of the Pb sources in the sedimentary rock-hosted can be established, Pb isotopic compositions of late Proterozoic and earliest Paleozoic clastic rocks not exposed near the deposits also need to be determined.

Pb isotopic compositions of eugeoclinal and miogeoclinal rocks plot as partly overlapping fields consistent with their in part common source regions and sedimentologic evidence (fig. 2). There is a considerable range in present-day Pb isotopic compositions, with $^{206}\text{Pb}/^{204}\text{Pb}$ ranging from 18.1 to 25.3 and a sympathetic range of $^{207}\text{Pb}/^{204}\text{Pb}$ between 15.57 and 16.0 (table 2; fig. 2b). Within this range, miogeoclinal calcareous rocks have low $^{206}\text{Pb}/^{204}\text{Pb}$ whereas the Pb isotopic compositions of eugeoclinal siliciclastic rocks span nearly the entire range of $^{206}\text{Pb}/^{204}\text{Pb}$. On the $^{207}\text{Pb}/^{204}\text{Pb}$ versus $^{206}\text{Pb}/^{204}\text{Pb}$ evolution diagram (fig. 2b), the eugeoclinal and miogeoclinal rocks scatters about a 700-Ma reference isochron defined by siliciclastic rocks of the Snow Canyon Formation. This 700-Ma reference isochron has no chronologic significance for these Paleozoic rocks but suggests some heterogeneity of initial Pb isotopic compositions of the fine-grained clastic rocks. It also emphasizes the influence of Precambrian craton detritus in these rocks.

A Pb isotopic distinction between miogeoclinal and eugeoclinal sedimentary rocks is particularly evident in the $^{208}\text{Pb}/^{204}\text{Pb}$ values (fig. 2a). Calcareous miogeoclinal rocks form a field that lies slightly below but parallel to the average

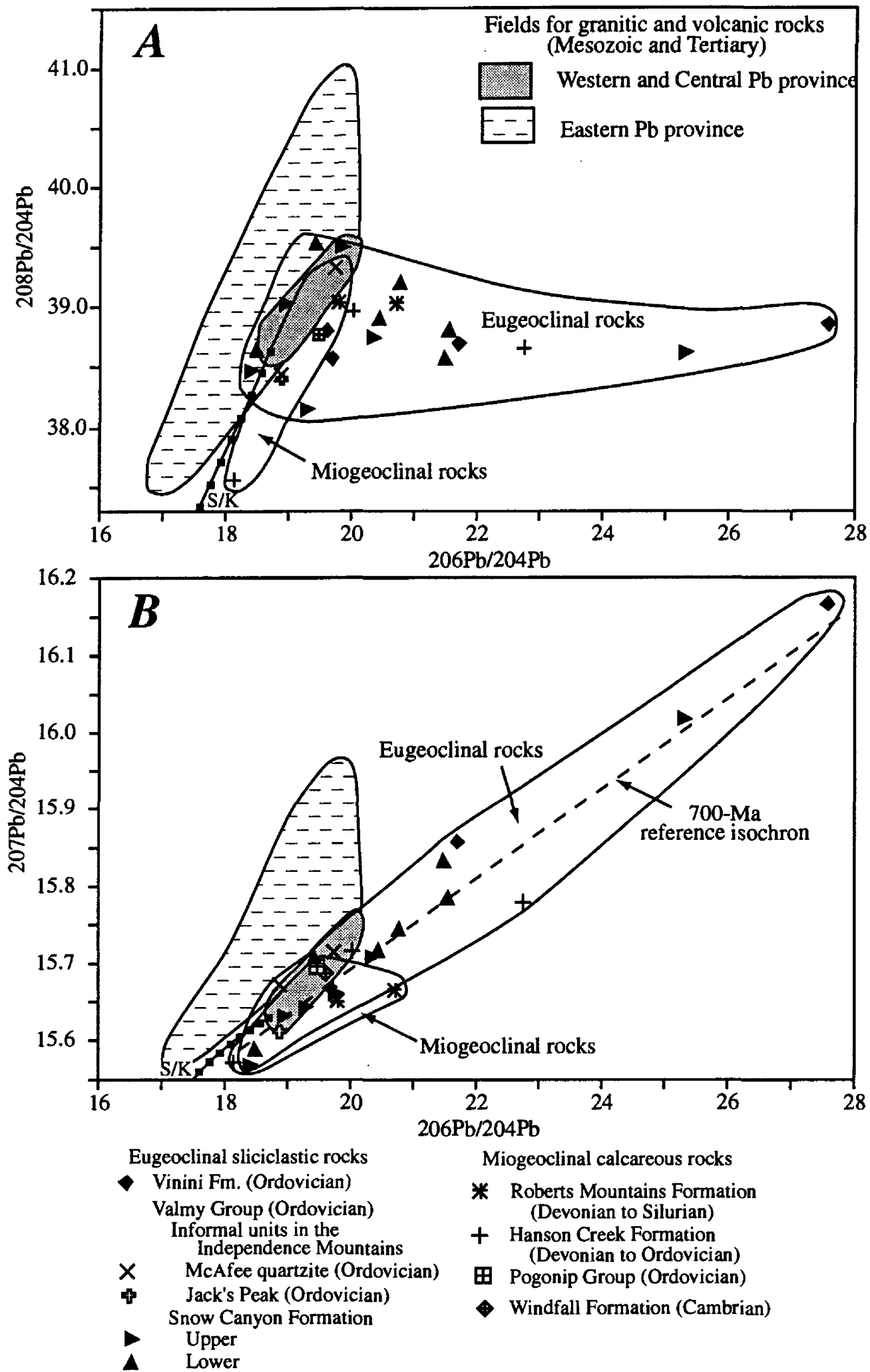


Figure 2: Pb isotopic compositions of potential Pb sources in sedimentary-rock-hosted Au deposits in northern Nevada. (A) $^{208}\text{Pb}/^{204}\text{Pb}$ versus $^{206}\text{Pb}/^{204}\text{Pb}$ and (B) $^{207}\text{Pb}/^{204}\text{Pb}$ versus $^{206}\text{Pb}/^{204}\text{Pb}$ evolution diagrams. Fields for the Pb isotopic provinces is from Wooden and others (1997; this volume and references therein). Rocks of Jack's Peak and the McAfee quartzite are informal units found at high stratigraphic levels in the Ordovician Valmy Group only in the Independence Mountains (D.T. Wilton, 1998 oral commun.). S/K, average crustal growth curve of Stacey and Kramers (1975).

ORE MINERALS

crustal growth curve of Stacey and Kramers (1975). This suggests a Th/U value close to average crust, or about 4. In contrast, $^{208}\text{Pb}/^{204}\text{Pb}$ values of eugeoclinal siliciclastic rocks vary over a narrow range between 38.1 and 39.5 despite a large range in $^{206}\text{Pb}/^{204}\text{Pb}$ between 18.3 and 25.3 (table 2; fig. 2A). Pb isotopic compositions of the eugeoclinal rocks plot in a field that overlaps the average crustal growth curve and the higher $^{208}\text{Pb}/^{204}\text{Pb}$ part of the miogeoclinal rock field, but more importantly the eugeoclinal rock field extends outward toward higher $^{206}\text{Pb}/^{204}\text{Pb}$ over the limited range of $^{208}\text{Pb}/^{204}\text{Pb}$. The limited range of $^{208}\text{Pb}/^{204}\text{Pb}$ in eugeoclinal rocks requires highly variable but generally low Th/U values less than the average crustal value of about 4. Time-integrated growth since deposition accounts for the variability in the $^{206}\text{Pb}/^{204}\text{Pb}$.

There are several explanations for the low but variable Th/U values in the siliciclastic eugeoclinal rocks. An increasing percentage of limestone can produce variable and low Th/U in sedimentary rocks (Rye and others, 1974; Goldhaber and others, 1995 and references therein). However, this explanation is untenable for the eugeoclinal siltstone, sandstone, and chert, as these rocks lack significant carbonate material in contrast to the dominantly calcareous miogeoclinal rocks. Island arc rocks and oceanic rift basalts represent two other environments where rocks can have low Th/U values (Tatsumoto, 1978; Allègre and others, 1986). Conceivably, detritus from these environments known to have been present along the coast of North America in the Paleozoic (Miller and others, 1992; Poole and others, 1992) could impart low Th/U values to the eugeoclinal rocks. In this scenario, variable Th/U values in the siliciclastic eugeoclinal rocks resulted from mixtures of detritus from different geologic environments. One clastic source was characterized by Th/U ~ 4, like the one contributing to the miogeoclinal rocks, that was shed from the craton to the east. A second clastic source was derived from fringing volcanic oceanic island arcs and back-arcs. Abundant phosphorite and organic matter are two other sedimentary environments where low Th/U values can be established (Kesler et al, 1994). Both characterize the Paleozoic clastic sequences particularly miogeoclinal rocks in northern Nevada. Just what is the explanation for the low Th/U trends is not known, but the tendency toward low Th/U is a distinctive attribute of the eugeoclinal sedimentary rocks. It reflects time-integrated growth since deposition in the Paleozoic, any modification of the Pb isotopic compositions during diagenesis in the Paleozoic, and subsequent low-grade regional metamorphism, plutonism, and hydrothermal circulation in the Mesozoic and Tertiary (Arehart and others, 1993a; Phinney and others, 1996; Ferdock and others, 1997; Groff and others, 1997).

At low values of $^{206}\text{Pb}/^{204}\text{Pb}$, eugeoclinal and miogeoclinal sedimentary rocks overlap the field for igneous rock in the central Pb Provinces, but only a limited part of the field for the eastern Pb province.

Au in sedimentary rock-hosted Au deposits is present in arsenian-rich rims on pyrite or as small arsenian pyrite grains in a siliceous groundmass (Arehart and others, 1993c; Cline and others, 1997; Ferdock and others, 1997). While pyritiferous rocks are abundant in the deposits, the complex relationship between ore-related arsenian pyrite and older non-ore pyrite precludes analyzing those minerals in bulk for their Pb isotopic compositions. Microanalytical techniques, in progress, are required to obtain Pb isotopic compositions of these complex minerals. Instead, other sulfide minerals, such as orpiment, realgar, and stibnite, that were deposited during the waning stage of hydrothermal activity (Cline and others, 1997; Ferdock and others, 1997) serve as proxies. Their Pb isotopic compositions can be analyzed using bulk mineral samples (see table 1 for analytical data and techniques). Some orpiment and realgar contain micro-inclusions of auriferous arsenian pyrite (Simon and others, 1997), hence any Pb isotopic composition of these minerals provides indirect constraints on Pb isotopic compositions of the hydrothermal fluid.

During this initial survey, Pb isotopic compositions were determined from eight sulfide minerals from seven samples (table 1). Four sulfide samples were of orpiment, realgar, marcasite, and stibnite formed as part of the paragenetic sequence at the Getchell deposit and in the Jerritt Canyon Mining District. Attempts to analyze orpiment, realgar, and stibnite from the Betze-Post deposit failed due to the lack of measurable Pb in these minerals. Similar results were obtained from orpiment and realgar from Getchell and Jerritt Canyon Mining District. Failure to detect Pb during analysis of realgar from Getchell using the SHRIMP confirms the low to negligible Pb contents of at least this sulfide mineral (R.M. Tosdal, 1997 unpublished data). From the Betze-Post deposit, Pb isotopic compositions were also determined on galena and pyrite (sample BMV, table 1) from one of the quartz-sericite-pyrite-base metal veins cutting the Goldstrike stock, and from pyrite (sample SP93-528, table 1) in thermally metamorphosed rocks adjacent to the stock. As sulfides in the quartz-sericite-pyrite veins are related to the stock, their Pb isotopic compositions record the magmatic-derived hydrothermal fluids. The paragenesis of pyrite in the hornfels aureole is enigmatic, as the pyritiferous whole-rock contains elevated arsenic concentrations typical of a sedimentary rock-hosted Au deposit, but also has low Au concentrations. The last sulfide from Betze-Post is from a 2 cm-in-diameter "framboid-like" marcasite (sample SP96-7033, table 1) interpreted to be a late hydrothermal mineral in the fringes of the deposit (S.G. Peters, 1996 unpublished data).

Pb isotopic compositions of sulfides regardless of paragenesis and location overlap the field for plutonic rocks from the eastern part of the central Pb Province (the higher $^{206}\text{Pb}/^{204}\text{Pb}$ portion of the field for the western and central Pb

provinces on fig. 3), but largely plot at higher $^{206}\text{Pb}/^{204}\text{Pb}$ values outside the field for igneous rocks from the eastern Pb Province. Sulfide Pb isotopic compositions also overlap the fields for miogeoclinal and eugeoclinal sedimentary rocks on the $^{208}\text{Pb}/^{204}\text{Pb}$ versus $^{206}\text{Pb}/^{204}\text{Pb}$ diagram (fig. 3A), but plot for the most part at higher $^{207}\text{Pb}/^{204}\text{Pb}$ at a given $^{206}\text{Pb}/^{204}\text{Pb}$ than do the miogeoclinal sedimentary rocks (fig. 3B). Orpiment and realgar from Getchell, located at the transition between the western and central Pb Province, have Pb isotopic compositions noticeably higher ($^{208}\text{Pb}/^{204}\text{Pb} > 39.020$; $^{206}\text{Pb}/^{204}\text{Pb} > 15.781$; $^{206}\text{Pb}/^{204}\text{Pb} > 19.929$; table 1) than those known for the Cretaceous Osgood Mountains stock (Pb isotopic compositions of K-feldspar: $^{208}\text{Pb}/^{204}\text{Pb} = 38.867$; $^{207}\text{Pb}/^{204}\text{Pb} = 15.685$; $^{206}\text{Pb}/^{204}\text{Pb} = 19.073$) (J.L. Wooden, 1996 unpublished data), the nearest igneous rocks; these granodioritic rocks were not genetically linked to the Au deposit (Groff and others, 1997) but they would represent approximate Pb isotopic compositions of magmatically derived Pb in this part of Nevada. In contrast, galena and pyrite from an igneous-related quartz-sericite-pyrite vein within the Goldstrike stock plot within the appropriate part of the field for the central Pb isotopic province that is consistent with their geographic positions. Pyrite from the hornfels aureole to the Goldstrike stock has similar $^{208}\text{Pb}/^{204}\text{Pb}$ and $^{207}\text{Pb}/^{204}\text{Pb}$ values as the igneous-related sulfides but has a higher $^{206}\text{Pb}/^{204}\text{Pb}$ values more typical of the miogeoclinal and eugeoclinal sedimentary rocks.

Igneous-related sulfides from the Betze-Post deposit seem to anchor the lower $^{206}\text{Pb}/^{204}\text{Pb}$ end of a diffuse sulfide array (fig. 3). Sulfides from the sedimentary rock-hosted Au deposits, except for a stibnite from the Jerritt Canyon Mining District, plot at higher $^{206}\text{Pb}/^{204}\text{Pb}$ values along this diffuse array that is anchored at the high $^{206}\text{Pb}/^{204}\text{Pb}$ end by late(?) marcasite from the Betze-Post deposit. The marcasite has very high $^{206}\text{Pb}/^{204}\text{Pb}$ (average=28.9) and $^{207}\text{Pb}/^{204}\text{Pb}$ (average=16.19) but a correspondingly low $^{208}\text{Pb}/^{204}\text{Pb}$ (38.9-39.2). With increasing $^{206}\text{Pb}/^{204}\text{Pb}$ values, sulfides from the sedimentary-rock-hosted Au deposits have Pb isotopic compositions that diverge from the fields for miogeoclinal rocks (fig. 3B). They do, however, lie completely within the field defined for Paleozoic eugeoclinal rocks on the $^{208}\text{Pb}/^{204}\text{Pb}$ versus $^{206}\text{Pb}/^{204}\text{Pb}$ diagram (fig. 3A). A similar tendency is shown on the $^{207}\text{Pb}/^{204}\text{Pb}$ versus $^{206}\text{Pb}/^{204}\text{Pb}$ diagram, except for the sulfides from Getchell which plot above the field for the eugeoclinal rocks (fig. 3B). Clearly, the available Pb isotopic composition of sulfides are more similar to those of the eugeoclinal rocks than to miogeoclinal rocks.

PRELIMINARY CONSTRAINTS OF Pb SOURCES IN THE SEDIMENT-HOST AU DEPOSITS

Limited Pb isotopic data from sulfides in the Getchell

deposits and in the Jerritt Canyon Mining District provide preliminary constraints on Pb sources in sedimentary rock-hosted Au deposits. Based on the data available, Pb in the deposits seemingly reflects mixing of Pb isotopic sources, a conclusion that is consistent with other fluid constraints (summarized by Arehart, 1996). One end member is a lower $^{206}\text{Pb}/^{204}\text{Pb}$ source characterized by Th/U and U/Pb values similar to igneous rocks present in the western and central Pb Province. The other end member or higher $^{206}\text{Pb}/^{204}\text{Pb}$ source is characterized by low but variable Th/U and elevated U/Pb like that present in the siliciclastic eugeoclinal rocks. Local contribution of Pb from calcareous miogeoclinal rocks hosting the deposits seemingly is precluded by two observations. One observation is that Pb isotopic compositions of orpiment, realgar, and stibnite from sedimentary-rock-hosted deposits lie at consistently higher $^{207}\text{Pb}/^{204}\text{Pb}$ for a given $^{206}\text{Pb}/^{204}\text{Pb}$ than do the calcareous miogeoclinal rocks. Two, the tendency of the Pb isotopic compositions of gold-ore-related sulfides to vary within (fig. 3A) or toward (fig. 3B) the field for eugeoclinal siliciclastic rocks, argues that these rocks, or rocks of similar Pb isotopic composition, provided one component of Pb in these deposits. This conclusion confirms the suggestion of Young-Mitchell and Titley (1996) whereby the relative Au-enrichment in eugeoclinal siliciclastic rocks makes them an attractive Au source. Unfortunately, the lack of Pb isotopic data for other potential sedimentary sources of Pb (see above) makes this hypothesis tentative until the appropriate Pb isotopic data is available. As the gold-ore-related sulfides mimic the tendency to low and variable Th/U of the eugeoclinal rock, we can also infer that the sulfides are relatively young.

The nature of the lower $^{206}\text{Pb}/^{204}\text{Pb}$ source in the gold-ore-related sulfides is at present speculative. As the mixing trends in the sulfides seems to be anchored in the Pb isotopic compositions of central Pb Province igneous rocks, a magmatic source is possible. However, derivation of this component of Pb from magmas suffers from two observations. One is the observation that the high $^{206}\text{Pb}/^{204}\text{Pb}$ mixing component in the sedimentary rock-hosted sulfides is not the host calcareous sedimentary rocks as would be expected in a simple magmatic-hydrothermal model where mixing is between a magmatic fluid and local country rocks. Rather, rocks more similar to the siliciclastic eugeoclinal rocks, which lie at high structural level, provided the sedimentary-rock Pb component. The second observation is that Pb in the Getchell sulfides are too radiogenic in terms of $^{207}\text{Pb}/^{204}\text{Pb}$ and $^{208}\text{Pb}/^{204}\text{Pb}$ to have been derived from igneous rocks in that part of Nevada (see above), and then mixed with Pb from the low but variable Th/U source. It is also important to emphasize that neither of these observations absolutely precludes Pb contribution from a magma.

Alternatively, it is possible that an unknown source containing the appropriately elevated $^{207}\text{Pb}/^{204}\text{Pb}$ values contributed the lower $^{206}\text{Pb}/^{204}\text{Pb}$ source. This source could be other sedimentary rocks at depth, perhaps of late Proterozoic and earliest Cambrian age, that contain detritus from Archean

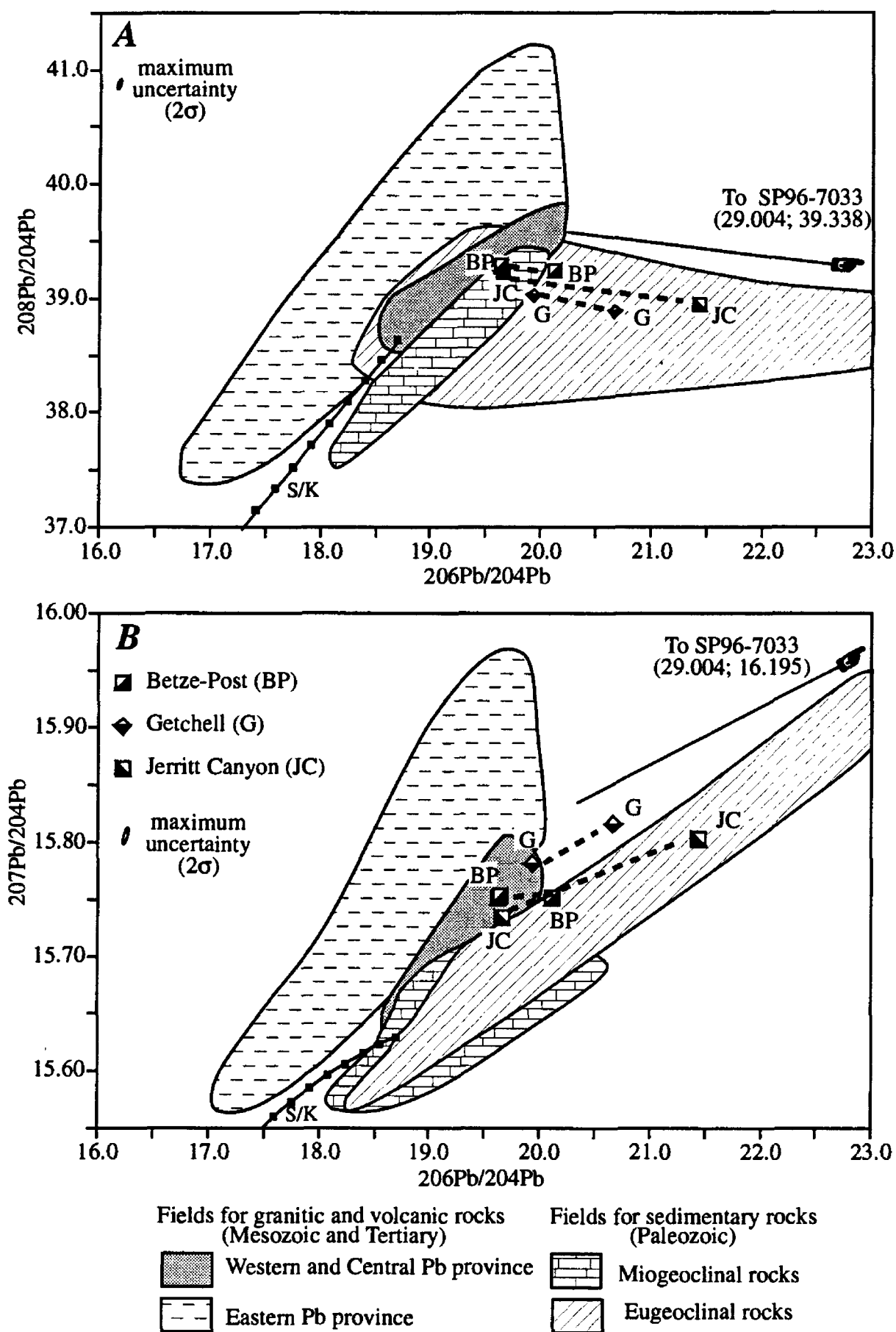


Figure 3: (A) $^{208}\text{Pb}/^{204}\text{Pb}$ versus $^{206}\text{Pb}/^{204}\text{Pb}$ and (B) $^{207}\text{Pb}/^{204}\text{Pb}$ versus $^{206}\text{Pb}/^{204}\text{Pb}$ evolution diagrams comparing Pb isotopic compositions of ore minerals from Getchell and Betze-Post deposits and from the Jerritt Canyon Mining District to potential sources of Pb in these minerals. Heavy dashed tie lines connect samples from the same deposit or mining district. S/K, average crustal growth curve of Stacey and Kramers (1975). B, Betze-Post; G, Getchell; JC, Jerritt Canyon Mining District.

rocks, such as the Wyoming Province (Wooden and Mueller, 1988; Farmer and Ball, 1997) or from a cratonic region even farther to the north (Gehrels and others, 1995). Conversely, this source could have been in the deep crust and have been fluids in Pb isotopic equilibrium with the thinned cratonic basement that underlies the late Proterozoic and Paleozoic

clastic sequences in the central Pb Province. These rocks are also inferred to have contributed Pb to the granitic magmas that intruded the crust (Wooden and others, 1997, this volume). We cannot discriminate between these possibility at this time.

Mixing of two Pb isotopic sources during evolution of the hydrothermal systems presumably took place near or at

the site of ore deposition in order to maintain their isotopic distinctions. Fluid mixing in sedimentary-rock-hosted deposits are common phenomenon and may include mixing of magmatic and sedimentary rock Pb during convective circulation around a cooling stock (Richards and others, 1991), or mixing at the site of ore deposition of basinal fluids traveling through different aquifers (Goldhaber and others, 1995). For the case of sedimentary-rock-hosted Au-Ag deposits in northern Nevada, identification of both Pb components in this mixing model awaits much additional data. However, it is certain that at least one component of Pb is derived from sedimentary rocks similar in Pb isotopic composition to the relatively Au-enriched eugeoclinal rocks (Young-Mitchell and Titley, 1996). Whether these rocks provided Pb to the waning stages of the hydrothermal system via descending circulating meteoric water (Kuehn and Rose, 1995) or via flowing fluids from reservoir rocks at depth or laterally is not known.

ACKNOWLEDGMENTS

We thank Dick Nanna and Getchell Gold, Barrick Goldstrike Mines, Inc., and Independence Mining Company for access to their mines for the samples reported herein, and for the many geologic discussions over the years. Greg Ferdock also provided samples from the Betze-Post Mine. We also gratefully acknowledge the efforts of Chuck Holdsworth for the chemical preparations necessary for the Pb isotopic analyses.

REFERENCES CITED

- Allègre, C.J., Dupré, B., and Lewin, E., 1986, Thorium/Uranium ratio of the Earth: *Chemical Geology*, v. 56, p. 219-227.
- Arehart, G.B., 1996, Characteristics and origin of sediment-hosted disseminated gold deposits: a review: *Ore Geology Reviews*, v. 11, p. 383-403.
- Arehart, G.B., Foland, K.A., Naeser, C.W., and Kesler, S.E., 1993a, $^{40}\text{Ar}/^{39}\text{Ar}$, K/Ar, and fission track geochronology of sediment-hosted disseminated gold deposits at Post/Betze, Carlin Trend, northeastern Nevada: *Economic Geology*, v. 88, p. 622-646.
- Arehart, G.B., Elderidge, C.S., Chryssoulis, S.L., and Kesler, S.E., 1993b, Ion microprobe determination of sulfur isotope variations in iron sulfides from the Post/Betze sediment-hosted disseminated gold deposits, Nevada, USA: *Geochimica et Cosmochimica Acta*, v. 57, p. 1505-1519.
- Arehart, G.B., Chryssoulis, S.L., and Kesler, S.E., 1993c, Gold and arsenic in iron sulfides from sediment-hosted disseminated gold deposits: Implications for depositional processes: *Economic Geology*, v. 88, p. 171-185.
- Arribas Jr., A., and Tosdal, R.M., 1994, Isotopic composition of Pb in ore deposits of the Betic Cordillera, Spain: Origin and relationship to other European deposits: *Economic Geology*, v. 89, p. 1074-1093.
- Christensen, O.D., 1993, Carlin trend geologic overview, *in* Christensen, O.D., ed., *Gold deposits of the Carlin Nevada: Society of Economic Geologists Guidebook Series*, v. 18, p. 12-26.
- Cline, J.S., Hofstra, A., Landis, G., and Rye, R., 1997, Ore fluids at the Getchell, Carlin-type gold deposit, north-central Nevada, *in* Vikre, P., Thompson, T.B., Bettles, K., Christensen, O., Parratt, R., eds., *Carlin-type gold deposits field conference: Society of Economic Geologist Guidebook Series*, v. 28, p. 155-166.
- Cunningham, C.G., 1988, The relationship between some disseminated gold deposits, the western edge of the Precambrian craton, and paleothermal anomalies in Nevada, *in* Schafer, R.W., Cooper, J.J., and Vikre, P.G., eds., *Bulk mineable precious metal deposits of the western United States; Symposium proceedings: Reno, Nevada, Geological Society of Nevada*, p. 35-48.
- Davidson, J.P., 1996, Deciphering mantle and crustal signatures in subduction zone magmatism, *in* Bebout, G.E., Scholl, D.W., Kirby, S.H., and Platt, J.P., eds., *Subduction: Top to Bottom: American Geophysical Monograph 96*, p. 251-262.
- Emsbo, P., Hofstra, A.H., Park, D., Zimmerman, J.M., and Snee, L., 1996, A mid-Tertiary age constraint on alteration and mineralization in igneous dikes on the Goldstrike Property, Carlin Trend, Nevada: *Geological Society of America Abstracts with Programs*, v. 28, p. A-476.
- Farmer, G.L., and Ball, T.T., 1997, Sources of Middle Proterozoic to early Cambrian siliciclastic sedimentary rocks in the Great Basin: A Nd isotope study: *Geological Society of America Bulletin*, v. 109, p. 1193-1205.
- Ferdock, G.C., Castor, S.B., Leonardson, R.W., and Collins, T., 1997, Mineralogy and paragenesis of ore stage mineralization in the Betze gold deposit, Goldstrike Mine, Eureka County, Nevada, *in* Vikre, P., Thompson, T.B., Bettles, K., Christensen, O., Parratt, R., eds., *Carlin-type gold deposits field conference: Society of Economic Geologist Guidebook Series*, v. 28, p. 75-86.
- Foley, N.K., and Ayuso, R.A., 1994, Lead isotope compositions as guides to early gold mineralization. The North Amethyst vein system, Creede District, Colorado: *Economic Geology*, v. 89, p. 842-1859.
- Gehrels, G.E., and Dickinson, W.R., 1995, Detrital zircon provenance of Cambrian to Triassic mio-geoclinal and eugeoclinal strata in Nevada: *American Journal of Sciences*, v. 295, p. 18-48.
- Goldhaber, M.B., Church, S.E., Doe, B.R., Aleinikoff, J.N., Brannon, J.C., Podosek, F.A., Mosier, E.L., Taylor, C.D., and Gent, C.A., 1995, Lead and sulfur isotope investigation of Paleozoic sedimentary rocks from the southern midcontinent of the United State: Implications for paleohydrology and ore genesis of the southeast Missouri lead belts: *Economic Geology*, v. 90, p. 1875-1910.
- Groff, J.A., Heizler, M.T., McIntosh, W.C., and Norman, D.I., 1997, ^{40}Ar - ^{39}Ar dating and mineral paragenesis for Carlin-type gold deposits along the Getchell Trend, Nevada: Evidence for Cretaceous and Tertiary gold mineralization: *Economic Geology*, v. 92, p. 601-622.
- Heyl, A.V., Landis, G.P., and Zartman, R.E., 1974, Isotopic evidence for the origins of Mississippi Valley-type mineral deposits: A review: *Economic Geology*, v. 69, p. 997-1006.
- Hofstra, A.H., Daly, W.E., Birak, D.J., and Doe, T.C., 1991, Geologic framework and genesis of Carlin-type gold deposits in the Jerritt Canyon district, Nevada, U.S.A., *in* Ladeira, E.A., ed., *BRAZIL GOLD '91, The economics, geology, geochemistry and genesis of gold deposits: Rotterdam, A.A. Balkema*, p. 77-87.
- Hofstra, A.H., 1995, Timing and duration of Carlin-type gold deposits in Nevada and Utah—Relation to back-arc extension and

- magmatism: Geological Society of America Abstracts with Programs, v. 27, no. 6, pp. A-329.
- Hofstra, A.H., 1997, Isotopic composition of sulfur in Carlin-type gold deposits: Implications for genetic models, *in* Vikre, P., Thompson, T.B., Bettles, K., Christensen, O., Parratt, R., eds., Carlin-type gold deposits field conference: Society of Economic Geologist Guidebook Series, v. 28, p. 119-130.
- Ilchik, R.P., and Barton, M.D., 1997, An amagmatic origin of Carlin-type gold deposits: *Economic Geology*, v. 92, p. 269-288.
- Keuhn, C.A., and Rose, A.W., 1995, Carlin gold deposit, Nevada: Origin in a deep zone of mixing between normally pressured and over pressured fluids: *Economic Geology*, v. 90, p. 17-36.
- Kesler, S.E., Cummings, G.L., Krstic, D., and Appold, M.S., 1994, Lead isotope geochemistry of Mississippi Valley-type deposits of the southern Appalachians: *Economic Geology*, v. 89, p. 307-321.
- Leonardson, R.W., and Rahn, J.E., 1996, Geology of the Betze-Post gold deposits, Eureka County Nevada, *in* Coyner, A.R., and Fahey, P.L., eds., Geology and ore deposits of the American Cordillera: Geological Society of Nevada Symposium Proceedings, Reno/sparks, Nevada, April, 1995, p. 61-94.
- Miller, E.L., Miller, M.M., Stevens, C.H., Wright, J.E., and Madrid, R., 1992, Late Paleozoic paleogeographic and tectonic evolution of the western U.S. Cordillera, *in* Burchfiel, B.C., Lipman, P.W., and Zoback, M.L., eds., The Cordilleran Orogen: Conterminous U.S.: Boulder, Colorado, Geological Society of America, The Geology of North America, v. G-3, p. 57-106.
- Phillips, G.N., and Powell, R., 1993, Link between gold provinces: *Economic Geology*, v. 88, p. 1084-1098.
- Phinisey, J.D., Hofstra, A.H., Snee, L.W., Roberts, T.T., Dahl, A.R., and Loranger, R.J., 1996, Evidence for multiple episodes of igneous and hydrothermal activity and constraints on the timing of gold mineralization, Jerritt Canyon District, *in* Coyner, A.R., and Fahey, P.L., eds., Geology and ore deposits of the American Cordillera: Geological Society of Nevada Symposium Proceedings, p. 15-39.
- Poole, F.G., Stewart, J.H., Palmer, A.R., Sandberg, C.A., Madrid, R.J., Ross, Jr., R.J., Hintze, L.F., Miller, M.M., and Wrucke, C.T., 1992, Latest Precambrian to latest Devonian time; Development of a continental margin, *in* Burchfiel, B.C., Lipman, P.W., and Zoback, M.L., eds., The Cordilleran Orogen: Conterminous U.S.: Boulder, Colorado, Geological Society of America, The Geology of North America, v. G-3, p. 9-56.
- Powell, R., Will, T.M., and Phillips, G.N., 1991, Metamorphism in Archaean greenstone belts: Calculated fluid compositions and implications for gold mineralization: *Journal of Metamorphic Geology*, v. 9, p. 14-150.
- Richards, J.P., McCulloch, M.T., Chappell, B.W., and Kerrich, R., 1991, Sources of metals in the Porgera gold deposit, Papua New Guinea: Evidence from alteration, isotope and noble gas geochemistry: *Geochimica et Cosmochimica Acta*, v. 55, p. 565-580.
- Rye, D.M., Doe, B.R., and Delevaux, M.H., 1974, Homestake gold mine, South Dakota: II. Lead isotopes, mineralization ages, and source of lead in ores of the northern Black Hills: *Economic Geology*, v. 69, p. 814-822.
- Seedorf, E., 1991, Magmatism, extension, and ore deposits of Eocene to Holocene age in the Great Basin; mutual effects and preliminary proposed genetic relationships, *in* Raines, G.L., Lisle, R.E., Schafer, R.W., and Wilkinson, W.H., eds., Geology and ore deposits of the Great Basin, Symposium Proceedings: Geological Society of Nevada, v. , p. 133-178.
- Sillitoe, R.H., and Bonham, H.F., 1990, Sediment-hosted gold deposits—Distal products of magmatic-hydrothermal systems: *Geology*, v. 18, p. 157-161.
- Simon, G., Kesler, S.E., and Chryssoulis, S.L., 1997, Partitioning of gold between arsenian pyrite and As-sulfides in sediment-hosted micron gold deposits: Geological Society of America Abstracts with Programs, v. 29, no. 6, p. A-207.
- Stacey, J.S., and Kramers, J.D., 1975, Approximation of terrestrial lead isotope evolution by a two-stage model: *Earth and Planetary Science Letters*, v. 26, p. 207-221.
- Stewart, J.H., 1980, Geology of Nevada: Nevada Bureau of Mines and Geology, Special Publication 4, 136 p.
- Tatsumoto, M., 1978, Isotopic compositions of lead in oceanic basalt and its implication to mantle evolution: *Earth and Planetary Science Letters*, v. 38, p. 63-87.
- Teal, L., and Jackson, M., 1997, Geologic overview of the Carlin Trend gold deposits and description of recent deep discoveries: Society of Economic Geologist Newsletter, no. 31.
- Theodore, T.G., 1998, Geology of pluton-related gold mineralization at Battle Mountain, Nevada: Tucson, Arizona, University of Arizona and U.S. Geological Survey Center for Mineral Resources Monograph 2 (in press).
- Titley, S.R., 1991, Phanerozoic ocean cycles and sedimentary-rock-hosted gold ores: *Geology*, v. 9, p. 645-648.
- Tosdal, R.M., and Wooden, J.L., 1997, Granites, Pb isotopes, and the Carlin and Battle Mt.-Eureka trends, Nevada: Geological Society of America Abstracts with Programs, v. 29, no. 6, p. A-61.
- Wooden, J.L., and Mueller, P.A., 1988, Pb, Sr, and Nd isotopic compositions of a suite of Late Archean igneous rocks, eastern Beartooth Mountains: Implications for crust-mantle evolution: *Earth and Planetary Science Letters*, v. 87, p. 59-72.
- Wooden, J.L., Tosdal, R.M., and Kistler, R.W., 1997, Pb and Sr isotopic mapping of crustal structure in the Northern Great Basin, *in* Vikre, P., Thompson, T.B., Bettles, K., Christensen, O., Parratt, R., eds., Carlin-type gold deposits field conference: Society of Economic Geologist Guidebook Series, v. 28, p. 47-53.
- Wooden, J.L., Tosdal, R.M., and Kistler, R.W., this volume, Pb isotopic mapping of crustal structure in the northern Great Basin and relationships to Au deposit trends, *in* Tosdal, R.M., ed., 1998, Toward a better understanding of the Au metallogeny of northern Nevada: U.S. Geological Survey Open-File Report.
- Wright, J.E., and Wooden, J.L., 1991, New Sr, Nd, and Pb isotopic data from plutons in the northern Great Basin: Implications for crustal structure and granite petrogenesis in the hinterland of the Sevier thrust belt: *Geology*, v. 19, p. 456-460.
- Wright, J.E., and Snoke, A.W., 1993, Tertiary magmatism and mylonitization in the Ruby-East Humboldt metamorphic core complex, north-eastern Nevada: U-Pb geochronology and Sr, Nd, and Pb isotope geochemistry: *Geological Society of America Bulletin*, v. 105, p. 935-952.
- Young-Mitchell, M.N., and Titley, S.R., 1996, Origins and consequences of gold enrichments in Lower Paleozoic organic-rich strata: Geological Society of America Abstracts with Programs, v. 28, no. 7, p. A-86.
- Zartman, R.E., 1974, Lead isotopic provinces in the cordillera of the western United States and their geologic significance: *Economic Geology*, v. 69, p. 792-805.

REGIONAL ANALYSIS OF THE DISTRIBUTION OF GOLD DEPOSITS IN NORTHEAST NEVADA USING NURE ARSENIC DATA AND GEOPHYSICAL DATA

By Boris B. Kotlyar, Donald A. Singer, Robert C. Jachens, and Ted G. Theodore

ABSTRACT

Regional geochemical surveys, gravity surveys, and magnetic surveys examined by means of modern computer-contouring methods employing various normalization and filtering techniques provide additional insight into crustal processes of metallogenesis. Regional-scale distribution patterns of stream-sediment arsenic anomalies in northeast Nevada bear striking similarities to some important mineralized trends and to some isostatic residual gravity anomalies and their gradients. The gravity anomalies and their bounding gradients, which primarily result from density distributions in the pre-Cenozoic rocks of the middle and upper crust, and their coincidence with linear zones of apparently enriched arsenic suggests that arsenic, as well as precious metals, also may have been derived from the middle and upper crust. However, other broad areas of apparently elevated arsenic concentrations show no indication of the presence of metal deposits. In addition, a map of residual magnetic potential anomalies indicates that magnetic rocks in the middle and upper crust—most likely late Tertiary in age—also must play an important role in the eventual distribution of some hot-spring gold-silver deposits.

INTRODUCTION

Regional-scale geochemical surveys, which were completed by the National Uranium Resource Evaluation (NURE) Program in the 1970's in northeast Nevada, can provide valuable information to a number of earth-science disciplines. However, this information is most powerful when the data are treated by modern computer methodologies and compared with regional geophysical surveys. For example, these data in northeast Nevada can provide fundamental information about: (1) geochemical background metal content of soils and stream sediments prior to much of the widespread gold mining in this part of Nevada (useful for ongoing environmental investigations); (2) regional metal distributions requisite for site-specific and mining district-scale geochemical studies; (3) the regional extent of metallotects such as the Cortez trend (also termed the Battle

Mountain-Eureka trend) of mineral deposits, and (4) linkages between deep-seated crustal structures and metals channeled along them. In this report, we focus on the last three.

Soil and stream-sediment geochemical data from the NURE program (Hoffman and Marsh, 1994), and a recently released digital version of the same data (Hoffman and Buttleman, 1994) is the multipurpose database examined herein. In spite of the recognized shortcomings of the geochemical data, including different sampling techniques, variability in density of sampling, different size fractions used for analysis, and different laboratories with different analytical sensitivities, the data can be a source of abundant information if treated properly (see also, McGuire and others, 1994; King, 1996; King and others, 1996).

For the present study, NURE data in northeast Nevada in the areas of the Carlin, Cortez, and Getchell gold trends were selected for study, including the McDermitt, Winnemucca, Millet, Wells, and Elko 1°X 2° quadrangles (fig. 1). From all elements analyzed in these areas, arsenic specifically was selected for our study, primarily because of: (1) its presence in a wide variety of minerals in many base- and precious-metal deposits in the region, and (2) the large number of samples in which arsenic contents were determined at acceptable lower determination levels. In the Ely 1°X 2° quadrangle, which is immediately south of the Elko quadrangle (fig. 1), samples were collected but not analyzed by the NURE Program. The NURE samples in the five selected quadrangles include three types of samples: wet stream-sediment samples, and dry stream-sediment samples, and soil samples.

From the original 4,758 samples with detectable arsenic in the five quadrangles, 4,256 samples were extracted and interpolated to a square grid by means of a routine based on the principal of minimum curvature (Briggs, 1974; see also, Kotlyar and others, 1995). However, the arsenic data from these quadrangles first were transformed. With trace-element geochemistry, small but important variations may be compressed into a relatively narrow range while other variation is spread out over a range wider than its importance justifies (Masters, 1993). Another reason to transform the data is that tests of significance of correlation coefficients are not valid for skewed distributions. For these reasons, we have used a logarithmic (base 10) transformation on the data (table 1A).

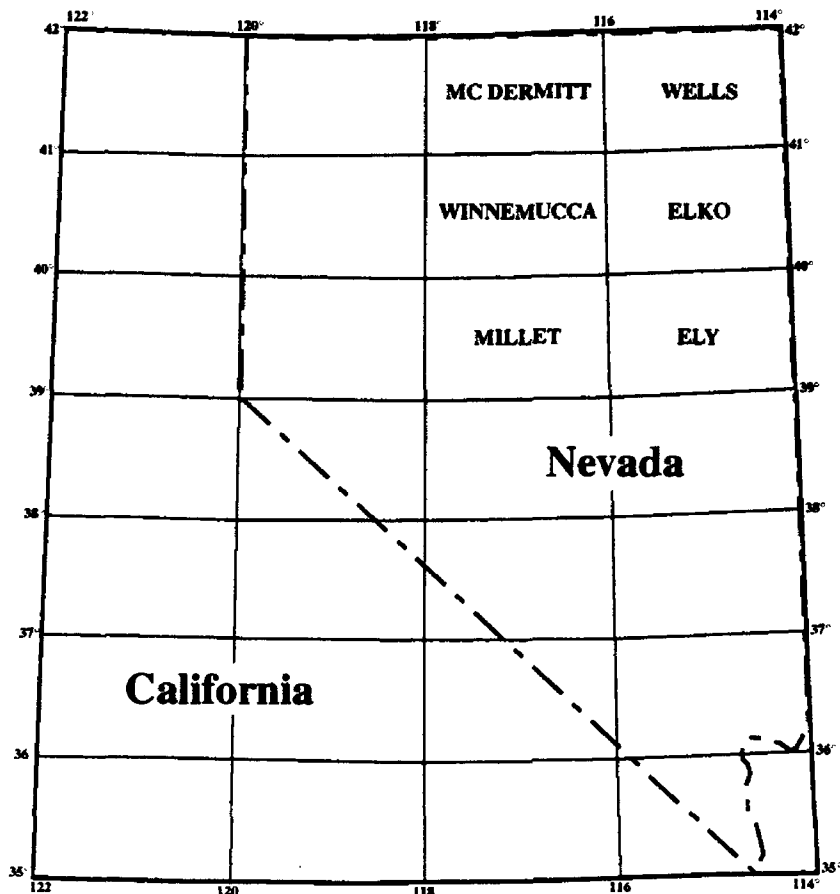


Figure 1. Index map showing location of six 1° X 2° quadrangles discussed in this report.

Histograms of the log transformed data for arsenic typically show a spike on the left (fig. 2) representing values substituted by the analyst for lower limit of detection or censored data. If the number of cases affected by this substitution represents more than a few percent of the number of samples, this practice can introduce biases in contoured values. For this reason, we have removed all such values (502 samples) in the following transformations and in contouring.

For arsenic, the transformed values were standardized or normalized to a Z-score by subtracting the subset's mean and dividing by its standard deviation: $(X_c - X_{\text{mean}})/X_{\text{standard deviation}}$, where all values are logarithms and X_c is the concentration for arsenic in an analyzed sample. Various descriptive statistics in the transformed database used to generate the elemental distribution diagrams also are given in table 1. This process removes all effects of different means and measurement scales and facilitates the comparison of the spatial patterns of elements among the five quadrangles. Histograms of the normalized As data approximate lognormal distributions (fig. 2B). Kotlyar and others (1995) discuss the gridding procedures employed and the various filter parameters used.

A computer-contoured plot for arsenic shows that the above-described transformation technique results in a relatively even distribution of arsenic across all of the quadrangles investigated (fig. 3). Boundary effects are absent with the possible exception of the data from the Elko 1° X 2° quadrangle. Areas shown in white represent areas excluded from the contouring procedures because of an absence of samples.

DISCUSSION

Elevated concentrations of arsenic, where arsenic contents are greater than scaled values of 0.0, are present in the general area of known gold, mercury and antimony deposits of various types (figs. 3 and 4). However, the distribution of arsenic also forms individual anomalies and trends, which conform closely to the major known gold trends in the region, including the Carlin, Cortez, and Getchell trends. With the exception of a group of Comstock- and Sado-type deposits in the southwestern corner of the Millet quadrangle, hot-spring Au-Ag deposits at Buckskin, and distal-disseminated Ag-Au deposits in the northwest part of the Wells 1° X 2° quadrangle (fig. 3), all other gold deposits are in areas where regional stream-sediment arsenic contents are inferred to have values greater than scaled values of 0.0. Nonetheless, many areas have arsenic anomalies or trends wherein regional stream-sediment values are greater than scaled values of 0.0 (fig. 3). These areas include:

- (1) to the south-east of the Dixie hot-spring gold deposit;
- (2) to the north-northeast and south-southwest of the Austin sediment-hosted Au deposit in the Millet quadrangle;
- (3) to the northwest of the Goldbanks hot spring gold deposit in the Winnemucca quadrangle;
- (4) to the north and northeast of the Bald Mountain sediment-hosted gold deposit;
- (5) to the north-northeast of the Gnome and Rain sediment-hosted gold deposits (fig. 4) in the Winnemucca and Elko quadrangles;
- (6) to the north and northwest of the Kinsley sediment-hosted gold deposit near the southeast corner of the Elko quadrangle;
- (7) to the east of Bootstrap and Dee sediment-hosted gold deposits (fig. 4) in the McDermitt quadrangle;
- (8) to the east of the Getchell and Rabbit Creek sediment-hosted gold deposits in the McDermitt quadrangle, although a part of this anomaly may reflect wind-blown contamination from the dumps at Getchell.

Generalized arsenic anomalies and their trends at the regional scale apparently have mainly four orientations, including northwest (Cortez and Carlin), northeast (Gold Bartonkin Springs and others), north-northeast (Getchell, Austin, and Independence Range), and east-northeast (to the east of Getchell). These arsenic trends also are characterized by relatively pronounced changes of orientation along an "arsenic boundary" present in the central part of the region (fig. 3). To the northwest of this boundary, many of the arsenic anomalies have a northwest orientation, whereas to the southeast of the boundary, many of the arsenic anomalies have a northeast orientation.

Table 1. Descriptive statistics of arsenic in NURE soil and stream-sediment samples in five 1° X 2° quadrangles in northeast Nevada. Data from Hoffman and Buttleman (1994). *A*, logarithmic data (base 10); *B*, Normalized Z-score data without censored values (see text).

A. Logarithmic data

Arsenic	McDermitt	Winnemucca	Millet	Wells	Elko
Mean	3.617	3.531	3.89	0.266	3.192
Std. Dev	0.226	1.25	0.692	0.309	1.019
Count	1383	692	793	58	1832
Minimum	3	1.544	1.845	0	-0.301
Maximum	4.643	5.769	5.75	1.079	4.544
Coef. Var.	0.062	0.354	0.178	1.164	0.319
Range	1.643	4.225	3.905	1.079	4.845
Sum Squares	18163.274	9708.826	12376.939	9.532	20561.296
Skewness	0.141	-0.711	-1.585	0.771	-2.727
Kurtosis	0.454	-1.121	2.643	-0.531	6.226
Median	3.602	4.085	4.005	0.151	3.477
Mode	3.602	1.544	1.845	0	3.477
10% Tr. Mean	3.612	3.599	4.008	0.231	3.447

B. Normalized Z-score data

Arsenic	McDermitt	Winnemucca	Millet	Wells	Elko
Mean	0	0	0	0	0
Std. Dev.	1	1	1	1	1
Count	1383	489	691	19	1674
Minimum	-2.73	-2.545	-1.547	-1.005	-1.98
Maximum	4.542	3.832	5.101	2.455	4.221
Range	7.272	6.377	6.647	3.46	6.201
Skewness	0.141	0.679	1.341	1.025	0.243
Kurtosis	0.454	0.746	2.741	0.485	0.928
Median	-0.066	-0.09	-0.208	-0.287	-0.064
10% Tr. Mean	-0.021	-0.063	-0.112	-0.085	-0.002

A number of earlier studies compared the distribution of mineral deposits in the region with geophysical fields, and showed that a correlation between gradients in gravity fields and some of the gold trends, in particular the Cortez trend (Grauch and others, 1995). In the remainder of this report, we will compare the regional distribution of arsenic anomalies and loci of mineral districts with regional gravity and magnetic patterns.

Figure 5 shows the gravity field of the study area, modified to emphasize those parts of the field most likely to be related to features in the middle and upper crust (see also, Saltus and Jachens, 1995). Two corrections were added to the standard Bouguer gravity to produce the map shown in figure 5. First, the strong regional gravity variations produced by deep-seated density distributions that isostatically support the topography were removed by direct calculation, assuming an Airy-

Heiskanen model of isostatic compensation (Simpson and others, 1986). The resulting map (see map of isostatic residual gravity anomalies in Saltus and Jachens, 1995) emphasizes gravity anomalies from density distributions in the middle and upper crust. A second correction was added to the isostatic residual gravity, one designed to eliminate the pervasive pattern of gravity lows that are caused by the low-density deposits contained in the Cenozoic basins throughout the region. This correction was determined by iteratively partitioning the isostatic residual gravity field into a "basin" component and a "basement" component (Jachens and Moring, 1990). The "basement" gravity component, shown in figure 5, approximates the gravity field that would have been measured if the Cenozoic deposits did not exist, and thus reflects the density distributions in the pre-Cenozoic rocks of the middle and upper crust. Coincidence of arsenic anomalies and their

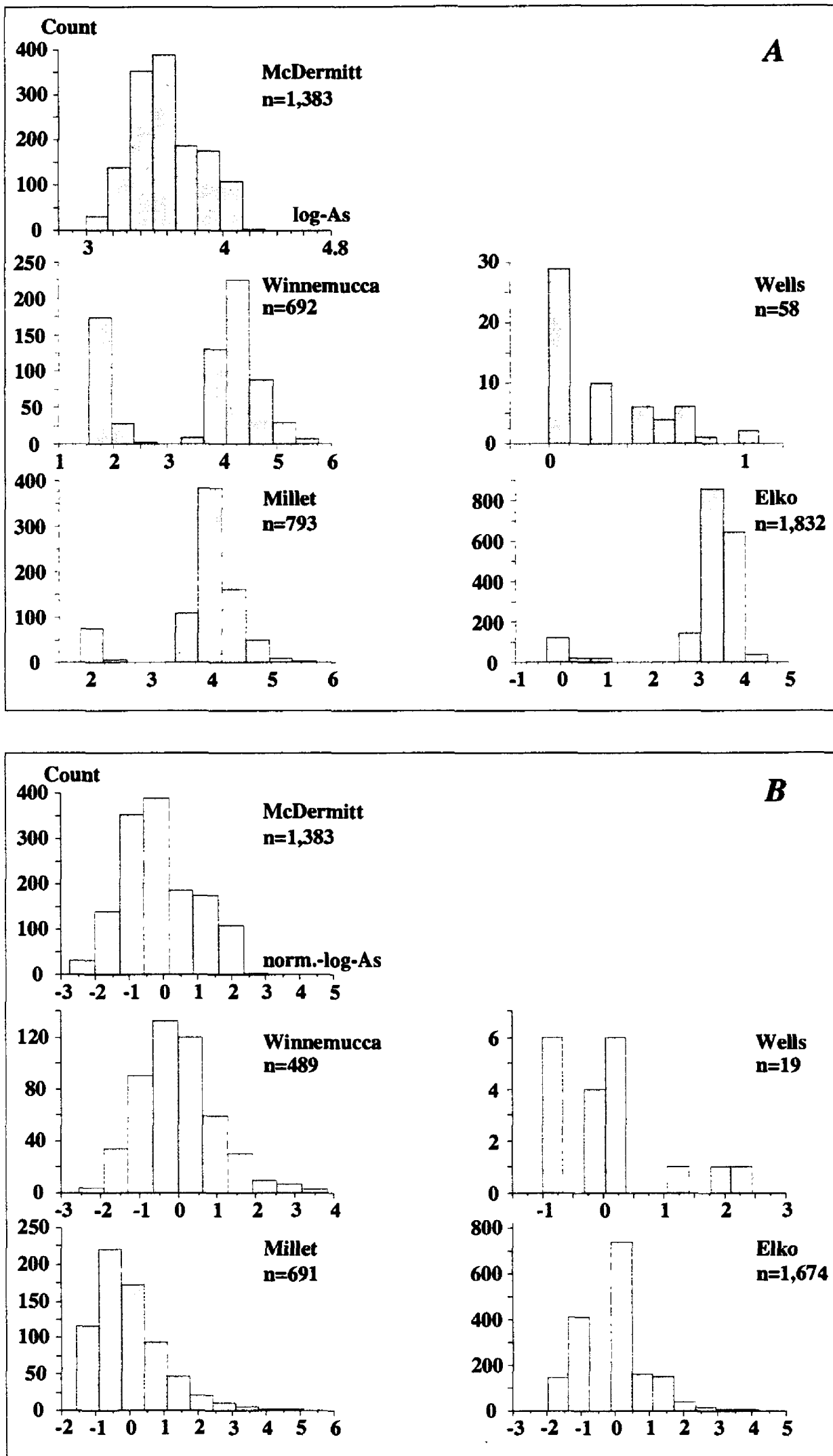


Figure 2. Frequency distributions of (A) logs (base 10) of arsenic contents (ppm) and (B) normalized logs of arsenic contents (see text), with censored data removed in sediment samples in McDermitt, Wells, Winnemucca, Elko, and Millet 1° X 2° quadrangles, Nevada.

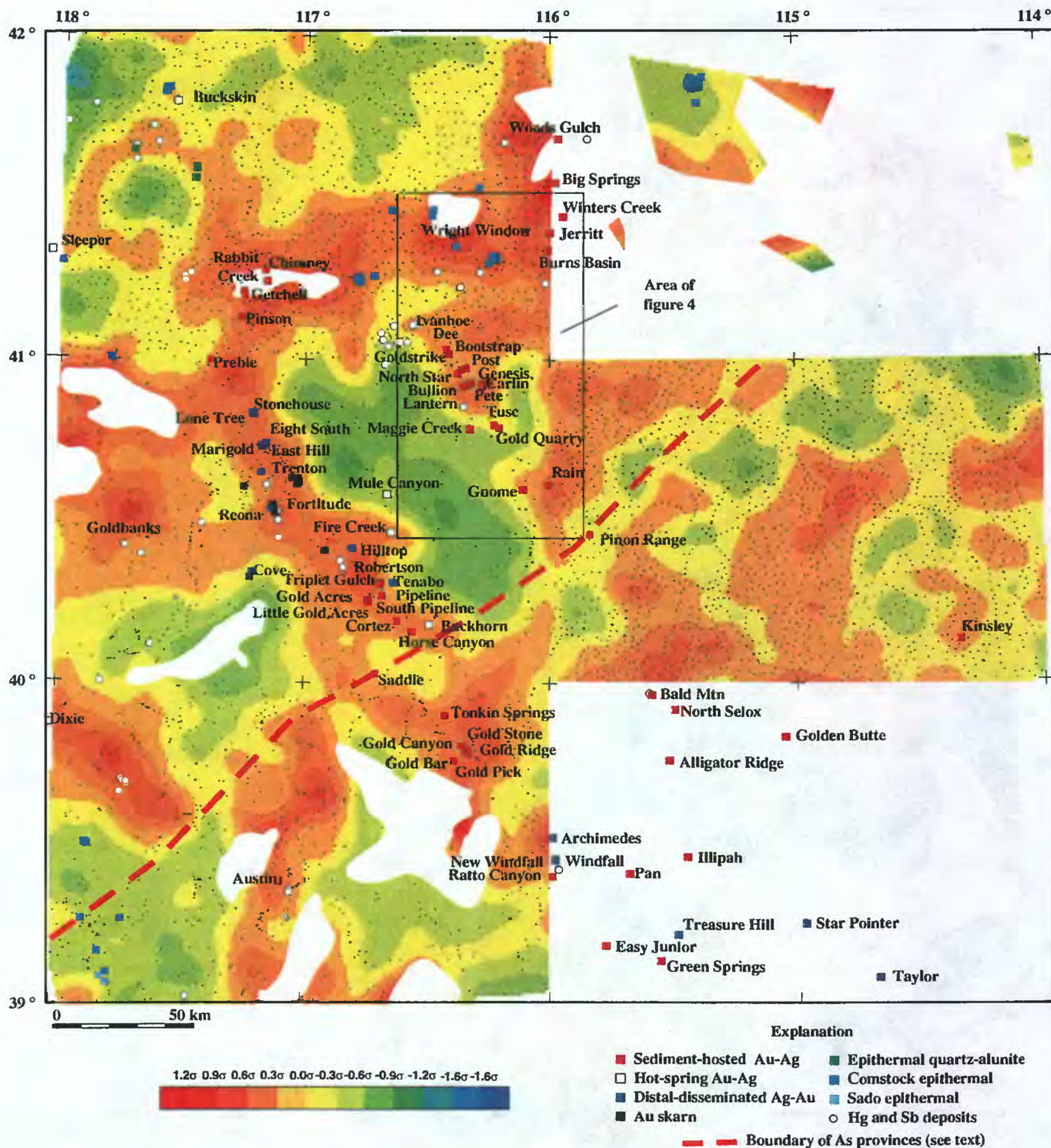


Figure 3. Distribution of normalized logs for arsenic contents in sediment samples, northeast Nevada. Dots are sample locations of analyzed samples. Reported arsenic contents gridded (1,000-m-wide cells) and filtered ($z = 5,000$ m) (see Kotlyar and others, 1995), resulting in contours showing standard deviations (s) of log-transformed metal concentrations from the mean. Unpatterned, areas without analyzed samples. Deposit types from U.S. Geological Survey Mineral Resource Data System (MRDS) (see also Sherlock, and others, 1996). Arsenic data modified from Hoffman and Buttleman (1994).

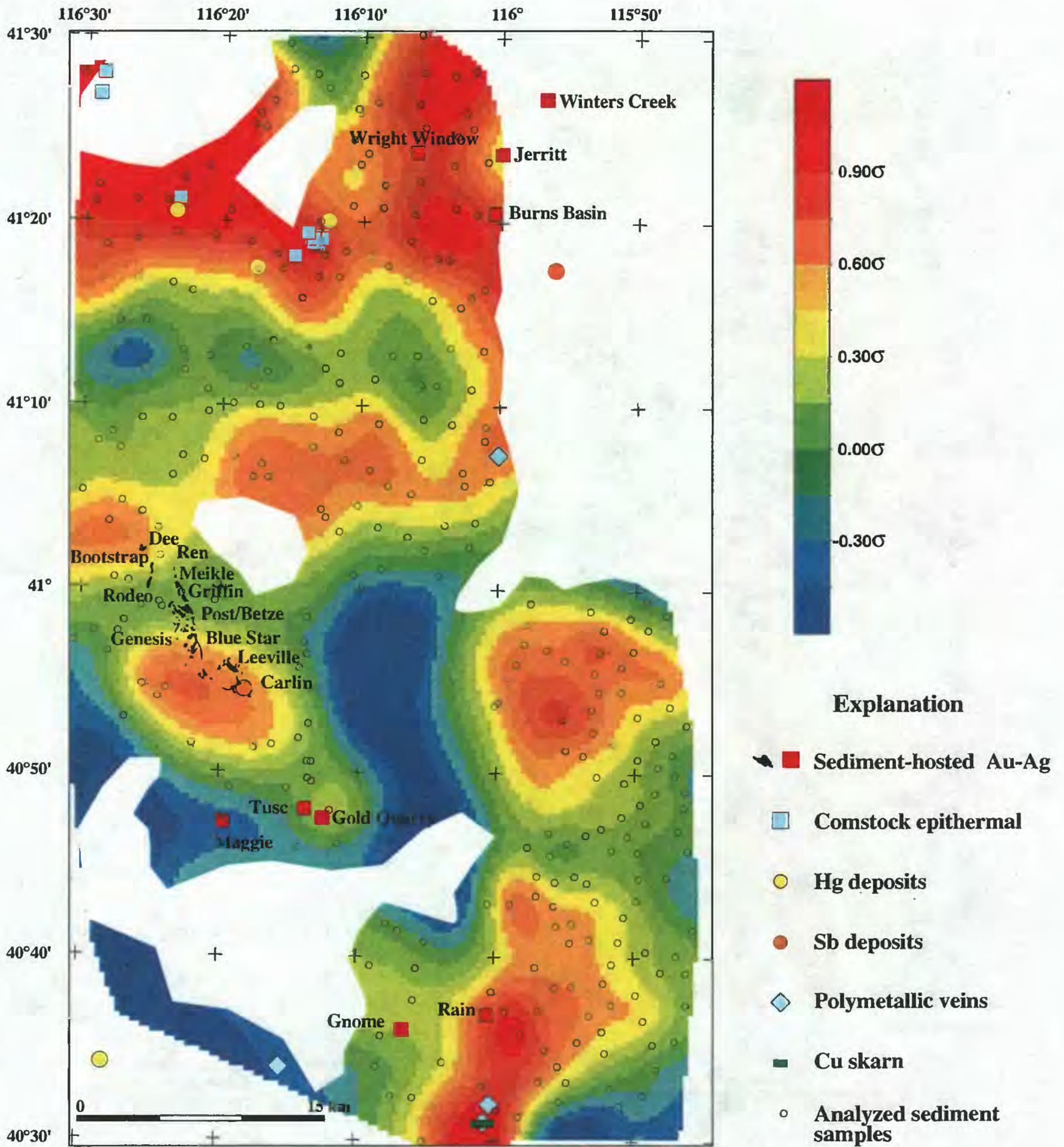


Figure 4. Distribution of normalized logs for arsenic contents in sediment samples near Carlin trend and surrounding area, Nevada (500-m-wide cells gridding, and $z = 3,000$ m), (see Kotlyar and others, 1995). Surface projection of sediment-hosted Au-Ag orebodies from S. G. Peters (written, commun., 1997). Deposit type and source of geochemical data same as figure 3.

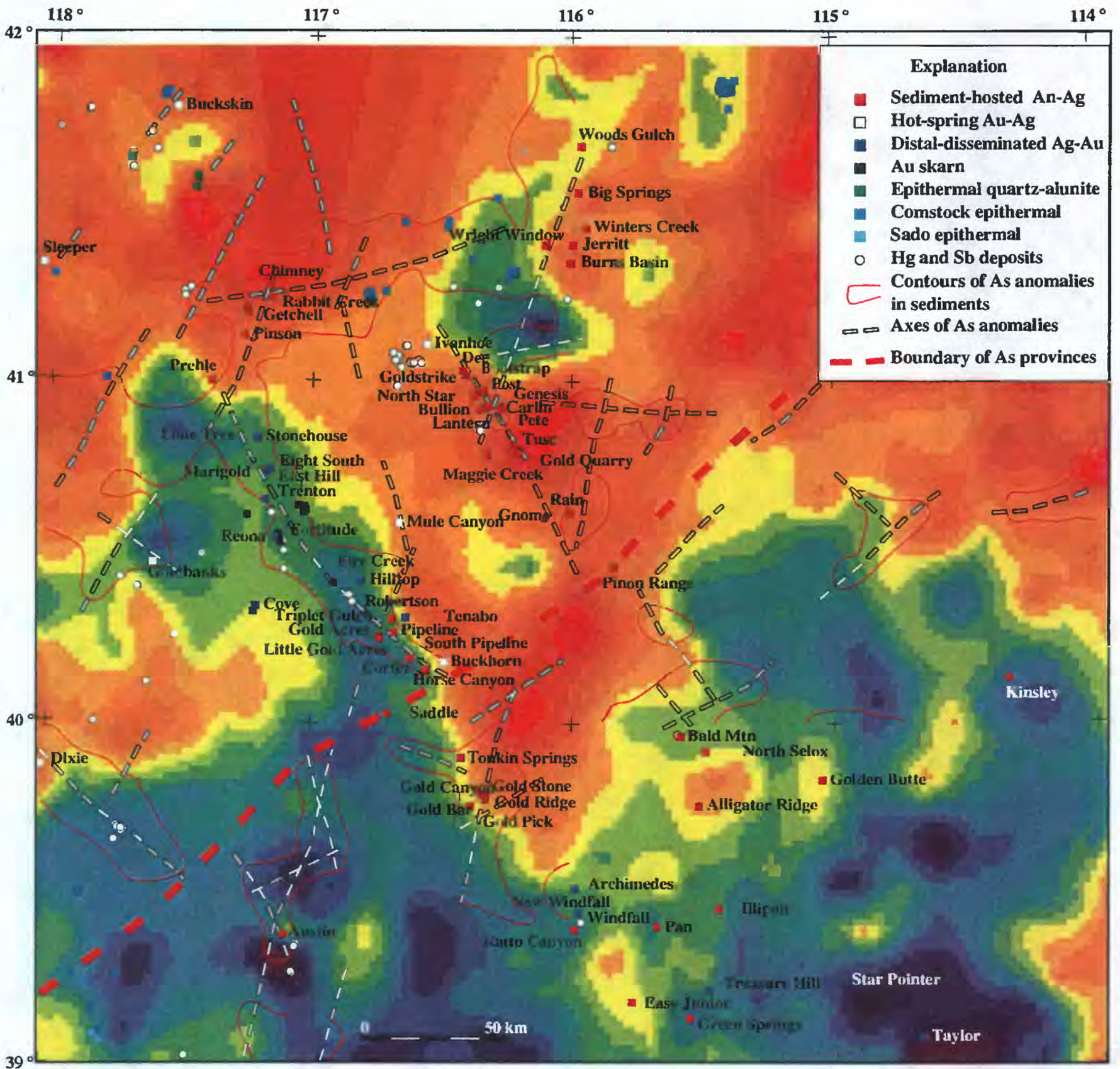


Figure 5. Map showing isostatic residual gravity of the pre-Cenozoic basement rocks of northern Nevada (after Saltus and Jachens, 1995), gold, mercury and antimony deposits, as well as contours and axes of arsenic anomalies from soil and stream sediment samples. Warm colors mark areas with rock in the middle and upper crust that are denser than those in areas marked by cool colors.

trends with linear trends defined by precious-metal deposits as well as density distributions in the middle and upper crust suggests derivation of arsenic and precious metals from these crustal levels.

In general, gravity anomalies and their gradients are characterized by three major trends, including northwest, northeast, and east-northeast, which orientations are similar to the known gold trends in northeast Nevada, as well as the orientations of the patterns of the regional arsenic anomalies (fig. 5). Comparison of gravity data and distribution of gold

deposits and arsenic anomalies shows that:

- (1) the southern part of the Cortez trend, which is comprised mostly of sediment-hosted gold deposits, coincides with a well-developed gravity gradient (fig. 5; see also, Grauch and others, 1995). Farther to the northwest along the Cortez trend, however, the bulk of the mineral deposits diverge away from the gravity gradient, and are situated in areas that have a negative gravity anomaly.
- (2) sediment-hosted gold deposits in the southern part of the Getchell trend correlate with the same gravity gradient,

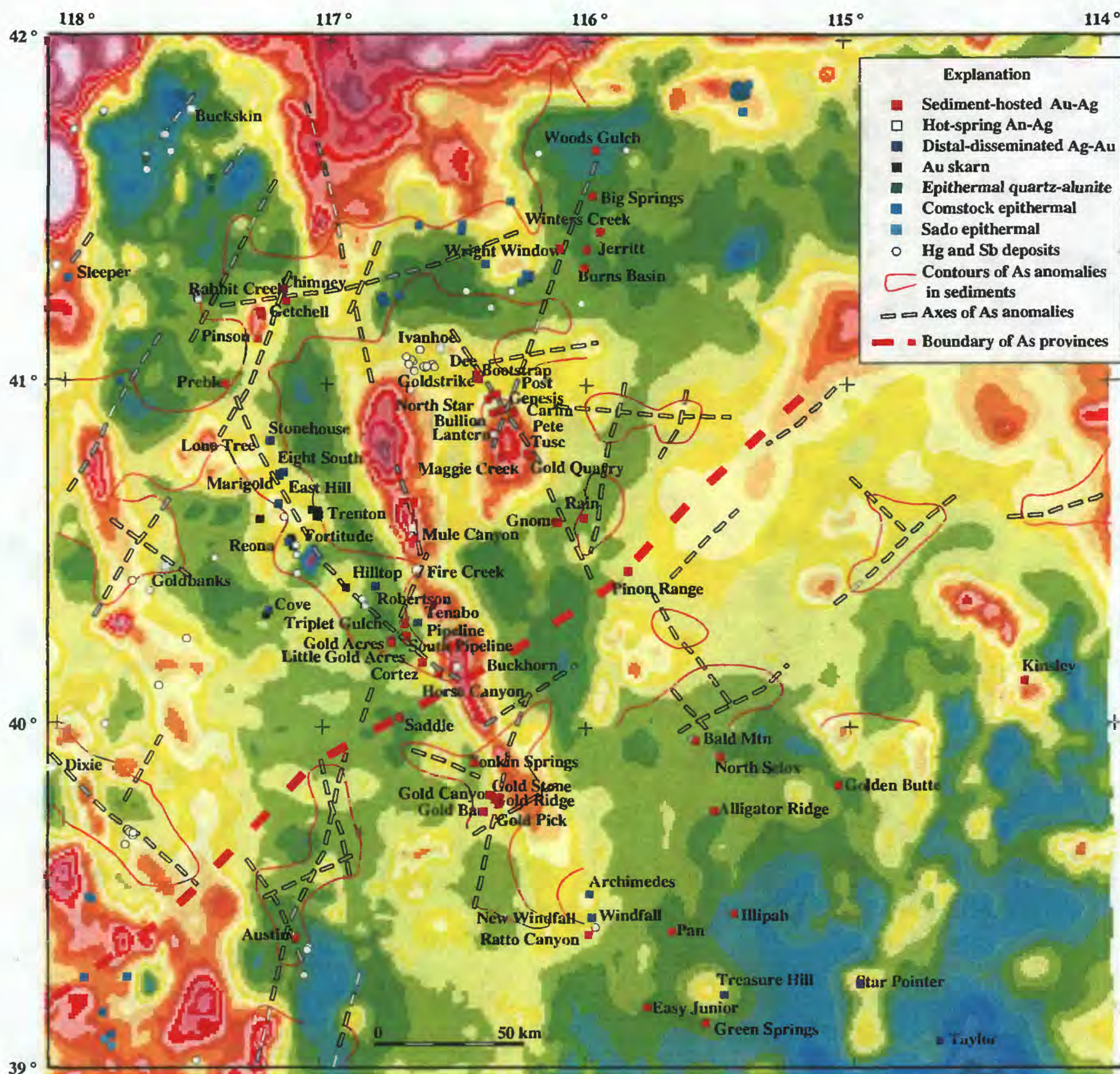


Figure 6. Map showing residual magnetic potential (pseudogravity) anomalies of northern Nevada, and gold, mercury and antimony deposits, as well as contours and axes of arsenic anomalies from soil and stream sediment samples. Warm colors mark areas with rock in the middle and upper crust that are more magnetic than those in areas marked by cool colors.

but they extend to the northeast at high angles to the gravity gradient and well away from the trace of the gravity gradient (fig. 5). A generalized axis of anomalous arsenic roughly correlates with the deposits along the Getchell trend, however. Similar relations are present near the sediment-hosted gold-silver deposits (including Burns Basin, Jerritt, Big Springs) in the northern Independence Mountains (fig. 5).

(3) gold deposits along the Carlin trend occur in areas where regional stream-sediment arsenic anomalies are present and they also are in an area of elevated gravity.

Figure 6 shows a map that reflects the regional distribution of magnetic rocks within the study area. It was derived from the magnetic map of Nevada (Hildenbrand and Kucks, 1988) by a procedure meant to emphasize the volume distribution of magnetization in the middle and upper crust. First, the map of magnetic anomalies was transformed to a map of magnetic potential anomalies (pseudogravity anomalies of Baranov, 1957), both to eliminate asymmetry of the anomalies caused by the inclination of the main geomagnetic field, and to emphasize the parts of the anomalies produced by the deeper

parts of the magnetic bodies. Second, the longest wavelengths of the magnetic potential anomalies (MPA) were suppressed in order to focus more closely on anomalies from sources in the middle and upper crust. This was accomplished by applying the following numerical filter: Residual MPA=MPA-MPA (upward continued 15 km).

The process of upward continuation 15-km selectively suppresses anomalies with wavelengths shorter than 100 km, anomalies that mostly are produced by sources in the middle and upper crust. By subtracting the upward continued magnetic potential anomalies from the original magnetic potential anomalies, the map of residual magnetic potential anomalies shown in figure 6 focuses on the distribution of magnetic rocks in the middle and upper crust.

Comparison of these magnetic data (fig. 6) with distributions of gold deposits and patterns of arsenic anomalies shows that there are at least two types of relations. First, strong elongate north-northwest magnetic anomalies correspond with mafic volcanic rocks of Tertiary age. Miocene hot-spring deposits are present along the northern Nevada rift, and these deposits include Buckhorn, Fire Creek, and Mule Canyon. In addition, much of the northern Nevada rift also coincides with the axis of an arsenic anomaly (fig. 6). Second, local magnetic highs coincide with a number of Mesozoic plutons and nearby sediment-hosted gold deposits, as well as some of distal-disseminated Ag-Au deposits in the northern part of the Cortez trend. However, a significant number of the gold deposits in the region, including those in the northern Independence Range, southern part of the Cortez trend, Austin, and sediment-hosted Au-Ag deposits in the Ely 1° X 2° quadrangle are located in areas that have regionally extensive negative magnetic anomalies.

CONCLUSIONS

Regional geochemical surveys, gravity surveys, and magnetic surveys examined by means of modern computer-contouring methods employing various normalization and filtering techniques provide additional insight into crustal processes of metallogenesis. Regional-scale distribution patterns of arsenic anomalies in northeast Nevada bear striking similarities to many important mineralized trends and to some isostatic residual gravity anomalies and their gradients. The gravity anomalies and their gradients primarily result from density distributions in the middle and upper crust and their coincidence with linear zones of apparently enriched arsenic suggests that arsenic, as well as precious metals, also may have been derived from the middle and upper crust. However, broad areas of apparently elevated arsenic concentrations also show no indication of metal deposits. In addition, a map of residual magnetic potential anomalies indicates that magnetic rocks in the middle and upper crust—most likely late Tertiary in age—also must play an important role in the eventual distribution of some hot spring Au-Ag deposits.

REFERENCES CITED

- Baranov, V., 1957, A new method for interpretation of aeromagnetic maps: *Geophysics*, v. 22, p. 359-383.
- Hildenbrand, T.G., and Kucks, R.P., 1988, Total intensity magnetic anomaly map of Nevada: Nevada Bureau of Mines and Geology Map Series 93A, scale 1:1,000,000.
- Hoffman, J.D., and Buttleman, Kim, 1994, National geochemical data base: National uranium resource evaluation for the conterminous United States: U.S. Geological Survey Digital Data Series DDS-18-A, 1 CD.
- Hoffman, J.D., and Marsh, S.P., 1994, National geochemical data base, in Carter, L.M., Toth, M., I. and Day, W., eds., USGS research on mineral exploration, 1994; Part A, Program and abstracts, p. 62-64.
- Jachens, R.C., and Moring, B.C., 1990, Maps of the thickness of Cenozoic deposits and the isostatic residual gravity over basement for Nevada: U.S. Geological Survey Open-File Report 90-404, 15 p., 2 sheets, scale 1:1,000,000.
- Jachens, R.C., Moring, B.C., and Schruben, P.G., 1996, Thickness of Cenozoic deposits and isostatic residual gravity over basement, in Singer, D.A., ed., An analysis of Nevada's metal-bearing mineral resources: Nevada Bureau of Mines and Geology Open-File Report 96-2, p. 2-1 to 2-10.
- King, H.D., 1996, Interpretation of reconnaissance geochemical data from the Bureau of Land Management's Winnemucca District and Surprise Resource Area, northwest Nevada and northeast California: U.S. Geological Survey Open-File Report 96-533, 36 p.
- King, H.D., Fey, D.L., Motooka, J.M., Roushey, B.H., and McGuire, D.J., 1996, Analytical data and sample locality map of stream-sediment and soil samples from the Winnemucca-Surprise Resource Assessment Area, northwest Nevada and northeast California: U.S. Geological Survey Open-File Report 96-062A, paper version, 341 p.; 96-062B, Diskette version.
- Kotlyar, B.B., Theodore, T.G., and Jachens, R.C., 1995, Re-examination of rock geochemistry in the Copper Canyon area, Lander County, Nevada: U.S. Geological Survey Open-File Report 95-816, 47 p.
- Masters, T., 1993, Practical neural network recipes in C++: San Diego, California, Academic Press, Inc., 493 p.
- McGuire, D.J., and Albino, G.V., 1994, Arsenic and antimony anomalies in NURE sediments show mineralized areas in northwestern Nevada, in Carter, L.M., Toth, M., I. and Day, W., eds., USGS research on mineral resources—1994; Part A, Program and abstracts, p. 62-64.
- Saltus, R.W., and Jachens, R.C., 1995, Gravity and basin-depth maps of the Basin and Range province, western United States: U.S. Geological Survey Geophysical Investigations Map GP-1012, scale 1:2,500,000.
- Sherlock, M.G., Cox, D. P., and Huber, D.F., 1996, Known mineral deposits in Nevada, in Singer, D.A., ed., An analysis of Nevada's metal-bearing mineral resources: Nevada Bureau of Mines and Geology Open-File Report 96-2, Chapter 10, p.10.1-10.38, 2 sheets, scale 1:1,000,000. (Also available at: www.nbmng.unr.edu/ofr962.)
- Simpson, R.W., Jachens, R.C., Blakely, R.J., and Saltus, R.W., 1986, A new isostatic residual gravity map of the conterminous United States with a discussion on the significance of isostatic residual anomalies: *Journal of Geophysical Research*, v. 91, p. 8,348-8,372.

SOIL GAS STUDIES ALONG THE CARLIN TREND, EUREKA AND ELKO COUNTIES, NEVADA

By Howard McCarthy *and* Emmet McGuire

ABSTRACT

Soil gases were sampled at 175 sites along widely-spaced traverses that crossed the Carlin Trend in north-central Nevada. Inorganic and organic soil gases including H₂, O₂, CO₂, and hydrocarbon gases, were analyzed using a truck-mounted mass spectrometer. The objective of these measurements was to test the possibility that gases might reveal faults that controlled the localization of gold deposits along this linear trend. Soil gases were sampled at 1-1.5 km intervals along traverses that extended 16-31 km on both sides of the hypothetical center line of the Carlin Trend, and for about 80 km in a north-south direction from Carlin on the south to the Willow Creek drainage on the north. CO₂ and H₂ soil-gas anomalies were found 8-11 km west of the hypothetical center line of the Carlin Trend. H₂ and more limited CO₂ gas anomalies were also found 3-11 km east of the trend line on two of the traverses. These gas anomalies may result from leakage along faults that have genetic significance in localization of the Carlin Trend. Both CO₂ and H₂ are produced in the deep crust or mantle, and deep-seated regional faults may be indicated by these gas anomalies. The anomalies extend as far north as the Willow Creek drainage suggesting that the trend may continue northward, beyond the known gold deposits.

INTRODUCTION

Many geologists have attempted to explain the linear pattern of gold deposits that occur along the Carlin Trend (Roberts, 1960; Roberts, 1966; Shawe, 1991). Shawe (1991) stated "The linearity of the gold trends and concentration of igneous rocks along them suggest that deep-penetrating regional structures controlled the emplacement of magmas generated in the lower part of the crust or upper mantle." Based on Pb and Sr isotope ratios, Wooden and others (1997) infer that both the Carlin and Battle Mountain mineral belts were localized along crustal scale regional faults. The considerable length of the Carlin Trend (about 185 km from the Dee Mine on the north to the Alligator Ridge Mine on the south) suggests deep-seated structural control. Northwest-striking faults of limited extent have been mapped along the Carlin Trend (Roberts and others, 1967); however, through-going faults of regional extent have not been identified.

Gases produced at depth migrate to the surface, commonly

along faults, because the faults are usually more permeable than the surrounding rock. Gases measured at the surface have been used to map concealed faults (Kasimov and others, 1979; Scherbakov and Koslova, 1986; McCarthy and Hardyman, 1996). Linear, narrow gas anomalies are found over high-angle faults and linear, broad or asymmetric gas anomalies over low-angle faults (Fridman, 1990). Assuming that deep-seated structures may exist along the Carlin Trend, the soil gas studies reported here were undertaken to test the possibility that they might be revealed by surface gas measurements. Although considerable thicknesses of Quaternary sediments and Tertiary volcanic rocks overlie the basement Paleozoic rocks that host the gold deposits on the Carlin Trend, gases have been found to migrate from depth to the surface through similar types of overburden (McCarthy and others, 1968; Kasimov and others, 1979).

SAMPLING AND ANALYTICAL PROCEDURES

Gases were sampled along traverses that followed roads crossing the Carlin Trend (figs. 1-3). Sample intervals were 1 to 1.5 km and some traverses extended 16-32 km on both sides of the north-northwest-striking line shown on figures 1-3, which represents the approximate center of the Carlin Trend. These traverses extended from the town of Carlin on the south to the Willow Creek drainage on the north, a distance of about 80 km. Gases were sampled by driving a hollow steel probe into the ground to a depth of 75 cm and extracting soil air from that depth. The samples were analyzed at each site using a truck-mounted mass spectrometer (McCarthy and Bigelow, 1990). Analytical reproducibility is ± 30 percent. A paper copy of the analytical data is printed, and along with the latitude and longitude of the site location, recorded on a floppy disk to permit plotting of individual gas species.

Individual atomic or molecular gas species are analyzed in the mass spectrometer and converted to concentration by comparison with standard gases of known composition. The concentration of the gases are expressed as volume of gas per volume of air (v/v). A detailed description of the mass spectrometer and its operation is given by McCarthy and Bigelow (1990).

The intervals selected for contours on figures 1-3, are based on concentrations that are considered anomalous. For

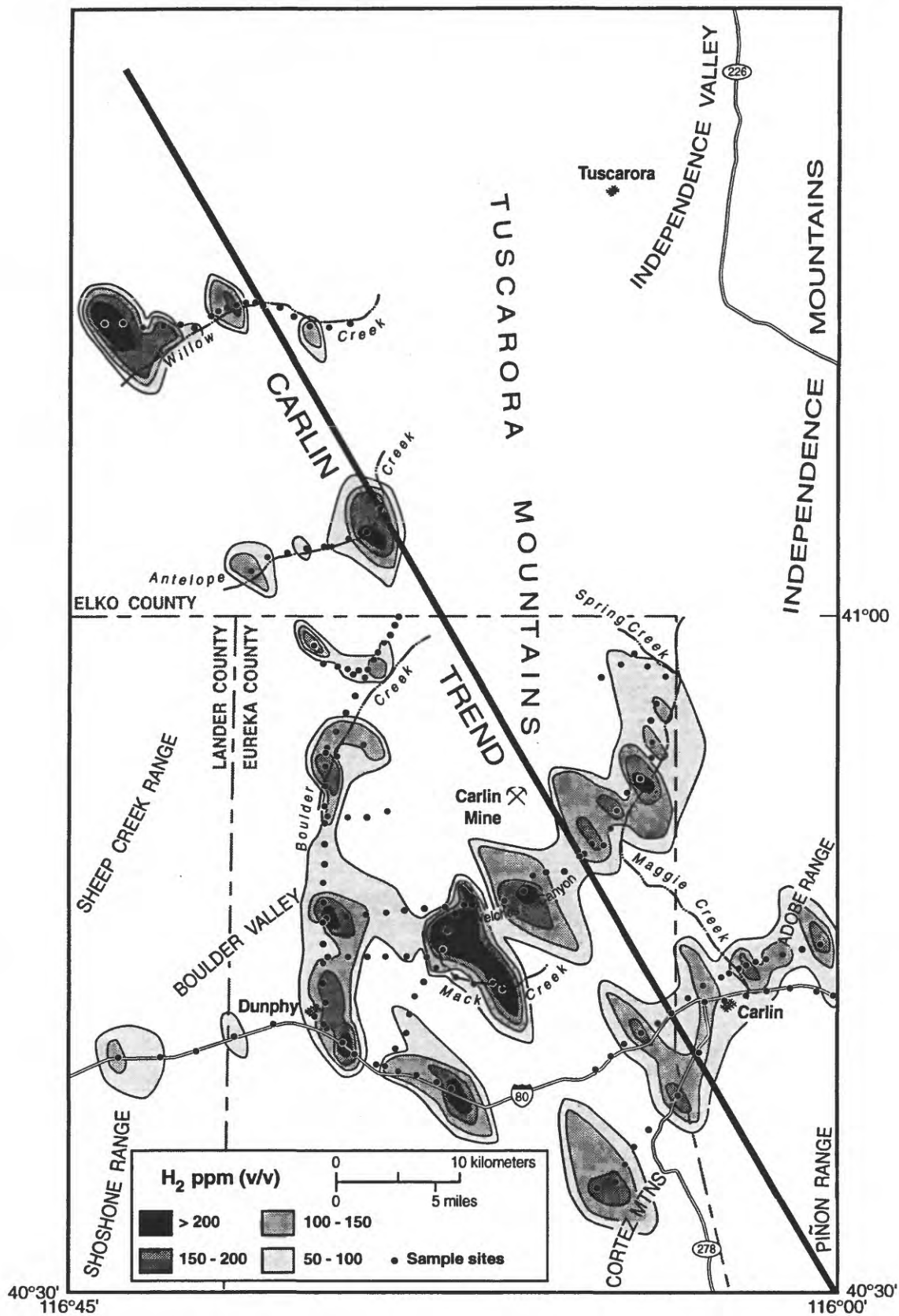


Figure 1. Contour map of H₂ in soil gas samples along the Carlin trend, Eureka and Elko Counties, Nevada.

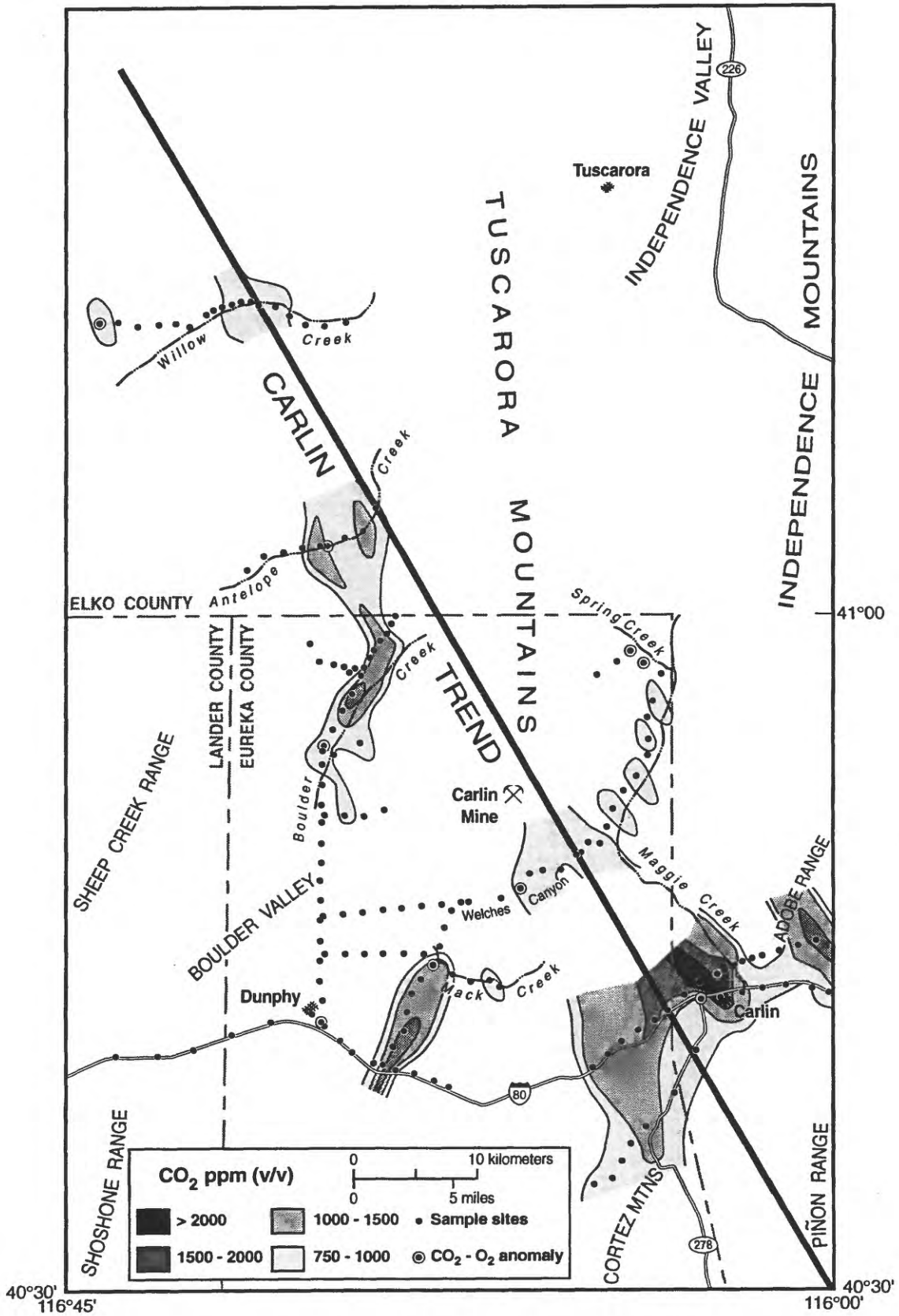


Figure 2. Contour map of CO₂ in soil gas samples along the Carlin trend, Eureka and Elko Counties, Nevada.

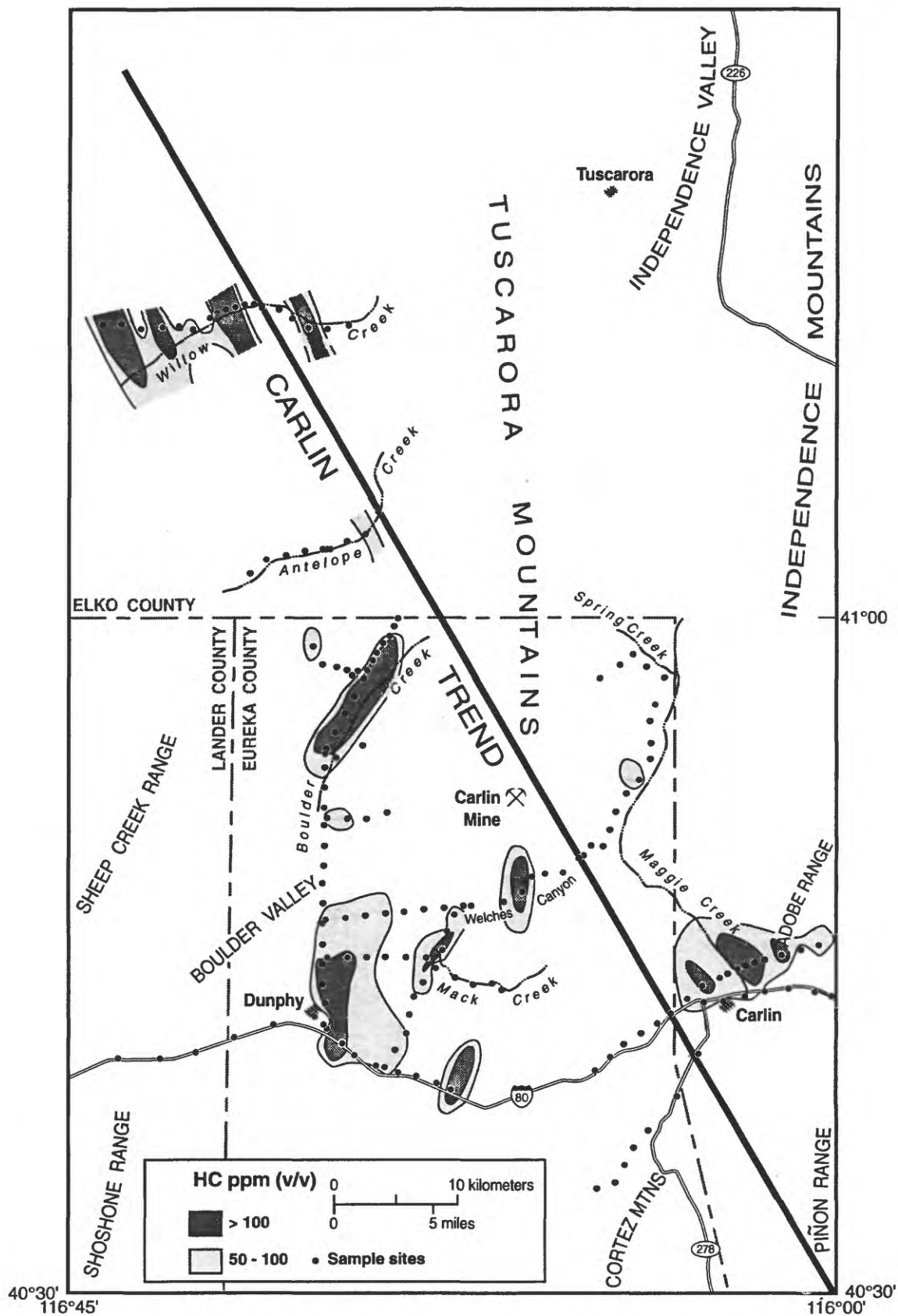


Figure 3. Contour map of hydrocarbon gases (HC) in soil gas samples along the Carlin trend, Eureka and Elko Counties, Nevada.

example, the background concentration of CO₂ in air is 350 ppm (Rose and others, 1979); approximately twice that concentration was selected as anomalous, and is the minimum contour shown on figure 2. The minimum concentration considered anomalous for H₂ and contoured on figure 1 is 50 ppm, and for the combined hydrocarbon gases (HC on figure 3) is 50 ppm.

RESULTS

Two of the gases measured in this study, H₂ and CO₂, are of particular interest because both of these gases can be derived from the deep crust and mantle (Krauskopf, 1967; Neal and Stanger, 1983; Shcherbakov and Kozlova, 1986; Barnes and others, 1978). Thus, these gases could indicate deep-seated faults.

The results for H₂, CO₂, and C₂H₅⁺ (an ion fragment that represents both propane and butane) were plotted on maps and contoured to show patterns of anomalous concentrations (figs. 1-3). Individual H₂ gas anomalies were connected by contours based on levels of concentration (fig. 1) and suggest possible northwest-striking linear alignments; however, northeast-striking alignments are also possible; the latter alignments may only reflect the sampling along roads. The linear continuity of any of these anomalies can only be confirmed (or negated) by additional sampling traverses between those reported in this study.

As shown by the data, H₂ gas anomalies were found 8 to 11 km west of the line on the figures indicating the approximate center of the Carlin Trend. A similar, but less continuous, alignment of CO₂ and H₂ gas anomalies were found about 3 to 11 km east of the trend line. If connected, these anomalies would reflect linear alignments that are approximately parallel to the Carlin Trend line. Two anomalies for both H₂ and CO₂ cross the Carlin Trend line; one is just north of the town of Carlin and the other extends from Welches Canyon on the west to the Maggie Creek drainage on the east. The latter anomaly coincides with a north-northeast-striking fault zone as mapped by Peters (this volume).

At several sites, high concentrations of CO₂ coincide with low concentrations of O₂, a combination that is commonly associated with oxidizing sulfide minerals (Lovell and others, 1983). In field studies cited by Lovell and Hale (1983) up to 9 percent CO₂ (v/v) and corresponding low levels of O₂ were found in soil gas samples over massive sulfide mineralization in Ireland, Scotland, Spain, and the United States. This process results from oxidation of sulfide minerals (in the cases cited above sphalerite, galena, chalcopyrite, and pyrite) producing acid solutions that react with carbonate minerals producing CO₂. McCarthy and others (1986) found similar high CO₂ and low O₂ anomalies in soil gases over the Crandon massive-sulfide ore deposit in northern Wisconsin. Carlin-type disseminated gold deposits commonly contain only 4 to 5 percent sulfide minerals (mostly pyrite), and consequently have

less pronounced CO₂ and O₂ anomalies (McCarthy and others, 1989). East of the trend line, this combination of CO₂ and O₂ anomalies are found near the town of Carlin, and along Spring Creek near its confluence with Maggie Creek. West of the trend line they occur at six sites: along Mack Creek, in Welches Canyon, 1.6 km southeast of Dunphy, 22 km north of Dunphy where the road heading north from Dunphy crosses Boulder Creek, along Antelope Creek 5 km west of the Trend line, and along Willow Creek 5 km west of the trend line. These anomalous sites (circled on fig. 2) may reflect oxidizing sulfide minerals in bedrock.

Anomalous concentrations of volatile hydrocarbons in soil gas samples (fig. 3) are found: at several sites in Boulder Valley north and east of Dunphy, at several sites extending 8 km east-northeast from the town of Carlin, at several sites 8 to 11 km west of the Carlin Trend line in the Boulder Creek drainage, and at several sites along the Willow Creek drainage. Hydrocarbon gas anomalies are associated with base metal deposits (Disnar, 1990) and with gold deposits (Ilchik and others, 1986; McCarthy and others, 1989). Carbonaceous material is a common constituent of Carlin-type gold deposits (Percival and others, 1988), and maturation of this organic matter could produce hydrocarbon gases. These gases may be used as exploration guides to gold and other types of mineral deposits.

All of the gas anomalies noted above probably result from gases migrating along faults in Paleozoic basement rocks. The inferred depth to Paleozoic bedrock based on modeling of gravity data (Saltus and Jachens, 1995) varies from about 1.8 km in the Antelope Creek basin to 4.5 km in the Maggie Creek basin. The depth to basement in Boulder Valley is about 3 km in the south and decreases to 1.6 km in the north. Studies have shown that gases migrate to the surface from such depths through valley-fill sediments (McCarthy and Hardyman, 1996) and through volcanic rocks (McCarthy and others, 1968).

In a study conducted in the Sheep Creek Range, north of Battle Mountain, Nevada, mercury vapor was detected through 300 m of volcanic rocks overlying mineralized Paleozoic basement rocks. Here, sphalerite and galena from a prospect pit in the underlying Paleozoic rocks contained several ppm of Hg, which appears to be the source of the Hg vapor detected at the surface. The Hg anomalies were found along faults in the volcanic rocks indicating that the Hg migrated as a vapor along the faults. These studies demonstrate that gases can migrate to the surface through volcanic or alluvial overburden.

DISCUSSION

The linear alignment of anomalous concentrations of H₂ and CO₂ as contoured on figures 1 and 2 probably result from leakage along faults that could have genetic significance in localization of the Carlin Trend. Both H₂ and CO₂ (as well as other gases) are common constituents of the following mantle-

derived fluids-(1) volcanic emanations (Mason and Moore, 1981); (2) submarine rift zones (Welhan and Craig, 1979); (3) continental rift zones (Coveney and others, 1987); and (4) ophiolites (Neal and Stanger, 1983). Both CO₂ and H₂ could reflect faults that penetrate to the deep crust or mantle. But, both can also have shallow sources (Sugisaki and others, 1983, Lovell and others, 1983).

HYDROGEN

According to Kasimov and others (1979), hydrogen emanating from faults in Kazakhstan came from great depth. However, Sugisaki and others (1983) have found several volume percent H₂ in both shallow and deep faults with historical movement, which they attribute to the reduction of water by reactive rock surfaces along the faults.

CARBON DIOXIDE

According to Barnes and others (1978), "CO₂ is thought generally to come from three different sources: (1) organic material, (2) metamorphism of marine carbonate rocks, and (3) the mantle." Carbon dioxide is a significant constituent of volcanic emanations and mid-ocean ridge gases, and isotopic measurements indicate that some of this CO₂ is derived from the mantle (Hoefs, 1997). Faults are commonly more permeable than the surrounding rock and provide conduits for fluids to migrate from depth (Shcherbakov and Kozlova, 1986). It is possible that the gases measured in this study migrate along faults that extend to the mantle.

Methane is commonly produced along with CO₂ when organic matter decomposes (Tan, 1994); however, anomalous concentrations of both methane and CO₂ are found in only 5 of the 175 soil gas samples in this study. We therefore conclude that most of the CO₂ anomalies reported here do not result from the decomposition of organic matter.

It is possible that the CO₂ found in the soil gas samples is produced by metamorphism of carbonate rocks. Although carbonate rocks do not crop out where CO₂ anomalies are found, they do crop out in the Tuscarora Mountains near the Carlin Mine (Roberts and others, 1967), and they underlie the volcanic rocks and the upper plate siliciclastic rocks of the Roberts Mountains allochthon. Thus, CO₂ in the soil gas samples may result from prior or continuing metamorphism of carbonate rocks.

A fourth possible source of CO₂ is reaction of acid solutions with carbonate rocks or minerals. Sulfuric acid is formed when oxygenated ground waters react with sulfide minerals, such as pyrite, which commonly is present in Carlin-type gold deposits. The resulting acidic fluid reacts with carbonate host rock, and CO₂ is produced. Oxygen is consumed in this reaction, and when lowered concentrations

of O₂ are found in soil gas samples that have increased concentrations of CO₂, oxidizing sulfide minerals in rocks below surficial deposits are indicated. The CO₂ generated in this reaction process has been documented by several investigators (Lovell and others, 1983, McCarthy and others, 1986).

OTHER GASES

Hydrocarbon gases are also associated with base and precious metal mineral deposits (Disnar, 1990; McCarthy and others, 1989; Taylor and others, 1981). It has been known for some time that hydrocarbons are associated with sediment-hosted gold deposits (Kesler and others, 1990; Ilchik and others, 1986). According to some investigators, volatile hydrocarbons are produced by thermal maturation of organic matter in the host or wall rock, with heat provided by ore-bearing hydrothermal solutions. However, evidence from Carlin-type deposits elsewhere indicates that hydrocarbons were present before the gold-bearing fluids were introduced, as at Alligator Ridge (Ilchik and others, 1986). Even if petroleum hydrocarbons were present before the introduction of gold-bearing fluids, the hydrocarbons would be subject to further maturation and production of gases by hydrothermal solutions that were introduced later. Volatile hydrocarbons (alkanes) have been found in soil gases at all Carlin-type gold deposits investigated (McCarthy, 1989; and unpublished data). The hydrocarbon gases (HC) plotted in figure 3 are combined C₃ and C₄ alkanes.

These and other C₂ + alkanes are of thermogenic origin (Hunt, 1979), and could have been produced by thermal maturation of organic matter by hydrothermal solutions (Welhan, 1988). Although methane (CH₄) is also produced thermogenically, about 80 volume percent of methane in air is biogenic (Enhalt, 1974), hence it may be misleading as a guide to hydrothermal ore deposits. Hydrocarbon gas anomalies were found at several sites in the study area and these sites may indicate concealed gold deposits. Six of the sites with hydrocarbon gas anomalies also have CO₂-O₂ anomalies.

These gas studies compliment geophysical studies in the area. A northwest-trending H₂ anomaly near the foot of Welches Canyon corresponds with the location of a deep crustal fault as interpreted from magnetotelluric measurements (Rodriguez, 1997).

CONCLUSIONS

Linear patterns of H₂ and CO₂ in soil gas were found 8 to 11 km both east and west of the hypothetical center line of the Carlin Trend, and are parallel to it. This alignment probably results from leakage of gases along faults. If so, these faults may represent regional structures that influenced the localization of the Carlin Trend and the gold deposits along it.

These gas anomalies extend to the northwest about 10 km beyond the known gold deposits along the Trend. Anomalies typical of oxidizing sulfide minerals (high CO₂ and low O₂) are found at two sites north of the known gold deposits, one on Antelope Creek and one on Willow Creek. The Willow Creek anomaly has a coincident hydrocarbon gas anomaly. The gas anomalies reported here may also be produced by volcanic-hosted gold or base-metal deposits. These findings indicate that the Carlin Trend may extend to the northwest and perhaps contain additional mineral deposits.

REFERENCES CITED

- Barnes, I., Irwin, W.P., and White, D.E., 1978, Global distribution of carbon dioxide discharges, and major zones of seismicity: U.S. Geological Survey Open-File Report 78-39, 12 p.
- Coveney, R.M., Jr., Goebel, E.D., Zeller, E.J., Dreschhoff, G.A.M., and Angino, E.E., 1987, Serpentinization and the origin of hydrogen gas in Kansas: American Association of Petroleum Geologists Bulletin, v. 71, no. 1, p. 39-48.
- Disnar, J.R., 1990, Volatile hydrocarbons in Ba-Zn-Pb ore genesis: analysis and use in mineral exploration: Journal of Geochemical Exploration, v. 38, p. 205-224.
- Enhalt, D.H., 1974, The atmospheric cycle of methane: Tellus, v. 26, p. 58-70.
- Fridman, A.I., 1990, Application of naturally occurring gases as geochemical pathfinders in prospecting for endogenetic deposits: Journal of Geochemical Exploration, v. 38, nos. 1-2, p. 1-11.
- Hoefs, J., 1997, Stable isotope geochemistry: New York, Springer-Verlag, 201 p.
- Hunt, J.M., 1979, Petroleum geochemistry and geology: San Francisco, W.H. Freeman and Company, 617 p.
- Ilchik, R.P., Brimhall, G.H., and Schull, H.W., 1986, Hydrothermal maturation of indigenous organic matter at the Alligator Ridge gold deposits: Nevada, Economic Geology, v. 81, p. 113-130.
- Kasimov, N.S., Kovin, M.L., Proskurykov, Y.V., and Shmel'kova, 1979, Geochemistry of the soils of fault zones (exemplified by Kazakhstan): Soviet Soil Science, v. 11, p. 397-406.
- Kesler, S.E., Gerdenich, M.J., Steininger, R.C., and Smith, C., 1990, Dispersion of soil gas around micron gold deposits: Journal of Geochemical Exploration, v. 38, nos. 1-2, p. 117-132.
- Krauskopf, K., 1967, Introduction to geochemistry: New York, McGraw Hill, Inc., 721 p.
- Lovell, J.S. and Hale, M., 1983, Application of soil-air carbon dioxide and oxygen measurements to mineral exploration: Transactions of the Institute of Mining and Metallurgy, v. 92, p. 28-32.
- Lovell, J.S., Hale, M., and Webb, J.S., 1983, Soil air carbon dioxide and oxygen measurements as a guide to concealed mineralization in semi-arid and arid regions: Journal of Geochemical Exploration, v. 19, p. 305-317.
- Mason, Brian and Moore, C.B., 1981, Principles of Geochemistry: New York, John Wiley and Sons, 344 p.
- McCarthy, J.H., Jr., Vaughn, W.W., Learned, R.E., and Meuschke, J.L. 1968, Experiments with mercury in soil gas and air applied to mineral exploration: Mining Engineering, v. 20, no. 12, p. 46-47.
- McCarthy, J.H., Jr., and Bigelow, R.C., 1990, Multiple gas analyses using a mobile mass spectrometer: Journal of Geochemical Exploration, v. 38, p. 233-245.
- McCarthy, H. and Hardyman, R., 1996, Mapping concealed faults in basins by measurement of naturally occurring gases, in Coyner, A.R. and Fahey, P.L., eds., Geology and Ore Deposits of the American Cordillera: Geological Society of Nevada Symposium Proceedings, Reno/Sparks, Nevada, April 1995, p. 757-768.
- McCarthy, J.H., Jr., Lambe, R.N., and Dietrich, J.A., 1986, A case study of soil gases as an exploration guide in glaciated terrain: Economic Geology, v. 81, p. 408-420.
- McCarthy, J.H., Jr., Erdman, J.A., Lovering, T.G., and Bettles, K.H., 1989, Evaluation of multiple geochemical sample media at the Betze gold deposit, Eureka County, Nevada: U.S. Geological Survey Circular 1035, p. 45-46.
- Neal, C. and Stanger, G., 1983, Hydrogen generation from mantle source rocks in Oman: Earth and Planetary Science Letters, v. 66, p. 315-320.
- Percival, T.J., Bagby, W.C., and Radtke, A.S., 1988, Physical and chemical features of precious metal deposits hosted by sedimentary rocks in the western United States, in Schafer, R.W., Cooper, J.J., and Vikre, P.G., eds., Bulk mineable precious metal deposits of the western United States: Geological Society of Nevada, p. 11-34.
- Peters, S.G., this volume, Evidence for the Crescent Valley-Independence lineament, north-central Nevada, in Tosdal, R.M., ed., Contributions to the gold metallogeny of northern Nevada: U.S. Geological Survey Open-File Report.
- Roberts, R.J., 1960, Alinements of mining districts in north-central Nevada: U.S. Geological Survey Professional Paper 400-B, p. B17-B19.
- Roberts, R.J., 1966, Metallogenic provinces and mineral belts in Nevada: Nevada Bureau of Mines and Geology, Report 13, p. 47-72.
- Roberts, R.J., Montgomery, K.M., and Lehner, R.E., 1967, Geology and mineral resources of Eureka County, Nevada: Nevada Bureau of Mines and Geology Bulletin 64, 152 p.
- Rodriguez, B.D., 1997, Deep regional resistivity structure across the Carlin trend, in Vikre, P., Thompson, T.B., Bettles, K., Christensen, O., and Parratt, R., eds., Carlin type gold deposits: Society of Economic Geologists, Guidebook Series, Volume 28, p. 39-45.
- Rose, A.W., Hawkes, H.E., and Webb, J.S., 1979, Geochemistry in mineral exploration: New York, Academic Press, 657 p.
- Saltus, R.W. and Jachens, R.C., 1995, Gravity and basin-depth maps of the Basin and Range province, western United States: U.S. Geological Survey, Map GP-1012, 1:2,500,000 scale.
- Shcherbakov, A.V. and Kozlova, N.D., 1986, Occurrence of hydrogen in subsurface fluids and the relationship of anomalous concentrations to deep faults in the USSR: Geotectonics, v. 20, p. 120-128.
- Shawe, D.R., 1991, Structurally controlled gold trends imply large gold resources in Nevada, in Raines, G.L., Lisle, R.E., Schafer, R.W., and Wilkinson, W. Geology and Ore Deposits of the Great Basin, Symposium Proceedings: Geological Society of Nevada, v. 1, p. 199-212.
- Sugisaki, R., Ido, M., Takeda, H., Isobe, Y., Hayashi, Y., Nakamura, N., Satake, H., and Mizutani, Y., 1983, Origin of hydrogen and carbon dioxide in fault gases and its relation to fault activity:

Journal of Geology, v. 91, no. 3, p. 239-258

Tan, K.H., 1994, *Environmental soil science*: New York, Marcel Dekker, Inc., 304 p.

Taylor, C.H., Kessler, S.E., and Cloke, P.L., 1981, Sulfur gases produced by the decomposition of sulfide minerals: application to geochemical exploration: *Journal of Geochemical Exploration*, v. 17, p. 165-186.

Welhan, J.A. and Craig, H., 1979, Methane and hydrogen in East Pacific Rise hydrothermal fluids: *Geophysical Research Letters*,

v. no. 11, p. 829-831.

Welhan, J.A., 1988, Origins of methane in hydrothermal systems: *Chemical Geology*, v. 71, no. 1/3, p. 183-198.

Wooden, J.L., Tosdal, R.M., and Kistler, R.W., 1997, Pb and Sr isotopic mapping of crustal structure in the Northern Great Basin, *in* Vikre, P., Thompson, T.B., Bettles, K., Christensen, O., and Parratt, R., eds., *Carlin-type gold deposit*: Society of Economic Geologists, Guidebook Series, Volume 28, p. 47-51.

PLUTON-RELATED GOLD IN THE BATTLE MOUNTAIN MINING DISTRICT—AN OVERVIEW

By Ted G. Theodore

The Battle Mountain Mining District includes four Tertiary porphyry Cu and three Cretaceous stockwork Mo systems, as well as a large number of distal-disseminated Ag–Au deposits (Doebrich and Theodore, 1996; Theodore, 1998). This is the main site of pluton-related mineral occurrences in the northern Great Basin, and it is an area of substantial recent production of Au by Battle Mountain Gold Co., Marigold Mining Co., and Newmont Mining Ltd. Historically, the Battle Mountain Mining District intermittently has produced metals over a span of about 120 years. It has yielded approximately 3.5 million oz Au since 1978 when production shifted from base and precious metals to precious metals. Prior to 1978, production of Au from large-scale mining operations, which began in 1967, was mostly as a byproduct of production of Cu from two separate porphyry systems centered at Copper Canyon and at Copper Basin (see section below entitled “Regional Implications of Large Distal-disseminated Precious-metal Deposits, Battle Mountain Mining District, Nevada”). Study of pluton-related Au provides a geologic and geochemical baseline for these types of deposits to which others may refer during evaluations of mineral resources in similar geologic terranes—this includes the Humboldt River Drainage study currently (1998) being investigated by the U.S. Geological Survey. Previous investigations by the U.S. Geological Survey in the mining district elucidated a linkage between a geologic terrane where distal-disseminated Ag–Au deposits (Cox and Singer, 1992) predominate in the northern part, and the porphyry Cu and stockwork Mo systems predominate in the southern part (Theodore, 1998).

Porphyry systems are generally large volumes of rock characterized by disseminated concentrations of chalcopyrite (CuFeS_2), bornite (Cu_5FeS_4), molybdenite (MoS_2), or Au—as well as a number of other prograde and secondary sulfide minerals—in intensely fractured rocks filled by stockwork veins or disseminated grains in hydrothermally altered porphyritic intrusions and (or) in their hydrothermally altered adjacent wall rock (Peters and others, 1996). In the Battle Mountain Mining District, the Tertiary porphyry Cu systems contain relatively high concentrations of Au compared to porphyry Cu systems elsewhere in the southwestern United States. Much mineralized rock in these systems owes its origin to fluids that were expelled during the process of crystallization of genetically associated magma, typically present locally in intrusive centers that represent composites of a number of closely associated igneous phases. In the Battle Mountain Mining District, some recent studies suggest that source

magma(s) responsible for generation of the important mineralized system at Copper Canyon crystallized at considerable depths, and that these magmas expelled mineralizing fluids which were focused by small, shallow-seated igneous bodies which had risen high into the crust (Kotlyar and others, 1998). Supergene-altered equivalents of many of these deposits also may be important economically because of enrichment processes that have a tendency to enhance their Cu grades. The Copper Basin area of the Battle Mountain Mining District is an excellent example of a site where secondary enrichment of Cu prevailed on the margins of a large Cretaceous stockwork Mo system (Theodore and others, 1992). Nonetheless, porphyry types of mineralized systems tend to be developed preferentially in generally shallow-level geologic environments. Further, a continuum exists among porphyry Cu deposits, skarn deposits, and polymetallic vein deposits (see also, Carten and others, 1993; Titley, 1993; Pierce and Boehm, 1995)—all of which are widespread in the Battle Mountain Mining District.

The mining district is near the northwest terminus of the Battle Mountain-Eureka mineral belt in north-central Nevada, where many porphyry systems are situated at broad intersections of north-south- and northwest-striking structures (Doebrich and Theodore, 1996). The mining district also includes, in its southern part, the Copper Canyon Au-enriched, skarn-related porphyry Cu system which has been site of 10 relatively recent discoveries of peripheral Au–Ag orebodies—one being the 2 million oz Au Fortitude gold skarn (Wotruba and others, 1986), which was in production between 1982 and 1993. If porphyry Cu systems also are present under some clusters of Au deposits in the northern part of the mining district, then as many as nine porphyry centers may be present in the mining district. This remarkable concentration of pluton-related mineralized systems results from a number of district- and regional-scale metallotects (Doebrich and Theodore, 1996; Peters and others, 1996). Consequently, study of pluton-related Au in the mining district currently involves, in part, three-dimensional evaluation and analysis of metal zonation in approximately 2,500 drill holes, which are being studied collaboratively with geologists from Battle Mountain Gold Co. This study will provide a well-grounded foundation for evaluating subtle base- and precious-metal anomalies in exposures well beyond orebodies in porphyry Cu, skarn-related environments (see also, Kotlyar and others, 1998). Some preliminary results of a three-dimensional evaluation in the Copper Canyon part of the mining district are presented in the

paper below entitled "Multilevel Geochemical Patterns at the Fortitude Gold Skarn, Battle Mountain Mining District, Nevada," which demonstrates the complexities of metal distributions around large Au deposits in pluton-related geologic environments.

REFERENCES CITED

- Carten, R.B., White, W.H., and Stein, H.J., 1993, High-grade granite-related molybdenum systems: classification and origin, *in* Kirkham, R.V., Sinclair, W.D., Thorpe, R.I., and Duke, J.M., eds. Mineral deposit modeling: Geological Association of Canada Special Paper 40, p. 521-554.
- Cox, D.P., and Singer, D.A., 1992, Grade and tonnage model of distal disseminated Ag-Au, *in* Bliss, J.D., ed., Developments in mineral deposit modeling: U.S. Geological Survey Bulletin 2004, p. 20-22.
- Doeblich, J.L., and Theodore, T.G., 1996, Geologic history of the Battle Mountain Mining District, Nevada, and regional controls on the distribution of mineral systems, *in* Coyner, A.R., and Fahey, P.L., eds., Geology and ore deposits of the American Cordillera: Geological Society of Nevada Symposium Proceedings, Reno/Sparks, Nevada, April, 1995, v. 1, p. 453-483.
- Kotlyar, B.B., Theodore, T.G., Singer, D.A., Moss, Ken, Campo, A.M., and Johnson, S.D., 1998, Geochemistry of the gold skarn environment at Copper Canyon, Nevada: *Economic Geology* (in press).
- Peters, S.G., Nash, J.T., John, D.A., Spanski, G.T., King, H.D., Connors, K.A., Moring, B.C., Doeblich, J.L., McGuire, D.J., Albino, G.V., Dunn, V.C., Theodore, T.G., and Ludington, Steve, 1996, Metallic mineral resources in the U.S. Bureau of Land Management's Winnemucca District and Surprise Resource Area, northwest Nevada and northeast California: U.S. Geological Survey Open-File Report 96-712, 147 p.
- Pierce, F.W., and Bolm, J.G., eds., 1995, Porphyry copper deposits of the American Cordillera: Tucson, Arizona, Arizona Geological Society Digest, v. 20, 656 p.
- Theodore, T.G., 1998, Geology of pluton-related gold mineralization at Battle Mountain, Nevada: Tucson, Arizona, University of Arizona and U.S. Geological Survey Center for Mineral Resources, Monograph 2 (in press)
- Theodore, T.G., Blake D.W., Loucks, T.A., and Johnson, C.A., 1992, Geology of the Buckingham stockwork molybdenum deposit and surrounding area, Lander County, Nevada, *with a section on* Potassium-argon and $^{40}\text{Ar}/^{39}\text{Ar}$ geochronology of selected plutons in the Buckingham area, by E.H., McKee, *and a section on* Economic geology, by T.A. Loucks and C.A. Johnson, and a section on Supergene copper deposits at Copper Basin, by D.W. Blake, *and a section on* Mineral chemistry of Late Cretaceous and Tertiary skarns, by J.M. Hammarstrom: U.S. Geological Survey Professional Paper 789-D, 307 p.
- Titley, S.R., 1993, Characteristics of porphyry copper occurrence in the American southwest, *in* Kirkham, R.V., Sinclair, W.D., Thorpe, R.I., and Duke, J.M., eds., Mineral deposit modeling: Geological Association of Canada Special Paper 40, p. 433-464.
- Wotruba, P.R., Benson, R.G., and Schmidt, K.W., 1986, Battle Mountain describes the geology of its Fortitude gold-silver deposit at Copper Canyon: *Mining Engineering*, July 1986, v. 38, no. 7, p. 495-499.

LARGE DISTAL-DISSEMINATED PRECIOUS-METAL DEPOSITS, BATTLE MOUNTAIN MINING DISTRICT, NEVADA

By Ted G. Theodore

ABSTRACT

Apparent transitions between two major classes of metal deposits in the Battle Mountain Mining District, porphyry Cu and stockwork Mo deposits, on the one hand, and high level distal-disseminated Ag–Au deposits, on the other hand, reflect a contrast in paleodepths of deposit formation on either side of the Miocene Oyarbide fault. This fault, a significant northeast-striking, post-mineral fault in the mining district, displaces downwards its northwestern block at least 700 m—geologic relations suggest that final displacements along this fault only can be constrained geologically to sometime during the last 17 to 14 m.y., possibly at roughly the same time as the less-than-9–Ma displacements recorded along the similarly trending Midas, Nev., trough, which is approximately 40 km to the north.

INTRODUCTION

The extraordinarily varied and copious metal endowment of the Battle Mountain Mining District (fig. 1) results from the location of the mining district in a shallow-seated geologic environment at the intersection of regional-scale metallotects of several ages (Roberts and Arnold, 1965; Theodore, 1992; see also, Doebrich and others (1996) for a summary). The term Battle Mountain Mining District used in this report differs from that used by Tingley (1992) by expanding the area to include the Buffalo Valley Mining District and the northern part of the Buffalo Mountain Mining District, which includes mineralized rock in the general area of Lone Tree Hill (fig. 1). Recent precious-metal discoveries in the northern part of the Battle Mountain Mining District have resulted in recognition of a fundamental difference between deposits in the northwest and southeast parts of the district. The discoveries generally are not closely associated genetically with intrusive rocks, and include approximately 1 million oz Au near the Eight South deposit, a probable 1 million oz Au in three other deposits (Trenton, Valmy, North Peak; Felder, 1997), and approximately 5 million oz Au in the Lone Tree deposits (fig. 1; see also, Bloomstein and others, 1998). However, in the southeast parts of the mining district many exposed metal-bearing plutons of Late Cretaceous and middle Tertiary ages contribute

significantly to the overall metal endowment of the mining district, and result in at least seven porphyry Cu and stockwork Mo systems being present (Theodore and others, 1992; Doebrich and others, 1996). The economically most significant area of precious metal-mineralized rock in the southeast part of the mining district is at Copper Canyon, where approximately 5 million oz Au have been delineated (Theodore, 1998; see also section below entitled “Multilevel Geochemical Anomalies at the Fortitude Gold Skarn, Battle Mountain Mining District, Nevada”). At Copper Canyon, gold-bearing skarns are present in a widespread 39–Ma skarn-related, porphyry copper system, including the Fortitude gold skarn (approximately 2 million oz Au, Wotruba and others, 1986; Myers, 1994).

The Late Cretaceous and middle Tertiary intrusive rocks, which are present throughout the southeast part of the mining district, are calc-alkaline and shallow seated—they were emplaced into a complex array of Paleozoic rocks that subsequently were broken by a number of post-mineral faults during the late Tertiary. The middle Tertiary magmatism also roughly coincides temporally with initiation of extension in the region, although much extension in north-central Nevada culminated somewhat later when a shift from calc-alkaline to bimodal magmatism occurred about 17 my ago (Seedorff, 1991; see also, Doebrich and Theodore, 1996). The mining district includes the prominent northeast-striking, northwest-dipping post-mineral Oyarbide fault, which displaced its hanging wall approximately 700 m (fig. 1). The Oyarbide fault is classified by Dohrenwend and Moring (1991) as a young, post-17–Ma, deeply penetrating block fault that, in part, juxtaposes Quaternary alluvium against bedrock.

DISTRIBUTION PATTERNS OF ORE DEPOSITS

Several metallized district-scale northwest and north-south structural trends characterize the known major orebodies and their genetically related granitic, *sensu lato*, rocks (Blake and others, 1979; Doebrich, 1995; Doebrich and others, 1996), and the major clusters of orebodies are present at their intersections.

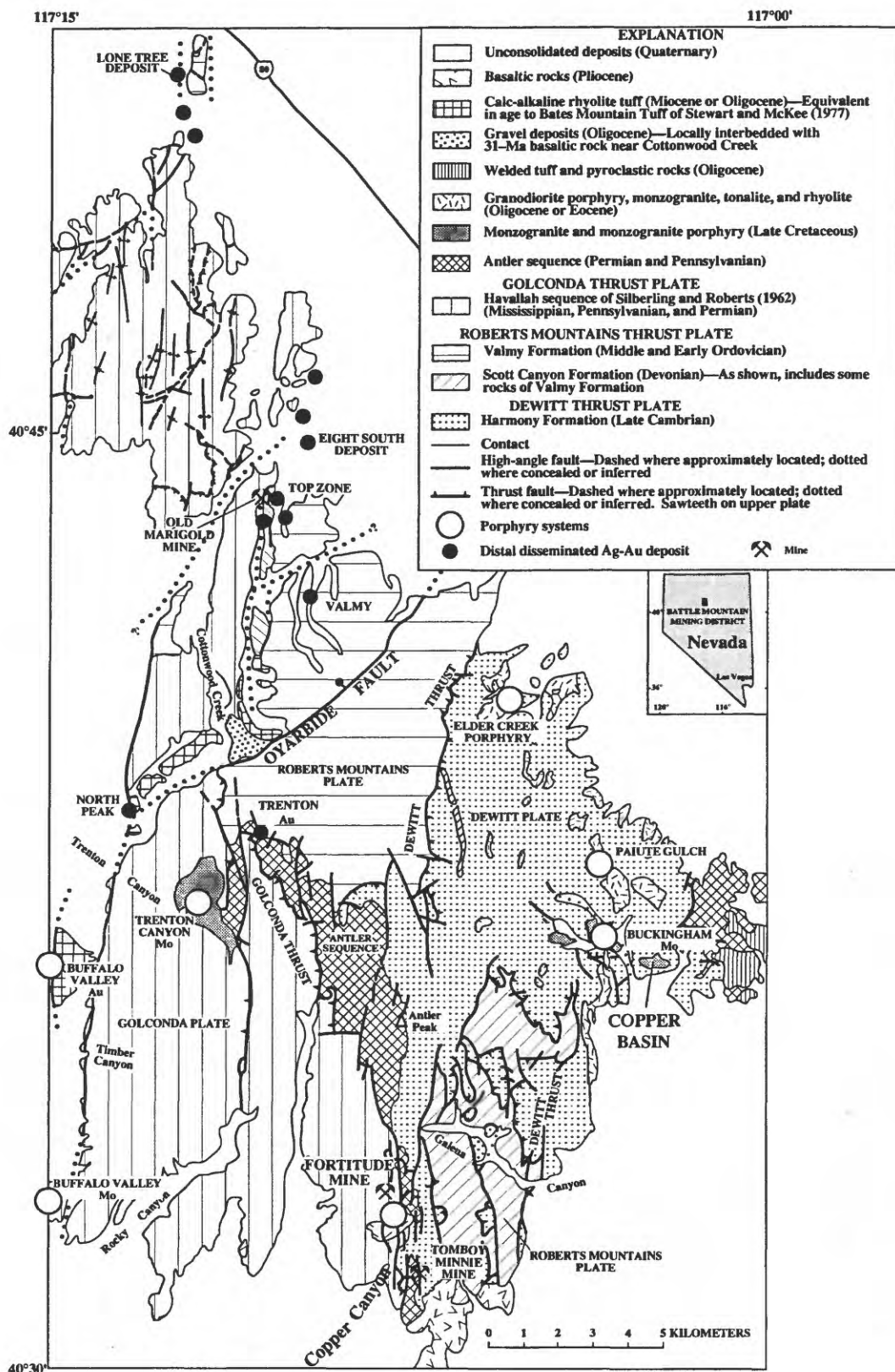


Figure 1. Geology of the Battle Mountain Mining District. Modified from Roberts (1964), Theodore (1991), and Doebrich (1995).

Other important regional-scale metallogenes also impact the mining district, and these include: (1) a Late Cretaceous magmatic arc resulting from trench-related magmatism in a continental margin mobile belt (for example, Westra and Keith, 1981), (2) a highly mineralized trend, the northwest-trending Eureka mineral belt of Shawe and Stewart (1976), previously termed the "Eureka-Battle Mountain mineral belt" by Roberts (1966) and also referred to as the "Battle Mountain gold belt" by Madrid and Roberts (1991), and (3) an apparently 5- to 8-km-wide, loosely constrained, north-south mineralized trend, termed the "Rabbit Creek-Marigold mineral belt," that includes the large number of Au-Ag deposits in the general area of the Eight South deposit. The latter metallized trend essentially extends about 50 km farther to the north where it terminates in the Twin Creeks Au-Ag deposit (Bloomstein and others, 1991) northeast of the Carlin-type (Berger, 1986) precious-metal deposits at Getchell.

The geology and geochemistry of a number of precious-metal deposits in the northwest part of the Battle Mountain Mining District (fig. 1) also provide specific insight into inferred regional patterns of their distribution, as well as their ages, even though many of these deposits apparently do not have clear-cut spatial and genetic ties to felsic plutons and have not been dated radiometrically. The dominant theme, however, that is repeated through all of the deposits in the northwest part of the mining district is the importance of faults and fractures as major contributing components to their overall genesis. Nonetheless, large volumes of rock in many of these precious-metal deposits contain disseminated ore which results from a bleeding out from mineralized faults and fractures that act as feeders to deliver metal-bearing fluids to chemically and (or) physically receptive sites.

About 15 precious-metal deposits are mostly present south of the Eight South deposit in the hanging wall of the Oyarbide fault (fig. 1). All of these deposits are probably best classified as distal-disseminated Ag-Au deposits (Cox and Singer, 1992), and owe their origins to relatively far-traveled, hypogene Au-bearing fluids emanating from buried porphyry Cu systems somewhat akin to the evolution of immiscible fluids described for porphyry systems (Hedenquist and Lowenstern, 1994; Albino, 1994). The Eight South Au deposit (Graney and McGibbon, 1991; McGibbon and Wallace, 1997) was the first of these recent discoveries near the Old Marigold Mine (fig. 1). The Eight South deposit is completely oxidized and, compared to most pluton-related systems, apparently has a relatively high Au/Ag ratio of 1 in its ore, as well as anomalous concentrations of As, Sb, Hg, Tl, and especially Ba—geochemical signatures that suggest that this deposit may be a Carlin-type precious-metal system (Graney and McGibbon, 1991). However, Au/Ag ratios prior to oxidation may have been different. Oxidation in the general area of the Eight South deposit may have been taking place for as long as approximately 23 m.y. (Theodore, 1998)—possibly enhanced by the fact that the site of the deposit, at one time, was elevated

approximately 700 m relative to its present position (D.H. McGibbon, oral commun., 1996). Classification of these deposits as distal-disseminated Ag-Au, nonetheless, is provisional and assumes that Carlin-type deposits are not pluton-related. Recent discovery of Au-mineralized rock associated with abundant oxide Cu at the Mike deposit along the Carlin trend, Nev. (Teal and Jackson, 1997)—approximately 75 km east of the Battle Mountain Mining District—may require a revision of classification schemes involving Carlin type deposits and distal disseminated Ag-Au deposits, particularly if it is demonstrated that evolved magmatic fluids are the dominant fluids involved in generation of the bulk of the Carlin-type deposits. However, if it turns out that Cu in the Mike deposit is unrelated temporally to the Au, then the Cu may be associated with some type of system other than a Carlin type.

The distal-disseminated Ag-Au deposits in the Battle Mountain Mining District cluster in sedimentary rocks and represent mineral occurrences at various levels vertically in large magmatic-hydrothermal systems as described by Albino (1994) (fig. 1). These 15 deposits—not all shown on figure 1—have many notable differences, some as described above, compare to the deposits used by Cox and Singer (1992) to construct the original distal-disseminated Ag-Au model. This deposit model, regardless, definitely belongs to the porphyry Cu or pluton-related mineralizing environment, and this model has a strong affiliation with upper crustal magmatism. An underestimation of base-metal contents of mineralized systems in the hanging wall of the Oyarbide fault also has contributed to their problematic classification. Nonetheless, the Lone Tree deposits appear to have an increase in base-metal content in the lower benches so that they are now (1998) beginning to display chemical and physical attributes—as well as fluid-inclusion signatures (Theodore, 1998)—characteristic of distal-disseminated Ag-Au deposits. Many of the deposits have elevated contents of K₂O (sericite) associated with Au-mineralized rock (Bloomstein and others, 1991)—large-scale additions of K₂O are not as common in most classic Carlin-type deposits. Some difficulty of classifying Au deposits in the Lone Tree and Marigold areas involves the protracted oxidation, probably lasting as long as 23 m.y., which may have altered significantly base- and precious-metal ratios from their preoxidation values.

The best evidence to assign these deposits to a pluton-related environment includes (1) the setting of the deposits in the pluton-related geologic environment of the Battle Mountain Mining District, (2) sericitically altered dikes in direct association with sericitically altered and Au-mineralized rock in some of the deposits, and (3) magmatic isotopic signatures of hydrothermal barite associated with Au-mineralized rock (Howe and others, 1995; Theodore, 1998). Sulfur isotopic ratios of hydrothermal barites—values of $\delta^{34}\text{S}$ clustering tightly at approximately +10 per mil—that are associated with several of these Au deposits clearly indicate a significant

magmatic component to ore-forming fluids (Howe and others, 1995). This contrasts to well-studied Carlin-type systems elsewhere (Hofstra and others, 1988, 1989; Arehart, 1996; Ilchik and Barton, 1997).

Vertically stacked, large porphyry Cu systems contain peripheral distal-disseminated Ag–Au deposits in the northwest part of the Battle Mountain Mining District, similar to deposits elsewhere referred to as distal epithermal gold deposits (Jones, 1992). These deposits represent the predominantly structurally controlled, high level parts of porphyry Cu systems, probably inboard from the more common Ag–rich deposits. Metal zoning in the most outermost parts of these systems is complicated because absolute differences in precious-metal abundances are difficult to quantify due to intense oxidation (see above). The distal-disseminated Ag–Au deposits are analogous to polymetallic vein deposits, and may be considered to be variants of them (Cox and Singer, 1992); however, distal-disseminated Ag–Au deposits differ from polymetallic veins in their disseminated nature whose style of ore can be dispersed sufficiently to have generated deposits as large as approximately 83 million tonnes as at Cove, Nev. (Cox and Singer, 1992). They differ, as well, in absence of concentrations of Pb and Zn comparable to that found in most polymetallic veins, although the Ag–rich Cove deposit includes relatively high contents of Pb.

Changes in elemental ratios brought about by oxidation in these deposits cause high-level occurrences to have Carlin-type geochemical signatures. Indeed, Albino (1993) points out that the common enrichment of As, Sb, and Hg in both Carlin-type systems and distal-disseminated Ag–Au deposits partly results from these elements having the ability to be transported as bisulfide complexes. In addition, Albino (1993) points out that many distal-disseminated Ag–Au deposits are enriched in Mn, whereas some Carlin-type deposits, in fact, may be leached of Mn. The Au deposits in the down-faulted terrane north of the Oyarbide fault represent high-level parts of large mineralized hydrothermal systems, which formed mostly in calcareous sedimentary rocks near the paleosurface. The two clusters of Au deposits near Lone Tree Hill and the Eight South deposit (fig. 1) result probably from two separate porphyry Cu centers buried beneath them.

I do not mean to imply, however, that distal-disseminated Ag–Au deposits cannot be present south of the Oyarbide fault—actually the Trenton Canyon Au deposits (fig. 1) probably are examples of such deposits (Felder, 1998). Any pluton-related mineralizing system, which is similar geologically to those previously described, and which is emplaced at somewhat greater overall paleodepths south of the Oyarbide fault, also should have the potential of forming distal-disseminated Ag–Au deposits. However, Sillitoe (1994) suggests that the two types gold deposit, distal-disseminated Ag–Au as well as Carlin type, should instead be considered

as two broad, genetic varieties of a single category of deposits. Previously, Sawkins (1990) also suggested that Carlin-type deposits result from fluids that emanated from buried felsic to chemically intermediate intrusive rocks and were channeled along deeply penetrating faults to sites where metal deposition occurred. These suggestions disregard the apparent different geologic processes that currently are envisioned by many to have been involved in generation of the two types of deposits: largely magma-equilibrated fluids associated with the former, and mostly evolved meteoric and (or) metamorphic fluids associated with the latter (Arehart, 1996; Ilchik and Barton, 1997), as well as major differences in salinity of the ore-forming fluids. Further, Carlin-type deposits commonly may have formed at paleodepths greater than the distal-disseminated Ag–Au deposits—400 to 800 bars (Peters and others, 1996)—the latter form typically in high-level parts of a Au–enriched pyritic envelope surrounding a porphyry Cu system. Intensely fractured rocks with abundant Au–bearing iron oxides along fractures are present in many of the distal-disseminated Ag–Au deposits in the Battle Mountain Mining District.

Even the age of Carlin deposits, including those that have been investigated intensely for as many as 30 years, remains enigmatic, both along the Carlin trend and along the Getchell trend. Perhaps, the deposits along the Carlin trend owe their origins to long-lived circulation of hot, Au–bearing fluids—perhaps as long as 100 m.y. Post-14–Ma hot fluids deposited quartz-adularia assemblages along joints and fractures in the Miocene Carlin Formation in the northern part of the Carlin trend (Fleck and others, this volume). Similar mineral assemblages (plus Hg) are present in highly recrystallized outcrops near the headframe of the Meikle Mine, one of the economically most important Au deposits along the Carlin trend (Teal and Jackson, 1997).

CONCLUSION

The seeming transition between two major classes of deposits in the Battle Mountain Mining District, porphyry Cu and stockwork Mo deposits, on the one hand, and distal-disseminated Ag–Au deposits, on the other hand, reflects a contrast in paleodepths of deposit formation on either side of the Oyarbide fault. This fault is a significant northeast-striking, post-mineral fault in the mining district (fig. 1). It displaces downwards its northwestern block at least 700 m—geologic relations suggest that final displacements along this fault only can be constrained geologically to sometime during the last 17 to 14 m.y., possibly at roughly the same time as the less-than-9–Ma displacements recorded along the similarly trending Midas, Nev., trough, which is approximately 40 km north of the mining district (Wallace and Hruska, 1991; see also Doebrich and Theodore, 1996).

REFERENCES CITED

- Albino, G.V., 1993, Application of metal zoning to gold exploration in porphyry copper systems by B.K. Jones: comments: *Journal of Geochemical Exploration*, v. 48, no 3, p. 359–366.
- 1994, Time-pH-fO₂ paths of hydrothermal fluids and the origin of quartz-alunite-gold deposits, *in* Berger, B.R., ed., *Advances in research on mineral resources, 1994: U.S. Geological Survey Bulletin 2081*, p. 33–42.
- Arehart, G.B., 1996, Characteristics and origin of sediment-hosted disseminated gold deposits: a review: *Ore Geology Reviews*, v. 11, no. 6, p. 383–403.
- Berger, B.R., 1986, Descriptive model of carbonate-hosted Au–Ag, *in* Cox, D.P., and Singer, D.A., eds., *Mineral deposit models: U.S. Geological Survey Bulletin 1693*, p. 175.
- Blake, D.W., Theodore, T.G., Batchelder, J.N., and Kretschmer, E.L., 1979, Structural relations of igneous rocks and mineralization in the Battle Mountain Mining District, Lander County, Nevada, *in* Ridge, J.D., ed., *Papers on mineral deposits of western North America: International Association on the Genesis of Ore Deposits Symposium, 5th, Snowbird-Alta, Utah, 1978, Proceedings: Nevada Bureau of Mines and Geology Report 33*, p. 87–99.
- Bloomstein, E.I., Braginton, B.L., Owen, R.O., Parratt, R.L., Raabe, K.C., and Thompson, W.F., 1998, Lone Tree gold deposit, *in* Theodore, T.G., *Geology of pluton-related gold mineralization at Battle Mountain, Nevada: Tucson, Arizona, University of Arizona and U.S. Geological Survey Center for Mineral Resources, Monograph 2* (in press)
- Bloomstein, E.I., Massingill, G.L., Parratt, R.L., and Peltonen, D.R., 1991, Discovery, geology, and mineralization of the Rabbit Creek gold deposit, Humboldt County, Nevada, *in* Raines, G.L., Lisle, R.E., Schafer, R.W., and Wilkinson, W.H., eds., *Geology and ore deposits of the Great Basin, Symposium Proceedings: Reno, Nevada, Geological Society of Nevada*, p. 821–843.
- Cox, D.P., and Singer, D.A., 1992, Grade and tonnage model of distal disseminated Ag–Au, *in* Bliss, J.D., ed., *Developments in mineral deposit modeling: U.S. Geological Survey Bulletin 2004*, p. 20–22.
- Doebrich, J.L., 1995, Geology and mineral deposits of the Antler Peak 7.5-minute quadrangle, Lander County, Nevada: *Nevada Bureau of Mines and Geology Bulletin 109*, 44 p.
- Doebrich, J.L., and Theodore, T.G., 1996, Geologic history of the Battle Mountain Mining District, Nevada, and regional controls on the distribution of mineral systems, *in* Coyner, A.R., and Fahey, P.L., eds., *Geology and ore deposits of the American Cordillera: Geological Society of Nevada Symposium Proceedings, Reno/Sparks, Nevada, April, 1995*, v. 1, p. 453–483.
- Doebrich, J.L., Wotruba, P.R., Theodore, T.G., McGibbon, D.H., and Felder, R.P., 1996, Field trip guidebook for Trip H—Geology and ore deposits of the Battle Mountain Mining District, *in* Green, S.M., and Struhsacker, Eric, eds., *Field Trip Guidebook Compendium: Reno, Nevada, Geological Society of Nevada, Geology and Ore Deposits of the American Cordillera*, p. 327–388.
- Dohrenwend, J.C., and Moring, B.C., 1991, Reconnaissance photogeologic map of young faults in the Winnemucca 1° by 2° quadrangle, Nevada: *U.S. Geological Survey Miscellaneous Field Studies Map MF-2175*, 1 sheet, 1:250,000.
- Felder, R.P., 1998, Geology, mineralization, and exploration history of the Trenton Canyon project, *in* Theodore, T.G., *Geology of pluton-related gold mineralization at Battle Mountain, Nevada: Tucson, Arizona, University of Arizona and U.S. Geological Survey Center for Mineral Resources, Monograph 2* (in press).
- Fleck, R.J., Theodore, T.G., Sarna-Wojcicki, Andrei, and Meyer, C.E., (this volume), Age and possible source of air-fall tuffs of the Miocene Carlin Formation, northern Carlin trend, *in* Tosdal, R.M., ed., *Contributions to the gold metallogeny of northern Nevada: U.S. Geological Survey Open-File Report*.
- Graney, J.R., and McGibbon, D.H., 1991, Geological setting and controls on gold mineralization in the Marigold Mine area, Nevada, *in* Raines, G.L., Lisle, R.E., Schafer, R.W., and Wilkinson, W.H., eds., *Geology and ore deposits of the Great Basin, Symposium Proceedings: Reno, Nevada, Geological Society of Nevada*, p. 865–874.
- Hedenquist, J.W., and Lowenstem, J.B., 1994, The role of magmas in the formation of hydrothermal ore deposits: *Nature*, v. 370, p. 519–527.
- Hofstra, A.H., Landis, G.P., Rye, R.O., Birak, D.J., Dahl, A.R., Daly, W.E., and Jones, M.B., 1989, Geology and origin of the Jerritt Canyon sediment-hosted disseminated gold deposits, Nevada, *in* Schindler, K.S., ed., *USGS Research on Mineral Resources—1989, Programs and Abstracts: U.S. Geological Survey Circular 1035*, p. 30–32.
- Hofstra, A.H., Northrop, H.R., Rye, R.O., Landis, G.P., and Birak, D.J., 1988, Origin of sediment-hosted disseminated gold deposits by fluid mixing—Evidence from jasperoids in the Jerritt Canyon gold district, Nevada, U.S.A., *in* Goode, A.D.T., and Bosma, L.I., eds., *Bicentennial Gold 88, Extended Abstracts, Oral Programme: Geological Society of Australia, Abstract Series no. 22*, p. 284–289.
- Howe, S.S., Theodore, T.G., and Arehart, G.B., 1995, Sulfur and oxygen isotopic composition of vein barite from the Marigold mine and surrounding area, north-central Nevada: Applications to gold exploration: *Geology and Ore deposits of the American Cordillera, Symposium, Reno/Sparks, Nevada, April 10–13, 1995, Program with Abstracts*, p. A39.
- Ilchik, R.P., and Barton, M.D., 1997, An amagmatic origin of Carlin-type gold deposits: *Economic Geology*, v. 92, no. 3, p. 269–288.
- Jones, B.K., 1992, Application of metal zoning to gold exploration in porphyry copper systems: *Journal of Geochemical Exploration*, v. 43, no. 2, p. 127–155.
- Madrid, R.J., and Roberts, R.J., 1991, Origin of gold belts in north-central Nevada, *in* Madrid, R.J., Roberts, R.J., and Mathewson, David, *Stratigraphy and structure of the Battle Mountain gold belt and their relationship to gold deposits, Field Trip 15, in* Buffa, R.H., and Coyner, A.R., eds., *Geology and ore deposits of the Great Basin: Reno, Nevada, Geological Society of Nevada, Fieldtrip Guidebook Compendium*, v. 2, p. 927–939.
- McGibbon, D.H., and Wallace, A.B., 1998, Geology of the Marigold Mine area, *in* Theodore, T.G., *Geology of pluton-related gold mineralization at Battle Mountain, Nevada: Tucson, Arizona, University of Arizona and U.S. Geological Survey Center for Mineral Resources, Monograph 2* (in press)
- Myers, G.L., 1994, Geology of the Copper Canyon-Fortitude skarn system, Battle Mountain, Nevada: *Pullman, Washington,*

- Washington State University, Ph.D. dissertation, 338 p.
- Roberts, R.J., 1964, Stratigraphy and structure of the Antler Peak quadrangle, Humboldt and Lander Counties, Nevada: U.S. Geological Survey Professional Paper 459-A, 93 p.
- 1966, Metallogenic provinces and mineral belts in Nevada: Nevada Bureau of Mines Report 13, part A, p. 47-72.
- Roberts, R.J., and Arnold, D.C., 1965, Ore deposits of the Antler Peak quadrangle, Humboldt and Lander Counties, Nevada: U.S. Geological Survey Professional Paper 459-B, 94 p.
- Sawkins, F.J., 1990, Metal deposits in relation to plate tectonics, 2nd Edition: Berlin, Springer-Verlag, 461 p.
- Seedorff, Eric, 1991, Magmatism, extension, and ore deposits of Eocene to Holocene age in the Great Basin—mutual effects and preliminary proposed genetic relationships, *in* Raines, G.L., Lisle, R.E., Schafer, R.W., and Wilkinson, W.H., eds., *Geology and ore deposits of the Great Basin, Symposium Proceedings: Reno, Nevada*, Geological Society of Nevada, p. 133-178.
- Shawe, D.R., and Stewart, J.H., 1976, Ore deposits as related to tectonics and magmatism, Nevada and Utah: *Society of Mining Engineers of AIME Transactions*, v. 260, p. 225-231.
- Sillitoe, R.H., 1994, Indonesian mineral deposits—introductory comments, comparisons, and speculations, *in* Van Leeuwen, T.M., Hedenquist, J.W., James, L.P., and Dow, J.A.S., eds., *Mineral deposits in Indonesia—Discoveries of the past 25 years: Journal of Geochemical Exploration*, v. 50, nos. 1-3, p. 1-11.
- Teal, Lewis, and Jackson, Mac, 1997, Geologic overview of the Carlin trend gold deposits: *Society of Economic Geology Newsletter*, no. 31, p.1, 13-25.
- Theodore, T.G., 1991, Preliminary geologic map of the Valmy quadrangle, Humboldt County, Nevada: U.S. Geological Survey Open-File Report 91-430, 11 p. (1 sheet, 1:24,000).
- 1998, Geology of pluton-related gold mineralization at Battle Mountain, Nevada: Tucson, Arizona, University of Arizona and U.S. Geological Survey Center for Mineral Resources, Monograph 2 (in press)
- Theodore, T.G., Blake, D.W., Loucks, T.A., and Johnson, C.A., 1992, Geology of the Buckingham stockwork molybdenum deposit and surrounding area, Lander County, Nevada, *with a section on Potassium-argon and ⁴⁰Ar/³⁹Ar geochronology of selected plutons in the Buckingham area*, by E.H. McKee, *and a section on Economic geology*, by T.A. Loucks and C.A. Johnson, *and a section on Supergene copper deposits at Copper Basin* by D.W. Blake, *and a section on Mineral chemistry of Late Cretaceous and Tertiary skarns*, by J.M. Hammarstrom: U.S. Geological Survey Professional Paper 798-D, 307 p.
- Tingley, J.V., 1992, Mining districts of Nevada: Nevada Bureau of Mines and Geology Report 47, 124 p.
- Wallace, A.R., and Hruska, D.C., 1991, Miocene volcanic rocks and gold deposits, Gold Circle (Midas) district and Ivanhoe gold deposit, *in* *Geology and ore deposits of the Getchell trend and northern Nevada rift, northern Nevada*, *in* Buffa, R.H., and Coyner, A.R., eds., *Geology and ore deposits of the Great Basin: Reno, Nevada, Geological Society of Nevada, Field Trip Guidebook Compendium*, v. 1, p. 382-388.
- Westra, Gerhard, and Keith, S.B., 1981, Classification and genesis of stockwork molybdenum deposits: *Economic Geology*, v. 76, no. 4, p. 844-873.
- Wotruba, P.R., Benson, R.G., and Schmidt, K.W., 1986, Battle Mountain describes the geology of its Fortitude gold-silver deposit at Copper Canyon: *Mining Engineering*, July 1986, v. 38, no. 7, p. 495-499.

MULTILEVEL GEOCHEMICAL PATTERNS AT THE FORTITUDE GOLD SKARN, BATTLE MOUNTAIN MINING DISTRICT, NEVADA

By Boris B. Kotlyar and Ted G. Theodore

ABSTRACT

Distribution of elevated contents of proximal (Cu, Au, Ag) and distal (Pb, Zn) metals around the Fortitude Au skarn reveals that a prominent Pb–Zn halo mantles the distal parts of the orebodies, more or less duplicating, at large scale, the district-scale relations between proximal and distal metals previously recognized in production data from widespread polymetallic veins. The geochemical haloes that surround the Fortitude orebodies are complicated and multilevel, including mushroom- and pillar-shaped parts. In addition, present-day topography impacted significantly these geometrically complex haloes as exemplified by apparent removal by erosion of part of a Pb locus near the northern end of the Fortitude orebodies. Further, mineralized rocks of the Pennsylvanian and Permian Antler sequence at the Nevada Mine are inferred to represent the northern leading edge of mineralized rocks that make up the Fortitude and Phoenix deposits in the Antler sequence farther to the south. Finally, Pb–Zn ores at the 700-ft level in the Copper Canyon underground mine, as well as a reversal in district metal zoning at the Tomboy–Minnie Au–skarn deposits, are inferred to be related to another site in the southern part of the Copper Canyon area near the Midas Au skarn where influx of mineralizing fluids occurred. Both of these sites where influx of metals may have occurred may be related to apices of mineralized cupolas of altered granodiorite.

INTRODUCTION

Geochemical data from mineralized drill core into the Fortitude Au skarn (the largest producer of Au in the Battle Mountain Mining District) define deposit-scale metal distribution patterns around skarn zones which are related to a 38- to 40-Ma skarn-related, porphyry Cu system at Copper Canyon (fig. 1; Wotruba and others, 1986; Myers, 1994; Kotlyar and others, 1997). Mining of ores from the Lower Fortitude deposit occurred between 1984 and 1993. Gold-skarn mineralized rocks in the Lower Fortitude deposit contained approximately 2.1 million oz Au, and are largely restricted to the generally flat-lying Pennsylvanian and Permian Antler Peak Limestone—middle formation of the Pennsylvanian and Permian Antler sequence—present below

the Golconda thrust. These rocks extend at depth below the Golconda thrust as much as 1,000 m from the northern contact of an altered 38- to 40-Ma granodiorite at the core of the system (fig. 1; Wotruba and others, 1986; Myers, 1994).

A north-south geochemical profile was studied, through the two major orebodies that comprise the Lower Fortitude Au skarn: Orebody I, proximal to the altered granodiorite of Copper Canyon, and the other distal, II (fig. 2). The Copper Canyon area also includes the Phoenix Au skarn immediately south of the Fortitude deposit (deposit no. 3, fig. 1)—the Phoenix deposit contains at least 900,000 oz Au (Doebrich and others, 1996; see also, Kotlyar and others, 1998), and is currently (early 1998) being permitted for mining. A number of drill holes that were analyzed for Cu, Au, Ag, Pb, and Zn in the general area of the Fortitude deposits were selected for study of their metal distributions at depth around the two major orebodies that make up the Lower Fortitude (fig. 2). The Nevada Mine, near the north end of the cross section, is a polymetallic replacement and vein occurrence hosted in rocks of the Antler sequence, which were exposed in a structural window through the Golconda thrust (Theodore and Blake, 1975). The Nevada Mine produced about 273 oz Au and 28,000 oz Ag from 1902 to 1948 (Roberts and Arnold, 1965).

These studies form a small part of a protracted examination of the behavior of Au in pluton-related geologic environments. This examination, in part, is designed to provide a better understanding of geometric relations of highly zoned mineralized systems in these environments that are widespread throughout much of northern Nevada (Peters and others, 1996). A more detailed description of these relations is presented by Kotlyar and others (1998).

COMPUTER-CONTOURING PROCEDURES

Down-hole gridding and filtering procedures were used to establish loci of Au, Cu, Ag, Pb, and Zn metallization in 982 drill-core samples analyzed along a north-south section through the Lower Fortitude orebodies (fig. 2). The computer-contouring procedures follow those described by Kotlyar and others (1995, 1998). The “Au” symbol, for example, is placed visually at the center of gravity of normalized, gridded, and

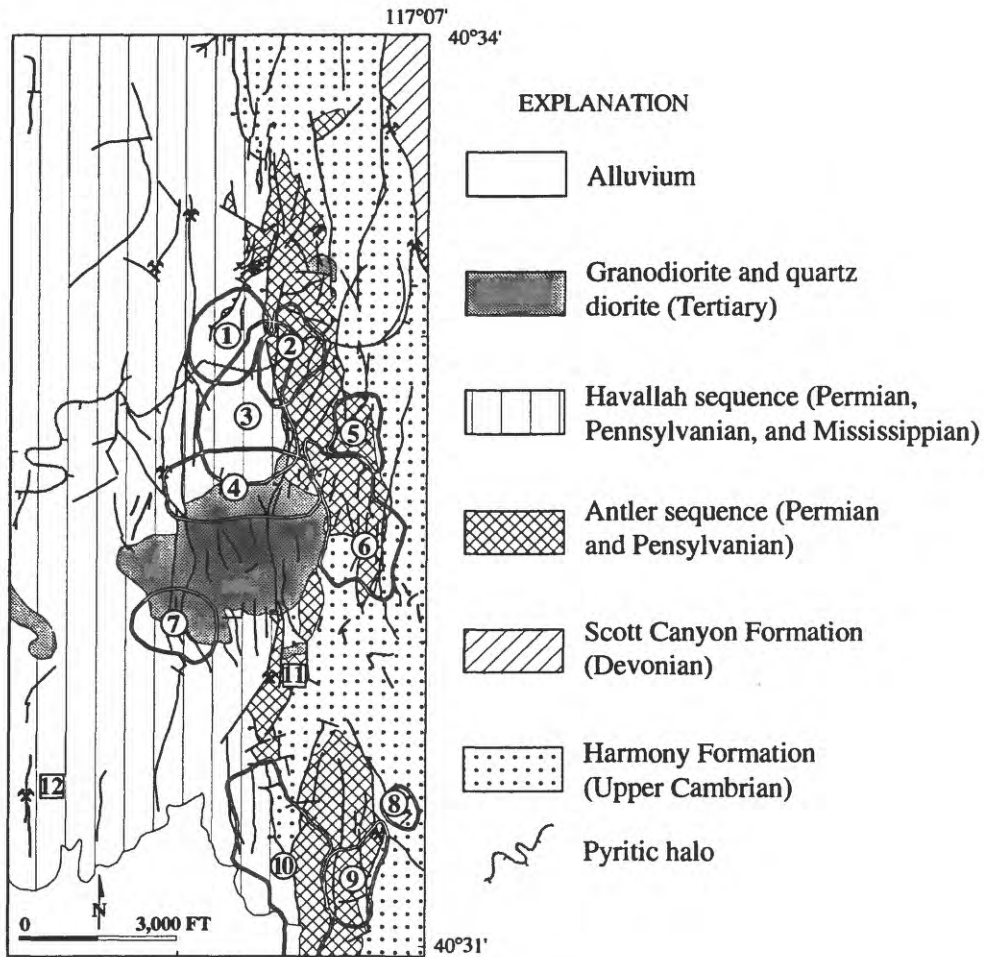


Figure 1. Geology of the Copper Canyon area, Battle Mountain Mining District, Nevada. Modified from Theodore and Blake (1975). Deposit nos. 1–12 are deposits discussed in report. 1, Lower Fortitude; 2, Upper Fortitude; 3, Phoenix; 4, West Orebody; 5, Northeast Extension; 6, East Orebody; 7, Reona; 8, Minnie; 9, Tomboy; 10, Midas; 11, Copper Canyon underground (Cu–Pb–Zn); 12, Wilson-Independence (Au–Ag). Deposit nos. in circles indicate large Au–Ag deposits mined by open-pit methods; squares, deposits mined by underground methods.

filtered data for Au—contours are in standard deviations. Greater intensity gray shades indicate higher deviation from the mean Au content across the plane of the section. Normalization of the data involved calculation of $(X_C - X_{Mean}) / X_{Standard\ Deviation}$, where all values are logarithms and X_C is the concentration for a selected element in an analyzed sample, resulting in contours showing deviations (σ) from the mean. The locus of Au-mineralized rock along the section is compared with loci of other metals, established by using the same technique, and shows a progression, respectively, from south to north of Au, Cu, Ag, Pb, and Zn loci of mineralized rock (fig. 2). These loci are more or less coincident with the projected trace of the Lower Fortitude orebodies onto the cross section—the locus for Au is at the proximal end; that is, proximal to the granodiorite of Copper Canyon (fig. 1), and Zn is at the distal end (fig. 2). Thus, zonation of metals around

the Fortitude orebodies may be grouped into a proximal suite (Cu, Au, Ag) and into a distal one (Pb, Zn).

Examination of analyzed drill-core samples showed that mineralized rock that surrounds the Fortitude orebodies also comprises multilevel and complex metal contents—a relation that was not that readily obvious during examination of untreated raw data. A lower level Au anomaly, made up of rocks inferred to contain as much as 0.25σ Au, is present well below the Lower Fortitude orebodies, and this lower anomaly comprises two parts: (1) a mushroom-shaped part elongated north-south, and (2) a pillar-shaped part which connects the lower anomaly with Au concentrations centered just below the Lower Fortitude orebodies (fig. 2B). In contrast to the other metals examined, two widely separate loci of equally intense Pb-mineralized rocks are present along the section: an upper one that may be arcuate shaped with parts removed

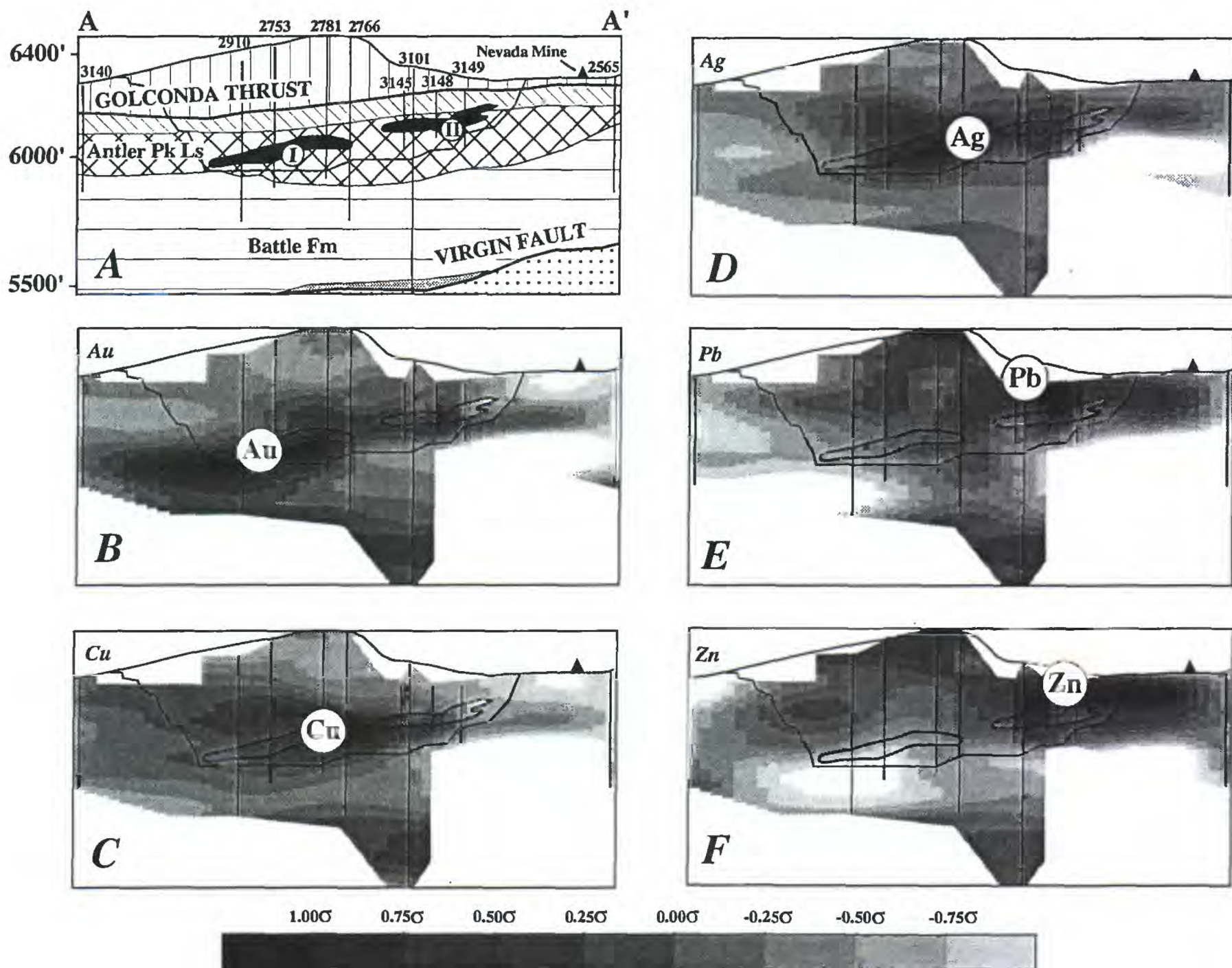


Figure 2. Geology (A) and normalized, gridded, and filtered (see text) distributions of Au (B), Cu (C), Ag (D), Pb (E), and Zn (F) in a north-south profile through the Lower Fortitude gold skarn deposit, Nevada. Explanation for A same as figure 1, except diagonal-lined pattern, Permian Edna Mountain Formation; doubly diagonal-lined pattern, Pennsylvanian and Permian Antler Peak Limestone; horizontal lined pattern, Pennsylvanian Battle Formation. Black, projection of ore in Lower Fortitude to plane of section. More densely shaded patterns (in B–F) represent higher standard deviations (σ) as shown in graduated gray scale. Circled chemical symbols represent respective loci for most intensely concentrated presence of proximal (Cu, Au, Ag) and distal metals (Pb, Zn). I, Southern orebody of Lower Fortitude; II, Northern orebody of Lower Fortitude.

by erosion above the north end of the Lower Fortitude orebodies—our preferred interpretation—and a lower one that is mushroom shaped deep below the Lower Fortitude orebodies and connected to the upper anomaly by a pillar-shaped part (fig. 2E). This lower level Pb anomaly below the Fortitude orebodies is associated spatially with the lower level Au anomaly. The lower level Pb anomaly at the Fortitude orebodies probably is analogous to Pb–Zn–Ag mineralized rock in the 700-level at the Copper Canyon underground mine (Roberts and Arnold, 1965). Further evaluation of these data

by comparing computer-contoured distributions with untransformed metal concentrations in the drill holes reveals that the statistically defined anomalies found are not artifacts of the contouring procedures employed (Kotlyar and others, 1998).

A three-dimensional configuration of gold-metallized rock in the southern parts of the Lower and Upper Fortitude deposits also was constructed on the basis of Au contents in exploration drill holes by Battle Mountain Gold Co. (fig. 3). The three-dimensional 1-ppm Au outer halo that surrounds the Fortitude

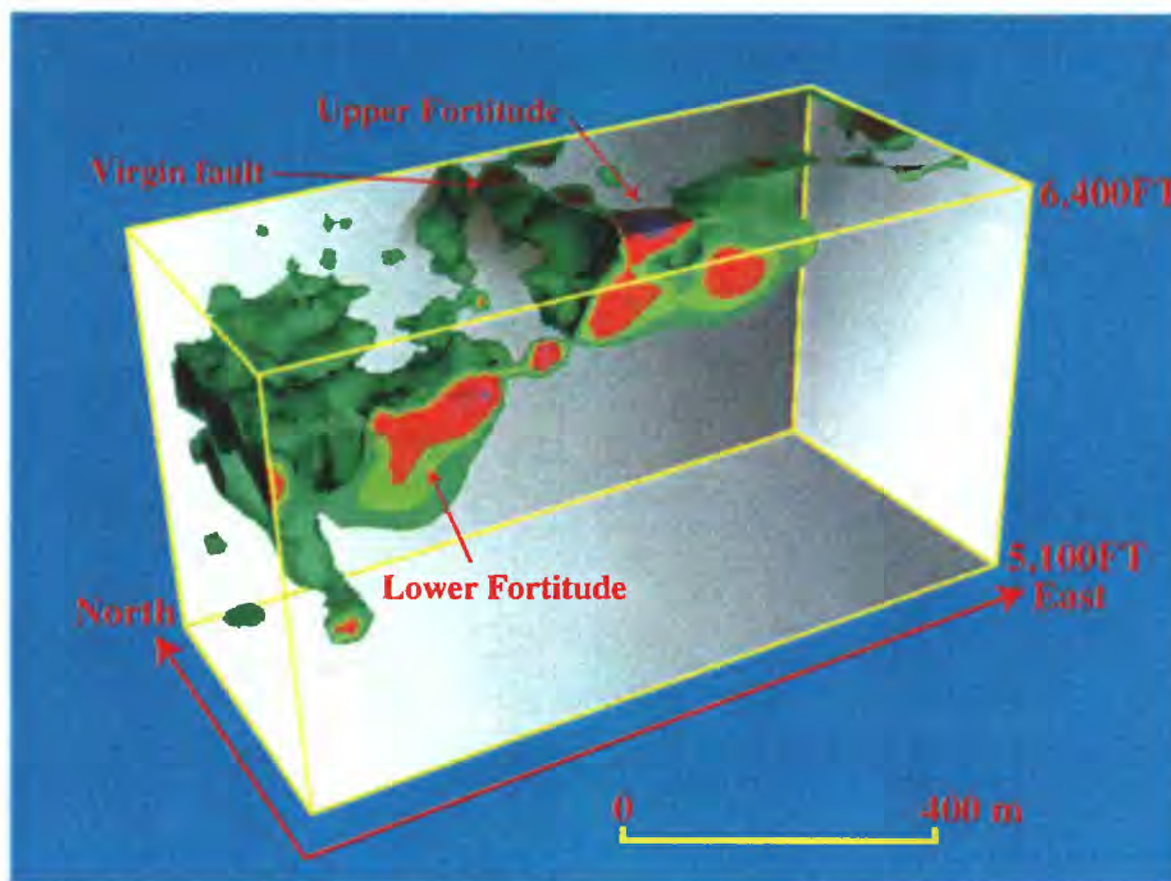


Figure 3. Block diagram showing three dimensional configuration of roughly southern one-third of Lower and Upper Fortitude Au-skarn orebodies and approximate trace of Virgin fault. Depicted outermost halo comprised of 1-ppm Au.

orebodies is much more complex than previously envisioned—compare with figure 2A—and the geometry of this halo primarily reflects distribution of chemically receptive rocks in the premineral calcareous Antler sequence below the Golconda thrust (fig. 2A). These rocks predominantly were broken and displaced by premineral normal movements along the Virgin fault and numerous other contemporaneous north-south striking faults in the Copper Canyon area (fig. 1). Cumulative displacements along these faults, including the significant Copper Canyon fault, are approximately 400 m, west blocks down.

CONCLUSIONS

Distribution of elevated contents of proximal (Cu, Au, Ag) and distal (Pb, Zn) metals around the Fortitude Au skarn reveals that a prominent Pb-Zn halo mantles the distal parts of the orebody, more or less duplicating, at large scale, the district-scale relations between proximal and distal metals previously recognized by Roberts and Arnold (1965) in production data from widespread polymetallic veins. The geochemical haloes that surround the Fortitude orebodies are complicated and multilevel, including mushroom- and pillar-shaped parts. In addition, topography impacted significantly these geometrically complex haloes as exemplified by apparent removal by erosion of part of a Pb locus concentrated near the northern end of the Fortitude orebodies. Further, mineralized rocks of the Antler sequence at the Nevada Mine (fig. 2) are

inferred to represent the northern leading edge of mineralized rocks that make up the Fortitude and Phoenix deposits in the Antler sequence farther to the south. The Pb-Zn ores at the 700-ft level in the Copper Canyon underground mine (deposit no. 11, fig. 2) and the reversal in district metal zoning at the Tomboy-Minnie deposits (Theodore and Blake, 1986) are inferred to be related to another site in the southern part of the Copper Canyon area where influx of mineralizing fluids occurred. This site appears to be somewhere near the Midas deposit (deposit no. 10, fig. 2). Both sites where influx of metals may have occurred, one beneath the Lower Fortitude deposits and the other beneath the Midas, may be related to apices of mineralized cupolas of altered granodiorite physically separate from the altered granodiorite of Copper Canyon which lies astride the major tectonic blocks (fig. 1; see also Kotlyar and others, 1998).

Primary dispersion haloes for Cu, Ag, Pb, and Zn in the Fortitude deposit are quite analogous to those reported at the Nikolaevskoye polymetallic skarn in the Former Soviet Union (Beus and Grigorian, 1977)—apparently Au is not present in the Nikolaevskoye polymetallic skarn, however. The Nikolaevskoye polymetallic skarn—a generally shallow-dipping orebody at approximately 700- to 1,000-m depths below the surface—contains sphalerite, galena, pyrite, and pyrrhotite in a hedenbergite skarn. Particularly analogous to the Fortitude deposits, Pb and Zn make up a well-developed halo quite distal to the Nikolaevskoye orebody by occurring as much as 850 m above it. Copper is confined tightly to the orebody, as is Ni and much of the Sn in the system. However,

the distributions of Ag and As at the Nikolaevskoye polymetallic skarn largely mimic the distribution of Pb, which differ somewhat from those that we found at the Fortitude. Nevertheless, the vertical extent of the multielement dispersion surrounding the Nikolaevskoye deposit is comparable to the Fortitude.

Finally, metal distributions in a porphyry environment must be considered relative to their configurations in three-dimensional space. Presence or absence of metals should be evaluated carefully by considering (1) non-orthogonal prograde fluid paths during metallization; and (2) the potential influence of prograde metal zonations—some quite subtle—from other nearby loci of mineralized rock. Filtering and gridding procedures turned out to be a wonderful tool, in our judgment, to enhance the syntheses of enormous amounts of geochemical data at Copper Canyon, and to model, thereby, concepts of fluid flow.

REFERENCES CITED

- Beus, A.A., and Grigorian, S.V., 1977, Geochemical exploration methods for mineral deposits: Wilmette, Illinois, Applied Publishing, Ltd., 287 p.
- Doebrich, J.L., Wotruba, P.R., Theodore, T.G., McGibbon, D.H., and Felder, R.P., 1996, Field trip guidebook for Trip H—Geology and ore deposits of the Battle Mountain Mining District, *in* Green, S.M., and Struhsacker, Eric, eds., Field Trip Guidebook Compendium: Reno, Nevada, Geological Society of Nevada, U.S. Geological Survey and Sociedad Geologica de Chile, Geology and Ore Deposits of the American Cordillera, p. 327–388.
- Kotlyar, B.B., Theodore, T.G., and Jachens, R.C., 1995, Re-examination of rock geochemistry in the Copper Canyon area, Lander County, Nevada: U.S. Geological Survey Open-File Report 95–816, 47 p.
- Kotlyar, B.B., Theodore, T.G., Singer, D.A., Moss, Ken, Campo, A.M., and Johnson, S.D., 1998, Geochemistry of the gold skarn environment at Copper Canyon, Battle Mountain Mining District, Nevada: Economic Geology (in press).
- Myers, G.L., 1994, Geology of the Copper Canyon-Fortitude skarn system, Battle Mountain, Nevada: Pullman, Washington, Washington State University, Ph.D. dissertation, 338 p.
- Peters, S.G., Nash, J.T., John, D.A., Spanski, G.T., King, H.D., Connors, K.A., Moring, B.C., Doebrich, J.L., McGuire, D.J., Albino, G.V., Dunn, V.C., Theodore, T.G., and Ludington, Steve, 1996, Metallic mineral resources in the U.S. Bureau of Land Management's Winnemucca District and Surprise Resource Area, northwest Nevada and northeast California: U.S. Geological Survey Open-File Report 96–712, 147 p.
- Roberts, R.J., and Arnold, D.C., 1965, Ore deposits of the Antler Peak quadrangle, Humboldt and Lander Counties, Nevada: U.S. Geological Survey Professional Paper 459–B, 94 p.
- Theodore, T.G., and Blake, D.W., 1975, Geology and geochemistry of the Copper Canyon porphyry copper deposit and surrounding area, Lander County, Nevada: U.S. Geological Survey Professional Paper 798–B, p. B1–B86.
- Theodore, T.G., Howe, S.S., Blake, D.W., and Wotruba, P.R., 1986, Geochemical and fluid zonation in the skarn environment at the Tomboy-Minnie gold deposits, Lander County, Nevada: Journal of Geochemical Exploration, v. 25, p. 99–128.
- Wotruba, P.R., Benson, R.G., and Schmidt, K.W., 1986, Battle Mountain describes the geology of its Fortitude gold-silver deposit at Copper Canyon: Mining Engineering, July 1986, v. 38, no. 7, p. 495–499.

NEW STUDIES OF TERTIARY VOLCANIC ROCKS AND MINERAL DEPOSITS, NORTHERN NEVADA RIFT

By Alan R. Wallace and David A. John

ABSTRACT

The northern Nevada rift is a long, narrow, north-northwest-trending alignment of middle Miocene volcanic and hypabyssal rocks and epithermal gold-silver and mercury deposits formed during west-southwest to east-northeast extension. New mapping is underway in three areas along the rift: the Ivanhoe district, the southern Sheep Creek Range, and the Mule Canyon area at the north end of the Shoshone Range. In the Ivanhoe district, Tertiary rocks range in age from late Eocene to middle Miocene, whereas Tertiary rocks in the other two areas are mostly Miocene in age. Compositions are varied in all three locations; a substantial part of the volcanic rocks in the Sheep Creek Range and northern Shoshone Range is dacitic, in contrast to the more basaltic composition that dominates most of the rift. At Ivanhoe, which is on the eastern margin of the rift, both northwest- and northeast-striking faults are common and are mutually crosscutting. Faulting there produced moderate to major amounts of Miocene tilting, with some evidence for 20° of pre-middle Miocene tilting. In the Sheep Creek Range and Mule Canyon area, the dominant faults strike north-northwest, consistent with the rest of the rift; east-northeast-striking faults are related to middle Miocene and younger northwest-directed extension. Oligocene rocks at Mule Canyon dip steeply to the east and northeast, whereas overlying Miocene volcanic rocks dip gently to the southeast. Ore deposits at Ivanhoe (mercury and gold) and Mule Canyon (gold) formed in syn-volcanic hot-spring environments during the middle Miocene, similar to other deposits along the rift. The gold deposits are low-sulfidation, quartz-adularia veins and disseminations in volcanic rocks.

INTRODUCTION

The northern Nevada rift was the site of middle Miocene igneous activity and related precious-metal mineralization. It extends approximately 500 km in a north-northwest direction from east-central Nevada to near the Nevada-Oregon border. The rift appears as a readily visible, fairly narrow positive anomaly on regional aeromagnetic maps that reflects the presence of abundant intrusive mafic rocks (Zoback and Thompson, 1978; Blakely and Jachens, 1991).

Although a general relationship between volcanism, faulting,

and mineralization along the rift has been known for some time, relatively little is known about the exact timing and interaction between these events. New mapping along the rift has focused on the southern Sheep Creek Range and northern Shoshone Range area, both near Battle Mountain, Nev., and the Ivanhoe mining district 60 km northeast of Battle Mountain (fig. 1). Mapping in the Sheep Creek/northern Shoshone Range area was initiated to study the volcano-tectonic framework of the newly developed Mule Canyon gold deposit. The Ivanhoe study has served to understand a similar framework for the Hollister gold and Ivanhoe mercury deposits and to expand previous studies of Miocene volcanic rocks and structures in the Snowstorm Mountains and Midas mining district 25 km to the northwest (Wallace, 1993). The intent of both projects is to improve the understanding of the rift and the mineral deposits that formed along it.

REGIONAL GEOLOGIC SETTING

The northern Nevada rift formed in the relatively narrow time span of 16 Ma to 14 Ma (Zoback and others, 1994). Mafic, mantle-derived magmas were emplaced along a deep-seated, north-northwest-trending fracture system that cut Paleozoic, middle Tertiary, and early Miocene formations. This crustal flaw either formed or was reactivated during a change in stress fields related to the northward migration of the Mendocino triple junction along the west coast of North America (Zoback, 1989). The magmas were intruded as closely spaced dike swarms and erupted as lava flows. Dikes and lava flows are abundant in the northern half of the rift, but they are less common to absent in the southern half. The rocks were mostly tholeiitic basalts and basaltic andesites with affinities to contemporaneous lava flows exposed in the Steens Mountains of southern Oregon and the Columbia River Plateau farther north. Locally derived pyroclastic rocks are interbedded with flows in the Snowstorm Mountains (Wallace, 1993), and dacite flows and intrusive rocks are common in the southern Sheep Creek and northern Shoshone Ranges (see below). Rift-related magmatism ceased at about 14 Ma (Zoback and others, 1994). Extensive felsic volcanic rocks related to the Yellowstone hot spot blanketed the rift-related rocks in the northern third of the rift.

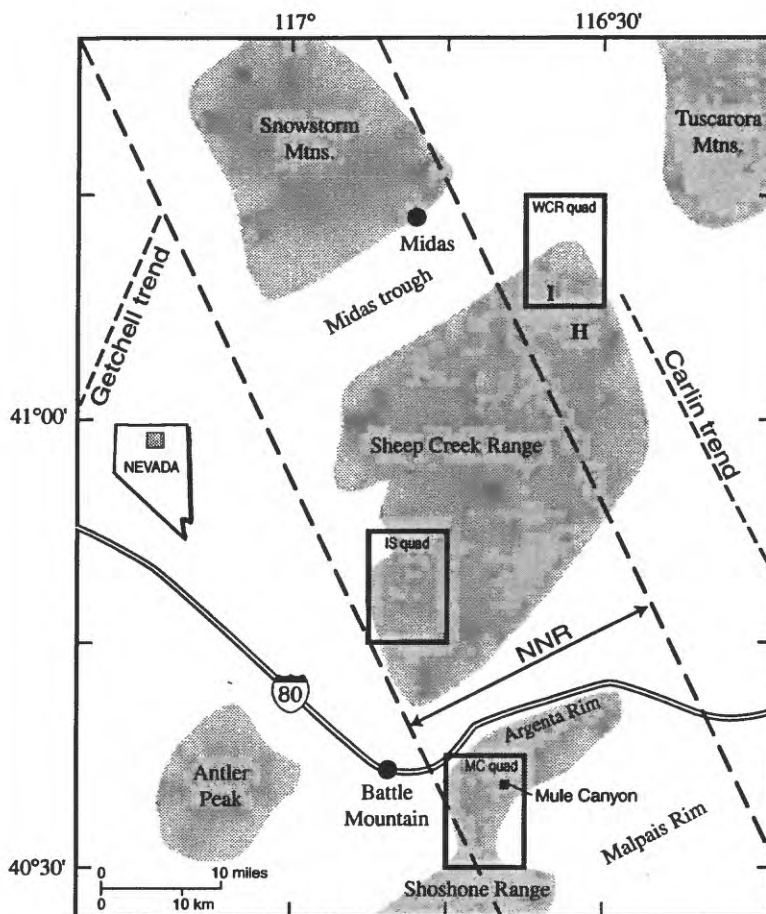


Figure 1. Index map showing geographic features mentioned in text, as well as the Willow Creek Reservoir (WCR), Izenhoo Spring (IS), and Mule Canyon (MC) 7-1/2-minute quadrangles. I, Ivanhoe district; H, Hollister mine; NNR, northern Nevada rift (approximate boundary).

Extension during rifting was in an east-northeast to west-southwest direction. Based on the orientations of rift-related dikes and faults in the younger volcanic sequence, this extension direction persisted until sometime after 10 Ma but before 6 Ma (Wallace, 1991; Zoback and Thompson, 1978; Zoback and others, 1994). At that point, a change in plate motions rotated the extension direction to a northwest-southeast orientation. Along the northern Nevada rift, this change disrupted the rift and formed a series of fault-bounded, east-northeast-oriented grabens. These grabens are spectacularly exposed along the Midas trough, at the north end of the Shoshone Range, and along the northern flank of the Cortez Range. This extension has continued into the

Quaternary, as indicated by faults in Quaternary alluvium on the west side of the Sheep Creek and Shoshone Ranges and especially along the mountain front of the Shoshone Range.

Mineral deposits related to the northern Nevada rift include Comstock-type gold-silver vein deposits, hot-spring gold deposits, and hot-spring mercury deposits. Isotopic dates on the gold deposits range from 15-15.5 Ma, indicating syn-volcanic mineralization. The mercury deposits, such as those at Ivanhoe, have not been dated but geologically appear to be the same age as or slightly younger than the gold deposits. Mined gold deposits include, from north to south, Buckskin-National, Midas, Hollister (Ivanhoe), Mule Canyon, Fire Creek, and Buckhorn; unmined altered and geochemically anomalous

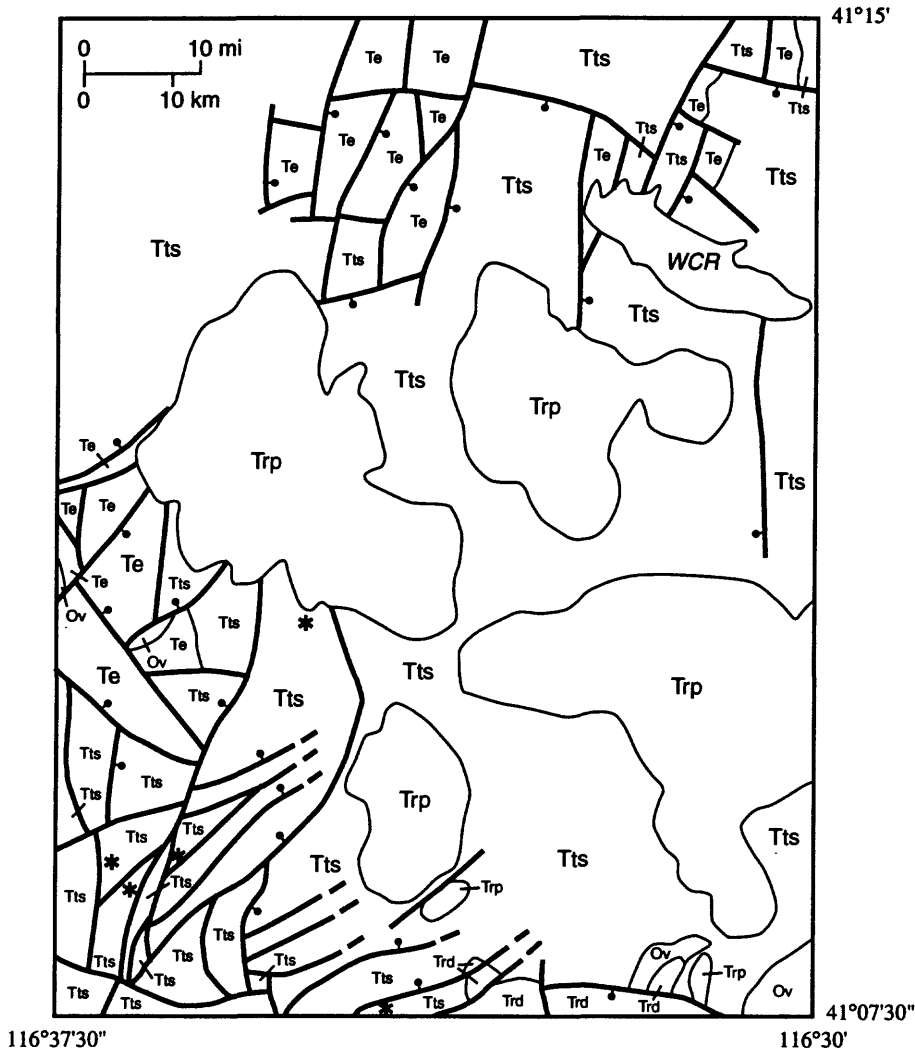


Figure 2. Generalized bedrock geologic map of the Willow Creek Reservoir quadrangle. Units (same labels as in figure 3, except as noted): Ov, Ordovician Valmy Formation; Te, Eocene volcanic rocks (Twt and Td of figure 3); Trd, Miocene rhyodacite; Trp, Miocene rhyolite porphyry; Tts, Miocene tuffs, tuffaceous sediments, andesite, and rhyolite (Ttsl, Ttsu, Tvt, Ta, and Trf of figure 3). WCR, Willow Creek Reservoir; *, mercury deposit. Heavy lines are faults, with ball and bar on downthrown side. The Hollister gold deposit is 1 km south of the center of the southern boundary of the quadrangle. Geology mapped by A.R. Wallace in 1996 and 1997.

volcanic rocks are common along the length of the rift.

IVANHOE DISTRICT

The Ivanhoe mining district is along the east margin of the northern Nevada rift and at the northwestern projection of the world-class Carlin gold trend. It is the site of the Hollister

open-pit gold mine and numerous small mercury deposits. Current work has focused on the Willow Creek Reservoir 7-1/2-minute quadrangle (fig. 2). Previous studies in the area include a short description of the general geology and mercury deposits (Bailey and Phoenix, 1944), a description of the geology of the Hollister mine area (Bartlett and others, 1991), and unpublished mapping, sampling, and drilling programs by several mining companies.

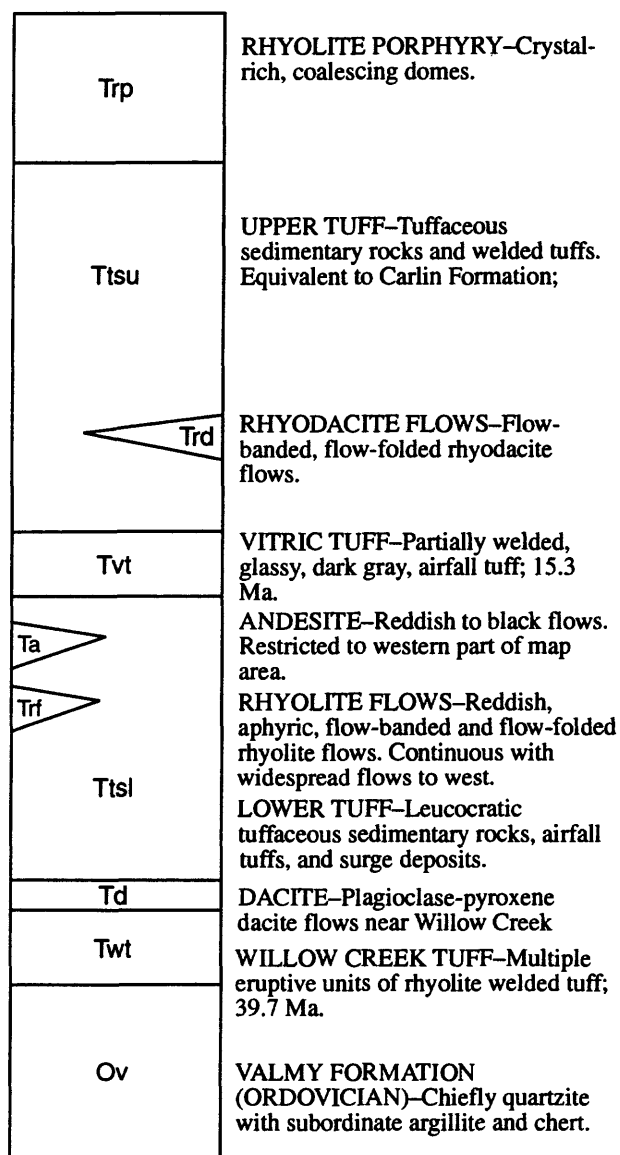


Figure 3. Stratigraphic section for Willow Creek Reservoir quadrangle. Reconnaissance mapping in rest of Ivanhoe district (A.R. Wallace, unpub. mapping, 1997) indicates the same sequence throughout the district. Thicknesses not to scale but show approximate relative thicknesses of units.

STRATIGRAPHY

Rock units in the Ivanhoe area include Paleozoic sedimentary rocks and Tertiary volcanic, sedimentary, and intrusive rocks. A generalized stratigraphic section is shown in figure 3. The Paleozoic rocks include quartzite, quartzite breccias, and phyllite of the Ordovician Valmy Formation. Exposures are limited, although exploration drilling shows that the Valmy Formation is present at variable depths throughout the district (Bartlett and others, 1991).

The oldest Tertiary unit in the area is the informally named

Willow Creek tuff. The tuff is composed of several crystal-rich cooling units, the uppermost of which is densely welded. Phenocrysts include sanidine, smoky quartz, plagioclase, and biotite. The rock is a rhyolite, based upon an average SiO₂ content of 73.8 weight percent. The age of the rhyolitic tuff is 39.7 ± 0.1 Ma (⁴⁰Ar/³⁹Ar date on sanidine) and, based upon age and petrographic similarities, it was erupted from the Big Cottonwood Creek caldera 35 km to the east-northeast in the Tuscarora Mountains (Henry and others, this volume). It crops out extensively in the northern part of the study area but is concealed in the main part of the Ivanhoe district and absent at the Hollister mine (Bartlett and others, 1991). In the northern part of the district, dacite to andesite flows (average SiO₂ is 60 weight percent), dated at 37.7 ± 0.1 Ma (⁴⁰Ar/³⁹Ar date on biotite), overlie the Willow Creek tuff. Approximately 4 km east of the Hollister mine, a weakly altered dacite porphyry of unknown but possibly Eocene age intrudes the Valmy Formation.

Airfall tuffs and waterlain tuffaceous sedimentary rocks overlie the welded tuff and dacite in the northern part of the district and the Valmy at the Hollister mine. A distinctive vitric welded tuff (trachydacite: 67 weight percent SiO₂, 6 weight percent K₂O) near the middle of the section is 15.29 ± 0.06 Ma (⁴⁰Ar/³⁹Ar date on sanidine). The tuffaceous sedimentary rocks beneath the vitric tuff (the "lower tuffs") are thickest to the north and locally are absent at the Hollister mine; the age of these strata is being studied. Tuffaceous sedimentary rocks and ash-flow tuffs above the vitric tuff (the "upper tuffs") are correlative with the lower units of the middle Miocene Carlin Formation, which yield ages of about 14.5-15.1 Ma in the Santa Renia Fields quadrangle immediately to the southeast (Fleck and others, this volume).

Two volcanic units interbedded with the lower tuff sequence are restricted to the western part of the district (fig. 3). The older of the two is an aphyric, flow-banded rhyolite (74 weight percent SiO₂) lava flow sequence that thickens to the west. The younger unit is a massive to vesicular andesite (55 weight percent SiO₂) several meters to tens of meters beneath the vitric tuff. The andesite pinches out to the east and is absent in the eastern half of the Willow Creek Reservoir quadrangle. The unit is petrographically similar to and equivalent in age to a widespread andesite unit in the western Snowstorm Mountains (Wallace, 1993).

Rhyodacite lava flows ("Craig rhyolite" of Bartlett and others, 1991) represent the dominant volcanic unit east and southeast of the Hollister mine. These flow units are massive to flow folded, and flow tops locally are extremely lithophysal. Although the contact is poorly exposed, the rhyodacite is thought to overlie the lowermost units of the upper tuff (fig. 3). Isotopic dating of this unit is in progress.

The youngest volcanic unit in the Ivanhoe area is a crystal-rich rhyolite (73 weight percent SiO₂). The rhyolite forms exogenous domes that, due to their relative resistance, dominate the landscape in the northern part of the area (figs. 2 and 3).

The domes are composed of constructive accumulations of flows that emanated from central vents, with adjacent domes coalescing into composite domes. The flows contain fluorite and topaz in the groundmass and vesicles, and elevated tin values are present in all analyzed samples. Although the Ivanhoe domes have not been dated (work is in progress), they are similar to domes in the Snowstorm Mountains and northern Sheep Creek Range that have ages of 14.0 to 14.6 Ma (Wallace, 1993; Zoback and Thompson, 1978). The anomalous tin concentrations are similar to those of domes near Izzenhood Ranch in the northern Sheep Creek Range, where wood and placer tin have been reported in and near rhyolite domes (Fries, 1942).

South from about the latitude of the Hollister mine (fig. 1), the Valmy Formation is overlain directly by rocks as young as the rhyolite porphyry domes. This relationship contrasts with those in areas to the north where a thick section of Eocene and younger rocks overlies the Paleozoic basement. Bartlett and others (1991) identified a "paleotopographic ridge" of Paleozoic rocks beneath Tertiary rocks at the Hollister mine area. There, the high is overlain by the upper part of the lower tuffs and in places by the andesite, with a substantial part of the lower tuffs and all of the Willow Creek tuff absent. To the southeast in the Santa Renia Fields area, Carlin Formation units equivalent to and younger than the upper tuffs overlie the Paleozoic basement (T.G. Theodore, oral commun., 1997). These relations indicate that, during much of the middle Tertiary, the area north of Hollister was a topographic low that progressively filled with tuffs and sediments as tuffs that had been deposited on surrounding highlands were eroded. Based upon the ages of the lowermost Carlin Formation, this basin did not fill and expand laterally until about 15 Ma.

Structure

The dominant structures in the Ivanhoe area are high-angle normal faults (fig. 2). The principal strike is northeast near Willow Creek Reservoir, where the faults both cut and are cut by west-northwest-striking faults. Both northeast- and northwest-striking faults are common in the western and southwestern parts of the district. The fault sets in these areas are mutually cross cutting, but the northeast-striking faults generally are younger than the northwest faults. At the Hollister mine, detailed studies indicate similar orientations and relative ages (Bartlett and others, 1991).

Faults in the Snowstorm Mountains have somewhat similar orientations. The older faults have a north-northwest orientation and were active from about 16 to 10 Ma (Wallace, 1993). Younger faults have an east-northeast trend and formed sometime after 10 Ma and before 6 Ma (Zoback and Thompson, 1978). The southern end of the Snowstorm Mountains is marked by the east-northeast-trending Midas trough, with vertical offsets along bounding faults of as much

as 1000 m. The master fault along the northern margin of the trough splays into at least four lesser faults just west of Midas and dies as a structural entity east of Midas. The southern structural margin of the trough extends to the extreme northwest margin of the Ivanhoe area. However, major high-angle, east-northeast-trending normal faults do not project eastward beyond that point. These relations suggest that offset along the master fault may have been taken up by the numerous northeast-trending faults in the Ivanhoe area, similar to the scenario at Midas.

Movement along the northeast-striking faults produced notable southeasterly dips in the volcanic rocks. Tilting is most pronounced in the northwest part of the district, where the Eocene Willow Creek tuff was tilted by as much as 53° to the southeast. Near Willow Creek reservoir (fig. 2), faulting repeated the volcanic section at least eight times. Going east, each fault block has a shallower dip than the block to the west, with dips decreasing eastward from 40° to 10°. The extensive faulting did not preserve a complete stratigraphic section, but limited evidence suggests that Eocene rocks dip approximately 20° more than the overlying tuffaceous sediments. If confirmed, as much as 20° of tilting took place prior to deposition of the tuffaceous sediments, and as much as 25° of tilting took place after deposition of the 15.3 Ma vitric tuff and overlying beds of the upper tuffs unit. Although fault blocks throughout much of the district have dips between 15° and 25°, the dips decrease district-wide from the steep dips in the north to horizontal in the middle Miocene Carlin Formation along Antelope Creek 20 km to the south.

A growing body of evidence indicates that gold deposits along the Carlin trend formed at about 42-38 Ma, about the same time that the Willow Creek tuff was emplaced (Emsbo et al., 1996). As exposed at Willow Creek Reservoir, the base of the tuff therefore marks the paleosurface at that time. That area has an elevation of 1650 m and the average elevation of the exposed Carlin deposits is about 1850 m, an elevation difference of only 200 m. The gold deposits along the Carlin trend formed at depths of 3 to 4.5 km (Lamb and Cline, 1997). This suggests the two areas have undergone several kilometers of post-Eocene differential offset, with the Carlin trend rising relative to the Willow Creek Reservoir area. Some, but likely not all, of the offset took place along the northeast-striking faults in the Ivanhoe area. Some of this displacement may have taken place in the Oligocene, accounting for the basin north of the Hollister mine.

Mineral deposits

The Ivanhoe district contains hot-spring mercury and hot-spring gold deposits (Bailey and Phoenix, 1944; Bartlett and others, 1991; Deng, 1991; Hollister and others, 1992). At the Hollister gold mine and nearby areas, gold deposits directly underlie mercury deposits. Company-confidential data from

several sources indicate anomalous gold near some mercury deposits elsewhere in the district.

Silicification related to the gold and mercury mineralization is widespread throughout the district and has several forms. Opal and chalcedony partially to completely replaced tuffaceous sediments in the upper and lower tuffs. The most favorable horizon was the tuffaceous sequence between the andesite flows and the vitric tuff. Tuffaceous beds in the upper tuffs locally were silicified as well, particularly at the Rimrock and Silver Cloud mines in the northern and southern parts of the district, respectively. The andesite and vitric tuff in places are altered near the silicified tuffs, although fresh vitric tuff locally overlies silicified tuffs. Broad areas of the rhyodacite flows east of the Hollister mine are pervasively silicified, and rhyolite porphyry domes near the Rimrock mine and east of the Hollister mine also are altered.

Siliceous sinter deposits are preserved at several mercury mines and prospects. Most of these are in the stratigraphic interval between the andesite and vitric tuff. However, like the replacement silica, some sinters formed during deposition of the upper tuffs. In places, distinguishing a sinter from a replacement body is difficult, and the two forms may represent a vertical continuum, as suggested by Bartlett and others (1991). Elongate vents and feeders at several mercury deposits suggest that hydrothermal fluids ascended faults which were subsequently reactivated and thereby exposing the deposits.

The mercury deposits in the silicified tuffs consist of cinnabar and metacinnabar in the opaline rocks. Other sulfides are not evident in surface workings, but drill cuttings contain pyrite. The deposits are relatively small and were mined intermittently between 1915 and 1973; 2,180 flasks of mercury were produced (LaPointe and others, 1991).

The Hollister gold deposit contains several orebodies that underlie mercury-bearing sinters and silicified zones. Ore horizons are in the lower tuffs directly beneath the andesite and locally in the upper tuffs where the andesite is absent (Bartlett and others, 1991). Some ore is present in the andesite and in the Valmy Formation. Grade distributions shown by Bartlett and others (1991) indicate northeast- and northwest-trending fault-related ore controls, and the andesite and replacement silica bodies served as hydrologic barriers to ascending gold-bearing fluids.

The gold and mercury deposits likely formed from the same hydrothermal system. Adularia from the Hollister deposit yielded a K-Ar age of 15.1 ± 0.4 Ma (Bartlett and others, 1991), consistent with the 15.3 Ma age of the altered vitric tuff. However, surface sinters beneath the vitric tuff and weak silicification in the younger rhyolite porphyry domes indicate that the mineralizing process may have spanned several hundred thousand to perhaps a million years. Similarly, gold mineralization in the Midas district took place at about 15.3 Ma (recalculated from McKee and others (1976) using modern decay standards), and sinter deposits several kilometers

northeast of the district formed in younger volcanic rocks.

SOUTHWESTERN SHEEP CREEK RANGE

New studies in the Sheep Creek and Shoshone Ranges have focused on the Izzenhood Spring 7-1/2 minute quadrangle in the southwestern part of the Sheep Creek Range, and on the Mule Canyon 7-1/2 minute quadrangle in the northernmost part of the Shoshone Range (fig. 1). These areas lie astride the northern Nevada rift. The Mule Canyon quadrangle contains the Mule Canyon mine, the largest known hot-spring gold deposit in the rift.

Stratigraphy

Rock units in the southwestern part of the Sheep Creek Range include Paleozoic sedimentary rocks and Miocene igneous rocks. These rocks are overlain by Quaternary surficial deposits that mantle much of the northeastern part of the Izzenhood Spring quadrangle (fig. 4).

Paleozoic sedimentary rocks

Lower Paleozoic sedimentary rocks crop out along the west flank of the Sheep Creek Range, which includes the southwest corner in the Izzenhood Spring quadrangle (fig. 4). They form more extensive outcrops in the adjacent Stony Point and Russells quadrangles. Paleozoic rocks consist of the Ordovician Valmy Formation and the Devonian Slaven Chert. The Valmy Formation consists of interbedded chert, quartzite, sandstone, siltstone, and argillite. The Slaven Chert consists of medium-gray to black chert, less abundant sandstone, argillite, and greenstone, and local beds of black barite. Both formations are complexly juxtaposed by thrust faults.

Miocene igneous rocks

Miocene igneous rocks unconformably overlie the Paleozoic rocks and cap most of the Sheep Creek Range. In the Izzenhood Spring quadrangle, a sequence of four major rock units has been identified: basalt-dacite unit, porphyritic dacite, porphyritic rhyolite, and olivine basalt.

Basalt-dacite unit

The oldest igneous rocks in the southwestern Sheep Creek Range consist of aphanitic to sparsely porphyritic basalt, basaltic andesite, andesite, and trachydacite lava flows that form cliffs along the west flank of the range and much of the uplands of the Izzenhood Spring quadrangle (fig. 4). These rocks consist of numerous thin lava flows that range in composition from basalt to trachydacite (about 47 to 66 weight percent SiO₂) (fig. 5). More than 20 flow units are present in

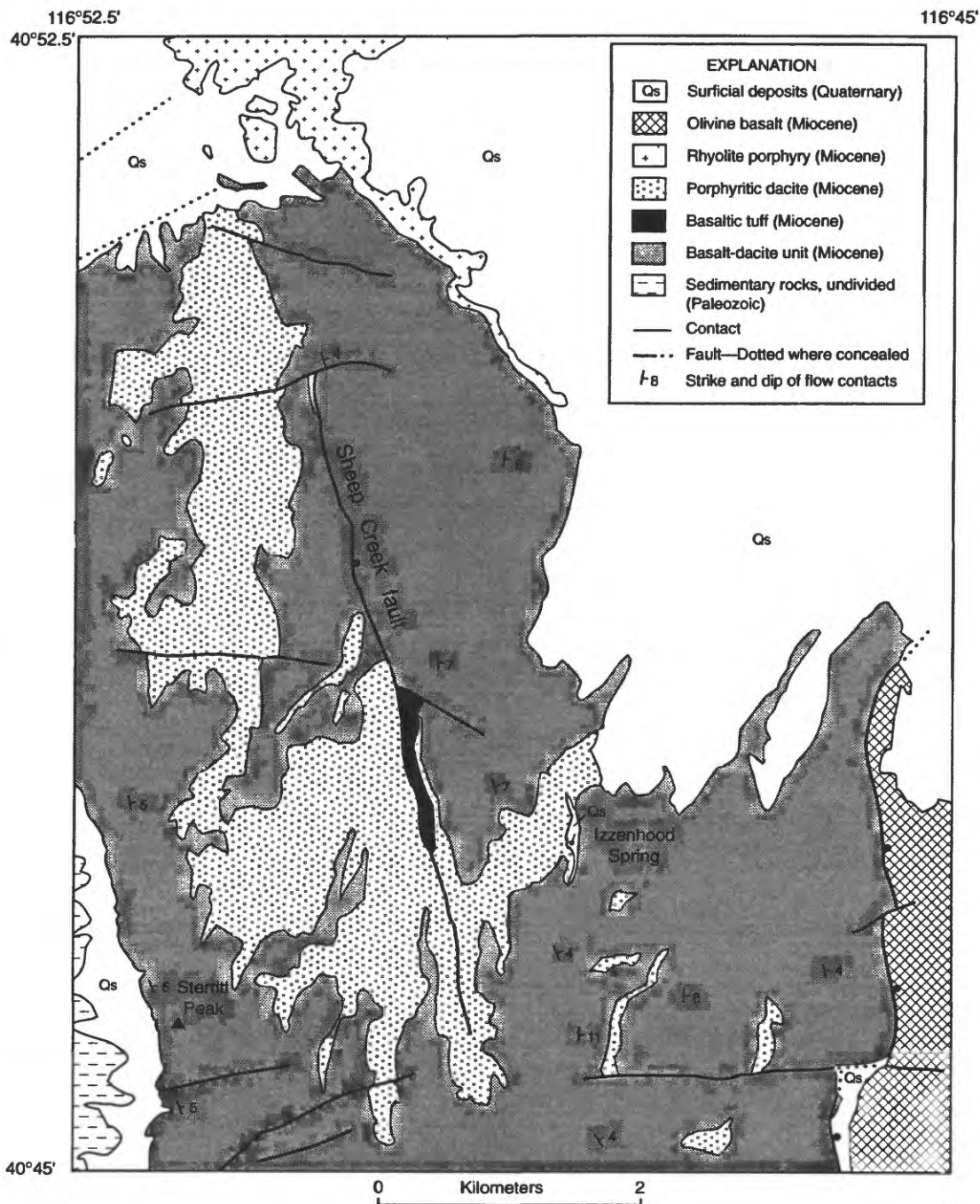


Figure 4. Generalized geologic map of the Izenhood Spring 7-1/2 minute quadrangle. Geology mapped by D.A. John and C.T. Wrucke in 1997.

the 150- to 200-meter-high cliffs exposed along the western edge of the range, and many other flows are present farther east. Individual flows are marked by glassy, highly vesicular flow bases and tops and devitrified, massive flow interiors. All rocks in this sequence are aphyric to sparsely porphyritic, containing <2 volume percent phenocrysts. Basalt and basaltic andesite flows contain fine- to medium-grained plagioclase

and (or) clinopyroxene phenocrysts in intergranular to intersertal groundmasses of plagioclase, clinopyroxene, and magnetite. Trachydacite lava flows commonly also contain sparse sieve-textured sanidine phenocrysts and have trachytic to pilotaxitic groundmasses. On the east side of the Sheep Creek fault, several areas of basaltic tuff as much as 120 m thick underlie porphyritic dacite lava flows and a dacite sill

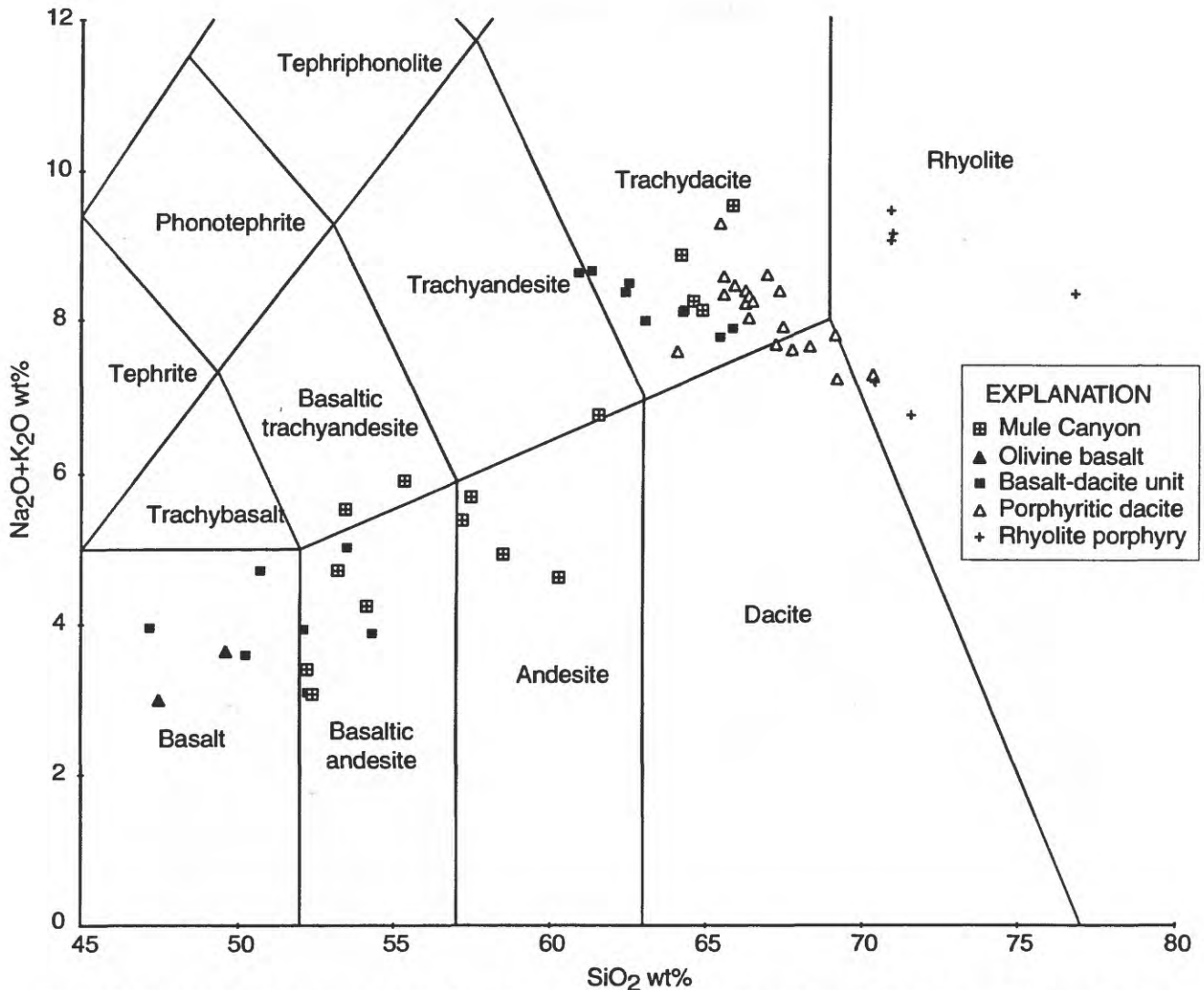


Figure 5. Total alkali-silica diagram for rocks in the Izzenhood Spring quadrangle and from the Mule Canyon mine area, northern Shoshone Range. Major-element oxides recalculated to 100 percent volatile-free. Rock names are IUGS classification (Le Bas and others, 1986).

(fig. 4). The tuffs are dark brown to brick red, finely bedded, poorly to densely welded, and nearly aphyric. They are very similar to pyroclastic units (lapilli ash tuffs) in the Mule Canyon mine that there host much of the gold mineralization (Thomson and others, 1993; Serenko, 1995).

Chemical and petrographic analyses indicate that there is no regular pattern of compositional variation with stratigraphic position in this sequence. However, the lowest flows in the sequence have basalt to basaltic andesite compositions, whereas most of the upper parts of the sequence have more silicic compositions. Basalts locally are present in the upper parts of the sequence. In addition, there is an apparent gap in compositions between about 54 to 61 weight percent SiO₂ in the Sheep Creek Range (fig. 5). Rock units in the Mule Canyon

area in the northern Shoshone Range have SiO₂ contents in this compositional gap (see below).

McKee and Silberman (1970) reported a whole-rock K-Ar age of 15.2 ± 0.5 Ma (recalculated using modern decay constants) on a lava flow collected along the crest of the Sheep Creek Range about 1 km south of the Izzenhood Spring quadrangle. Additional K-Ar and ⁴⁰Ar/³⁹Ar dating of this and other Tertiary units in the southwestern Sheep Creek Range is underway.

Porphyritic dacite unit

Much of the central part of the Izzenhood Spring quadrangle is underlain by bodies of porphyritic dacite (fig. 4). Most of these rocks form the uppermost parts of a large

dacite stock that is inferred to underlie much of the southwestern part of the Sheep Creek Range. Thick sequences of lava flows of similar composition and appearance are present in the northern Shoshone Range, principally in the Mule Canyon quadrangle, along the Argenta Rim, and on much of the upper slopes of the Malpais Rim farther to the south (fig. 1; Struhsacker, 1980; Thomson and others, 1993).

The texture of the porphyritic dacite varies significantly. Margins of the intrusions are black vitrophyres. Locally, the upper few meters of the vitrophyre is strongly vesiculated, forming a scoriaceous-like rock. The vitrophyre grades downward and inward into irregular zones of spherulitic devitrification characterized by abundant reddish-brown spherulites that are 0.5 to 6 cm in diameter. The spherulitic zones grade downward and inward to massive, dark-red to lavender-gray, devitrified dacite that is subhorizontally layered, giving the rock the appearance of lava flows. The dacite generally contains 5 to 20 percent phenocrysts consisting of plagioclase, clinopyroxene, magnetite, and minor olivine. The phenocrysts range in size from 0.1 to 4 mm but are mostly <1 mm. The phenocrysts commonly occur in small glomeroporphyritic clots.

Chemical analyses of the porphyritic dacite indicate a relatively restricted range of composition between about 64 to 69 weight percent SiO₂, making the rocks trachydacites and dacites, according to the IUGS chemical classification (fig. 5). These rocks have notably high K₂O contents (fig. 6) that are comparable to compositions reported by Struhsacker (1980) for similar lava flows in the Malpais Rim area about 30 km to the southeast. No radiometric ages are available at present for the porphyritic dacite unit in the Sheep Creek Range, but Struhsacker (1980) reported a K-Ar age of 16.1±0.6 Ma for a lava flow in the Malpais Rim area.

Rhyolite porphyry unit

Coarse-grained rhyolite porphyry domes and related lava flows crop out in the northwest corner of the Izzenhood Spring quadrangle (fig. 4). These rocks are the southernmost part of a large rhyolite dome field that forms much of the area between the Sheep Creek Range and the Midas trough about 35 km to the northwest (fig. 1; Stewart and Carlson, 1978; Stewart and McKee, 1977; Wallace, 1993).

In the Izzenhood Spring quadrangle, rhyolite porphyry is both intrusive and extrusive; the northern half of the porphyry is in domes that intrude the basalt-dacite unit, whereas the southern half of these exposures are lava flows that overlie the basalt-dacite unit. The intrusive rocks are devitrified, commonly strongly flow banded, and spectacularly jointed, as described by Stewart and McKee (1977, p. 46-47). Extrusive parts of the unit are chilled against the underlying basalt-dacite unit forming black vitrophyre that grades upward into red to pinkish-gray, devitrified, subhorizontally flow-banded rock.

The rhyolite porphyry contains about 15 to 30 percent seriate phenocrysts of sanidine, quartz, plagioclase, and fayalitic(?) olivine in glassy to microcrystalline groundmasses. Feldspar and rounded quartz phenocrysts are as much as 8 mm across. McKee and Silberman (1970) reported sanidine K-Ar ages of 14.2 and 14.3 Ma (recalculated) for rhyolite porphyry flow domes about 7 km north of the Izzenhood Spring quadrangle.

Olivine basalt unit

The southeastern part of the Izzenhood Spring quadrangle is underlain by dark-gray to black olivine basalt lava flows that are downfaulted against the basalt-dacite unit (fig. 4). The basalt flows make up most of the large tableland of the Sheep Creek Range to the northeast (Stewart and McKee, 1977). They contain scattered, small (<2 mm) olivine phenocrysts in a fine-grained, subophitic groundmass of plagioclase, clinopyroxene, and magnetite. They also contain abundant, very fine-grained vesicles, producing a spongy texture. No radiometric ages are available for this unit in the Izzenhood Spring quadrangle, but McKee and Silberman (1970) reported a whole-rock K-Ar age of 10.3 Ma (recalculated using modern decay constants) for a possibly correlative olivine basalt lava flow farther northeast in the Sheep Creek Range.

Surficial deposits

Late Quaternary surficial deposits cover most of the northeastern quarter of the Izzenhood Spring quadrangle and are extensively exposed on the west side of the quadrangle (fig. 4). The most extensive units are thin(?) deposits of caliche and eolian silt and sand that cover a pediment surface in the northeast quarter of the quadrangle. Prominent sand dunes and other alluvial deposits are present in the northwest corner of the quadrangle, and extensive talus deposits are present along the west edge of the quadrangle, where they cover the contact between Paleozoic sedimentary rocks and the basalt-dacite unit.

Late Cenozoic structure

The Sheep Creek Range is a gently east-tilted horst formed by late Cenozoic Basin and Range faulting. The range is bounded on the west by a north-northwest-striking fault with late Quaternary displacement (Dohrenwend and Moring, 1991) that parallels the northern Nevada rift and results in nearly 1 km of topographic relief between the crest of the range and the Humboldt River valley to the west (fig. 1). Total offset on this fault estimated using gravity data is 2 to 2.5 km (D.A. Ponce, oral commun., 1997). This range-bounding fault may be a reactivated middle Miocene fault that was active during formation of the northern Nevada rift. The Sheep Creek Range has undergone relatively little post-middle Miocene tilting.

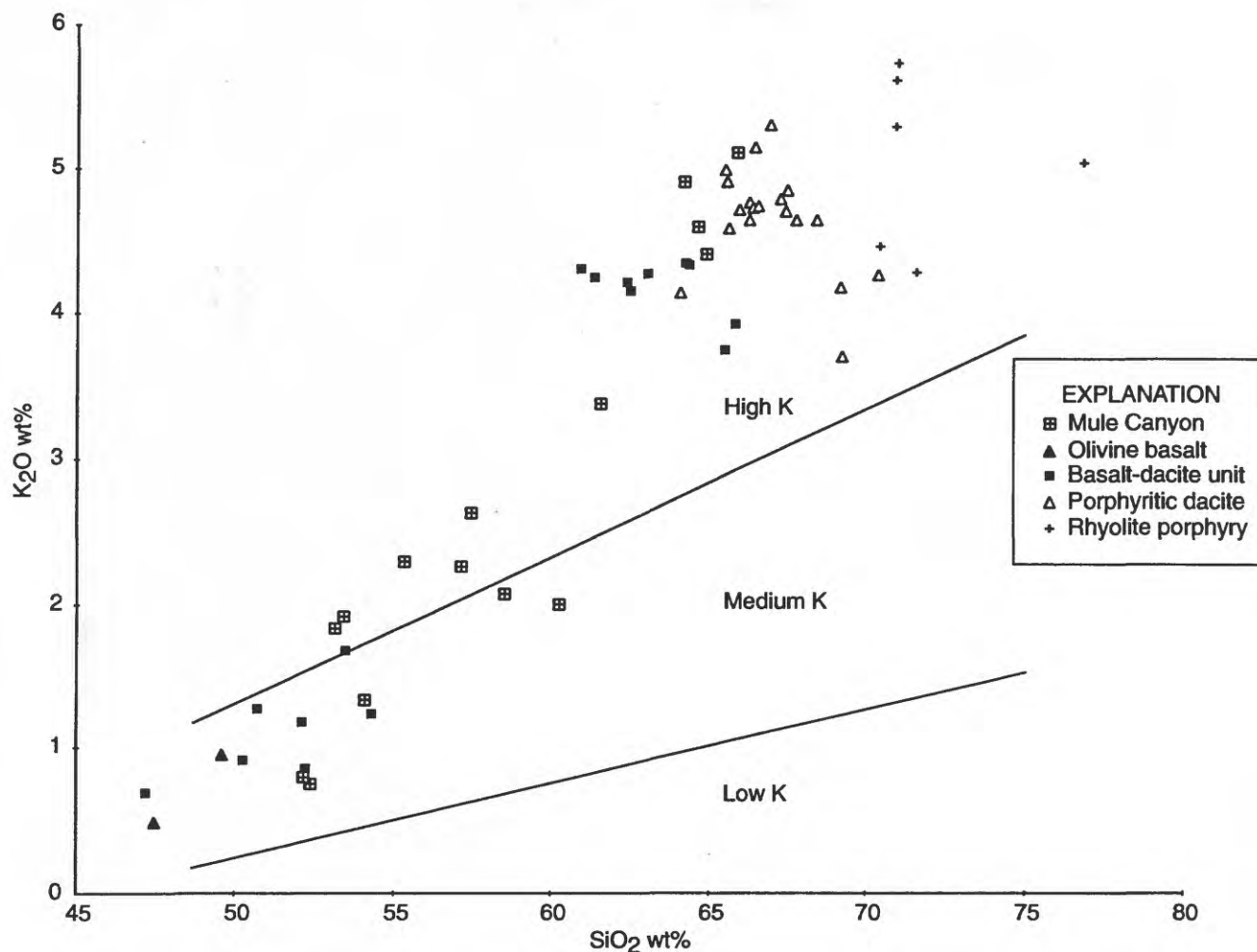


Figure 6. K₂O-silica diagram for rocks in the Izzehood Spring quadrangle and from the Mule Canyon mine area, northern Shoshone Range. Major-element oxides recalculated to 100 percent volatile-free. High-, medium-, and low-potassium fields from LeMaitre and others (1989).

Average dips on lava flows in the basalt-dacite unit are about 5° east, with strikes ranging from about N30°W to N-S (fig. 4). The structure of the Izzehood Spring quadrangle is dominated by high-angle normal faults. Relatively few faults have been mapped in the Miocene igneous rocks in the quadrangle, probably due in part to the lack of marker units. Two orientations of high-angle faults are evident: north- to north-northwest and east-northeast to east-southeast (fig. 4). The east-northeast-striking faults generally appear to cut the north-northwest-striking faults and are subparallel to young faults at the southern end of the Sheep Creek Range and the Argenta and Malpais Rims to the south (fig. 1; Stewart and McKee, 1977; Dohrenwend and Moring, 1991). The north-northwest-striking faults parallel the northern Nevada rift and probably influenced emplacement of the large porphyritic dacite stock that is elongated in this direction (fig. 4).

The most prominent fault in the Izzehood Spring

quadrangle is the N20°W-striking Sheep Creek fault in the upper parts of Sheep Creek (fig. 4). The fault dips about 70° east and is traceable along strike for 7 km. It is truncated on the north by an east-northeast-striking fault and appears to die out to the south (fig. 4). For much of its length, the fault juxtaposes the porphyritic dacite unit on the west with the basalt-dacite unit on the east. A prominent north-striking fault in the southeast corner of the quadrangle drops the olivine basalt unit against the basalt-dacite unit (fig. 4). This fault is offset in several places by east- to east-northeast-striking faults.

Zoback and others (1994) have shown that the east-northeast-striking faults reflect a change in the regional stress regime that began at about 10 Ma. North-northwest-striking faults characteristic of the northern Nevada rift formed during a period of extension when the least principal stress direction was oriented approximately N65-70°E. Between about 10 to 6 Ma, the least principal stress direction rotated approximately

40° clockwise, and the northeast- to east-northeast faults bounding the southern end of the Sheep Creek Range and the northeast end of the Shoshone Range (Argenta Rim) formed in this modern, approximately N70°W extension direction. The east-northeast-striking faults, such as those forming the Argenta Rim, are dominantly left-lateral oblique-slip faults that laterally displace the northern Nevada rift as much as 3.5 km along the Argenta Rim (Zoback and others, 1994).

Mineral Deposits

No mineral deposits or areas of hydrothermal alteration are present in the Tertiary rocks in the Izzenhood Spring quadrangle. Numerous prospect pits, several open-pit mines, and an underground mine are present in the Paleozoic rocks along the southwestern flank of the Sheep Creek Range, primarily in the Russells and Stony Point quadrangles. Most of the prospects and open pits were dug for bedded barite deposits in the Devonian Slaven Chert. However, little, if any, barite was produced from these workings. The underground workings are at the Snowstorm Mine in the Stony Point quadrangle. This mine produced silver-lead-gold ore at various times beginning in 1910.

NORTHERN SHOSHONE RANGE

Studies in the northern Shoshone Range, including collaborative work with Newmont Gold Company in the Mule Canyon mine area, are just beginning. Consequently, the following discussion is limited to new observations and preliminary interpretations. Studies in the northern Shoshone Range are focused on the Mule Canyon 7-1/2 minute quadrangle and include geologic mapping of the quadrangle based on mapping provided by Newmont Gold Co. for their claim block in and around the Mule Canyon mine and new mapping by C.T. Wrucke and D.A. John, petrographic, geochemical, and radiometric dating studies of Tertiary igneous rocks, and petrographic and SEM studies of hydrothermal alteration and gold mineralization in the Mule Canyon mine.

Tertiary Stratigraphy

Tertiary stratigraphy in the Mule Canyon quadrangle is more complex than it is in the southern Sheep Creek Range and includes early Oligocene to early Miocene volcanic and sedimentary rocks, in addition to middle Miocene igneous rocks related to the northern Nevada rift (Stewart and McKee, 1977; Struhsacker, 1980; Thomson and others, 1993). The oldest unit is the approximately 34-Ma Caetano Tuff, a regionally widespread, but only locally exposed, rhyolite ash-

flow tuff that unconformably overlies Lower Paleozoic sedimentary rocks in the western part of the quadrangle. The Caetano Tuff is overlain by a poorly exposed sequence of Oligocene or early Miocene sedimentary rocks, including debris flows, conglomerate, sandstone, siltstone, and minor fresh-water limestone. The sedimentary rocks are overlain by thick sequences of middle Miocene igneous rocks related to the northern Nevada rift, which were deposited mostly into narrow, north-northwest-elongated grabens that were developing during volcanism. From oldest to youngest, these units include the Mule Canyon mine sequence, a series of mafic to intermediate composition lava flows and pyroclastic rocks that host most of the gold mineralization in the Mule Canyon deposit; basaltic andesite lava flows ("shear-banded normal flows"); porphyritic dacite lava flows; aphyric dacite lava flows ("roddy-platy dacite"); and capping basalt lava flows. In contrast to most of the lava flows in the southwestern Sheep Creek Range, the Mule Canyon sequence was erupted from nearby sources, including small cinder and spatter cones and other vents. Numerous north-northwest-trending dikes intrude the older rocks and probably were feeders for the lava flows. Some of these dikes intrude faults that controlled hydrothermal alteration and gold mineralization in the Mule Canyon mine, and the dikes are thought to be closely related to gold mineralization (Thomson and others, 1993; Eric Saderholm, oral commun., 1997).

Most of the Tertiary rocks in the Mule Canyon mine area are poorly dated, and new K-Ar and ⁴⁰Ar/³⁹Ar dating of these rocks and of hydrothermal alteration is in progress. Available K-Ar ages suggest that the upper part of the Mule Canyon mine sequence and the overlying basaltic andesite and dacite lava flows are about 16 to 17 Ma and that the capping basalt lava flows are about 10.6 Ma (see Thomson and others, 1993). However, no samples collected in the Mule Canyon quadrangle have been dated.

Preliminary chemical analyses suggest a fairly wide range of rock compositions in the Mule Canyon mine area between about 52 to 66 weight percent SiO₂, indicating that these rocks are similar to rocks in Sheep Creek Range (figs. 5 and 6). Interestingly, no rocks analyzed to date have basaltic compositions using the IUGS classification (Le Bas and others, 1986). Rocks thought to be most closely associated with gold mineralization here (mafic dikes) have basaltic andesite compositions.

Cenozoic structural history

Late Cenozoic structure in the Mule Canyon quadrangle is dominated by north-northwest- and east-northeast-striking high-angle faults that border two narrow north-northwest elongated grabens. These faults and grabens and rocks that fill the grabens are surface expressions of the northern Nevada rift (Struhsacker, 1980; Thomson and others, 1993; Serenko,

1995). In addition, the steep dips of the early Oligocene Caetano Tuff suggest that there were two periods of tilting that probably were related to several episodes of extensional faulting during development of the rift.

In the Mule Canyon area, the northern Nevada rift is about 13 to 16 km wide and is bounded by N15-30°W-striking high-angle normal faults, the West fault on the west and the Dunphy Pass fault on the east (Struhsacker, 1980; Thomson and others, 1993). A third, subparallel fault in the Mule Canyon mine area divides the western part of the rift into two grabens. These faults were active during formation of the rift, and volcanic rocks erupted during rift formation were deposited into grabens bounded by these faults. The Mule Canyon mine sequence is mostly limited to the western graben, which is about 2 to 3 km wide, whereas the eastern part of the rift is primarily filled by the overlying dacite and capping basalt units.

Northeast- to east-northeast-striking-faults generally crosscut the north-northwest-faults. Some of these faults, such as the faults that form the Malpais and Argenta Rims and are present in Whirlwind Valley, have late Quaternary displacement (Wallace, 1979; Struhsacker, 1980; Dohrenwend and Moring, 1991; Zoback and others, 1994). Other, older northeast-striking faults were active during gold mineralization at Mule Canyon, and high-grade gold ore was deposited at the intersection of some of these faults with the north-northwest-striking faults.

In the Mule Canyon quadrangle, there is a pronounced angular unconformity between the Caetano Tuff and the overlying Mule Canyon mine sequence. Isolated outcrops of the Caetano Tuff on the west side of the quadrangle strike N10-30°W and dip 35-75°NE. At least part of the overlying Oligocene to early Miocene sedimentary rock sequence also has steep northeast dips. In contrast, the Mule Canyon mine sequence and overlying rocks have shallow (10-20°) southeast dips, probably resulting from late Miocene and younger, northeast-striking faults at the Malpais and Argenta Rims (Struhsacker, 1980). The regional extent and exact age of the earlier tilting event are unknown. Oligocene rocks are absent in the southwestern Sheep Creek Range, and the Caetano Tuff only has gentle dips (<30°) on the east side of Battle Mountain Range 25 km to the west.

Mule Canyon deposit

Reconnaissance work to date includes petrographic and geochemical studies of igneous host rocks in the Mule Canyon mine area and petrographic and SEM studies of samples from two high-grade (>1 oz/ton Au) ore zones. Preliminary observations of these ore zones are summarized below and generally are similar to relations reported by Thomson and others (1993) and Serenko (1995). These observations suggest that there may have been multiple pulses of gold deposition and multiple generations of arsenic minerals.

Ore in the North Zone is hosted by mafic "normal" lava flows near the top of the Mule Canyon mine sequence and by

mafic dikes. High-grade ore (as much as 30 oz/ton Au) is confined to narrow breccia zones near the margins of the dikes. Breccia fragments are pervasively altered to fine-grained adularia + quartz + pyrite and(or) marcasite ± minor arsenopyrite. Marcasite in breccia fragments is locally rimmed by arsenopyrite and silver selenides. At least three stages of brecciation are evident. Early breccia matrix is fine-grained pyrite cut by quartz + electrum ± pyrite. Late breccia matrix is quartz + minor pyrite. Much of the high-grade ore is oxidized, and visible and microscopic electrum has only been found in oxidized rocks in close association with Fe-oxides or jarosite. Electrum forms irregular crystals as much as 0.25 mm long (fig. 7A). Electrum composition ranges from about 70 to 80 weight percent gold and varies within single crystals. Minor argentite is present in gold-bearing breccia matrix.

High-grade ore in the Main pit (as much as 40 oz/ton Au) is in narrow zones at the intersection of N10-30°W-trending, steeply dipping dikes and faults and N30°E-striking faults. High-grade ore is primarily present in the margins of mafic dikes where they intrude mafic "flow tongue" units and lapilli ash tuffs in the upper part of the Mule Canyon mine sequence. The ore is unoxidized and locally contains as much as 20 weight percent sulfur (Eric Saderholm, oral commun., 1997). High-grade ore samples contain multiple generations of narrow (mm- to a few cm-wide) veins that cut intensely altered wallrock. Wallrocks in ore samples are pervasively replaced by adularia ± sericite + pyrite/marcasite or arsenopyrite (fig. 7B). Adularia is locally altered to sericite, making the rock highly friable. Adularia alteration is surrounded by broad zones of argillic and propylitic alteration (Thomson and others, 1993; Serenko, 1995) that contain much lower gold contents. At least 4 generations of veins are evident in high-grade ore samples. From oldest to youngest, they are: (1) narrow pyrite or marcasite ± quartz, (2) quartz + adularia + pyrite or marcasite, (3) vuggy quartz + pyrite locally containing arsenopyrite or arsenian pyrite inclusions ± minor adularia (figs. 7C to 7E), and (4) thicker (cm) quartz + coarse-grained pyrite or marcasite locally containing argentite inclusions. Arsenian pyrite locally rims marcasite in type 2 veins (fig. 7F). Sphalerite inclusions locally are present in marcasite (fig. 7F). Chalcopyrite and tetrahedrite locally are present in type 4(?) veins. No gold has been detected in these samples using petrographic and SEM techniques. Serenko (1995) also was unable to detect gold using these techniques in similar types of samples, but on the basis of laser-ablation ICP analyses, he suggested that gold is contained in arsenopyrite.

DISCUSSION

The current studies demonstrate several new facts about the volcanic rocks, structures, and deposits along the northern Nevada rift. These include: (1) rift-related magmas were not simply mafic in composition, but rather consisted also of intermediate-composition and locally felsic magmas; (2) pre-

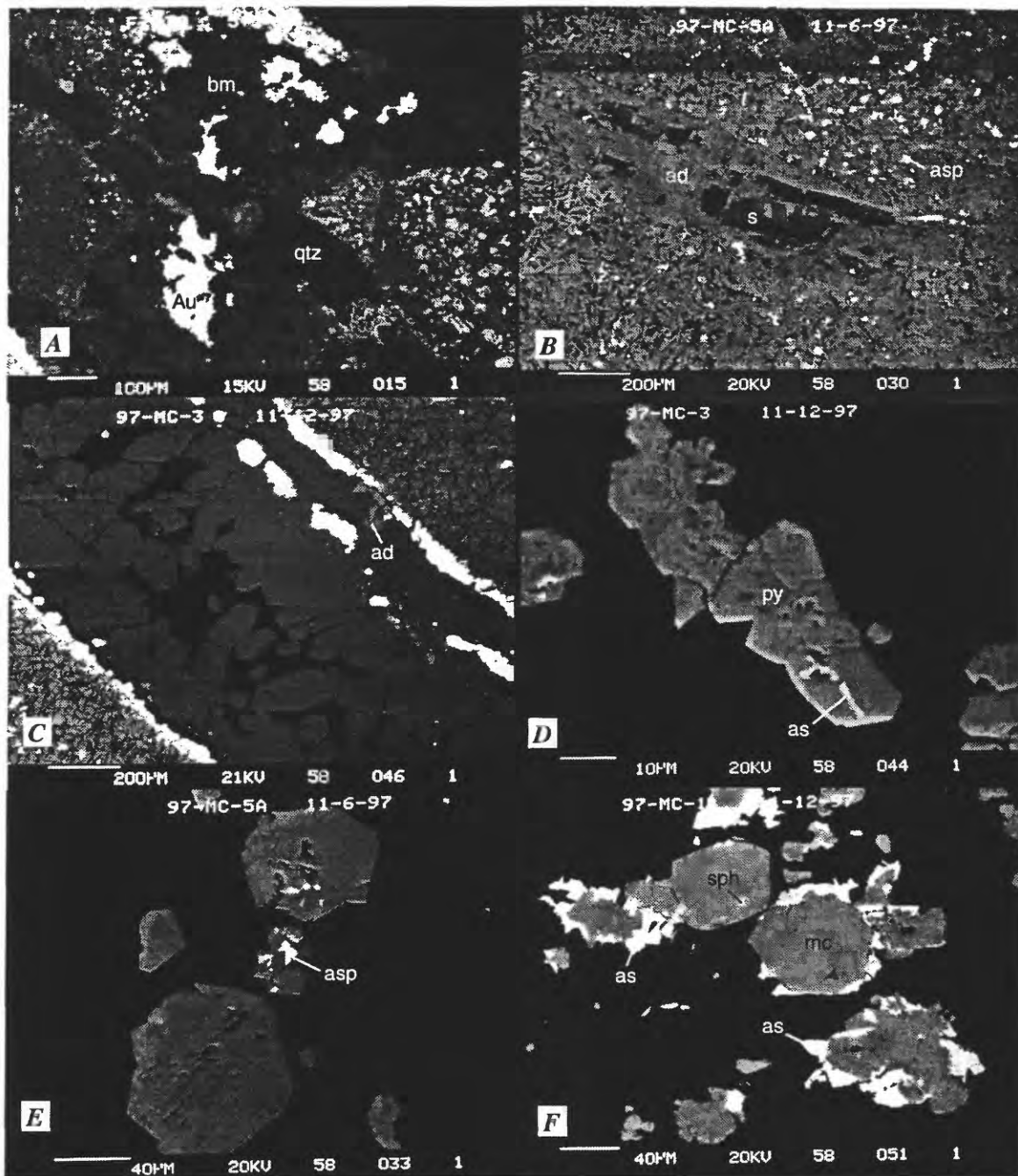


Figure 7. Back-scattered, scanning electron microscope images of ore textures from the Mule Canyon deposits. (A) Coarse electrum (Au) in quartz-adularia breccia matrix (bm) crosscut by barren quartz veinlet (qtz). Breccia fragments altered to adularia (ad) + quartz. Surface outcrop from North zone. (B) Adularized mafic dike from Main pit. Fine laths of adularia replace the groundmass and coarser adularia (ad) replaces a plagioclase phenocryst. Dark areas of the phenocryst are sericite (s). Disseminated, fine-grained arsenopyrite (asp) in groundmass. (C) Vuggy quartz + adularia + pyrite vein from high-grade ore in Main pit. Symmetric vein containing an outer band of pyrite + adularia (ad), an inner zone of pyrite + adularia, and terminated quartz that fills the center of the vein. Wallrock is pervasively altered to adularia + sericite (dark laths). (D) Enlargement of (C) showing white zones of arsenian pyrite (as) in pyrite (py) along outer edge of vuggy quartz-adularia-pyrite vein. (E) Marcasite (mc) crystals containing inclusions of arsenopyrite (asp). Quartz-marcasite vein from Main pit. (F) Arsenic-rich (as) rims on marcasite crystals in quartz vein from Main pit. Sphalerite inclusions (sph) are also present in marcasite crystals.

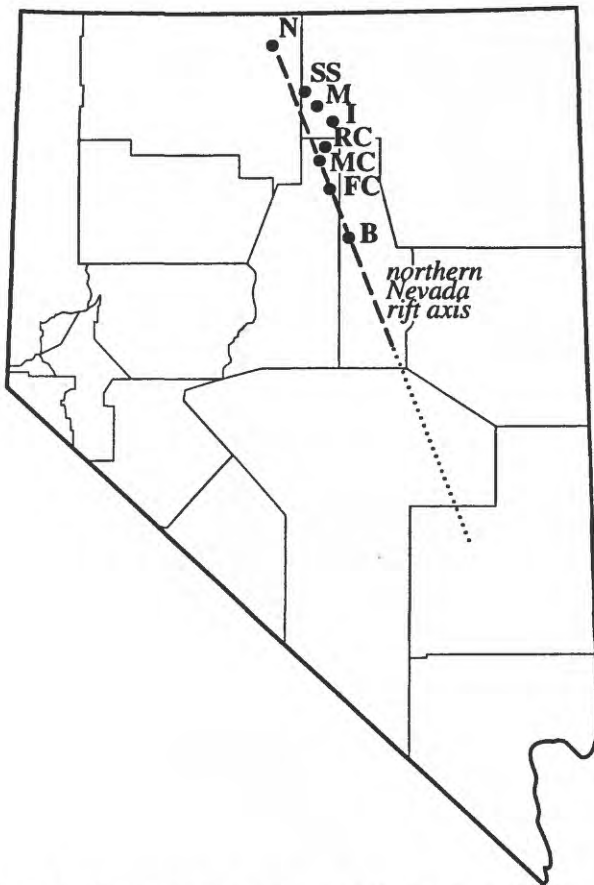


Figure 8. Distribution of epithermal and hot-spring gold, silver, and mercury deposits and occurrences associated with the northern Nevada rift. Dashed line is axis of aeromagnetic anomaly associated with rift; dotted extension is continuation of anomaly with no surface expression of rift (Blakely and Jachens, 1991). N, National/Buckskin; SS, Snowstorm Mountain; M, Midas; I, Ivanhoe, RC, Rock Creek; MC, Mule Canyon; FC, Fire Creek; B, Buckhorn.

rift extension and block tilting took place between the early Oligocene and middle Miocene, producing a paleotopography marked by numerous highlands and basins; (3) rifting produced an elongate, fault-controlled basin in which rift-related volcanic rocks accumulated; and (4) high-grade, near-surface epithermal gold deposits, locally associated with hot-spring mercury deposits, formed along rift-related faults during volcanic activity.

Previous discussions of magmas related to the rift describe them as predominantly basaltic in composition, with minor rhyolite and dacite (Zoback and Thompson, 1978; Zoback and others, 1994), and basalts indeed are common along the rift. However, as shown herein, substantial amounts of intermediate-composition igneous rocks were also emplaced during rifting. This especially is true in the Mule Canyon and southern Sheep Creek Range areas, where dacites are common, and in the Ivanhoe area, where a unit described previously as

a basalt (Bartlett and others, 1991) has an andesitic composition. Additionally, felsic pyroclastic and intrusive rocks are interbedded with rift-related basalt flows in the Snowstorm Mountains (Wallace, 1993), and early-rift rhyolite flows are present at Ivanhoe. As a result, the rift does not fit into a strict bimodal petrogenetic model, but instead includes a wide range of magma types.

Based on evidence at Mule Canyon and Ivanhoe, faulting and block tilting took place sometime between the early Oligocene and middle Miocene. At Mule Canyon, shallow-dipping Miocene basalt flows overlie steeply dipping Oligocene tuffs. At Ivanhoe, tilting of as much as 20° took place after the late Eocene and before the eruption of middle Miocene volcanic rocks. Faulting related to this event likely produced an irregular middle Tertiary paleotopography, with highlands in the Sheep Creek Range, Carlin-Hollister, and Snowstorm Mountains areas, and a basin between Hollister and the Snowstorm Mountains. Pre-middle Tertiary volcanic rocks were stripped from the highlands, and tuffaceous sediments accumulated in the basins. In northeastern Nevada, the major tectonic event during this period was extensional faulting at about 20 Ma, although relatively little tilting was associated with that event (Thorman and others, 1991).

Rift-related faulting produced a north-northwest-trending graben or series of grabens in which volcanic rocks accumulated. Dikes and elongate intrusions were emplaced along many of the faults, producing dikes swarms in many locations (Zoback and others, 1994). In the Snowstorm Mountains, the trough was approximately 30 km wide, based upon the distribution of rift-related flows (Wallace, 1993). The graben was deepest along its central axis and shallower to the east and west, with flows thinning and pinching out in both directions, as at Ivanhoe. The 30-km-wide surface expression of the trough contrasts with the 3- to 5.5-km-wide magnetic anomaly that represents the magmatic feeder system for the volcanic rocks (Zoback and others, 1994). In the Mule Canyon area, the graben is only 10 to 15 km wide, and is shallower to the west than to the east. The dike swarm that is associated with that segment of the rift is 2-3 km wide and is in the western part of the graben.

Gold deposits associated with the rift (fig. 8) formed in shallow epithermal to hot spring environments. The epithermal deposits formed along faults (Midas), and along the margins of rift-related dikes (Mule Canyon). The Hollister deposit, which directly underlies a hot-spring mercury deposit, is disseminated in Miocene tuffaceous sedimentary rocks. All deposits formed in the narrow time interval of 15 to 15.5 Ma. The epithermal deposits are low-sulfidation, quartz-adularia systems. The Mule Canyon deposit contains gold-rich, arsenical rims on pyrite, similar to sedimentary rock-hosted deposits in the Carlin trend. In contrast, the Midas deposit contains very little arsenic and abundant selenium, and gold is present as electrum and native gold.

ACKNOWLEDGMENTS

Eric Saderholm of Newmont Gold Ltd. provided much information on the Mule Canyon deposit. Chris Henry of the Nevada Bureau of Mines and Geology provided three new $^{40}\text{Ar}/^{39}\text{Ar}$ dates on rocks from the Ivanhoe district. Analyses were performed at the New Mexico Geochronological Laboratory under the direction of Bill McIntosh; all dates are relative to an age of 520.4 Ma for Mmhb-1. Helpful reviews of the manuscript were provided by R.J. Fleck, C.D. Henry, and C.T. Wrucke. Susan Tingley drafted some of the figures.

REFERENCES CITED

- Bailey, E.H., and Phoenix, D.A., 1944, Quicksilver deposits in Nevada: Nevada Bureau of Mines and Geology Bulletin 41, 206 p.
- Bartlett, M.W., Enders, M.S., and Hruska, D.C., 1991, Geology of the Hollister gold deposit, Ivanhoe district, Elko County, Nevada, in Raines, G.L., Lisle, R.E., Schafer, R.W., and Wilkinson, W.H., eds., Geology and ore deposits of the Great Basin, Symposium Proceedings: Geological Society of Nevada, p. 957-978.
- Blakely R.J., and Jachens, R.C., 1991, Regional study of mineral resources in Nevada—insights from three-dimensional analysis of gravity and magnetic anomalies: Geological Society of America Bulletin, v. 103, p. 795-803.
- Deng, Q., 1991, Geology and trace element geochemistry of the Hollister gold deposit, Ivanhoe District, Elko County, Nevada: El Paso, University of Texas at El Paso, Ph.D. thesis, 313 p.
- Dohrenwend, J.C., and Moring, B.C., 1991, Reconnaissance photogeologic map of young faults in the Winnemucca 1° by 2° quadrangle, Nevada: U.S. Geological Survey Miscellaneous Field Studies Map MF-2175, scale 1:250,000.
- Emsbo, P., Hofstra, A., Park, D., Zimmerman, J.M., and Snee, L., 1996, A mid-Tertiary age constraint on alteration and mineralization in igneous dikes on the Goldstrike property, Carlin trend, Nevada: Geological Society of America Abstracts with Programs, v. 28, p. A476.
- Fleck, R.J., Theodore, T.G., Sarna-Wojcicki, A., and Meyer, C.E., this volume, Age and possible source of air-fall tuffs of the middle Miocene Carlin Formation, in Tosdal, R.M., ed., Contributions to the gold metallogeny of northern Nevada: U.S. Geological Survey Open-File Report.
- Fries, C., Jr., 1942, Tin deposits of northern Lander County, Nevada: U.S. Geological Survey Bulletin 931-L, p. 279-294.
- Henry, C.D., Boden, D.R., and Castor, S.B., this volume, Eocene volcanism and related precious-metal mineralization, Tuscarora Mountains, Elko County, Nevada, in Tosdal, R.M., ed., Contributions to the gold metallogeny of northern Nevada: U.S. Geological Survey Open-File Report.
- Hollister, V., Hruska, D., and Moore, R., 1992, A mine-exposed hot spring deposit and related epithermal gold resource: Economic Geology, v. 87, p. 421-424.
- Lamb, J.B., and Cline, J., 1997, Depths of formation of the Meikle and Betze/Post deposits, in Vikre, P., Thompson, T.B., Bettles, K., Christensen, O., and Parratt, R., eds., Carlin-type gold deposits field conference: Society of Economic Geologists Guidebook Series, v. 28, p. 101-107.
- LaPointe, D.D., Tingley, J.V., and Jones, R.B., 1991, Mineral resources of Elko County, Nevada: Nevada Bureau of Mines and Geology Bulletin 106, 236 p.
- Le Bas, M.J., LeMaitre, R.W., Streckeisen, A., and Zanettin, B., 1986, A chemical classification of volcanic rocks based on the total alkali-silica diagram: Journal of Petrology, v. 27, p. 745-750.
- Le Maitre, R.W., Bateman, P.C., Dudek, A., Keller, J., Lameyre, Le Bas, M.J., Sabine, P.A., Schmid, R., Sorensen, H., Streckeisen, A., Woolley, A.R., and Zanettin, B., 1989, A classification of igneous rocks and glossary of terms: Oxford, Blackwell, xx p.
- McKee, E.H., and Silberman, M.L., 1970, Geochronology of Tertiary igneous rocks in central Nevada: Geological Society of America Bulletin, v. 81, p. 2317-2328.
- McKee, E.H., Tarshis, A.L., and Marvin, R.F., 1976, Summary of radiometric ages of Tertiary volcanic and selected plutonic rocks in Nevada. Part V: northeastern Nevada: Isochron/West, v. 16, p. 15-27.
- Serenko, T.J., 1995, Nature of gold mineralization at Mule Canyon, Lander County, Nevada, U.S.A.: Transactions of the Institute of Mining and Metallurgy, v. 104, section B, p. B99-B110.
- Stewart, J.H., and Carlson, J.E., 1978, Geologic map of Nevada: U.S. Geological Survey, scale 1:500,000.
- Stewart, J.H., and McKee, E.H., 1977, Geology and mineral deposits of Lander County, Nevada, with a section on mineral deposits by Harold K. Stager: Nevada Bureau of Mines and Geology Bulletin 88, 106 p.
- Struhsacker, E.M., 1980, The geology of the Beowawe geothermal system, Eureka and Lander Counties, Nevada: Earth Science Laboratory Division, University of Utah Research Institute, Report ESL-37, 78 p.
- Thomson, K., Brummer, J.E., Caldwell, D.A., McLachlan, C.D., and Schumacher, A.L., 1993, Geology and geochemistry of the Mule Canyon gold deposit, Lander County, Nevada: Society for Mining, Metallurgy, and Exploration, Inc., Preprint 93-271, 10 p.
- Thorman, C.H., Ketner, K.B., Brooks, W.E., Snee, L.W., and Zimmermann, R.A., 1991, Late Mesozoic-Cenozoic tectonics in northeastern Nevada, in Raines, G.L., Lisle, R.E., Schafer, R.W., and Wilkinson, W.H., eds., Geology and ore deposits of the Great Basin, Symposium Proceedings: Geological Society of Nevada, p. 25-45.
- Wallace, A.R., 1991, Effect of late Miocene extension on the exposure of gold deposits in north-central Nevada, in Raines, G.L., Lisle, R.E., Schafer, R.W., and Wilkinson, W.H., eds., Geology and ore deposits of the Great Basin, Symposium Proceedings: Geological Society of Nevada, p. 179-183.
- Wallace, A.R., 1993, Geologic map of the Snowstorm Mountains and vicinity, Elko and Humboldt Counties, Nevada: U.S. Geological Survey Miscellaneous Investigations Map I-2394, scale 1:50,000.
- Wallace, R.E., 1979, Map of young fault scarps related to earthquakes in north central Nevada: U.S. Geological Survey Open-file Report 97-1554, scale 1:125,000.
- Zoback, M.L., 1989, State of stress and modern deformation of the northern Basin and Range province: Journal of Geophysical Research, v. 94, no. B6, p. 7105-7128.
- Zoback, M.L., McKee, E.H., Blakely, R. J., and Thompson, G.A., 1994, The northern Nevada rift: Regional tectono-magmatic relations and middle Miocene stress direction: Geological Society of America Bulletin, v. 106, p. 371-382.
- Zoback, M.L., and Thompson, G.A., 1978, Basin and Range rifting in northern Nevada: clues from a mid-Miocene rift and its subsequent offsets: Geology, v. 6, p. 111-116.

GEOLOGY AND MINERALIZATION OF THE EOCENE TUSCARORA VOLCANIC FIELD, ELKO COUNTY, NEVADA

By Christopher D. Henry, David R. Boden, and Stephen B. Castor

ABSTRACT

The Tuscarora volcanic field is the largest remnant of Eocene magmatism in Nevada. Detailed geologic mapping reveals that at least five major volcanic centers formed in a ~450 km² area in the southeastern part of the Tuscarora volcanic field during a remarkably intense period of magmatism between ~39.9 and 39.3 Ma. (1) The Pleasant Valley volcanic complex erupted andesitic to dacitic lava flows and minor pyroclastic rocks at ~39.9-39.7 Ma. (2) The Mount Blitzen volcanic center, which formed between 39.8 and 39.7 Ma, is a 11x6-km fault-bounded basin filled with dacitic domes, small-volume pyroclastic flows erupted from the domes, and reworked deposits. (3) The Big Cottonwood Canyon caldera, a ≥15-km diameter rhyolitic ash-flow caldera, lies just north of and truncates the Mount Blitzen center and erupted at ~39.7 Ma. (4) The Mount Neva intrusive episode consists of a granodiorite stock, numerous dacitic intrusions, and abundant, northeast-striking, andesitic to low-silica rhyolitic dikes. The granodiorite and dacites were emplaced along the margins of the Mount Blitzen center, and the dikes intruded throughout the center, between 39.5 and 39.3 Ma. These intrusions probably represent continued activity of the Mount Blitzen center. (5) Andesitic to dacitic lava flows, similar to those of the Pleasant Valley complex, erupted east of the Big Cottonwood Canyon caldera at ~39.3 Ma.

Gold-silver deposits at Tuscarora lie along and just outside the southeastern margin of the Mount Blitzen center, are closely associated with volcanism, and constitute the oldest Tertiary volcanic-hosted epithermal mineralization in Nevada. Two deposit types are present: (a) base-metal-bearing, high-grade Ag-Au veins (Ag/Au ~310) that lie in the northern and eastern parts of the district, and (b) base metal-poor Au-Ag veins and stockworks (Ag/Au ~25) that lie in the southern and western parts of the district. The deposits are hosted by dacites of the Mount Neva intrusive episode and reworked tuffs of the Pleasant Valley complex. ⁴⁰Ar/³⁹Ar dates on six samples of adularia, four from Au-rich and two from Ag-rich veins, range narrowly from 39.32±0.14 (2σ) to 39.14±0.13 Ma, with all but one ≥39.24 Ma. The location and timing of

mineralization are consistent with hydrothermal circulation having been driven by intrusions of the Mount Neva episode. Both the near surface volcanic rocks and deeper Paleozoic rocks are prospective for additional deposits.

INTRODUCTION

Geologic mapping of the Tuscarora volcanic field is part of a broader project to understand Eocene magmatism and tectonism in northeastern Nevada (fig. 1). The Tuscarora volcanic field is interesting in itself; it represents some of the oldest Tertiary magmatism in Nevada, is the largest Eocene volcanic field in Nevada, and has significant mineral potential. Epithermal gold-silver deposits at Tuscarora are clearly associated with igneous activity and structure of the Tuscarora volcanic field. Our geologic mapping is also intended to help address potential environmental concerns if large-scale mining becomes warranted in the area. Another particularly important goal is to understand the relation between Eocene magmatism and tectonism and Carlin-type gold deposits in the region (fig. 1; Henry and Boden, 1997). The Tuscarora volcanic field lies just north of major gold deposits of the Carlin trend and west of deposits in the Independence Mountains (fig. 1). The age and origin of these deposits remain controversial (e.g., Sillitoe and Bonham, 1990; Arehart and others, 1993; Kuehn and Rose, 1995; Thorman and others, 1995; Ilchik and Barton, 1997), but evidence is growing that many deposits in the Carlin trend, Independence Mountains, and adjacent areas formed in the Eocene (Hofstra, 1995; Emsbo and others, 1996; Leonardson and Rahn, 1996; Phinisey and others, 1996; Rota, 1996; Groff and others, 1997).

This work briefly summarizes results of detailed mapping of the Mount Blitzen (Henry and Boden, 1998) and Tuscarora quadrangles and the southern two thirds of the Toe Jam Mountain quadrangle (area covered in fig. 2). This mapping documents at least five voluminous volcanic-intrusive centers in the southern part of the Tuscarora volcanic field (figs. 1 and 2). ⁴⁰Ar/³⁹Ar dates show that the five centers developed between approximately 39.9 and 39.3 Ma during a brief,

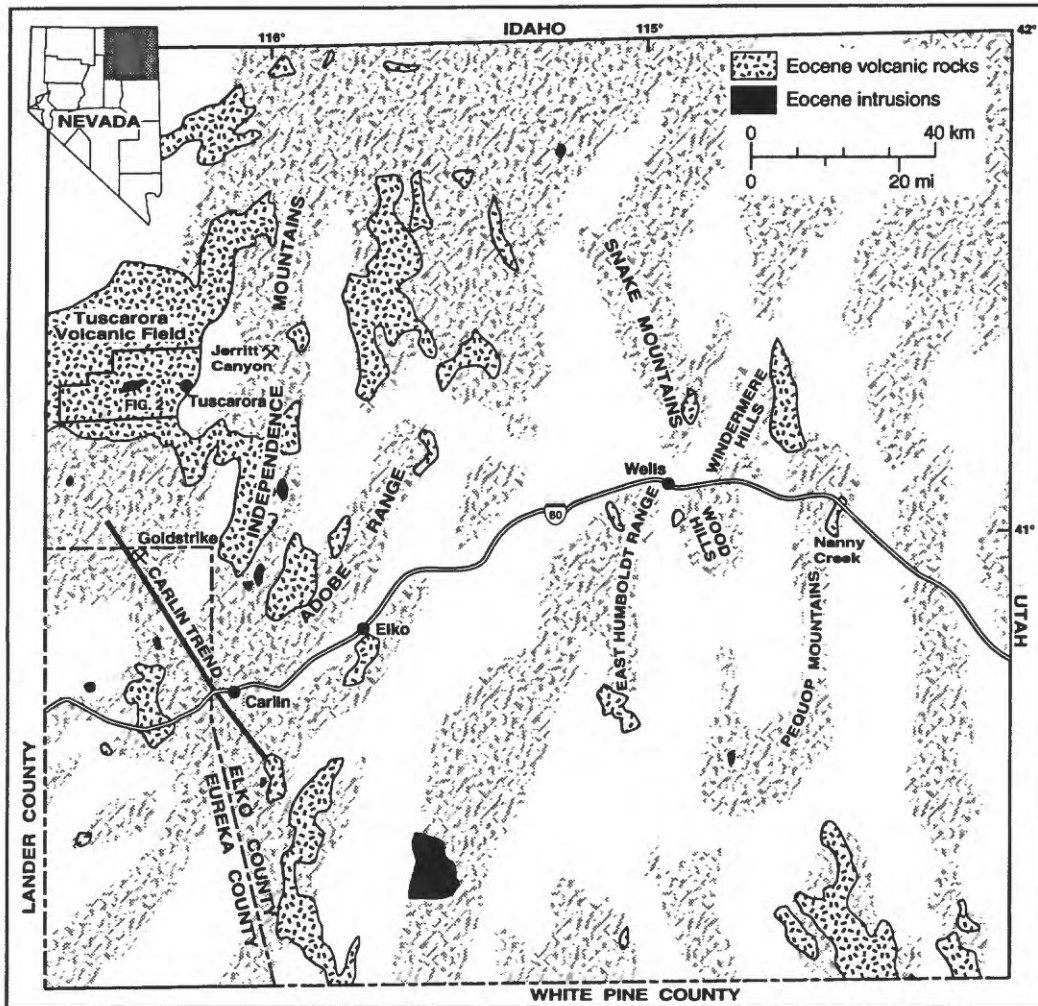


Figure 1. Location map showing generalized distribution of Eocene volcanic and intrusive rocks in northeastern Nevada, especially the Tuscarora volcanic field. Note that Eocene magmatism was particularly intense around the Carlin trend and Independence Mountains.

intense period of magmatism. Precious-metal mineralization at Tuscarora formed at about 39.3 Ma, contemporaneous with a major intrusive episode of the Tuscarora volcanic field, and is the oldest Tertiary volcanic-hosted epithermal deposit in Nevada.

PALEOZOIC ROCKS

The Tuscarora volcanic field formed in an area of complexly deformed Lower Paleozoic rocks that constitute the upper plate (or western assemblage) of the Roberts Mountains allochthon (Roberts, 1964). Upper-plate rocks were deposited in relatively deep water off what was then the western margin of the North American continent and thrust southeastward over

generally coeval sedimentary rocks (lower-plate or eastern assemblage) deposited on the craton (Miller and others, 1992; Poole and others, 1992). Two distinct packages of Paleozoic rocks crop out in the Tuscarora volcanic field (fig. 2). A northern package contains boudins of quartzite in a matrix of siltstone and chert. Based on regional data, the quartzite almost certainly is correlative with the Ordovician Valmy Formation (Churkin and Kay, 1967; Miller and Larue, 1983; Coats, 1987). However, a thin limestone unit within the quartzite-bearing package north of Tuscarora contains Devonian conodonts (Coats, 1987), so younger rocks are present. A southern package consists of siltstone, chert, and minor sandstone and limestone; A. E. Saucier (personal communication, 1997) found Silurian to Devonian conodonts in three samples. Both sequences were folded and thrust southeastward before Eocene

volcanism. We interpret the presence of a major thrust fault that places the northern package over the southern one (fig. 2). Carbonate-bearing, lower-plate rocks, which are the major hosts for gold deposits in the Carlin trend and Independence Mountains, do not crop out in the Tuscarora area but should underlie the Roberts Mountains thrust, probably at present-day depths of ~3 km.

THE TUSCARORA VOLCANIC FIELD

Previous reconnaissance work in the Tuscarora volcanic field indicated that several volcanic centers were active between about 42 and 38 Ma (Berger and others, 1991; Crawford, 1992; Boden and others, 1993). Volcanism appears to have been in part contemporaneous with extension in the region (Clark and others, 1985; Brooks and others, 1995), although the amount and significance of extension within the Tuscarora volcanic field remain uncertain.

At least five major episodes of Eocene magmatism occurred in the southern Tuscarora volcanic field in a remarkably intense period of activity between about 39.9 and 39.3 Ma (fig. 2; Henry and Boden, 1997, 1998). From oldest to youngest, these episodes are: (1) andesitic to dacitic lava flows and tuffaceous sedimentary rocks of the Pleasant Valley volcanic complex (~39.9-39.7 Ma); (2) dacitic domes, small-volume pyroclastic-flow deposits, and epiclastic deposits of the Mount Blitzen volcanic center (~39.8-39.7 Ma); (3) rhyolitic ash-flow tuff of the Big Cottonwood Canyon caldera (39.7 Ma); (4) a granodiorite pluton and andesitic to rhyolitic dikes and small intrusions of the Mount Neva intrusive episode (39.5-39.3 Ma); and (5) andesitic to dacitic lava flows of Sixmile Canyon (~39.3 Ma). Field, petrographic, chemical, and $^{40}\text{Ar}/^{39}\text{Ar}$ age data indicate that each of the five major sequences consists of genetically related rocks erupted from sources in the southern Tuscarora volcanic field. Two rhyolitic lavas erupted at about 35 Ma in the western part of the area of figure 2 and represent a sixth episode of local, but distinctly younger and volumetrically minor, activity.

Slightly older Tertiary volcanic rocks, including three rhyolitic or dacitic ash-flow tuffs, underlie rocks of the Pleasant Valley complex to the west. A dacitic tuff that directly underlies Pleasant Valley rocks is 39.84 ± 0.10 (2σ) Ma. These tuffs are absent in the central and eastern parts of the area of figure 2, where Pleasant Valley rocks rest directly upon Paleozoic rocks or upon basal Tertiary conglomerate. The source areas of these tuffs, although unknown, were probably not within the southern Tuscarora volcanic field.

Pleasant Valley Volcanic Complex

The Pleasant Valley volcanic complex, the oldest major volcanic sequence of the Tuscarora volcanic field, consists of

andesitic to dacitic lava flows and lesser pyroclastic and volcaniclastic rocks (fig. 2). These rocks crop out extensively in the southern parts of the Mount Blitzen and Toe Jam Mountain quadrangles and continue several kilometers farther south. Lavas total about 300 m thick in the southern part of the Mount Blitzen quadrangle but become increasingly interbedded with volcaniclastic deposits and wedge out northeastward toward Tuscarora. Lavas rest directly upon basal Tertiary conglomerate in the Mount Blitzen quadrangle and upon the slightly older ash-flow tuff sequence to the west and south. Known sources include several dacite lava domes in the southwestern part of Pleasant Valley outcrop, a pyroclastic(?) center in the southern part, and several shallow intrusions in the southwest that were probable feeders for the flows. $^{40}\text{Ar}/^{39}\text{Ar}$ dates on two lava flows and the immediately underlying dacitic tuff indicate that Pleasant Valley lavas erupted between about 39.9 and 39.7 Ma (fig. 3).

Mount Blitzen Volcanic Center

Previous reconnaissance studies called the large Mount Blitzen volcanic center (fig. 2) a stratovolcano (Berger and others, 1991), a caldera (Cruson and Limbach, 1985; Crawford, 1992), or a volcano-tectonic graben (Boden and others, 1993). The Mount Blitzen center is a fault-bounded basin filled with dacitic intrusive and extrusive rocks. The basin is approximately 11 by 6 km; however, it is truncated on the north by the younger Big Cottonwood Canyon caldera, and the original extent in that direction is unknown. Most boundaries are high-angle faults.

The Mount Blitzen center is filled with a thick sequence of dacitic domes (Tbd) and the dacitic tuff of Mount Blitzen (Tbt), which consists of small-volume pyroclastic-flow and epiclastic deposits. Domes occur throughout the center and are most abundant along the margins; a few intrude older rocks outside the center. Pyroclastic rocks are petrographically similar to the domes and probably erupted from them. Epiclastic rocks consist mostly of very coarse to fine fragments of domes and tuff and represent reworking of the primary volcanic rocks. Both pyroclastic and epiclastic rocks contain megabreccia blocks of the dacitic domes, older andesite probably of the Pleasant Valley complex, and, rarely, Paleozoic rocks that were shed from the margins of the center. The composite tuff of Mount Blitzen is at least 1 km thick and could be several kilometers thick. The tuff was tilted into a northeast- to east-northeast-striking anticline through the middle of the center; with some complexity, dips on both limbs average about 35 to 40° (fig. 2). Therefore, oldest rocks are exposed in the middle of the center and are progressively younger outward. However, the base is not exposed and complex stratigraphy, lack of marker beds, and uncertainty in repetition by faults preclude determining an accurate thickness.

Imprecise $^{40}\text{Ar}/^{39}\text{Ar}$ dates on biotite from samples of

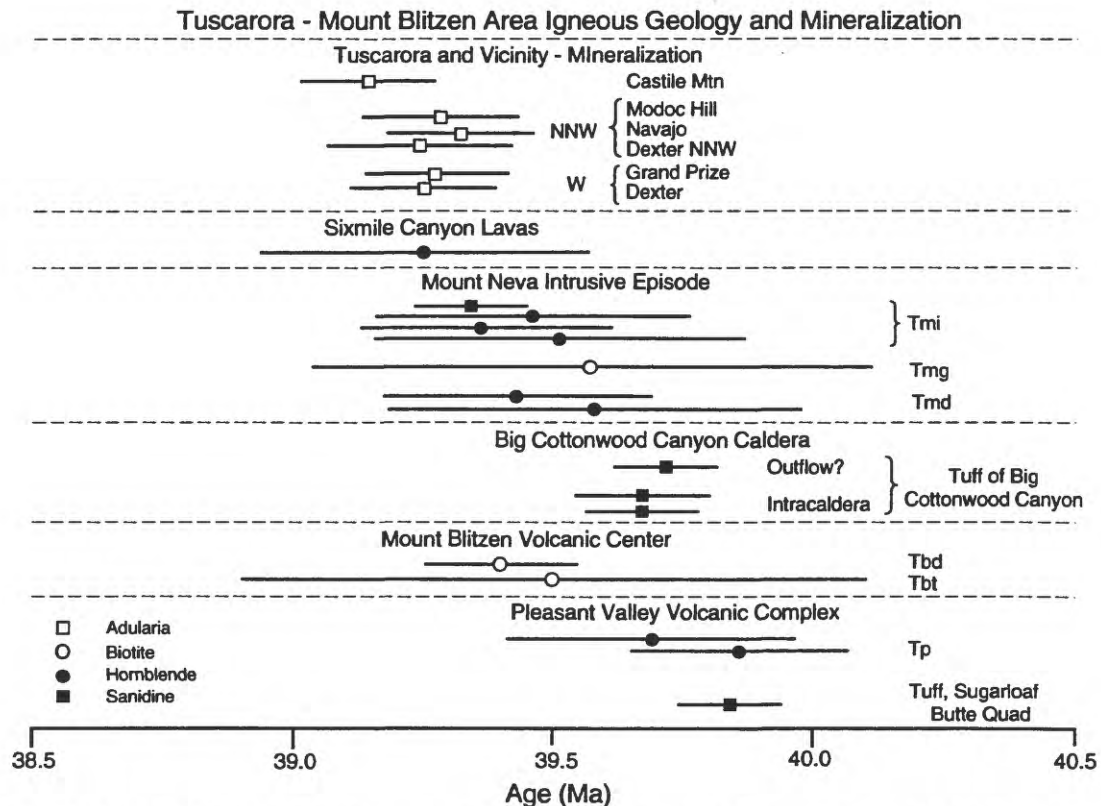


Figure 3. $^{40}\text{Ar}/^{39}\text{Ar}$ dates ($\pm 2\sigma$) of igneous rocks and mineralization in the Tuscarora volcanic field. Rocks are in stratigraphic order determined from field relations. Sanidine and adularia give the most precise and accurate dates, hornblende is next, and biotite is less precise.

dacitic domes and tuff and, more importantly, dates on sanidine from older and younger rocks bracket activity in the Mount Blitzen center between about 39.8 and 39.7 Ma (fig. 3).

Big Cottonwood Canyon Caldera

The Big Cottonwood Canyon caldera is a large, rhyolitic ash-flow caldera that lies north of and truncates the Mount Blitzen volcanic center (fig. 2). The caldera margin is marked by the juxtaposition of thick intracaldera tuff of Big Cottonwood Canyon (Tct) against Paleozoic rocks and tuff of Mount Blitzen. The caldera extends at least 15 km east-west and an unknown distance to the north, outside the mapped area. All tuff shown on figure 2 lies within the caldera, is lithic-rich, densely to moderately welded, and unless repeated by unrecognized faults, may be several kilometers thick, based on its somewhat irregular 15° to 25° westward dip across the caldera. Tuff near the caldera margin contains abundant debris lenses and individual blocks of andesite, probably of the Pleasant Valley complex, tuff of Mount Blitzen, and Paleozoic rocks up to several hundred meters in diameter. Ponding of the tuff within the caldera and presence of megabreccia show

that caldera collapse occurred contemporaneously with ash-flow eruption. Correlative outflow tuff crops out approximately 25 km to the southeast, in the southeastern part of the Tuscarora quadrangle, and a similar distance to the southwest near Willow Creek Reservoir (Wallace and John, this volume). $^{40}\text{Ar}/^{39}\text{Ar}$ dates on sanidine from two samples of intracaldera tuff are identical at 39.67 Ma; outflow tuff at Willow Creek Reservoir gives an age of 39.72 Ma (fig. 3).

Mount Neva Intrusive Episode

The Mount Neva pluton, several other irregularly shaped intrusions, and innumerable dikes were emplaced into and immediately adjacent to the Mount Blitzen volcanic center (fig. 2). Dikes of the Mount Neva episode cut the tuff of Big Cottonwood Canyon, so they and probably the other intrusions postdate formation of the Big Cottonwood Canyon caldera.

Intrusions of the Mount Neva episode developed in three distinct pulses: (1) early porphyritic dacite (Tmd), (2) the Mount Neva granodiorite (Tmg), and (3) late dikes (Tmi). Early dacites form numerous irregularly shaped intrusions along the western, southern, and eastern margins of the Mount Blitzen

volcanic center and a few dikes within the center. These intrusions are particularly abundant along the southeastern margin of the center in the Tuscarora mining district. This distribution indicates that the intrusions rose along the faults that bound the center.

The Mount Neva granodiorite (Tmg), the largest intrusion of the area, cuts across the southwestern margin of the Mount Blitzen volcanic center. It is about 5 km by 1 to 2 km, elongate east-northeast, and has steep contacts with surrounding rocks.

Numerous late dikes, ranging in composition from andesite to low-silica rhyolite, were the last manifestations of the Mount Neva episode. Although we mapped five types on the basis of phenocryst assemblage and inferred composition, all dikes are shown as a single unit on figure 2. These dikes are most abundant in a broad, northeast-striking band through the middle of the Mount Blitzen center, where they intrude tuff of Mount Blitzen (Tbt) and coincide with the northeast-striking anticline. Dikes die out within three to four kilometers north and south of the Mount Blitzen center. Both the dikes and the anticline coincide with a prominent aeromagnetic anomaly. Based on these data, we interpret the dikes to be apophyses from a large, underlying intrusion.

$^{40}\text{Ar}/^{39}\text{Ar}$ dates on representatives of all three intrusive pulses indicate that the Mount Neva intrusive episode may have begun as early as about 39.5 Ma and lasted until 39.3 Ma (fig. 3). On the basis of spatial coincidence and similar rock compositions, we interpret the Mount Neva episode to be a late phase of activity of the Mount Blitzen volcanic center.

The physical characteristics and evolution of the Mount Blitzen center and Mount Neva intrusive episode are similar to those of many calderas. Indeed, Cruson and Limbach (1985) and Crawford (1992) designated the Mount Blitzen center a caldera. It is a deep, fault-bounded basin filled with a thick sequence of tuff that commonly contains megabreccia. The preserved basin is roughly circular, although its original dimensions are uncertain because it is truncated on the north. The late intrusions of the Mount Neva episode are similar to late activity recognized in almost all calderas. The anticline that developed in the tuff of Mount Blitzen, if resulting from emplacement of the underlying intrusion, is somewhat similar to resurgent domes in many calderas. The Mount Blitzen center is different from most calderas in that the tuff consists of complexly interbedded, small-volume pyroclastic flows and epiclastic rocks. These deposits contrast with the thick, massive intracaldera tuff that is typical of most calderas, for example, the tuff of Big Cottonwood Canyon. Also, the anticline is far more elongate and steeper than typical resurgent domes.

Sixmile Canyon Lavas

The youngest major volcanic episode in this area consists of dacitic to andesitic lava flows and minor tuffs that crop out

north of Tuscarora and east of the Big Cottonwood Canyon caldera (fig. 2). Although rock types are similar to those of the Pleasant Valley volcanic complex, Sixmile Canyon lavas are faulted down against and, in one location, overlie the tuff of Big Cottonwood Canyon. Along with a single $^{40}\text{Ar}/^{39}\text{Ar}$ date on hornblende of 39.25 ± 0.31 Ma (fig. 3), the field relations show that the Sixmile Canyon lavas are younger than Pleasant Valley rocks. Compositional, petrographic, and age similarities suggest the lavas may be extrusive counterparts to dacitic rocks of the Mount Neva intrusive episode.

A group of dacitic lava flows that crop out in the northeastern part of the Toe Jam Mountain quadrangle (dacites of the Falcon Mine; fig. 2) may be contemporaneous with the Sixmile Canyon lavas. These rocks have been only briefly studied but are younger than the tuff of Big Cottonwood Canyon and older than 35.3-Ma rhyolite lava

35-Ma Rhyolitic Volcanism

Two rhyolite lava flows erupted in the western part of the mapped area at about 35 Ma. A small (1.5 x 0.5 km) lava dome and associated tuff erupted along the southern margin of the Big Cottonwood Canyon caldera. Although it lies on the ring fracture of the caldera, its age of 35.05 ± 0.10 Ma shows that it is much too young to be genetically related to caldera magmatism. A much larger but possibly composite flow (~8 km in diameter) appears to have erupted from a vent in the northeastern part of the Toe Jam Mountain quadrangle and flowed to the south and west. A sample from near the possible vent area gives an age of 35.29 ± 0.10 Ma.

EXTENSION IN AND AROUND THE TUSCARORA VOLCANIC FIELD

The Tuscarora volcanic field formed in the Eocene during probable northwest-directed extension, some of the earliest Tertiary extension in the region (Clark and others, 1985; Brooks and others, 1995; Janecke and others, 1997). However, details on timing, amount, and significance of early to mid-Tertiary extension in the Tuscarora volcanic field are not fully resolved (Henry and Boden, 1998). Most Eocene rocks in the Mount Blitzen and Tuscarora quadrangles are nearly flat lying or dip gently and appear negligibly extended. Uncertainty about the influence of extension centers on the origin of the fault-bounded Mount Blitzen volcanic center and the northeast-striking anticline in the tuff of Mount Blitzen (fig. 2). Our favored interpretation is that the Mount Blitzen center resulted dominantly from volcanic subsidence and the anticline from magmatic resurgence. Northwest-directed extension is manifest by the northeast strike of the anticline and Mt Neva dike swarm. Alternatively, the Mount Blitzen center is a tectonic graben and the anticline a result of tilting by

displacement along oppositely dipping normal faults that form the western and eastern margins of the center.

A later episode of extension definitely occurred between about 35 and 15 Ma and affected the Toe Jam Mountain quadrangle and areas farther west. A transition zone between less extended rocks to the east and moderately extended rocks to the west strikes northward through the eastern part of the quadrangle. Rocks of the Pleasant Valley complex in the southeastern part of the quadrangle are approximately flat lying. To the west, Pleasant Valley rocks and rocks at least as young as the 35.3-Ma rhyolite lava flow are tilted eastward, typically between 25° and 35°, and repeated by a series of west-dipping normal faults. A 15.3-Ma dacitic ash-flow tuff unconformably overlies the tilted rocks in the southwestern corner of the quadrangle. This Miocene tuff dips approximately 5° eastward, which indicates still later, but minor extension.

PRECIOUS-METAL DEPOSITS AT TUSCARORA

Productive deposits at Tuscarora occur along and just outside the southeastern margin of the Mount Blitzen volcanic center (fig. 2). Total production, from early working of placer deposits and subsequent discovery of silver-rich veins to recent mining of the Dexter gold-silver stockwork zone by open-pit methods, is about 200,000 oz gold and 7.5 million oz silver along with 7 tons Cu and 70 tons Pb (LaPointe and others, 1991). Other nearby areas of mineral deposits, which had little or no production, include mercury workings at Berry Basin, west of Tuscarora, and at the Red Bird (Silverado) mine just north of Tuscarora.

Lode deposits at Tuscarora are of two types: silver-rich deposits and gold deposits (Nolan, 1936). Silver-rich deposits are restricted to a relatively small area north and east of Tuscarora, whereas gold deposits occur in a larger area that extends southwest from Tuscarora (fig. 4). The two types overlap west of the Dexter pit, but paragenetic relations are unknown. Steeply to moderately dipping veins are present in both deposit types. The silver deposits are mainly along the north-northwest to northwest striking Navajo-Commonwealth vein system and the east-northeast striking Grand Prize-Argenta vein system (fig. 4). Gold deposits are along the north-northeast to north-northwest striking Modoc and Eureka vein systems, but are also associated with stockwork veining at the Dexter mine and in the Battle Mountain area (fig. 4).

Although both deposit types belong to the quartz-adularia (low sulfidation) epithermal class, they have somewhat different ore and gangue mineral assemblages, alteration patterns, and geochemistry. Quartz and adularia are gangue minerals for both types, but calcite, base-metal sulfides, and manganese minerals are more abundant in the silver-rich deposits. Ore minerals in unoxidized samples from the silver-rich deposits consist mainly of pyrrargyrite and acanthite with

minor electrum. Electrum and acanthite are the main ore minerals in the gold deposits.

Silver/gold ratios based on production records ranged from four or five for the gold deposits to 150 in the silver-rich deposits (Nolan, 1936). On the basis of samples collected for this study, mean silver/gold is about 25 for gold deposits and 300 for silver-rich deposits (table 1). The two types form distinct fields on a scatter plot of silver against gold (fig. 5), but there is some overlap, mainly for samples from the Modoc mine and the southern part of the Navajo vein. Gold and silver are strongly correlative in both deposit types (fig. 5), although some oxidized samples are highly enriched in silver relative to gold.

Samples of silver-rich ore commonly have high calcium and magnesium concentrations relative to those for the gold deposits, probably reflecting higher carbonate content, and base metals are generally high in the former and low in the latter (table 1, fig. 5). Samples from the silver-rich deposits commonly contain more than 1 ppm selenium to a maximum of 78 ppm, whereas samples from the gold deposits generally have less than 1 ppm. Arsenic, antimony, and mercury are moderately to strongly enriched in samples from both types of deposits; bismuth, molybdenum, and tellurium are generally low (table 1). Thallium is slightly enriched in both types.

Main host rocks for the precious-metal deposits are early porphyritic dacites (Tmd) of the Mount Neva intrusive episode and dacitic lavas and tuffaceous sediments of the Pleasant Valley complex. East-northeast-striking silver-rich veins (e.g., the Grand Prize and Argenta veins) are subparallel to dikes of the Mount Neva episode, and north-northwest-striking veins (e.g., the highly productive Navajo vein) are subparallel to right-lateral transfer faults that make up part of the southeastern margin of the Mount Blitzen center (figs. 2 and 4).

Silver-rich ore consists mainly of sulfide-bearing replacement veins, although late-stage barren comb quartz veins are also present. Gold ore consists of or is associated with comb quartz fissure veins that locally contain sulfide minerals. In places, as at the recently productive Dexter mine, low-grade gold ore occurs as relatively large areas of silicified rock and stockwork veins. As noted by Nolan (1936), silver-rich ore is associated with relatively narrow zones of quartz-adularia-clay alteration, whereas gold is associated with widespread quartz-adularia-clay alteration.

A reconnaissance fluid-inclusion study indicates that the silver-rich Grand Prize vein formed from nonboiling fluids at 245°–255°C (J. Cline, personal communication, 1993). By contrast, a sample of Dexter gold ore contains two populations of fluid inclusions; one with variable liquid/vapor ratios suggestive of boiling and homogenization temperatures of 200°–220°C, and another with constant liquid/vapor ratios and homogenization temperatures of 225°–250°C. Under these conditions, and assuming hydrostatic or hydrodynamic gradients and minor amounts of dissolved CO₂, inferred paleodepths of trapping range from about 200 to 400 m (Haas,

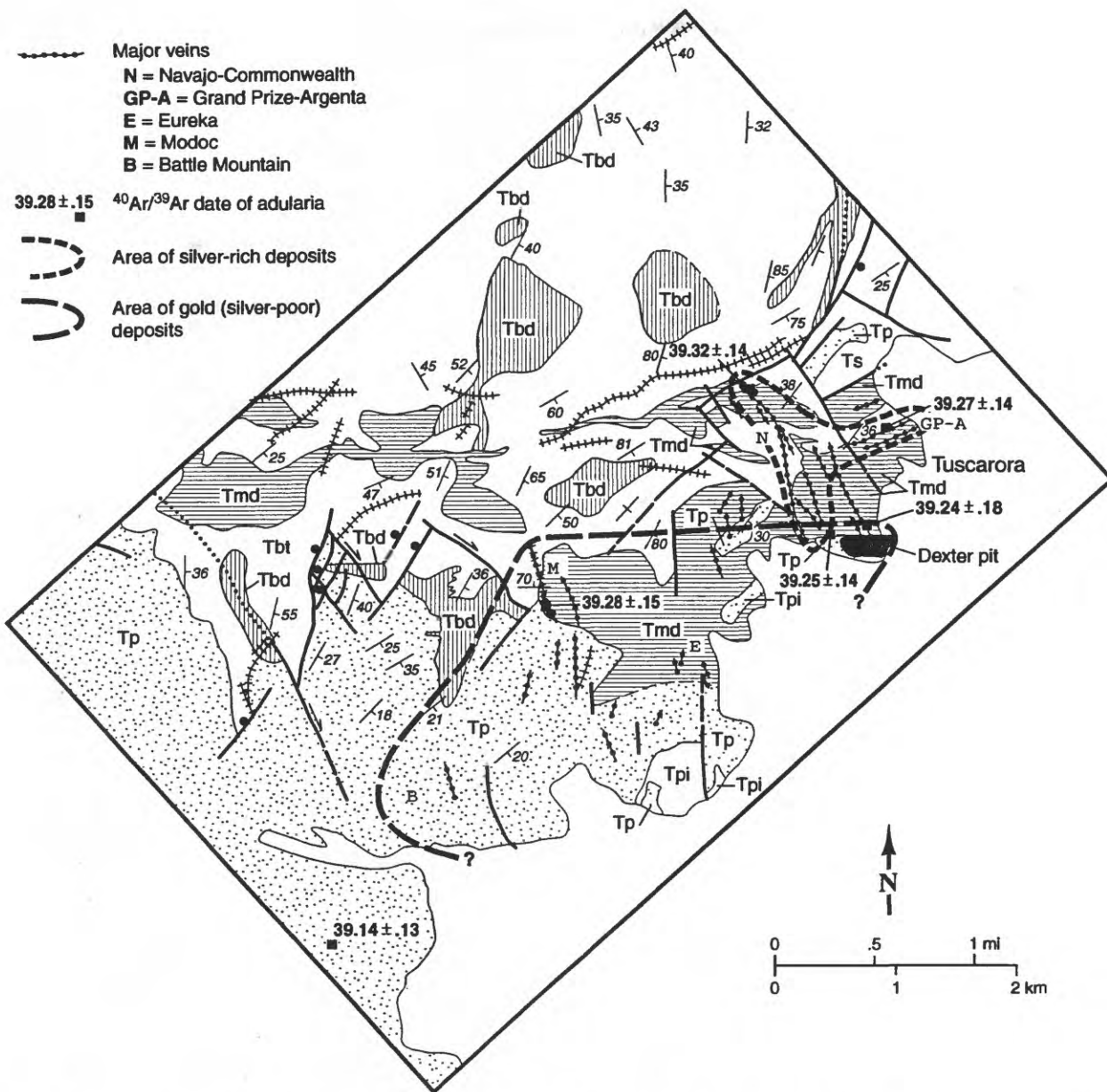


Figure 4. Geologic map of the Tuscarora mining district, showing major veins, $^{40}\text{Ar}/^{39}\text{Ar}$ ages of adularia, and general areas of the silver-rich and silver-poor deposits. Geologic units are as in figure 2.

1971; Hedenquist and Henley, 1985, Bodnar and others, 1985).

$^{40}\text{Ar}/^{39}\text{Ar}$ dates on six samples of adularia, four from areas of gold stockwork zones and two from silver-rich veins, have a narrow range between 39.32 ± 0.14 (2σ) to 39.14 ± 0.13 Ma, with all but one ≥ 39.24 Ma (fig. 3). All ages are indistinguishable within their analytical uncertainties and allow two hypotheses relating the two types of mineralization. Either both types of mineralization formed concurrently and are zoned counterparts, or each type represents temporally separate, compositionally distinct hydrothermal events, albeit closely spaced in time (within about 100,000 years). This is not an

unreasonably brief time in light of data from modern geothermal fields, where measured flow rates and fluid compositions indicate that a million ounces of gold can be transported in about 500 to 600 years (Seward, 1989; Krupp and Seward, 1987). If 10 percent of transported gold is deposited, a million-ounce gold deposit could be produced in as little as 5,000 to 6,000 years. Indeed, $^{40}\text{Ar}/^{39}\text{Ar}$ data from the giant volcanic-hosted gold-silver deposit at Round Mountain (18 million ounces of gold) indicate that this deposit formed in less than 100,000 years and probably less than 50,000 years (Henry and others, 1996, 1997).

Table 1. Geochemical characteristics of Tuscarora area mineral deposits (n=48).

	Ag/Au	Ag ppm	As ppm	Au ppm	Ba ppm	Bi ppm	Ca %	Cu ppm	Fe ppm	Hg ppm
Silver-Rich Deposits										
Mean	309.2	486.4	246.5	1.48	695	0.64	2.60	19.09	4.99	0.58
Median	106.7	31.4	108	0.341	494	0.61	0.15	11.4	2.73	0.256
High	2054	4854	1515	24.7	2019	1.23	24.71	92.4	19.15	5.03
Low	12.1	0	14	0.003	49	0.34	0.04	1.1	0.67	0.017
Gold Deposits										
Mean	24.8	69.77	809.3	3.659	859.8	0.53	0.06	7.71	1.51	0.687
Median	11.9	2.78	47.9	0.208	700	0.48	0.06	5.83	1.35	0.404
High	147	777	8901	17.7	1502	1.04	0.16	20	6.26	2.28
Low	1.4	<0.02	5.1	0.016	89	0.39	0.01	2.22	0.29	0.024
	Li ppm	Mn ppm	Mo ppm	Pb ppm	Sb ppm	Se ppm	Te ppm	Tl ppm	V ppm	Zn ppm
Silver-Rich Deposits										
Mean	26.7	4152	9.02	434.5	35.81	5.99	0.2	1.69	41.0	451.9
Median	23	301	3.54	87.6	7.43	1.58	0.18	1.47	33	90.2
High	68	56482	56.6	3745	355	77.9	0.66	5.69	141	5699
Low	6	32	1.08	16	0.8	0	0	0.87	4	4.3
Gold Deposits										
Mean	49.4	202	5.33	50.5	61.63	2.09	0.22	1.38	18.8	49.3
Median	40	23	2.53	18.4	4.75	0.26	0.12	1.21	18	5.72
High	108	1071	26.6	463	656	23.8	1.8	2.24	45	398
Low	23	7	1.16	1.78	1.56	0	0	0.7	6	2.48

We believe that the silver-rich and gold deposits are not zoned counterparts but represent discrete hydrothermal events that were closely spaced in time. This is supported by the consistent and distinctive mineralogical and geochemical characteristics of both deposit types over large areas with little spatial overlap. In any case, the timing and location of both styles of precious-metal deposits are consistent with hydrothermal circulation having been driven by intrusions of the Mount Neva episode, in particular the early dacites.

The deposits at Tuscarora are volcanic hosted and epithermal, but siliceous, upper-plate Paleozoic rocks that are present in the walls of both the Mount Blitzen volcanic center and Big Cottonwood Canyon caldera underlie the volcanic host rocks. More prospective, carbonate-bearing, lower-plate rocks, which are the principal hosts for Carlin-type deposits, underlie the siliceous rocks, probably at depths no greater than the inferred 3- to 4-km paleodepths of Carlin ore bodies (Kuehn and Rose, 1995; Leonardson and Rahn, 1996; Lamb and Cline, 1997). For example, these rocks crop out and host gold deposits in the Independence Mountains just 15 to 20 km to the east. The dacite intrusions of the Mount Neva episode, which we interpret to have driven

hydrothermal circulation, must intrude the Paleozoic rocks. The hydrothermal fluids that generated volcanic-hosted deposits at Tuscarora almost certainly interacted with these deeper seated rocks. Although specific conditions of alteration at depth are speculative, the hydrothermal system could have generated Carlin-type, distal-disseminated, skarn, or manto deposits in the lower-plate rocks. With the major exception of relatively high silver/gold, the trace element signature of Tuscarora deposits is similar to that of Carlin-type deposits: moderate to high levels of arsenic, antimony, mercury, and thallium and generally low levels of base metals and magmatic components such as bismuth, tellurium, and molybdenum.

In summary, the precious-metal deposits at Tuscarora are located along and mainly just outside the southeastern margin of the Mount Blitzen volcanic center. The productive, east-northeast- and north-northwest-striking veins in the district are subparallel to dikes and north-northwest faults that both transect and in part bound the Mount Blitzen volcanic center. The orientations of these structures and senses of displacement are consistent with a modest amount of northwest-directed extension. Ore deposition occurred at or near the close of a major pulse of volcanic activity in the region and is temporally and spatially associated with the early dacite intrusions of the

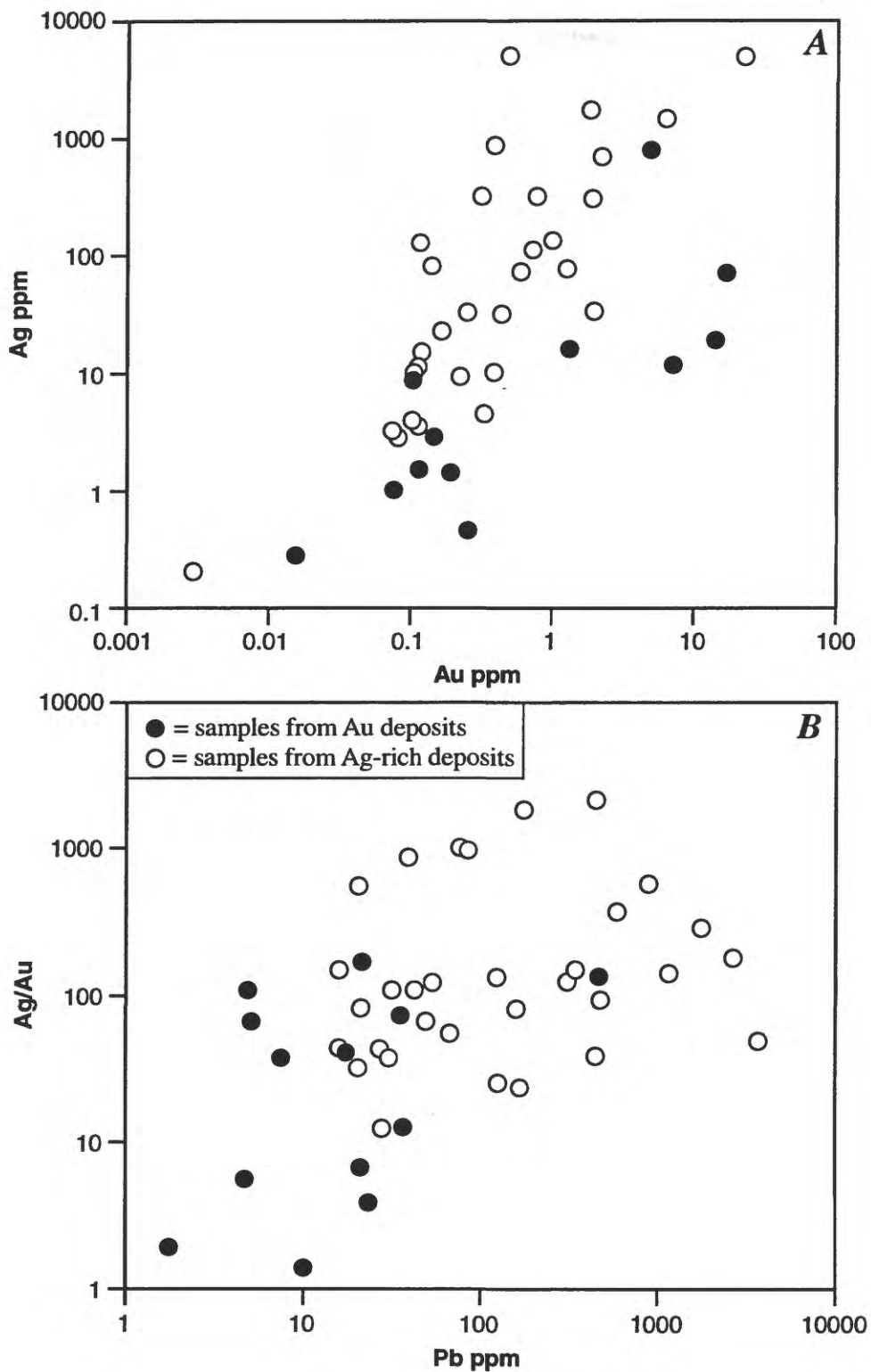


Figure 5. Scatter plots of A, Au versus Ag, and B, Ag/Au versus Pb. Ag-rich deposits have similar Au contents, but generally much higher Ag contents, than do Au or Ag-poor deposits. Ag-rich deposits also have higher Pb concentrations than do Ag-poor deposits.

Mount Neva intrusive episode. These intrusions are inferred to be the heat source that drove hydrothermal fluids that produced the deposits at Tuscarora. Mineral deposits at Tuscarora consist of silver-rich and silver-poor ore that we consider to represent two separate, short-lived hydrothermal events closely spaced in time, i.e., both having formed, as indicated from precise $^{40}\text{Ar}/^{39}\text{Ar}$ dating, within about 100,000 years.

ACKNOWLEDGMENTS

Geologic mapping of the Tuscarora volcanic field was supported by the STATEMAP program (Contracts 1434-HQ-96-AG-01502 and 1434-HQ-97-AG-01766) and Nevada Gold project of the U.S. Geological Survey and by Homestake Mining Company and Newcrest Resources, Inc. $^{40}\text{Ar}/^{39}\text{Ar}$ ages were determined by CDH in the Geochronology Laboratory of the New Mexico Bureau of Mines and Mineral Resources, under the guidance of Bill McIntosh and Matt Heizler. We thank Jean Cline for fluid inclusion data and Alan Wallace and David John for thorough, constructive reviews.

REFERENCES CITED

- Arehart, G. B., Foland, K. A., Naeser, C. W., and Kesler, S. E., 1993, $^{40}\text{Ar}/^{39}\text{Ar}$, K/Ar, and fission track geochronology of sediment-hosted disseminated gold deposits at Post-Betze, Carlin trend, northeastern Nevada: *Economic Geology*, v. 88, p. 622-646.
- Berger, B. R., Ridley, W. I., and Tingley, J. V., 1991, Interrelationship of mineralization, volcanism, and tectonism, northern Tuscarora Mountains, Elko County, Nevada, in Thorman, C. H., ed., Some current research in eastern Nevada and western Utah: U.S. Geological Survey Open-file Report 91-386, p. 13-19.
- Boden, D. R., Struhsacker, E. M., and Wright, B. A., 1993, Structurally controlled volcanism and contrasting types of mineralization, Tuscarora mining district and vicinity, Nevada: *Geological Society of America Abstracts with Programs*, v. 25, no. 6, p. 11.
- Bodnar, R. J., Reynolds, T. J., and Kuehn, C. A., 1985, Fluid inclusion systematics in epithermal systems, in Berger, B. R., and Bethke, P. M., eds., *Geology and Geochemistry of Epithermal Systems*, *Reviews in Economic Geology*, v. 2, p. 73-98.
- Brooks, W. E., Thorman, W. E., and Snee, L. W., 1995, The $^{40}\text{Ar}/^{39}\text{Ar}$ ages and tectonic setting of the middle Eocene northeast Nevada volcanic field: *Journal of Geophysical Research*, v. 100, p. 10,403-10,416.
- Churkin, M., Jr., and Kay, M., 1967, Graptolite-bearing Ordovician siliceous and volcanic rocks, northern Independence Range, Nevada: *Geological Society of America Bulletin*, v. 78, p. 651-668.
- Clark, T. M., Ehman, K. D., and Axelrod, D. I., 1985, Late Eocene extensional faulting in the northern Basin and Range province, Nevada: *Geological Society of America Abstracts with Programs*, v. 17, no. 6, p. 348.
- Coats, R. R., 1987, *Geology of Elko County, Nevada*: Nevada Bureau of Mines and Geology Bulletin 101, 112 p.
- Crawford, K. S., 1992, *The geology of the Tuscarora mining district, Elko County, Nevada*: M. S. thesis, University of Nevada, Reno, 85 p.
- Cruson, M. G., and Limbach, F. W., 1985, Progress report, Cow Creek prospect, Elko County, Nevada: Nevada Bureau of Mines and Geology Open-file report, File 75, Item 11, 21 p.
- Emsbo, P., Hofstra, A., Park, D., Zimmerman, J. M., and Snee, L., 1996, A mid-Tertiary age constraint on alteration and mineralization in igneous dikes on the Goldstrike property, Carlin trend, Nevada: *Geological Society of America Abstracts with Programs*, v. 28, p. A-476.
- Groff, J. A., Heizler, M. T., McIntosh, W. C., and Norman, D. I., 1997, $^{40}\text{Ar}/^{39}\text{Ar}$ dating and mineral paragenesis for Carlin-type gold deposits along the Getchell trend, Nevada: Evidence for Cretaceous and Tertiary gold mineralization: *Economic Geology*, v. 92, p. 601-622.
- Haas, J. L., Jr., 1971, The effect of salinity on the maximum thermal gradient of a hydrothermal system at hydrostatic pressure: *Economic Geology*, v. 66, p. 940-946.
- Hedenquist, J. W., and Henley, R. W., 1985, Hydrothermal eruptions in the Waiotapu geothermal system, New Zealand: Their origin, associated breccias, and relation to precious metal mineralization: *Economic Geology*, v. 80, p. 1640-1668.
- Henry, C. D., and Boden, D. R., 1997, Eocene magmatism of the Tuscarora volcanic field, Elko County, Nevada, and implications for Carlin-type mineralization, in Vikre, P., Thompson, T. B., Bettles, K., Christensen, O., and Parratt, R., eds., *Carlin-type gold deposits field conference: Society of Economic Geologists Guidebook Series*, v. 28, p. 193-202.
- Henry, C. D., and Boden, D. R., 1998, Geologic map of the Mount Blitzen quadrangle, Elko County, northeastern Nevada: Nevada Bureau of Mines and Geology Map 110.
- Henry, C. D., Castor, S. C., and Elson, H. B., 1996, Geology and $^{40}\text{Ar}/^{39}\text{Ar}$ geochronology of volcanism and mineralization at Round Mountain, Nevada, in Coyner, A. R., and Fahey, P. L., eds., *Geology and Ore Deposits of the American Cordillera: Geological Society of Nevada Symposium Proceedings, Reno/Sparks, Nevada, April, 1995*, p. 283-307.
- Henry, C. D., Elson, H. B., McIntosh, W. C., Heizler, M. T., and Castor, S. B., 1997, Brief duration of hydrothermal activity at Round Mountain, Nevada determined from $^{40}\text{Ar}/^{39}\text{Ar}$ geochronology: *Economic Geology*, v. 92, p. 807-826.
- Hofstra, A. H., 1995, Timing and duration of Carlin-type gold mineralization in Nevada and Utah - Relation to back-arc extension and magmatism: *Geological Society of America Abstracts with Programs*, v. 27, p. A-329.
- Ilchik, R. P., and Barton, M. D., 1997, An amagmatic origin of Carlin-type gold deposits: *Economic Geology*, v. 92, p. 269-288.
- Janecke, S. U., Hammond, B. F., Snee, L. W., and Geissman, J. W., 1997, Rapid extension in an Eocene volcanic arc: Structure and paleogeography of an intra-arc half graben in central Idaho: *Geological Society of America Bulletin*, v. 109, p. 253-267.
- Krupp, R. E., and Seward, T. M., 1987, The Rotokawa geothermal system, New Zealand: An active epithermal gold-depositing environment: *Economic Geology*, v. 82, p. 1109-1129.
- Kuehn, C. A., and Rose, A. W., 1995, Carlin gold deposits, Nevada: Origin in a deep zone of mixing between normally pressured

- and over pressured fluids: *Economic Geology*, v. 90, p. 17-36.
- Lamb, J. B., and Cline, J., 1997, Depths of formation of the Meikle and Betze/Post deposits, *in* Vikre, P., Thompson, T. B., Bettles, K., and Parratt, R., eds., Carlin-type gold deposits field conference: Society of Economic Geologists Guidebook Series, v. 28, p. 101-107.
- LaPointe, D. D., Tingley, J. V., and Jones, R. B., 1991, Mineral resources of Elko County, Nevada: Nevada Bureau of Mines and Geology Bulletin 106, 236 p.
- Leonardson, R. W., and Rahn, J. E., 1996, Geology of the Betze-Post gold deposits, Eureka County, Nevada, *in* Coyner, A. R., and Fahey, P. L., eds., Geology and Ore Deposits of the American Cordillera: Geological Society of Nevada Symposium Proceedings, Reno/Sparks, Nevada, April, 1995, p. 61-94.
- Miller, E. M., and Larue, D. K., 1983, Ordovician quartzite in the Roberts Mountains allochthon, Nevada: Deep sea fan deposits derived from cratonic North America, *in* Stevens, C. H., ed., Pre-Jurassic rocks in western North American suspect terranes: Society of Economic Paleontologists and Mineralogists, Pacific Section, Special Publication, p. 91-102.
- Miller, E. M., Miller, M. M., Stevens, C. H., Wright, J. E., and Madrid, R. J., 1992, Late Paleozoic paleogeographic and tectonic evolution of the western U.S. Cordillera, *in* Burchfiel, B. C., Lipman, P. W., and Zoback, M. L., eds., The Cordilleran Orogen: Conterminous U.S.: Boulder, Colorado, Geological Society of America, The Geology of North America, v. G-3, p. 57-106.
- Nolan, T. B., 1936, The Tuscarora mining district, Elko County, Nevada: University of Nevada Bulletin, v. 30, 36 p.
- Phinisey, J. D., Hofstra, A. H., Snee, L. W., Roberts, T. T., Dahl, A. R., and Loranger, R. J., 1996, Evidence for multiple episodes of igneous and hydrothermal activity and constraints on the timing of gold mineralization, Jerritt Canyon district, Elko County, Nevada, *in* Coyner, A. R., and Fahey, P. L., eds., Geology and Ore Deposits of the American Cordillera: Geological Society of Nevada Symposium Proceedings, Reno/Sparks, Nevada, April, 1995, p. 15-39.
- Poole, F. G., Stewart, J. H., Palmer, A. R., Sandberg, C. A., Madrid, R. J., Ross, R. J., Jr., Hintze, L. F., Miller, M. M., and Wrucke, C. T., 1992, Latest Precambrian to latest Devonian time; Development of a continental margin, *in* Burchfiel, B. C., Lipman, P. W., and Zoback, M. L., eds., The Cordilleran Orogen: Conterminous U.S.: Boulder, Colorado, Geological Society of America, The Geology of North America, v. G-3, p. 9-56.
- Roberts, R. J., 1964, Stratigraphy and structure of the Antler Peak quadrangle, Humboldt and Lander Counties, Nevada: U.S. Geological Survey Professional Paper 459-A, 93 p.
- Rota, J. C., 1996, Gold Quarry: a geologic update, *in* Green, S. M., and Struhsacker, E., eds., Geology and Ore Deposits of the American Cordillera: Geological Society of Nevada Field Trip Guidebook Compendium, Reno/Sparks, Nevada, April, 1995, p. 157-166.
- Seward, T. M., 1989, The hydrothermal chemistry of gold and its implications for ore formation: Boiling and conductive cooling as examples, *in* Keays, R. R., Ramsay, W. R. H., and Groves, D. I., eds., The Geology of Gold Deposits: The Perspective in 1988, *Economic Geology Monograph* 6, p. 398-404.
- Sillitoe, R. H., and Bonham, H. F., Jr., 1990, Sediment-hosted gold deposits; distal products of magmatic-hydrothermal systems: *Geology*, v. 18, p. 157-161.
- Thorman, C. H., Brooks, W. E., Snee, L. W., Hofstra, A. H., Christensen, O. D., and Wilton, D. T., 1995, Eocene-Oligocene model for Carlin-type deposits in northern Nevada: Geological Society of Nevada Symposium, April, 1995, Reno/Sparks, Nevada, p. 75.
- Wallace, A. R., and John, D. A., this volume, New studies of Tertiary volcanic rocks and mineral deposits, northern Nevada rift *in* Tosdal, R. M., ed., Contributions to the gold metallogeny of the northern Nevada: U.S. Geological Open-File Report .